



University of  
**BRISTOL**

# **Developing A New Class of Molecular Machine: Light-Fuelled Single-Bond Rotors**

Oliver M. Bayley

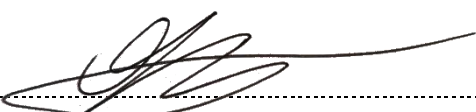
Supervisor: Dr Beatrice Collins

School of Chemistry, September 2023

*A dissertation submitted to the University of Bristol in accordance with the requirements for award of  
the degree of Ph.D. in the Faculty of Science.*

## **Authors Declaration**

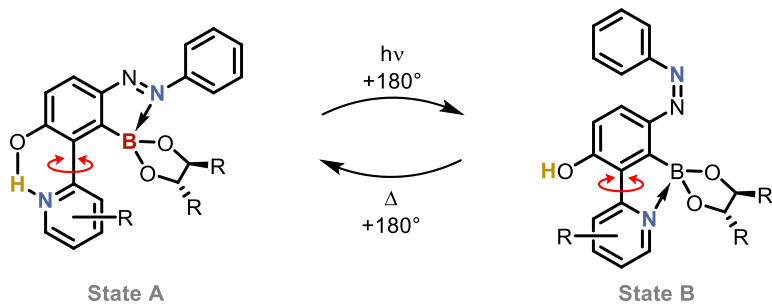
I declare that the work in this thesis was carried out in accordance with the requirements of the *University's Regulations and Code of Practice for Research Degree Programmes* and that it has not been submitted for any other academic award. Except where indicated by specific reference in the text, the work is the candidate's own work. Work done in collaboration with, or with the assistance of, others, is indicated as such. Any views expressed in the report are those of the author.

SIGNED:  DATE: 29/09/2023

## Abstract

Due to the central role of molecular machines in biological systems, chemists have long sought to create synthetic equivalents, for the development of future nanoscale technologies.<sup>1</sup> For molecular machines to play a diverse role in these technologies, a variety of machines which exhibit different types of motion or use different types of fuels are needed. The research herein details new work towards the development of a novel class of molecular machine which uses light to drive rotation around an inherently non-light-responsive single C–C bond. While many classes of molecular machines have been developed, as discussed in chapter 1, the class of light-fuelled single-bond rotor is yet to be realized.

In our design, light controlled formation of one of two competing N–B bonds allows switchable control over two 180° rotary states of a borylated azo-biaryl scaffold (states A and B). In the lowest energy state (state A), the azo nitrogen should form a dative bond with the boronic ester while the pyridine nitrogen should form an intramolecular hydrogen bond. Upon UV irradiation, the light responsive azobenzene moiety can undergo *E*-to-*Z* photoisomerization, breaking the N<sub>azo</sub>–B bond. This should in turn cause the pyridine ring to undergo a 180° rotation around the central C–C bond to form a new N<sub>pyr</sub>–B bond (state B). Upon thermal relaxation back to the *E* isomer, the azobenzene nitrogen outcompetes the pyridine nitrogen for boronic ester binding, causing the pyridine ring to undergo a second 180° rotation, reforming the lower energy initial state (State A). If the chirality of the biaryl axis can be controlled using a chiral boronic ester, it opens the possibility of controlling the trajectory of these pyridyl ring rotations and would provide the foundations for a light-fuelled single-bond rotor.



To better understand the central N<sub>azo</sub>–B and N<sub>pyr</sub>–B bonds, azobenzene and biaryl-pyridine model systems were synthesized, with their study described in chapters 2 and 3. These studies provided novel insights into the nature of these N–B bonds, their involvement in photochemical processes and demonstrated that chiral boron ligands had the ability to influence the chirality of the biaryl axis.

As discussed in chapter 4, the multistep synthesis of the target azo-biaryl proved challenging but ultimately successful and was used to make a variety of differently substituted azo-biaryl scaffolds. In chapter 5 a selection of these scaffolds were studied by  $^{11}\text{B}$  and  $^{15}\text{N}$  NMR, compared against other benchmarking standards, and the NMR data used to understand how the balance between intramolecular bonds can be controlled by the pyridyl substitution. These findings are then used to identify a suitable motor candidate in which the  $\text{N}_{\text{azo}}-\text{B}$  bond formation is favoured in state A. Having established methods of favouring the  $\text{N}_{\text{azo}}-\text{B}$  bond formation in state A, the photoswitching between these N–B bonds was investigated and shown to be a viable process. Due to rapid rates of thermal relaxation in the hydroxy azobenzenes, the research shifted towards the development of new UV-Vis and NMR equipment which allowed the azobenzene systems to be monitored under constant irradiation. Finally, the new avenues of research stemming from this work, the ongoing efforts and the future of the project are discussed in chapter 6.

## Acknowledgements

First and foremost, I like to thank Dr. Beatrice Collins for her fantastic guidance and support throughout the duration of my PhD. Your creativity and drive have been truly inspirational to be around, and your resolute attention to detail has definitely pushed me to improve in all aspects of chemistry, for which I am hugely grateful! I feel extremely fortunate to have been given the opportunity to work on such a creative and diverse project and to have been able to do so amongst a group with such a range of projects. You have been a fantastic mentor and I have hugely appreciated that your door was always open for a chat, chemistry or otherwise.

PhDs are never easy tasks, so I am extremely thankful to my family for their encouragement and support through thick-and-thin, especially to my partner Dani. Dani, you have constantly been a massive support throughout this time, and I know that my time here has been made better because of you. I'm really lucky to have you in my life.

I was very fortunate to have been able to work with such a sociable group who have made my day-to-day experience all the better, particularly the Friday nights. There has been a number of people pass through the group during my time, all of whom I would like to thank but a particular thanks goes to Aidan, Michael, Greg, Connah, Jordan, Emma, Liv, Charlotte, Jamie, Sarah and Nick. Aidan, thanks for leading the way in the group's early days when it felt like the blind leading the blind, you took on a ton of responsibility and really led by example. I hope your new role treats you well and brings in enough Avios points to keep taking first-class flights. Michael, it's been great working beside you over the past few years and I hope the final stretch of the thesis writing goes well. Still have my fingers crossed that your NFT makes you rich one of these days. Connah, you were one of the first people I met here and you've been one of my closest mates since, thanks for falling victim to a few spoons lunches that went longer than intended. Jordan, thanks for all of the French chats, it's been great having the opportunity to dust off what French I can pull out, and thanks for all the chemistry advice, you've been a life saver more times than I'd like to admit. I hope Manchester treats you well. Emma, thanks for being a crazy little sister. I'm going to miss your chaos and I'm looking forward to seeing you and Connah in Amsterdam. I hope you and Liv enjoy being the 'old' PhDs now that I'm gone. Liv, I hope you keep being a solve-all cheat for the crossword and

I'm looking forward to seeing your and Jordan's paper. Charlotte, it was great chatting F1 with you and I hope your job in Oxford is going well. Jamie, wish you'd joined the group earlier! it's been great having you around in the lab, at the pub, and on the football field. Good luck with organizing the Wednesday football. Sarah, you've been shockingly sane for a PhD student, don't let Emma's insanity infect you too much. Good luck with the next few years.

I would also like to give a particular mention to Ben, Dawn, Chris and Sam from the Bower, Aggarwal and Lennox groups. You guys have been really sound lot and have much made my time in Bristol way more fun. I'm looking forward to seeing you all in Amsterdam. I would also like to thank the chem football group, particularly Alex, for organizing a midweek football game which has been a great way of breaking up the week.

I would also like to thank the technical staff at the University of Bristol for their help throughout my studies. I am especially grateful to Paul Laurance, who has been a lifeline for all NMR work. Thanks also go to Dr. Chris Williams (NMR), Sam Ferrins (NMR/MS), Dr. Paul Gates (MS), Dr. Hazel Sparkes (School of Chemistry X-ray Crystallography Service) and Dr. Natalie Pridmore (School of Chemistry X-ray Crystallography Service) for their help with NMR, MS and X-ray crystallography. I would also like to thank Tony Rogers for keeping the labs running as well as Paul Egan, Mark Wiltshire, and Vincent Reardon at stores.

A huge thanks goes to Paul Pringle for the significant amount of safety management work he took on to keep the school open for research during the COVID pandemic.

In order to conduct research, access to published literature is essential. As such, I would also like to thank Alexandra Elbakyan for helping to remove all barriers in the way of science.

## Table of Contents

<b>Authors Declaration .....</b>	<b>i</b>
<b>Abstract .....</b>	<b>ii</b>
<b>Acknowledgements .....</b>	<b>iv</b>
<b>Chapter 1 Introduction .....</b>	<b>1</b>
1.1    Preface.....	1
1.1.1    Terminology .....	1
1.1.2    Introduction Overview.....	3
1.2 <i>Chemically Fuelled Single-Bond Rotors</i> .....	4
1.2.1    Pioneering Work Towards Chemically Fuelled Motion.....	4
1.2.2    Protecting Group Rotary Motors .....	6
1.2.3    Redox Cycle Rotary Motor .....	9
1.2.4    Lactonization-Hydrolysis Rotary Motors .....	10
1.2.5    Summary of Chemically Fuelled Single-Bond System Development .....	13
1.3 <i>Light-Fuelled Motion</i> .....	14
1.4 <i>Light Fuelled Double Bond Systems</i> .....	16
1.4.1    Four-Step Alkene Rotor Systems .....	16
1.4.2    Two-Stroke Imine System .....	17
1.4.3    Hula Twist Systems.....	18
1.4.4    Summary of Light Fuelled Double Bond System Development .....	20
1.5 <i>Light Gated Free-Rotation Around Single-Bond Axes</i> .....	21
1.5.1    Steric Control of Rotation.....	21
1.5.2    Coordination Control of Rotation .....	23
1.5.3    Summary of Light Controlled Non-Directional Single-Bond Systems .....	24
1.6 <i>Light-Fuelled Single-Bond Switching</i> .....	25
1.6.1    Switching Ferrocene Scissors .....	25
1.6.2    Switching Biaryl Scissors.....	26
1.6.3    Summary of Light Controlled Single-Bond Oscillation Systems .....	27
1.7 <i>Motion Transmission from Alkene Motors to C–C Single-Bonds</i> .....	28
1.7.1    Summary of Alkene Motor Motion Transmission to C–C Single-Bonds.....	30
1.8 <i>Project Aims</i> .....	31
<b>Chapter 2 Azobenzene Model Systems .....</b>	<b>35</b>
2.1 <i>Introduction</i> .....	35
2.2 <i>Photoswitch Ligand Identification</i> .....	37

<i>2.3 Synthesis of Boryl-Azobenzene Switches.....</i>	<i>38</i>
<i>2.4 Assessment of N<sub>azo</sub>-B Bond and Photoisomerization.....</i>	<i>40</i>
<i>2.4.1 Formation of N<sub>azo</sub>-B Bond in E Isomer.....</i>	<i>40</i>
<i>2.4.2 Photoswitching and PSS Assessment .....</i>	<i>43</i>
<i>2.4.3 Loss of N<sub>azo</sub>-B Bond in Z Isomer .....</i>	<i>45</i>
<i>2.4.4 Lewis Acidity Testing via Pyridine Binding .....</i>	<i>46</i>
<i>2.4.5 Pyridine Nucleophile Effect on the Boryl-Azobenzene PSS .....</i>	<i>47</i>
<i>2.5 Summary of Chapter 2.....</i>	<i>48</i>
<b><i>Chapter 3 Biaryl Model Systems.....</i></b>	<b><i>50</i></b>
<i>3.1 Introduction .....</i>	<i>50</i>
<i>3.1.1 N<sub>azo</sub>-B Bond Formation and Tuning .....</i>	<i>50</i>
<i>3.1.2 Chirality Transfer and Rotation Barrier Effects.....</i>	<i>51</i>
<i>3.2 Synthesis of Axially Strained Borylated Biaryls.....</i>	<i>52</i>
<i>3.3 Analysis of the N<sub>pyr</sub>-B Bond Strength and Formation.....</i>	<i>53</i>
<i>3.4 Chirality Transfer and Rotation Barrier Effects .....</i>	<i>54</i>
<i>3.5 Hydrogen Bond Formation and Effect on the Rotation Barrier .....</i>	<i>57</i>
<i>3.6 Summary of Chapter 3.....</i>	<i>59</i>
<b><i>Chapter 4 Synthesis of the Borylated Azo-Biaryl Scaffold .....</i></b>	<b><i>60</i></b>
<i>4.1 Proposed Retrosynthesis.....</i>	<i>60</i>
<i>4.2 Synthesis.....</i>	<i>61</i>
<i>4.2.1 Initial Attempt via Late-Stage C-H Functionalization .....</i>	<i>61</i>
<i>4.2.2 Synthesis via Boron Protection.....</i>	<i>70</i>
<i>4.3 Summary of Chapter 4.....</i>	<i>82</i>
<b><i>Chapter 5 Analysis of Motor and Comparison to Analogues and Standards. ....</i></b>	<b><i>83</i></b>
<i>5.1 N<sub>azo</sub>-B vs N<sub>pyr</sub>-B bonding .....</i>	<i>83</i>
<i>5.2 Intramolecular Bond Assessment .....</i>	<i>83</i>
<i>5.2.1 Control Systems and Benchmarking of <sup>11</sup>B and <sup>15</sup>N NMR Shifts .....</i>	<i>83</i>
<i>5.2.2 Influence of Pyridyl Substitution on N-B Bond Formation.....</i>	<i>87</i>
<i>5.2.3 Hydrogen Bond Formation .....</i>	<i>92</i>
<i>5.3 Photochemical Studies .....</i>	<i>94</i>
<i>5.4 Equipment Development and Model System Benchmarking .....</i>	<i>101</i>
<i>5.4.1 UV-Vis Spectroscopy .....</i>	<i>101</i>
<i>5.4.2 NMR Spectroscopy .....</i>	<i>110</i>
<i>5.5 Preliminary Studies of the Boryl-Azo-Biaryl 187b .....</i>	<i>116</i>

<i>5.6 Summary of Chapter 5</i> .....	<i>117</i>
<b>Chapter 6 Conclusions and Future Work</b> .....	<b>119</b>
<i>6.1 Model Systems</i> .....	<i>119</i>
<i>6.2 Synthesis and Bonding Analysis</i> .....	<i>121</i>
<i>6.3 Equipment development</i> .....	<i>123</i>
<i>6.4 Remaining Work</i> .....	<i>125</i>
<b>Chapter 7 Appendix</b> .....	<b>128</b>
<i>List of Abbreviations</i> .....	<i>128</i>
<i>List of Figures</i> .....	<i>132</i>
<i>List of Schemes</i> .....	<i>137</i>
<i>List of Tables</i> .....	<i>140</i>
<b>Chapter 8 Experimental Data</b> .....	<b>141</b>
<i>8.1 General Experimental Details</i> .....	<i>141</i>
<i>8.2 General Synthetic Procedures</i> .....	<i>144</i>
<i>8.3 Compound Data</i> .....	<i>148</i>
<i>8.4 Photochemistry</i> .....	<i>242</i>
<i>8.4.1 Photochemistry – Initial Irradiation Experiments</i> .....	<i>242</i>
<i>8.4.2 Photochemistry - Online UV-Vis Experiments</i> .....	<i>243</i>
<i>8.4.3 Photochemistry – <i>in situ</i> NMR Experiments</i> .....	<i>245</i>
<i>8.4.4 Photochemistry –Photostationary States Established by <sup>1</sup>H NMR</i> .....	<i>246</i>
<i>8.5 XRD Crystallographic data</i> .....	<i>255</i>
<i>8.6 Supplementary Data and Optimization Tables</i> .....	<i>258</i>
<i>8.6.1 C–H Borylation Testing</i> .....	<i>258</i>
<i>8.6.2 Azobenzene-TIDA NMR</i> .....	<i>259</i>
<i>8.6.3 Second Hindered Suzuki cross-coupling Ligand Screen</i> .....	<i>260</i>
<i>8.6.4 Addition of Water to Twisted H-bonding Compound 194</i> .....	<i>261</i>
<i>8.6.5 Python Script for UV-Vis data acquisition.</i> .....	<i>262</i>
<b>References</b> .....	<b>266</b>

## **Chapter 1 Introduction**

### **1.1 Preface**

Over the past three decades, substantial research has been conducted into developing artificial molecular machines which mimic motion observed in biological systems and the macroscopic world.<sup>1-4</sup> As the development of synthetic molecular machines are heavily inspired by life-critical biological systems, such as the rotating ATP (Adenosine triphosphate) synthase motor or kinesin walker proteins, they hold huge potential for the development of new artificial processes, new materials and new technologies.<sup>5, 6</sup> The significance of these endeavours was recognized by the award of the 2016 Nobel Prize in Chemistry to B. L. Feringa, J. F. Stoddart and J. P. Sauvage for “the design and synthesis of molecular machines”.<sup>7-11</sup>

#### **1.1.1 Terminology**

To effectively discuss artificial molecular machines, it is useful to define the terms ‘machine’, ‘switch’ and ‘motor’. To this end, the definitions proposed by Leigh and co-workers from their 2015 and 2017 reviews of the field are used herein.<sup>1,3,12</sup> Following these definitions, a *molecular machine* is defined as any molecular-scale system in which stimulation triggers the controlled motion of (sub)molecular components with respect to other components of the system. A *molecular switch* is a subtype of molecular machine which reversibly shifts between two (or more) states, undoing any mechanical work upon return to the original state.<sup>13</sup> A *molecular motor* is also a subtype of molecular machine, but crucially, once it returns to its original state, the work performed is not undone,<sup>12</sup>

To understand the difference between *molecular motors* and *molecular switches* the concept of *microscopic reversibility* must be addressed. In a *microscopically reverse* process, the return to the initial state occurs *via* the exact opposite pathway to the forwards pathway. Since it is the exact opposite process, it therefore undoes any work achieved by the forwards process. This plays an important role in molecular machines, particularly in molecular motors, as a machine which undergoes the microscopic reverse reactions/pathways to return to the initial state cannot generate any net work. This is of no impact to molecular switches as, by definition, they need not generate any net work and always return to the initial state *via* the microscopically reverse pathway.<sup>1,3</sup>

The difference between a *molecular switch* and a *molecular motor* in terms of *microscopic reversibility* is illustrated by a simple three state system shown in Figure 1. In Figure 1a, for the *molecular switch* to go from the starting state **A** to the final state **C**, it must pass through state **B** following the path **A** → **B** → **C**. For the system to return to the starting state **A**, it must proceed *via* the opposite path **C** → **B** → **A**. As the return path is the exact opposite to the initial path (i.e. the *microscopic reverse* pathway) any work performed by the **A** → **B** → **C** process must be undone by the subsequent **C** → **B** → **A** reversion. In the case of the *molecular motor* shown in Figure 1b, the system can follow the same **A** → **B** → **C** path to go from starting state **A** to the final state **C**, but unlike the *molecular switch*, the *molecular motor* is able to return directly to the starting state **A** following the path **C** → **A**. This path is not the exact opposite of the initial **A** → **B** → **C** path (i.e. **C** → **A** is not the *microscopic reverse* of **A** → **B** → **C**) meaning any work performed by the **A** → **B** → **C** process is not undone by the subsequent **C** → **A** process.

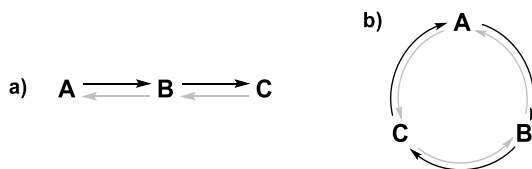


**Figure 1.** a) Representation of a molecular **switch** with the microscopically reverse pathway in grey. b) Representation of a molecular **motor** with the microscopically reverse pathway in grey.

Due to the importance of axial chirality to this work, it is important to clarify the terminology used herein. Consistent with the IUPAC guidelines, the *axial chirality* descriptors  $R_a$  (or  $R_{ax}$ ) and  $S_a$  (or  $S_{ax}$ ) are assigned according to the CIP assignment rules which define the substituent priorities on the axial unit, with the additional rule that the two near substituents have higher priority than the far ones (Figure 2a).<sup>14, 15</sup> The *helicity* descriptors  $M$  (*Minus*) and  $P$  (*Plus*) are used to describe the helical chirality of the molecules based on their screw axis (Figure 2b). Throughout this work the *helicity* descriptors  $M$  and  $P$  are used in a manner consistent with their use in helicene and alkene motor systems (Figure 2c and d).<sup>14, 15</sup> Defining *axial chirality* and *helicity* also facilitates a more accurate description of the complex systems discussed in Chapters 1 and 2.

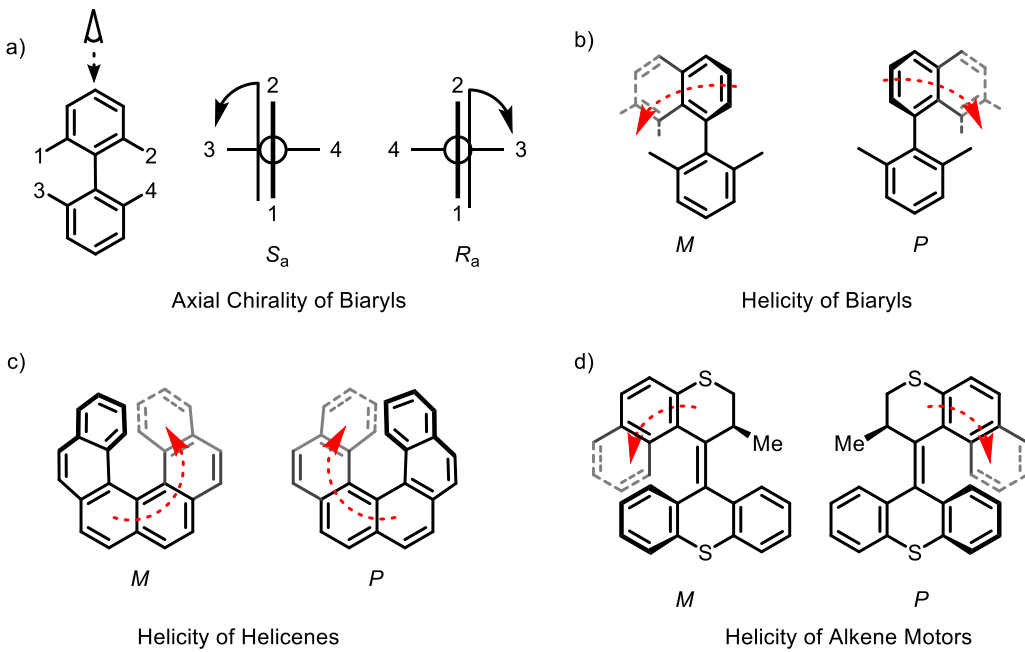


**Figure 2.** a) IUPAC recommended axial chirality terminology for biaryl systems. b) Helicity terminology for biaryl systems used herein. c) IUPAC recommended helicity terminology used in helicene systems. d) Helicity terminology used in alkene motor systems.

### 1.1.2 Introduction Overview

While many molecular machines have been developed (including light-driven overcrowded alkenes,<sup>16-20</sup> mechanically interlocked catenanes,<sup>21-23</sup> linear rotaxanes,<sup>24-26</sup> and molecular walkers,<sup>27, 28</sup>), achieving controlled motion around rotationally labile single-bond axes remains a formidable task. This introduction focusses on the development of the molecular rotors, which are currently divided into the chemically fuelled single-bond rotors (section 1.2) and the light-driven alkene rotors (section 1.4). Some examples of using light to influence motion around rotationally labile axes are examined and discussed in sections 1.5, 1.6 and 1.7, and drawing upon these seminal works a novel design for a new class of molecular machine, a light-driven single-bond rotor, is proposed in section 1.8.

## **1.2 Chemically Fuelled Single-Bond Rotors**

### **1.2.1 Pioneering Work Towards Chemically Fuelled Motion**

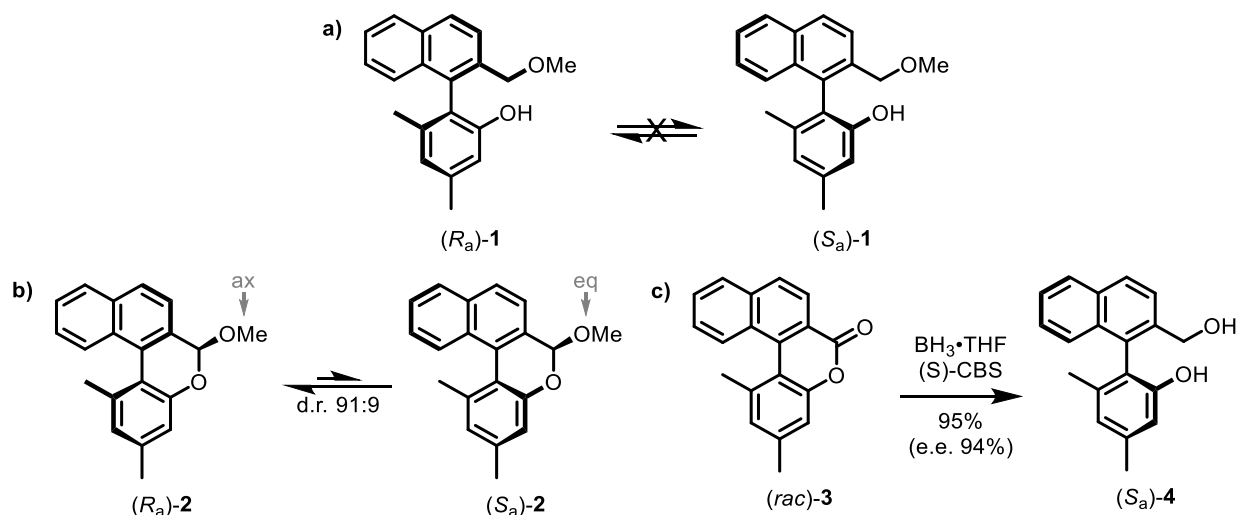
Single-bonds, particularly C–C single-bonds, are arguably the most fundamental moiety in organic chemistry and consequently, developing systems that can control the motion around these fundamental and rotationally labile bonds has been of significant interest to many chemists. The development of C–C single-bond rotors is the central focus of section 1.2, but a short summary of the work leading to the development of the first C–C single-bond rotors is briefly discussed to provide a context to their development.

Early pioneering from Iwamura and Mislow in 1988 reported one of the first systems to demonstrate that single bond rotation could be influenced by the steric interlocking of molecular components. Using an interlocked di-trptycene system, they were able to create molecular gears in which rotation about one bond caused coupled rotation about a second linked bond.<sup>29-32</sup> Although rotation in these systems was driven entirely by random Brownian motion, the use of carefully designed steric interactions to control bond rotation represented a milestone in the development of molecular rotors. Subsequently, a series of triptycene systems capable of greater rotational control were reported by Kelly and co-workers between 1994 and 2000, culminating in their phosgene powered triptycene ratchet.<sup>33-35</sup> This ratchet was the first example of unidirectional rotation powered by coupling steric encumbrance with selective, chemically fuelled steric barrier lowering, although the system was limited to performing 120° of rotation.

Although the bond rotation in Kelly and co-workers systems was limited, this was another landmark step in the field and highlighted that achieving unidirectional rotation was heavily reliant on the consumption of a fuel (so as not to violate the second law of thermodynamics).<sup>36</sup> Understanding the fuelling and subsequent energy dissipation of these systems has not only been crucial to the molecular machines field but has been of significant importance to the development of all out-of-equilibrium systems. Early work in 2003 from Mock and co-workers had shown it is possible to drive autonomous chemically-fuelled oscillation by anhydride formation and subsequent hydrolysis but in more recent years work from the groups of Di Stefano and Hartley have significantly expanded the out-of-equilibrium

field. The out-of-equilibrium systems pioneered by Hartley and coworkers have since played a pivotal role in the development of the systems described in section 1.2.4.<sup>37-40</sup>

Although the studies were not initially aimed towards the development of molecular machines, methodology work by Bringmann and co-workers had shown that biaryl compounds possessed a number of key features which made them ideal candidates for molecular machine scaffolds. Particularly, the biaryls systems possessed the ability to create tuneable steric barriers to single-bond rotation which could be selectively lowered by the formation of a five- or six-membered bridge between the upper and lower halves (Scheme 1, **1** vs **2**).<sup>41-46</sup> These systems had also shown that point chirality could influence the atropdiastereomeric preference of the bridged biaryls (Scheme 1b). Equally, chiral nucleophiles or chiral reducing agents could selectively form one atropisomer from racemic bridged biaryl material *via* dynamic kinetic resolution (DKR) (e.g., Scheme 1c).<sup>47</sup>



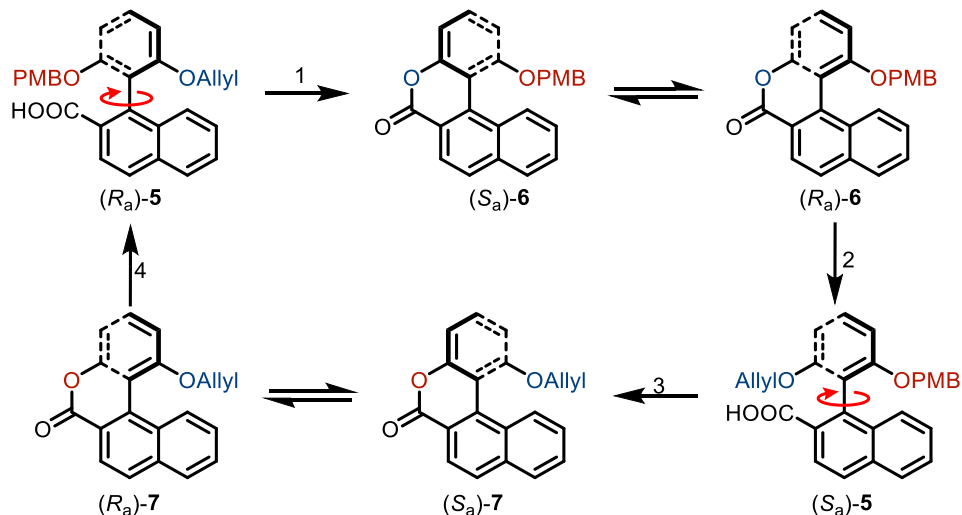
**Scheme 1.** Bringmann and co-workers 6-membered-bridge-containing biaryl which exhibited a diastereomeric preference based on the point chirality of the methoxy group.<sup>42</sup>

Inspired by these studies, Branchaud and co-workers proposed a series of biaryl based molecular rotors which used a lactonization, enantioselective nucleophilic ring opening and subsequent re-lactonization to drive a unidirectional rotation.<sup>42, 43, 45</sup> Unfortunately, due to fast single bond rotation and nucleophile cleavage issues, unidirectional rotation greater than 180° was never observed in these systems. While these systems were ultimately unable to achieve

controlled and unidirectional 360° rotation, they were significant advances in molecular rotor design as they highlighted the potential of biaryl scaffolds to be used in controlling single bond rotation.

### 1.2.2 Protecting Group Rotary Motors

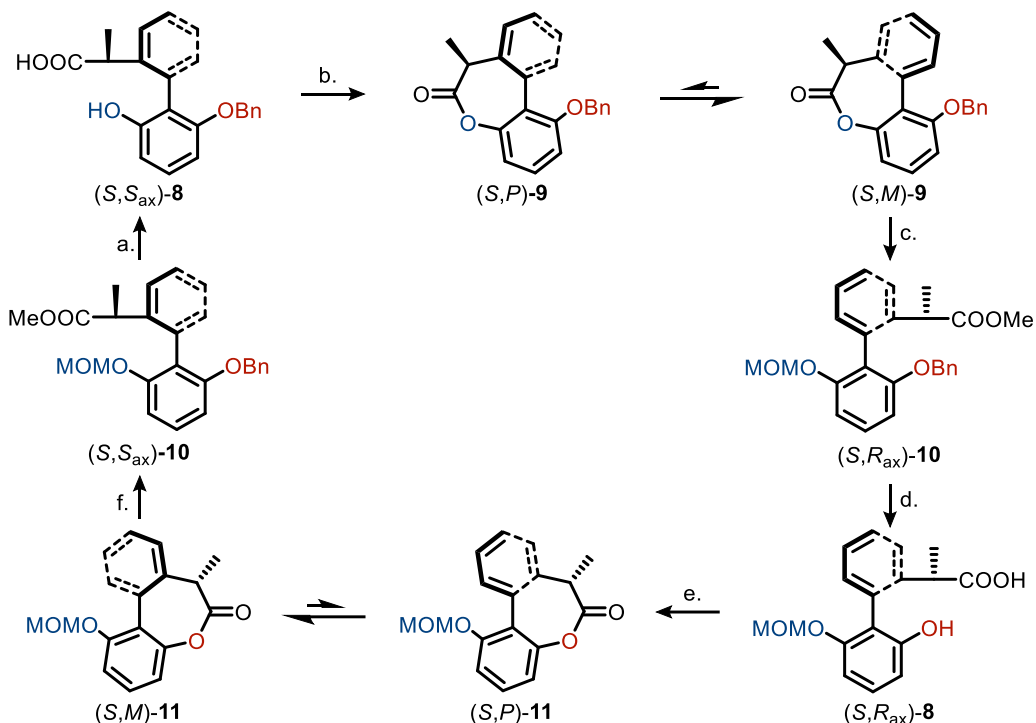
In 2005 Feringa and co-workers reported the first molecular motor capable of unidirectional 360° rotation around a single bond (Scheme 2).<sup>44</sup> Following from Bringmann and Branchaud's studies, the tetra-*ortho* substituted biaryl system had large barriers to rotation which could be overcome by the introduction of a lactone bridge to facilitate crossing of the biaryl axis. Using the DKR procedure pioneered by Bringmann and co-workers, Feringa and co-workers were able to atropselectively reduce the configurationally labile lactone using a CBS (Corey–Bakshi–Shibata) catalyst to get a single atropisomer.<sup>48, 49</sup> By employing orthogonal phenol protecting groups, they were then able to use a deprotection, lactonization, CBS reduction and reprotection strategy to operate the biaryl motor with exquisite (>90%) unidirectional efficiency. This protecting group strategy was not only useful for improving the net directionality of the system but was also crucial in allowing analysis of the motor's operation.



**Scheme 2.** Feringa and co-workers' first unidirectional single-bond rotary motor. (1) Allyl deprotection and lactonization; (2) Asymmetric lactone reduction, reinstatement of the allyl protecting group and oxidation to reform the carboxylic acid; (3) para-Methoxy benzyl deprotection and lactonization; (4) Asymmetric lactone reduction, reinstatement of the PMB protecting group and oxidation to reform the carboxylic acid.<sup>44</sup>

Starting from the doubly protected (*R*<sub>a</sub>)-**5**, allyl deprotection and subsequent DCC mediated coupling of the newly exposed phenolic hydroxy group led to the formation of lactone (*S*<sub>a</sub>)-**6**. This lactone was able to freely interconvert between (*S*<sub>a</sub>)-**6** and (*R*<sub>a</sub>)-**6** *via* bridge facilitated ring crossover, generating a racemic mixture of the two enantiomers. Selective CBS reduction of this mixture, followed by reinstallation of the allyl group and oxidation of the remaining primary alcohol, led to the generation of (*S*<sub>a</sub>)-**5** with high atroposelectivity (e.e. = 93.6%). PMB deprotection of this compound led to rotation and spontaneous lactonization to form a racemic mixture of lactones (*S*<sub>a</sub>)-**7** and (*R*<sub>a</sub>)-**7**. Finally, a second stereoselective CBS reduction, PMB re-protection and subsequent oxidation, regenerated the starting compound (*R*<sub>a</sub>)-**5** (e.e. = 80.6%), in an overall yield of 21% over the 10 steps to complete the 360° rotation.<sup>44</sup>

Following the same protecting group strategy, Feringa and co-workers produced a second biaryl system **8-11** (Scheme 3), which used a similar tri-*ortho* substituted scaffold with two orthogonally protected phenol groups.<sup>50</sup> While the new system used the same protecting group and lactone bridging strategy as **5-7** (Scheme 2), the directionality of the new system **8-11** was governed by a chiral substituent on the lactone bridge. This chirality meant that upon lactonization of **8** to form a pair of non-thermodynamically degenerate atropdiastereomers (*S,P*)-**9/11** and (*S,M*)-**9/11** (Scheme 1b), which could freely interconvert *via* rotation about the biaryl axis, a preference for one of the two diastereomers would arise. This preference could then be used to drive the directionality of the operational cycle. Using internal chirality was a notable change from the previous system **5-7** as now an external source of chirality (previously the CBS catalyst) was not required for directional rotation. While external chirality was no longer required, it did mean that the direction of the motor’s rotation was fixed and could not be changed during operation, as it could be in rotor **5-7** by swapping the (*R*)-CBS for the (*S*)-CBS catalyst.



**Scheme 3.** Feringa and co-workers most recent 6-step biaryl rotor. a) MOM and Ester deprotection b) EDCI lactonization. c) hydrolysis and MOM protection d) Bn and Ester deprotection e) EDCI lactonization. f) hydrolysis and Bn protection.<sup>50</sup>

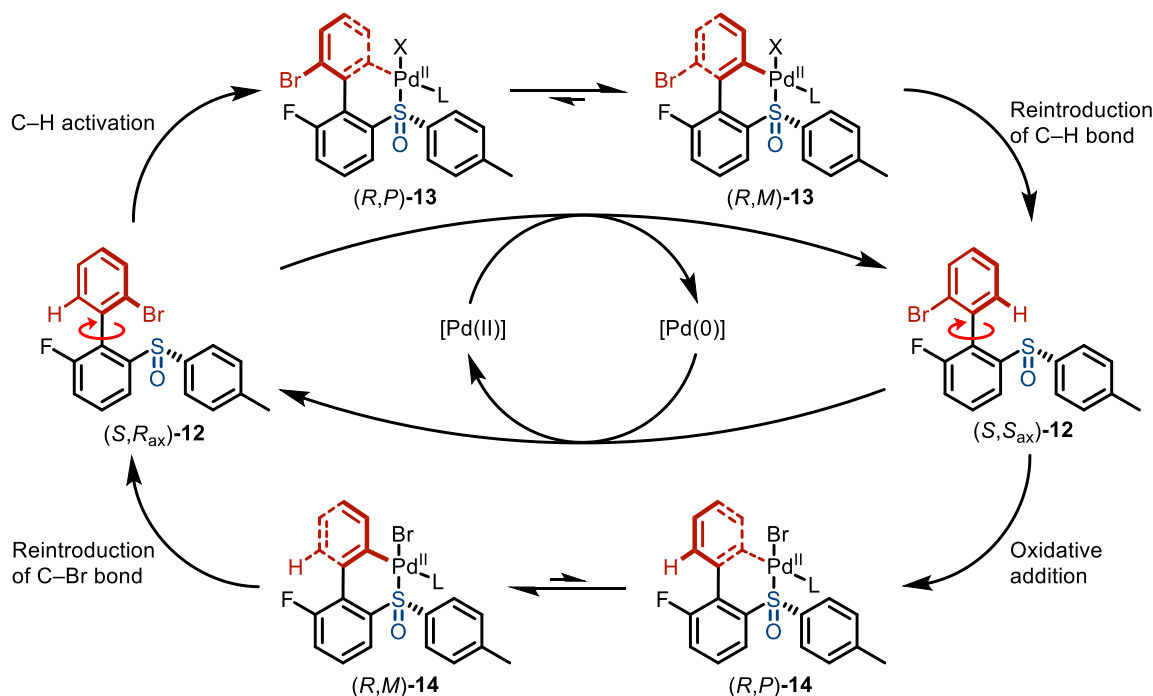
Starting from  $(S,S_{ax})\text{-}10$ , treatment with HCl then NaOH (Scheme 3, Step a.) resulted in the deprotection of the phenol and carboxylic acid to give  $(S,S_{ax})\text{-}8$ . Subsequent treatment with the coupling reagent EDCI afforded the lactone bridged biaryl, which could freely interconvert between the *P*-atropisomer  $(S,P)\text{-}9$  and the *M*-atropisomer  $(S,M)\text{-}9$  at room temperature. Due to an energy preference for the *M*-isomer over the *P*-isomer, upon lactone cleavage and subsequent reprotection of the diastereomeric mixture, only a single atropisomer (Scheme 3  $(S,R_{ax})\text{-}10$ ) was generated. This compound was then selectively deprotected to form  $(S,R_{ax})\text{-}8$  which upon treatment with EDCI formed lactone  $(S,P)\text{-}11$  which thermally relaxes to  $(S,M)\text{-}11$ . Lactone cleavage and subsequent phenol protection then led to the regeneration of  $(S,S_{ax})\text{-}10$ , thereby completing the  $360^\circ$  rotation.

While the above biaryl systems represented significant advancements in single-bond rotor design, they required sequential addition of multiple fuels (i.e. require multiple different reactions) and many purifications by an experimentalist to operate. This severely limits the potential applications and utility of the motor due to the impracticality of operating a system requiring constant experimental input. Practical synthetic molecular devices should be operable with minimal experimental input, i.e., they need to operate virtually or perfectly autonomously.

As the nature of the protecting group strategy will always require sequential operational steps and multiple incompatible fuels, other strategies must be investigated in which all steps of the rotary cycle can occur in the same medium.

### 1.2.3 Redox Cycle Rotary Motor

In a significant step towards autonomous motor operation, Feringa and co-workers developed a unidirectional rotor based on a palladium redox cycle, which was fuelled by a hydride reducing agent and an oxidant (Scheme 4).<sup>46</sup> The successful operation of this system is underpinned by the ability of sulfoxide to direct palladium reactivity, the inherent reactivity of the palladium centre in each oxidation state to insert into either C–Br or C–H bonds, and the ability of the chiral sulfoxide to impart directionality to the rotary cycle.



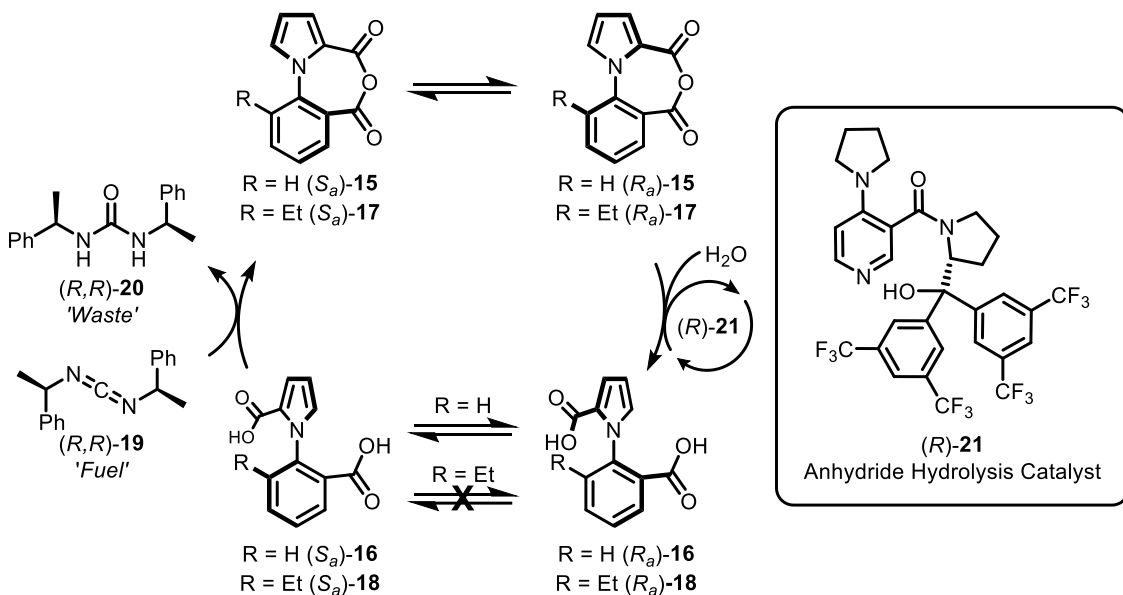
**Scheme 4.** Feringa and co-workers' palladium mediated unidirectional single-bond rotary motor.<sup>46</sup>

Starting from  $(S,R_{ax})\text{-12}$ , treatment with a Pd(II) complex leads to C–H activation and metalation to generate palladacycle  $(R,P)\text{-13}$ . Like the previous lactones **5-7** and **8-11** (Scheme 2 and Scheme 3),  $(R,P)\text{-13}$  is configurationally labile, which due to the chiral sulfoxide centre, facilitates the thermal relaxation of  $(R,P)\text{-13}$  to the lower energy diastereomer  $(R,M)\text{-13}$ . Subsequent treatment of the palladacycle mixture with sodium triacetoxyborohydride induces

reductive elimination and reintroduction of a C–H bond to afford exclusively compound (*S,S<sub>ax</sub>*)-**12**, representing a directional 180° rotation from (*S,R<sub>ax</sub>*)-**12**. After exchanging ligands, the resulting Pd(0) complex underwent oxidative addition into the C–Br bond of (*S,S<sub>ax</sub>*)-**12**, forming a second pair of interconverting palladacycles ((*R,P*)-**14** and (*R,M*)-**14**) with a preference for the lower energy diastereomer (*R,M*)-**14**. Subsequent treatment of this diastereomeric mixture with N–Bromosuccinimide (NBS) then resulted in oxidation of the Pd(II) complex, followed by reductive elimination and reformation of the C–Br bond. This then led to the exclusive regeneration of the starting compound (*S,R<sub>ax</sub>*)-**12** to complete the cycle. It is worth noting that the change in chirality descriptors in Scheme 4 associated with palladium insertion/removal are due to the new assignment priority of palladium according to CIP rules, rather than a change in the point chirality of the sulfoxide centre.

#### **1.2.4 Lactonization-Hydrolysis Rotary Motors**

Achieving autonomous operation in 2022, Leigh and co-workers reported the first autonomous, chemically-fuelled, single bond rotor **15–18** (Scheme 5). Based on work by Hartley and co-workers, as well as Boekhoven and co-workers, which had shown that dicarboxylic acids could catalyse the fuel to waste process of carbodiimides, the rotor reported by Leigh and co-workers exploited the same anhydride formation-hydrolysis operational cycle.<sup>38–40, 51, 52</sup> In this system the directionality of the cycle was imparted by atroposelectively hydrolysing the interconverting anhydride rotamers (*S<sub>a</sub>*)-**15/17** and (*S<sub>a</sub>*)-**15/17** using a chiral organocatalyst (*R*)-**21**. Much like the first protecting group rotor **5–7** (Scheme 2), the directionality of the rotation was controlled by an external chiral catalyst. This meant that by using the opposite enantiomer of the chiral catalyst the direction of rotation could be reversed.



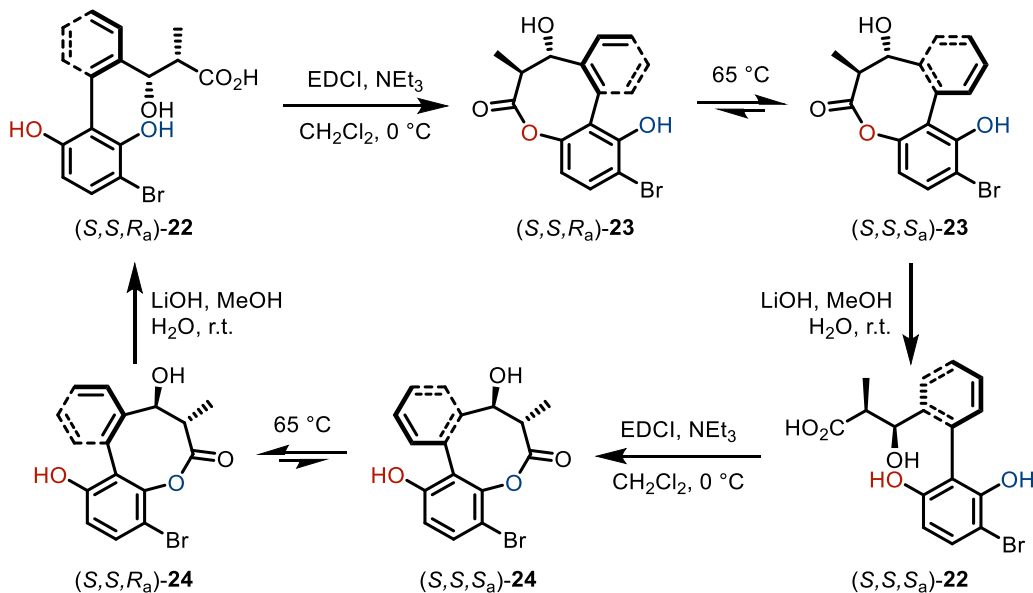
Scheme 5. Leigh and co-worker's autonomous carbodiimide fuelled anhydride hydrolysis motor.<sup>51</sup>

Starting from the diacid (*S<sub>a</sub>*)-16, reaction with the chiral carbodiimide fuel (*R,R*)-19 activates the diacid to form the anhydride (*S<sub>a</sub>*)-15. Due to the anhydride bridge between the upper and lower rings in compound 15, it has a low rotational energy barrier allowing free interconversion between (*S<sub>a</sub>*)-15 and (*R<sub>a</sub>*)-15. Enantioselective hydrolysis of (*R<sub>a</sub>*)-15 mediated by chiral organocatalyst (*R*)-21 then affords (*R<sub>a</sub>*)-16, representing a 180° rotation from the starting material. It is important to note that the rotation during the first 180° occurs with the crossing of the two dicarboxylic acid substituents relative to one another. Once hydrolysed to the diacid, the two dicarboxylic acid substituents are no longer able to pass over each other and therefore any further rotation must be around the opposite face. As (*R<sub>a</sub>*)-16 is *di-ortho* substituted, the energy barrier to rotation about the biaryl axis to regenerate the starting (*S<sub>a</sub>*)-16 isomer is low, allowing the 360° rotary cycle to be completed purely by thermal rotation.

Whilst the configurational instability of 16 is essential to motor operation, this feature also prevents direct monitoring of directional rotation. To assess the directionality of their system, Leigh and co-workers also studied the tri-*ortho* substituted motor analogue 18, which possesses a higher energy barrier to rotation and is configurationally stable. This enabled observation of changes in the proportion of *S<sub>a</sub>*-18 and *R<sub>a</sub>*-18 during anhydride formation and hydrolysis reactions, facilitating the assessment of these steps' stereoselectivity. In summary, whilst 16 is capable of undergoing a complete 360° rotation, its directionality is not directly assessable,

whilst **18**, whose directionality can be monitored, cannot be a motor due to its inability to complete the 360° rotation. This highlights how the dynamic nature of autonomous, out-of-equilibrium systems makes their analysis very challenging, and why model systems and computational proofs become necessary proofs for the assessment of directionality in motors operating under these regimes.

In the same year, a second but since retracted, carbodiimide-hydrolysis system was published by the Feringa group in which lactone formation and hydrolysis was used to drive the rotary cycle (Scheme 6).<sup>53</sup> In a similar manner to the second protecting group rotor **8-11** (Scheme 3), the directionality of the system was controlled by the integration of chiral substituents into the lactone arm. While this rotor relied on the same principle of using carbodiimide fuelled cyclization followed by subsequent hydrolytic cleavage, this system had the key advantage that the intermediates of the rotary cycle were stable at room temperature allowing each step of the cycle to be analysed directly.



**Scheme 6.** Feringa and co-worker's carbodiimide fuelled lactone hydrolysis motor.<sup>53</sup>

Starting from  $(S,S,R_a)$ -**22**, EDCI-mediated cyclization leads to the formation of lactone  $(S,S,R_a)$ -**23**, which upon heating freely interconverts with lactone  $(S,S,S_a)$ -**23**. This results in the accumulation of the thermodynamically favoured diastereomer  $(S,S,S_a)$ -**23**, which hydrolytically ring opens to form  $(S,S,S_a)$ -**22** in the presence of lithium hydroxide. A second

EDCI mediated cyclization leads to (*S,S,S<sub>a</sub>*)-**24**, which upon heating isomerises to form (*S,S,R<sub>a</sub>*)-**24**. A final hydrolysis step with lithium hydroxide then reforms the starting material (*S,S,R<sub>a</sub>*)-**22** to complete the 360° rotary cycle. As the cyclization and hydrolysis steps are non-enantioselective, directionality in this system is conferred by the energy difference between the diastereomers of **23** and **24** and their dynamic thermodynamic resolutions.

While the system was shown to undergo a directional 360° rotation, making it a functional molecular rotor, the article was retracted due to the waste products preventing continued and autonomous operation. Follow-up experiments on this system found that fuel consumption caused the system to become basic, and that the addition of acid after each cyclization step was required for continuous motor operation. This retraction highlighted how developing chemically fuelled molecular machines requires not only identifying compatible fuel sources to drive out-of-equilibrium motion, but also overcoming issues associated with the accumulation of waste products of motor operation.

### 1.2.5 Summary of Chemically Fuelled Single-Bond System Development

Over many decades, the development of this class of molecular rotor has been exceedingly challenging with the seminal work from Kelly and co-workers followed by Branchaud and coworkers, showing that achieving a chemically-fuelled unidirectional 360° rotation is a formidable task (Section 1.2.1). The protecting group strategy employed by Feringa and co-workers (Section 1.2.2) highlighted the challenge of finding chemically compatible fuels. As the operation of these protecting group motors used a sequence of mutually incompatible synthetic steps, a further system which improved on the catalytic-like behaviour of these rotors was developed (Section 1.2.3). This system was a landmark in moving more towards rotors which act more as fuel-to-waste catalysts which use the dissipated energy to drive their molecular scale motion. Finally, drawing upon precedented chemically-fuelled out-of-equilibrium reaction networks, lactonization-hydrolysis rotors were developed which used mutually compatible fuels, ultimately resulting in the first example of an autonomous chemically-fuelled rotor (Section 1.2.4).

### **1.3 Light-Fuelled Motion**

As discussed in section 1.2, a common challenge posed by chemically fuelled systems is identifying mutually compatible fuel inputs, chemical intermediates, and waste products. In *light* of this, fuel sources which do not have significant compatibility issues or lead to the accumulation of waste products are highly desirable. Light is therefore an attractive fuel for molecular motion in future technologies as not does it overcome the self-reactivity issues associated with chemical fuels, but as it is a massless fuel source, it also does not result in the accumulation of fuel waste.<sup>4, 54, 55</sup> Light is also a desirable fuel from an ecological standpoint, as it avoids the use of toxic compounds, heavy metals or depletable feedstocks and produces a minimal amount of waste.<sup>4, 56</sup>

Although light is a practical fuel source for molecular machines, a large array of chemical reactions can arise from photon absorption and subsequent excited-state decay, including: isomerization, dimerization, addition, rearrangement, cyclization, proton transfer, or redox processes. Since light-responsive molecular machines require large amplitude changes to occur upon photon absorption, ideally with a lack of other photochemical side reactions, the development of these motors has been heavily reliant on the exploitation of well-established photochromatic moieties (Figure 3).<sup>56</sup> While these photochromatic moieties typically operate as switches, through careful modification and integration into larger systems, they may be used as rotors, or made to power ratchets such as pseudo-rotaxanes.<sup>17-19, 25, 56, 57</sup> Based not only on their ability to photoisomerize under irradiation, but also on their repetitive operation, clean photoinduced processes, fatigue-resistance, ease of synthetic generation and ease of functionalization, stilbene **25**, azobenzene **26**, indigo **27**, thioindigo **28** and dithienylethene **29/30** are exceedingly useful photochromophores. As such, these moieties or their derivatives can be found in many light-fuelled molecular machines.<sup>56</sup>

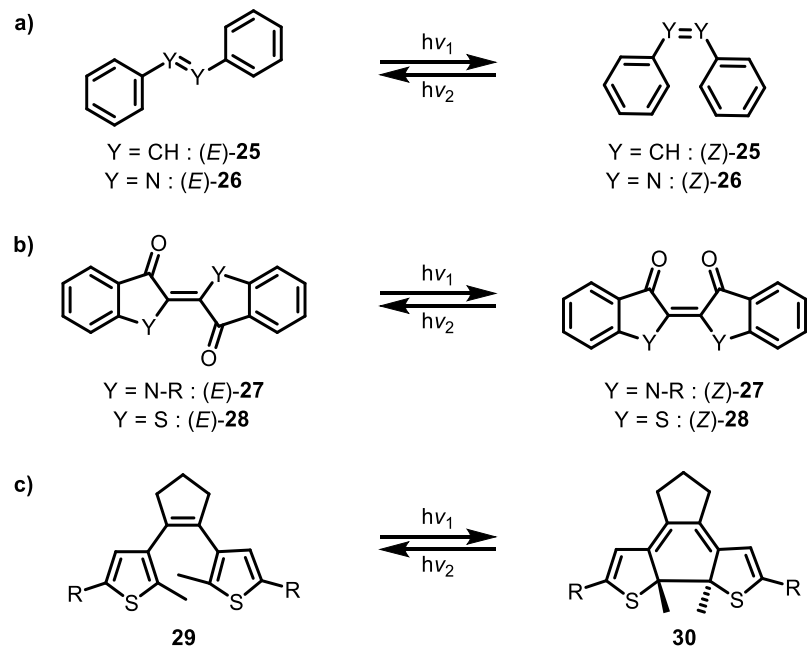
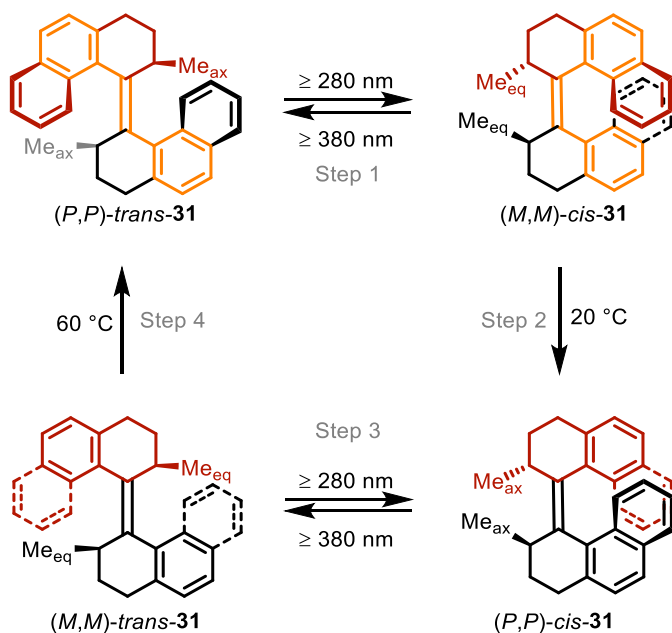


**Figure 3.** Common photoresponsive compounds used in artificial systems. (a) Stilbene ( $Y = \text{CH}$ ) and Azobenzene ( $Y = \text{N}$ ); (b) Indigos ( $Y = \text{NR}$  where  $R = \text{any alkyl or aryl group}$ ) and Thioindigo ( $Y = \text{S}$ ); (c) dithienylethenes.

## 1.4 Light Fuelled Double Bond Systems

### 1.4.1 Four-Step Alkene Rotor Systems

In 1999 the first light-driven molecular motor capable of performing unidirectional 360° rotation was reported by Feringa and co-workers (Scheme 7).<sup>19</sup> This motor was designed to exploit the out-of-plane C–C double bond rotation observed in the photoisomerization of stilbene. Although stilbene can rotate both clockwise and anticlockwise, by introducing new steric interactions which force the alkene into a non-planar helical shape, the direction of the rotation during the photoisomerization process can be controlled. Through the incorporation of two methyl groups (Scheme 7, (*P,P*)-*trans*-31 **Me<sub>ax</sub>** in light red and light grey) which can occupy pseudo-equatorial (**Me<sub>eq</sub>**) or pseudo-axial (**Me<sub>ax</sub>**) positions, an energy preference is generated for one helicity over the other. These conformationally labile methyl groups are key to the directional operation of the motor as they generate metastable intermediates which, *via* crossing of the upper and lower halves, thermally relax to the lower energy conformations. This process is now known as a thermal helix inversion (THI).



**Scheme 7.** Operation of the first light-driven unidirectional molecular motor. Stilbene moiety highlighted in orange in first step.<sup>19</sup>

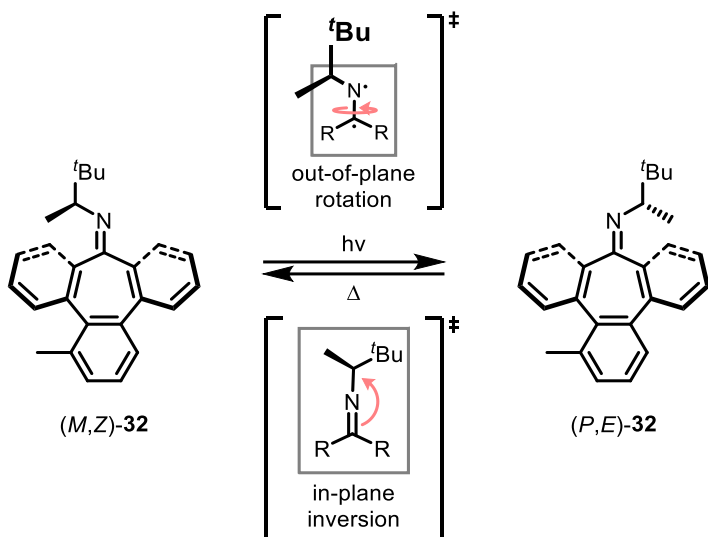
Putting this into operation, photoirradiation of the (*P,P*)-*trans*-31 isomer, at  $\lambda > 280$  nm, results in a unidirectional 180° double bond rotation (and thereby an inversion of helicity) to give the (*M,M*)-*cis*-31 isomer (Scheme 7, Step 1). The (*M,M*)-*cis*-31 isomer then

undergoes a THI at 20 °C, driven by the conformational preference of the methyl groups, to give the (*P,P*)-*cis*-**31** isomer (Scheme 7, Step 2). The (*P,P*)-*cis*-**31** isomer then photoisomerizes under constant  $\lambda > 280$  nm irradiation, resulting in a second unidirectional 180° rotation to generate the (*M,M*)-*trans*-**31** isomer (Scheme 7, Step 3). This isomer then undergoes a final THI at 60 °C to give the starting (*P,P*)-*trans*-**31** isomer (Scheme 7, Step 4).

This seminal four-step operating principle of sequential photoisomerizations and thermal helix inversions has led to the development of many other light-fuelled rotors derived from this scaffold. This includes the second and third generation alkene motors, the oxindole motors, the imine motors, the first generation hemithioindigo motors as well as a variety of theoretical computational-based motors.<sup>16, 17, 20, 58-70</sup> Further design modifications to these motors included decreasing the amount of chiral information required, increasing the rate of rotation, changing the wavelength of irradiation, symmetrizing the THI steps, improving quantum yield and more. Many of these systems also introduced ways to control these changes dynamically, for example systems in which different chelating metal ions controlled THI rates, or where the operating wavelength could be changed by light-controlled conjugation.<sup>71, 72</sup>

#### **1.4.2 Two-Stroke Imine System**

While the four-step photoisomerization-THI operational cycle has become the most common light-fuelled rotary cycle, other systems have been developed which exploit different modes of mechanical motion. The first of these alternative light-driven systems were imine motors from Greb and Lehn.<sup>68</sup> While these systems could also operate *via* the same four-step pathway as the alkene motors, as nitrogen also has the ability to undergo an in-plane inversion, the imine motors were also able to undergo a non-microscopically reverse two-step rotary cycle (Scheme 8). In this cycle, (*M,Z*)-**32** was irradiated at 254nm, inducing excitation of an electron from the  $\pi$ -to- $\pi^*$  orbital of the C=N bond. This caused out-of-plane rotation around the C–N bond, generating (*P,E*)-**32** (Scheme 8, top). Upon heating, the imine underwent a thermally induced in-plane inversion at nitrogen to return to (*M,Z*)-**32** (Scheme 8, bottom). As the first step occurred *via* out-of-plane rotation while the second occurred *via* in-plane inversion, the two steps were non-microscopically reverse, allowing the system to operate as a molecular rotor.

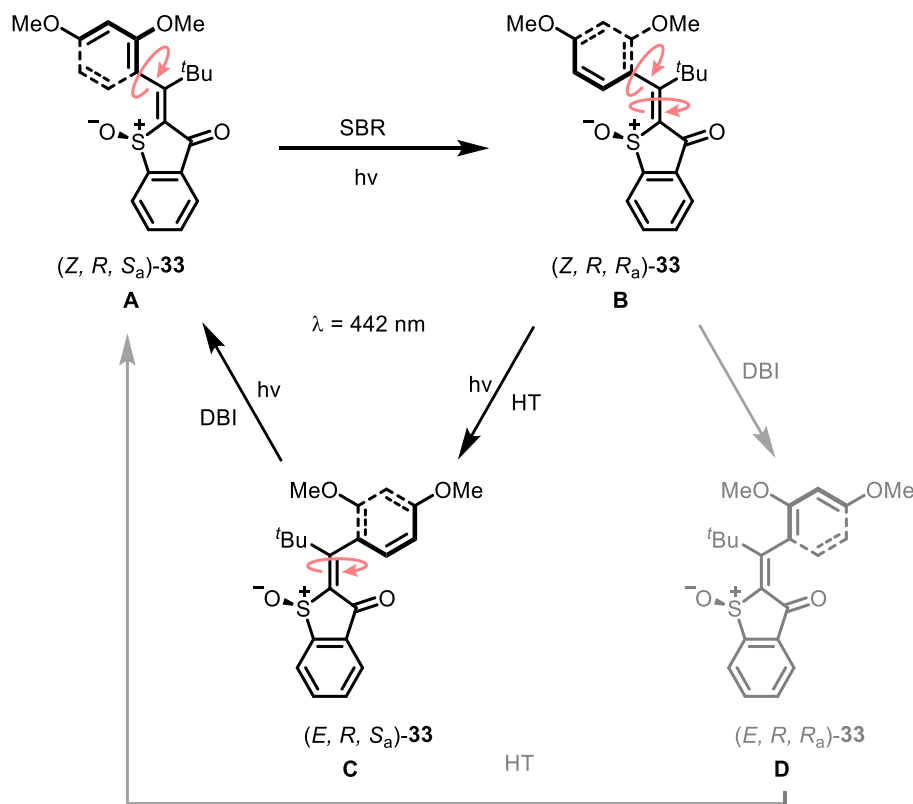


**Scheme 8.** Two-stroke imine rotor which operates through sequential non-microscopically reverse out-of-plane rotation and subsequent in-plane inversion.<sup>68</sup>

### 1.4.3 Hula Twist Systems

Similar to the imine motors in which a new operational cycle was developed by exploiting new molecular scale motion, Dube and co-workers developed additional hemithioindigo systems in which linked single and double bond rotation would occur *via* a “hula twist”.<sup>64, 67, 73</sup> Of particular interest was a three-state photon-only system which operated *via* an independent single bond rotation, independent double bond rotation and a linked hula twist. In this system, the single bond between the alkene and dimethoxy-aryl ring possesses a significant degree of double bond character, due to conjugation, making it mildly photoactive. Starting from (*Z, R, S<sub>a</sub>*)-33, irradiation ( $\lambda = 442$  nm) triggers single bond rotation (SBR) of the alkene-aryl single bond to generate (*Z, R, R<sub>a</sub>*)-33 (Scheme 9, SBR step). Under the same wavelength of irradiation, the compound then undergoes a photochemically induced hula twist (HT) in which both the double and single bonds rotate synchronously to give (*E, R, S<sub>a</sub>*)-33 (Scheme 9, HT step). Finally, double bond isomerization (DBI) occurs, again under the same wavelength of irradiation, to regenerate (*Z, R, S<sub>a</sub>*)-33 (Scheme 9, DBI step). As there were multiple possible pathways through which this motor system could operate, it is important to distinguish between the terms monodirectional, defined as the preference for one cycle against all others, and unidirectional, defined as the preference for one cycle against the corresponding reverse cycle. For example, if the DBI step occurred before the HT step the system would instead pass through conformation (*E,R,R<sub>a</sub>*)-33 rather than (*E,R,S<sub>a</sub>*)-33, making a second, competing operational pathway (Scheme 9, grey cycle). If the first cycle which passes through

intermediate (*E,R,S<sub>a</sub>*)-33 is defined as A→B→C→A as long as the forwards pathway occurs more readily than the reverse pathway A←B←C←A it is considered a unidirectional operational cycle. By comparison if the second cycle which passes through intermediate (*E,R,R<sub>a</sub>*)-33 is defined as A→B→D→A, the motor is only considered monodirectional if it preferentially operates through either the A→B→C→A or the A→B→D→A cycle. As each intermediate was stable at room temperature their conformation could be identified unequivocally and their isomerization behaviour studied individually. Using the quantum yields for each transformation, both the monodirectionality and unidirectionality of the system could be established. By doing this, they found that the photon only system was able to not only exhibit a unidirectional cycle but at the operating temperature (-50 °C) it was also monodirectional.



**Scheme 9.** Photon-only molecular rotor. SBR = single bond rotation, DBI = double bond isomerization, HT = Hula twist.<sup>64</sup>

#### **1.4.4 Summary of Light Fuelled Double Bond System Development**

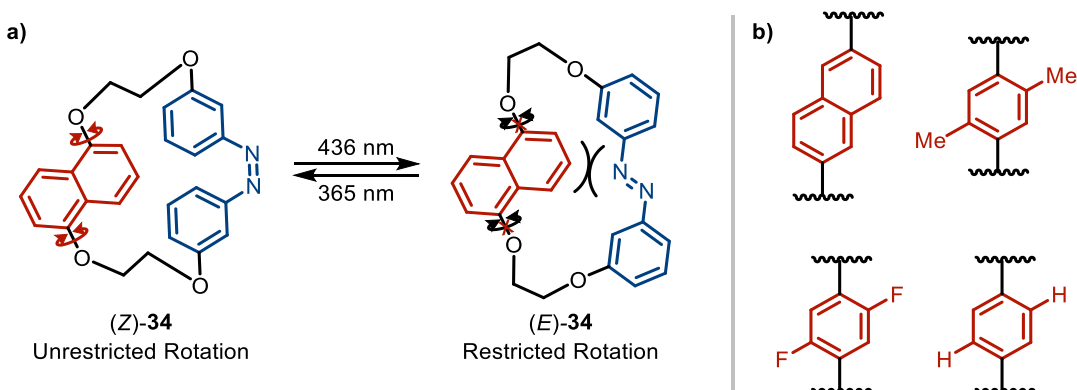
The highly successful development of double bond rotors over the past two decades has produced a plethora of autonomous rotors. Through continuous improvement of Feringa and co-workers' first alkene rotor, highly effective alkene rotor scaffolds have been developed, as well as designs with structural modification which allow greater control over the motor's rate of rotation. Recently, new alkene rotor scaffolds, mechanisms of action, and trajectories of molecular motion have also been reported. Overall, the development of these double bond rotors has shown, and continues to show, incredible new approaches to harnessing molecular scale motion.

## 1.5 Light Gated Free-Rotation Around Single-Bond Axes

As discussed section 1.4, light-fuelled rotors have implemented photochromic moieties into the core of the motor scaffolds, making the light responsive double bond the axis of rotational motion. However, other studies have instead employed photochromic moieties to control rotation at distal axes. In these systems, irradiation causes a photochromic moiety to undergo a geometric change which alters the motion of a remote, rotating single bond attached to a ‘rotor’ unit. The influence of photoisomerization on the motion of the rotor unit occurs by means of either steric modulation (Section 1.5.1), or *via* a coordination process (Section 1.5.2).

### 1.5.1 Steric Control of Rotation

Initial studies into sterically-controlled, light-gated rotation systems led to the development of multiple molecular gyroscopes.<sup>74-79</sup> These included macrocyclic systems from Tamaoki and co-workers composed of an aryl rotor unit (Scheme 10a, red) and an azobenzene (Scheme 10a, blue) linked *via* an ether spacer (Scheme 10a, black).<sup>74, 75</sup>

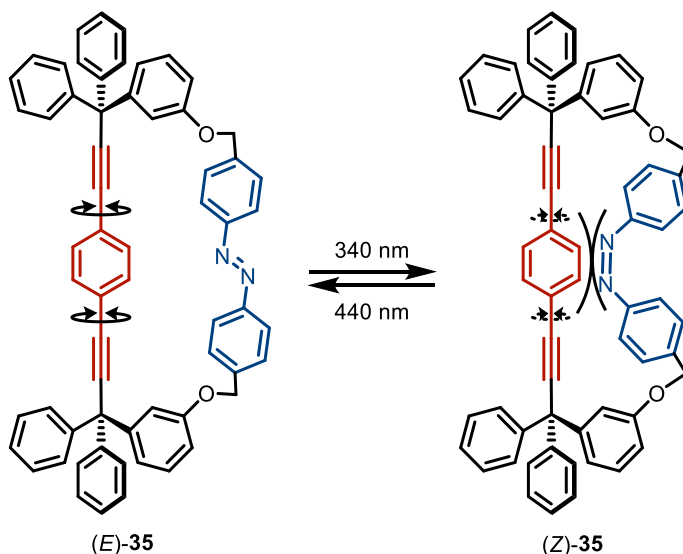


**Scheme 10.a)** Gyroscope systems from Tamaoki and co-workers in which the rate of rotation could be controlled by the state of the azobenzene photoswitch. b) different aryl ring rotors used in Tamaoki and co-workers gyroscopes.<sup>74-76, 78</sup>

By exploiting the large amplitude change caused by the photoisomerization of azobenzene, the steric hindrance experienced by the central aryl rotor (Scheme 10, red) can be selectively increased or decreased. When the azobenzene moiety is in the *Z* configuration the aryl ring can freely rotate (Scheme 10a, **(Z)-34**), however, under irradiation with 436 nm light the azobenzene isomerises to **(E)-34**, which significantly increases the steric interactions between the azobenzene and the aryl rotor (Scheme 10a, **(E)-34**). This increases the energy

barrier to rotation of the central aryl rotor, thereby slowing its rotation. By altering the size of the central aryl rotor, the difference between the steric interactions in the *E* and *Z* azobenzene states can be fine-tuned to achieve different types of control over the rotation. For example, the dimethyl rotor (Scheme 10b, top right) freely rotates in the *Z* state but not in the *E* state, whereas the difluoro-rotor (Scheme 10b, bottom left) exhibits fast rotation in the *Z* state and slow rotation in the *E* state.

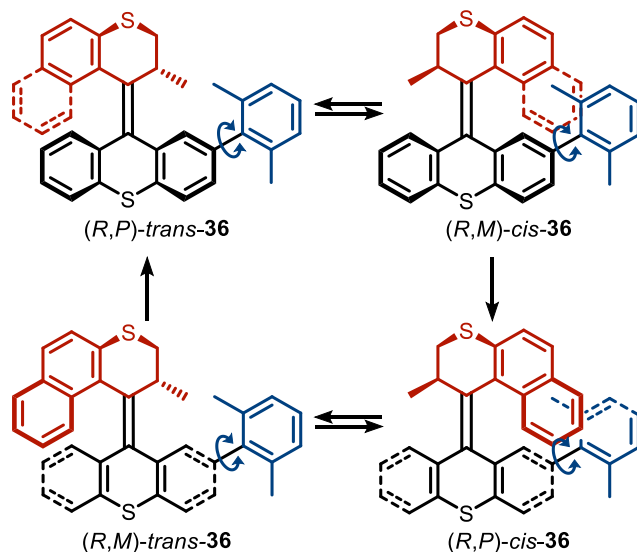
Following the same design principles, Garibay and co-workers developed gyroscope **35**, which used azobenzene switching to alter the rotation speed of a central aryl ring (Scheme 11).<sup>77</sup> In contrast to Tamaoki and co-workers' systems, for **35** in the *E* configuration of the azobenzene the steric clashes between the central rotor and the azobenzene were minimized allowing the phenyl to rotate freely while in the *Z* configuration the steric clashes increased causing the phenyl to rotate more slowly. This system highlighted how the same design principles could be applied to different molecular architectures.



**Scheme 11.** Garibay and co-workers gyroscope system.<sup>77</sup>

Going beyond a simple two-state system, Feringa and co-workers developed the molecular gearbox **36** which used a second-generation alkene motor to control the rotation of a pendant biaryl to a greater degree (Scheme 12).<sup>80</sup> Due to the different steric interactions between the xylyl group (Scheme 12, blue) and the rotor (Scheme 12, red) in each of the four states, the barrier to rotation of the xylyl group varies accordingly. As the energy barriers—

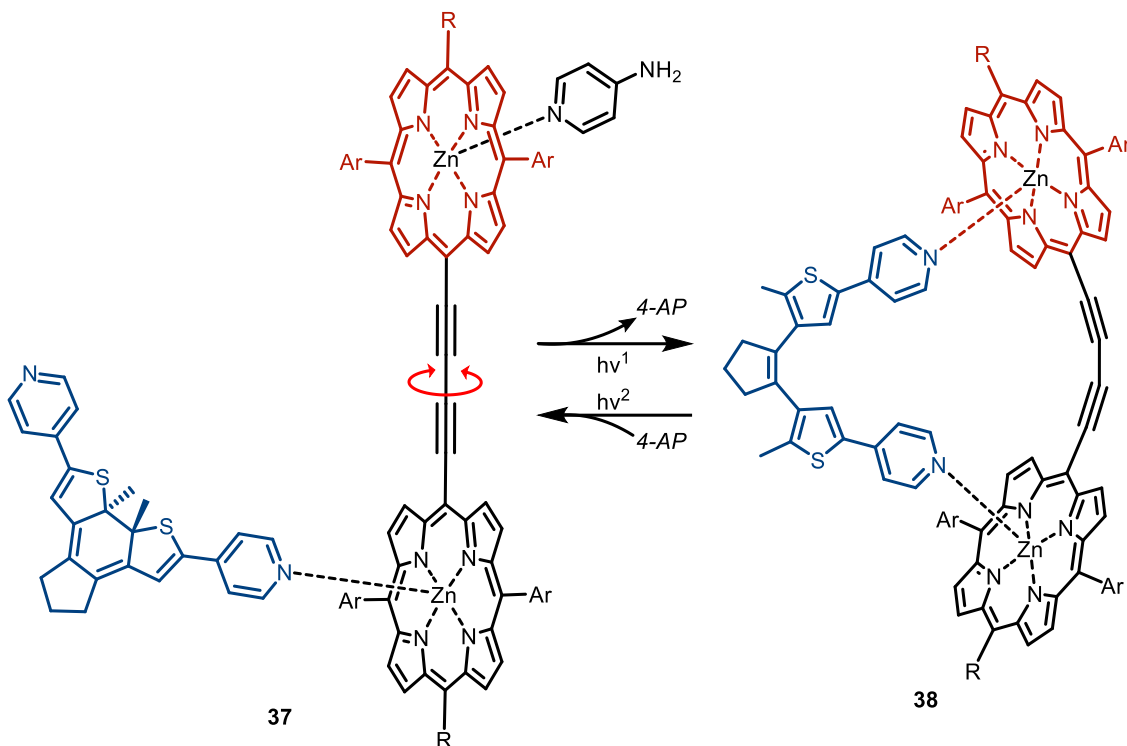
and therefore rates of rotation—were different in all four states, the ‘gear’ system could switch incrementally between four different rates of xylyl ring rotation. Using EXSY (EXchange SpectroscopY) NMR, the operation of the ‘molecular gearbox’ could be directly observed with the rates of xylyl ring rotation from highest to lowest following the order *(R,P)-cis-36* > *(R,M)-cis-36* > *(R,P)-trans-36* > *(R,M)-trans-36*.



**Scheme 12.** Overcrowded alkene gearbox system with freely rotating xylyl ring in blue, rotor in red and stator in black.<sup>80</sup>

### 1.5.2 Coordination Control of Rotation

While many molecular gyroscopes operate through steric interactions (Section 1.5.1), other systems have been developed in which complexation between a Lewis base and metal ion allows or disallows the free-rotation of a rotor unit.<sup>81,82</sup> For example, the supramolecular complex **37/38** developed by Andreasson and co-workers, demonstrated control of C–C single-bond rotation could be achieved in a linear diporphyrin complex using zinc porphyrin complexation with a diarylethene photoswitch (Scheme 13).<sup>81</sup>



**Scheme 13.** Andreasson and co-workers photoswitchable supramolecular complex. Ar = Si(C<sub>6</sub>H<sub>13</sub>)<sub>3</sub>, R = 3,5-di-*tert*-butyl-1-ethynylbenzene. 4-AP = 4-aminopyridine.<sup>81</sup>

In this system, two zinc porphyrin moieties are connected *via* a series of single and triple C–C bonds, which act as a freely rotating central axis. In the diarylethene’s closed-ring configuration **37**, the diarylethene coordinates with only one of the two zinc porphyrin moieties allowing the second zinc porphyrin to rotate freely. In the diarylethene’s open-ring configuration **38**, the diarylethene coordinates with both zinc porphyrin rings, preventing free rotation of the two moieties relative to each other. While this system offers no control over the direction of rotation, like the previous molecular gyroscopes (Section 1.5.1), it does offer the ability to control the rate of thermal rotation.

### 1.5.3 Summary of Light Controlled Non-Directional Single-Bond Systems

The molecular gyroscopes and gearboxes outlined above demonstrated how light can control the rate of non-directional rotation about single bond, through either dative bond formation or steric interactions. Whilst the inability of these systems to effect directional rotation precludes their further development into molecular motors, they still provide useful insights into the use of photoswitches for controlling single-bond rotation.

## 1.6 Light-Fuelled Single-Bond Switching

### 1.6.1 Switching Ferrocene Scissors

In the pursuit of light-fuelled, directionally controlled rotation, Aida and co-workers designed a pair of “molecular scissors” (Figure 4, **39**) in which an azobenzene ‘handle’ (Figure 4, blue) was linked to a ferrocene ‘pivot’ (Figure 4, orange) and used to move the terminal aryl ring ‘blades’ (Figure 4, green).<sup>83</sup>

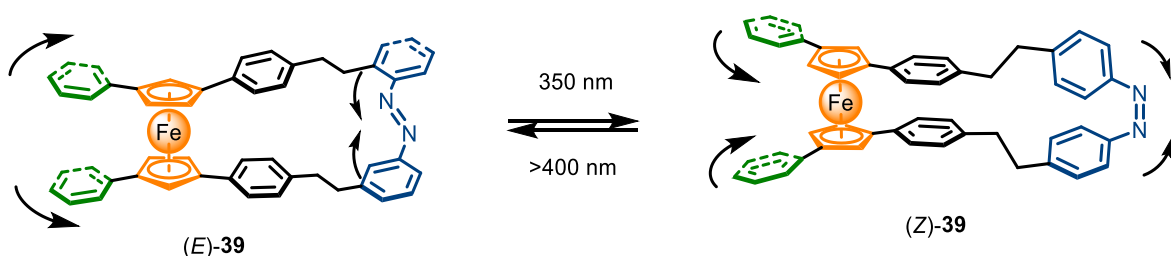
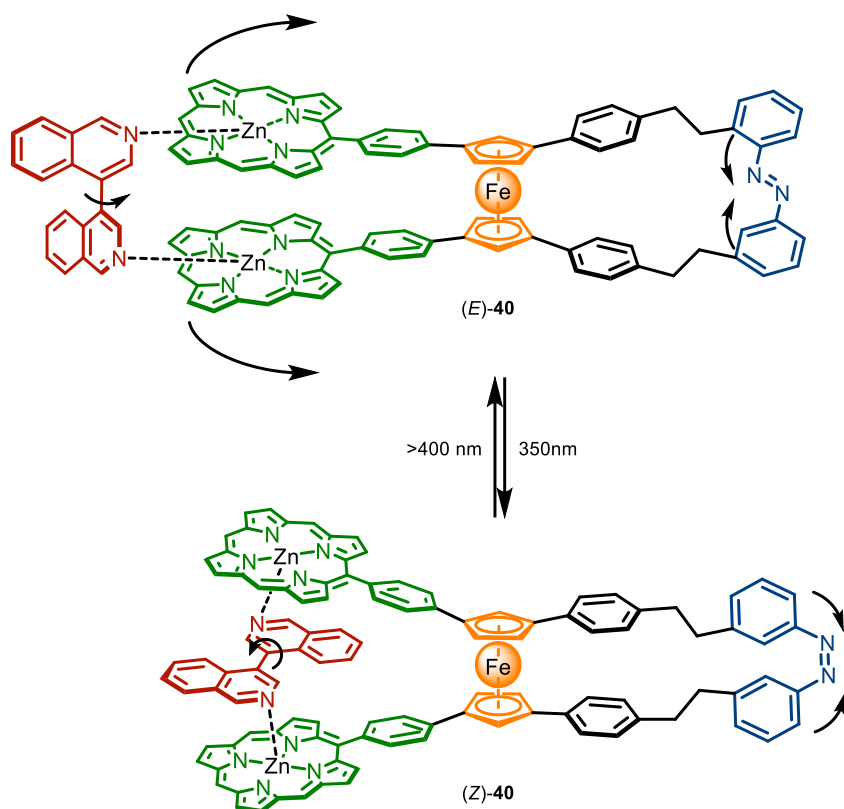


**Figure 4.** Molecular Scissors from Aida and co-workers.<sup>83</sup>

By coupling the azobenzene to a ferrocene pivot, the large-scale translational motion associated with azobenzene *E/Z* photoisomerization could be converted to rotary motion around a Cp–Fe–Cp axis.<sup>84</sup> Irradiation of (*E*)-**39** with 350 nm light induced isomerization to (*Z*)-**39**, bringing the phenyl rings of the azobenzene handle (Figure 4, blue) together. As the two rings of the azobenzene were linked to the upper and lower halves of the ferrocene unit, this movement in turn caused rotation of the two Cp rings of the ferrocene unit relative to each other. This in turn caused the linked ‘scissor blade’ phenyl rings (Figure 4, green) to open by pivoting away from each other about the rotationally labile Cp–Fe–Cp axis of the linked ferrocene unit. Using a combination of DFT calculations, <sup>1</sup>H NMR and CD Spectra, Aida and co-workers proved that upon azobenzene *E/Z* isomerization, the bite angle of the molecular scissor’s blades changed by ~49°.<sup>83, 85, 86</sup> This system was a significant development in directionally controlling motion around a rotational axis as it was the first example to demonstrate that the translational motion of an azobenzene could be converted into rotational motion around a labile axis. While this work showed that directional rotational motion could be controlled by the translational motion of azobenzene isomerization, the angular range of rotation was very limited and, as reclosing the molecular scissors was the microscopic reverse of opening them, they could not perform any net work through successive operations.

### 1.6.2 Switching Biaryl Scissors

Extending the previous molecular scissor design (Figure 4, **39**) to include dative bond formation, a host-guest system was developed which focused on the translation of the molecular scissor's motion to a second guest moiety (Scheme 14, **40**). In this system, a zinc porphyrin was added to the molecular scissor blades (Scheme 14, green) allowing coordination between the scissors and a nitrogenous base compound (Scheme 14, red).<sup>87</sup> By coordinating the scissors with a nitrogenous bidentate rotor, the scissor's opening/closing action is converted into a mechanical twisting of the guest rotor system. This allows the *E/Z* azobenzene photoswitching to induce a unidirectional clockwise, and subsequent anticlockwise, rotation around the nitrogenous rotor's C–C single-bond.



Scheme 14. Aida and co-workers' host-guest system.<sup>87</sup>

While **40** additionally incorporated the use of dative bonds and controlled rotation around a C–C single bond axis into its design, it presented many of the same limitations as **39**. As it remained true that the scissors could only be closed *via* the microscopically reverse pathway of opening, although the induced C–C bond rotation was directional during each

isomerization, no net directional rotation could be achieved. Further scissor-type systems capable of long-distance signal transduction have also been developed, incorporating different photoswitches or more axes of rotation. However, none have overcome the issue of limited rotational range or have been capable of performing progressive rotation.<sup>88</sup>

### **1.6.3 Summary of Light Controlled Single-Bond Oscillation Systems**

These systems have successfully demonstrated the ability to convert translational motion arising from the isomerization of a photoswitch to directional rotary motion around one or more labile axes. While they are able to achieve directional motion through isomerization processes, the switch-like nature of the systems meant the return to the initial state was always *via* the microscopically reverse pathway, preventing any net directional rotation from being achieved in these systems.

## 1.7 Motion Transmission from Alkene Motors to C–C Single-Bonds

The final class of light-fuelled, single-bond rotation systems to be discussed in this introduction are the rotary motion transmission systems. These systems couple and transfer rotation from a light-fuelled double bond rotor axis to a biaryl single bond axis. The first of these systems, from Feringa and co-workers, integrated a biaryl moiety directly into the rotor of a 2<sup>nd</sup> generation alkene motor (Figure 5a, **41**).<sup>89</sup> Doing so brought the stator of the alkene rotor (Figure 5, black) into close proximity with the lower half of the biaryl moiety (Figure 5 red), resulting in steric interactions which could influence the movement of the biaryl axis.

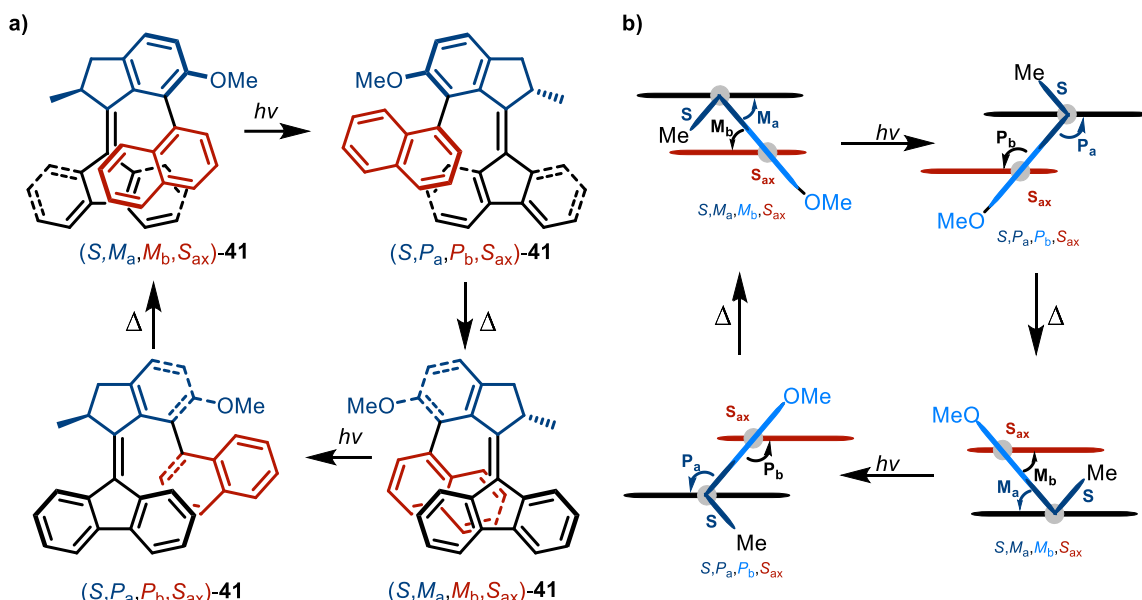
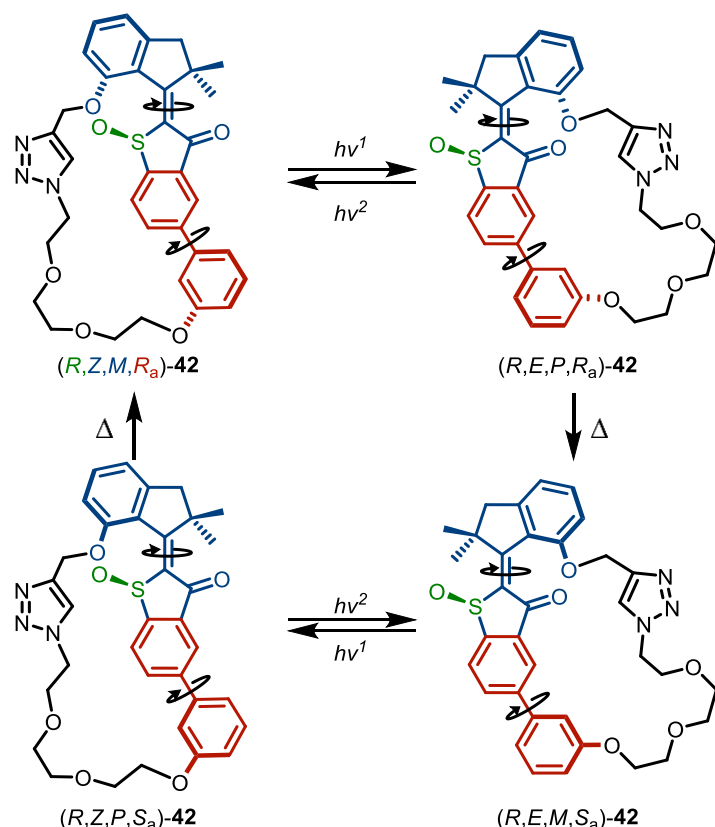


**Figure 5.** a) Schematic representation of the operational cycle using 2D structures. Naming follows: (point chirality of Me group)-(Helicity of alkene)-(Helicity of biaryl axis)-(axial chirality of biaryl axis)-**compound number** b) Top down view of the  $S_{ax}$  cycle highlighting the point chirality (*S*), helicity of alkene rotor ( $M_a/P_a$ ), helicity of the biaryl ( $M_b/P_b$ ) and axial chirality of the biaryl ( $R_b$ ).<sup>89</sup>

Starting from  $(S, M_a, M_b, S_{ax})\text{-}41$  (Figure 5a), irradiation of the system causes the isomerization of the alkene bond leading to the generation of  $(S, P_a, P_b, S_{ax})\text{-}41$  which upon heating, undergoes a THI to generate  $(S, M_a, M_b, S_{ax})\text{-}41$ . Irradiation of this system then forms  $(S, P_a, P_b, S_{ax})\text{-}41$ , which also undergoes another THI to reform  $(S, M_a, M_b, S_{ax})\text{-}41$ . As the central alkene motor rotates through this cycle, the same side of the naphthyl paddle (red biaryl lower half) remains facing the fluorenyl unit (Figure 5, black stator of alkene motor). This means that as the motor rotates the helicity of the alkene axis is mirrored by the biaryl axis allowing the biaryl's helicity to also be controlled throughout this cycle. While the helicity of the biaryl changes throughout, the axial chirality of the biaryl is retained as no crossover event occurs at

the biaryl axis (Figure 5b, change of black  $M_b/P_b$  to match blue  $M_a/P_a$  in each step without a change to the red  $S_{ax}$ ). See section 1.1.1 for more detail on the difference between *axial chirality* and *helicity*. Although control over the biaryl rotation was limited to less than 180°, and the changes to the helicity were reversed in each step meaning no net work could be achieved, this was a landmark design in demonstrating directional control over a biaryl axis through coupling to a unidirectional alkene motor.

In 2018, a second motion transmission system was reported by Dube and co-workers, where the light-fuelled unidirectional 360° rotation of a hemithioindigo motor could be transferred to a reporter biaryl axis. In this system, a biaryl unit (Scheme 15, red) was integrated into the lower half of a 1<sup>st</sup> generation hemithioindigo motor (Scheme 15, blue) with the upper half of the motor linked to the lower half of the biaryl *via* an ethylene glycol chain (Scheme 15, black).<sup>90, 91</sup> As the light-fuelled motor rotated unidirectionally around the central axis, the attached ethylene glycol chain would force the biaryl moiety attached at the other end to rotate in a synchronous fashion around the biaryl axis.



**Scheme 15.** Linked biaryl-hemithioindigo system from Dube and co-workers. Naming follows: (point chirality of the sulfoxide)-(geometry of the alkene bond)-(helicity of alkene rotor)-(axial chirality of biaryl)-**compound number**.<sup>92</sup>

This was a landmark study as it was the first example of light-fuelled unidirectional 360° rotation around a biaryl axis. While compound **42** did achieve light-fuelled unidirectional rotation around a biaryl axis, in a similar manner to an engine and a wheel, the rotary motion was initiated by the hemithioindigo motor (engine) and subsequently transferred to a distal and otherwise passive axis (wheel) where the motion was then be observed. As the rotary motion of the biaryl axis in compound **42** is not being initiated at the biaryl axis, but rather at a separate motor axis and then transferred to the otherwise passive biaryl axis, it is not considered a C–C single-bond motor like previously discussed chemically-fuelled rotors in section 1.2.

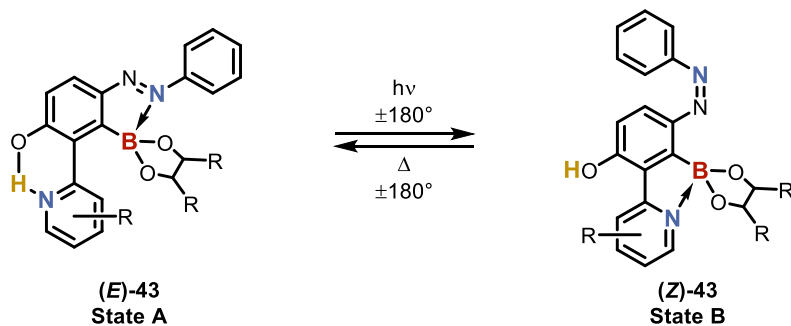
Further developments of this system have also been reported which demonstrate that introduction of bulk to the biaryl can force the system to operate *via* a 6-step pathway where the biaryl can only rotate after the hemithioindigo has undergone the THI.<sup>93, 94</sup> These later systems have also shown that coupling of the biaryl to the hemithioindigo motor increase the rate of biaryl rotation compared to a similarly substituted unlinked biaryl.<sup>93</sup>

### **1.7.1 Summary of Alkene Motor Motion Transmission to C–C Single-Bonds**

While the first alkene motors transmission systems could only vary rates of C–C bond rotation (e.g. Scheme 12, **36**), more recent developments from Feringa and co-workers (Figure 5, **41**) and Dube and co-workers (Scheme 15, **42**) have achieved a significantly higher level of control over biaryl rotation. Although the naphthalene paddle system **41** from Feringa and co-workers could not achieve a controlled crossover of the biaryl axis, and was therefore limited to sub-180° biaryl rotation, it was an innovative development highlighting the difference between controlling axial chirality and helicity. The linked hemithioindigo system from Dube and co-workers was a significant development in the field, as it represented the first example of observing autonomous and unidirectional 360° rotation around a C–C bond. However, as the rotary motion in this system was not initiated at the C–C single-bond axis, with the biaryl instead reporting the rotary motion generated by the hemithioindigo motor, a light fuelled rotary motor where rotary motion is initiated at the C–C single-bond remains an unreported phenomenon.

## 1.8 Project Aims

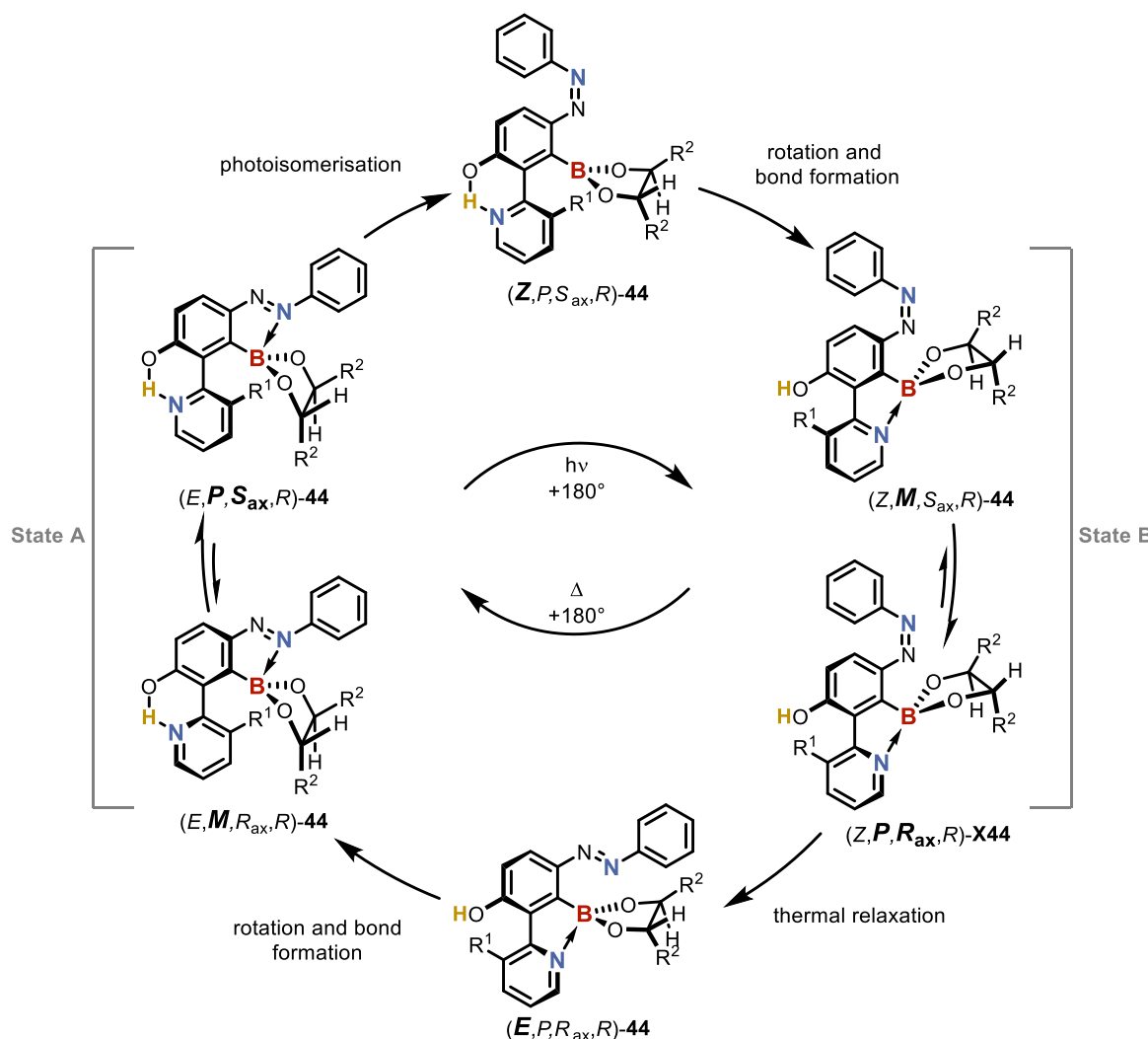
Molecular rotors have undergone extensive developments in the past two decades with a plethora of designs which exhibit different operating mechanisms or use different types of fuel. Despite this, the molecular rotors all currently fall into one of two classes: chemically-fuelled single bond rotors (Section 1.2) or light-fuelled double bond rotors (Section 1.4). While a significant number of methods have been developed to control single bond rotation with light (Sections 1.5, 1.6 and 1.7), no light-fuelled single bond rotors have yet emerged. Drawing on the knowledge gained from sections 1.2 to 1.7, a new two state system in which two  $180^\circ$  rotary states can be controlled with light is proposed (Scheme 16). In this system, the azobenzene unit in the borylated-azo-biaryl scaffold **43** is proposed to control the formation of the two possible intramolecular N–B bonds. By exploiting the azobenzene unit’s geometry change upon photoisomerization, the balance between the N–B bond formation can be controlled by light, in turn giving control over two  $180^\circ$  rotary states (Scheme 16, State A and State B).



**Scheme 16.** Proposed borylated-azo-biaryl system in which interconversion between two  $180^\circ$  rotary states can be controlled using light.

Based on work by Kawashima and co-workers, in the lowest energy state (State A) a  $\text{N}_{\text{azo}}-\text{B}$  bond is proposed to form between the azobenzene unit and a pendant boronic ester leaving the pyridine stator free to form a hydrogen bond with a phenol on the upper half of the motor.<sup>95-98</sup> Upon irradiation and isomerization to the *Z* isomer, the  $\text{N}_{\text{azo}}-\text{B}$  bond is broken leaving the p-orbital of the boron empty. As formation of the  $\text{N}_{\text{pyr}}-\text{B}$  bond is more favourable than formation of the pyridine-phenol hydrogen bond, the pyridine should undergo a  $180^\circ$  rotation around the central axis to form a new  $\text{N}_{\text{pyr}}-\text{B}$  bond (State B).<sup>99-102</sup> As the higher energy *Z* azobenzene is thermally unstable, it is able to thermally relax back to the *E* isomer, regenerating the  $\text{N}_{\text{azo}}-\text{B}$  bond and breaking the  $\text{N}_{\text{pyr}}-\text{B}$  bond. Finally, the pyridine ring should undergo a second  $180^\circ$  rotation around the central axis to reform the hydrogen bond, returning to its initial state (state A).

Realizing this two-state system (Scheme 16) would be a significant achievement, however, to be considered a molecular machine, the system also requires unidirectional control of the trajectory of the  $180^\circ$  rotation between the two rotary states. To this end, a chiral ligand bound to the boron centre is proposed to form diastereomers in both state A and state B. Since diastereomers are non-thermodynamically degenerate, this creates an energetic preference for one of the diastereomers in each state. If the diastereomers can interconvert, then a complete  $360^\circ$  rotatory cycle might be achievable, where the trajectory of the rotation is guided by the energy preference induced by the chiral ligand in both states A and B (akin to the biaryl systems **8-11**, **12-14** and **22-24** in section 1.2). This would in turn enable the system to undergo net unidirectional rotation around the central C–C axis, constituting the first light-fuelled single bond rotor (Scheme 17).



**Scheme 17.** Proposed borylated-azo-biaryl system in which directional  $360^\circ$  rotation could be achieved using light. Naming follows: (azobenzene geometry)-(helicity of the biaryl)-(axial chirality of biaryl)-(point chirality of the ligand)-**compound number**.

Starting from (*E,M,R<sub>ax</sub>,R*)-**44**, interconversion between (*E,M,R<sub>ax</sub>,R*)-**44** and (*E,P,S<sub>ax</sub>,R*)-**44** is proposed to occur readily, facilitated by the lower rotation barrier induced by the hydrogen bond. Due to the fixed chirality of the boron ligand, there should be a preference for (*E,P,S<sub>ax</sub>,R*)-**44**. Upon irradiation, the azobenzene isomerises to the *Z* isomer, breaking the N<sub>azo</sub>–B bond to form (*Z,P,S<sub>ax</sub>,R*)-**44**. Driven by the energetic preference to form the stronger N<sub>pyr</sub>–B bond rather than the phenol-pyridine hydrogen bond, the pyridine ring undergoes same-face rotation (i.e. a change in helicity but not in axial chirality) around the central bond to form (*Z,M,S<sub>ax</sub>,R*)-**44**. (*Z,M,S<sub>ax</sub>,R*)-**44** then interconverts with its diastereomer (*Z,P,R<sub>ax</sub>,R*)-**44**, with a preference for (*Z,P,R<sub>ax</sub>,R*)-**44** due to the fixed chirality of the boron ligand. It is important to note that in both states (Scheme 17 State A and State B), it is proposed that the same biaryl helicity is favoured as the chirality of the boron remains unchanged. From (*Z,P,R<sub>ax</sub>,R*)-**44**, thermal relaxation of the azobenzene then leads to the reformation of the *E* isomer (*E,P,R<sub>ax</sub>,R*)-**44**. In this state the azobenzene nitrogen then rebinds to the boron centre, reforming the N<sub>azo</sub>–B bond and breaking the N<sub>pyr</sub>–B bond. Subsequent same-face rotation of the pyridine around the central bond occurs to reform the hydrogen bond and make (*E,M,R<sub>ax</sub>,R*)-**44**, completing the rotary cycle. Understanding whether the chiral boron ligand can induce directional rotation in such a system also requires an in depth understanding of the thermodynamic and kinetic control of the system, and is discussed further in section 6.4.

Realization of this system would represent an entirely new class of light-driven single-bond rotor. As the proposed system is fuelled by light and heat, there are no chemical fuel or waste compatibility issues that could interfere with autonomous motion, a potential that has already been highlighted by Credi and co-workers' autonomous autothreading pseudo-rotaxane.<sup>25</sup> Although achieving autonomy in this system is beyond the scope of this project, it is of significant interest for any proposed designs to be capable of this feat.

As this project involves a high degree of complexity, very limited literature precedent and many entirely untested elements, model systems were made to better understand key features of the proposed design before embarking on analysis of the complete system (Figure 6). To probe the proposed N<sub>azo</sub>–B bond formation and breakage requirements, as well as test the effect of the N<sub>azo</sub>–B bond on the photochemical behaviour, model boryl-azobenzenes (Figure 6, **44a**) were generated with the results discussed Chapter 2. Similarly, to better

understand the formation requirements of the N<sub>pyr</sub>–B bond, the effect on the barrier to rotation and the ability to influence the chirality of the biaryl axis, model biaryl systems (Figure 6, **44b**) were generated with the results discussed in Chapter 3. Once these elements were better understood, a more complete motor design and synthetic route to the target system could be developed, which is discussed further in Chapter 4. Although the proposed scaffold is already a non-trivial synthetic target, the synthetic route must also be adequately modular to enable rapid late-stage changes and fine tuning of the motor. Finally, analysis of the motor scaffolds **44** and comparison against the model systems or other structurally related analogues was performed using equipment and techniques developed from model studies, work that is discussed further in Chapter 5.

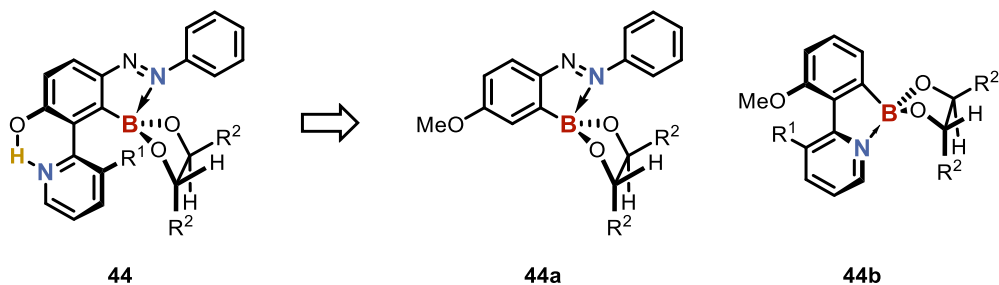


**Figure 6.** Breakdown for the analysis of the proposed system using boryl-azobenzene and boryl-biaryl-pyridine models.

## Chapter 2 Azobenzene Model Systems

### 2.1 Introduction

As discussed in section 1.8, formation of the N<sub>azo</sub>–B bond in the proposed motor is crucial for achieving state A, as otherwise the pyridine ring will remain bound to the boron centre preventing rotation of the central bond from occurring. Conversely, it is also crucial that the N<sub>azo</sub>–B bond can be broken during the photoisomerization step otherwise the system will remain stuck in state A. This would again lead to no rotation around the central bond as the pyridine would remain bound to the phenol. As the system is reliant on the ability to reversibly form the N<sub>azo</sub>–B bond, understanding the behaviour of this bond was quickly identified as a crucial step towards realizing the system. Findings from Kawashima and co-workers' studies into boryl azobenzene systems had suggested that the electronics of the boron ligand play a key role in determining the presence or strength of the N<sub>azo</sub>–B bond (Figure 7).<sup>97</sup> This in turn was found to have a strong effect on the ability of the azobenzene to undergo photoisomerization.

In line with the wider literature on N–B bonds, the strength of the N<sub>azo</sub>–B bond in a series of borylated azobenzenes was measured using the difference in the <sup>11</sup>B NMR chemical shift between the borylated azobenzene and the corresponding phenyl boronic ester (Figure 7, top left box showing  $\Delta\delta_B$  calculation).<sup>97</sup> This is a more reliable measure of bond strength than the direct assessment of the <sup>11</sup>B NMR shift as it helps to account for the differences caused by different ligands as well as variations between NMR instruments. Using this approach, Kawashima and co-workers demonstrated that azobenzene boronic acid **47**, pinacol boronic ester **48** or *o*-phenylenediamine boronic ester **49** were all unable to form a N<sub>azo</sub>–B bond. Conversely, they were also able to show that azobenzenes **46**, **50** and **51** were all able to form N<sub>azo</sub>–B bonds of varying strengths. While proving the formation of the N<sub>azo</sub>–B bond was significant in and of itself, Kawashima and co-workers also examined the ability of these systems to undergo photoisomerization. From this, they found that the systems with no N<sub>azo</sub>–B bond such as **47** were able to isomerise readily to the Z isomer, with a favourable PSS (*E*:*Z* 2:98) under 360 nm irradiation, while systems with strong N<sub>azo</sub>–B bonds, such as **50** or **51**, were unable to undergo *E*-to-Z isomerization. Fortunately, they also found that systems with weak N<sub>azo</sub>–B bonds, such as **46** were able to undergo *E*-to-Z isomerization resulting in a moderate-to-poor PSS (*E*:*Z* 65:35) under 360 nm irradiation in favour of the initial *E* isomer.

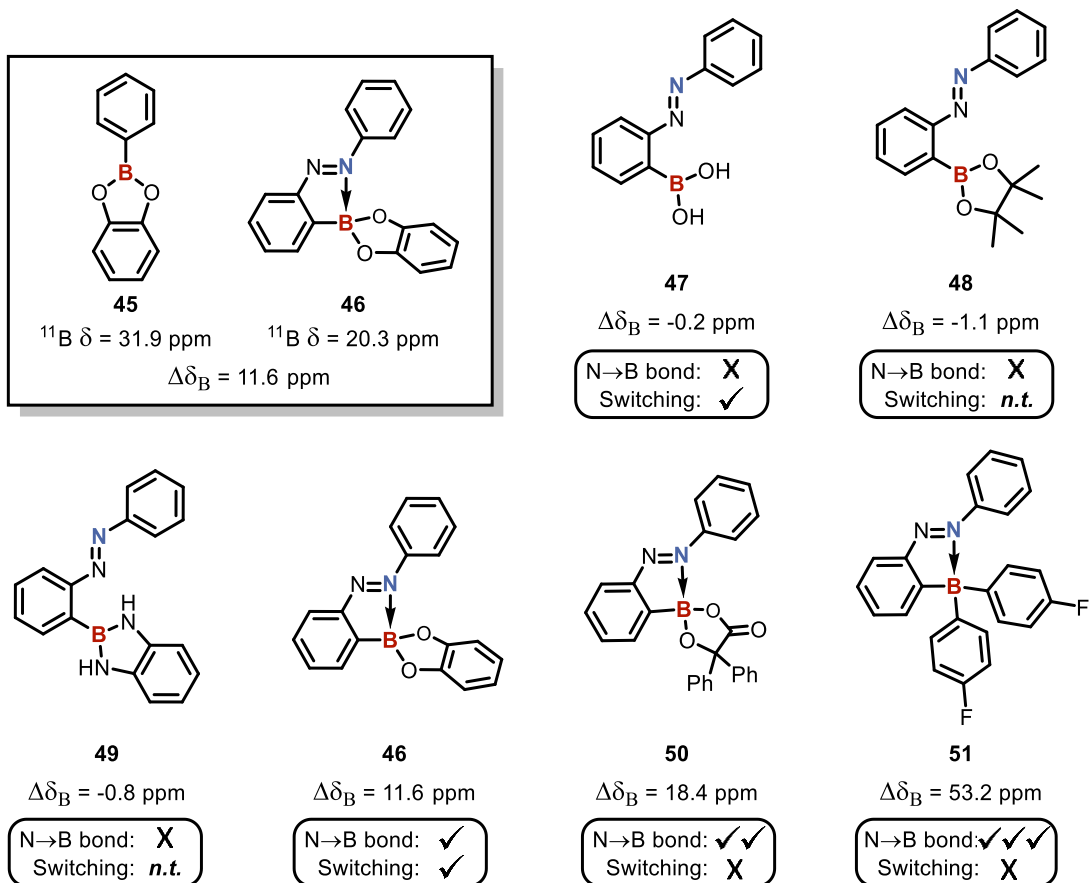


**Figure 7.** Summary of the borylated-azobenzene compounds made by Kawashima and co-workers with the relative difference in  $^{11}\text{B}$  NMR shift shown as a measure of  $\text{N}_{\text{azo}}-\text{B}$  bond strength. *n.t.* – not tested.<sup>97</sup>

From these results, it was proposed that the  $\text{N}_{\text{azo}}-\text{B}$  bond strength could be controlled by altering the amount of back-donation from the boron ligand into the p-orbital of the boron centre (Figure 8). In more electron withdrawn systems (e.g., carbon-based boryl-azobenzene **51**) less electron back-donation occurs from the ligand to the boron centre, allowing greater electron donation from the azobenzene nitrogen and leading to strong a  $\text{N}_{\text{azo}}-\text{B}$  bond (Figure 8, left). Conversely, highly electron-rich boron ligands (e.g., boronic acid azobenzene **47**) back-donate greater electron density into the p-orbital of the boron and prevent the azobenzene nitrogen from being able to donate electron density, thereby preventing the formation of the  $\text{N}_{\text{azo}}-\text{B}$  bond (Figure 8, right). Mildly reducing the electron back-donation by bringing the electron rich, boron bound atoms into conjugation (e.g., catechol boronic ester azobenzene **46**) means a less back-filled p-orbital, mild electron donation from the azobenzene, and formation of a weak  $\text{N}_{\text{azo}}-\text{B}$  bond (Figure 8, middle). Kawashima and co-workers then proposed two ways in which the strength of the  $\text{N}_{\text{azo}}-\text{B}$  bond may be related to the photochemical behaviour. In their first proposal they suggest that as the  $\text{N}_{\text{azo}}-\text{B}$  bond strength increases it causes a red shift of the *E* isomer (but not the *Z*) in turn causing greater overlap between the absorption maxima

of the *E* and *Z* isomers, leading to a PSS more heavily in favour of the *E* conformation. Alternatively, they also propose that photoisomerization could only occur from the tri-coordinated boron state and if the weaker N<sub>azo</sub>–B bonds are more dynamic in nature, it would allow isomerization of the temporarily formed tri-coordinated boron state to occur in system with weaker N<sub>azo</sub>–B bonds. While investigating this behaviour further is beyond the scope of this project, it is a particularly interesting aspect of these systems and is being studied further by another member of the Collins group, Connah Harris.

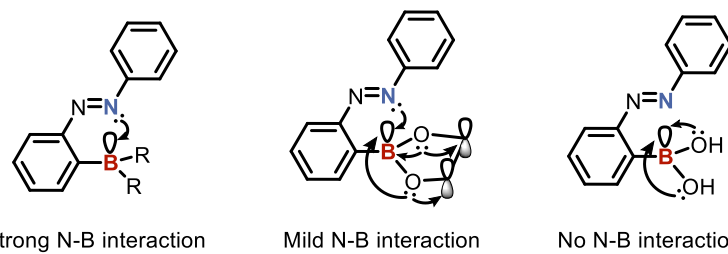


**Figure 8.** Proposed rationale for the N–B bond strength control based on electron donation into the empty p-orbital.

## 2.2 Photoswitch Ligand Identification

While the systems from Kawashima and co-worker's study (Figure 7) gave useful inspiration and an understanding of the limitations for these systems, the catechol ligand they identified for inducing a breakable N<sub>azo</sub>–B bond was non-chiral and therefore not suitable for our purposes.<sup>97</sup> It is also worth noting that not only is a chiral ligand needed for the proposed system (Scheme 17) but due to the possible rotation around the C–B bond, chirality that derives from C2 symmetry would greatly simplify the system but limits the pool of viable ligands. Furthermore, it was also desirable for the system identified to have a PSS in favour of the *Z* isomer so that the post-irradiation analysis could be done on the major species. With these requirements in mind, (+)-dimethyl-L-tartrate (DMT) **55** and (S)-BINOL **56** were selected for testing and α-hydroxyisobutyric acid **52**, pinacol **53** and catechol **54** were chosen for use as control systems (Figure 9).

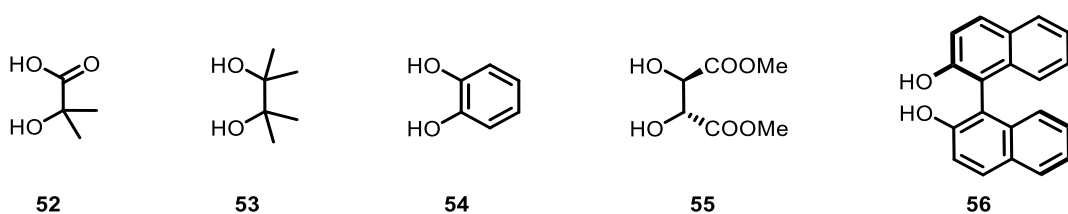


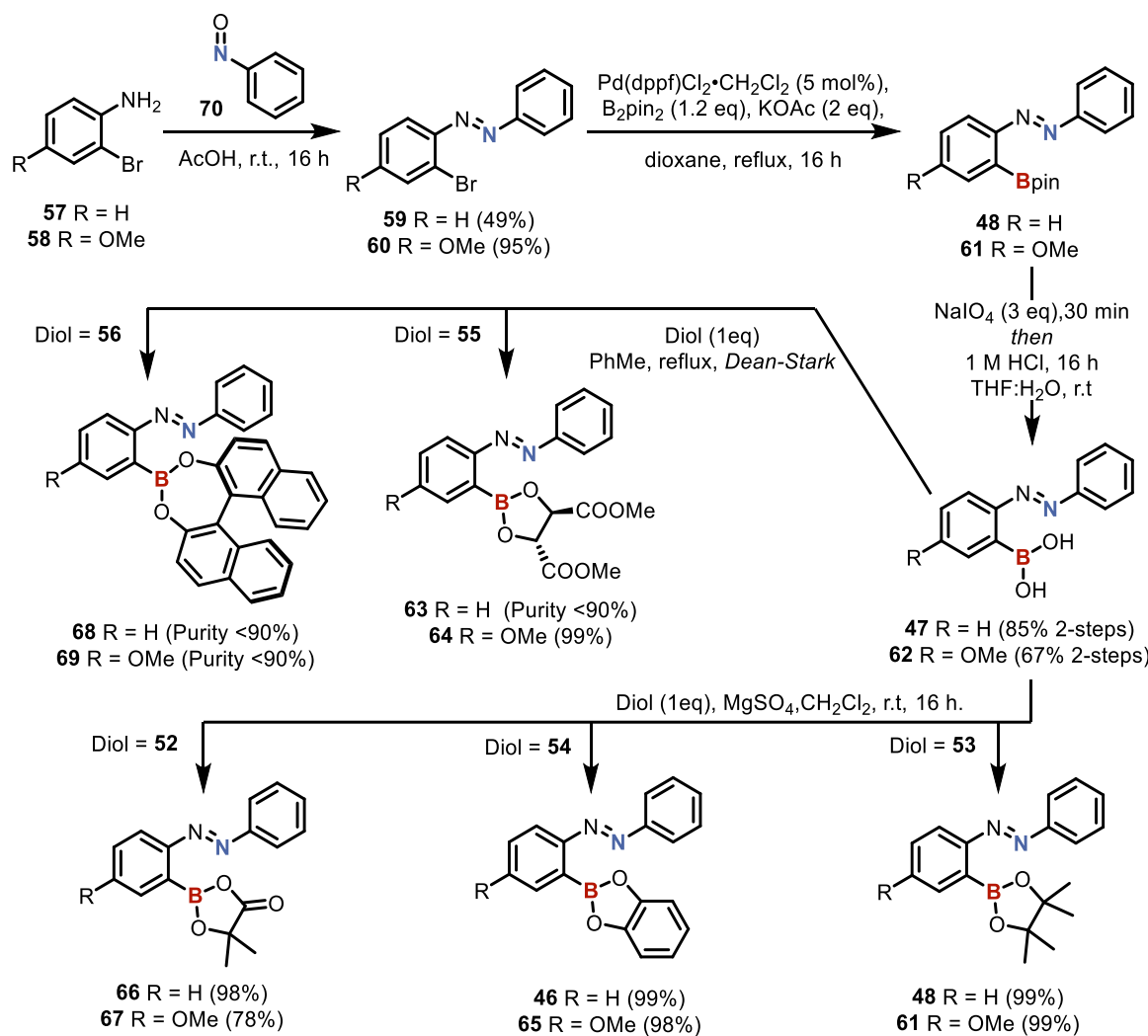
**Figure 9.** Diol ligands **52–56** initially selected for photoswitch testing.

The  $\alpha$ -hydroxyisobutyric acid-based system **52** was intended to act as a control for a strong N<sub>azo</sub>–B bond which prevents photoisomerization. The pinacol based system **53** would act as a control for a lack of the N<sub>azo</sub>–B bond and show clear photoisomerization behaviour. Finally, the catechol-based system **54** should display the desired photoswitching N<sub>azo</sub>–B bond behaviour described by Kawashima and co-workers and could be used to benchmark our results. Although Kawashima and co-workers assessed a great range of different ligands, they never investigated ligands which had any inductive electron withdrawal instead looking solely at conjugated systems. As such, (+)-DMT **55** was selected to investigate whether electron withdrawal *via* induction might be viable for inducing a weak N<sub>azo</sub>–B bond. The final ligand of interest, (*S*)-BINOL **56**, was suspected to exhibit a similar electron withdrawing effect to catechol but due to the axis of chirality might be a viable chiral ligand for driving the directionality of the proposed rotary cycle (Scheme 17).

### **2.3 Synthesis of Boryl-Azobenzene Switches**

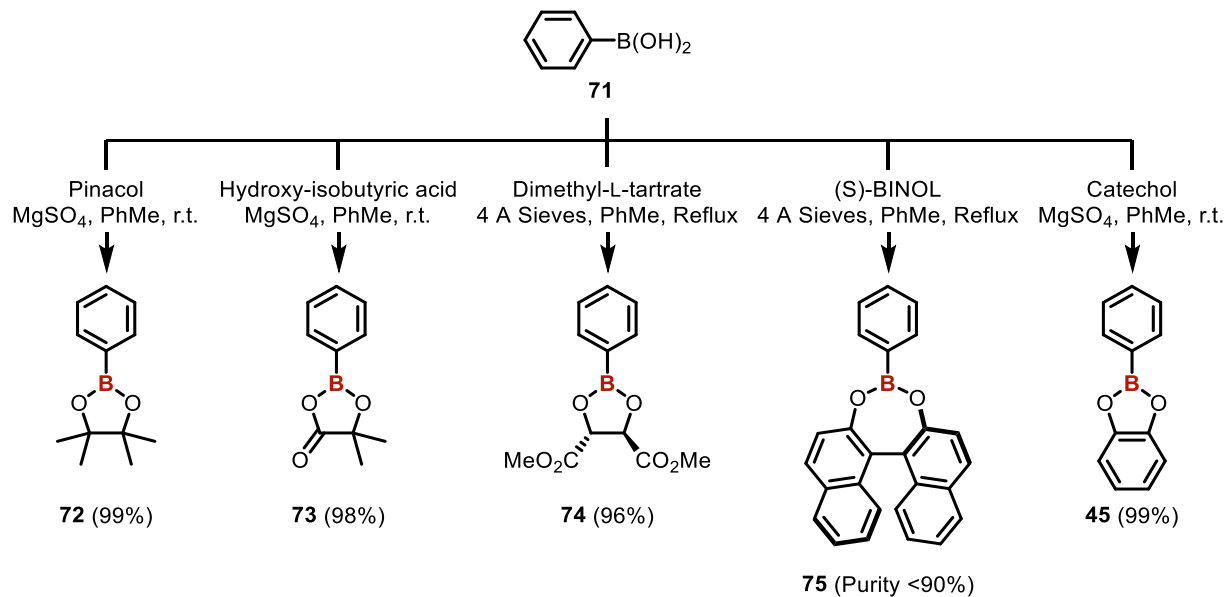
After selecting the ligands to test, synthesis of the borylated azobenzenes was initially undertaken following the procedure from Kawashima and co-workers.<sup>97</sup> Following this approach, haloanilines **57** and **58** were coupled to nitrosobenzene **70** *via* a Mills reaction to give azobenzenes **59** and **60**, in 48% and 95% yield respectively (Scheme 18, Step 1). Subsequent lithiation-borylation unfortunately resulted in a complex mixture of products due to the attack into the azo-bond.<sup>103, 104</sup> This issue was readily overcome by using a Miyaura borylation followed by pinacol deprotection (*via* Malaprade oxidative cleavage) to give azobenzenes **47** and **62** in 85% and 67% yield respectively over two steps (Scheme 18, Steps 2 and 3). It is worth noting that the azobenzene pinacol boronic esters **48** and **61** were unstable on silica gel making column chromatography problematic, but due to the clean conversion and high yield of the Miyaura borylation the material could be used directly in the next deprotection step without further purification. Coupling of the diol ligands (**52** - **56**) to the azobenzene boronic acids **47** and **62** *via* dehydrative coupling, resulted in the generation of the boryl-azobenzenes **48**, **61**, **46** and **63-69** in high yields. Unfortunately, purification of these compounds proved a significant challenge with azobenzenes **46** and **63-69** being highly water and silica sensitive and azobenzenes **48** and **61** being silica sensitive. However, as compounds **46**, **65**, **66** and **67** could be made in near quantitative yield and were crystalline solids they could be readily prepared *via* recrystallization. Unfortunately, due to their state as oils compounds **63** and **64** could not be purified by aqueous work-up, chromatography or

recrystallization and were therefore analysed without further purification. Compounds **68** and **69** which were unstable to water and silica were also analysed without further purification as their highly unstable nature meant any attempts at recrystallization, even under dry and inert conditions, resulted in partial hydrolysis of the product. Although compounds **48** and **61** were oils and unstable towards silica, they possessed high water stability and since they could be prepared in near quantitative yield, they were purified *via* simple aqueous workup. Due to these challenges, the  $^{11}\text{B}$  NMR data is presented for the purified compounds **46**, **65**, **66**, **67**, **48** and **61** while for compounds **63**, **64**, **68** and **69** it is presented from a mixture of the desired product, excess ligand, and residual starting material (**47** or **62**).



Scheme 18. Synthesis of the model borylated-azobenzenes used for ligand testing.

As discussed in section 2.1, the N<sub>azo</sub>–B bond strength is best measured by calculating the difference in <sup>11</sup>B NMR chemical shift ( $\Delta\delta_B$ ) between the borylated azobenzene and the corresponding phenyl boronic ester (i.e.  $\Delta\delta_B = \delta_{B(\text{phenyl boronic ester})} - \delta_{B(\text{azobenzene boronic ester})}$ ). As such, the phenyl boronic esters **72**–**74** and **45** were generated in high yield by coupling the boron ligands **52**–**56** to phenyl boronic ester **71** using the dehydrative esterification procedure (Scheme 19). Unfortunately, compound **75**, degraded very readily and was therefore analysed without further purification.



Scheme 19. Synthesis of phenyl boronic ester reference compounds.

## 2.4 Assessment of N<sub>azo</sub>–B Bond and Photoisomerization

### 2.4.1 Formation of N<sub>azo</sub>–B Bond in *E* Isomer

Using the borylated azobenzenes and the phenyl boronic ester systems, the presence or strength of the N<sub>azo</sub>–B bond was measured using the calculated  $\Delta\delta_B$  values (Table 1) where larger  $\Delta\delta_B$  values represent stronger N<sub>azo</sub>–B bonds. In line with expectations, no N<sub>azo</sub>–B bond was observed in the *E* isomer of the azobenzene pinacol ester or boronic acid compounds **47** ( $\Delta\delta_B = -0.9$  ppm, *lit.*  $\Delta\delta_B = -0.2$  ppm), **62** ( $\Delta\delta_B = -0.2$  ppm), **48** ( $\Delta\delta_B = -0.4$  ppm, *lit.*  $\Delta\delta_B = -1.1$  ppm) or **61** ( $\Delta\delta_B = -0.2$  ppm).<sup>97</sup> It is also worth noting that no difference in  $\Delta\delta_B$  was observed in these systems between the methoxy and non-methoxy equivalents (e.g., neither **48** nor **61** displayed a N<sub>azo</sub>–B bond). As expected, N<sub>azo</sub>–B bonds were observed in the *E* isomer of the isobutyric acid based azobenzenes **66** ( $\Delta\delta_B = 18.4$  ppm) and **67** ( $\Delta\delta_B = 20.4$  ppm) and in the

catechol based azobenzenes **46** ( $\Delta\delta_B = 11.7$  ppm, *lit.*  $\Delta\delta_B = 11.6$  ppm) and **65** ( $\Delta\delta_B = 15.1$  ppm). In both the isobutyric acid and catechol-based systems the methoxy substituted azobenzene displayed notably stronger N<sub>azo</sub>–B bonds than its unsubstituted counterpart (e.g., **67** shows a stronger bond than **66**). This indicated that while methoxy substitution at the *para*-position was unable to induce the formation of new N<sub>azo</sub>–B bonds in systems that would otherwise not form a N–B bond (e.g., **48**), the increased electron density due to the methoxy group still served to increase the bond strength of the N–B bond in systems which were already capable of forming these bonds (e.g., **46**). Turning to the DMT and BINOL systems, moderately strong N<sub>azo</sub>–B bonds were observed in compounds **63** ( $\Delta\delta_B = 8.4$  ppm), **64** ( $\Delta\delta_B = 13.8$  ppm), **68** ( $\Delta\delta_B = 12.5$  ppm) and **69** ( $\Delta\delta_B = 13.4$  ppm). From Kawashima and co-workers' study, compound **46** ( $\Delta\delta_B = 11.7$  ppm, *lit.*  $\Delta\delta_B = 11.6$  ppm) was known to have a N<sub>azo</sub>–B bond of the desired strength to allow photoswitching, while that of compound **50** (*lit.*  $\Delta\delta_B = 18.4$  ppm) was believed to be too strong. As the  $\Delta\delta_B$  values of the DMT and BINOL based systems **63**, **64**, **68** and **69** are all below that of **50** (*lit.*  $\Delta\delta_B = 18.4$  ppm) and similar to that of **46** (*lit.*  $\Delta\delta_B = 11.6$  ppm), the N<sub>azo</sub>–B bonds in these compounds are expected to be of the desired strength to allow photoswitching.

Ligand	R	Azo	Phenyl	$\delta_B$ (Azo)	$\delta_B$ (Phenyl)	$\Delta\delta_B^a$
Boronic Acid	H	(E)- <b>47</b>	<b>71</b>	28.9 <sup>b</sup>	28.0 <sup>b</sup>	-0.9
Boronic Acid	OMe	(E)- <b>62</b>	<b>71</b>	28.2 <sup>b</sup>	28.0 <sup>b</sup>	-0.2
Pinacol	H	(E)- <b>48</b>	<b>72</b>	30.4	30.0	-0.4
Pinacol	OMe	(E)- <b>61</b>	<b>72</b>	30.2	30.0	-0.2
$\alpha$ -Hydroxyisobutyric acid	H	(E)- <b>66</b>	<b>73</b>	14.6	33.0	18.4
$\alpha$ -Hydroxyisobutyric acid	OMe	(E)- <b>67</b>	<b>73</b>	12.6	33.0	20.4
Catechol	H	(E)- <b>46</b>	<b>45</b>	19.6	31.3	11.7
Catechol	H	(E)- <b>46</b>	<b>45</b>	21.4 <sup>c</sup>	31.3 <sup>c</sup>	9.9 <sup>c</sup>
Catechol	OMe	(E)- <b>65</b>	<b>45</b>	16.2	31.3	15.1
(+)-dimethyl L-tartrate	H	(E)- <b>63</b>	<b>74</b>	22.7 <sup>d</sup>	31.1	8.4
(+)-dimethyl L-tartrate	OMe	(E)- <b>64</b>	<b>74</b>	17.3	31.1	13.8
(S)-BINOL	H	(E)- <b>68</b>	<b>75</b>	12.6 <sup>d</sup>	25.1 <sup>de</sup>	12.5
(S)-BINOL	OMe	(E)- <b>69</b>	<b>75</b>	11.7 <sup>d</sup>	25.1 <sup>de</sup>	13.4

**Table 1.**  $^{11}\text{B}$  NMR chemical shifts of the *E* isomers of the boryl-azobenzenes in  $\text{CDCl}_3$  and the upfield shifts from their corresponding phenylboranes. The targeted systems of interest are highlighted in yellow. <sup>a</sup>  $\Delta\delta_B = \delta_B$  (phenylborane) -  $\delta_B$  (2-(phenylazo)phenylborane). <sup>b</sup> in  $\text{DMSO-d}_6$ . <sup>c</sup> in  $\text{C}_6\text{D}_6$ . <sup>d</sup> Data from <90% pure compound was used due to compound instability. <sup>e</sup> Data confirmed by ref 103.

To better understand these N<sub>azo</sub>–B bonds and test whether they had distinctive UV-Vis characteristics, as well as confirm the *E* isomers would absorb light at the desired irradiation wavelength (365 nm), a brief UV-Vis analysis of selected boryl-azobenzenes **47**, **48**, **63**, **64**,

**66** and **65** was performed (Figure 10). As mentioned in section 2.1, further work into the understanding of the photochemical properties of these boryl-azobenzenes, which includes more extensive UV-Vis analysis, is being conducted by fellow group member Connah Harris. As such, only a short discussion of the relevant properties of the UV-Vis spectra are discussed herein.

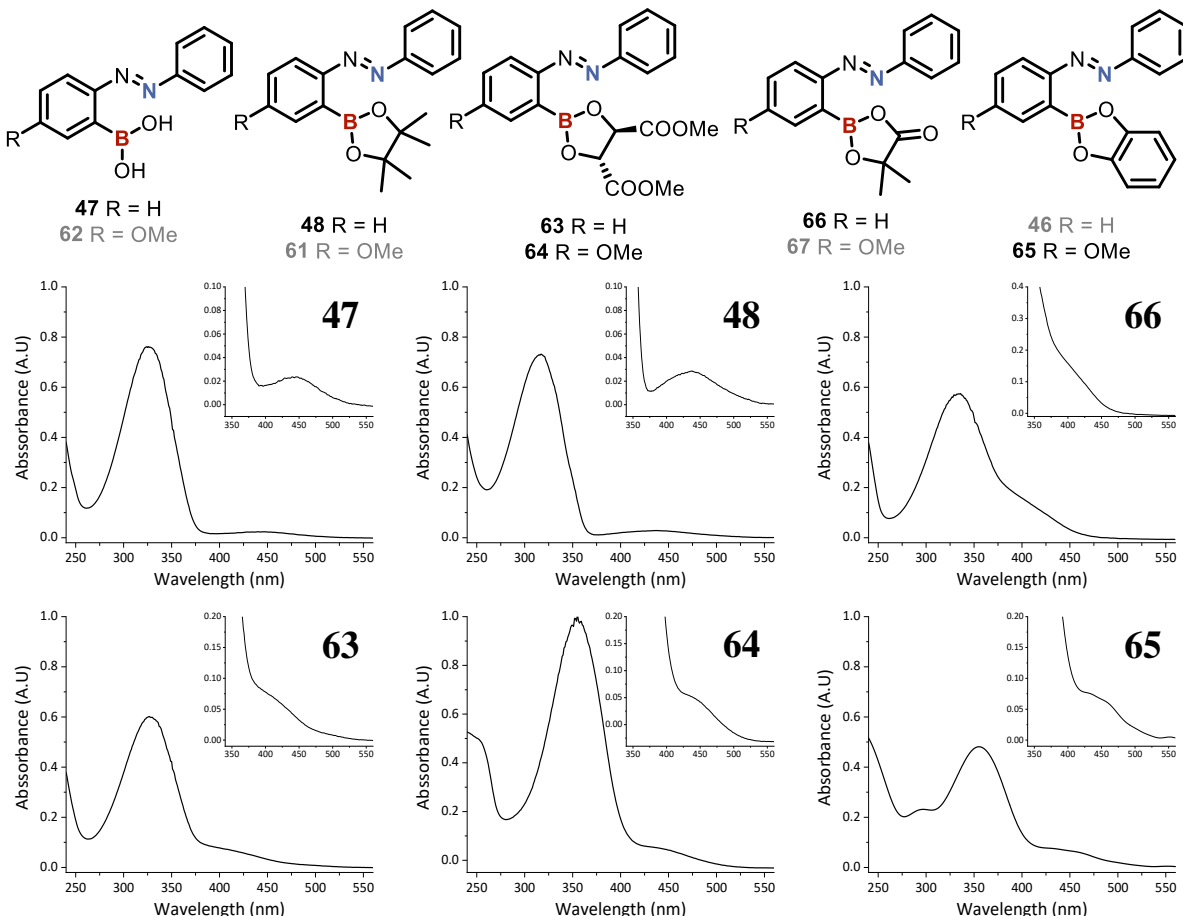


**Figure 10.** UV-Vis spectra in MeCN of selected boryl-azobenzenes **48**, **66**, **63**, **64** and **65**.

From the UV-Vis spectra it was apparent that the methoxy group caused a notable redshift of the  $\lambda_{\max}$  of the methoxy azobenzenes compared to the less substituted equivalents (e.g., **63**  $\lambda_{\max} = 327$  nm vs. **64**  $\lambda_{\max} = 356$  nm), which is in good agreement with the literature on other methoxy-substituted azobenzenes.<sup>105</sup> In line with Kawashima and co-workers' results, boronic acid **47** displayed two resolved peaks at 326 nm and 446 nm (*lit.* 326 nm and 444 nm) corresponding to the  $\pi-\pi^*$  and  $n-\pi^*$  transitions respectively. Similarly, pinacol-based **48** also displayed two resolved peaks at 317 nm and 438 nm (*lit.* 317 nm and 440 nm) again corresponding to the  $\pi-\pi^*$  and  $n-\pi^*$  transitions respectively. Compounds **63**, **64**, **66** and **65**

which had been identified as containing a N<sub>azo</sub>–B bond, exhibited peaks at 328 nm, 356 nm, 334 nm, 356 nm respectively, which all correspond to the respective π–π\* transition. Interestingly, rather than observe distinct peaks for the n–π\* transitions of these systems, they instead exhibited a shoulder on the peaks representing the π–π\* transition, a feature which was also observed by Kawashima and co-workers. This meant that not only did the N<sub>azo</sub>–B bonds display distinctive characteristics by NMR but also by UV-Vis giving another useful analytical handle. While the  $\lambda_{\text{max}}$  varied between the azobenzene systems, all had a sufficient absorption at 365 nm for the azobenzenes to be used for further photoisomerization work. Due to the challenging stability of the chiral compounds **63**, **64**, **68** and **69**, only compound **64** was carried into the subsequent studies as it possessed the required N<sub>azo</sub>–B bond, the N<sub>azo</sub>–B bond was of the desired strength, it possessed C<sub>2</sub> symmetric chirality at the boron centre, and the methoxy substitution most closely resembled the electronics of the proposed motor system.

#### 2.4.2 Photoswitching and PSS Assessment

Once the presence of the N<sub>azo</sub>–B bond had been ascertained in the *E* isomer of the DMT system **64**, the strength of the bond shown to be comparable to the known catechol system **46**, and light absorption at 365 nm proven, attention turned to assessing the photochemical behaviour. To do this, compounds **48**, **61**, **66**, **67**, **46**, **65** and **64** were irradiated in quartz NMR tubes using a basic irradiation set-up described in experimental section 8.4.1. Following irradiation at 365 nm or 430 nm, the photostationary state (PSS) composition of each compound was determined by integration of the <sup>1</sup>H NMR signals corresponding to the relative *E* and *Z* isomers (Table 2).

Ligand	R	Compound	N–B Bond	E : Z Ratio	
				$\lambda = 365 \text{ nm}$	$\lambda = 430 \text{ nm}$
Pinacol	H	<b>48</b>	✗	59 : 41	82 : 18
Pinacol	OMe	<b>61</b>	✗	10 : 90	71 : 29
α-Hydroxyisobutyric acid	H	<b>66</b>	✓	97 : 3	100 : 0
α-Hydroxyisobutyric acid	OMe	<b>67</b>	✓	100 : 0	-
Catechol	H	<b>46</b>	✓	89 : 11	99 : 1
Catechol	H	<b>46</b>	✓	80 : 20 <sup>a</sup>	95 : 5 <sup>a</sup>
Catechol	OMe	<b>65</b>	✓	89 : 11	100 : 0
(+)-dimethyl L-tartrate	OMe	<b>64</b>	✓	17 : 83	71 : 29

**Table 2.** Photostationary states of the boryl-azobenzenes after three hours of irradiation in CDCl<sub>3</sub> at 365 nm or 430 nm. The DMT system of interest is highlighted in yellow. <sup>a</sup> in C<sub>6</sub>D<sub>6</sub>

It was evident from the PSSs achieved under irradiation at 365 nm that both the presence of the N<sub>azo</sub>–B bond and the presence of the methoxy group had significant effects on the PSS. As expected, the pinacol based azobenzenes **48** and **61**, which contained no N<sub>azo</sub>–B bond isomerized readily under 365 nm irradiation with PSSs of 59:41 and 10:90 respectively. Conversely, compounds **66** and **67** which contained strong N<sub>azo</sub>–B bonds appeared not to isomerise or had a very poor PSS (*E*:*Z* ratio of 97:3). The notably more favourable PSS for the methoxy azobenzene **61** over azobenzene **48** was attributed to the red shift of the  $\lambda_{\text{max}}$  in the *E* isomer of **61**. This causes a greater absorption cross section between the absorbance of the *E* isomer of compound **61** and the excitation light (365 nm). By improving the absorption cross section, and therefore increasing the photon abortion by the *E* isomer at the wavelength of irradiation, the forwards *E*-to-*Z* isomerization process is improved. i.e. the molar absorption coefficient of compound *E*-**61** at the wavelength of irradiation is increased leading to a greater number of forwards photoisomerisation events. By improving the molar absorption coefficient (at the wavelength of excitation) of the *E* isomer more significantly than the *Z* isomer, the forwards *E*-to-*Z* isomerization process is improved more significantly than the reverse *Z*-to-*E* process. This then leads to a PSS more heavily in favour of the *Z* isomer.

Irradiation at 365 nm of the literature compound **46** in CDCl<sub>3</sub> led to a moderate-to-poor PSS of 89:11 (*E*:*Z*), which could be slightly improved to 80:20 (*E*:*Z*) when performed in C<sub>6</sub>D<sub>6</sub>. It is worth noting that while Kawashima and co-workers characterized their azobenzene systems in CDCl<sub>3</sub>, all of their irradiation studies were conducted in C<sub>6</sub>D<sub>6</sub> as they noted the azobenzenes were able to achieve more favourable PSSs in more non-polar solvents, particularly in deuterated cyclohexane.<sup>97</sup> In contrast to the pinacol-based systems (**48** and **61**), the catechol-based systems **65** and **46** displayed a slightly less favourable PSS in the methoxy substituted compound than in the less substituted compound. As the methoxy substitution had been shown to favour the photoisomerization (evidenced by the pinacol systems **61** vs **48**) while the N<sub>azo</sub>–B bond had been shown to disfavour photoisomerization (catechol system **46** vs pinacol system **48**), the less favourable PSS of **65** compared to **46** was attributed to the increased bond strength of the N<sub>azo</sub>–B bond.

Pleasingly, under 365 nm irradiation the DMT-based compound **64** showed a good PSS of 17:83 (*E*:*Z*) in favour of the desired *Z* isomer. This meant that compound **64** could not only

form the desired N<sub>azo</sub>–B bond in the *E* isomer and still isomerise to the *Z* isomer under irradiation, but it was able to form the desired *Z* isomer as the major species during the process. This made the DMT ligand very appealing for use in the final system.

While the ultimate goal was to have the reverse *Z*-to-*E* isomerization driven by thermal relaxation, the ability of these azobenzene systems to undergo the reverse *Z*-to-*E* photoisomerization using 430 nm irradiation was also investigated. For the pinacol based compounds **48** and **61**, reversion back to the *E* isomers occurred readily under irradiation at 430 nm with the PSS in favour of the desired *E* isomer for both compounds (82:18 and 71:29 respectively). The α-hydroxyisobutyric acid system **66** which had shown the formation of trace amounts of the *Z* isomer under 365 nm irradiation, returned exclusively to the *E* isomer upon irradiation at 430 nm. Similarly, both catechol systems **46** and **65** which showed minimal formation of the *Z* isomer under 365 nm irradiation, gave PSSs of almost exclusively *E* isomer under 430 nm irradiation (99:1 and 100:0 respectively). The DMT system of interest **64**, also reverted to the *E* isomer under 430 nm irradiation to give a PSS of 71:29 in favour of the desired *E* azobenzene. This meant that both the forwards *E*-to-*Z* isomerization and the reverse *Z*-to-*E* isomerization of the DMT system **64** could be achieved to give the desired isomer as the major species using 365 nm and 430 nm irradiation respectively. Interestingly, the PSS observed for the DMT azobenzene **64** under 430 nm irradiation (71:29) was an exact match to the PSS observed pinacol system **61** (71:29).

#### **2.4.3 Loss of N<sub>azo</sub>–B Bond in Z Isomer**

While the formation of the N<sub>azo</sub>–B bond had been demonstrated in the *E* isomer of azobenzene **64** and the photoswitching ability shown to be an improvement over the benchmarked systems (sections 2.4.1 and 2.4.2 respectively), the loss of the N<sub>azo</sub>–B bond in the *Z* isomer was still unproven. Irradiation of compounds **48**, **61**, **46**, **65** and **64** with 365 nm light to generate the corresponding *Z* isomers, then allowed the measurement of the Δδ<sub>B</sub> values for the *Z* isomers and therefore the assessment of the N<sub>azo</sub>–B bond (Table 3). From these Δδ<sub>B</sub> values, it is apparent that no N<sub>azo</sub>–B bond forms in either the *E* or the *Z* isomer of the pinacol-based compounds **48** or **61** as expected (Table 3, rows 1 and 2). In the catechol-based systems **46** and **65**, which do contain N<sub>azo</sub>–B bonds in the *E* isomer, isomerization to the *Z* isomer led to the loss of the N<sub>azo</sub>–B bonds, evidenced by the significant drop to near zero values of Δδ<sub>B</sub>.

(Table 3, rows 3 and 4). Similarly, the DMT-based system **E-64**, which exhibited a N<sub>azo</sub>–B bond of comparable strength to **E-46** and **E-65**, showed the same drop in Δδ<sub>B</sub> value indicating the loss of the N<sub>azo</sub>–B bond during the *E*-to-*Z* photoisomerization (Table 3, row 5). This would indicate that the chiral DMT based system **64**, is able to form the N<sub>azo</sub>–B bond in the *E* isomer, able to undergo photoisomerization at 365 nm or 430 nm to favour the desired isomer (*E* or *Z* respectively), and the isomerization is shown to break the N<sub>azo</sub>–B bond.

Azo	Ligand	R	Δδ <sub>B</sub> (E) <sup>a</sup>	Δδ <sub>B</sub> (Z) <sup>a</sup>
<b>48</b>	Pinacol	H	-0.4	-0.3
<b>61</b>	Pinacol	OMe	-0.2	0.5
<b>46</b>	Catechol	H	11.7	1.4
<b>46</b>	Catechol	H	9.9 <sup>b</sup>	0.6 <sup>b</sup>
<b>65</b>	Catechol	OMe	15.1	0.3
<b>64</b>	(+)-dimethyl L-tartrate	OMe	13.8	2.4

**Table 3.** <sup>11</sup>B NMR chemical shifts of the *Z* isomers of the boryl-azobenzenes in CDCl<sub>3</sub> and the upfield shifts from their corresponding phenylboranes. The DMT system of interest is highlighted in yellow. <sup>a</sup>Δδ<sub>B</sub> = δ<sub>B</sub> (phenylborane) - δ<sub>B</sub> (2-(phenylazo)phenylborane). <sup>b</sup> in C<sub>6</sub>D<sub>6</sub>.

#### 2.4.4 Lewis Acidity Testing *via* Pyridine Binding

While the formation and breakage of the N<sub>azo</sub>–B bond upon photoisomerization shows the occupancy of the p-orbital can be controlled using light, it does not necessarily prove modulation of pyridine coordination to the boron centre can be achieved. To prove this, and to prove the systems are also compatible with nitrogenous bases, boryl-azobenzenes **46**, **64** and **66** were irradiated in the presence of 1.3 equivalents of pyridine with the Δδ<sub>B</sub> values reported in Table 4. In the catechol system **46**, addition of pyridine caused a slight increase in the Δδ<sub>B</sub> value (Table 4, row 1. 9.9 ppm vs 13.5 ppm) indicating a small degree of pyridine coordination to the system in the *E* isomer. This might suggest that the N<sub>azo</sub>–B bond is moderately dynamic in nature allowing exchange between the internal N<sub>azo</sub>–B bond and the external N<sub>pyr</sub>–B bond. Although dynamic exchange may be observed, the system is still believed to exhibit more N<sub>azo</sub>–B bond character than N<sub>pyr</sub>–B bond character as the <sup>11</sup>B NMR shift (<sup>11</sup>B δ = 19.2 ppm) is more similar to the <sup>11</sup>B NMR shift of the pure *E*-**46** (<sup>11</sup>B δ = 21.4 ppm) than the phenyl boronic catechol ester **45** in the presence of pyridine (<sup>11</sup>B δ = 13.9 ppm). Importantly, upon irradiation of the *E*-**46** to generate the *Z* isomer, rather than a drop in the Δδ<sub>B</sub> value as was previously observed in the absence of pyridine (Table 4, row 1, 9.9 ppm to 0.6 ppm), in the presence of pyridine the Δδ<sub>B</sub> value instead increased (Table 4, row 1, 13.5 ppm to 20.4 ppm). Since no

$N_{\text{azo}}-\text{B}$  bond forms in the *Z* isomer (section 2.4.3), the increased  $\Delta\delta_B$  value in the pyridine system is indicative of the formation of the external  $N_{\text{pyr}}-\text{B}$  bond.<sup>98</sup> As there was a significant change in the  $\Delta\delta_B$  value upon photoisomerization, which is attributed to the formation of a new external  $N_{\text{pyr}}-\text{B}$  bond, there must be a significant difference in the ability of pyridine to coordinate to the boronic ester in the *E* and *Z* states. This would indicate that the azobenzene photoswitching is indeed able to modulate the Lewis acidity of the compound as desired.

Ligand	R	Azo	With Pyridine		Without Pyridine	
			$\Delta\delta_B(\text{E})^{\text{ab}}$	$\Delta\delta_B(\text{Z})^{\text{ab}}$	$\Delta\delta_B(\text{E})^{\text{a}}$	$\Delta\delta_B(\text{Z})^{\text{a}}$
Catechol	H	<b>46</b>	13.5 <sup>c</sup>	20.4 <sup>c</sup>	9.9 <sup>c</sup>	0.6 <sup>c</sup>
(+)-dimethyl L-tartrate	OMe	<b>64</b>	14.3	18.6	13.8	2.4
$\alpha$ -Hydroxyisobutyric acid	H	<b>66</b>	21.9	25.2	18.4	-

**Table 4.**  $\Delta\delta_B$  values of the E and Z isomers of boryl-azobenzenes **46**, **64** and **66** in  $\text{CDCl}_3$  (or  $\text{C}_6\text{D}_6$  where indicated) with or without 1.3 equivalents of pyridine present. The DMT system of interest is highlighted in yellow. <sup>a</sup>  $\Delta\delta_B = \delta_B(\text{phenylborane}) - \delta_B(2-(\text{phenylazo})\text{phenylborane})$ . <sup>b</sup> 1.3 equivalents of pyridine added. <sup>c</sup> in  $\text{C}_6\text{D}_6$ .

When comparing the chiral DMT system **64** to the catechol system **46** (Table 4, row 1 and row 2), the same trend is observed with the  $\Delta\delta_B$  value increasing upon *E*-to-*Z* photoisomerization rather than decreasing. In the presence of pyridine, the  $\Delta\delta_B$  value of the DMT system **64** increased from 14.3 ppm to 18.6 ppm upon photoisomerization but in the absence of pyridine the  $\Delta\delta_B$  value decreased from 13.8 to 2.4 (Table 4, row 2). Following the same reasoning as before, this would suggest the DMT system **64** was forming an internal  $N_{\text{azo}}-\text{B}$  bond in the *E* isomer and an external  $N_{\text{pyr}}-\text{B}$  bond in the *Z* isomer. As the DMT system **64** was capable of modulating the external  $N_{\text{pyr}}-\text{B}$  bond as a function of the azobenzene state, the DMT ligand would likely be viable for use in controlling the conversion between states A and B in the proposed motor system (Scheme 17). In the  $\alpha$ -hydroxyisobutyric acid system **66**, which contains a stronger  $N_{\text{azo}}-\text{B}$  bond, the same trend is observed with an increase in  $\Delta\delta_B$  value upon *E*-to-*Z* photoisomerization in the presence of pyridine (Table 4, row 3). This would suggest that the formation of the external  $N_{\text{pyr}}-\text{B}$  bond modulation can be achieved in multiple compounds which all use different ligands.

#### 2.4.5 Pyridine Nucleophile Effect on the Boryl-Azobenzene PSS

While testing the pyridine coordination to the boryl-azobenzenes (section 2.4.4), it was discovered that addition of pyridine also affected the PSS achieved by these systems. As shown

in Table 5, under 365 nm irradiation compounds **46**, **64** and **66** had previously shown PSSs of 80:20, 17:83 and 97:3 respectively, but upon addition of pyridine and subsequent irradiation, the PSSs improved to 27:73, 15:85 and 5:95 respectively. Interestingly, the systems with stronger N<sub>azo</sub>–B bonds were able to show the greatest improvement. This was most evident in compound **66** where in the absence of pyridine barely any *E*-to-*Z* photoisomerization was observed, while in the presence of pyridine near quantitative *E*-to-*Z* isomerization was displayed. These were particularly useful results as it showed that the more electron withdrawn ligands, which were believed to be detrimental to the photoswitching based on the results described in section 2.4.2, were actually viable ligands for these types of systems. This opened up more chemical space for ligand exploration and provided additional options should the DMT ligand prove unsuccessful in the proposed motor.

As in section 2.4.2, although the reverse *Z*-to-*E* isomerization was planned to be driven by thermal relaxation, the PSSs were also assessed under 430 nm irradiation. This was done to ensure that both the forwards and reverse photoisomerization behaviour could occur and that the reverse *Z*-to-*E* isomerization could be achieved photochemically in case it were required at a later stage in the project. While the addition of pyridine made the reverse *Z*-to-*E* isomerization slightly worse for all three compounds (**46**, **64** and **66**) achieving lower PSSs, the isomerization was still able to proceed in all cases to give the desired *E* isomer as the major product (Table 5).

Ligand	R	Azo	With Pyridine		Without Pyridine	
			E : Z Ratio $\lambda=365\text{ nm}$	E : Z Ratio $\lambda=430\text{ nm}$	E : Z Ratio $\lambda=365\text{ nm}^a$	E : Z Ratio $\lambda=430\text{ nm}^a$
Catechol	H	<b>46</b>	27:73 <sup>b</sup>	76:24 <sup>b</sup>	80:20 <sup>b</sup>	95:5 <sup>b</sup>
(+)-dimethyl L-tartrate	OMe	<b>64</b>	15:85	62:38	17:83	76:24
$\alpha$ -Hydroxyisobutyric acid	H	<b>66</b>	5:95	84:16	97:3	100:0

**Table 5.** PSS of boryl-azobenzenes **46**, **64** and **66** in CDCl<sub>3</sub> (or C<sub>6</sub>D<sub>6</sub> where indicated) with or without 1.3 equivalents of pyridine present. The DMT system of interest is highlighted in yellow. <sup>a</sup>1.3 equivalents of pyridine added. <sup>b</sup>In C<sub>6</sub>D<sub>6</sub>

## 2.5 Summary of Chapter 2

The boryl-azobenzenes **46**–**48** and **61**–**69** and the phenyl boronic ester counterparts **45** and **71**–**75** were successfully prepared (section 2.3) and used to assess the presence or strength of the N<sub>azo</sub>–B bond in the *E*-boryl-azobenzenes (section 2.4.1). Comparing the N<sub>azo</sub>–B bond

strengths against literature standards identified (+)-DMT as a viable ligand for inducing a N<sub>azo</sub>–B bond of the desired strength while also bearing the required C<sub>2</sub> symmetric chirality. Subsequent examination of the photostationary states (PSSs) under 365 nm and 430 nm irradiation revealed that the DMT-based system **64** not only possessed the ability to photoswitch but was able to do so with significantly improved efficiency compared to the literature example **46** (section 2.4.2). The breakage of the N<sub>azo</sub>–B bond upon isomerization to the Z isomer was confirmed (section 2.4.3) with further examination of systems **46**, **64** and **66** in the presence of pyridine revealing that not only could they modulate their Lewis acidity (section 2.4.4) but that the addition of pyridine also improved their photoswitching ability (section 2.4.5). The latter discovery is of particular interest as it opens new avenues for using more electron withdrawing ligands in these systems. A summary of the <sup>11</sup>B NMR and PSS data from this chapter is presented in Table 6.

Comp.	E : Z Ratio		E : Z Ratio		$\Delta\delta_B$	$\Delta\delta_B$	$\Delta\delta_B$	$\Delta\delta_B$
	$\lambda=365$ nm	$\lambda=430$ nm	$\lambda=365$ nm <sup>a</sup>	$\lambda=430$ nm <sup>a</sup>	(E)	(Z)	(E) <sup>a</sup>	(Z) <sup>a</sup>
<b>47</b>	-	-	-	-	-0.9	-	-	-
<b>62</b>	-	-	-	-	-0.2	-	-	-
<b>48</b>	59 : 41	82 : 18	-	-	-0.4	-0.3	-	-
<b>61</b>	9 : 91	71 : 29	-	-	-0.2	0.5	-	-
<b>66</b>	97 : 3	100 : 0	5:95	84:16	18.4	-	21.9	25.2
<b>67</b>	100 : 0	-	-	-	20.4	-	-	-
<b>46</b>	80 : 20 <sup>b</sup>	95 : 5 <sup>b</sup>	27 : 73 <sup>b</sup>	76:24 <sup>b</sup>	9.9 <sup>b</sup>	0.6 <sup>b</sup>	13.5 <sup>b</sup>	20.3 <sup>b</sup>
<b>46</b>	89 : 11	98 : 2	-	-	11.7	1.4	-	-
<b>65</b>	89 : 11	99 : 1	-	-	15.1	0.3	-	-
<b>63</b>	-	-	-	-	8.4	-	-	-
<b>64</b>	17 : 83	71 : 29	15:85	62:38	13.8	2.4	14.3	18.6
<b>68</b>	-	-	-	-	12.5	-	-	-
<b>69</b>	-	-	-	-	13.4	-	-	-

**Table 6.** Summary of the N–B bond and Photoisomerization data presented in chapter 2. The DMT system of interest is highlighted in yellow. <sup>a</sup>1.3 equivalents of pyridine added. <sup>b</sup>In C<sub>6</sub>D<sub>6</sub>

## Chapter 3 Biaryl Model Systems

### 3.1 Introduction

#### 3.1.1 N<sub>azo</sub>–B Bond Formation and Tuning

After investigating the behaviour of the N<sub>azo</sub>–B bond that is crucial to the design of the proposed system (Chapter 2), attention turned to the second dative bond of interest, the N<sub>pyr</sub>–B bond and the associated chirality transfer. As discussed in section 1.8, the formation of this bond is not only essential for the generation of state B (Section 1.8, Scheme 16 and Scheme 17) but it must also lower the barrier to rotation to allow the interconversion of the diastereomers in this state (Scheme 17, conversion between (Z,M,S<sub>ax</sub>,R)-**44** and (Z,P,R<sub>ax</sub>,R)-**44**). Dative N<sub>pyr</sub>–B bonds have been observed in many systems including helicenes, molecular organic frameworks (MOFs) or frustrated Lewis pairs (FLPs), however little-to-no evidence exists in the literature of N<sub>pyr</sub>–B bonds existing in axially strained (i.e. tri-*ortho*-substituted) biaryl-pyridine boronic esters.<sup>106-114</sup> In fact, studies by Lassaletta and co-workers have highlighted that axial strain is detrimental to the formation of the N<sub>pyr</sub>–B bonds in biaryl-pyridine boronic ester systems.<sup>115</sup> As shown in Figure 11, planar biaryl-pyridine systems, such as **76** and **77**, readily form N<sub>pyr</sub>–B bonds between the pyridine and the boron centre while systems where axial strain force the rings out of planarity, such as **78** and **79**, the N<sub>pyr</sub>–B bond formation is inhibited. While the studies on axially strained boronic ester systems have been limited to pinacol boronic esters, other borane systems, such as **80**, which employ more electron withdrawing mesityl groups (Mes) have been shown to form N<sub>pyr</sub>–B bonds in axially strained biaryl-pyridines. As there is a significant difference in the electronics of the boron centre between Bpin and B(Mes)<sub>2</sub> the formation of the N<sub>pyr</sub>–B bond in the axially strained system **80** was attributed to the more electron withdrawn boron (B(Mes)<sub>2</sub>) facilitating N<sub>pyr</sub>–B bond formation. As shown in Chapter 2, changing the electronics of the diol bound to the boron centre also has a significant effect on the electronics of the boron centre itself, in turn helping with the formation of N–B bonds. As such, investigations into using the DMT ligand to induce the desired N<sub>pyr</sub>–B bonds in these axially hindered biaryl pyridines was pursued.

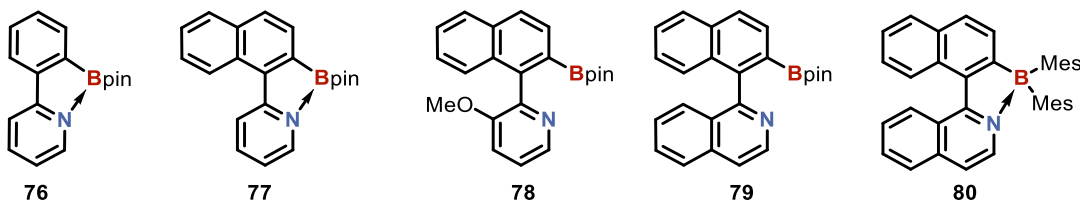


**Figure 11.** Literature systems which probe the extent of the N<sub>pyr</sub>–B bond in various biaryl-pyridines.

While achieving the formation of the required N<sub>pyr</sub>–B bond was an important objective, in order for the proposed motor system (Scheme 17) to work, the N<sub>pyr</sub>–B bond must be weaker than the N<sub>azo</sub>–B bond to allow the formation of state A. While the impact of the axial strain on the ability of the pyridine to act as a nucleophile was untested, the  $\Delta\delta_B$  values observed in section 2.4.4 indicated stronger N–B bonds were formed with the external pyridine rather than the azobenzene. As such, it was suspected that the biaryl-pyridines may be better nucleophiles than the azobenzenes and it was therefore of significant interest to test whether the N<sub>pyr</sub>–B bonds could be weakened by decreasing the nucleophilicity of the pyridine. To do this, models with varying pyridine ring substitution patterns were required to test the relationship between pyridine electron withdrawal and N<sub>pyr</sub>–B bond strength.

### 3.1.2 Chirality Transfer and Rotation Barrier Effects

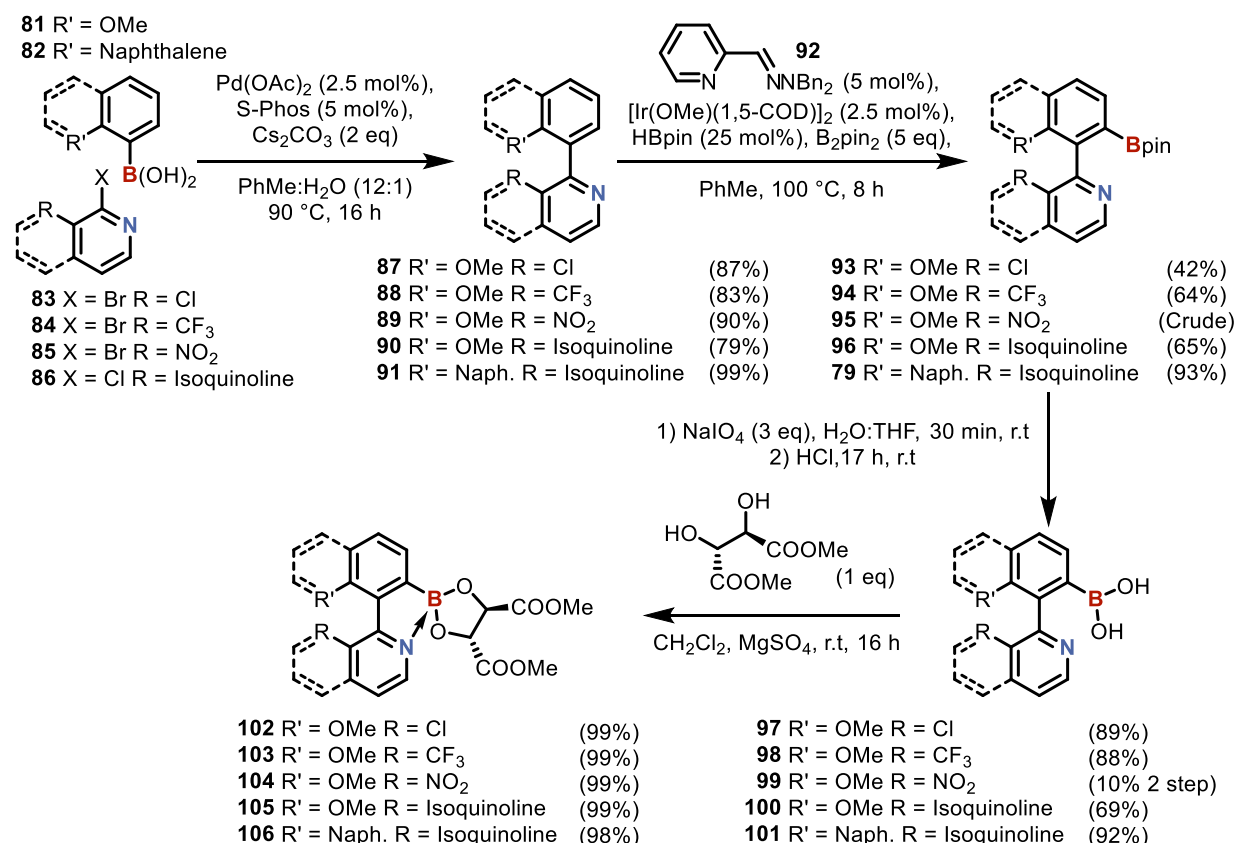
While formation of a N<sub>pyr</sub>–B bond of the correct strength is crucial, this bond must also have the effect of lowering the barrier to rotation enough to allow the interconversion of the two diastereomers in state B (Scheme 17). Although having a low rotational barrier is crucial for the diastereomer interconversion in states A and B, it is essential that the rotation barrier remains high in the unbound state to cause the pyridyl ring to rotate on the same face during the interconversion between states, i.e., the facile crossover of the upper and lower rings of the biaryl should only be possible when the N<sub>pyr</sub>–B bond or the hydrogen bond is present.

Although no rotation rate studies had been conducted on 5-membered boroles, similar studies have been done on other biaryl systems containing 5-membered phospholes, arsoles, cyclic iodonium salts and thiophenes.<sup>116-121</sup> These studies demonstrated that systems with a 5-membered bridging interaction have very low barriers to rotation and exhibit extremely fast racemization, typically requiring negative temperatures to be observed by NMR (sub-zero VT-NMR allows interconverting diastereomers with rotation barriers between ~40 kJ/mol to ~60 kJ/mol to be observed).<sup>122</sup> Conversely, borylated naphthyl-isoquinoline systems similar to **79** have been cleanly separated by chiral HPLC at room temperature implying they have significantly higher barriers to rotation (chiral-HPLC requires rotation barriers of ~95 kJ/mol or more for peak separation at room temperature).<sup>122, 123</sup> To ensure, the N<sub>pyr</sub>–B bond in the proposed system (Scheme 17) lowers the barrier to rotation, compared to the unbound state, and allows interconversion of the atropdiastereomers at room temperature, the rotation barriers of selected axially strained model biaryl-pyridines will be studied.

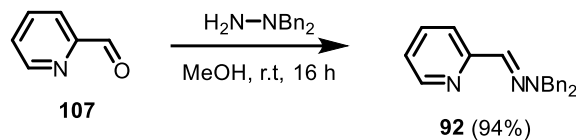
Demonstrating that the  $N_{\text{pyr}}-\text{B}$  bond can be formed, its strength modulated by structural changes to the pyridine, that it lowers the barrier to rotation and that it facilitates interconversion between diastereomers are all significant steps towards realizing the proposed motor but in order for the system to have directionality the DMT ligand (identified from the azobenzene studies in Chapter 2) must also be able to create a significant and measurable preference for one diastereomer over the other. Currently no literature examples of using borylated biaryls to control the chirality of the biaryl-pyridine axis have been demonstrated. Therefore, model systems designed to establish the chirality transfer must also be generated to test whether meaningful chirality transfer can be achieved.

### 3.2 Synthesis of Axially Strained Borylated Biaryls

To test the  $N_{\text{pyr}}-\text{B}$  bond formation requirements, the bond strength modulation by pyridine functionalization, the effect on the lowering of the barrier to rotation, the ability of the atropdiastereomers to interconvert at room temperature, and the ability to transfer chiral information from the boron centre to the biaryl axis, a series of biaryl pyridines were synthesized (Scheme 20).



Starting with a Suzuki-Miyaura cross-coupling between the commercially available boronic acids **81** and **82** and the commercially available pyridyl halides **83-86** the corresponding biaryl-pyridines **87-91** were generated in 79% - 99% yields (Scheme 20, step 1). Subsequent C–H borylation proved challenging with initial attempts using rhodium catalysis proving incompatible with the non-planar substrates (see experimental section 8.6.1, Scheme 43).<sup>124</sup> After synthesizing the required ligand **92** (Scheme 21), attention turned to the iridium-based C–H borylation developed by Lassaletta and co-workers, which was known to work with non-planar substrates.<sup>115</sup> After a short re-optimization (experimental section 8.6), the iridium-based C–H borylation was successfully used to generate the borylated biaryl-pyridines **79**, **93-96** (Scheme 20 step 2). In the case of compound **95**, due to challenges in separating the excess  $B_2\text{pin}_2$  from the product, the impure material was used directly in the next reaction and instead purified as the boronic acid. Using the same pinacol deprotection method as described in section 2.3, the boronic acids **97-101** were successfully generated (Scheme 20 step 3). Notably, the low 2-step yield for **99** was due to issues in the C–H borylation step rather than issues in the deprotection step. Subsequent dehydrative coupling of (+)-dimethyl L-tartrate to the biaryl-pyridine boronic acids **97-101** gave the boronic esters **102-106** all in quantitative yield (Scheme 20 step 4).



**Scheme 21.** Synthesis of the hemilabile ligand for the iridium-catalysed borylation.

### 3.3 Analysis of the $\text{N}_{\text{pyr}}-\text{B}$ Bond Strength and Formation

Once synthesized, the  $^{11}\text{B}$  NMR data of the borylated biaryl-pyridines **93-96** and **102-105** were used to assess the presence and strength of the  $\text{N}_{\text{pyr}}-\text{B}$  bonds (Figure 12). In line with literature, no  $\text{N}_{\text{pyr}}-\text{B}$  bonds were observed in the axially strained  $\text{Bpin}$  biaryl-pyridines **93-96**, with all showing near-zero  $\Delta\delta_{\text{B}}$  values ( $\Delta\delta_{\text{B}} = 0.4 \text{ ppm}, 0.6 \text{ ppm}, 0.4 \text{ ppm}$  and  $0.7 \text{ ppm}$  respectively). Crucially, the DMT-based biaryl-pyridines **102-105** all exhibited the desired  $\text{N}_{\text{pyr}}-\text{B}$  bond with  $\Delta\delta_{\text{B}}$  values between  $19.5 \text{ ppm}$  and  $17.8 \text{ ppm}$ . Interestingly, while the strength of the  $\text{N}_{\text{pyr}}-\text{B}$  bonds appeared to decrease (decrease in  $\Delta\delta_{\text{B}}$ ) as the electron withdrawal of the pyridine ring increased, the decrease in the  $\text{N}_{\text{pyr}}-\text{B}$  bond strength was not as prominent as was expected.<sup>125</sup> It is also worth noting that even in the more electron withdrawn systems **104** (R

$= \text{NO}_2$ ) and **103** ( $\text{R} = \text{CF}_3$ ), the  $\Delta\delta_B$  values are still larger than those of the azo system **64** indicating that the  $\text{N}_{\text{pyr}}\text{-B}$  bonds are still stronger than the  $\text{N}_{\text{azo}}\text{-B}$  bond.

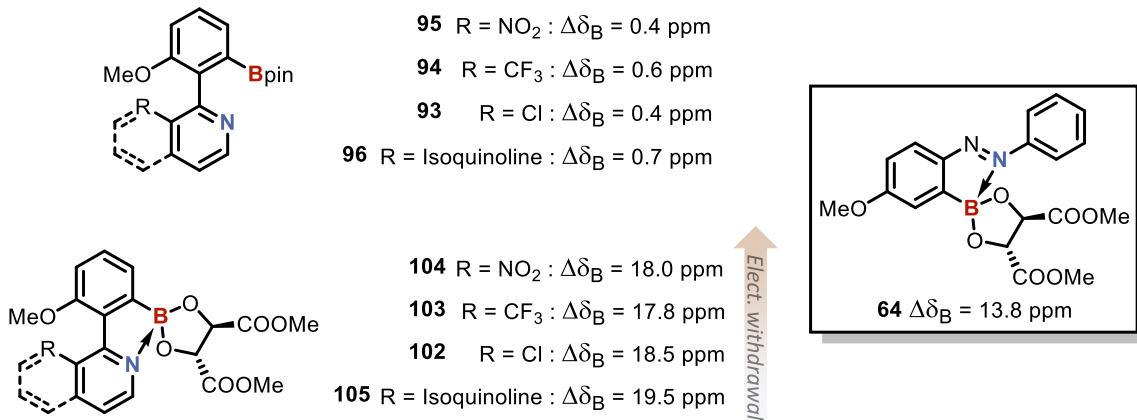


**Figure 12.**  $\Delta\delta_B$  values for biaryl-pyridines **93-96** and **102-105** used for the assessment of the  $\text{N}_{\text{pyr}}\text{-B}$  bonds.

While these studies had been unable to make the  $\text{N}_{\text{pyr}}\text{-B}$  bond weaker than the  $\text{N}_{\text{azo}}\text{-B}$  bond (based on the  $\Delta\delta_B$  value), they had shown that it was both possible to form the required  $\text{N}_{\text{pyr}}\text{-B}$  bond and possible to weaken the bond strength by increasing the electron withdrawal of the pyridine. As the models had already given a useful level of insight into forming and tuning the  $\text{N}_{\text{pyr}}\text{-B}$  bond, achieving a balance between  $\text{N}_{\text{pyr}}\text{-B}$  and the  $\text{N}_{\text{azo}}\text{-B}$  bond was made a focus for the later azo-biaryl scaffolds where the hydrogen bond would also help to achieve this balance.

### 3.4 Chirality Transfer and Rotation Barrier Effects

In addition to studying the formation and modulation of the  $\text{N}_{\text{pyr}}\text{-B}$  bond the effect of the  $\text{N}_{\text{pyr}}\text{-B}$  bond on the barrier to rotation was also investigated. Initial attempts to measure the barrier to rotation in biaryl-pyridines **102** or **105** proved unsuccessful as the barriers to rotation were so low that interconversion between the  $R_{ax}$  and  $S_{ax}$  atropisomers occurred too quickly to observe at  $-80^\circ\text{C}$  by NMR ( $\Delta G^\ddagger < 40 \text{ kJ/mol}$ ). Satisfactorily, biaryl-pyridine **106**, in which the *ortho* substituents induced a higher barrier to rotation than **102** or **105**, showed peak coalescences between  $-30^\circ\text{C}$  and  $-50^\circ\text{C}$  allowing for the measurement of the barrier to rotation (Figure 13).

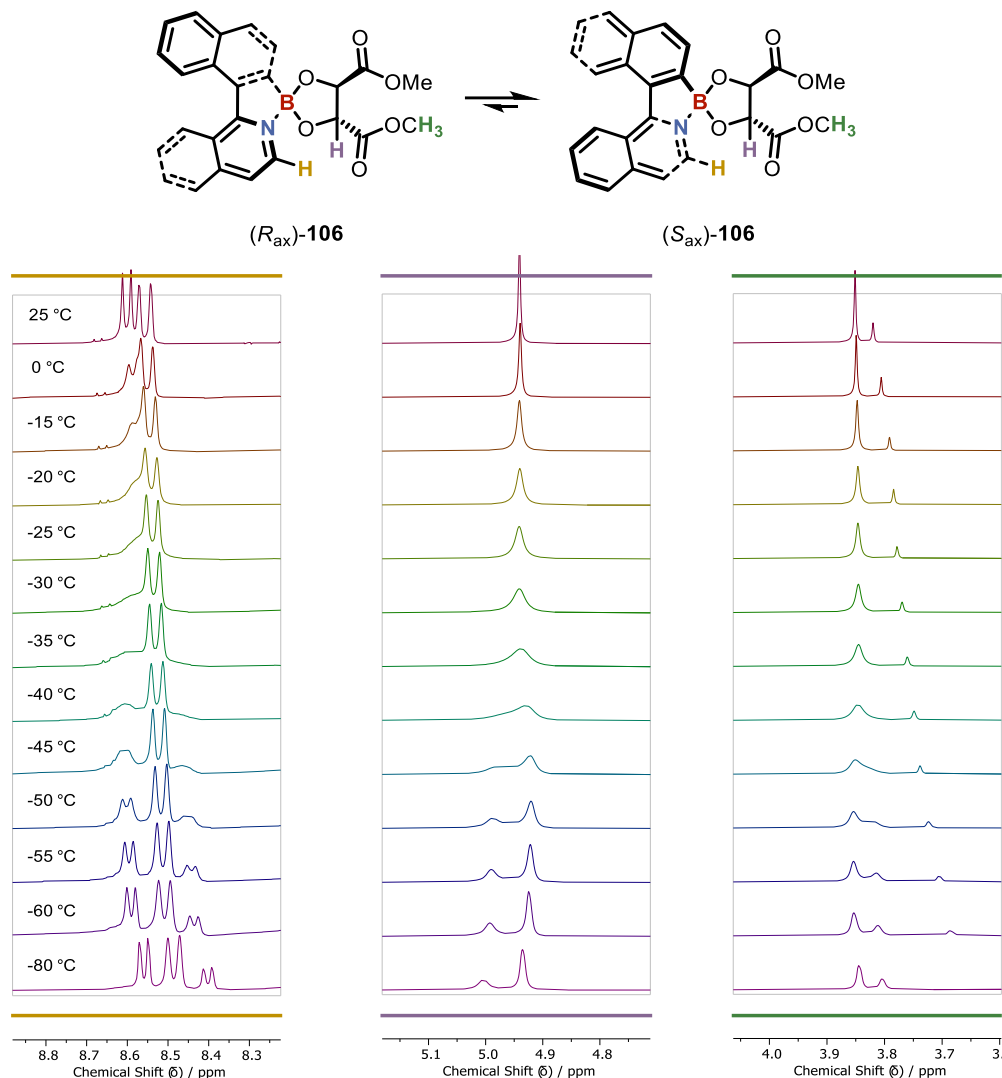


**Figure 13.** Low temperature VT-NMR study of **106** in  $\text{CD}_2\text{Cl}_2$  showing peak coalescence of the gold (left), purple (middle) and green (right) colour coded protons.

Rearranging the Eyring equation (Equation 1a) to solve for  $\Delta G^\ddagger$  (Equation 1b), allows for the calculation of the rotational barrier using the coalescence temperature (defined as the temperature at which the intensity of the trough between the two diastereomer peaks becomes equal to the intensity of the lowest peak) and the difference in  $^1\text{H}$  NMR peak shift between the diastereomers. Calculating the rotation barrier based on the shifts corresponding to the gold ( $T_c = -35$  °C and  $\Delta\delta = 0.16$  ppm), purple ( $T_c = -45$  °C and  $\Delta\delta = 0.06$  ppm) and green ( $T_c = -50$  °C and  $\Delta\delta = 0.04$  ppm) protons, gave rotation barrier values of 47.6 kJ/mol, 48.0 kJ/mol and 48.4 kJ/mol respectively. Known systematic errors common to VT-NMR may be present in these calculations (e.g., temperature dependant peak drift, uncalibrated temperature measurement, etc.) which have been estimated to account for 0.3 – 1 kJ/mol error in other systems.<sup>119, 126, 127</sup> As the variance in the calculated barriers to rotation for biaryl **106**

is within this margin of error ( $0.3 - 1 \text{ kJ/mol}$ ), the measurements can be considered in good agreement, and in good agreement of a barrier to rotation of  $48 \pm 0.4 \text{ kJ/mol}$ .

$$\text{a) } k_{ex} = \frac{\kappa k_B T_c}{h} e^{-\frac{\Delta G^\ddagger}{RT_c}} \quad \text{b) } \Delta G^\ddagger = RT_c \ln \left( \frac{\kappa k_B T_c}{k_{ex} h} \right) \quad \text{c) } k_{ex} = \frac{\pi \Delta \delta \nu_{(\text{Spectrometer})}}{\sqrt{2}}$$

**Equation 1.** a) The Eyring equation b) the Eyring equation rearranged to solve for  $\Delta G^\ddagger$  c) relationship between rate of exchange and peak separation at the coalescence temperature. Where  $k_{ex}$  is the rate of exchange between the diastereomers in Hz,  $\kappa$  is the transmission coefficient (1),  $k_B$  is the Boltzmann constant ( $1.38065 \times 10^{-23} \text{ J K}^{-1}$ ),  $T_c$  is the coalescence temperature in Kelvin,  $h$  is the Planck constant ( $6.62607 \times 10^{-34} \text{ J sec}$ ),  $\Delta G^\ddagger$  is the Gibbs energy of activation (i.e. the barrier to rotation),  $R$  is the ideal gas constant ( $8.31446 \text{ J K}^{-1} \text{ mol}^{-1}$ ),  $\Delta \delta$  is the difference in peak shift in ppm and  $\nu_{(\text{Spectrometer})}$  is the measurement frequency.

This barrier to rotation is also in good agreement with the data presented by Wild and co-workers which had shown that the barrier to rotation in similar arsole (**108**) or phosphole (**109**) systems was  $65 \pm 1 \text{ kJ/mol}$  or  $56 \pm 1 \text{ kJ/mol}$  respectively.<sup>119</sup> Following the same trend where the bridged-binaphthyls containing smaller nuclei in the 5-membered ring had smaller barriers to rotation, the borole system exhibited a smaller barrier to rotation than either of the phosphole or arsole systems (Figure 14), i.e., the smaller the heteroatom centre (covalent radius - boron =  $84 \pm 3 \text{ pm}$ , phosphorus =  $107 \pm 3 \text{ pm}$ , arsenic =  $119 \pm 4 \text{ pm}$ ) the smaller the 5-member ring and correspondingly, the lower the barrier to rotation.<sup>122</sup>

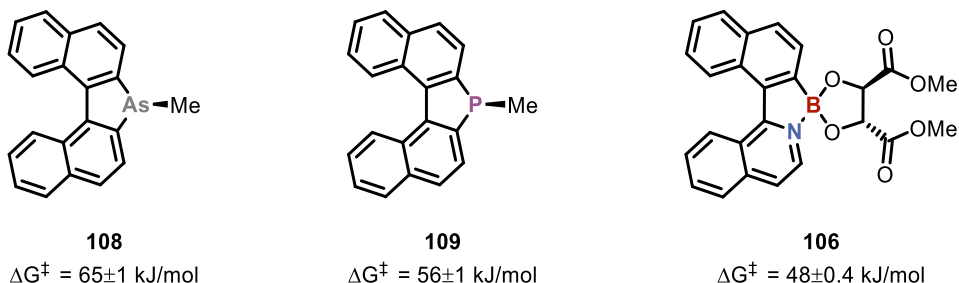


**Figure 14.** Comparison of the calculated barrier to rotation for compound **106** against the literature examples **108** and **109** from Wild and co-workers.<sup>119</sup>

It is also worth noting that while the chirality of the DMT was introduced to give directionality to the proposed motor, it also plays a critical role in facilitating the analysis of the system by VT-NMR, as this technique requires either diastereomers or enantiotopic protons to measure the barrier to rotation and is the only technique capable of measuring such low barriers to rotation.

While these studies demonstrated that the N<sub>pyr</sub>–B bound system had a low barrier to rotation and allowed facile interconversion of diastereomers ( $\Delta G^\ddagger = 48 \text{ kJ/mol}$ ,  $t_{1/2 \text{ rac}} = 29 \mu\text{s}$ ), it had not proven that the low barrier was due to the formation of the N<sub>pyr</sub>–B bond. To prove that the lowering of this barrier was caused by the bond formation, the Bpin system **79**, in which no N<sub>pyr</sub>–B bond formed, was used as a model for the barrier to rotation in the unbound state. To begin these investigations, a chiral HPLC method was developed to resolve the two enantiomers of the Bpin system **79**. As the two enantiomers could be cleanly separated by chiral HPLC at room temperature, the barrier to rotation must be greater than 95 kJ/mol ( $t_{1/2 \text{ rac}} > 1.4 \text{ h}$ ).<sup>122</sup> While time limitations meant that a single enantiomer of **79** was not purified for further racemization studies, the rotation around the biaryl axis in the unbound system **79** ( $\Delta G^\ddagger > 95 \text{ kJ/mol}$ ,  $t_{1/2 \text{ rac}} > 1.4 \text{ h}$ ) was at least orders of magnitude slower than the rotation around the biaryl axis in the N<sub>pyr</sub>–B bond forming system **106** ( $\Delta G^\ddagger = 48 \pm 0.4 \text{ kJ/mol}$ ,  $t_{1/2 \text{ rac}} = 29 \mu\text{s}$ ). As there is such a large difference in the calculated barriers to rotation between the naphthyl-isoquinoline system **106** which contains a N<sub>pyr</sub>–B bond, and the naphthyl-isoquinoline system **79** which contains no N<sub>pyr</sub>–B bond, the N<sub>pyr</sub>–B bond is likely causing the lowering of the barrier to rotation.

Another key element from these studies was the proof that the fixed chirality on the boron centre would create a preferred diastereomer. As observed in Figure 13, at temperatures below  $-55 \text{ }^\circ\text{C}$  the diastereomer peaks become clearly resolved with clear formation of a minor and major diastereomer. While this doesn't confirm which of the two diastereomers is favoured, based on the integration of the diastereomeric peaks corresponding to the gold, purple and green protons (Figure 13), a d.r of 1:1.9 could be established which indicated that the fixed chiral information from the ligand does cause a diastereomeric preference as desired.

### 3.5 Hydrogen Bond Formation and Effect on the Rotation Barrier

While studying the N<sub>pyr</sub>–B bond gives an understanding of the biaryl rotation in state B (Scheme 17) and the ability of the system to form state A, in order to understand the requirements for biaryl rotation in state A, the O–H–N hydrogen bond (H-bond) also needs to be understood. Fortunately, studies from Ott and co-workers had shown *via* XRD analysis that formation of a H-bond in twisted phenol-pyridines **110–112** can occur and that the protons (when visible) have distinctive shifts by <sup>1</sup>H NMR (Figure 15).<sup>128</sup> Although the barrier to biaryl

inversion was not measured in the study, the authors did note that the formation of the H-bond did appear to labilise the biaryl axis. As the enantiotopic protons (red protons in compounds **112** and **113**) of the 1,3-propylene fragment were distinguishable by  $^1\text{H}$  NMR in **113** but became indistinguishable in **112**, rotation around the biaryl axis must be occurring slower than the NMR timescale in **113** but faster than the NMR timescale in **112**. This would suggest that rotation rate is faster in **112** and therefore it possess a lower barrier to rotation. This study not only showed that the H-bonds do occur in biaryl-phenol-pyridines, it also proved that they have a distinctive analytical handle by  $^1\text{H}$  NMR and suggested the H-bond can labilise biaryl axes.

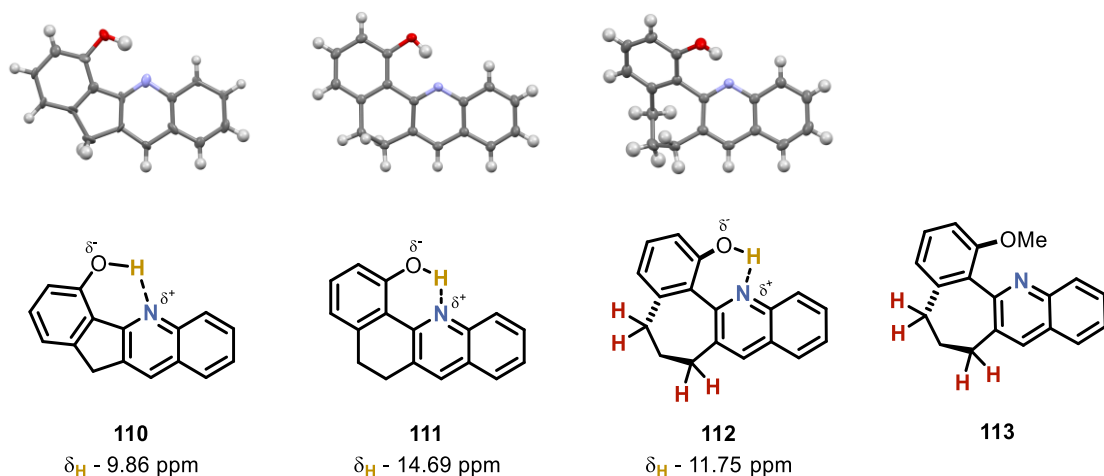


**Figure 15.** Twisted, prebound phenol-pyridines from Ott and co-workers.<sup>128</sup>

While the study from Ott and co-workers indicated the H-bond could labilise a biaryl axis in their systems, further studies by the groups of Smith, Brown and Stoltz have more accurately quantified the extent to which a H-bond is able to reduce the barrier to rotation in axially chiral naphthyl amide or naphthyl-isoquinoline systems (Figure 16).<sup>129-131</sup> In the naphthyl amide system, Smith and co-workers showed that upon deprotection of the atropoisomerically stable compound **115** ( $\Delta G^\ddagger = 129.3 \text{ kJ/mol}$ ,  $t_{1/2 \text{ rac}} = 163 \text{ years}$ ) to the hydroxy compound **114**, the barrier to rotation was drastically reduced due to the presence of the new H-bond interaction ( $\Delta G^\ddagger = 97.5 \text{ kJ/mol}$ ,  $t_{1/2 \text{ rac}} = 3.8 \text{ hours}$ ).<sup>129</sup> Similarly, independent racemization rate studies on compounds **116** and **117** by Brown and co-workers and Stoltz and co-workers have shown that the formation of a H-bond in naphthyl-isoquinoline systems is able to decrease the barrier to rotation from  $\Delta G^\ddagger = 124.2 \text{ kJ/mol}$  ( $t_{1/2 \text{ rac}} = 20 \text{ years}$ ) in compound **116** to  $\Delta G^\ddagger = 110.4 \text{ kJ/mol}$  ( $t_{1/2 \text{ rac}} = 29 \text{ days}$ ) in compound **117**.<sup>130, 131</sup> This showed that the

hydrogen bonding is capable of lowering the barriers to rotation across multiple types of systems and particularly in biaryl-pyridine systems.

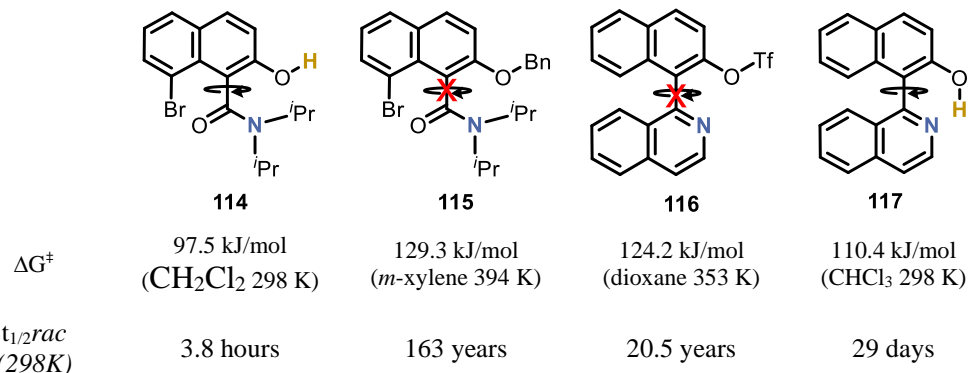


**Figure 16.** Barriers to rotation and half-lives of racemization at room temperature of various naphthyl phenols.

As the hydrogen bond had been comprehensively studied in the literature, with its existence proven, an analytical handle identified, the influence on the rotation barrier established and studies on systems similar to the proposed motor present in the literature, it was decided that developing further model systems for this interaction was unnecessary. As such, assessment of this bond would to be left until either the synthesis of the final motor scaffold was achieved, or until more structurally similar synthetic intermediates were made.

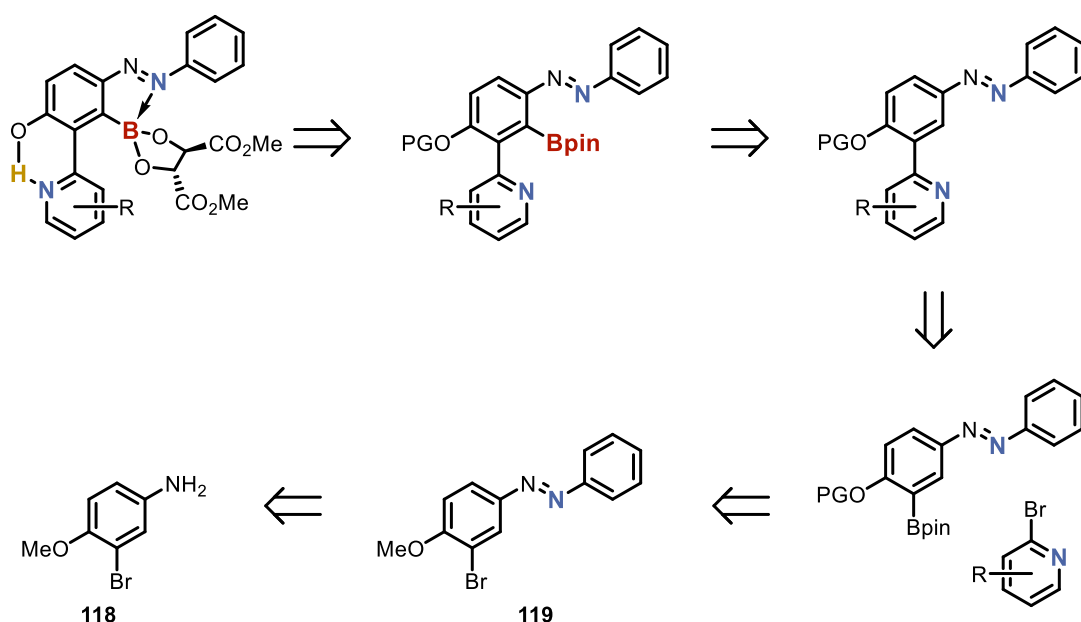
### 3.6 Summary of Chapter 3

After developing a synthetic route that allowed the generation of biaryl-pyridines **102–106**, it was confirmed that the  $\text{N}_{\text{pyr}}\text{–B}$  bond could be formed in boronic esters using electron withdrawing ligands and that the strength of the bond could be modulated to a small degree by varying the electronics of the pyridine ring. Subsequent studies with these compounds showed that not only did the formation of the  $\text{N}_{\text{pyr}}\text{–B}$  bond lower the barrier to rotation but also that the fixed chirality of the boron ligand would impart a diastereomeric preference to the biaryl-pyridine. While the studies on the  $\text{N}_{\text{pyr}}\text{–B}$  bond in model systems were crucial due to the lack of literature precedent, the other biaryl bridging interaction, the hydrogen bond, already had a significant amount of literature precedent in similar systems and therefore model systems for this interaction were not developed.

## Chapter 4 Synthesis of the Borylated Azo-Biaryl Scaffold

### 4.1 Proposed Retrosynthesis

Using similar methodology to that used in the synthesis of the azobenzenes and the biaryl pyridines (sections 2.3 and 3.2), a retrosynthetic analysis was proposed for the initial generation of the motor scaffold (Scheme 22). In this retrosynthetic route, it was proposed that the motor scaffold could be accessed from the protected Bpin-azo-biaryl *via* a global deprotection and dehydrative coupling of the tartrate ligand (Scheme 22, step 1). The borylated-azo-biaryl could in turn be accessed *via* C–H borylation (Scheme 22, step 2), using the same iridium catalysed method as was used in the biaryl-pyridine synthesis (Section 3.2, Scheme 20). The azo-biaryl backbone could be accessed from the Suzuki-Miyaura cross-coupling of the borylated azobenzene and a suitable bromo pyridine (Scheme 22, step 3). The choice of coupling partner in this system is particularly important as 2-boryl-pyridines are known to undergo extremely rapid proto-deborylation meaning that, although it adds a step to the longest linear sequence, the borylated coupling partner needed to be the azobenzene.<sup>132</sup> The borylated azo coupling partner could be made from bromo-azobenzene **119** *via* Miyaura borylation with a potential change of protecting group (Scheme 22, step 4). Finally, the bromo-azobenzene **119** could be made *via* the Mills reaction of bromoaniline **118** as had been used in the synthesis of the previous azo compounds (section 2.3).

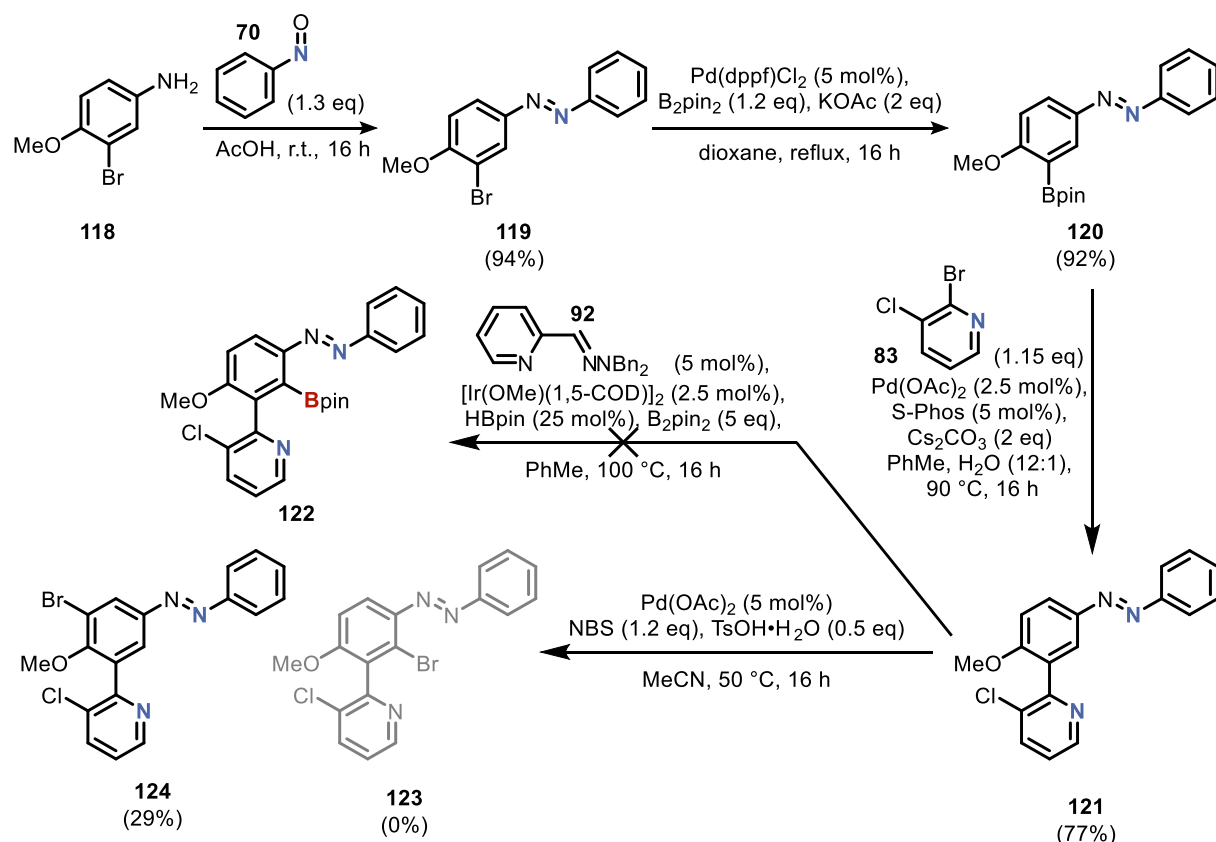


**Scheme 22.** Retrosynthetic strategy for the generation of the proposed borylated azo-biaryl where PG = protecting group.

## 4.2 Synthesis

### 4.2.1 Initial Attempt via Late-Stage C–H Functionalization

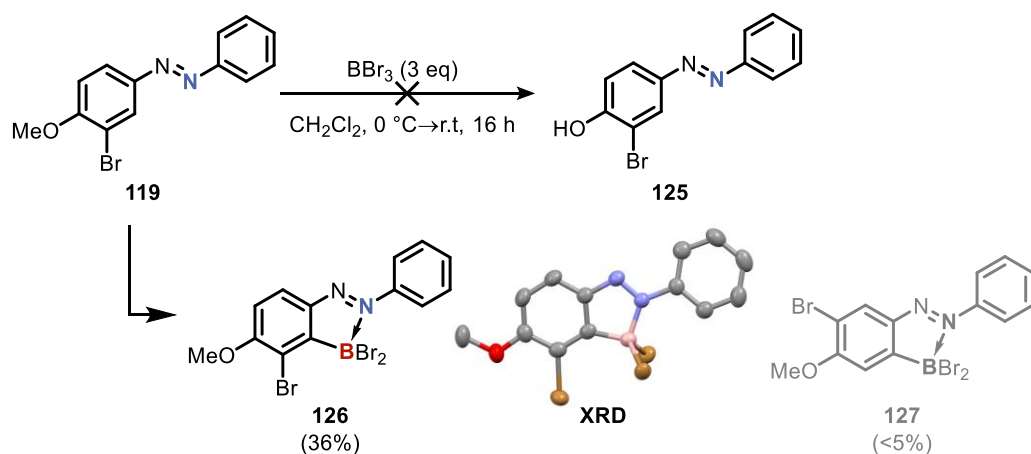
Following the proposed retrosynthetic strategy (Scheme 22), a Mills reaction was performed to generate azobenzene **119** in 94% yield which was then subjected to a Miyaura borylation to generate the borylated azobenzene **120** in 92% yield. Notably, unlike the previous Bpin azobenzenes **48** or **61** (section 2.3), compound **120** was stable on silica gel allowing purification *via* column chromatography. Compound **120** was then coupled to bromo-pyridine **83** *via* Suzuki cross-coupling to generate the azo-biaryl **121** in 77% yield. Unfortunately, subsequent attempts at the C–H borylation using the pyridine-directed iridium-catalysed borylation proved unsuccessful with no starting material conversion observed. This was attributed to the large steric bulk of the azobenzene adjacent to the site of desired C–H functionalization preventing insertion of the iridium into the C–H bond (Scheme 23).<sup>123</sup> As the other pyridine C–H borylation methodologies using lower period metals (e.g., Rh or Ru catalysed C–H borylations) appeared incompatible with non-planar biaryl-pyridine systems, attention instead turned to using the azobenzene as a directing group for the C–H functionalization.<sup>115, 124, 133</sup>



**Scheme 23.** Synthesis of biaryl-azobenzene **121** and attempted functionalizations.

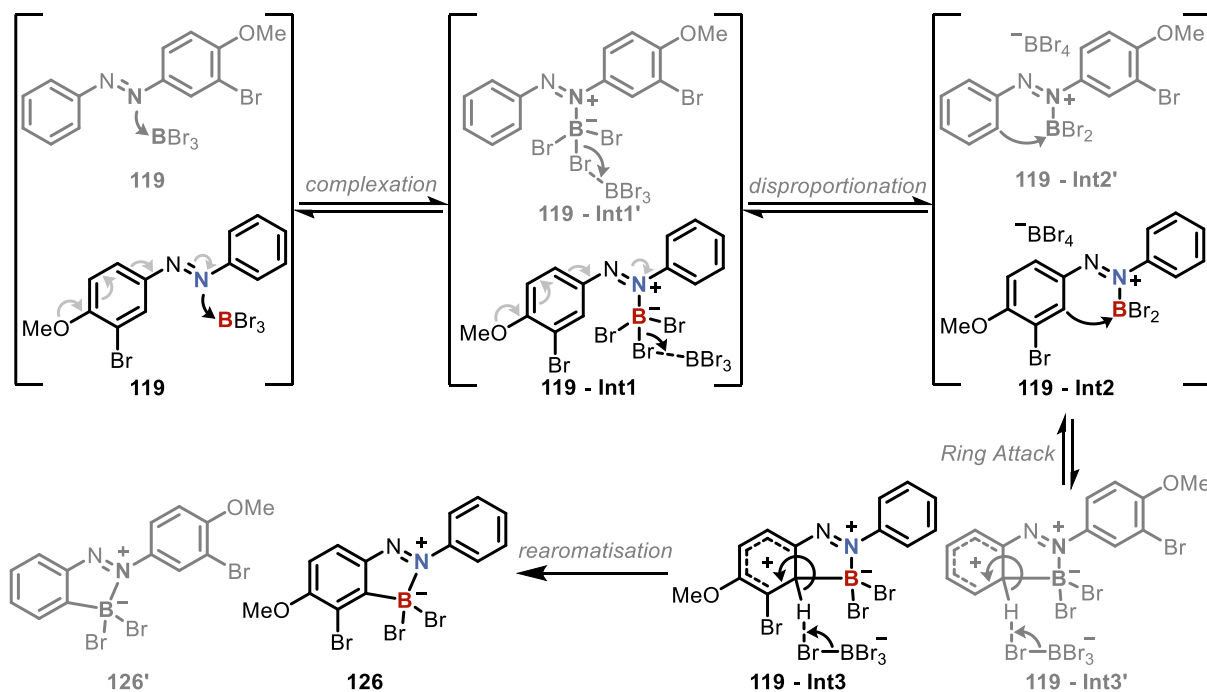
Azobenzenes have been used extensively in the literature as directing groups for palladium-catalysed C–H halogenations, acetoxylations and hydroxylations using electrophilic reagents (chlorine, NBS, NIS, bisacetoxyiodobenzene, Oxone, etc).<sup>134–138</sup> While there have been several examples of these functionalizations, almost all of the examples used symmetrical azobenzene substrates and had limited chemical diversity in the substrate scope. This made it challenging to predict the regioselectivity of the reaction in a non-symmetric and more functionalized scaffold such as compound **121**. As the reaction conditions for these ligand-less functionalizations were nearly identical (palladium acetate, an electrophile and in some cases an acid/base additive), similar regioselectivity outcomes were expected from each method. As such, a C–H bromination was performed to test whether functionalization occurred on the electron rich or electron poor aryl ring, and if it occurred on the electron rich ring, whether it could functionalise at the more sterically hindered position (Scheme 23, **123**). Unfortunately, while some C–H bromination was found to occur on the electron rich ring, only a single regioisomer was observed in which the functionalization occurred at an undesired site to form compound **124** with no trace of the desired product **123**. As the electrophilic palladium-catalysed functionalization approach appeared to generate the undesired product, attention then turned to other methods of azobenzene directed functionalization.

Curiously, while testing demethylation conditions for compound **119**, a new and unexpected reactivity was observed where boron tribromide ( $\text{BBr}_3$ ), rather than perform the expected demethylation, underwent a metal-free C–H borylation directed by the azobenzene (Scheme 24, **126**).



**Scheme 24.** Unexpected C–H borylation identified during the attempted methoxy deprotection. Single-crystal XRD structure drawn with ellipsoids at 90% probability and hydrogen atoms omitted for clarity.

Although there was no literature precedent for this reaction in azobenzenes at the time, similar metal free  $\text{BBr}_3$  borylations had been observed in which imines, amides, amines or pyridines had been used as directing groups for C–H borylation of aromatic rings.<sup>114, 139–145</sup> It should be noted that the azobenzene directed  $\text{BBr}_3$  borylation has since been published by Shigeno and co-workers on a small pool of symmetric substrates.<sup>146</sup> While  $\text{BBr}_3$  borylations had already been observed, what was particularly interesting about the C–H borylation in the case of the asymmetric azobenzene **119** was that not only did it functionalise the more electron rich ring as desired, but it also functionalized the more sterically encumbered position to form the unusual 1,2,3,4-tetra-substituted ring. This was a particularly important discovery as achieving selectivity for the sterically hindered position had been identified as a key challenge in using the azobenzene to direct the C–H functionalization. Based on  $^1\text{H}$  NMR of the crude reaction mixture, functionalization occurred exclusively on the electron rich aryl ring and preferentially at the more hindered position over the less hindered position in a ~10:1 ratio (**126:127**). To understand the observed regioselectivity a more thorough study of the reaction mechanism is required. Drawing on mechanistic work from Chatani and co-workers, a potential mechanism for the reaction is proposed in Scheme 25.<sup>142, 147</sup>



Scheme 25. Proposed  $\text{S}_{\text{EAr}}$  type mechanism for the azobenzene directed  $\text{BBr}_3$  borylation.

In the first step of the proposed mechanism, complexation between the nucleophilic azobenzene nitrogen and the highly Lewis acidic  $\text{BBr}_3$  forms the Lewis adduct **119-Int1** or **119-Int1'** (Scheme 25, step 1).<sup>147</sup> This adduct then undergoes a disproportionation step with another molecule of  $\text{BBr}_3$  to generate a tri-coordinate and again Lewis acidic boron species **119-Int2/119-Int2'** (Scheme 25, step 2). This species should then undergo an  $\text{S}_{\text{EAr}}$  type reaction, forming a Wheland intermediate (arenium ion) **119-Int3/119-Int3'** (Scheme 25, step 3) followed by its deprotonation to rearomatize the aryl ring, leading to the irreversible generation of the borylated azobenzene **126/ 126'** (Scheme 25, step 4).

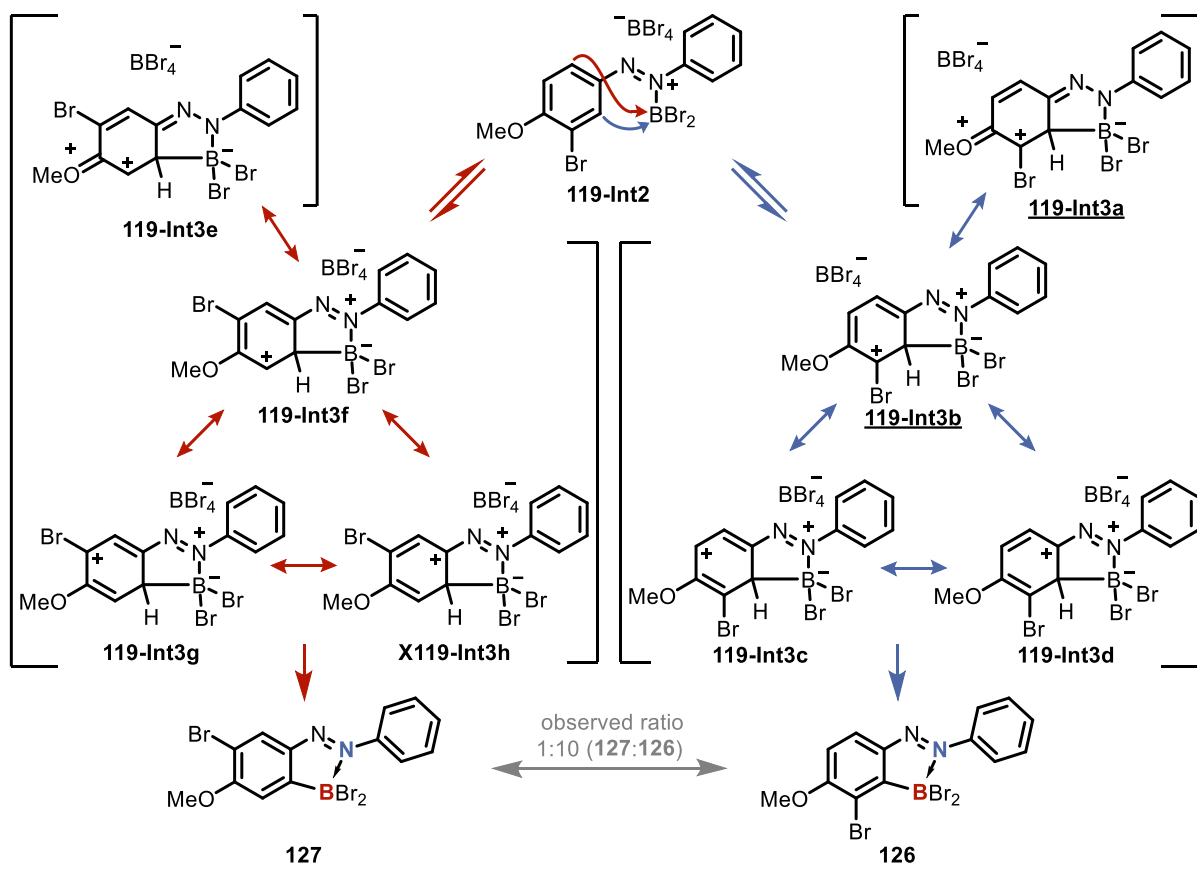
Based on this mechanism, it is unsurprising to see selectivity for the electron rich ring as  $\text{S}_{\text{EAr}}$  reactions are well established to occur more readily in electron rich systems.<sup>148</sup> Although electron rich aryl rings undergo  $\text{S}_{\text{EAr}}$  reactions more readily, the electron donating substituents typically direct substitution to the *ortho* or *para* positions relative to the electron donating group. By contrast, the substitution in this reaction is observed at the *meta* position relative to the electron rich methoxy group. Multiple rationales for this selectivity (i.e., formation of **126** over **126'**) can be proposed, based on both the ground state stabilization and lower transitions state energies during each step, but without deeper mechanistic studies it is not possible to establish exactly which step, or combination of steps, confers the observed regioselectivity.

To provide a general proposal for the observed selectivity, the proposed mechanism is further examined. In the first step, the conjugation between the distal azo nitrogen and the *para* methoxy group (Scheme 25, light grey arrows of bottom **119**) makes the distal nitrogen more nucleophilic. This should lower the transition state energy, and therefore the activation energy, for the complexation at the distal nitrogen relative to complexation by the other non-conjugated azo nitrogen (Scheme 25, top). This would then lead to preferable formation of **119-Int1** over **119-Int1'**. Subsequently due to the same methoxy conjugation the positive charge in the Lewis adduct **119-Int1** is better stabilized than in **119-Int1'** making **119-Int1** the lower energy intermediate. Again, the methoxy conjugation should lower the activation energy for the disproportionation step as the greater electron density at the nitrogen centre should favour the loss of the bromide. This would then favour disproportionation from **119-Int1** over **119-Int1'** leading preferable formation for **119-Int2**. Again **119-Int2** should be lower in energy than **119-**

**Int2'** due to the better positive charge stabilization. Subsequently, the nucleophilic attack by the aryl ring into the electrophilic  $\text{BBr}_2$  species should occur from **119-Int2** more preferably than **119-Int2'** due to the increased electron density of the aryl ring, leading to a preference for the generation of **119-Int3**. Intermediate **119-Int3** should be more stable **119-Int3'** due to the improved charge stabilization of the Wheland intermediate by the bromine centre (carbocation stabilized by tertiary centre and adjacent electron density of the bromine). The final and irreversible deprotonation and rearomatization of the preferred intermediate **119-Int3** would then form **126**, leading to the observed regioselectivity (i.e. formation of **126** over **126'**). In this way the reaction pathway through intermediates **Int1**, **Int2** and **Int3** is proposed to be more favourable than the reaction pathway through intermediates **Int1'**, **Int2'** and **Int3'** but without deeper mechanistic study the contribution of each step towards the observed regioselectivity cannot be established.

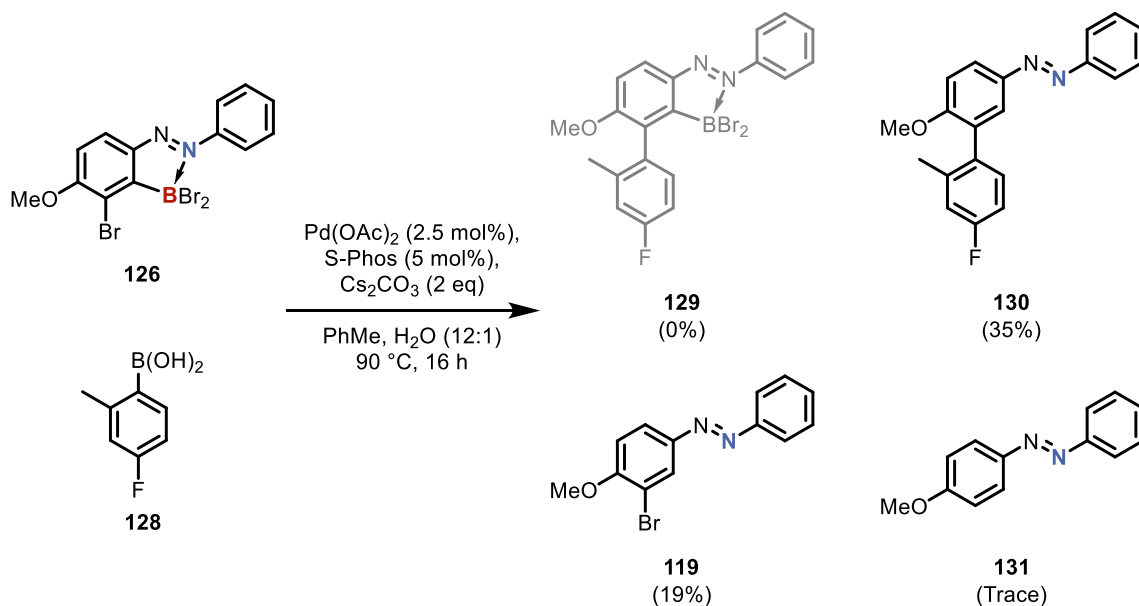
To propose a rationale for the observed regioselectivity for the hindered site over the unhindered site (i.e., formation of **126** over formation of **127**), a closer examination of the  $\text{S}_{\text{EAr}}$  step (Scheme 25, ring attack and rearomatization) is required. Based on the proposed stability of the resonance forms achievable in the Wheland intermediates and the proposed ability to equilibrate between these states, a possible rationale for the observed regioselectivity is proposed. As shown in Scheme 26, multiple resonance forms of the Wheland intermediates are possible with the positive charge(s) localized to different centres of the molecule. As is well established, carbocations (i.e., positively charged carbon ions) are the most stabilized when the positive charge is located on a more substituted centre (i.e., a tertiary carbocation is more stable than a secondary carbocation) and when adjacent substituents have lone pairs capable of  $\pi$ -donation.<sup>149-152</sup> This would make the resonance structures **119-Int3a**, **119-Int3b**, **119-Int3d**, **119-Int3g** and **119-Int3h**, where the positive charge is at a pi-donating tertiary centre, more stable than the resonance structures **119-Int3c**, **119-Int3e** and **119-Int2f** where the positive charge localized to an electronically neutral secondary centre. Another element to consider is that, as mentioned previously, the positively charged azo nitrogen can also be in conjugation with the *para* methoxy group (e.g., conversion between **Int3b** and **Int3a**). This conjugation is only possible in the intermediates **119-Int3a**, **119-Int3b**, **119-Int3e** and **119-Int3f** as this conjugation is broken in the other resonance forms due to the migration of the double bond (e.g., no movement of electrons is possible between the positively charged azo nitrogen and the *para* methoxy group in **119-Int3c** without first returning to **119-Int3b**). As **119-Int3a** and

**119-Int3b** are the only two resonance structures in which the azo-methoxy conjugation is retained, and have the positive charge generated from the S<sub>E</sub>Ar step localized to a pi-donating tertiary centre, they are likely the most energetically favoured of all of the possible resonance structures. If the system is able to equilibrate between the two Wheland intermediates (Scheme 26, resonance forms in brackets), then the intermolecular deprotonation/rearomatization should occur from the lowest energy state (i.e., **119-Int3a**/**119-Int3b**) which would then lead to the observed regioselectivity for **126**. It should be noted that this is a speculative proposal for the observed regioselectivity, and more comprehensive mechanistic studies are required to elucidate the exact behaviour of this system. Although there is value in probing the regioselectivity of this reaction through deeper mechanistic studies, particularly for the purpose of developing other reactions capable of achieving the challenging 1,2,3,4-tetra substitution pattern, due to time constraints, efforts were instead focused towards using this reaction to generate the desired borylated-azo-biaryl substrates.



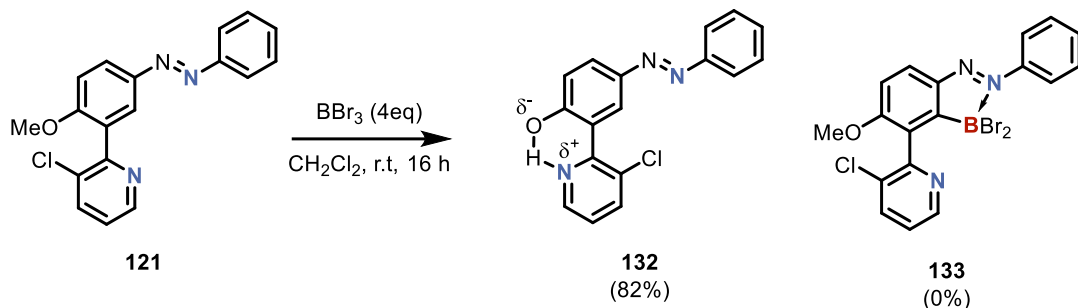
**Scheme 26.** Possible resonance forms of the Wheland intermediates that are accessible during the S<sub>E</sub>Ar step with the two forms that are proposed to be the most stable underlined.

As the  $\text{BBr}_3$  borylation was able to introduce a boron centre in the desired position to generate boryl-azobenzene **126**, the first strategy towards using this borylation was to test whether the  $\text{BBr}_2$  functional group was compatible with palladium catalysed reactions such as a Miyaura borylation or Suzuki-Miyaura cross-coupling. Unfortunately, subjecting compound **126** to the same Suzuki cross-coupling conditions used in the biaryl or azo-biaryl syntheses (Scheme 20 and Scheme 23 respectively) gave moderate-to-poor conversion of starting material and led to the loss of the  $\text{BBr}_2$  functional group with none of the desired product **129** being observed (Scheme 27).



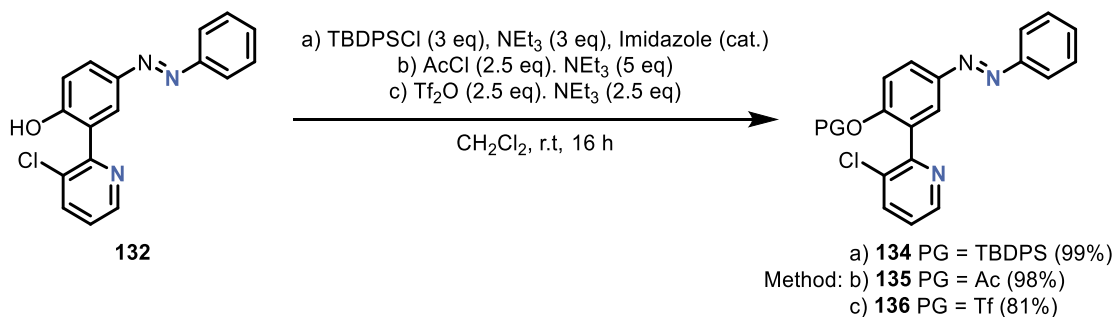
**Scheme 27.** Test Suzuki-Miyaura Cross-coupling to assess the compatibility of the  $\text{BBr}_2$  functional group with palladium catalysed reactions.

As the  $\text{BBr}_2$  functional group appeared to be incompatible with palladium catalysed reactions, meaning the borylation could not be done at an early stage and the  $\text{BBr}_2$  group taken through the synthesis, the borylation was instead tested on the azo-biaryl scaffold **121** (Scheme 28). Unfortunately, rather than give the desired borylated product **133**, only the deprotection of the methoxy group was observed, to give compound **132** in 82% yield. While compound **132** was not the desired product, it still proved useful for assessing the formation of the desired intramolecular H-bond in the azo-biaryl scaffold ( $\delta_{\text{H}} = 12.56$  ppm in **132** vs.  $\delta_{\text{H}} = 4.86$  ppm in phenol) and for generating other protected-azo-biaryls to test protecting group stability towards  $\text{BBr}_3$ .



**Scheme 28.** Attempted  $\text{BBr}_3$  borylation on the azo-aryl-scaffold.

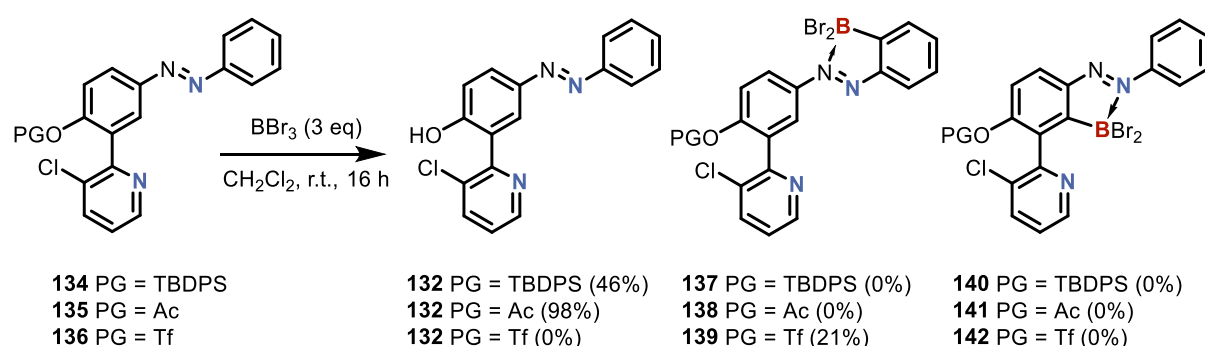
Although the methoxy group was labile, which appeared to inhibit any borylation, literature precedent from other total syntheses had shown that in certain cases acetyl (Ac),<sup>153</sup> triisopropylsilyl (TIPS),<sup>154</sup> triethylsilyl (TES),<sup>155</sup> and tosyl (Ts)<sup>156</sup> groups could remain intact during a boron tribromide mediated methoxy deprotection. As such, the stability of the acetyl (Ac), *tert*-butyl diphenylsilyl (TBDPS) or triflyl (Tf) protecting groups toward BBr<sub>3</sub> was tested. Although the literature precedent used the TIPS or TES protecting groups, the TBDPS group was selected in this case as it is known to be more stable towards acidic conditions (~7 fold more stable than TIPS and ~78,000 fold more stable than TES).<sup>158</sup> The triflyl (Tf) group was also chosen over the tosyl (Ts) as it was expected to have similar stability towards BBr<sub>3</sub>, as both are sulfonyl based functional groups, but the triflyl would have more useful analytical properties (i.e., it allows <sup>19</sup>F NMR analysis to be used and gives less complex <sup>1</sup>H NMR spectra). As such, the azo-biaryls **134-136** were prepared in high yields (82-98%) from **132** using well-established procedures (Scheme 29).<sup>158</sup>



**Scheme 29.** Preparation of **134**, **135** and **136** to test the protecting group stability towards BBr<sub>3</sub>.

Subjecting the three azo-biaryls **134-136** to the  $\text{BBr}_3$  borylation unfortunately gave none of the desired products **140-142** (Scheme 30). Instead, the TBDPS protected compound **134** and the acetyl protected compound **135** regenerated the deprotected phenol **132** as the major

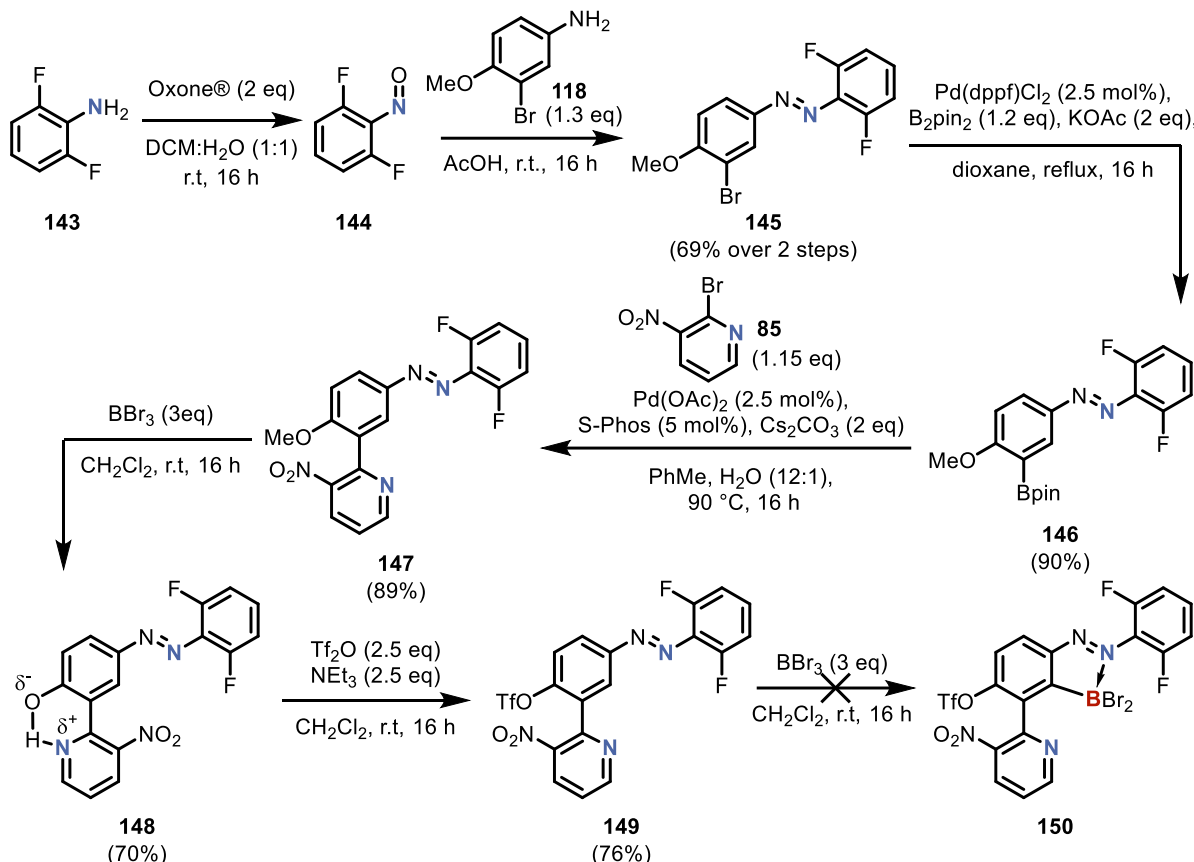
product in both cases. Notably the acetyl protected compound **135** underwent cleaner deprotection to regenerate phenol **132** in 98% yield whereas the reaction on the TBDPS substrate **134** had a lower conversion of starting material, contained a greater number of unidentified (non–borylated) side products and generated phenol **132** in a lower 46% yield. Interestingly, while the triflate protected compound **136** did not form the desired product **142**, it still underwent a borylation reaction to instead introduce the boron species on the opposite ring and form the borylated product **139** in 21% yield (Scheme 30).



Scheme 30. Attempted  $\text{BBr}_3$  borylation of the protected azo-biaryls **134**–**136**.

As the borylation had occurred on the opposite aryl ring of the azobenzene, it was proposed that a blocking group strategy could be used where fluorine groups would be introduced to the distal azobenzene ring to prevent the C–H borylation and instead force the borylation to occur on the desired ring. To do this, another azo-biaryl scaffold was generated as shown in Scheme 31. Starting from 2,6-difluoroaniline **143**, the oxidation of the aniline to the nitroso was performed using Oxone® to generate the volatile species **144** which, without further purification, was reacted with aniline **118** in a Mills reaction to form the azobenzene **145** in a 69% yield over two steps (Scheme 31, steps 1 and 2). The Miyaura borylation of azobenzene **145** then generated the borylated azobenzene **146** in 90% yield which was subsequently coupled to the bromopyridine **85** via a Suzuki-Miyaura cross-coupling, to give the azo-biaryl **147** in 92% yield (Scheme 31, steps 3 and 4). Subsequent  $\text{BBr}_3$  mediated deprotection then formed compound **148** in 70% yield with the proton involved in the H-bond exhibiting a  $^1\text{H}$  NMR shift  $\sim$ 1 ppm further upfield compared to the shift observed in the previous phenol-pyridine **132** (**148**  $\delta_{\text{H}} = 11.45$  ppm, **132**  $\delta_{\text{H}} = 12.56$  ppm). This difference was attributed to the decreased nucleophilicity of the nitro substituted pyridine weakening the H-bond compared to the chloro substituted pyridine. Compound **148** was then treated with

triflic anhydride to form the triflyl protected species **149** in 76% yield. Unfortunately, attempts at the borylation of the triflyl protected species **149** proved unsuccessful with no conversion of the starting material observed.



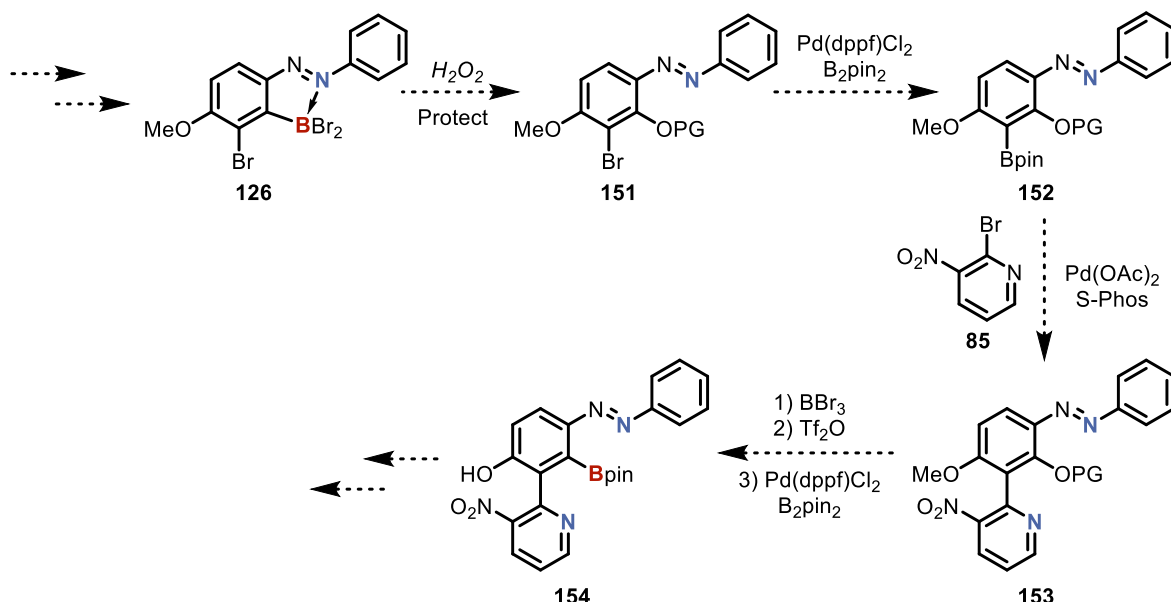
**Scheme 31.** Synthesis of the fluorinated azo-biaryl scaffold.

As it appeared that the late-stage functionalization of the azo-biaryl scaffolds to form the 1,2,3,4-tetra substituted ring was not viable, attention instead shifted towards finding ways of using the early-stage  $\text{BBr}_3$  borylation to achieve the 1,2,3,4-tetra substitution. By converting the  $\text{BBr}_2$  group into a masked functional handle, it could potentially be taken through the synthesis and converted to a boronic ester at a later synthetic stage.

#### 4.2.2 Synthesis *via* Boron Protection

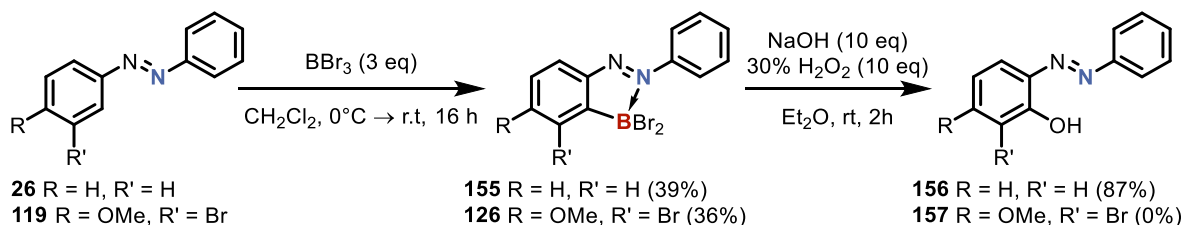
As mentioned above, although the  $\text{BBr}_3$  borylation gave the desired regioselectivity in azobenzene **119**, carrying the unprotected  $\text{BBr}_2$  functional group through the synthesis, which involved multiple palladium catalysed reactions, appeared non-viable. As such, attention

shifted to methods of masking the functionality by converting the  $\text{BBr}_2$  species into a different functional group that could then be converted back into a boronic ester at a later stage. To this end, the first proposed approach was to convert the  $\text{BBr}_2$  group into a protected hydroxy group that could later be converted into a pseudo-halide (e.g., OTf, OMs, ONs, etc) and subsequently borylated via a late-stage Miyaura borylation to introduce the desired boronic ester (Scheme 32).



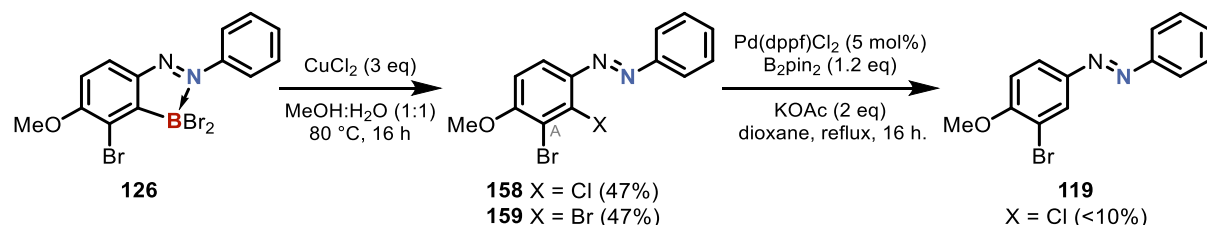
**Scheme 32.** Proposed synthetic approach to the borylated-azo-biaryl scaffold **158** using hydroxylation as a masking group strategy.

Initial attempts at the hydroxylation on azobenzene **155**, which could be prepared from azobenzene **26** in 39% yield, showed good promise with the hydrogen peroxide oxidation cleanly forming azobenzene **156** in 87% yield (Scheme 33). Unfortunately, attempts at the hydroxylation on the desired substrate **126**, afforded complex mixtures from which none of the desired hydroxy azobenzene **157** could be observed (Scheme 33).



**Scheme 33.**  $\text{H}_2\text{O}_2$  mediated hydroxylations of boryl-azobenzenes **155** and **126**.

Following the same approach, it was proposed that instead of the hydroxylation, a halide group could be used to mask the  $\text{BBr}_2$  functionality and be carried through the synthesis with the same late stage Miyaura borylation making the desired boronic ester. To achieve this, copper-mediated halogenations and subsequent Miyaura borylations were investigated to test whether the  $\text{BBr}_2$  functionality could be converted to a halide and whether the desired regioselectivity would be obtained in the subsequent Miyaura borylation (Scheme 34).<sup>159</sup> It is important that the borylation of the di-halogenated azobenzenes was selective for the lower bromine centre (marked A in **158** and **159** in Scheme 34) so that the subsequent Suzuki cross-coupling would afford the desired azo-biaryl scaffold (e.g., Scheme 32 **153**). Using identical methodology to Chattpadhyay and co-workers, the chlorination and bromination reactions were carried out using  $\text{CuCl}_2$  and  $\text{CuBr}_2$  respectively to give both halo-azobenzenes **158** and **159** in 47% yield.<sup>159</sup> Both the dibromo and the chloro-bromo azobenzenes were generated to test whether any site selectivity arose due to the steric environment during the Miyaura borylation of dibromo azobenzene **159** or whether site selectivity would require two different halogens (e.g., **158**). To test the viability of the Miyaura borylation, chloro-azobenzene **158** was subjected to the borylation conditions which gave none of the desired borylation product, no proto-debrominated product and a small amount of the proto-dechlorinated product **119** (<10%).



**Scheme 34.** Testing of copper-mediated halogenation and borylation reactions on these substrates.

As there was no sign of any carbon–bromine bond activation while there was evidence of carbon–chlorine bond activation (which is known to be more challenging),<sup>160</sup> it was proposed that the azobenzene was overriding the difference in reactivity between these bonds and instead directing the oxidative insertion towards the adjacent carbon–halogen bond (i.e., the carbon–chlorine bond of **158**). As it appeared that the azobenzene was overriding the Miyaura borylation’s selectivity for site A, which was required if the newly introduced halogen was to be carried through the synthesis, it appeared that this approach was not viable.

Taking inspiration from the MIDA (methyliminodiacetic acid) boronates developed by the group of Martin Burke (Figure 17a), which have been used to mask boron functionality and perform orthogonal Suzuki cross-couplings, it was proposed that malonic acid could potentially be used in a similar manner for our system.<sup>161-163</sup> While the MIDA esters were initially considered, they were postulated to face steric issues with the pendant azobenzene and potentially have issues with binding competition for the boron centre between the nitrogen of the azobenzene and the nitrogen of the MIDA group (Figure 17b). The lowered reactivity and improved stability of the MIDA boronates is known to arise from the presence of the N–B bond between the amine of the MIDA and the boron centre and as such, having a competing N–B bond may be detrimental to the desired protecting properties. To test the viability of the malonic acid as a protecting group, the malonic acid disodium salt was coupled to the borylated azobenzene species **126** to generate azobenzene **162** (Figure 17c). While the formation of **162** could be observed by <sup>1</sup>H and <sup>11</sup>B NMR, in line with the previous boryl-azobenzenes (section 2.3), the malonic ester compound **162** was not stable towards silica gel or aqueous conditions. As the compound was unstable and could not be purified, meaning it would not function as a useful protecting group in the synthesis, it was decided that the malonic boronic ester strategy was not viable.

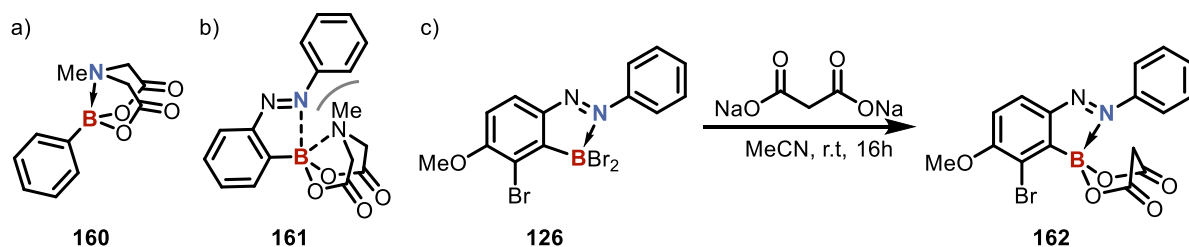
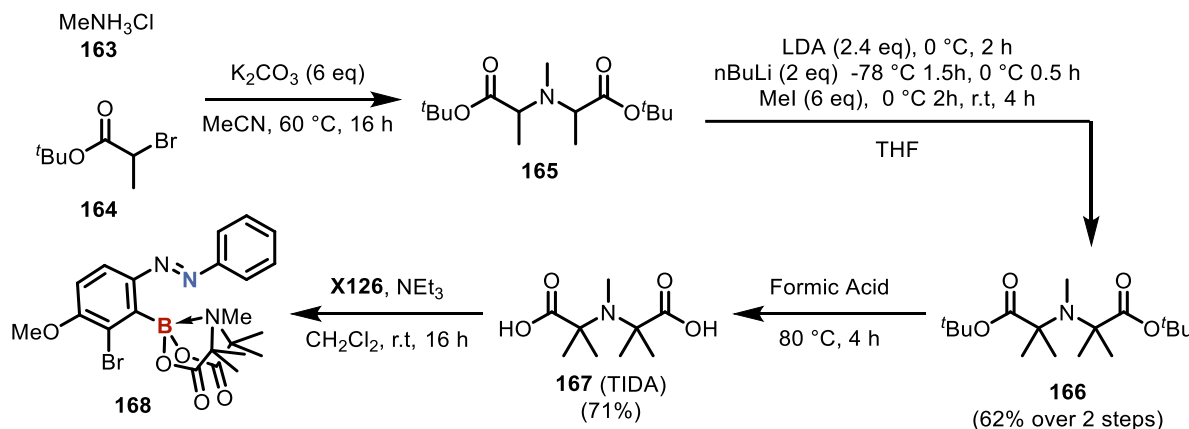


**Figure 17.** a) Generic phenyl MIDA boronate. b) Azobenzene MIDA boronate highlighting the steric clash and the competition for N–B bond formation. c) Attempted synthesis of the proposed malonic acid substitute.

Although the MIDA strategy was initially sidelined due to the suspected issues around steric bulk and competitive N–B bond formation, as the proposed malonic acid boronic esters had proven unstable, the MIDA strategy was tested using the newer and more stable TIDA (tetramethyl *N*-methylinodiacetic acid) masking group.<sup>164</sup> Although the TIDA group is not commercially available, it could be synthesized in three steps following a published synthetic route and coupled directly to compound **162** (Scheme 35). Starting from methylammonium chloride **163**, coupling of two equivalents of bromo-ester **164** formed diester **165** which was carried directly into the subsequent methylation step to give ester **166** in 62% yield over two

steps (Scheme 35, steps 1 and 2). Deprotection with formic acid then generated TIDA **167** in 71% yield which was then coupled to the borylated azobenzene **126** to generate the TIDA complex **168**.

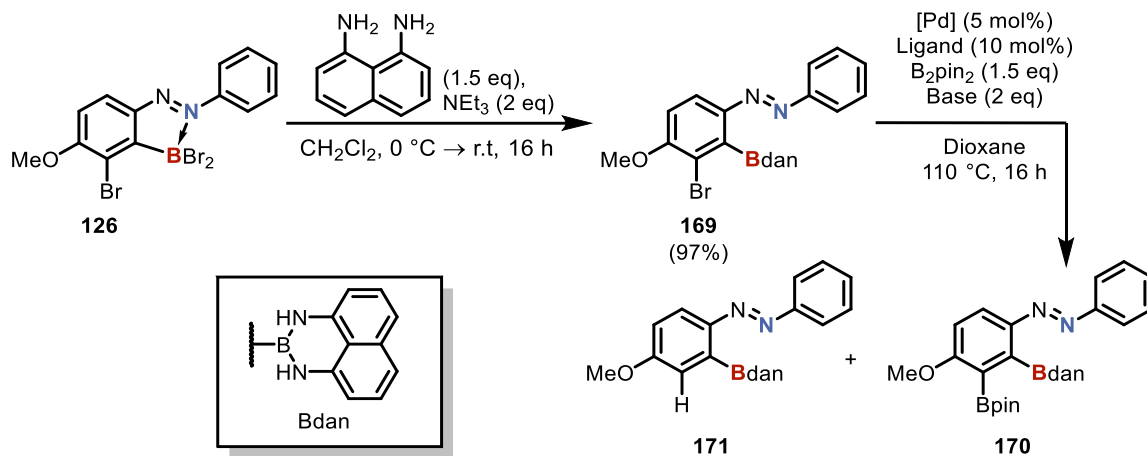


**Scheme 35.** Synthesis of the TIDA protecting group and subsequent coupling to the boryl azobenzene.

While the TIDA complex **168** proved notably more stable than the malonic ester **162**, with negligible degradation during aqueous work-up, it still proved unstable towards silica gel making further purification challenging. It should also be noted that the steric bulk of the TIDA group also caused severely restricted rotation around the C-B bond in the molecule resulting in poorly resolved  $^1H$  NMR spectra at room temperature and required the spectra to be acquired  $100^\circ C$  for clean resolution (see section 8.6.2). Due to both the moderately poor stability and the requirement for performing the spectroscopic analysis at  $100^\circ C$ , the TIDA approach was sidelined in favour of a different boron masking group approach.

While research on boron masking groups has largely focused on the MIDA and TIDA groups developed by Burke and co-workers, the diamino-naphthalene (dan) group has also been shown by Sugimoto and co-workers to be a viable masking group for boron with a resistance to hydrolysis more than 10 fold better than the MIDA boronates.<sup>165, 166</sup> As such, the Bdan azobenzene **169** was generated to test its stability and analytical properties as well as test whether it could allow orthogonal palladium-catalysed reactions to be performed (Scheme 36). Subjecting boryl azobenzene **126** to 1,8-diaminonaphthalene (dan) and triethylamine afforded the Bdan azobenzene **169** in 97% yield, which could be cleanly analysed by  $^1H$  NMR at room temperature and was stable to both water and silica gel (Scheme 36, step 1). While the increased

stability of the BdAN compound **169** was extremely promising, the BdAN group still needed to be tolerant of the subsequent Miyaura borylation conditions (Scheme 36, step 2).



**Scheme 36.** Synthesis of BdAN azobenzenes to test the dan masking group approach.

To test the compatibility of the BdAN group in compound **169** with the Miyaura borylation conditions, a series of different palladium sources, palladium ligands and inorganic bases were screened and presented in Table 7. While achieving orthogonality with the BdAN group was already a notable challenge, Miyaura borylations and Suzuki cross-couplings are well-known to be especially challenging in sterically encumbered substrates.<sup>167-169</sup> As such, the screening was not only aimed at identifying compatible conditions with the BdAN masking strategy, but also to identify conditions that are capable of achieving the borylation on such a sterically challenging substrate. In line with this, the major challenge faced in the conditions screening was not the loss/degradation of the BdAN group but rather preventing the formation of the undesired proto-debrominated side product **171**. While formation of the product **171** is not desirable, it is still a useful indicator of oxidative insertion into the C–Br bond and shows the BdAN group is stable under the reaction conditions.

## Chapter 4 – Synthesis of Borylated Azo-Biaryl Scaffolds

Entry	Pd source	Ligand	Base	Conversion (%) <sup>a</sup>	<b>171</b> (%) <sup>a</sup>	<b>170</b> (%) <sup>a</sup>	Mass Bal. (%)
1	Pd <sub>2</sub> (dba) <sub>3</sub>	SPhos	KOAc	100	71	0	71
2	Pd(OAc) <sub>2</sub>	SPhos	KOAc	100	96	0	96
3	PdCl <sub>2</sub>	SPhos	KOAc	20	13	0	93
4	PdCl <sub>2</sub> (PPh <sub>3</sub> ) <sub>2</sub>	SPhos	KOAc	91	75	17	101
5	Pd(OAc) <sub>2</sub>	XPhos	KOAc	100	93	0	93
6	Pd(OAc) <sub>2</sub>	CyJohnPhos	KOAc	100	90	0	90
7	Pd(OAc) <sub>2</sub>	tBuPPh <sub>2</sub>	KOAc	73	58	21	106
8	Pd(OAc) <sub>2</sub>	PPh <sub>3</sub>	KOAc	10	3	12	105
9	Pd(OAc) <sub>2</sub>	dppp	KOAc	4	0	0	96
10	Pd(OAc) <sub>2</sub>	dppe	KOAc	4	0	0	96
11	PdCl <sub>2</sub> (PPh <sub>3</sub> ) <sub>2</sub>	tBuPPh <sub>2</sub>	KOAc	29	9	19	99
12	PdCl <sub>2</sub> (PPh <sub>3</sub> ) <sub>2</sub>	tBuPPh <sub>2</sub>	NaOAc	0	0	0	100
13	PdCl <sub>2</sub> (PPh <sub>3</sub> ) <sub>2</sub>	tBuPPh <sub>2</sub>	K <sub>2</sub> CO <sub>3</sub>	100	4	77	81

**Table 7.** Miyaura borylation condition screening with the optimal conditions highlighted in yellow. <sup>a</sup> Reported yields are calculated by <sup>1</sup>H NMR using 1,3,5-trimethoxy benzene as an internal standard.

From the reaction screening, some notable trends were observed. Firstly, even though a separate ligand was added to the palladium pre-catalyst and pre-mixed to form the active catalyst species, the pre-catalyst played a significant role in determining the reaction outcome as shown in Table 7 entries 1-4. From these entries, the reactions using Pd<sub>2</sub>(dba)<sub>3</sub> and Pd(OAc)<sub>2</sub> were shown to form the proto-debrominated product **171** in high yields, the reaction using PdCl<sub>2</sub> formed **171** in poor yield due to a lack of conversion, and the reaction using PdCl<sub>2</sub>(PPh<sub>3</sub>)<sub>2</sub> was able to form both the proto-debrominated product **171** in high yield and the desired borylated product **170** in low yield. Unsurprisingly, changing the phosphine ligand also had a significant effect on the reaction outcome (Table 7, entries 5-10) with the reactions using Buchwald ligands (SPhos, XPhos, CyJohnPhos)<sup>170, 171</sup> giving high yields of the proto-debrominated product **171**, reactions using the bisphosphine ligands (dppp, dppe) giving little to no conversion, and the reactions using monophosphine ligands (PPh<sub>3</sub> and tBuPPh<sub>2</sub>) giving low yields of the desired product.

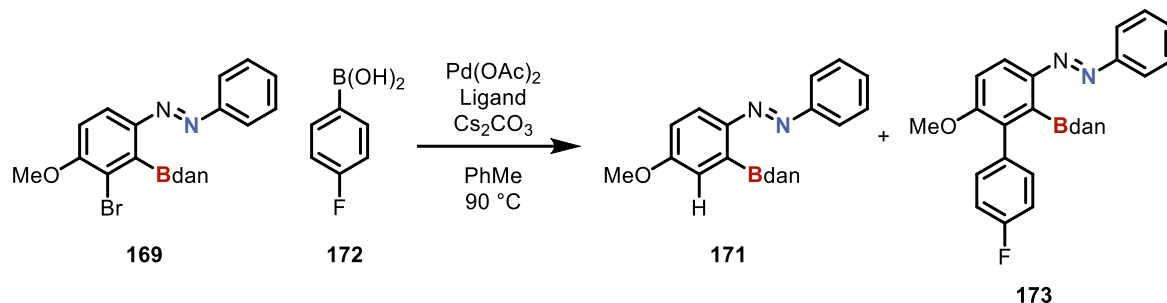
Interestingly, although the reaction using the tBuPPh<sub>2</sub> ligand gave a higher yield of **170** and much greater conversion than the reaction using PPh<sub>3</sub>, the reaction using PPh<sub>3</sub> gave significantly better selectivity for the borylated product **170** over the proto-dehalogenated product **171** (Table 7 entries 7 and 8). Curiously, when using both the PdCl<sub>2</sub>(PPh<sub>3</sub>)<sub>2</sub> pre-catalyst, which was identified as the best pre-catalyst for formation of product **170** (entries 1-4) and the tBuPPh<sub>2</sub> ligand which was identified as the best ligand for formation of product **170** (entries 5-10), no improvement in yield was observed with a similar yield obtained to those in entries 4 and 7 (Table 7 entry 11). Although the yield of the desired product remained ~20%

for entry 11, a very significant improvement in selectivity for the desired borylated product **170** was observed. As shown in entries 11-13, changing the inorganic base also had a significant impact on the reaction with the stronger base  $K_2CO_3$  significantly increasing the yield of the borylated product from 19% to 77% without increasing the amount of de-halogenated product. This was a particularly curious result as  $K_2CO_3$  and other similarly strong bases are typically avoided in Miyaura borylation reactions due to their ability to facilitate a subsequent Suzuki-cross coupling between the borylated product and the halogenated starting material (e.g., cross-coupling of **169** and **170**).<sup>172</sup> While this is a common concern in simpler systems, the dimerized product was not observed in these reactions, which was proposed to be due to the significant steric bulk of this system disfavouring the possible Suzuki (dimerization) reaction. As the Suzuki dimerization was disfavoured, the stronger  $K_2CO_3$  base could then be used. Although Miyaura borylations (unlike Suzuki cross couplings) are not normally reliant on the formation of boronate species to achieve transmetalation, it was proposed that using the stronger base  $K_2CO_3$ , the  $B_2Pin_2$  boronate species could be generated which would improve the transmetalation process.<sup>172</sup> As the formation of both compounds **170** and **171** indicated a facile oxidative insertion step while the more prevalent formation of **171** over **170** indicated a poor subsequent transmetalation, improving the transmetalation step *via* boronate formation could explain the improved yield caused by the stronger  $K_2CO_3$  base.

While the assessment of Miyaura borylation conditions was underway, a small screen of ligands for the subsequent Suzuki cross-coupling reaction was also performed between azobenzene **169** and fluorophenyl boronic acid **172** (Scheme 37 and Table 8). Although the coupling partners were the inverse of those planned in the synthesis (Section 4.1, Scheme 22), this was not considered problematic as the reaction was performed to test the stability of the BdAn group under the reaction conditions. This cross-coupling and the planned cross-coupling would also proceed through a common intermediate, meaning the conditions identified from these screens could still be of potential use for the planned synthetic route. From the conditions assessed, triphenylphosphine ( $PPh_3$ ) was identified as the most suitable ligand (entry 5) with the other ligands showing lower conversion of starting material (entries 1-4). In the case of CyJohnPhos (entry 3), the proto-dehalogenated product was also observed. Notably, the yields and mass balances calculated by  $^1H$  NMR (using a 1,3,5-trimethoxy benzene internal standard) were lower than was expected based on the conversion of the reaction, especially when compared with the calculated mass balances of the Miyaura borylation screen above (Table 7).

## Chapter 4 – Synthesis of Borylated Azo-Biaryl Scaffolds

The lower-than-expected mass balances were proposed to be attributable to the poorer solubility of compound **173** in  $\text{CDCl}_3$ , also explaining the improved isolated yield (isolated yield - 87%, NMR yield - 77%). With suitable cross-coupling conditions identified for the model system, attention turned to the synthesis of the desired boryl-azo-biaryl scaffold.



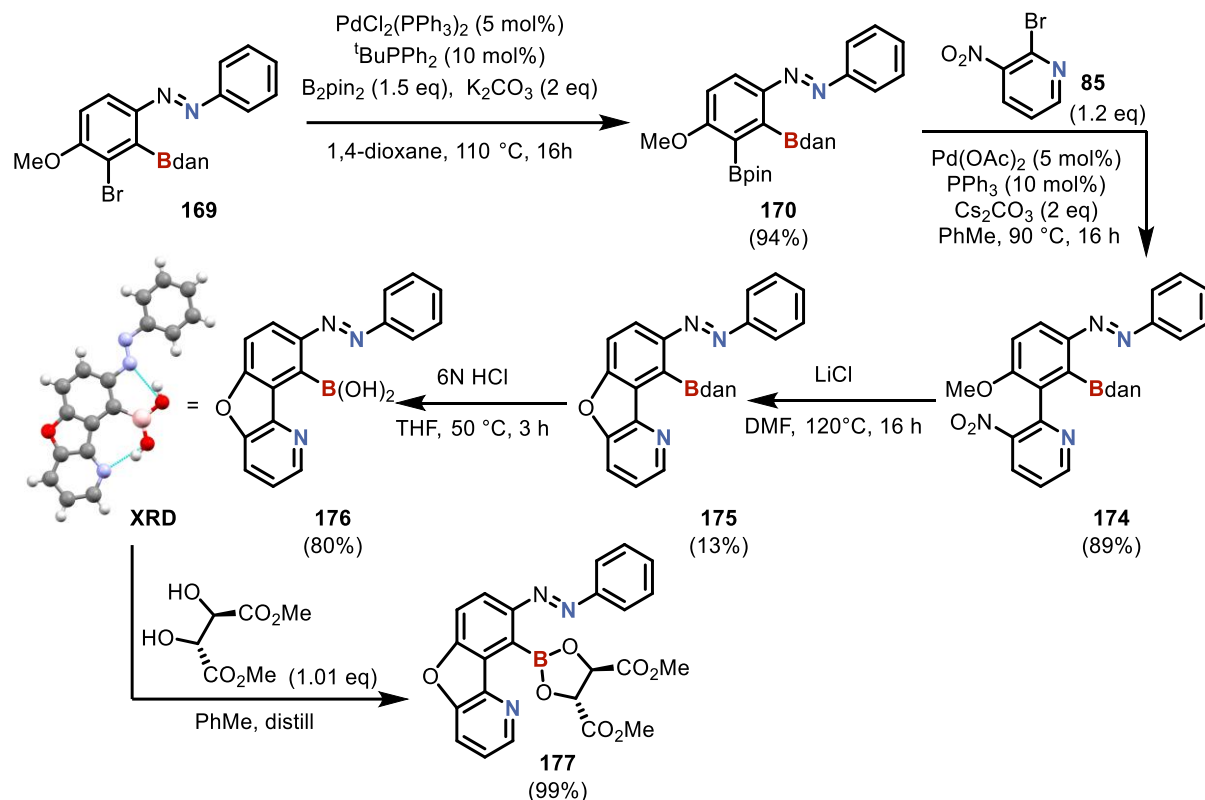
**Scheme 37.** Model Suzuki cross-coupling for testing Bdan orthogonality.

Entry	Pd source	Ligand	Conversion (%) <sup>a</sup>	171 (%) <sup>a</sup>	173 (%) <sup>a</sup>	Mass Bal. (%) <sup>a</sup>
1	Pd(OAc) <sub>2</sub>	SPhos	76	0	58	82
2	Pd(OAc) <sub>2</sub>	Xphos	56	0	42	86
3	Pd(OAc) <sub>2</sub>	CyJohnPhos	86	15	51	80
4	Pd(OAc) <sub>2</sub>	tBuPPh <sub>2</sub>	78	0	63	85
5	Pd(OAc) <sub>2</sub>	PPh <sub>3</sub>	100	0	77 (87)	77

**Table 8.** Suzuki cross-coupling ligand testing with the optimal conditions highlighted in yellow. <sup>a</sup> Reported yields are calculated by <sup>1</sup>H NMR using 1,3,5-trimethoxy benzene as an internal standard. Isolated given in parentheses.

With the Bdan group identified as stable and unreactive in the palladium catalysed reactions, and the conditions for a high yielding Miyaura borylation and subsequent Suzuki cross-coupling identified, the synthesis of the first boryl-azo-biaryl was commenced (Scheme 38). Subjecting compound **169** (synthesis shown in Scheme 23, Scheme 24 and Scheme 36) to the Miyaura borylation conditions identified from the screening above (Table 7), the diborylated azobenzene **170** could be prepared in 94% yield and subsequently subjected to the Suzuki cross-coupling with 2-bromo-3-nitropyridine **85** to generate the boryl-azo-biaryl **174** in 89% yield. Attempts at the methoxy deprotection using  $\text{BBr}_3$ ,  $\text{BF}_3\bullet\text{OEt}_2$ , TMSI,  $\text{AlCl}_3$ , NaI in combination with  $\text{AlCl}_3/\text{FeCl}_3/\text{CeCl}_3$  or NaSEt proved unsuccessful while treatment of compound **174** with LiCl gave boryl-azo-biaryl **175** in 13% yield (Scheme 38, step 6). Running the LiCl reaction for longer or at higher temperature to increase the yield instead resulted the loss of the Bdan group. Deprotection of the Bdan group in compound **175** using 6N HCl then gave the boronic acid **176** in 80% yield. Single crystals of **176** suitable for X-ray diffraction analysis were grown and used to confirm the structure (Scheme 38). Although the cyclic

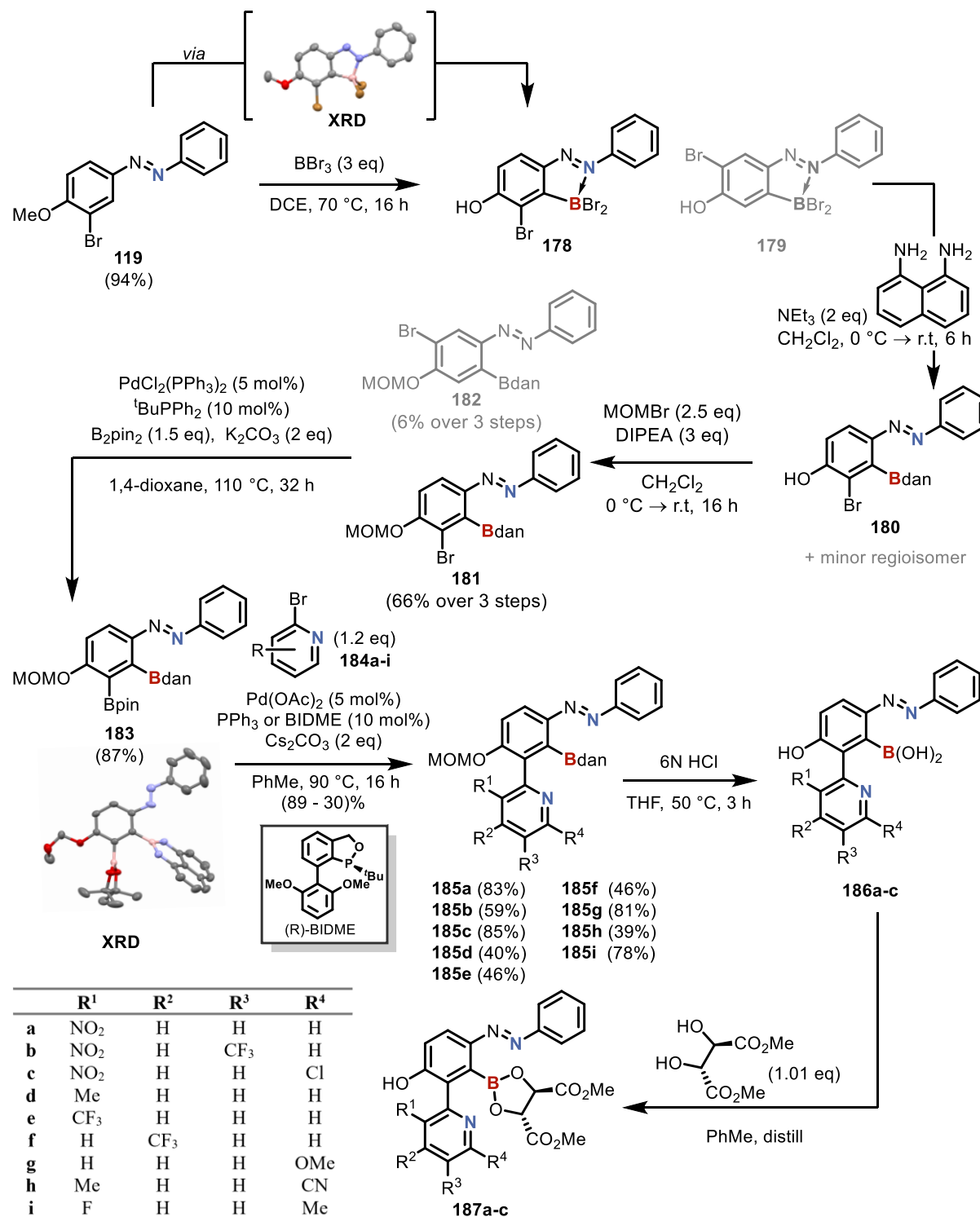
product was not the desired phenolic biaryl, as was shown by the XRD analysis, it was still a useful scaffold for analysis as it possessed a photoswitchable azobenzene and a competitive pyridine moiety. As such, the synthesis was completed with the dehydrative coupling of the DMT ligand to give the final boryl-azo-biaryl **177** in quantitative yield (Scheme 38, step 8).



**Scheme 38.** Synthetic route to the cyclized boryl-azo-biaryl **177**. Single-crystal XRD structure drawn with ellipsoids at 90% probability and hydrogen atoms omitted for clarity.

As the cyclized product **177** was not the initially desired target, due to the lack of possible rotation around the central C–C bond, work towards the synthesis of the freely rotating phenol system was undertaken. To test whether the LiCl deprotection would be viable with a differently substituted pyridyl ring, the LiCl methoxy demethylation was tested on compounds **87**, **88**, **89**, (the Cl, CF<sub>3</sub> and NO<sub>2</sub> model biaryls from section 3.2). Unfortunately, these systems showed no signs of the desired demethylation with the NO<sub>2</sub> substrate **89** showing traces of the cyclization product. As the demethylation could not be achieved using any of the other demethylation methods once the boron centre had been installed, a new synthetic route was developed in which deprotection was performed at an earlier stage of the synthesis (Scheme 39).

Starting with the previously discussed Mills reaction to form **119**, the  $\text{BBr}_3$  borylation was investigated further in an attempt to achieve both the metal-free borylation and the methoxy deprotection in the same step. After investigating different solvents and temperatures, it was found that changing the solvent to 1,2-dichloroethane (DCE) and increasing the reaction temperature to 70 °C led to both the desired borylation and the subsequent demethylation, giving the borylated phenol azobenzene **178** as the major product in a 10:1 ratio with the minor regioisomer **179** (Scheme 39, step 1). Compound **178** was exceedingly insoluble in all common organic solvents making not only purification but also analysis challenging. It was therefore carried directly into the next reaction. Subsequent coupling of the dan protecting group gave compound **180** which was again carried directly into the next reaction due to challenging solubility issues (Scheme 39, step 2). Protection of the hydroxyl group with the methoxymethyl ether (MOM) group then gave the major product **181** in 66% yield (over 3 steps) and the minor regioisomer **182** in 6% yield (Scheme 39, step 3). Subjecting the protected azobenzene **181** to the Miyaura borylation conditions then gave the diborylated species **183** in 87% yield (Scheme 39, step 4). Single crystals of **183** were grown and used to confirm the structure by X-ray diffraction analysis. It is also worth noting that while the yield of the reaction was equally as high as the methoxy substrate **169**, the rate of reaction was significantly slower requiring 32 hours rather than the previous 16 hours. The subsequent Suzuki coupling with the bromopyridines **184a-i** then gave the boryl-azo-biaryls **185a-i** in varying yields (39% - 85%). While the Suzuki cross-coupling reactions using  $\text{PPh}_3$  were viable with the 3-nitro-pyridines (e.g., **184a** or **184c**) or pyridines with a small  $\text{R}^1$  substituent (e.g., **184g**), these conditions proved unsuccessful in cross-couplings bromopyridines containing a Me or  $\text{CF}_3$  group in the 3-position (e.g., **184d** or **184e**). This was attributed to the steric clash between the bromopyridines and boryl-azobenzene inhibiting the reaction with the 3-Me or 3- $\text{CF}_3$  pyridines while in the 3-nitro-pyridines, coordination between the oxygen of the nitro group and the palladium catalyst stabilized the oxidative insertion intermediate allowing the sterically congested Suzuki reaction to take place.<sup>173, 174</sup> To achieve the cross-coupling with the more challenging 3-Me or 3- $\text{CF}_3$  pyridines, a short ligand screen was performed (section 8.6.3, Table 11) which identified BIDME as the only viable ligand for these cross couplings. With the Suzuki cross-coupling conditions identified to make all of the desired boryl-azo-biaryls **185a-i**, a variety of scaffolds could be quickly generated at a late stage in the synthesis. The ability to perform the cross-coupling at a later stage of the synthesis should not be underestimated, as it allows the effect of the pyridine substitution to be quickly studied, which is an important consideration since the exact desired design of the motor was not known.



**Scheme 39.** Divergent synthetic route used to generate boryl-azo-biaryl scaffolds **187a-d**. Single-crystal XRD structure drawn with ellipsoids at 90% probability and hydrogen atoms omitted for clarity.

Using the boryl-azo-biaryls **185a-c**, global deprotection using 6N HCl generated the boronic acids **186a-c** which, due to their poor solubilities in common organic solvents, were directly coupled to DMT without further purification to give the boronic esters **187a-c**. The

stability of these boronic esters proved particularly challenging with any attempts at their purification resulting in degradation. Due to the low stability of these compounds, they were analysed directly as a crude mixture in the presence of excess DMT to disfavour the hydrolysis back to the boronic acid material. This also meant that both the global deprotection and the final dehydrative coupling had to form the desired products with clean conversion and in high yield. While this was initially challenging, a high yield and clean conversion could be achieved by increasing the temperature and decreasing the reaction time of the HCl deprotection step and driving the subsequent dehydrative coupling to completion using either a Dean Stark or distillation apparatus. In this way, the boryl-azo-biaryls **187a-c** were prepared and could be used for examining the effect of the pyridine substitution on the motor behaviour.

### 4.3 Summary of Chapter 4

While the initial attempts at the synthesis of the boryl-azo-biaryls by late-stage functionalization all proved unsuccessful (section 4.2.1), a novel reaction was discovered in which the azobenzene could direct a  $\text{BBr}_3$  mediated borylation. This reaction was found to occur with the desired regioselectivity to form an otherwise challenging to access 1,2,3,4-tetra substituted aryl ring. After hydroxy protecting group or azo blocking group strategies proved unsuccessful, attempts at using boron masking groups were investigated. From these strategies the dan masking group was found to be the most viable and was used to make a variety of boryl-azo-biaryls. While the first attempts at the synthesis resulted in an unexpected cyclization to form azobenzene **175**, a subsequent synthetic route using a MOM protecting group strategy eventually proved successful with the late-stage Suzuki cross coupling, enabling the synthesis of multiple boryl-azo-biaryl scaffolds.

## **Chapter 5 Analysis of Motor and Comparison to Analogues and Standards.**

### **5.1 N<sub>azo</sub>–B vs N<sub>pyr</sub>–B bonding**

As discussed in section 1.8, to prevent the proposed motor system from becoming stuck in a pyridine bound state (Scheme 17, state B), it is crucial that in the *E*-geometry the N<sub>azo</sub>–B bond is more favoured than the N<sub>pyr</sub>–B bond. Since the boron ligand had already been selected to provide the optimal azobenzene photoisomerization properties, as well as the desired chirality transfer to the biaryl, the balance between the N<sub>azo</sub>–B and N<sub>pyr</sub>–B bonds should ideally be achieved without requiring any changes to the boron ligand. Due to the synthetic accessibility and the availability of sites for functionalization, the balance of the N–B bonds should ideally be achieved by alterations to the pyridine ring rather than the azobenzene unit. With a synthetic route capable of generating a range of azo-biaryls bearing differently substituted pyridine rings (Scheme 38 and Scheme 39), the effect of the pyridyl substitution on the balance between the N<sub>azo</sub>–B and N<sub>pyr</sub>–B bonds in the lowest energy states azo-biaryl scaffolds can be studied.

### **5.2 Intramolecular Bond Assessment**

#### **5.2.1 Control Systems and Benchmarking of <sup>11</sup>B and <sup>15</sup>N NMR Shifts**

While the analysis of the N–B bonds in the azobenzene and biaryl model systems from sections 2.4 and 3.3 had been done by <sup>11</sup>B NMR, this was no longer suitable for the newer azo-biaryls as there were two potential N–B bonds that could be formed with the same boron centre. As such, attention turned to characterising these systems using both <sup>11</sup>B and <sup>15</sup>N HMBC NMR analysis. <sup>15</sup>N NMR is a particularly challenging technique due to both the poor gyromagnetic ratio (~2.5-fold lower than <sup>13</sup>C and ~10-fold lower than <sup>1</sup>H) and the low natural abundance (0.37%) of the <sup>15</sup>N nucleus making it a particularly insensitive nucleus for NMR study.<sup>175</sup> Although <sup>14</sup>N is much more abundant (99.6%), the quadripolar nature of the nucleus makes the peak widths exceedingly broad in non-symmetric compounds (e.g., <sup>14</sup>N peak width for urea >125 ppm) and ultimately makes it unsuitable for our purposes.<sup>175, 176</sup> While the poor NMR sensitivity of the <sup>15</sup>N nucleus typically requires the nitrogen centres to be isotopically enriched for direct 1D NMR, more sensitive 2D techniques, particularly (<sup>1</sup>H-)<sup>15</sup>N HMBC, can be used to establish the <sup>15</sup>N shifts in non-isotopically enriched samples.<sup>175</sup> Although <sup>15</sup>N HMBC is able to greatly improve the sensitivity, it does face other challenges, particularly in that some of the experimental parameters for observing the magnetization transfer between the

$^1\text{H}$  and  $^{15}\text{N}$  nucleus are unknown and vary based on the nitrogen environment and by compound.<sup>175, 177-180</sup> To understand how the  $^{15}\text{N}$  HMBC improves sensitivity while being limited by parameter identification, an understanding of the HMBC technique (and pulse sequence) is required. In a basic HMQC/HMBC experiment, an RF (radio frequency) pulse, at the frequency corresponding to the  $^1\text{H}$  nucleus, excites the  $^1\text{H}$  nuclei of the compound into a high energy state (Figure 18, first pulse in  $^1\text{H}$  channel).<sup>177-180</sup> After a time delay ( $\Delta_1$ , Figure 18), an RF pulse at the frequency corresponding to the hetero-nucleus ( $^{13}\text{C}$ ,  $^{15}\text{N}$ , etc...) causes zero and double quantum coherences for any  $^1\text{H}$  nuclei  $J$ -coupled to the pulsed hetero-nuclei (Figure 18, first black pulse in the heteronucleus channel). This means the resonances of the protons coupled to the pulsed heteronuclei will have greater or lesser resonances than the non-coupled protons, i.e., magnetization transfer from the pulsed heteroatom to the high energy proton nuclei causes changes in resonance of the heteroatom-coupled  $^1\text{H}$  nuclei. This is then followed by the evolution phase (Figure 18,  $t_1$ ) during which a second RF pulse on the  $^1\text{H}$  frequency serves to remove the resonances of the excited  $^1\text{H}$  nuclei which have no heteroatom correlations to allow visualization of only the protons which have heteroatom couplings (Figure 18, second pulse on the  $^1\text{H}$  channel). Finally, a second pulse on the heteroatom frequency (Figure 18, second black pulse in the heteronucleus channel) serves to convert the magnetization of interest into observable single-quantum magnetization for detection (Figure 18, free induction decay/FID measurement). The standard pulse sequence for the HMBC is near identical to the HMQC sequence described but also includes a pulse during the  $\Delta_1$  phase which serves to remove the 1-bond H-X correlations (Figure 18, grey pulse on the heteroatom frequency).<sup>177-180</sup>

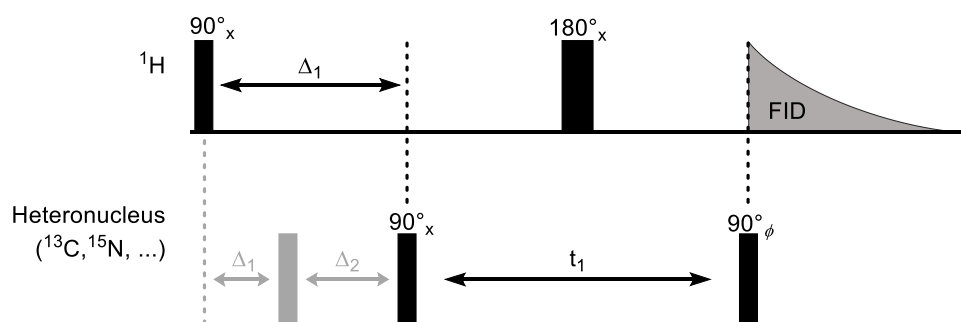


**Figure 18.** General pulse sequence for HMQC/HMBC NMR experiments. HMBC experiment differs only by the inclusion of the RF pulse in grey which serves to remove the 1-bond correlations.

There are two key elements to note in the pulse sequence of these NMR experiments. First, since the HMQC/HMBC experiments excite and detect the highly NMR active  $^1\text{H}$

nucleus, the NMR sensitivity is significantly improved compared to the direct excitation and detection of the heteronucleus of interest (in this case  $^{15}\text{N}$ ).<sup>181</sup> The second important element is that the magnetization transfer is controlled by the timing between the initial RF pulse on the  $^1\text{H}$  frequency and the RF pulse on the heteronuclei frequency. For any changes to be observed on the proton frequency, the time delay ( $\Delta_1$ ) must match the equivalent *J*-coupling of the  $^1\text{H}$ -heteronuclei interaction in order for magnetization to be transferred from the excited heteronucleus to the  $^1\text{H}$  nucleus.<sup>180</sup> In the case of the  $^{15}\text{N}$  HMBC, this  $\Delta_1$  delay needs to match the *J*-coupling between the  $^1\text{H}$  and the  $^{15}\text{N}$  nuclei for a correlation to be observed. Since the *J*-coupling between the proton and nitrogen of interest is unknown, the required  $\Delta_1$  delay for the HMBC/HMQC experiment is also unknown. This can mean that no correlations are observed in the  $^{15}\text{N}$  HMBC due to issues in identifying the required  $\Delta_1$  delay rather than there being a lack of a coupling between the two nuclei in the compound. Although the  $^{15}\text{N}$  HMBC can be more challenging, and not all of the desired correlations are always identified, this technique is still an exceptionally powerful tool for understanding the nitrogen environments in the compounds of interest and is essential for interpreting the intramolecular bonding in systems such as the boryl-azo-biaryls discussed herein.

As there is very little literature against which to benchmark the azo-biaryl systems, in part due to the challenges in performing  $^{15}\text{N}$  NMR analysis, a series of positive and negative control systems were analysed by both  $^{15}\text{N}$  and  $^{11}\text{B}$  NMR. These systems were then to be used as references for interpreting the N–B bond formation in the borylated-azo-biaryls systems. As shown in Figure 19 with compounds **188**, **26** and **64**, the azobenzene nitrogens have characteristic shifts around 500 ppm (499–508 ppm) which get shifted significantly upfield upon formation of a  $\text{N}_{\text{azo}}\text{–B}$  bond. The  $^{15}\text{N}$  shift of the bonding nitrogen shifts upfield to 400 ppm while the adjacent nitrogen shifts upfield to 478 ppm. The observed upfield shift is in agreement with other literature studies on  $^{15}\text{N}$  labelled azobenzene, where protonation to the conjugate acid or oxidation to the azoxybenzene caused upfield shifts of ~150 ppm.<sup>182</sup> It is also helpful that the formation of the N–B bond gives characteristic shifts at both azo nitrogens, as this gives two analytical handles for N–B bond assessment. This is particularly useful since, as mentioned above, it is not always trivial to identify parameters that allow the observation of the  $^{15}\text{N}$  HMBC correlations. As such, having a greater number of analytical handles gives a greater chance of identifying parameters in which at least one correlation can be observed.

Examining the pyridine systems, the  $^{15}\text{N}$  shifts of the pyridyl nitrogens were also found to be equally characteristic of N–B bond formation. In the substituted pyridines **188**, **184c** and **88** the  $^{15}\text{N}$  shifts were around 325 ppm (323, 325 and 324 ppm respectively) while the pyridines exhibiting either a H-bond (**192**) or an  $\text{N}_{\text{pyr}}\text{–B}$  bond (**104**) had  $^{15}\text{N}$  shifts further upfield at 317 ppm and 252 ppm respectively. While the shift caused by the H-bond was not large in magnitude, the shift caused by the  $\text{N}_{\text{pyr}}\text{–B}$  bond was very distinctive and could function as a clear analytical handle. Interestingly, while the pyridines **188**, **184c** or **88** exhibited very similar  $^{15}\text{N}$  chemical shifts, the simple pyridine **189** had a slightly more upfield shift of 309 ppm. While it was not one of the key analytical targets, the nitro group could also be identified by  $^{15}\text{N}$  HMBC in compounds **188**, **184c** and **104**, and was found to have chemical shifts around 370 ppm (373 ppm, 365 ppm and 371 ppm respectively). Given the unexpected cyclization encountered during the development of the synthetic routes (Scheme 38, step 6), it is also useful to be able to confirm the presence of the nitro group in these molecules.

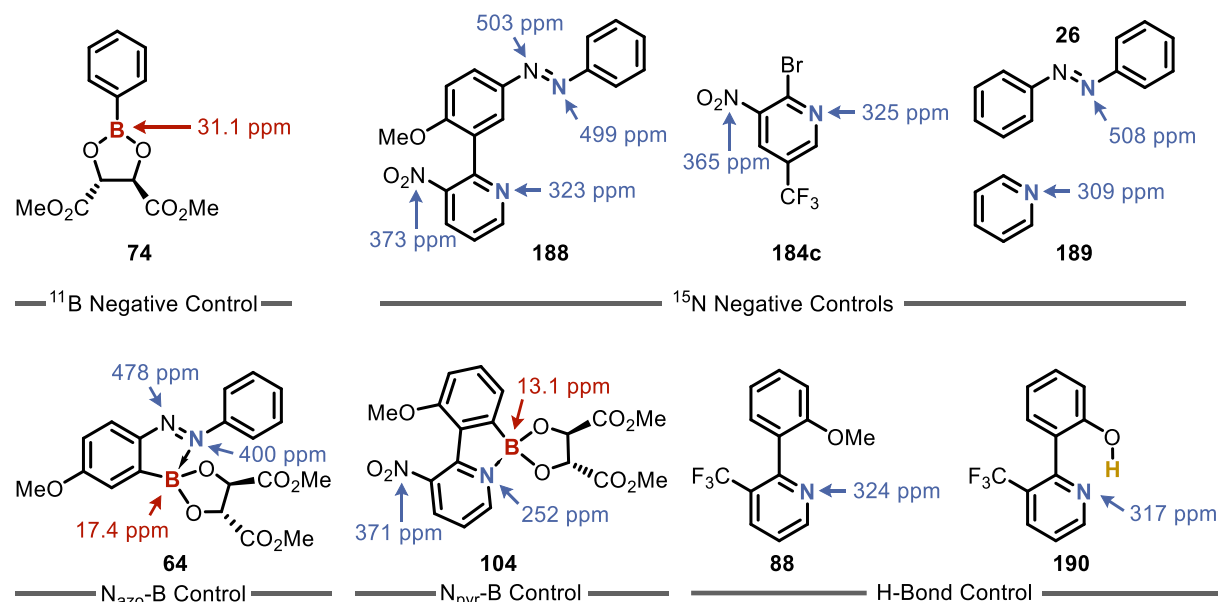


**Figure 19.**  $^{11}\text{B}$  and  $^{15}\text{N}$  NMR control systems used to analyse the intramolecular bonding present in the azo-biaryl systems.

While the  $^{15}\text{N}$  shifts are crucial for understanding which of the two N–B bonds are formed, the  $^{11}\text{B}$  NMR still serves as a useful analytical handle to confirm that the bond has formed with the desired boron centre. Using the DMT boronic ester **74** as a model for a lack of a N–B bond, the  $^{11}\text{B}$  shift of 31.1 ppm can be considered diagnostic of a tricoordinate boron species, which upon formation of a  $\text{N}_{\text{azo}}\text{–B}$  bond (**64**) or  $\text{N}_{\text{pyr}}\text{–B}$  bond (**104**) causes a significant upfield shift to 17.4 ppm or 13.1 ppm respectively.

### 5.2.2 Influence of Pyridyl Substitution on N–B Bond Formation

With highly characteristic shifts identified for the boron and nitrogen centres involved in the  $\text{N}_{\text{azo}}\text{-B}$  bonds, the  $\text{N}_{\text{pyr}}\text{-B}$  bonds and in the unbound state, the bonding in the boryl-azo-biaryl scaffolds was investigated (Figure 20). Looking first to the cyclized compound **177**, the  $^{15}\text{N}$  shifts of the azo nitrogens (476 ppm and 393 ppm) are shifted significantly upfield compared to the negative control systems **188** (503 ppm and 499 ppm) and **26** (508 ppm) shown in Figure 19, but are in good agreement with the  $\text{N}_{\text{azo}}\text{-B}$  bond control **64** (478 ppm and 400 ppm). This would strongly suggest the presence of the desired  $\text{N}_{\text{azo}}\text{-B}$  bond. Examining the  $^{15}\text{N}$  chemical shift of the pyridyl nitrogen of **177** (303 ppm), a slight upfield shift is observed in comparison to the negative controls **188** (323 ppm) and **184c** (325 ppm), but it is in good agreement with the chemical shift of pyridine **189** (309 ppm). The  $^{15}\text{N}$  shift of the pyridyl nitrogen is also significantly further downfield than the shift of the  $\text{N}_{\text{pyr}}\text{-B}$  bond control **104** (252 ppm) suggesting a lack of a  $\text{N}_{\text{pyr}}\text{-B}$  bond. The  $^{11}\text{B}$  NMR shift for compound **177** (22.2 ppm) is also significantly further upfield than the negative control **74** (31.1 ppm), downfield from the  $\text{N}_{\text{pyr}}\text{-B}$  bond control **104** (13.1 ppm), and a reasonable match to  $\text{N}_{\text{azo}}\text{-B}$  bond control **64** (17.4 ppm) suggesting the formation of the  $\text{N}_{\text{azo}}\text{-B}$  bond. From these  $^{15}\text{N}$  and  $^{11}\text{B}$  NMR shifts it is very likely that the desired  $\text{N}_{\text{azo}}\text{-B}$  bond had formed in the cyclized compound **177** in preference to the  $\text{N}_{\text{pyr}}\text{-B}$  bond.

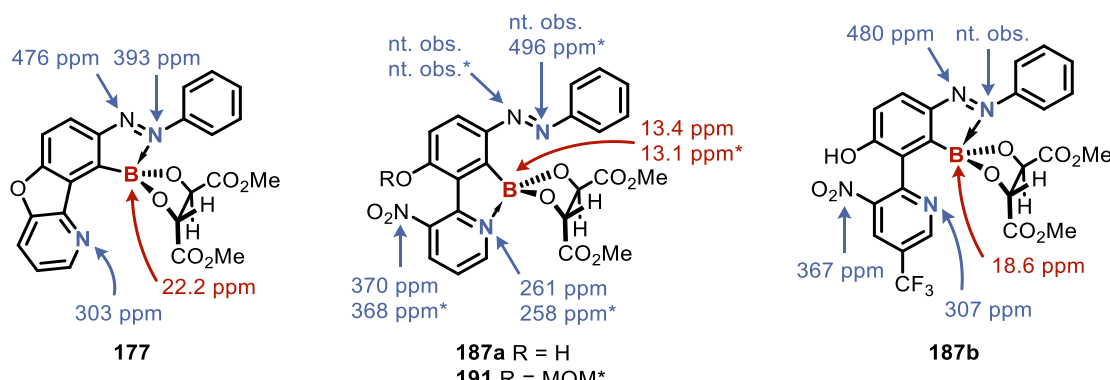


Figure 20.  $^{11}\text{B}$  and  $^{15}\text{N}$  NMR data for selected boryl-azo-biaryl compounds.

Examining the nitro substituted boryl-azo-biaryls **187a** and **191**, the nitro group nitrogens were identified with  $^{15}\text{N}$  shifts at 370 ppm and 368 ppm respectively. These are in good agreement with the control systems **184c**, **188** and **104** (365 ppm, 373 ppm and 371 ppm respectively) shown in Figure 19, indicating that no cyclization has occurred. The  $^{15}\text{N}$  shifts of

the pyridine nitrogens of **187a** and **191** (261 ppm and 258 ppm respectively) were significantly upfield of the negative controls **188**, **184c**, **88** and **189** (323 ppm, 325 ppm, 324 ppm and 309 ppm respectively) and in good agreement with the N<sub>pyr</sub>–B bond control **104** (252 ppm), indicating the presence of the N<sub>pyr</sub>–B bond in the lowest energy state of azo-biaryls **187a** and **191**. Unfortunately, issues were encountered when trying to identify the <sup>15</sup>N shifts of the azo nitrogens, in part due to the poor solubility of the compounds limiting the sample concentration, with only one nitrogen identified in compound **191**. Although only one <sup>15</sup>N shift was identified, the shift of 496 ppm at the distal nitrogen was in good agreement with the negative controls **188** (499 ppm) and **26** (508 ppm) and significantly downfield from the corresponding nitrogen of the N<sub>azo</sub>–B bond control **64** (400 ppm), indicating the lack of a N<sub>azo</sub>–B bond. In line with this, the <sup>11</sup>B NMR shifts of compounds **187a** and **191** (13.4 ppm and 13.1 ppm respectively) are both upfield of the negative control **74** (31.1 ppm) and the N<sub>azo</sub>–B control **64** (17.4 ppm) but in good agreement with the N<sub>pyr</sub>–B control **104** (13.1 ppm), further suggesting formation of the N<sub>pyr</sub>–B bond over the N<sub>azo</sub>–B bond in compounds **187a** and **191**. Based on these <sup>15</sup>N and <sup>11</sup>B NMR shifts, it is believed that the undesired N<sub>pyr</sub>–B bond formed in preference to the desired N<sub>azo</sub>–B bond in the nitro substituted azo-biaryls **187a** and **191**.

Examining the <sup>11</sup>B and <sup>15</sup>N shifts of boryl-azo-biaryl **187b**, the <sup>15</sup>N shift of the nitro group nitrogen was identified at 367 ppm, which matches the control systems **184c**, **188** and **104** (365 ppm, 373 ppm and 371 ppm respectively) and confirms the lack of cyclization. The <sup>15</sup>N shift of the pyridyl nitrogen was also identified at 307 ppm which is slightly further upfield than the negative controls **188** (323 ppm) and **184c** (325 ppm) but is a close match to the pyridine **189** (309 ppm) and the previous N<sub>azo</sub>–B bond forming azo-biaryl **177** (303 ppm). This shift is significantly further downfield than the N<sub>pyr</sub>–B bond control **104** (252 ppm) or the N<sub>pyr</sub>–B bond forming azo-biaryls **187a** or **191** (261 ppm or 258 ppm). Based on these shifts, compound **187b** is unlikely to be forming a N<sub>pyr</sub>–B bond. As before, identification of the <sup>15</sup>N shifts for the azo nitrogens proved challenging, but one of the two azo nitrogens could be identified with a <sup>15</sup>N shift at 480 ppm. This was significantly further upfield than the <sup>15</sup>N shifts for the corresponding nitrogens in the negative control compounds **188** (503 ppm) and **26** (508 ppm) but was in good agreement with the N<sub>azo</sub>–B bond control **64** (478 ppm) and N<sub>azo</sub>–B bond forming azo-biaryl **177** (476 ppm). These shifts would suggest the presence of the N<sub>azo</sub>–B bond in the lowest energy conformation of **187b**. Looking to the <sup>11</sup>B NMR data, the <sup>11</sup>B shift (18.6 ppm) is upfield of the negative control **74** (31.1 ppm), downfield from the N<sub>pyr</sub>–B bond

control **104** (13.1 ppm) and a close match to the N<sub>azo</sub>–B bond control **64** (17.4 ppm), again suggesting the lack of a N<sub>pyr</sub>–B bond and the formation of the N<sub>azo</sub>–B bond. As the <sup>15</sup>N shifts of the pyridyl nitrogen, the azo nitrogen and the <sup>11</sup>B shift of the boron centre all suggest the lack of a N<sub>pyr</sub>–B bond and the formation of a N<sub>azo</sub>–B bond, it is highly likely that the desired N<sub>azo</sub>–B bond is forming in the boryl-azo-biaryl **187b**.

As is apparent in Figure 20, the <sup>15</sup>N shifts of the azo nitrogens were notably more challenging to identify than the nitro or pyridyl nitrogens and require further investigation. Although the <sup>15</sup>N shifts of the azo nitrogens could be identified in the control systems **188** and **26**, the boryl-azo-biaryls **177**, **187a**, **191** and **187b** had significantly poorer solubility which limited the sample concentration and made the detection of the insensitive <sup>15</sup>N more challenging than it was in the control systems. Further work investigating the ideal Δ<sub>1</sub> delay (i.e., the expected <sup>1</sup>H-<sup>15</sup>N *J*-coupling) to visualise the azo <sup>15</sup>N shifts at these low sample concentrations would be highly beneficial, as well as the incorporation of a <sup>15</sup>N labelled nitrogen nucleus into the azo group to allow easier detection *via* <sup>15</sup>N HMBC and potentially direct detection *via* 1D <sup>15</sup>N NMR.

To serve as further confirmation of the proposed N<sub>azo</sub>–B bonding the <sup>13</sup>C chemical shifts of the carbon centres bound to the azo unit were also examined. As shown in Figure 21, in the control systems which exhibit a N<sub>azo</sub>–B bond (**64**, **67** and **65**), the <sup>13</sup>C chemical shift of the azo-substituted carbon in the borylated ring is observed around 151 ppm (150.7 ppm, 150.6 ppm and 150.4 ppm respectively) while the <sup>13</sup>C chemical shift of the equivalent carbon in the distal ring is observed around 144 ppm (146.4 ppm, 144.2 ppm and 143.9 ppm respectively). Conversely, in the control systems which exhibit no N<sub>azo</sub>–B bond (**61**, **185a** and **185f**), the <sup>13</sup>C chemical shift of the azo-substituted carbon in the borylated ring is still observed around 151 ppm (151.0 ppm, 151.0 ppm and 150.9 ppm respectively) but the <sup>13</sup>C chemical shift of the equivalent carbon in the distal ring is instead observed further downfield around 153 ppm (153.0 ppm, 151.8 ppm and 153.4 ppm respectively). From this it would appear that the formation of the N<sub>azo</sub>–B bond causes a distinctive shift of the distal carbon's chemical shift, causing it to shift from being downfield of the proximal carbon to becoming upfield of the proximal carbon. Based on this trend, the upfield <sup>13</sup>C chemical shift of the distal carbon centre (148.1 ppm) relative to the proximal carbon centre (152.3 ppm) of boryl-azo-biaryl **177**, would

suggest that the desired  $\text{N}_{\text{azo}}-\text{B}$  bond has formed, supporting the findings from  $^{11}\text{B}$  and  $^{15}\text{N}$  studies. Examination of the  $^{13}\text{C}$  chemical shifts of boryl-azo-biaryl **187b** also reveals the same trend, with the  $^{13}\text{C}$  chemical shift of the distal carbon centre (149.6 ppm) further upfield than the proximal carbon centre (150.5 ppm). This again supports the claim from the  $^{11}\text{B}$  and  $^{15}\text{N}$  studies that the desired  $\text{N}_{\text{azo}}-\text{B}$  bond has formed in boryl-azo-biaryl **187b**. Finally, the downfield  $^{13}\text{C}$  chemical shift of the distal carbon centre (153.1 ppm) relative to the proximal carbon centre (148.7 ppm) of boryl-azo-biaryl **187a** would suggest that no  $\text{N}_{\text{azo}}-\text{B}$  bond is present, again, supporting the findings from  $^{11}\text{B}$  and  $^{15}\text{N}$  studies.

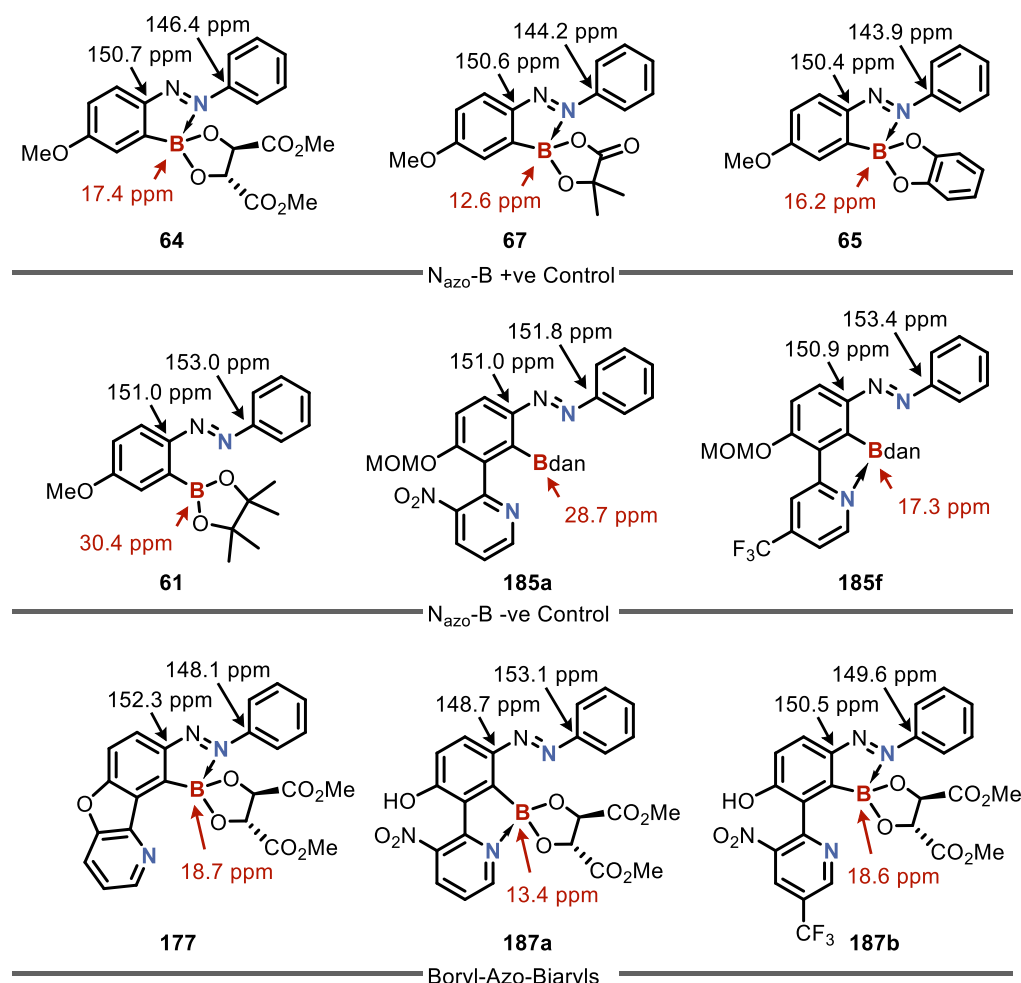


**Figure 21.**  $^{13}\text{C}$  shifts of control systems and boryl-azo-biaryls used to analyse the intramolecular bonding present in the azo-biaryl systems.

From the boryl-azo-biaryl **187a**, it is apparent that in the case where the pyridine ring sits in a favourable conformation for binding and has only one electron withdrawing unit on the pyridyl ring, the undesired  $\text{N}_{\text{pyr}}-\text{B}$  bond prevails over the desired  $\text{N}_{\text{azo}}-\text{B}$  bond. Conversely, in systems with exceedingly electron deficient pyridyl rings such as **187b**, or in systems in

which the pyridine ring is geometrically constrained to keep the pyridyl nitrogen further from the boron centre (i.e., cyclized **177**), the N<sub>azo</sub>–B bond appears to dominate over the N<sub>pyr</sub>–B bond. While this gives useful insight into using both the pyridyl electronics and geometry constraints to bias the system towards forming one of the two N–B bonds, it doesn't provide an understanding of how the substituent positioning on the pyridyl ring affects these bonds. To this end, boryl-azo-biaryl systems **185e–f**, which contained the masked BdAn boron species and varied substituent positioning on the pyridyl ring were examined (Figure 22).

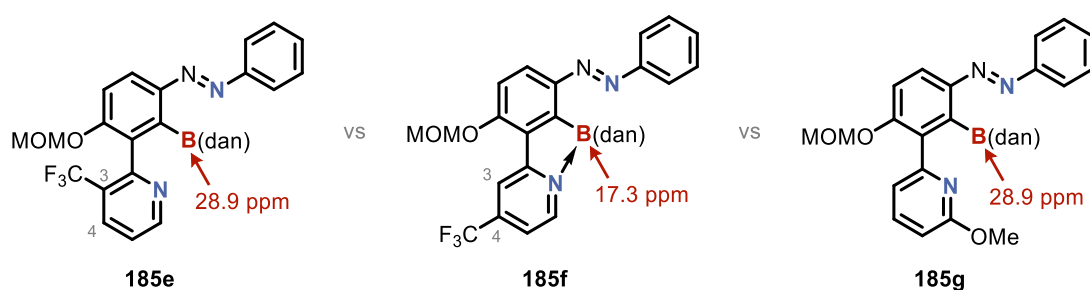


**Figure 22.**  $^{11}\text{B}$  NMR data for selected boryl-azo-biaryl compounds **185e–f** to assess the effects of substitution pattern.

As expected, no N–B bonds were observed in the 2-substituted boryl-azo-biaryl **185e**, with the  $^{11}\text{B}$  NMR shift of 28.9 ppm being characteristic of the tricoordinate BdAn species. By contrast the 3-substituted boryl-azo-biaryl **185f** displayed a  $^{11}\text{B}$  shift of 17.3 ppm which is highly characteristic of a tetracoordinate boron species, suggesting the formation of a N–B bond. As the difference between compounds **185e** and **185f** is restricted to positional changes on the pyridyl ring substituent, with no changes to the azobenzene, the change in the boron environment should be attributable to the formation of a N<sub>pyr</sub>–B bond. The new bond formation is likely enabled by the change in the CF<sub>3</sub> group substitution from the 3-position to the 4-position allowing the biaryl to adopt a planar conformation, which is known from previous literature studies (section 3.1.1) to facilitate the N<sub>pyr</sub>–B bond formation.<sup>183</sup> Looking to the planar and electron rich boryl-azo-biaryl **185g**, no N<sub>pyr</sub>–B was observed with the  $^{11}\text{B}$  NMR shift of 28.9 ppm again being characteristic of the tricoordinate BdAn species. As both the increased electron density and the planarity should improve the ability of the pyridyl nitrogen to form a N<sub>pyr</sub>–B bond, the lack of N<sub>pyr</sub>–B bond is attributed to the steric crowding of the pyridyl nitrogen. As the steric crowding appears to significantly reduce the ability of the pyridine to bind to the boron centre, it has potential for being used to achieve a balance between the N<sub>azo</sub>–B and N<sub>pyr</sub>–B bonds.

From the bonding in these three systems (**185e**, **185f**, **185g**), two design principles were highlighted. Firstly, the biaryl twist (i.e., the barrier to rotation) is not only required for the final system to act as a rotor, but it also plays a key role in achieving a balance between the N<sub>azo</sub>–B bond and the N<sub>pyr</sub>–B bond. Secondly, comparing **185f** against **185g** would also suggest that substituents *ortho* to the pyridyl nitrogen are able to disfavour the N<sub>pyr</sub>–B bond formation through steric means, potentially providing another strategy towards controlling the balance between the N<sub>azo</sub>–B and N<sub>pyr</sub>–B bonds.

### 5.2.3 Hydrogen Bond Formation

While achieving a balance of the N–B bonds had been the central focus of the intramolecular bond analysis, it was also important to assess the formation of the H-bond, as this is also a key element of the proposed motor design (section 1.8, bridging interaction required to stabilise the biaryl axis in state A). As discussed in section 3.5, related H-bonds have been shown in the literature to lower the barrier to rotation in axially chiral compounds and exhibit diagnostic shifts by <sup>1</sup>H NMR.<sup>128–131</sup> Using some of the synthetic intermediates generated in Chapter 3 and Chapter 4, which contained the biaryl phenol-pyridine motif, further examination of these bonds was performed to better understand this interaction in structures more similar to the proposed motor. Upon examination of the simpler CF<sub>3</sub> biaryl **190** (Figure 23), a significant downfield shift was observed for the hydroxyl proton of **190** (10.29 ppm) relative to the hydroxyl proton of phenol **192** (4.86 ppm) with the shift being similar to the shifts observed by Ott and co-workers in their phenol derivatives (Figure 15, **110** δ<sub>H</sub> = 9.86 ppm, **113** δ<sub>H</sub> = 11.75 ppm and **112** δ<sub>H</sub> = 14.69 ppm).<sup>128</sup> As the diagnostic handle used for assessing the H-bond is an exchangeable hydroxyl proton, which can be challenging to visualise by <sup>1</sup>H NMR, the assessment of the H-bond was also tested via <sup>15</sup>N HMBC. Unfortunately, while the <sup>15</sup>N shift of phenol-pyridine **190** was slightly upfield of the shift observed in biaryl-pyridine **88**, the upfield shift was relatively minor (Δδ = 7 ppm) and was therefore a less distinctive analytical handle than the <sup>1</sup>H NMR shift.

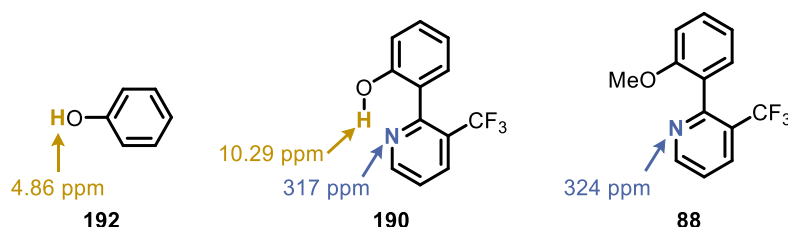


**Figure 23.** Comparison of the <sup>1</sup>H and <sup>15</sup>N shifts of the pyridyl-phenol biaryl **190** against the respective negative controls **192** and **88**.

With the  $^{15}\text{N}$  shifts shown to be less characteristic of the H-bond formation than the  $^1\text{H}$  shifts, the focus shifted to assessing the H-bonds present in the azo-biaryl scaffolds **132**, **193**, **148** and **194** by  $^1\text{H}$  NMR (Figure 24). From the  $^1\text{H}$  shifts in the azo-biaryls it was again apparent that the pyridine and phenol hydroxyl were forming a hydrogen bond, with the inclusion of the azobenzene unit *para* to the hydroxyl group causing the  $^1\text{H}$  shifts to be shifted further downfield (e.g., **190**  $\delta_{\text{H}} = 10.29$  ppm while **132**  $\delta_{\text{H}} = 12.57$  ppm or **193**  $\delta_{\text{H}} = 11.46$  ppm). As downfield  $^1\text{H}$  shifts are known to be indicative of stronger H-bonds,<sup>126</sup> this would indicate that the azobenzene increases the strength of the H-bond, potentially due to the known conjugation of the azobenzene and *para*-hydroxy systems which causes an increase in the acidity of the hydroxyl proton.<sup>128, 184-192</sup> Comparing azo-biaryls **193** and **132**, the  $^1\text{H}$  shifts would indicate a weaker H-bond in the nitro containing system **193** than in the chloro system **132** ( $\delta_{\text{H}} = 11.46$  ppm vs.  $\delta_{\text{H}} = 12.57$  ppm) suggesting that decreasing the electron density of the pyridyl ring has a significant effect on the H-bond strength.<sup>125</sup> Based on the  $^1\text{H}$  shifts of the nitro-azo-biaryls **193** and **148**, the difluorination of the azobenzene bears little effect on the hydrogen bond strength with the systems having  $^1\text{H}$  shifts of 11.46 ppm and 11.45 ppm respectively. Comparing the  $^1\text{H}$  shifts of the azo-biaryl **194** ( $\delta_{\text{H}} = 8.15$  ppm) against the less substituted azo-biaryl **193** ( $\delta_{\text{H}} = 11.46$  ppm), a significant upfield shift is observed, suggesting a weakened H-bond in the axially strained system. This is in line with the observations from the  $\text{N}_{\text{pyr}}-\text{B}$  bond studies where introducing substituents that force the biaryl out-of-plane weakens the intramolecular bond between the upper and lower rings (section 5.2.2). To give further confirmation of the H-bond presence in **194**, water was added to the sample to destabilise the potential H-bond with the corresponding and expected loss of the peak at 8.15 ppm observed (section 8.6.4, Figure 64).

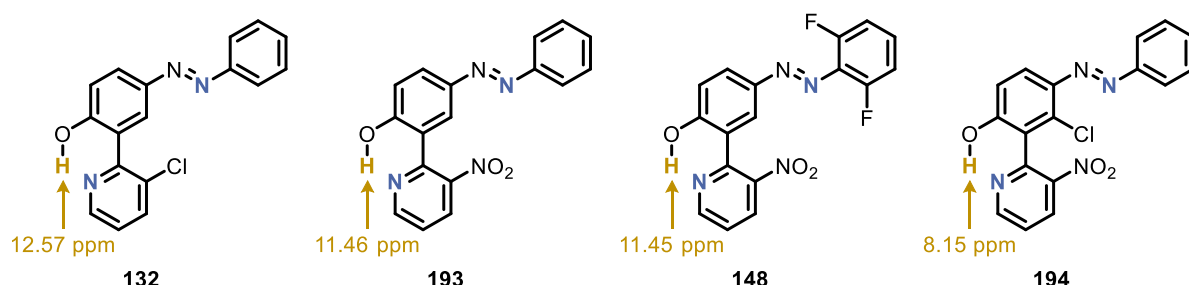


**Figure 24.** Comparison of the  $^1\text{H}$  shifts of azo-biaryls **132**, **193**, **148** and **194** corresponding to the protons involved in the H-bond interaction.

Although these studies provide good precedent for the formation of the desired H-bond in the azo-biaryl motor scaffolds, the H-bond is yet to be identified in any of the generated boryl-azo-biaryl motor candidates (compounds **187a** **187b** or **187c**). This may be attributable to the exchangeable protons of the excess DMT ligand exchanging with the proton of the azo-biaryl hydroxy group and preventing visualization by  $^1\text{H}$  NMR. Further work into identifying this bond in the final scaffolds is still needed and may require investigations into methods of slowing the potential proton exchange (e.g., low temperature NMR) or into methods of improving the compound stability so that purer samples without the excess DMT ligand can be obtained. While the H-bond is yet to be identified in the motor candidates, the study of these systems has been useful in proving that the H-bonds can form in a variety of different azo-biaryl scaffolds, that they have distinctive shifts by  $^1\text{H}$  NMR and that they show a slight but not unambiguously characteristic shift by  $^{15}\text{N}$  HMBC. These scaffolds have also shown that the presence of the azobenzene increases the strength of the H-bond, while forcing the biaryl out-of-plane decreases the H-bond strength.

### **5.3 Photochemical Studies**

Having established which of the N–B bonds were present in the borylated-azo-biaryl scaffolds, attention turned to the analysis of the photochemical behaviour and whether photoswitching between the two N–B bonds would be possible. Using the simplest of the scaffolds, compound **177**, irradiation of the azo-biaryl was performed at 365 nm using the irradiation setup described in section 8.4.1, and the system subsequently analysed by  $^1\text{H}$  and  $^{11}\text{B}$  NMR (Figure 25). While the irradiation studies described in section 2.4.2 had been conducted in  $\text{CDCl}_3$  (or in select cases  $\text{C}_6\text{D}_6$ ), the solvent for the irradiation studies of the boryl-azo-biaryls was changed to  $\text{MeCN-d}_3$  due to the formation of precipitate during the irradiation experiments in  $\text{CDCl}_3$ .

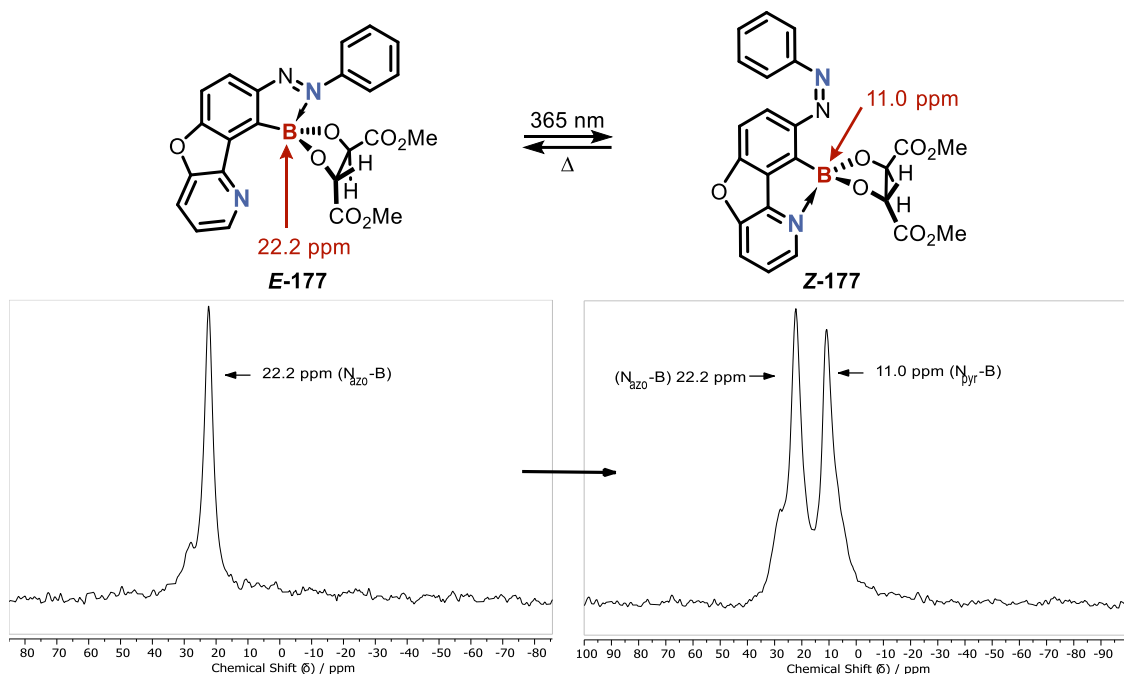


**Figure 25.** Photoswitching of borylated-azo-biaryl **177**.  $^{11}\text{B}$  NMR spectra pre (left) and post (right) irradiation at 365 nm showing the emergence of a new  $^{11}\text{B}$  peak at 11.0 ppm. For the sake of clarity, the  $^{11}\text{B}$  shift representing the  $\text{N}_{\text{azo}}-\text{B}$  bond in the post-irradiation spectra is manually referenced to 22.2 ppm to match the  $^{11}\text{B}$  shift observed in the pre-irradiation spectra.

From the  $^{11}\text{B}$  NMR spectra pre-irradiation (Figure 25, left) it was apparent that there was only a single N–B bound species which, from the studies above (section 5.2.2), was known to be the  $\text{N}_{\text{azo}}-\text{B}$  bond species. Post-irradiation, two distinct boron species were visible at 22.2 ppm and 11.0 ppm which were both characteristic of tetrahedral boron environments (Figure 25, right). The appearance of the new  $^{11}\text{B}$  peak at 11.0 ppm would strongly indicate the formation of a new N–B bond in the species generated upon irradiation. Based on the  $\text{N}_{\text{azo}}-\text{B}$  **64** (17.4 ppm) and  $\text{N}_{\text{pyr}}-\text{B}$  **104** (13.1 ppm) control systems discussed in section 5.2.1 (Figure 19), the  $\text{N}_{\text{pyr}}-\text{B}$  bond should have a  $^{11}\text{B}$  shift further upfield than that of the  $\text{N}_{\text{azo}}-\text{B}$  bond. Since the new bond must be different from the  $\text{N}_{\text{azo}}-\text{B}$  bond already identified in the initial state, the new upfield 11.0 ppm peak is likely characteristic of a  $\text{N}_{\text{pyr}}-\text{B}$  bond (Figure 25, right). It should be noted that due to the changes in the concentration of the starting *E* isomer, and changes to the sample composition, the  $^{11}\text{B}$  peak shift representing the  $\text{N}_{\text{azo}}-\text{B}$  bond in the pre and post irradiation spectra varies slightly (22.2 ppm pre-irradiation and 22.0 ppm post-irradiation). For the sake of clarity, the  $^{11}\text{B}$  shift representing the  $\text{N}_{\text{azo}}-\text{B}$  bond in the post-irradiation spectra is manually referenced to 22.2 ppm to match the  $^{11}\text{B}$  shift observed in the pre-irradiation spectra. While the formation of a  $\text{N}_{\text{pyr}}-\text{B}$  bond would generate a highly strained (6,5,5,6)-ring system, these types of motifs have been observed throughout the literature with a range of different

bridging groups (Figure 26a).<sup>193-197</sup> As these types of strained (6,5,5,6)-motifs have been observed in a range of compounds, and the post-irradiation  $^{11}\text{B}$  NMR data of compound **177** would suggest the presence of the desired  $\text{N}_{\text{pyr}}-\text{B}$  bond, it is believed that the desired  $\text{N}_{\text{pyr}}-\text{B}$  bond is present in the cyclized azo-biaryl **Z-177**. Interestingly, NMR studies undertaken by Trost and co-workers on the dihydribenzopentalene structure **195** had indicated that the compound adopted a bent structure with a  $\psi$  angle of  $114\pm6^\circ$  to accommodate for the large ring strain (Figure 26b). Conversely, their XRD studies had indicated that the compound is more planar ( $\psi$  unspecified) and that it was the increased bond angles of the aryl ring (Figure 26b,  $\theta$ ) and the shortened bond length of the central bond (Figure 26b, Å) which helped to accommodate the ring strain.<sup>193</sup>

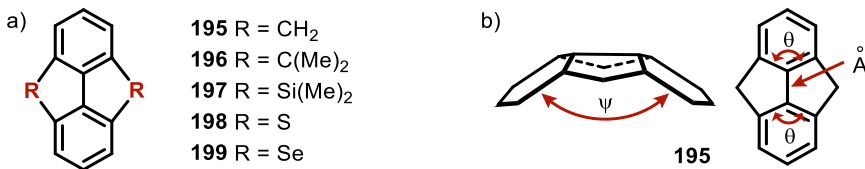


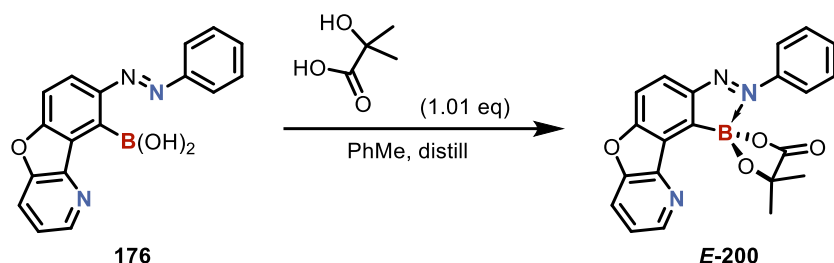
**Figure 26.** a) 6,5,5,6 ring systems reported in the literature. b) Trost and co-workers structural studies on compound **195**.<sup>193-197</sup>

During the irradiation experiment of **177**, new but poorly resolved peaks were also observed in the  $^1\text{H}$  NMR spectra in the regions characteristic of the *E*-to-*Z* isomerization. Interestingly, the poor resolution of the  $^1\text{H}$  NMR peaks was only observed with the new *Z*-isomer peaks while the peaks corresponding to the initial *E*-isomer remained clearly resolved throughout. Further work is required to understand the root cause of the poor peak resolution, but this may be attributable to the  $\text{N}_{\text{pyr}}-\text{B}$  bound conformation adopting a slightly bent structure (Figure 26b,  $\psi \neq 180^\circ$ ). Due to the presence of the chiral DMT ligand, the bent conformation would make the compound diastereomeric. If the system were able to interconvert between bent conformations ( $\psi = >180^\circ$  and  $<180^\circ$ ), and therefore interconvert between diastereomers, this would cause similar line shape broadening to that observed at the coalescence temperature of the rotation barrier studies described in section 3.4 (Figure 13). This might explain the poor resolution observed in the *Z*-isomer but further studies are required to further understand this phenomenon.

While the exact rate of thermal relaxation was not established during these experiments, it was found that the newly formed species was thermally unstable with different amounts of

the metastable isomer observed based on the time taken from the cessation of irradiation to the acquisition of the first NMR spectrum. This prevented the PSS composition and the rate of thermal relaxation from being determined and also meant that the  $^{15}\text{N}$  shifts could not be established, since the  $^{15}\text{N}$  HMBC requires long experiment times (>45min per run), especially at the low concentrations caused by the compound's poor solubility. It should be noted that when the sample was left to rest for 1 hour after the irradiation, the new signals attributed to the metastable Z isomer post-irradiation disappeared, with no other new peaks appearing. This would suggest the metastable intermediate post-irradiation relaxed back to the starting isomer as desired and that the peaks were not a photodegradation product.

To test whether photoswitching the N–B bonds of this scaffold would be possible with a more electron withdrawing ligand,  $\alpha$ -hydroxyisobutyric acid was coupled to the same cyclized azo-biaryl scaffold to generate boryl-azo-biaryl **200** (Scheme 40). As discussed in section 2.4.5, in the simplest of the azo systems the electron withdrawn  $\alpha$ -hydroxyisobutyric acid induced a strong  $\text{N}_{\text{azo}}\text{–B}$  bond which appeared to prevent the azobenzene photoisomerization. However, in the presence of a competing pyridine nucleophile, clean photoswitching behaviour could be observed. As such, it was proposed that in a system which contained an internal pyridine the same behaviour might be observed, allowing the use of more electron withdrawing ligands.



**Scheme 40.** Synthesis of  $\alpha$ -hydroxy-isobutyric acid based boryl-azo-biaryl **200**

Examining the  $^{11}\text{B}$  NMR spectrum of **200** prior to irradiation, a single peak was observed at 15.2 ppm (Figure 27, left spectrum). Upon irradiation at 365 nm, a second upfield peak emerged at 6.4 ppm (Figure 27, right spectrum). This is in line with the observations from previous system **177** (Figure 25) and would indicate that the  $\alpha$ -hydroxyisobutyric acid system **200** is not only capable of photoswitching but is likely photoswitching between the two

possible N–B bonds in the same manner as the DMT system **177**. Also in line with the findings from section 2.4.1, both peaks attributed to the  $\text{N}_{\text{azo}}\text{-B}$  and the  $\text{N}_{\text{pyr}}\text{-B}$  bonds in the  $\alpha$ -hydroxyisobutyric acid system **200** were shifted significantly upfield compared to the DMT system **177**, indicating that both the  $\text{N}_{\text{azo}}\text{-B}$  and the  $\text{N}_{\text{pyr}}\text{-B}$  bond were stronger in the isobutyric acid system **200**. The emergence of the new  $^{11}\text{B}$  peak at 28.3 ppm in the post-irradiation spectrum (Figure 27, right) was attributed to the slow hydrolysis back to the boronic acid due to the low hydrolytic stability of these boronic esters in solution.

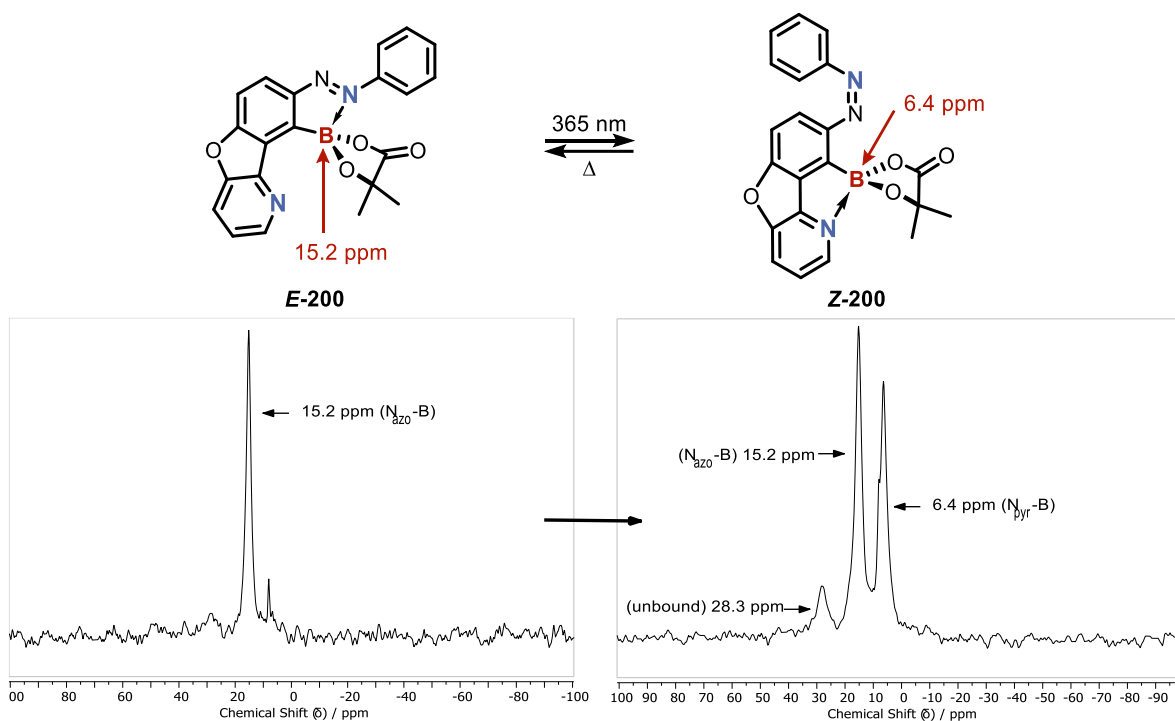


**Figure 27.** Photoswitching of borylated-azo-biaryl **200**.  $^{11}\text{B}$  NMR spectra pre (left) and post (right) irradiation at 365 nm showing the emergence of a new  $^{11}\text{B}$  peak at 6.4 ppm.

To investigate the effect of substituents *ortho* to the pyridyl nitrogen, the photochemical behaviour of compound **187c** was also investigated (Figure 28). While it was desirable to examine this effect in a planar and electron rich pyridyl system, attempts at the global deprotection of **185g** proved unsuccessful and as such compound **185c** which underwent the global deprotection more cleanly was investigated instead (Section 4.2.2, Scheme 39). While the deprotection of **185c** proceeded more cleanly, it still proved challenging to obtain a pure sample of the *E*-**187c** as not only was it hydrolytically unstable but also highly light sensitive. As such, rather than a pure sample, a mixture containing *E*-**187c** as the major species was irradiated with 365 nm light and subsequently analysed by NMR. In the pre-irradiation  $^{11}\text{B}$

NMR spectrum of the mixed material (Figure 28, left), three peaks were observed in a roughly 0.5:1:0.3 ratio; one at 29.9 ppm which is in the range characteristic of an unbound tricoordinate boron centre, one at 19.8 ppm which is in the range characteristic of the  $\text{N}_{\text{azo}}\text{-B}$  bond, and one at 9.3 ppm which is in the range characteristic of a  $\text{N}_{\text{pyr}}\text{-B}$  bond. Irradiation of this system with 365 nm light, then caused significant increases in the 29.9 ppm and 9.3 ppm peaks relative to the 19.8 ppm peak, changing the peak ratio to 0.8:1:0.5. Interestingly, the ratio of the 29.9 ppm peak to the 9.3 ppm peak remained very similar pre- and post- irradiation (1:1.7 pre-irradiation and 1:1.6 post-irradiation), suggesting they both grew equally in intensity relative to the 19.5 ppm peak. As above, due to changes in the concentration of the boron species, and changes to the general sample composition, a slight peak drift between the pre- and post- irradiation spectra is observed and has been manually corrected in the post-irradiation spectrum by setting the central peak to 19.8 ppm to match the pre-irradiation spectrum.

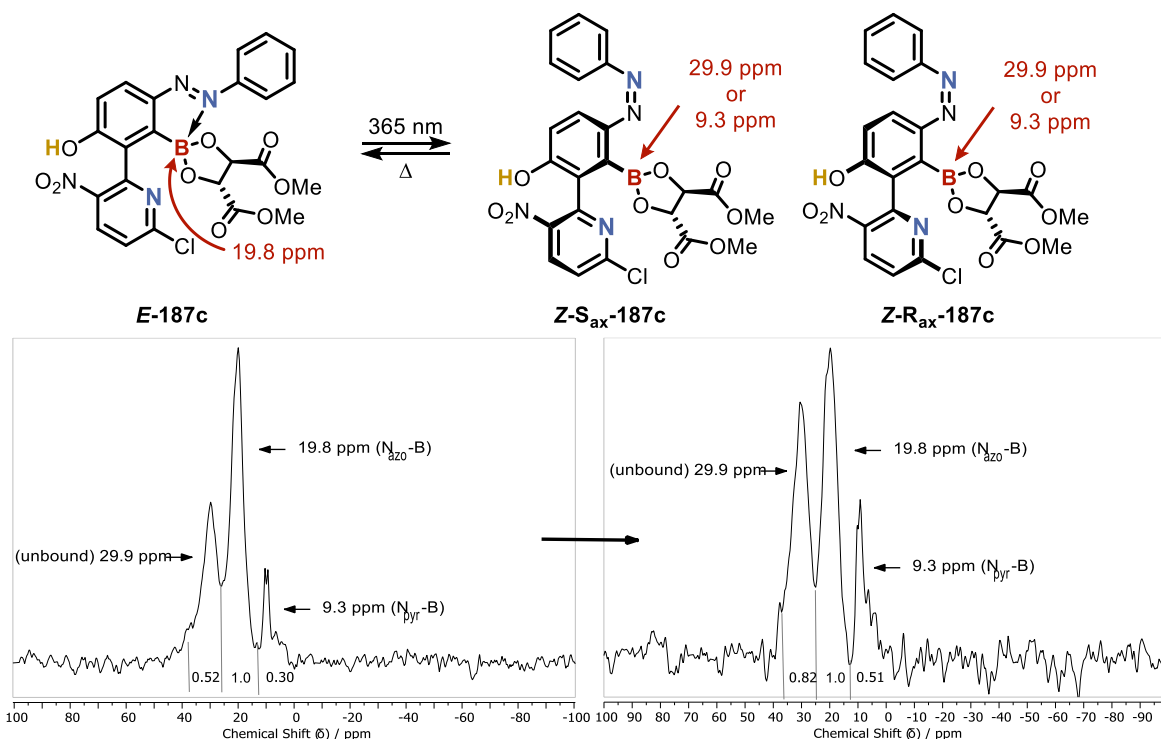


**Figure 28.** Photoswitching of borylated-azo-biaryl **187c**. <sup>11</sup>B NMR spectra pre (left) and post (right) irradiation at 365 nm showing a change in the ratios of the <sup>11</sup>B peaks.

As the 19.5 ppm peak, which is in the range typically indicative of a  $\text{N}_{\text{azo}}\text{-B}$  bond, is decreasing in intensity while both the 29.9 ppm and the 9.3 ppm peaks, which are in the ranges typically indicative of an unbound boron centre and a  $\text{N}_{\text{pyr}}\text{-B}$  bond respectively, are increasing and maintaining the same ~1:1.7 ratio, it would suggest that the azobenzene isomerization is

breaking the N<sub>azo</sub>–B bond and forming a mixture of both the unbound species and the N<sub>pyr</sub>–B bond forming species. As the ~1:1.7 ratio of the 29.9 ppm and 9.3 ppm peaks is notably similar to the d.r of 1:1.9 observed from the DMT model biaryl **106** from section 3.4 (Figure 13), it may be possible that the formation of the unbound and the N<sub>pyr</sub>–B bond forming species is affected by the chiral DMT ligand. One possible explanation is that upon isomerization of the azobenzene, which breaks the N<sub>azo</sub>–B bond and allows the N<sub>pyr</sub>–B bond to form, both the R<sub>ax</sub> and S<sub>ax</sub> isomers of compound **Z-187c** are generated. Due to the diastereomeric nature of this system, the R<sub>ax</sub> and S<sub>ax</sub> axial isomers will each experience different steric interactions with the DMT ligand. Based on the previous observations from section 5.2.2 (Figure 22), the steric interactions between the *ortho* pyridyl bulk and the boron centre/boron ligand are known to have an inhibitory effect on the ability of the pyridyl ring to form a N<sub>pyr</sub>–B bond. As these steric clashes would be different between the two isomers it may be possible that in one of the isomers the steric clash is too great to allow the N<sub>pyr</sub>–B bond formation, while in the other isomer the clash between the *ortho*-chloro group and the DMT ligand is reduced, allowing the system to form the N<sub>pyr</sub>–B bond. Further studies should be done using achiral N–B bond inducing boron ligands of different sizes, using highly electron withdrawing ligands which induce stronger N–B bonds, using pyridyl rings which contain larger and smaller *ortho* groups, as well as using pyridyl rings which allow the biaryl to be planar. This would give a much clearer understanding of the bonding present in this system, the effect of the steric interactions between the pyridyl ring and the boron ligand, and whether the bond formation was truly dependant on the chirality of the DMT ligand.

As these studies indicated that photoswitching between the N<sub>azo</sub>–B and N<sub>pyr</sub>–B bonds is possible in the boryl-azo-biaryls scaffolds **177** and **200**, and potentially in scaffold **187c**, attention turned to the photoswitching of the N–B bonds in compound **187b**. Compound **187b** was the prime motor candidate as not only was it theoretically able to rotate around the central C–C bond, but had also been shown to form the desired N<sub>azo</sub>–B bond in preference to the N<sub>pyr</sub>–B bond in the *E* isomer (section 5.2.2, Figure 20). Unfortunately, attempts at the photoswitching of **187b** using the experimental setup that had been used for the previous experiments (described in section 8.4.1) proved unsuccessful with no changes observed by <sup>11</sup>B or <sup>1</sup>H NMR after irradiation at 365 nm (Figure 29). As the cyclic compound **177** faced challenges with rapid thermal relaxation, and hydroxy azobenzenes are known to exhibit particularly rapid thermal relaxation, it was proposed that the lack of observed photoactivity may be attributable

to issues with the timeframes required for analysis rather than a lack of photoresponse in compound **187b**.<sup>187-190</sup> As such, attention shifted towards the development of new equipment that would allow these systems to be analysed more rapidly and under constant irradiation conditions.

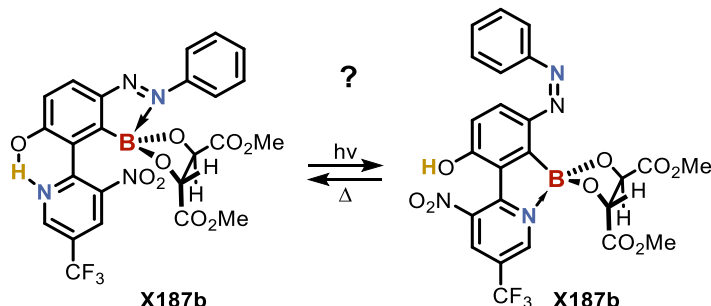


**Figure 29.** Desired but unobserved photoswitching of compound **187b**.

## 5.4 Equipment Development and Model System Benchmarking

### 5.4.1 UV-Vis Spectroscopy

To begin developing equipment capable of analysing the photochemical systems rapidly and under constant irradiation, attention first turned to UV-Vis spectroscopy. UV-Vis spectroscopy is well suited for custom development as, the light path for the analysis can be easily redirected allowing the equipment to be built around the sample housing and the sample remains accessible during analysis allowing simultaneous irradiation (unlike MS, HPLC, etc.). In addition, the data collection can be rapid since it uses light for analysis, and the equipment is cheap relative to other analytical instruments such as NMR, HPLC or MS.<sup>198-200</sup> UV-Vis spectroscopy is also particularly well suited for the study of azobenzenes as they have clear absorption bands which differ significantly upon isomerization, allowing for clear analysis of the photoisomerization process. The final design of this UV-Vis system is described in section 8.4.2.

There are two elements which underpin the utility of this design. Firstly, by using a spectrometer containing a Czerny-Turner design monochromator and a CCD array, broadband light can be used directly for sample analysis, dramatically increasing the collection speed (from minutes down to milliseconds). Secondly, by using a four-way cuvette and mount, the optical path for the sample irradiation is perpendicular to the optical path for analysis, allowing both the irradiation and data acquisition to take place concurrently (Figure 30).

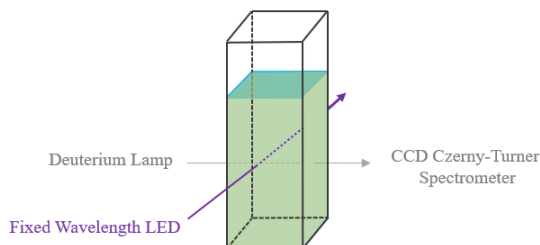
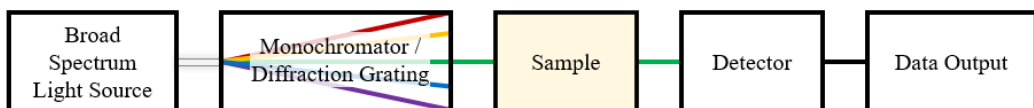


**Figure 30.** Perpendicular optical paths for irradiation and analysis.

To understand how the data collection speed is increased by this design it is important to compare the workflow of this system against that of a typical UV-Vis spectrometer (Figure 31). In a typical spectrometer (e.g., Agilent's Cary 5000), broad-spectrum light is generated using a deuterium, tungsten-halogen or xenon lamp which then passes through a monochromator which splits the broad-spectrum light into separate wavelengths (Figure 31a).<sup>200</sup> By mechanically rotating either the diffraction grating or a focusing lens in the monochromator, a single wavelength of light can be selectively focused onto the sample and subsequently used for analysis. Further rotation of the diffraction grating/focusing lens then allows the system to "step-through" each wavelength allowing the absorption to be measured at each subsequent wavelength. In this way, by stepping through each wavelength and measuring the absorbance at that wavelength a complete UV-Vis spectrum can be acquired. As such, acquisition of a complete spectrum requires each separate wavelength of light to be isolated by mechanical rotation in the monochromator, passed through the sample, and then measured individually.<sup>200</sup> For example, a spectrum ranging from 250 nm to 750 nm, requires five hundred separate, sequential measurements with mechanical refocusing at each wavelength. This is a time-consuming process causing spectra acquisition to take a significant amount of time. While these systems cannot capture complete spectra rapidly, they have still been used to monitor rapid absorption changes at a fixed wavelength.<sup>201</sup>

a) Simplified schematic of a Classical UV-Vis spectrometer design.



b) Simplified schematic of the UV-Vis system design built for rapid online analysis.

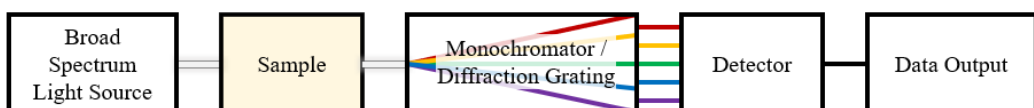


**Figure 31.** a) A simplified workflow of a typical UV-Vis spectrometer (e.g., Cary 5000) and b) A simplified workflow of the system built for the study of the azobenzene isomerization.

In contrast, rather than split the wavelengths of light prior to passing through the sample, with subsequent analysis of the absorption wavelength by wavelength (Figure 31a), the custom-built system described in Section 8.4.2 passes the broad-spectrum light from a deuterium lamp directly through the sample and then splits the wavelengths of the resulting light using a Czerny-Turner design monochromator (Figure 31b).<sup>199</sup> Once split into separate wavelengths, the light can then be analysed by a CCD detector array (Figure 32). A CCD array is a sensitive multi-channel photon detector which is divided into a large number of small light-sensitive areas (pixels) which interact with light to build up a charge, with brighter light or longer exposures generating a greater charge. By exposing each of these pixels to different wavelengths of light, the entire absorption spectrum can be established by measuring the charge generated by each pixel in response to a single pulse of broad-spectrum light. This means that a complete absorption spectrum can be acquired from a single measurement with no mechanical refocusing required, dramatically cutting down the acquisition time (from >1 minute down to as low as 1 ms). With such short acquisition times, the complete UV-Vis spectrum can be used to monitor the rapid isomerization processes.<sup>200</sup> As this setup is not confined to a spectrometer enclosure, it also has a far greater degree of modularity. Due to the custom-built nature of the system, data acquisition for the time resolved UV-Vis data below is handled by purpose-built Python scripts. The Python script for controlling the spectrometer and acquiring the time resolved UV-Vis spectra, is given in the appendix (section 8.6.5) and has been made available on GitHub (<https://github.com/is20508/UV-Vis.git>).

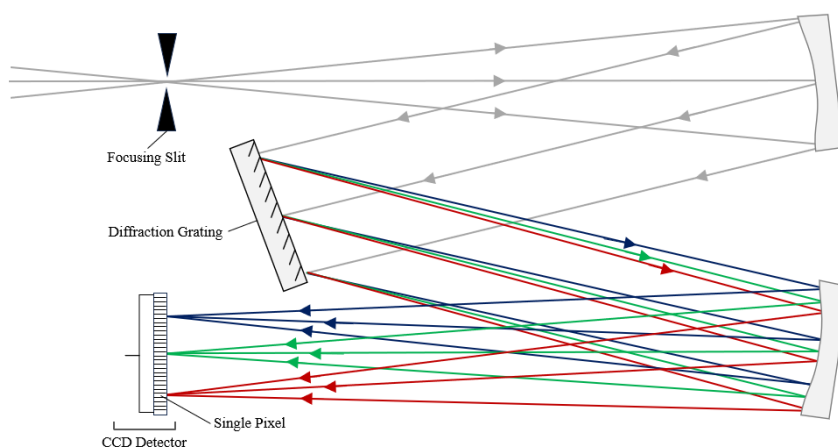


**Figure 32.** Czerny–Turner design monochromator, which separates a single beam of broad-spectrum light into the individual wavelengths where the intensities of each wavelength can be measured using a charge-coupled device (CCD).

To test whether the UV-Vis system was capable of monitoring fast relaxing systems as desired, the thermal relaxation of a model system, 2-hydroxy-azobenzene **156**, was studied (Figure 33). This was a particularly useful model for testing the equipment as 2-hydroxy-azobenzenes are known to undergo fast thermal relaxation at room temperature, with the half-lives for the metastable isomer in the range of milliseconds to minutes.<sup>187-190</sup> As the issues in detecting a photoresponse in compound **187b** were suspected to be attributable to the thermal relaxation occurring faster than the time it took to acquire the first NMR spectrum after cessation of irradiation, a model with a thermal relaxation rate in the seconds to minute regime was desirable.

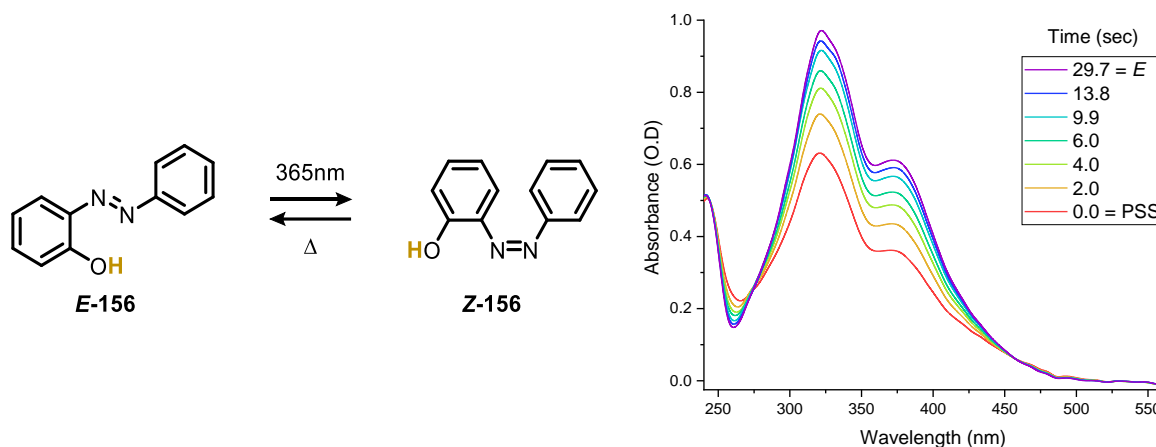


**Figure 33.** (left) Model 2-hydroxy-azobenzene **156** used to test the ability of the system to monitor switching behaviour. (right) Time resolved UV-Vis absorption spectrum of a 0.067 mM solution of **156** in MeCN during thermal relaxation at room temperature.

Using azobenzene **156**, a 67  $\mu$ M solution of **E-156** in acetonitrile (Figure 33b, top purple line) was irradiated at 365 nm ( $\lambda_{\text{max}}$  of **E-156** = 322 nm) until no further change in the absorption was observed, thereby reaching the photostationary state (PSS) (Figure 33b, bottom red line). Maintaining the sample at 25 °C, the irradiation was stopped, and the sample left to thermally relax back to the initial *E* isomer. Acquiring time resolved UV-Vis spectra during this process then allowed the spectral changes to be tracked and the half-life calculated. By monitoring the change in the absorbance at any given wavelength, an exponential decay curve can be generated from which the half-life of the metastable *Z*-isomer can be calculated using Equation 2a and b.

$$\text{a)} \quad y = A_1 e^{\left(\frac{-x}{t_1}\right)} \quad \text{b)} \quad t_{1/2} = t_1 \ln 2$$

**Equation 2.** a) Exponential decay equation b) half-life equation

Fitting decay functions (Equation 2a) to the changing absorbances at 324 nm or 380 nm, which correspond to the two  $\lambda_{\text{max}}$  peaks, gives the relaxation times ( $t_1$ ) of the Z-isomer which, using Equation 2b, then gives the respective half-lives ( $t_{1/2}$ ) for thermal relaxation. Based on the change in absorbance at 324 nm a half-life of 3.7 seconds was established while based on the change in absorbance at 380 nm a half-life of 4.0 seconds was established. These half-lives are in good agreement and would indicate that the calculated thermal relaxation is independent of the wavelength at which it is measured, as is essential. These measurements are also in good agreement with the relaxation timeframes expected based on other hydroxy azobenzene studies in the literature (0.4 – 50 seconds).<sup>188, 192</sup>

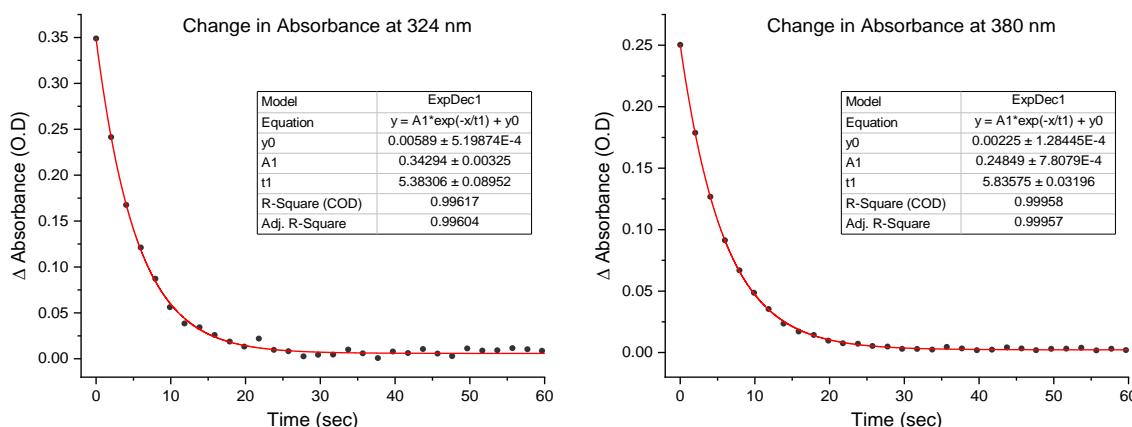


**Figure 34.** (left) The change in the absorbance at 324 nm of a 0.067 mM solution of **156** in MeCN during thermal relaxation. (right) The change in the absorbance at 380 nm of a 0.067 mM solution of **156** in MeCN during thermal relaxation.

Δ Absorbance defined as the difference between measured Absorbance and the Absorbance of the *E* isomer.

With the custom-built UV-Vis equipment shown to work for analysing simple azo systems which thermally relax on the second timescale, focus shifted towards using the equipment to study model systems that would be more reflective of the final motor. As such, the photoisomerization and subsequent thermal relaxation of the 4-hydroxy-chloro-azo-biaryl **132** was studied (Figure 35, left). As shown in Figure 35 (right), under 365 nm irradiation ( $\lambda_{\text{max}}$  of *E*-**132** = 346 nm) a significant change in the absorption spectra was observed going from the *E*-isomer (top purple line) to the PSS (bottom red line). Halting the irradiation and monitoring the thermal relaxation *via* time resolved UV-Vis spectroscopy, a rapid thermal relaxation response was observed with a notable increase in the intensity of the peak at 346 nm and a decrease in the intensity of the peak at 440 nm. Again, plotting the change in absorbance at these two wavelengths gives growth/decay curves which can be fitted with an exponential decay equation to calculate the half-life of the metastable Z isomer (Figure 36).

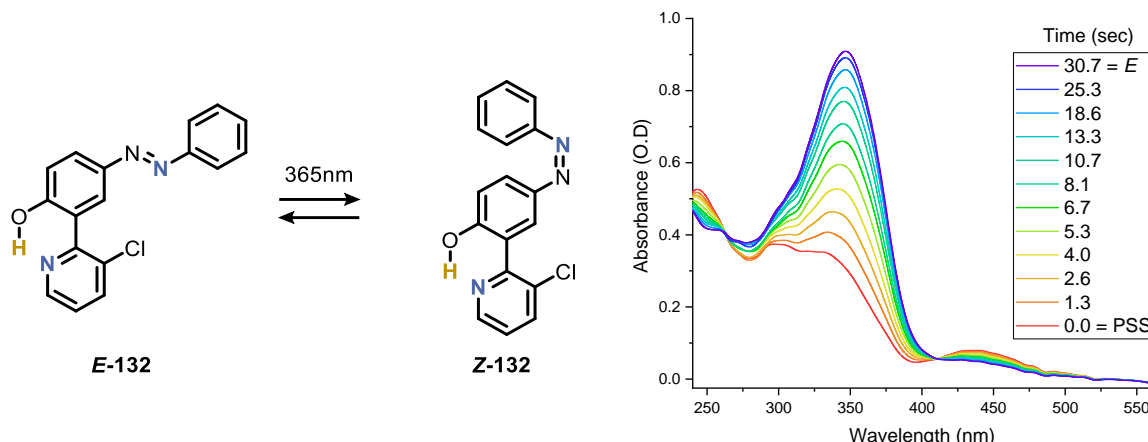


**Figure 35.** (left) Model hydroxy-azo-biaryl **132**. (right) Time resolved UV-Vis absorption spectrum of a 0.04 mM solution of **132** in MeCN during thermal relaxation at room temperature.

Calculating the thermal relaxation half-life ( $t_{1/2}$ ) of the *Z*-isomer based on the rate of change in the absorbance at 346 nm gives a half-life of 5.7 seconds, while calculation of the half-life based on the rate of change in absorbance at 440 nm gives a half-life of 6.4 seconds. These measurements are both in good agreement suggesting a half-life of six seconds ( $6.05 \pm 0.35$  sec). This is in a similar regime to that of the 2-hydroxy-azobenzene **156** as was expected based on the literature.<sup>188</sup> Also worthy of note is that the half-life measurements are in good agreement regardless of the size of the difference in absorbance (Figure 36, max  $\Delta$  Abs = 0.63 at 346 nm vs. max  $\Delta$  Abs = 0.03 at 440 nm) or the direction of change (growth or decay), highlighting the capability of this system for measuring these half-lives.

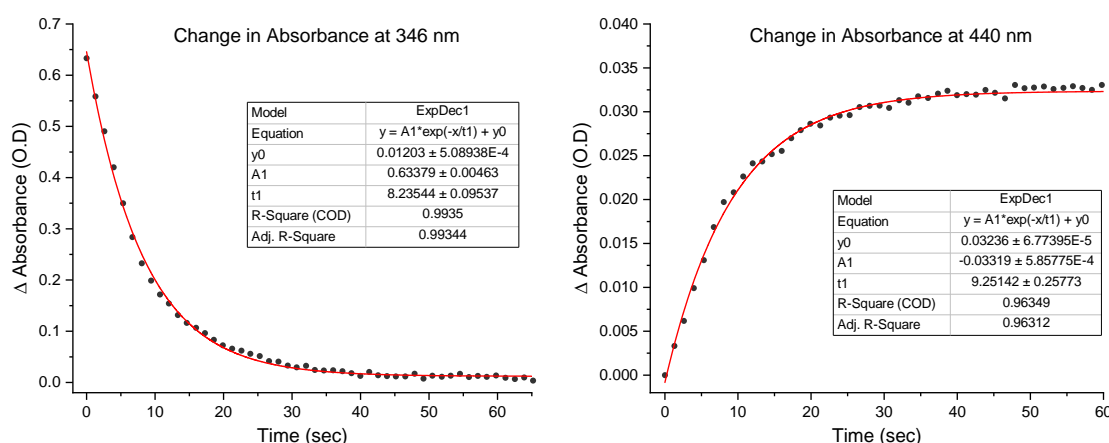


**Figure 36.** (left) The change in the absorbance at 346 nm of a 0.04 mM solution of **132** in MeCN during thermal relaxation. (right) The change in the absorbance at 440 nm of a 0.04 mM solution of **132** in MeCN during thermal relaxation.  $\Delta$  Absorbance defined as the difference between measured Absorbance and the Absorbance of the *E* isomer.

Looking to another model compound, 4-hydroxy-nitro-azo-biaryl **193**, which contained a nitro group in place of the previous chloro group, the photoswitching behaviour was again examined using time resolved UV-Vis spectroscopy (Figure 37). While a seemingly minor change, nitro benzenes are known to have significantly redshifted absorptions, and as such, it was of interest to test whether the introduction of the nitro group in the azo-biaryl system had any significant effect on the absorption properties or the photochemical behaviour.<sup>202</sup>

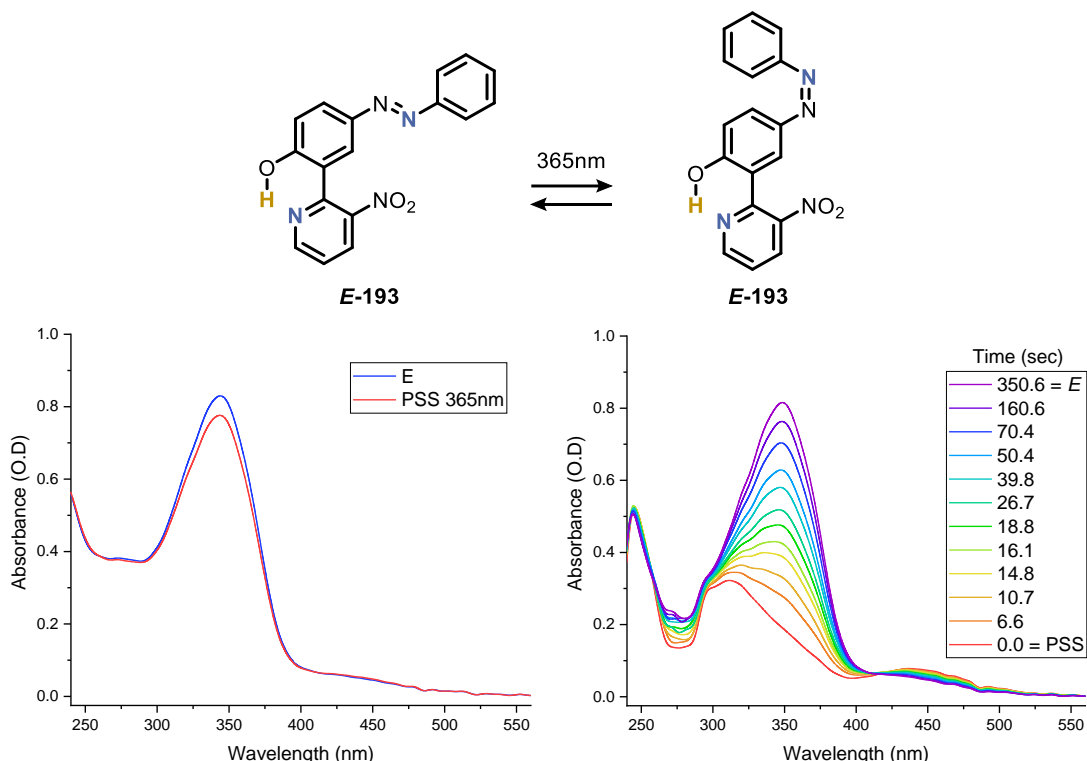


**Figure 37.** (top) Model hydroxy-azo-biaryl system **193**. (left) UV-Vis absorption spectrum of a 0.04 mM solution of **193** in MeCN pre and post irradiation. (right) Time resolved UV-Vis absorption spectrum of a 0.04 mM solution of **132** in THF during thermal relaxation at room temperature.

Unexpectedly, when irradiating a 0.04 mM solution of *E*-**193** in acetonitrile ( $\lambda_{\text{max}} = 343 \text{ nm}$ ) with 365 nm light, little-to-no photochemical response was observed (Figure 37, bottom left) but upon switching the solvent to THF ( $\lambda_{\text{max}} = 348 \text{ nm}$ ), a much more significant photochemical response was observed (Figure 37, bottom right). After irradiating the THF solution of *E*-**193** to reach the PSS (Figure 37, right, red line), the rate of thermal relaxation was measured using the time resolved UV-Vis spectrometry with the change in absorbance at 350 nm and 450 nm used to calculate the half-life of *Z*-**193**. Based on these changes, the half-lives of 30.0 seconds and 29.3 seconds were established respectively, which are in both in good agreement and suggest a thermal relaxation half-life of ~30 seconds (Figure

38). While this half-life is slightly longer than that of the structurally similar **Z-132** ( $t_{1/2} = 6$  s), these two half-lives have been calculated in two different solvents (THF vs. MeCN) and solvent choice is known to cause considerable change in the calculated thermal relaxation half-lives.<sup>188</sup> In a more extreme case, Velasco and co-workers have demonstrated a >74,000-fold decrease in the thermal relaxation half-life of their 4-hydroxy-azobenzenes when changing the solvent from toluene to ethanol.<sup>188</sup>

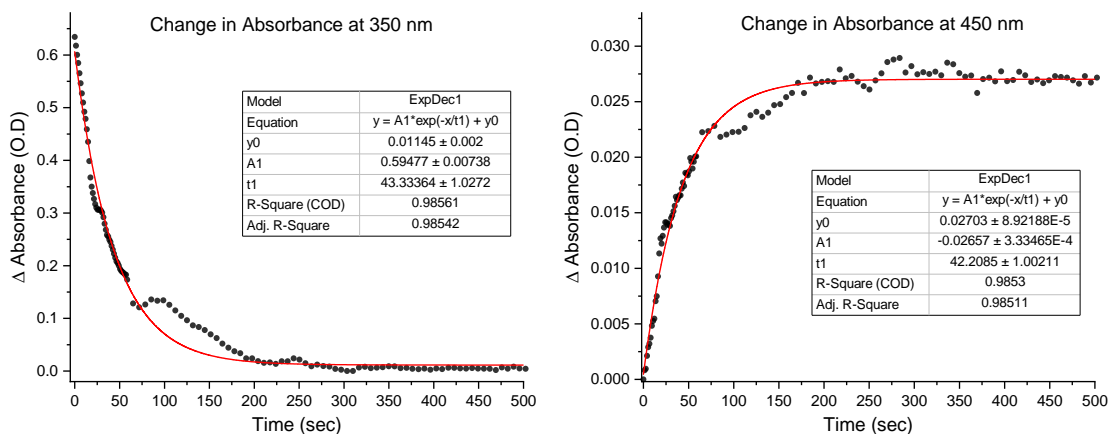


**Figure 38.** (left) The change in the absorbance at 350 nm of a 0.04 mM solution of **193** in THF during thermal relaxation.  
 (right) The change in the absorbance at 450 nm of a 0.04 mM solution of **193** in THF during thermal relaxation.  
 $\Delta$  Absorbance defined as the difference between measured Absorbance and the Absorbance of the *E* isomer.

While the change in absorbance at both 350 nm and 450 nm during thermal relaxation followed the expected exponential decay, the relaxation appeared to briefly stagnate at the 60 second mark (Figure 38, data points between 60 and 200 seconds). It is currently unknown whether this stalling is due to issues with the experimental setup, such as a lack of stirring causing localized heat pockets post-irradiation, or whether this stalling is attributable to unidentified reactivity properties of the compound itself. Further benchmarking of the system is still required with other systems which relax over similarly long time periods to test whether this stalling may be attributable to the equipment design. To ensure aggregation did not have an effect on the relaxation stalling, and ensure the concentrations being used for these experiments followed the Beer-Lambert law, the absorption spectra of **193** in THF was measured across a range of concentrations (Figure 39).<sup>203</sup> For the isomerization processes to be studied accurately, it is essential that the photoirradiation and analysis is being performed at concentrations that lie within the linear region of the Beer-Lambert regime (region where the absorbance is directly proportional to the concentration). The Beer-Lambert law ( $A = \varepsilon\ell c$ , where  $A$  is absorbance,  $\varepsilon$  is the molar absorptivity coefficient,  $\ell$  is the pathlength and  $c$  is

the concentration of the sample) assumes that the molecules absorbing radiation don't interact with each other and therefore deviation from this implies an interaction between analyte molecules (e.g., aggregation), making the analysis non-reflective of the system of study. By measuring the absorption spectra of the azo system **193** across a range of concentrations, a calibration curve, based on the change in absorbance at 348 nm ( $\lambda_{\text{max}} = 348 \text{ nm}$ ), can be generated to test the linearity of the relationship between the absorption and the concentration (Figure 39). From this, it was clear that there was a linear relationship between the absorbance and concentration of the sample up to the concentration used in the photoisomerization studies (40  $\mu\text{M}$ ). This meant the concentration used for the photoirradiation experiments is within the linear region of the Beer-Lambert regime, as required, and that compound aggregation should not have had any impact on the studies of **193**.<sup>203</sup>

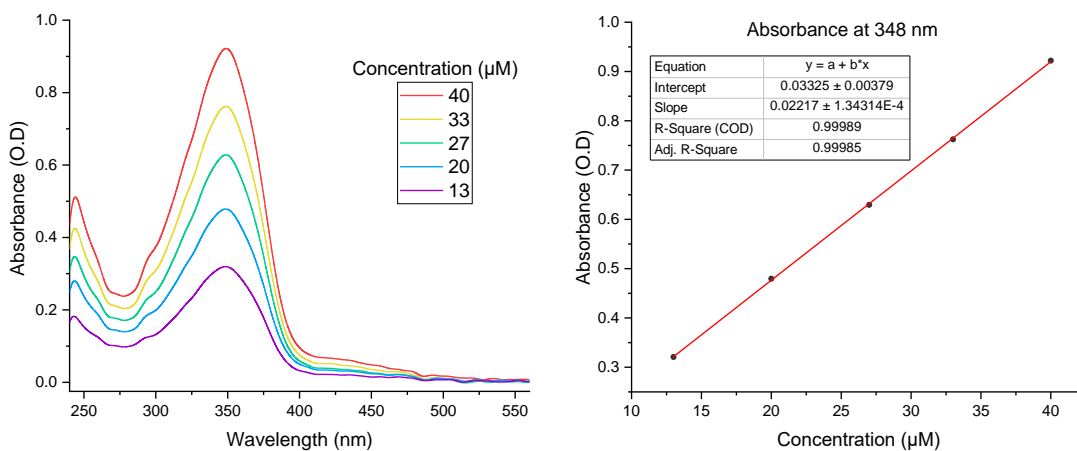


**Figure 39.** (left) Absorption spectra of E-193 across a range of concentrations and (right) the calibration curve of the absorbance versus concentration.

Although further studies into the cause of the photoisomerization inhibition of *E*-**193** in MeCN, and the brief stalling of the thermal relaxation after 60 seconds in THF are required, the study of **193** was particularly useful in highlighting the effect of the nitro group on the photochemical behaviour, the importance of solvent selection and for showing that these scaffolds are capable of photoisomerization and rapid thermal relaxation.

While there are still more developments to be made to the experimental setup, such as the inclusion of stirring, and more work remains to be done on studying the behaviour of the model systems, the UV-Vis equipment has been shown to be capable of acquiring data on short

timescales and under constant irradiation conditions. This has been extremely valuable for measuring the half-lives of the faster relaxing hydroxy azobenzenes and has allowed analysis of systems that could not have been studied using the previous setup (described in section 8.4.1). This equipment has also been useful for distinguishing between systems which lack a significant photochemical response, and systems in which fast thermal relaxation had previously prevented observation of the metastable intermediate.

### **5.4.2 NMR Spectroscopy**

The custom-built UV-Vis equipment has been particularly useful for enabling the visualization of the irradiation and thermal relaxation processes but, due to the nature of UV-Vis spectroscopy, the amount of information it can provide is limited. To gain a greater understanding of the photochemical processes, as well as the conformations and bonding of the metastable intermediates, attention turned to developing equipment which would allow the azo systems to be studied by NMR under constant irradiation. After testing light sources, fibre optic cables, focusing lenses and light-to-cable couplings, the system described in section 8.4.3 was built, allowing the irradiations to be performed directly in the NMR spectrometer.

Using the isomerization of azobenzene **26** as a model, a PSS of 37:63 (*E*:*Z*) under 365 nm irradiation was established using the previous experimental setup described in section 8.4.1. This was a particularly useful model system as the thermal relaxation ( $t_{1/2} = \sim 4$  hours) was slow enough to allow an accurate PSS to be established minutes after the cessation of irradiation.<sup>204</sup> Using this PSS as a benchmark, the ability of the new irradiation system (section 8.4.3) was tested. As shown in Figure 40, using the new equipment to irradiate fresh samples of azobenzene at varying concentrations directly inside the spectrometer, PSSs of 38:62 (1:1.62) and 40:60 (1:1.47) were established for the lower concentration samples (2mM and 5mM respectively). The observed PSSs in the 2mM (38:62) and 5mM (40:60) azobenzene solutions are both in good agreement with the PSSs established using the previous setup (37:63) suggesting the new setup was effective at achieving the desired *E*-to-*Z* isomerization, and crucially could do inside the spectrometer. Interestingly, in the higher concentration samples of 10mM and 20mM respectively, slower photoisomerization responses were observed and the established PSS of 37:62 was not reached after 10 minutes (Figure 40).

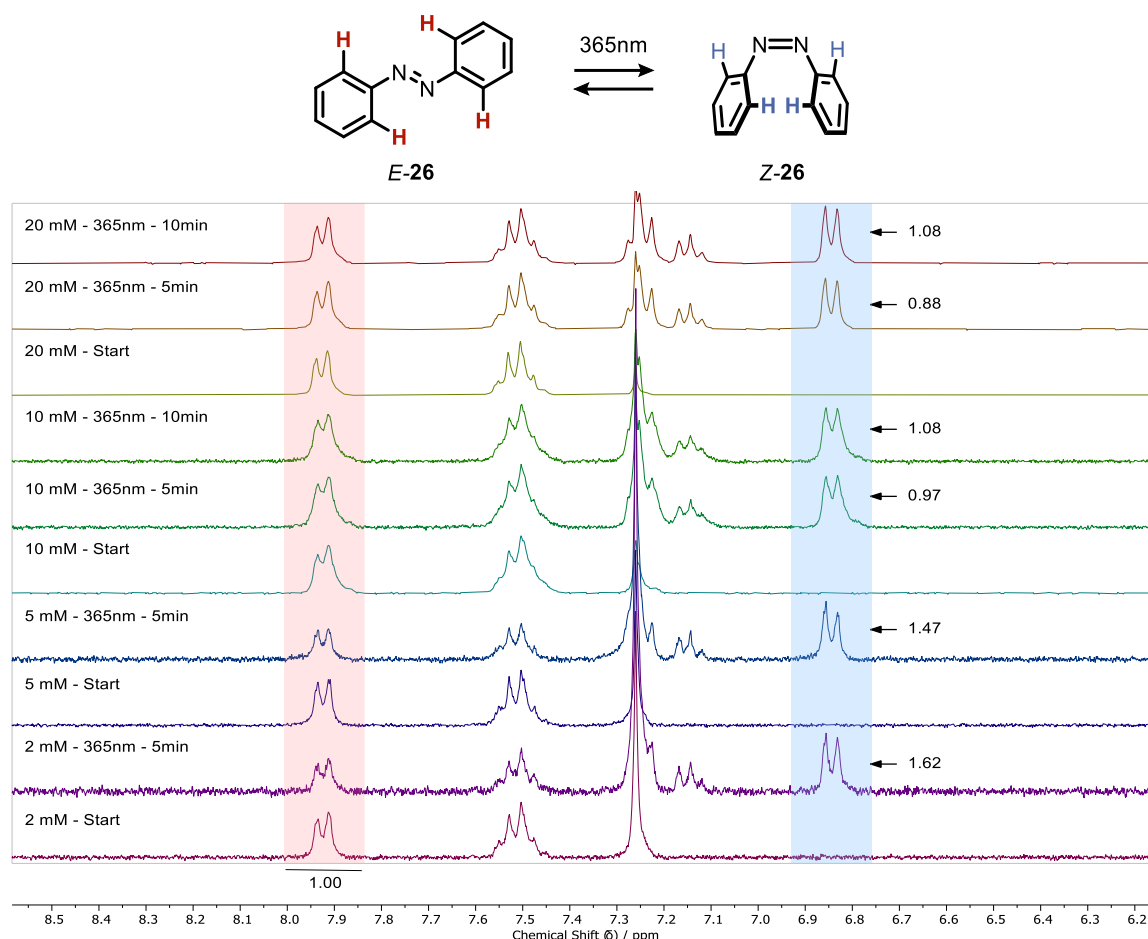


**Figure 40.** NMR irradiation of azobenzene **26** at varying concentrations using the new NMR irradiation equipment. Highlighted doublet peaks at ~7.9 ppm in red and ~6.8 ppm in blue, represent the four protons *ortho* to the azo unit in the *E* and *Z* isomers respectively and are used to establish the PSS composition.

The photoisomerization of azobenzene should not be a concentration dependant behaviour and since the irradiation at the higher concentrations shows lower *E*:*Z* ratios after longer periods of irradiation, a secondary effect must be impacting the photoisomerization. Two sources were identified for having the potential to cause this behaviour. First, if azobenzene **26** formed aggregates at the higher sample concentrations (10mM or 20mM), this would cause a significant change in the azobenzenes photophysical properties leading to altered photoisomerization responses.<sup>205, 206</sup> Second, the higher concentration samples may cause greater attenuation of the excitation light, and if the light source is weak, this would prevent enough photons penetrating through the sample thereby reducing the photoresponse in the parts of the sample further from the light source (akin to the primary inner filter effect).<sup>207</sup>

To test whether aggregation of the azobenzene might be occurring at the higher sample concentrations ( $>10$  mM), a concentration assay was performed (Figure 41). Monitoring the change in absorption at 376 nm (Figure 41, black arrow) across a range of concentrations, a calibration curve was generated which showed a linear relationship between the concentration and absorption up to concentrations of  $\sim 15$  mM (Figure 41, right). Due to equipment limitations, the optical path length for the analysis was fixed at 1 cm meaning that at the tested concentrations, the measured absorbances were exceedingly high ( $>1.0$ ) even at the lowest point of absorption (376 nm). Since absorbance is proportional to the optical path length and concentration according to the Beer-Lambert law  $A = \varepsilon\ell c$ , a shorter optical path would allow higher concentrations to be measured while keeping the absorbance below 1.0 (i.e 10% light transmittance since  $A = -\log(T)$ ). The current equipment is capable of accurately calculating absorbances up to 2.0, corresponding to 1% light transmittance through the sample, but it would still be ideal to investigate the  $>10$  mM sample concentrations using a shorter optical path length to improve the light transmittance and allow more accurate analysis.

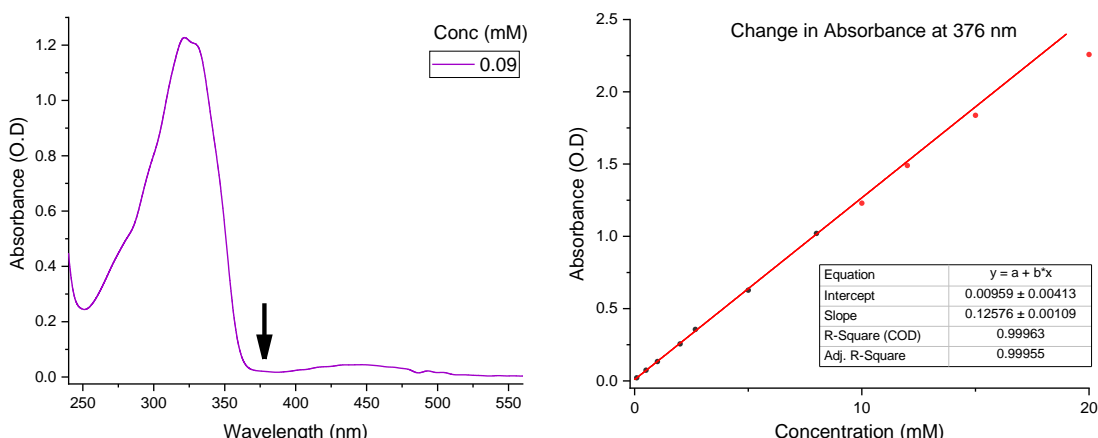


**Figure 41.** Study of azobenzene **26** absorbance at 376 nm across a range of concentrations to test for potential aggregation at the concentrations used for the NMR studies. Linear trendline is fitted based on the data points in black.

Based on the concentration calibration curve shown in Figure 41, there is a clear linear relationship between the absorbance and the sample concentration up to  $\sim 15$  mM indicating that no aggregation occurs at these sample concentrations of 15 mM or below. The final concentration measured at 20 mM deviates significantly from the linear trend, but due to the low light transmission caused by the high absorbance (if  $A = 2.5$  then  $T = 0.3\%$ ), deviation from the linear trend may be attributed to issues in detection rather than compound aggregation. Further investigation using a shorter optical path length is required to establish the linearity at

these concentrations. As azobenzene aggregation did not appear to be occurring at sample concentrations below 15 mM, it would not explain the slow photoisomerization response observed in the 10 mM solution when using the newer NMR irradiation equipment. As such, the light attenuation needs to be investigated further.

As long as no molecular changes to the azobenzene occur upon the change in concentration (e.g., aggregation, protonation, etc.), the quantum yield must remain unchanged. As the quantum yield remains unchanged upon the change in concentration, but a lower rate of *E*-to-*Z* photoisomerization is observed, this must be attributable to a lower number of photons being absorbed by the azobenzene since the quantum yield ( $\Phi$ ) equals the number of events divided by the number of photons absorbed. As mentioned above, if the sample concentration is increased it will cause more photons to be absorbed at the interface between the light source and the sample. This decreases the number of photons that permeate through the solution (i.e., increased sample attenuation), in turn, causing fewer photons to reach the molecules that are further from the light source. With a lower power output from the light source, fewer photons are emitted per second (by definition) and therefore the impact of the increased sample attenuation is larger with lower power light sources. The power output of the new NMR irradiation system has not yet been established but work into calculating the photon flux of the system (*via* potassium ferrioxalate actinometry) is planned.<sup>207</sup> Based on the power output of the light sources listed by the supplier (ThorLabs), the light source used for the *in-situ* NMR irradiation setup (15.5 mW using a Ø400  $\mu\text{m}$  Fiber) is approximately 80-fold less powerful than the light source being used for the previous photochemical experiments described in sections 8.4.1 and 8.4.2 (1290 mW). It should be noted that while these power outputs describe the number of photons emitted by the light source itself, it does not necessarily describe the number of photons that reach the sample in the experimental setups, hence the need for actinometry. As the light source for the NMR irradiation setup is less powerful, it would be expected that this system is more affected by the light attenuation of the sample. Further studies into establishing and increasing the power output of the equipment would be useful for facilitating the analysis of higher concentration samples. Although there appears to be some undesired sample concentration limitations to the NMR irradiation setup, at the lower concentrations (2 mM and 5 mM) the irradiation system is able to induce the desired *E*-to-*Z* photoswitching behaviour and can be used to study the photoisomerization of azobenzenes by NMR under constant irradiation.

To test whether this system could be used to study faster relaxing systems, irradiation of the fast relaxing 2-hydroxy-azobenzene **156** at room temperature was performed. Unfortunately, no photoisomerization was observed in this system which was believed to be attributable to the fast rate of thermal relaxation.<sup>208</sup> As discussed above, it was suspected that the power output of the NMR irradiation equipment was low due to the low power output of the light source. As such, the NMR irradiation equipment is likely to have a low photon flux (number of photons emitted per second per unit area). If the photon flux of the system is low, then the number *E*-to-*Z* photoisomerization events induced by the light source must be accordingly low. Although, upon photon absorption, the photochemical processes of the photoisomerisation is exceedingly fast, if there is a lack of photons to excite the compound, the number of *E*-to-*Z* photoisomerization events occurring per second will be low. This means that generating a significant population of the metastable isomer will take more time. Since this system was known to have a fast thermal relaxation half-life ( $t_{1/2} = 4$  s, section 5.4.1), it may be possible that the fast rate of thermal relaxation (*Z*-to-*E*) and low photon flux, prevent the buildup of the metastable *Z* isomer, in turn, preventing observation by NMR. This might indicate that further studies into increasing the power output of the system (as mentioned above) may be essential for monitoring the photoisomerization of the faster relaxing azobenzenes at room temperature. Further studies performing the isomerization at lower temperatures to slow the thermal relaxation would also provide useful insights for the later analysis of the motor system.

To test whether photoisomerization might be achieved on the motor candidate **187b** using the NMR irradiation equipment, the irradiation of the more stable synthetic intermediate **185b** was performed. As shown in Figure 42, upon irradiation of **185b** at 365 nm using the NMR irradiation equipment, a slow *E*-to-*Z* photoisomerization response was observed. It should be noted that this test was conducted before the concentration dependence study described above and needs to be repeated at lower concentrations. While the isomerization was slow, and a PSS under 365nm irradiation was not established, the appearance of the new peaks characteristic of the *Z*-isomer does show that a photoisomerization response can be observed in these types of scaffolds using the new equipment (Figure 42, purple trace). This is preliminary work and requires further study but does serve as a useful indication that these more heavily functionalized scaffolds retain the ability to photoswitch.

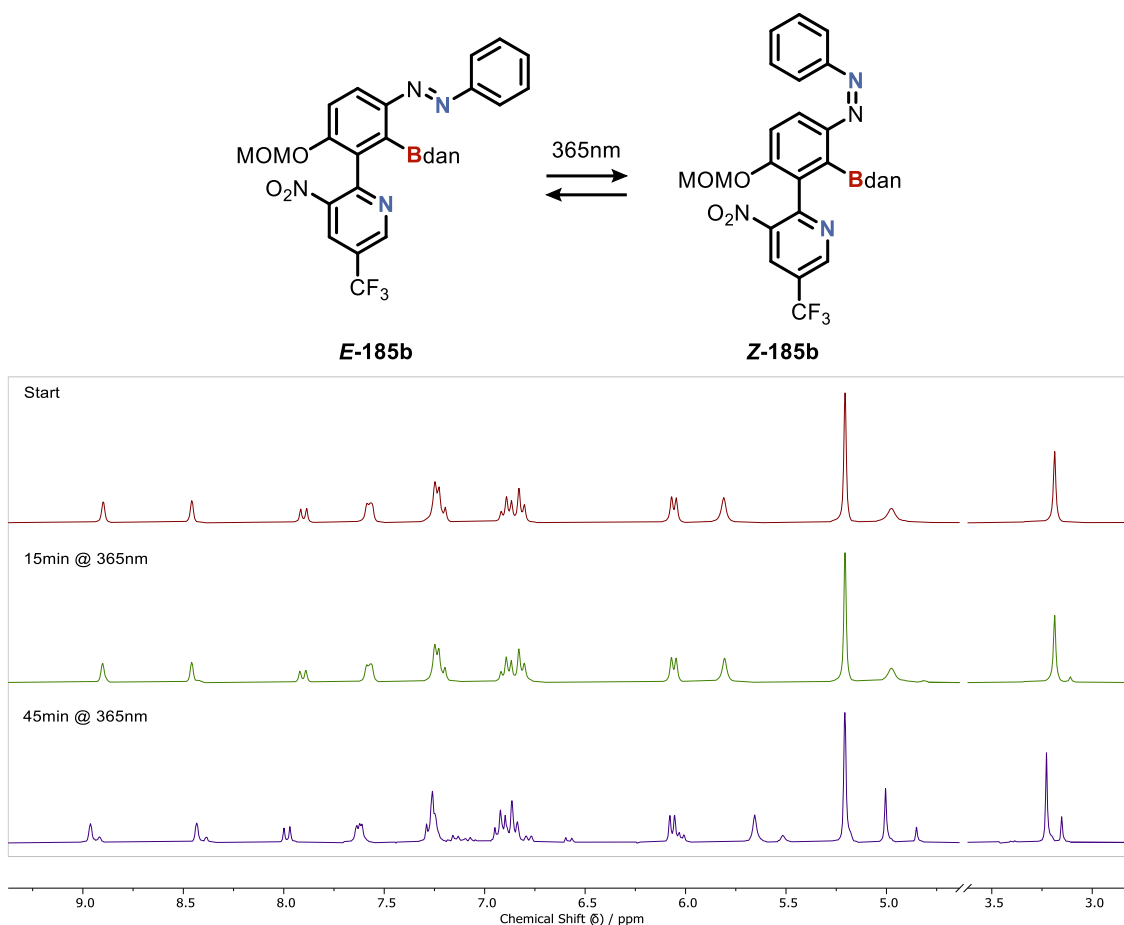


**Figure 42.** NMR study of azobenzene **185b** under constant irradiation in  $\text{CD}_2\text{Cl}_2$  showing the emergence of new peaks corresponding to the generation of the Z-isomer

Early work into the development of a system capable of performing irradiation experiments inside the NMR spectrometer has shown that at low sample concentrations, photoisomerization of azobenzene can be achieved and that these systems reach the same PSS as the benchmark provided by the system used in the previous irradiation studies. Photoswitching studies on the faster relaxing 2-hydroxy-azobenzene system **156** have shown that more work is required before the irradiation system can be used to study fast thermally relaxing systems at room temperature and suggests that increasing the power output of the system may be crucial for future studies. While it is highly likely that cooling the fast-relaxing systems to suppress the thermal relaxation would also allow the Z-isomer state to be observed, it would be useful to be able to observe the Z-isomer state at room temperature as cooling of the final motor systems is also likely to cause the diastereomers to emerge, complicating the spectral analysis. In a preliminary study, boryl-azo-biaryl scaffold **185b** also appears to exhibit

the desired photoisomerization using the NMR irradiation equipment, indicating that these highly substituted systems are still photoactive and can be studied using the new equipment.

## **5.5 Preliminary Studies of the Boryl-Azo-Biaryl **187b****

Now that a system capable of performing fast analysis under constant irradiation was available, motor candidate **187b** was re-examined using the new UV-Vis system (Figure 43). Irradiation of a THF mixture containing *E*-**187b** and DMT (used to help prevent dissociation of the ligand in **187b**) at 365 nm, resulted in a significant change in absorption, rapidly reaching the PSS (Figure 43, top red line down to bottom orange line). Halting the irradiation and monitoring the thermal relaxation using the UV-Vis system, showed that the system quickly relaxed back to the starting *E*-isomer within a matter of minutes. It should be noted that the timings for this experiment are presented as estimates due to an error in the timings of the data collection. Although the timings are not exact, and therefore a thermal relaxation half-life was not calculated, this behaviour was significant as it showed that not only was the desired motor scaffold **187b** light responsive, but that it also readily underwent the desired thermal relaxation. Also of note, was the shoulder-like peak around 425 nm (Figure 43), which from the previous studies (section 2.4.1) is known to be indicative of a N<sub>azo</sub>–B bond further supporting the formation of the desired N<sub>azo</sub>–B bond in compound **187b**. Analysis of this system should ideally be repeated using the improved data collection script given in section 8.6.5 so that the thermal relaxation half-life may be calculated. Although this data is preliminary, it represents an important milestone in proving that the primary motor candidate **187b** exhibits both photoisomerisation and thermal relaxation.

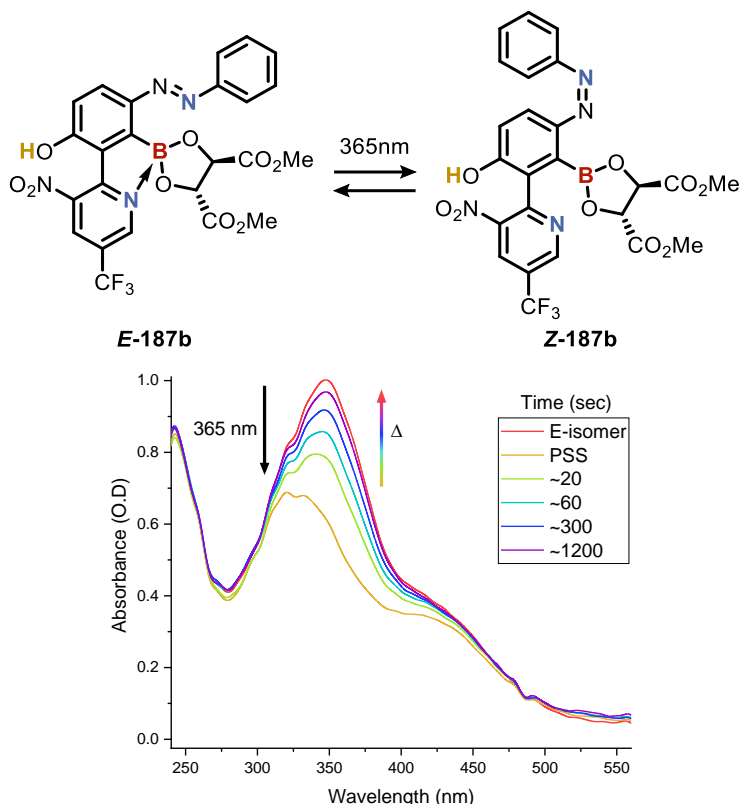


**Figure 43.** Preliminary study on the motor candidate **187b** in THF showing irradiation at 365 nm to reach the PSS and subsequent thermal relaxation at room temperature.

## 5.6 Summary of Chapter 5

Having established the need for new methods of N–B bond assessment in the boryl-azo-biaryl systems, attention turned to  $^{15}\text{N}$  HMBC where a series of model systems were studied to establish the expected shifts of the different nitrogen environments in differently bound states (section 5.2). With unambiguous and distinctive  $^{15}\text{N}$  shifts for the assessment of each nitrogen environment identified, the  $^{15}\text{N}$  shifts of the boryl-azo-biaryls **177**, **187a**, **191** and **187b** were measured and used to characterise the N–B bonds present in the lowest energy states. Based on this, **187b** was identified as the most suitable motor candidate as it possessed both the desired N–B bond in the lowest energy state and the potential to rotate around the central C–C bond (as opposed to **177**, which showed the desired bonding but did not have the ability to rotate). Further studies into the photoswitching behaviour of the azo-biaryls showed that the cyclized compound **177** was able to successfully photoswitch between the  $\text{N}_{\text{azo}}\text{-B}$  and  $\text{N}_{\text{pyr}}\text{-B}$  bonds, showing that this type of switching behaviour is possible and can be achieved in these azo-biaryl scaffolds. Initial attempts at the photoswitching of the motor candidate **187b** showed no signs of isomerisation prompting the development of new equipment (section 5.3). As the lack of observed photoresponse in **187b** was believed to be due to rapid thermal

relaxation, the development of the new equipment focused on being able to perform the analysis quickly and under constant irradiation (section 5.4). This led to the development of new UV-Vis equipment capable of acquiring time-resolved UV-vis spectra, as well as the development of new equipment for performing irradiations inside a NMR spectrometer. Both systems require further optimization and study, but the early benchmarking work shows that, within certain limits, these systems are both capable of performing the desired photoisomerizations with simultaneous monitoring. Preliminary work using these systems also suggests that the desired motor candidate **187b** is able to undergo both the desired photoswitching and the rapid (minute timeframe) thermal relaxation (section 5.5). This holds promise for future work as not only does the desired switching behaviour appear to be exhibited by candidate **187b**, but there is now equipment capable of analysing this behaviour.

## Chapter 6 Conclusions and Future Work

### 6.1 Model Systems

As the proposed motor system had a high degree of complexity with little literature precedent to underpin many design elements, two types of model system (the azo models and the biaryl models) were investigated to better understand the bonding, behaviour, and analytical properties of the proposed motor system. As discussed in Chapter 2, the study of the azo models gave useful insights into the relationships between the electron withdrawal of the boron ligand, the strength of the  $\text{N}_{\text{azo}}\text{-B}$  bond, and the observed photoswitching ability of the azobenzene (Figure 44). Through these studies, (+)-DMT was identified as the most viable candidate for use as a ligand in the proposed motor. Further ultrafast and computational studies are currently underway, led by Prof. Andrew J Orr-Ewing and A. Prof. Basile Curchod, which focus on understanding how the formation of different strength  $\text{N}_{\text{azo}}\text{-B}$  bonds affect the excited state dynamics of these azo systems.

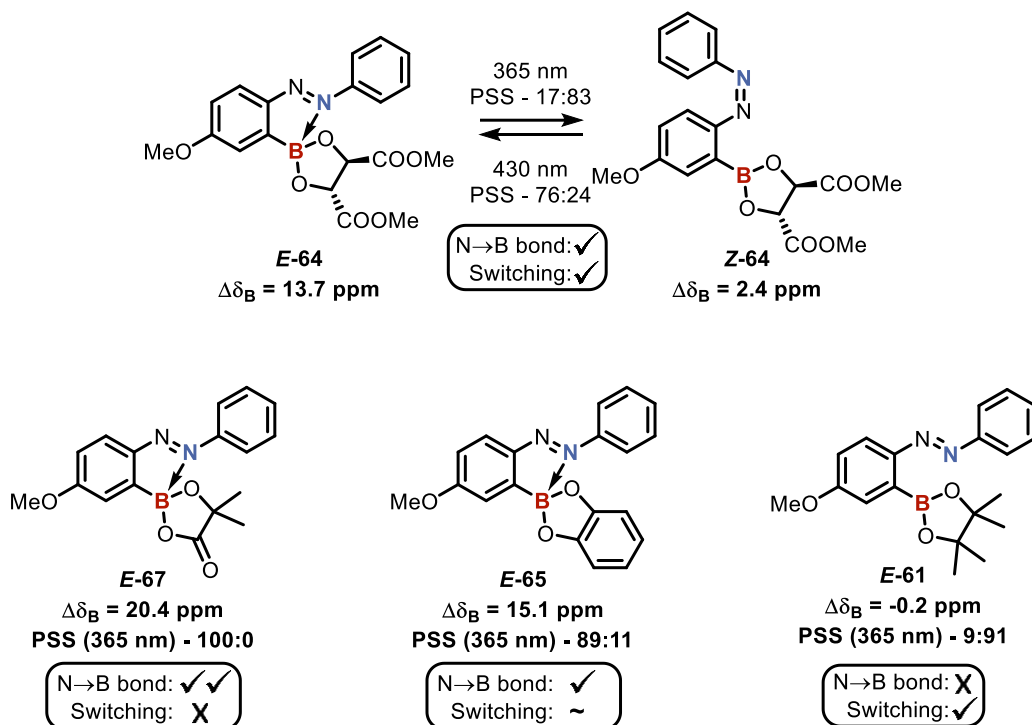


**Figure 44.** Summary of the investigations into the azo model systems from chapter 2.

While the studies on the azo systems gave a useful degree of insight into the requirements for the  $\text{N}_{\text{azo}}\text{-B}$  bond formation as well as the effect on the photochemical properties, the studies on the biaryl model systems, discussed in Chapter 3, also gave

particularly useful insights into tuning the strength of the N<sub>pyr</sub>–B bonds, how the formation of these bonds affects the barrier to rotation and showed that it is possible to use chiral ligands on the boron centre to influence the chirality of the biaryl axis (Figure 45).

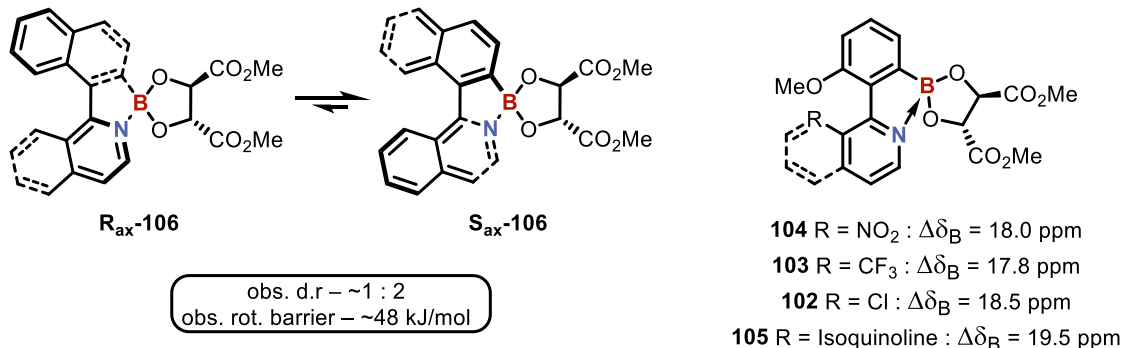
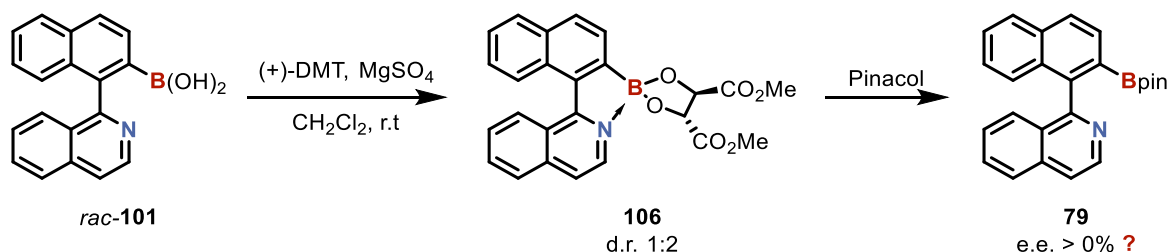


**Figure 45.** Summary of the investigations into the biaryl pyridine model systems from chapter 3.

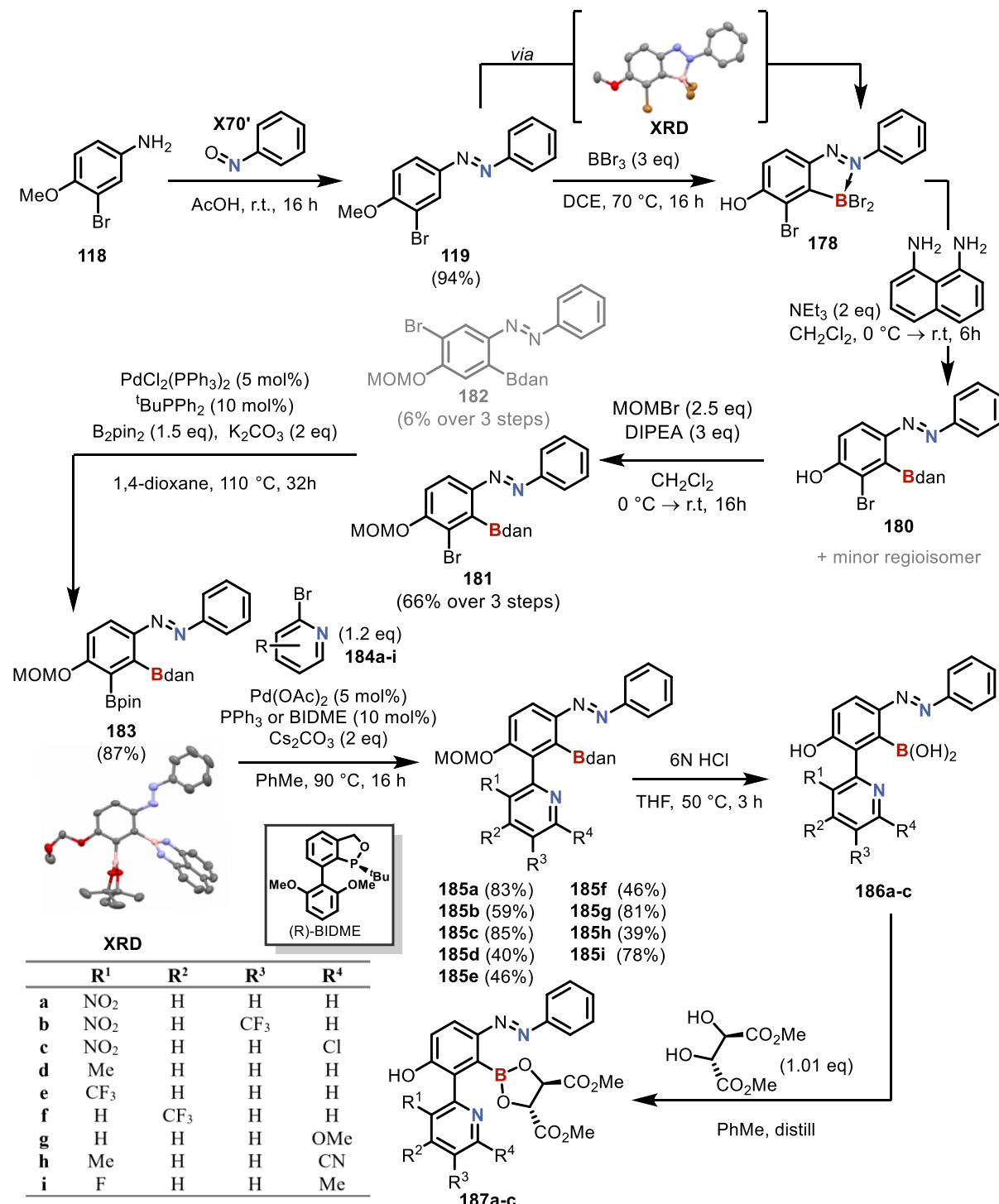
Based on the findings from Chapter 3, investigations have begun into performing a thermodynamic deracemization by exploiting the ability of the biaryl pyridines to form N<sub>pyr</sub>–B bonds (Scheme 41). In the proposed system, the dehydrative coupling of the chiral ligand to the racemic boronic acid generates compound **106** which from the studies in section 3.4 is known to be labile around the biaryl axis and have a preference for one of the two diastereomers. Treatment with pinacol then causes substitution of the DMT ligand for the pinacol due to the greater stability of the pinacol boronic ester, generating compound **79**.<sup>209</sup> Due to the electronics of the pinacol ligand, the N<sub>pyr</sub>–B bond is broken, causing a significant increase in the barrier to rotation and preventing the two atropisomers of **79** from interconverting at room temperature. If the d.r. from **106** can be retained during the pinacol substitution, it may be possible to achieve enantioenrichment of **79**. Further work into this is ongoing but it highlights the potential use of these findings beyond the proposed molecular motor discussed herein.



**Scheme 41.** Proposed thermodynamic deracemization by exploiting the selective rotation barrier lowering caused by the formation of a N<sub>pyr</sub>–B bond.

## 6.2 Synthesis and Bonding Analysis

Having worked through various synthetic approaches, a serendipitously discovered borylation methodology played a central role in the synthesis of the desired boryl-azo-biaryl scaffolds. A late-stage Suzuki coupling allows a multitude of different boryl-azo-biaryl scaffolds to be rapidly generated which could then be used for further analysis (Scheme 42).



Scheme 42. Final synthetic route to the boryl-azo-biaryl scaffolds as described in chapter 4.

As discussed in Chapter 5 (sections 5.2.1 and 5.2.2), using  $^{15}\text{N}$  HMBC and  $^{11}\text{B}$  NMR the  $^{15}\text{N}$  and  $^{11}\text{B}$  shifts of a series of boryl-azo-biaryls were measured and compared against various controls to establish which N–B bonds were present. From this, the desired  $\text{N}_{\text{azo}}\text{–B}$  bond was found to form in the lowest energy states of compounds **187b** and **177** (Figure 46).

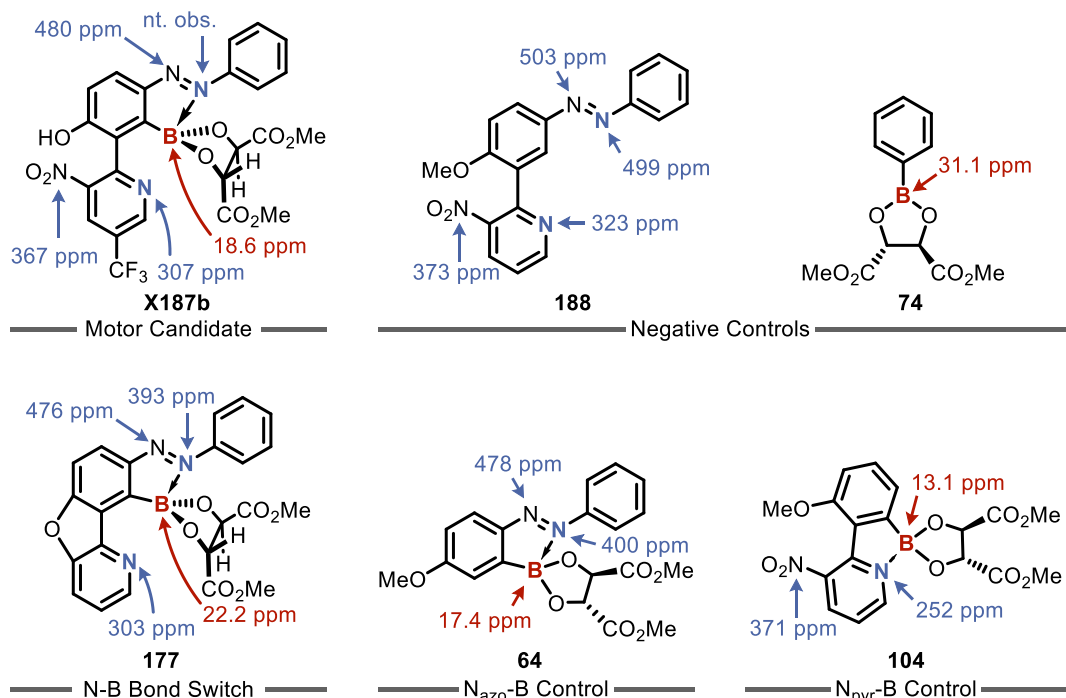


**Figure 46.** Summary of the  $^{11}\text{B}$  and  $^{15}\text{N}$  analysis from chapter 5.

While establishing the  $^{15}\text{N}$  shifts of the azobenzene played a crucial role in understanding the intramolecular bonding, significant challenges were faced when trying to identify the shifts for the azo nitrogens. To better analyse the proposed motor candidate **187b**, incorporation of a  $^{15}\text{N}$  nucleus into the azobenzene unit (Figure 46, **187b** blue azo nitrogen) would be highly desirable. This would not only allow better confirmation of the bonding in the lowest energy state but could allow the use of direct-detect  $^{15}\text{N}$  NMR and potentially allow the monitoring the  $^{15}\text{N}$  chemical shift during the irradiation studies. Although it may be costly,  $^{15}\text{N}$  isotope labelling of this position is viable using  $^{15}\text{N}$ -aniline (~£250/g – Sigma Aldrich) to form the  $^{15}\text{N}$  labelled nitrosobenzene ( $^{15}\text{N}$ -) **70**. This compound could then be carried through the synthetic route shown in Scheme 42 to generate ( $^{15}\text{N}$ )-**187b**.

Having established the intramolecular bonding *via*  $^{15}\text{N}$  and  $^{11}\text{B}$  NMR analysis, photoisomerization studies of the boryl-azo-biaryl **177** were performed which investigated the changes to the N–B bonds by  $^{11}\text{B}$  NMR. These studies suggest that the system is able to switch between the  $\text{N}_{\text{azo}}\text{-B}$  and  $\text{N}_{\text{pyr}}\text{-B}$  bonds upon irradiation, even when using a more electron withdrawing ligand to induce stronger  $\text{N}_{\text{azo}}\text{-B}$  bonds that were shown in Chapter 2 to be more challenging to break.

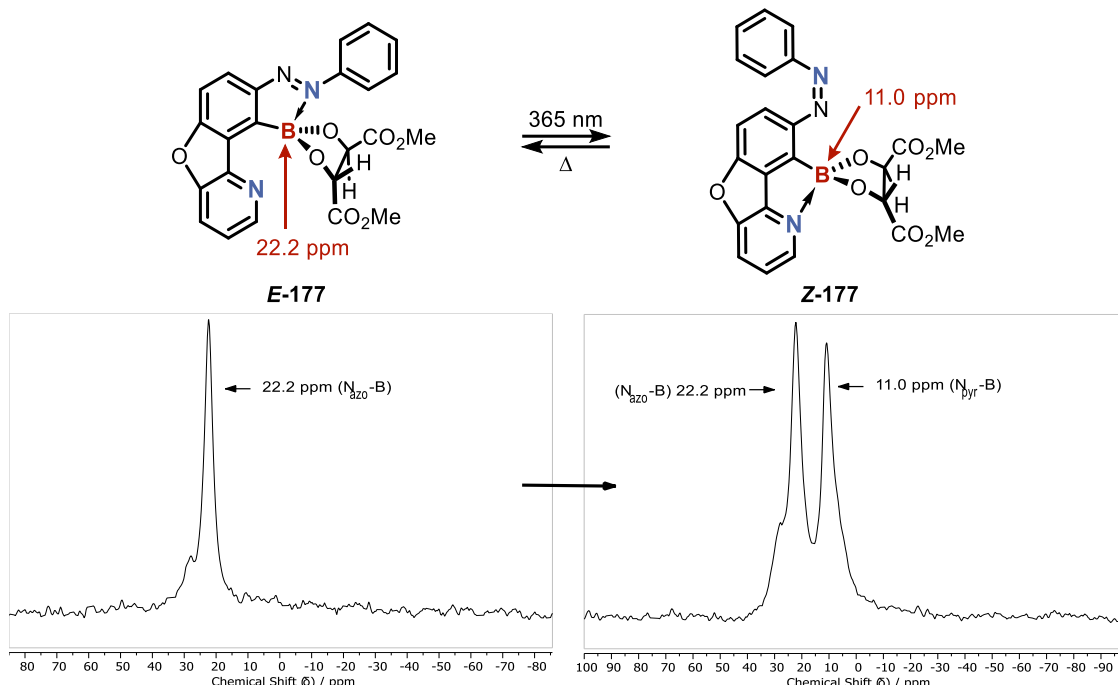


**Figure 47.** Example of the N–B bond photoswitching observed in borylated-azo-biaryl **177** upon irradiation at 365 nm.

Interestingly the photoisomerization studies of the *ortho*-blocked scaffold **187c** indicated that the azobenzene could photoswitch and break the  $\text{N}_{\text{azo}}\text{-B}$  bond and hinted at the possibility of the subsequent  $\text{N}_{\text{pyr}}\text{-B}$  bond formation being controlled by the chirality of the boron ligand. Further studies into these types of *ortho*-blocked scaffolds would be of significant value both for understanding the interaction between the chiral ligand and the biaryl axis, as well as for identifying new ways of controlling the balance between  $\text{N}_{\text{azo}}\text{-B}$  and  $\text{N}_{\text{pyr}}\text{-B}$  bond formation.

### 6.3 Equipment Development

Having tested the photoisomerisation of motor candidate **187b** and observing no changes by NMR, new analytical equipment was built to study these azo systems under

constant irradiation (section 5.4). Looking first to UV-Vis spectrometry (section 5.4.1), a new, highly modular, system was built based on using broad-spectrum light for sample analysis as described in sections 5.4.1 and 8.4.2. Using this equipment, the thermal relaxation of a variety of hydroxy azobenzenes was studied and the equipment demonstrated to be capable of monitoring both the azo systems under constant irradiation and during fast thermal relaxation (Figure 48). Further benchmarking of the UV-Vis system is still required so that it can be used for quantum yield measurements, with further developments such as the inclusion of a stirring system, and more user friendly software also being particularly valuable.

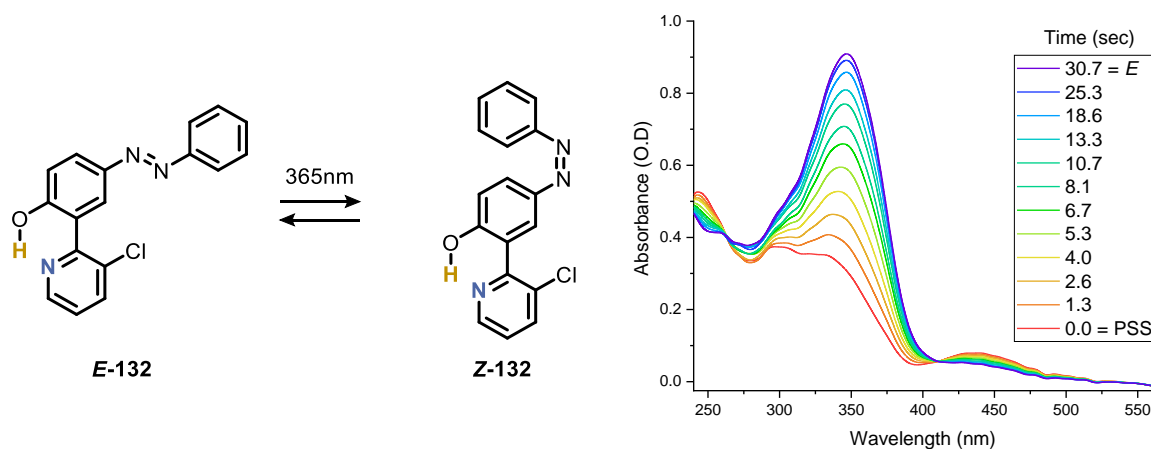


**Figure 48.** Example study of the fast-relaxing model azobenzene **132** ( $t_{1/2} = 6$  s) that could be studied *via* time-resolved UV-Vis spectrometry enabled by the newly built equipment as discussed in chapter 5.

To understand the photochemical behaviour of these systems beyond changes in their absorption spectra, a new experimental setup was developed to enable the irradiation of samples directly in the NMR spectrometer. At low sample concentrations ( $\leq 5$  mM), the equipment was shown to produce a photoisomerization response equivalent to that observed with the previous *ex-situ* equipment, showing that the equipment is capable of studying the azobenzene systems under constant irradiation. Further work measuring, and ideally increasing, the power output of the system is still required before being used to assess the photochemical behaviour of the motor candidate **187b**. Work to increase the power output of this system is particularly desirable as it would improve the ability of the system to study fast relaxing azobenzene systems at room temperature and might also allow the studies to be performed at higher sample concentrations. Increasing the sample concentrations is particularly desirable as due to the design of the system, the sample volume is limited meaning the  $^{11}\text{B}$  NMR analysis at low concentrations becomes particularly challenging.

## 6.4 Remaining Work

Summarizing the work above in the context of the proposed motor, an ideal boron ligand has been identified (Figure 49, R<sup>2</sup> identification), the ligand has been shown to influence the chirality of a biaryl axis (Figure 49, model of d.r. in state B), the required N<sub>azo</sub>–B and N<sub>pyr</sub>–B bonds have been shown to form (Figure 49, N–B bond formation in state A and state B), a desirable pyridyl ring to favour the N<sub>azo</sub>–B bond in state A has been identified (Figure 49, identification of R<sup>1</sup> and N<sub>azo</sub>–B bond formation in state A), the photoswitching between the two N<sub>azo</sub>–B and N<sub>pyr</sub>–B bonds has been shown to be possible in a cyclized model system (Figure 49, change of N–B bonds during state A and state B interconversion), the motor has been shown to be photoresponsive and able to undergo rapid thermal relaxation (Figure 49, state A and state B interconversion without proof of N<sub>pyr</sub>–B bond), and the newly built UV-Vis and NMR equipment has been shown to allow the monitoring of these systems under constant irradiation.

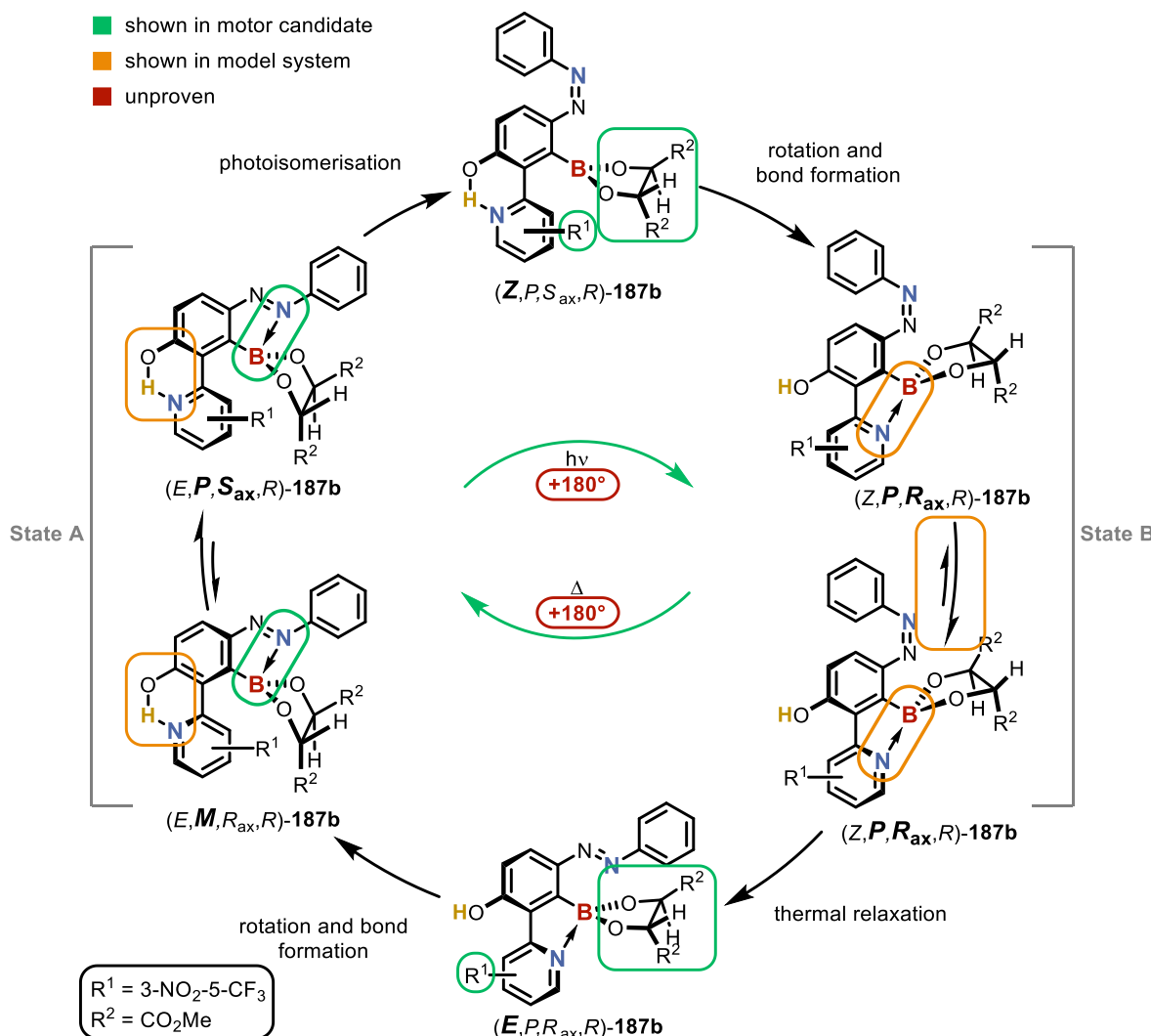


**Figure 49.** The proposed operational cycle presented in section 1.8 highlighting the different elements of the design that have been studied.

While the N<sub>pyr</sub>-B has been observed in model systems, and the preliminary time-resolved UV-Vis study indicates the motor candidate **187b** undergoes the required photoisomerization, the formation of the N<sub>pyr</sub>-B bond in **187b** remains unproven. Once the NMR irradiation equipment has been adequately benchmarked and optimized, it can be used to irradiate the motor candidate **187b**, generating the metastable Z-isomer, and allowing the presence of the N<sub>pyr</sub>-B bond to be assessed in state B.

As highlighted in Figure 49, the required H-bond has also been identified and studied in other similar model azo-biaryl scaffolds but has not yet been identified in the boryl-azo-biaryl scaffold **187b**. Further work into other analytical techniques, or into improving compound purity may be required in order to visualise the H-bond. It is critical that the H-bond forms in the lowest energy conformation of **187b** as this provides the drive for the rotation around the central C-C bond. As neither the H-bond nor the N<sub>pyr</sub>-B bond have yet been identified in **187b**, the rotation around the central C-C single bond in response to the photoisomerization still remains unproven.

The final element of this system which has been studied in model systems but not on compound **187b**, is the chirality transfer from the boron ligand to the biaryl axis (Figure 49, state B). In state A, the system should exhibit a 6-membered bridging interaction (H-bond) which lowers the barrier to rotation but does so to a far lesser extent than the 5-membered bridging interaction (N<sub>pyr</sub>-B bond) proposed in state B. As such, it is more likely that the energy barrier to rotation and the transfer of chirality will be observed in state A than it will be in state B when using low temperature NMR. Based on the failed attempts at measuring chirality transfer in compounds **102** and **105** (see section 3.2) it is likely that the barrier to rotation in Z-**187b** will be too low for the two separate axial isomers to be observed, even at -80 °C. Due to this, it is likely that the chirality transfer in state A can be established by low temperature NMR analysis of *E*-**187b** while the chirality transfer in state B will likely need to be assessed based on model systems and computational analysis.

To truly make this system a new class of rotary motor, the rotation around the central C-C bond must be net unidirectional. While the chirality of the boron ligand has been proposed to drive the unidirectional rotation by favouring one diastereomer in both state A and state B,

similar to the rotor systems described in section 1.2, this implies that the directionality of the rotation would be governed by differences in the energy levels of the ground state species. As each step will proceed through different transition states, it is also possible that the operational cycle of the motor could be governed by the differences in transition state energies. This means that a detailed understanding of the energy flow of the system, particularly in regard to the different transition state energies, will be essential in assessing the directionality of the rotor. Further computational work into the transition state, excited state, and ground state energies of the intermediates of this system are now being investigated under the guidance of A. Prof. Basile Curchod. This should provide a deeper understanding of the energy flow of this system and allow the directionality to be more clearly assessed.

The most significant challenge faced in the generation and analysis of these boryl-azo-biaryl systems has reliably been the poor compound stability and solubility. As such, it would be highly valuable to identify new methods of improving both of these factors. Identification of structural changes that will improve compound stability (or solubility) is often a challenging task and can require significant trial-and-error. Given the number of requirements for the design of the azo-biaryl motor scaffolds, there are limited positions at which functionalisation can be done without preventing the motors proposed operation. Equally, this provides particularly clear positions at which stability related functionalisation could be done. Investigations into using longer chain tartrate-based ligands (e.g., dioctyl-tartrate) may provide improved stability or introducing substituents on the upper azo ring may also identify a method of improving the stability (and solubility) of **187b**.

Significant steps towards the development of the first light-fuelled single bond rotor have now been made with several studies deriving from the discoveries made during this project currently underway. With a viable synthetic route, the analytical equipment ready, benchmarks from model studies established and the core design principles underpinning the proposed system validated, achieving the desired light-fuelled single bond rotor is within reach.

## Appendix

---

### Chapter 7 Appendix

#### List of Abbreviations

<b>δ</b>	NMR Chemical Shift (ppm)
<b>+ve</b>	Positively Charged
<b>-ve</b>	Negatively Charged
<b><sup>1</sup>H NMR</b>	Proton Nuclear Magnetic Resonance
<b><sup>11</sup>B NMR</b>	Boron-11 Nuclear Magnetic Resonance
<b><sup>13</sup>C NMR</b>	Carbon-13 Nuclear Magnetic Resonance
<b><sup>19</sup>F NMR</b>	Fluorine-19 Nuclear Magnetic Resonance
<b>Ac</b>	Acetyl
<b>APCI</b>	Atmospheric-Pressure Chemical Ionization
<b>aq.</b>	Aqueous
<b>Ar</b>	Aryl
<b>ATP</b>	Adenosine Triphosphate
<b>BINOL</b>	1,1'-Bi-2-naphthol
<b>Bn</b>	Benzyl
<b>BOC</b>	<i>tert</i> -Butoxycarbonyl
<b>Bpin</b>	Pinacol Boronic Ester
<b>br.</b>	Broad
<b>cat.</b>	Catalytic
<b>Calc.</b>	Calculated
<b>CBS</b>	Corey–Bakshi–Shibata
<b>CCD</b>	Charge Coupled Detector
<b>CIP</b>	Cahn–Ingold–Prelog
<b>Conc.</b>	Concentrated
<b>COSY</b>	<sup>1</sup> H- <sup>1</sup> H Homonuclear Correlation Spectroscopy
<b>Cp</b>	Cyclopentadienyl
<b>CPL</b>	Circularly Polarized Light
<b>COD</b>	1,5-Cyclooctadiene
<b>d</b>	Doublet
<b>DCC</b>	N,N'-Dicyclohexylcarbodiimide
<b>dd</b>	Doublet of Doublets
<b>ddd</b>	Doublet of Doublet of Doublets

## Appendix

---

<b>DFT</b>	Density Functional Theory
<b>DI</b>	De-ionized
<b>DIPEA</b>	N,N-Diisopropylethylamine
<b>DKR</b>	Dynamic Kinetic Resolution
<b>DMAP</b>	4-Dimethylaminopyridine
<b>DMT</b>	Dimethyl tartrate
<b>DMF</b>	<i>N,N</i> -dimethylformamide
<b>DMSO</b>	Dimethyl Sulfoxide
<b>DNA</b>	Deoxyribonucleic Acid
<b>dppf</b>	1,1'-Bis(diphenylphosphino)ferrocene
<b>d.r.</b>	Diastereomeric Ratio
<b>EDCI</b>	1-Ethyl-3-(3-dimethylaminopropyl)carbodiimide
<b>EDTA</b>	Ethylenediaminetetraacetic Acid
<b>e.e.</b>	Enantiomeric Excess
<b>EI</b>	Electron Ionization
<b>eq.</b>	Equivalents
<b>ESI</b>	Electrospray Ionization
<b>Et</b>	Ethyl
<b>FID</b>	Free induction decay
<b>FT-IR</b>	Fourier Transform Infrared Spectroscopy
<b>g</b>	Grams
<b>h</b>	Hours
<b>Hex</b>	Hexane
<b>HMBC</b>	Heteronuclear Multiple Bond Correlation Spectroscopy
<b>HPLC-MS</b>	High Pressure Liquid Chromatography–Mass Spectrometry
<b>HRMS</b>	High Resolution Mass Spectrometry
<b>HSQC</b>	Heteronuclear Single Quantum Correlation Spectroscopy
<b>Hz</b>	Hertz
<b>IUPAC</b>	International Union of Pure and Applied Chemistry
<b>J</b>	Coupling Constant
<b>L</b>	Ligand
<b>L.A.</b>	Lewis Acid
<b>m</b>	Multiplet

## Appendix

---

<b>M</b>	Moles per Litre
<b>Me</b>	Methyl
<b>MIDA</b>	N-methylimidodiacetic
<b>MOM</b>	Methoxymethyl Ether
<b>Mp</b>	Melting Point
<b>MS</b>	Mass Spectrometry
<b>m/z</b>	Mass to Charge Ratio
<b>NBS</b>	N-Bromosuccinimide
<b>NIS</b>	N-Iodosuccinimide
<b>NHC</b>	N-Heterocyclic Carbene
<b>NMR</b>	Nuclear Magnetic Resonance
<b>Nu</b>	Nucleophile
<b>Ph</b>	Phenyl
<b>pin</b>	Pinacol
<b>PMB</b>	<i>para</i> -Methoxybenzyl
<b>ppm</b>	Parts per Million
<b>PSS</b>	Photostationary State
<b>RBF</b>	Round Bottom Flask
<b>Rf</b>	Retention Factor
<b>RF</b>	Radio Frequency
<b>r.t.</b>	Room Temperature
<b>s</b>	Singlet
<b>sat.</b>	Saturated
<b>t</b>	Triplet
<b>TBC</b>	To be confirmed
<b><sup>t</sup>Bu</b>	<i>tert</i> -Butyl
<b>THF</b>	Tetrahydrofuran
<b>THI</b>	Thermal Helix Inversion
<b>TIDA</b>	tetramethyl <i>N</i> -methylimidodiacetic acid
<b>TMP</b>	2,2,6,6-Tetramethylpiperidine
<b>TLC</b>	Thin Layer Chromatography
<b>Ts</b>	Tosyl
<b>UV</b>	Ultraviolet

## **Appendix**

---

<b>Vis</b>	Visible
<b>VT</b>	Variable Temperature
<b>XRD</b>	X-Ray Diffraction

## Appendix

---

### List of Figures

Figure 1. a) Representation of a molecular switch with the microscopically reverse pathway in grey. b) Representation of a molecular motor with the microscopically reverse pathway in grey.....	2
Figure 2. a) IUPAC recommended axial chirality terminology for biaryl systems. b) Helicity terminology for biaryl systems used herein. c) IUPAC recommended helicity terminology used in helicene systems. d) Helicity terminology used in alkene motor systems. ....	3
Figure 3. Common photoresponsive compounds used in artificial systems. (a) Stilbene ( $Y = CH$ ) and Azobenzene ( $Y = N$ ); (b) Indigos ( $Y = NR$ where $R = \text{any alkyl or aryl group}$ ) and Thioindigo ( $Y= S$ ); (c) dithienylethenes.....	15
Figure 4. Molecular Scissors from Aida and co-workers.83 .....	25
Figure 5. a) Schematic representation of the operational cycle using 2D structures. Naming follows: (point chirality of Me group)-(Helicity of alkene)-(Helicity of biaryl axis)-(axial chirality of biaryl axis)-compound number b) Top down view of the Sax cycle highlighting the point chirality ( $S$ ), helicity of alkene rotor ( $Ma/Pa$ ), helicity of the biaryl ( $Mb/Pb$ ) and axial chirality of the biaryl ( $Rb$ ).89 .....	28
Figure 6. Breakdown for the analysis of the proposed system using boryl-azobenzene and boryl- biaryl-pyridine models.....	34
Figure 7. Summary of the borylated-azobenzene compounds made by Kawashima and co-workers with the relative difference in $^{11}B$ NMR shift shown as a measure of Nazo-B bond strength. n.t – not tested.97 .....	36
Figure 8. Proposed rationale for the N-B bond strength control based on electron donation into the empty p-orbital. .....	37
Figure 9. Diol ligands 52-56 initially selected for photoswitch testing. ....	37
Figure 10. UV-Vis spectra in MeCN of selected boryl-azobenzenes 48, 66, 63, 64 and 65. ....	42
Figure 11. Literature systems which probe the extent of the Npyr-B bond in various biaryl- pyridines. ....	50
Figure 12. $\Delta\delta B$ values for biaryl-pyridines 93-96 and 102-105 used for the assessment of the Npyr-B bonds.....	54
Figure 13. Low temperature VT-NMR study of 106 in $CD_2Cl_2$ showing peak coalescence of the gold (left), purple (middle) and green (right) colour coded protons. ....	55
Figure 14. Comparison of the calculated barrier to rotation for compound 106 against the literature examples 108 and 109 from Wild and co-workers.119 .....	56
Figure 15. Twisted, prebound phenol-pyridines from Ott and co-workers.128 .....	58
Figure 16. Barriers to rotation and half-lives of racemization at room temperature of various naphthyl phenols.....	59

## Appendix

---

Figure 17. a) Generic phenyl MIDA boronate. b) Azobenzene MIDA boronate highlighting the steric clash and the competition for N–B bond formation. c) Attempted synthesis of the proposed malonic acid substitute.....	73
Figure 18. General pulse sequence for HMQC/HMBC NMR experiments. HMBC experiment differs only by the inclusion of the RF pulse in grey which serves to remove the 1-bond correlations.	84
Figure 19. $^{11}\text{B}$ and $^{15}\text{N}$ NMR control systems used to analyse the intramolecular bonding present in the azo-biaryl systems.....	86
Figure 20. $^{11}\text{B}$ and $^{15}\text{N}$ NMR data for selected boryl-azo-biaryl compounds.....	87
Figure 21. $^{13}\text{C}$ shifts of control systems and boryl-azo-biaryls used to analyse the intramolecular bonding present in the azo-biaryl systems.....	90
Figure 22. $^{11}\text{B}$ NMR data for selected boryl-azo-biaryl compounds 185e-f to assess the effects of substitution pattern.	91
Figure 23. Comparison of the $^1\text{H}$ and $^{15}\text{N}$ shifts of the pyridyl-phenol biaryl 190 against the respective negative controls 192 and 88.....	92
Figure 24. Comparison of the $^1\text{H}$ shifts of azo-biaryls 132, 193, 148 and 194 corresponding to the protons involved in the H-bond interaction.	93
Figure 25. Photoswitching of borylated-azo-biaryl 177. $^{11}\text{B}$ NMR spectra pre (left) and post (right) irradiation at 365 nm showing the emergence of a new $^{11}\text{B}$ peak at 11.0 ppm. For the sake of clarity, the $^{11}\text{B}$ shift representing the Nazo–B bond in the post-irradiation spectra is manually referenced to 22.2 ppm to match the $^{11}\text{B}$ shift observed in the pre-irradiation spectra.....	95
Figure 26. a) 6,5,5,6 ring systems reported in the literature. b) Trost and co-workers structural studies on compound 195.193–197.....	96
Figure 27. Photoswitching of borylated-azo-biaryl 200. $^{11}\text{B}$ NMR spectra pre (left) and post (right) irradiation at 365 nm showing the emergence of a new $^{11}\text{B}$ peak at 6.4 ppm.	98
Figure 28. Photoswitching of borylated-azo-biaryl 187c. $^{11}\text{B}$ NMR spectra pre (left) and post (right) irradiation at 365 nm showing a change in the ratios of the $^{11}\text{B}$ peaks.	99
Figure 29. Desired but unobserved photoswitching of compound 187b.	101
Figure 30. Perpendicular optical paths for irradiation and analysis.	102
Figure 31. a) A simplified workflow of a typical UV-Vis spectrometer (e.g., Cary 5000) and b) A simplified workflow of the system built for the study of the azobenzene isomerization.	102
Figure 32. Czerny–Turner design monochromator, which separates a single beam of broad-spectrum light into the individual wavelengths where the intensities of each wavelength can be measured using a charge-coupled device (CCD).	103
Figure 33. (left) Model 2-hydroxy-azobenzene 156 used to test the ability of the system to monitor switching behaviour. (right) Time resolved UV-Vis absorption spectrum of a 0.067 mM solution of 156 in MeCN during thermal relaxation at room temperature.	104

## Appendix

---

Figure 34. (left) The change in the absorbance at 324 nm of a 0.067 mM solution of 156 in MeCN during thermal relaxation. (right) The change in the absorbance at 380 nm of a 0.067 mM solution of 156 in MeCN during thermal relaxation. $\Delta$ Absorance defined as the difference between measured Absorbance and the Absorbance of the E isomer. ....	105
Figure 35. (left) Model hydroxy-azo-biaryl 132. (right) Time resolved UV-Vis absorption spectrum of a 0.04 mM solution of 132 in MeCN during thermal relaxation at room temperature. ....	106
Figure 36. (left) The change in the absorbance at 346 nm of a 0.04 mM solution of 132 in MeCN during thermal relaxation. (right) The change in the absorbance at 440 nm of a 0.04 mM solution of 132 in MeCN during thermal relaxation. $\Delta$ Absorance defined as the difference between measured Absorbance and the Absorbance of the E isomer. ....	106
Figure 37. (top) Model hydroxy-azo-biaryl system 193. (left) UV-Vis absorption spectrum of a 0.04 mM solution of 193 in MeCN pre and post irradiation. (right) Time resolved UV-Vis absorption spectrum of a 0.04 mM solution of 132 in THF during thermal relaxation at room temperature. ....	107
Figure 38. (left) The change in the absorbance at 350 nm of a 0.04 mM solution of 193 in THF during thermal relaxation. (right) The change in the absorbance at 450 nm of a 0.04 mM solution of 193 in THF during thermal relaxation. $\Delta$ Absorance defined as the difference between measured Absorbance and the Absorbance of the E isomer. ....	108
Figure 39. (left) Absorption spectra of E-193 across a range of concentrations and (right) the calibration curve of the absorbance versus concentration. ....	109
Figure 40. NMR irradiation of azobenzene 26 at varying concentrations using the new NMR irradiation equipment. Highlighted doublet peaks at ~7.9 ppm in red and ~6.8 ppm in blue, represent the four protons ortho to the azo unit in the E and Z isomers respectively and are used to establish the PSS composition. ....	111
Figure 41. Study of azobenzene 26 absorbance at 376 nm across a range of concentrations to test for potential aggregation at the concentrations used for the NMR studies. Linear trendline is fitted based on the data points in black. ....	112
Figure 42. NMR study of azobenzene 185b under constant irradiation in CD <sub>2</sub> Cl <sub>2</sub> showing the emergence of new peaks corresponding to the generation of the Z-isomer.....	115
Figure 43. Preliminary study on the motor candidate 187b in THF showing irradiation at 365 nm to reach the PSS and subsequent thermal relaxation at room temperature. ....	117
Figure 44. Summary of the investigations into the azo model systems from chapter 2. ....	119
Figure 45. Summary of the investigations into the biaryl pyridine model systems from chapter 3. ....	120
Figure 46. Summary of the <sup>11</sup> B and <sup>15</sup> N analysis from chapter 5.....	122
Figure 47. Example of the N–B bond photoswitching observed in borylated-azo-biaryl 177 upon irradiation at 365 nm. ....	123

## Appendix

---

Figure 48. Example study of the fast-relaxing model azobenzene 132 ( $t^{1/2} = 6$ s) that could be studied via time-resolved UV-Vis spectrometry enabled by the newly built equipment as discussed in chapter 5.....	124
Figure 49. The proposed operational cycle presented in section 1.8 highlighting the different elements of the design that have been studied.....	125
Figure 52. Light intensity detected with MeCN or THF solutions used for UV-vis absorption spectra background.....	244
Figure 53. Photostationary State composition of Azobenzene 26 under 365 nm and 430 nm irradiation.....	246
Figure 54. Photostationary State composition of Azobenzene 64 under 365 nm and 430 nm irradiation.....	247
Figure 55. Photostationary State composition of Azobenzene 64 under 365 nm and 430 nm irradiation in the presence of pyridine. ....	248
Figure 56. Photostationary State composition of Azobenzene 61 under 365 nm and 430 nm irradiation.....	249
Figure 57. Photostationary State composition of Azobenzene 65 under 365 nm and 430 nm irradiation.....	250
Figure 58. Photostationary State composition of Azobenzene 66 under 365 nm and 430 nm irradiation in the presence of pyridine. ....	251
Figure 59. Photostationary State composition of Azobenzene 48 under 365 nm and 430 nm irradiation.....	252
Figure 60. Photostationary State composition of Azobenzene 49 under 365 nm and 430 nm irradiation.....	253
Figure 61. Photostationary State composition of Azobenzene 49 under 365 nm and 430 nm irradiation in the presence of pyridine. ....	254
Figure 62. Crystal structure of 126 with the anisotropic displacement parameters depicted at the 50% probability level and hydrogens omitted for clarity. ....	255
Figure 63. Crystal structure of 177 with the anisotropic displacement parameters depicted at the 50% probability level. Solvent molecule and hydrogens, except those on the heteroatoms, omitted for clarity.....	255
Figure 64. Crystal structure of 155 with the anisotropic displacement parameters depicted at the 50% probability level. Disorder and hydrogens omitted for clarity. ....	255
Figure 65. Crystal structure of 183 with the anisotropic displacement parameters depicted at the 50% probability level. Disorder and hydrogens, except those on the heteroatoms, omitted for clarity.....	256
Figure 64. Addition of excess water to compound 194 to disturb the H-bond thereby proving its presence in the anhydrous conditions. Borad peak corresponding to the H-bond in the top	

## **Appendix**

---

*spectrum (red label) shifts upfield and shows significant line broadening indicating the H-bond is disturbed by the presence of water. Significant upfield shifting is also observed for the peaks corresponding to the azo hydrogens labelled in orange and blue. ....261*

## Appendix

---

### List of Schemes

Scheme 1. Bringmann and co-workers 6-membered-bridge-containing biaryl which exhibited a diastereomeric preference based on the point chirality of the methoxy group. <sup>42</sup> .....	5
Scheme 2. Feringa and co-workers' first unidirectional single-bond rotary motor. (1) Allyl deprotection and lactonization; (2) Asymmetric lactone reduction, reinstallation of the allyl protecting group and oxidation to reform the carboxylic acid; (3) para-Methoxy benzyl deprotection and lactonization; (4) Asymmetric lactone reduction, reinstallation of the PMB protecting group and oxidation to reform the carboxylic acid. <sup>44</sup> .....	6
Scheme 3. Feringa and co-workers most recent 6-step biaryl rotor. a) MOM and Ester deprotection b) EDCI lactonization. c) hydrolysis and MOM protection d) Bn and Ester deprotection e) EDCI lactonization. f) hydrolysis and Bn protection. <sup>50</sup> .....	8
Scheme 4. Feringa and co-workers' palladium mediated unidirectional single-bond rotary motor. <sup>46</sup> .....	9
Scheme 5. Leigh and co-worker's autonomous carbodiimide fuelled anhydride hydrolysis motor. <sup>51</sup> 11	
Scheme 6. Feringa and co-worker's carbodiimide fuelled lactone hydrolysis motor. <sup>53</sup> .....	12
Scheme 7. Operation of the first light-driven unidirectional molecular motor. Stilbene moiety highlighted in orange in first step. <sup>19</sup> .....	16
Scheme 8. Two-stroke imine rotor which operates through sequential non-microscopically reverse out-of-plane rotation and subsequent in-plane inversion. <sup>68</sup> .....	18
Scheme 9. Photon-only molecular rotor. SBR = single bond rotation, DBI = double bond isomerization, HT = Hula twist. <sup>64</sup> .....	19
Scheme 10.a) Gyroscope systems from Tamaoki and co-workers in which the rate of rotation could be controlled by the state of the azobenzene photoswitch. b) different aryl ring rotors used in Tamaoki and co-workers gyroscopes. <sup>74-76, 78</sup> .....	21
Scheme 11. Garibay and co-workers gyroscope system. <sup>77</sup> .....	22
Scheme 12. Overcrowded alkene gearbox system with freely rotating xylyl ring in blue, rotor in red and stator in black. <sup>80</sup> .....	23
Scheme 13. Andreasson and co-workers photoswitchable supramolecular complex. Ar = Si(C <sub>6</sub> H <sub>13</sub> ) <sub>3</sub> , R = 3,5-di-tert-butyl-1-ethynylbenzene. 4-AP = 4-aminopyridine. <sup>81</sup> .....	24
Scheme 14. Aida and co-workers' host-guest system. <sup>87</sup> .....	26
Scheme 15. Linked biaryl-hemithioindigo system from Dube and co-workers. Naming follows: (point chirality of the sulfoxide)-(geometry of the alkene bond)-(helicity of alkene rotor)-(axial chirality of biaryl)-compound number. <sup>92</sup> .....	29
Scheme 16. Proposed borylated-azo-biaryl system in which interconversion between two 180° rotary states can be controlled using light. ....	31

## Appendix

---

Scheme 17. Proposed borylated-azo-biaryl system in which directional 360° rotation could be achieved using light. Naming follows: (azobenzene geometry)-(helicity of the biaryl)-(axial chirality of biaryl)-(point chirality of the ligand)-compound number. ....	32
Scheme 18. Synthesis of the model borylated-azobenzenes used for ligand testing. ....	39
Scheme 19. Synthesis of phenyl boronic ester reference compounds. ....	40
Scheme 20. Synthetic route to the borylated biaryl-pyridines 102-106 ....	52
Scheme 21. Synthesis of the hemilabile ligand for the iridium-catalysed borylation. ....	53
Scheme 22. Retrosynthetic strategy for the generation of the proposed borylated azo-biaryl where PG = protecting group. ....	60
Scheme 23. Synthesis of biaryl-azobenzene 121 and attempted functionalizations. ....	61
Scheme 24. Unexpected C–H borylation identified during the attempted methoxy deprotection. Single-crystal XRD structure drawn with ellipsoids at 90% probability and hydrogen atoms omitted for clarity. ....	62
Scheme 25. Proposed SEAr type mechanism for the azobenzene directed $BBr_3$ borylation. ....	63
Scheme 26. Possible resonance forms of the Wheland intermediates that are accessible during the SEAr step with the two forms that are proposed to be the most stable underlined. ....	66
Scheme 27. Test Suzuki-Miyaura Cross-coupling to assess the compatibility of the $BBr_2$ functional group with palladium catalysed reactions. ....	67
Scheme 28. Attempted $BBr_3$ borylation on the azo-biaryl-scaffold. ....	68
Scheme 29. Preparation of 134, 135 and 136 to test the protecting group stability towards $BBr_3$ . ....	68
Scheme 30. Attempted $BBr_3$ borylation of the protected azo-biaryls 134-136. ....	69
Scheme 31. Synthesis of the fluorinated azo-biaryl scaffold. ....	70
Scheme 32. Proposed synthetic approach to the borylated-azo-biaryl scaffold 158 using hydroxylation as a masking group strategy. ....	71
Scheme 33. $H_2O_2$ mediated hydroxylations of boryl-azobenzenes 155 and 126. ....	71
Scheme 34. Testing of copper-mediated halogenation and borylation reactions on these substrates. ....	72
Scheme 35. Synthesis of the TIDA protecting group and subsequent coupling to the boryl azobenzene. ....	74
Scheme 36. Synthesis of Bdan azobenzenes to test the dan masking group approach. ....	75
Scheme 37. Model Suzuki cross-coupling for testing Bdan orthogonality. ....	78
Scheme 38. Synthetic route to the cyclised boryl-azo-biaryl 177. Single-crystal XRD structure drawn with ellipsoids at 90% probability and hydrogen atoms omitted for clarity. ....	79
Scheme 39. Divergent synthetic route used to generate boryl-azo-biaryl scaffolds 187a-d. Single-crystal XRD structure drawn with ellipsoids at 90% probability and hydrogen atoms omitted for clarity. ....	81

## Appendix

---

<i>Scheme 40. Synthesis of <math>\alpha</math>-hydroxy-isobutyric acid based boryl-azo-biaryl 200.....</i>	97
<i>Scheme 41. Proposed thermodynamic deracemization by exploiting the selective rotation barrier lowering caused by the formation of a Npyr-B bond.Synthesis and bond Analysis.....</i>	120
<i>Scheme 42. Final synthetic route to the boryl-azo-biaryl scaffolds as described in chapter 4.....</i>	121
<i>Scheme 43. Rhodium catalysed borylation from Crudden and co-workers which was only viable on the planar biaryl-pyridine 201 with attempts at the borylation of 87 proving unsuccessful.</i>	124
.....	258

## Appendix

---

### List of Tables

Table 1. $^{11}\text{B}$ NMR chemical shifts of the E isomers of the boryl-azobenzenes in $\text{CDCl}_3$ and the upfield shifts from their corresponding phenylboranes. The targeted systems of interest are highlighted in yellow. a $\Delta\delta\text{B} = \delta\text{B} (\text{phenylborane}) - \delta\text{B} (2-(\text{phenylazo})\text{phenylborane})$ . b in $\text{DMSO-d}_6$ . c in $\text{C}_6\text{D}_6$ . d Data from <90% pure compound was used due to compound instability. e Data confirmed by ref 103.....	41
Table 2. Photostationary states of the boryl-azobenzenes after three hours of irradiation in $\text{CDCl}_3$ at 365 nm or 430 nm. The DMT system of interest is highlighted in yellow. a in $\text{C}_6\text{D}_6$ .....	43
Table 3. $^{11}\text{B}$ NMR chemical shifts of the Z isomers of the boryl-azobenzenes in $\text{CDCl}_3$ and the upfield shifts from their corresponding phenylboranes. The DMT system of interest is highlighted in yellow. a $\Delta\delta\text{B} = \delta\text{B} (\text{phenylborane}) - \delta\text{B} (2-(\text{phenylazo})\text{phenylborane})$ . b in $\text{C}_6\text{D}_6$ .....	46
Table 4. $\Delta\delta\text{B}$ values of the E and Z isomers of boryl-azobenzenes 46, 64 and 66 in $\text{CDCl}_3$ (or $\text{C}_6\text{D}_6$ where indicated) with or without 1.3 equivalents of pyridine present. The DMT system of interest is highlighted in yellow. a $\Delta\delta\text{B} = \delta\text{B} (\text{phenylborane}) - \delta\text{B} (2-(\text{phenylazo})\text{phenylborane})$ . b 1.3 equivalents of pyridine added. c in $\text{C}_6\text{D}_6$ .....	47
Table 5. PSS of boryl-azobenzenes 46, 64 and 66 in $\text{CDCl}_3$ (or $\text{C}_6\text{D}_6$ where indicated) with or without 1.3 equivalents of pyridine present. The DMT system of interest is highlighted in yellow. a1.3 equivalents of pyridine added. bIn $\text{C}_6\text{D}_6$ .....	48
Table 6. Summary of the N–B bond and Photoisomerization data presented in chapter 2. The DMT system of interest is highlighted in yellow. a1.3 equivalents of pyridine added. bIn $\text{C}_6\text{D}_6$ .....	49
Table 7. Miyaura borylation condition screening with the optimal conditions highlighted in yellow. a Reported yields are calculated by $^1\text{H}$ NMR using 1,3,5-trimethoxy benzene as an internal standard. .....	76
Table 8. Suzuki cross-coupling ligand testing with the optimal conditions highlighted in yellow. a Reported yields are calculated by $^1\text{H}$ NMR using 1,3,5-trimethoxy benzene as an internal standard. Isolated yield given in parentheses.....	78
Table 9. Crystal data and structure refinement. ....	257
Table 10. Short reoptimization of the borylation methodology from Lassaletta and co-workers to use more forcing conditions as it was noted in their paper that electron deficient pyridyl rings were more challenging to borylate. <sup>115</sup> .....	258
Table 11. Second screen of the hindered Suzuki cross-coupling with pyridine rings lacking an ortho Nitro substituent .....	260

### Chapter 8 Experimental Data

#### 8.1 General Experimental Details

*Reagents and solvents.* Reactions with air- or moisture-sensitive materials were carried out in dried glassware under a nitrogen atmosphere using standard Schlenk line techniques. Bulk solutions were evaporated under reduced pressure using a Büchi or IKA rotary evaporator. Unless otherwise stated, all reagents, catalysts, and solvents were obtained from commercial sources and were used without further purification. All anhydrous solvents were commercially supplied or, in the case of toluene, dichloromethane, diethyl ether, tetrahydrofuran, acetonitrile or hexane, provided by the communal stills of the School of Chemistry, University of Bristol (Anhydrous Engineering Ltd. modified Grubbs system of double alumina and alumina-copper catalysed drying columns).

*Chromatography.* Flash column chromatography was carried out using VWR silica gel 40–63 µm. Thin-layer chromatography (TLC) was performed using Merck aluminium-backed plates (Silica gel 60 F<sub>254</sub>). Compounds were visualized under UV light or by staining with Ceric ammonium molybdate (CAM).

*Nuclear magnetic resonance spectroscopy.* <sup>1</sup>H, <sup>13</sup>C, <sup>19</sup>F, <sup>11</sup>B and <sup>15</sup>N nuclear magnetic resonance (NMR) spectra were recorded using either 7.05 Tesla Jeol ECS spectrometer fitted with a 30TH5AT probe, a 9.4 Tesla Jeol ECS spectrometer fitted with a 40RO5AT probe, a 9.4 Tesla Jeol ECZ spectrometer fitted with a 40ROHFXS probe, a 11.75 Tesla Varian/Agilent VNMRS spectrometer fitted with an AutoX probe, a 11.75 Tesla Bruker Advance IIIHD spectrometer fitted with a DCH 500S1 *Cryo-probe* or a 14.1 Tesla Bruker Neo Spectrometer fitted with a TXO 600S3 *Cryo-probe*. <sup>1</sup>H and <sup>13</sup>C positive chemical shifts ( $\delta$ ) are referenced to CHCl<sub>3</sub> (<sup>1</sup>H: 7.26 ppm, <sup>13</sup>C: 77.2 ppm) C<sub>6</sub>D<sub>6</sub> (<sup>1</sup>H: 7.16 ppm, <sup>13</sup>C: 128.06 ppm), CD<sub>3</sub>OD (<sup>1</sup>H: 3.32 ppm, <sup>13</sup>C: 49.00 ppm), CD<sub>3</sub>CN (<sup>1</sup>H: 1.94 ppm, <sup>13</sup>C: 118.26 ppm) or DMSO-d<sub>6</sub> (<sup>1</sup>H: 2.50 ppm, <sup>13</sup>C: 39.5 ppm) and are given in parts per million (ppm) relative to tetramethylsilane. Peaks are described as singlets (s), doublets (d), triplets (t), quartets (q), pentets (pent), sextets (sext), heptets (hept) and multiplets (m). Coupling constants (J) are given in Hertz (Hz) and reported as observed. <sup>11</sup>B NMR spectra are obtained using thin wall quartz NMR tubes sourced

## Experimental

---

from Wilmad (unless otherwise stated) and are given in parts per million (ppm) relative to boron trifluoride etherate.  $^{15}\text{N}$  NMR shifts are obtained using  $^{15}\text{N}$ -HMBC to overcome the poor sensitivity issues arising from the low abundance (0.36%) and gyromagnetic ratio (~100-fold lower than  $^1\text{H}$ ) of the  $^{15}\text{N}$  nucleus. The  $^{15}\text{N}$  shifts are given in parts per million (ppm) relative to liquid ammonia. Where applicable, the NMR data is reported as: chemical shift (multiplicity, coupling constant(S), integral, assignment). NMR assignments are made according to spin systems, using two-dimensional (COSY, HSQC, HMBC) NMR spectroscopy to assist the assignment.

*Infrared spectroscopy.* Infrared (IR) spectra were recorded on a Perkin Elmer Spectrum Two FT-IR spectrophotometer as a thin film with selected absorption maxima ( $\nu$ ) reported in wavenumbers ( $\text{cm}^{-1}$ ).

*Mass spectrometry.* High resolution mass spectrometry (HRMS) spectra were recorded on a Thermo Scientific Exactive by Electron Ionization (EI), on a Bruker Daltonics micrOTOF II by Electrospray Ionization (ESI), on a Waters Synapt G2S by Nanospray, on a Thermo Scientific Orbitrap Elite by Atmospheric Pressure Chemical Ionization (APCI), or on a Bruker Daltonics UltrafleXtreme by Matrix-Assisted Laser Desorption Ionization (MALDI). In the cases where the reported compound contains Boron, Silicon, Chlorine or Bromine the masses are given for the  $^{11}\text{B}$ ,  $^{28}\text{Si}$ ,  $^{35}\text{Cl}$  or  $^{79}\text{Br}$  isotopes respectively.

*Melting points.* Melting points were recorded in degrees Celsius ( $^\circ\text{C}$ ), using a Gallenkamp melting point apparatus or a Cole-Parmer SMP50 automatic melting point apparatus and are reported uncorrected. Melting points denoted with “(dec.)” indicates decomposition of the compound at the given temperature.

*UV-Vis.* Spectra are recorded in ThorLabs’ quartz cuvettes using a custom experimental set-up described in section 8.4.2 and processed using OriginLabs’ Origin 2019b software package.

## Experimental

---

*Enantiomeric ratios.* Enantiomeric ratios were determined by HPLC on an Agilent Technologies 1260 Infinity with UV detection wavelength and Hexane:isopropanol (IPA) mixture ratios as indicated. Separations were performed at room temperature using the indicated column.

*Naming of Compounds.* Compound names are those generated by ChemBioDraw 20.0 software (PerkinElmer), following IUPAC nomenclature.

*X-ray crystallography.* X-ray diffraction experiments on **177** were carried out at 200(2) K on a Bruker APEX II diffractometer using Mo-K $\alpha$  radiation ( $\lambda = 0.71073 \text{ \AA}$ ) and collected using a CCD area detector. While **183** was carried out at 200(2) K (due to cracking at lower temperatures) and **126** and **155** were carried out at 100(2) K on a Bruker D8 Venture diffractometer using Mo-K $\alpha$  radiation ( $\lambda = 0.71073 \text{ \AA}$ ) and the data collected using a Bruker CPAD detector. Intensities were integrated in SAINT<sup>210</sup> and absorption corrections based on equivalent reflections were applied using SADABS.<sup>211</sup>

Structures were solved using ShelXT<sup>212</sup> and refined by full matrix least squares against F2 in ShelXL<sup>212, 213</sup> using Olex2.<sup>214</sup> All of the non-hydrogen atoms were refined anisotropically. While all of the hydrogen atoms were located geometrically and refined using a riding model, apart from the N-H protons in **183** and the O-H protons in **177** which were located in the difference map. Disorder was present in the whole or part of the molecule in **155** and **183** respectively, and in the solvent molecule of **177**. In each case, the occupancies of the fragments were determined by refining them against a free variable with the sum of the two sites set to equal 1 and relevant restraints and constraints were used to maintain sensible geometries and thermal parameters. While data quality was lower than desired for **183**, several crystals were tried and confirm the structure. The crystal structures are shown in Figure 60, Figure 61, Figure 62 and Figure 63 with the structure and refinement data given in Table 9

## Experimental

---

### 8.2 General Synthetic Procedures

#### General Suzuki Procedure A

In a flame-dried RBF, Pd(OAc)<sub>2</sub> (2.5 mol%) and S-Phos (5.0 mol%) were dissolved in toluene (~1 M *relative to Pd(OAc)<sub>2</sub>*) under an atmosphere of N<sub>2</sub>. The catalyst was left to stir at room temp for 2 h or until the mixture had darkened (light orange to dark brown/red).

In a separate RBF under N<sub>2</sub>, the aryl-boronic acid (1.15 eq.), the aryl-halide coupling partner, and Cs<sub>2</sub>CO<sub>3</sub> (2 eq.), were dissolved in a (1:13) solution of water and toluene (0.2 M), to which was added the catalyst solution. The reaction was then warmed to 90 °C in a pre-heated heating block and left to stir. After stirring for 16 h the reaction was cooled to room temperature, diluted with H<sub>2</sub>O (½ reaction volume), and extracted with CH<sub>2</sub>Cl<sub>2</sub> (3 × reaction volume). The organic layer was dried over MgSO<sub>4</sub>, filtered through Celite®, concentrated *in vacuo*, and the residue purified by column chromatography to give the biaryl product. If crystalline, the compound was then recrystallized from CHCl<sub>3</sub>.

#### General Suzuki Procedure B

To a flame-dried RBF, Pd(OAc)<sub>2</sub> (5 mol%) and PPh<sub>3</sub> (10 mol%) or *rac*-BIDME (10 mol%) were dissolved in toluene (~0.5 M *relative to Pd(OAc)<sub>2</sub>*) under an atmosphere of N<sub>2</sub>. The catalyst was left to stir at room temp for 2 h or until the mixture had darkened.

In a separate RBF under N<sub>2</sub>, the hindered-azo-Bpin (1.0 eq.), the aryl-halide coupling partner (1.2 eq.), and Cs<sub>2</sub>CO<sub>3</sub> (2 eq.), were dissolved in dry toluene (0.1 M), to which was added the catalyst solution. The reaction was then warmed to 85 °C in a pre-heated heating block and left to stir. After stirring for 16 h the reaction was cooled to room temperature, diluted with H<sub>2</sub>O (½ reaction volume), and extracted with CH<sub>2</sub>Cl<sub>2</sub> (3 × reaction volume). The organic layer was dried over MgSO<sub>4</sub>, filtered through Celite®, concentrated *in vacuo*, and the residue purified by column chromatography to give the biaryl product. If crystalline, the compound was then recrystallized from CHCl<sub>3</sub>.

### General Miyaura Borylation Procedure

To a flame-dried RBF,  $\text{PdCl}_2(\text{PPh}_3)_2$  (5 mol%) and  $\text{tBuPPH}_2$  (10 mol%) were dissolved in dioxane ( $\sim 0.5 \text{ M}$  relative to  $\text{Pd}(\text{OAc})_2$ ) under an atmosphere of  $\text{N}_2$  and the catalyst left to stir at room temp for 2 h.

In a separate RBF under  $\text{N}_2$ , the hindered-azo-bromide (1.0 eq.), the  $\text{B}_2\text{pin}_2$  (1.5 eq.), and  $\text{K}_2\text{CO}_3$  (2 eq.), were dissolved in dioxane (0.1 M), to which was added the catalyst solution. The flask was fitted with a reflux condenser (under  $\text{N}_2$ ), the reaction heated to reflux, and left to stir. After stirring for a time (16 h - 32 h) the reaction was cooled to room temperature, diluted with  $\text{H}_2\text{O}$  ( $\frac{2}{3}$  reaction volume), and extracted with  $\text{EtOAc}$  ( $3 \times$  reaction volume). The organic layer was dried over  $\text{MgSO}_4$ , filtered through Celite<sup>®</sup>, concentrated *in vacuo*, and the residue purified by column chromatography to give the biaryl product. If crystalline, the compound was then recrystallized from  $\text{CHCl}_3$ .

### General Ir Borylation Procedure

In a flame-dried J-Young tube,  $[\text{Ir}(\text{OMe})(\text{COD})]_2$  (2.5 mol%) and (*E*)-2-((2,2-dibenzylhydrazineylidene)methyl)pyridine (5.0 mol%) were dissolved in THF (0.03 M relative to  $[\text{Ir}(\text{OMe})(\text{COD})]_2$ ) the solution ultrasonicated and then left to stir for 2 h.

In a separate flame-dried RBF, the pyridine-biaryl substrate and  $\text{B}_2\text{pin}_2$  (5 eq) were placed under an atmosphere of  $\text{N}_2$  and dissolved in dry PhMe (0.1M). Neat HBpin (25 mol%) and the Ir catalyst solution (2.5 mol%) were then transferred into the RBF. The mixture was heated to 100 °C in a heating block and left to stir for 8 h. The reaction was then cooled to room temperature, filtered through a plug of Celite<sup>®</sup> and concentrated *in vacuo* to generate a crude oil. The oil was purified *via* column chromatography to give the borylated biaryl material.

## Experimental

---

### General Biaryl Boronic Ester Hydrolysis Procedure

The boronic pinacol ester was dissolved in THF (0.1 M) in a RBF capped with a pierced rubber septum (small scale) or a gas adaptor (large scale) to expose the reaction to air. Sodium metaperiodate (3 eq) was dissolved in DI water (0.3 M *relative to the periodate*) and added to the solution. After stirring for 30 minutes, 1 M HCl (*% of reaction volume*) was added, and the reaction left to stir for 14 h at room temperature. The reaction was then diluted with Et<sub>2</sub>O, neutralized to ~pH 5 using 2 M NaOH and sat. aq. NH<sub>4</sub>Cl, the aqueous layer separated, and the organic layer washed with 10% w/v sodium thiosulfate solution (×2) into a separate collecting flask. The organic layer was tested for peroxides using starch paper, reduced to half the volume *in vacuo*, and then extracted with 2 M NaOH (×4). The aqueous extracts were then neutralized using 2 M HCl and sat. aq. NH<sub>4</sub>Cl (5 mL). The aqueous layer was then extracted with Et<sub>2</sub>O (×5), the organic layer dried with MgSO<sub>4</sub>, filtered through Celite® and reduced *in vacuo* to give the pyridine boronic acid.

### General Boron Esterification Procedure A

Freshly prepared boronic acid was dissolved in CH<sub>2</sub>Cl<sub>2</sub> (0.1 M) to which the diol ligand (1.0 eq) and MgSO<sub>4</sub> were added. The mixture was then stirred for 24 h at room temperature. The reaction mixture was filtered through Celite® and subsequently reduced *in vacuo* to give the relevant boronic ester.

### General Boron Esterification Procedure B

Under a an atmosphere of N<sub>2</sub>, freshly prepared boronic acid and the relevant diol ligand, (1.0 eq) were dissolved in dry PhMe (0.025 M). The flask was then fitted with a Soxhlet extractor containing activated 4 Å molecular sieves and the reaction bought to reflux. The water generated by the reaction was then removed *via* passage of the azeotrope through the activated sieves in the Soxhlet extractor. After 10 h, the reaction mixture was cooled and reduced *in vacuo* to give the relevant azobenzene boronic ester.

## **Experimental**

---

### **General Mills Reaction Procedure**

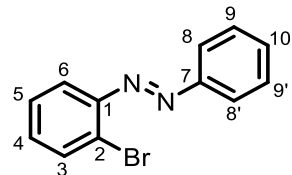
Functionalized aniline and nitrosobenzene (1.3 eq) were dissolved in glacial acetic acid (0.2 M) and the solution left to stir at room temperature for 24 h. The resulting mixture was diluted with EtOAc, washed with brine ( $\times 3$ ) and water ( $\times 2$ ). The organic layer was then dried with MgSO<sub>4</sub>, filtered through Celite<sup>®</sup>, and reduced *in vacuo*. The resulting oil was purified *via* silica gel chromatography to generate the relevant azobenzene.

## Experimental

---

### 8.3 Compound Data

#### (E)-1-(2-Bromophenyl)-2-phenyldiazene **59**



Synthesized according to the **General Mills Reaction** from 2-bromoaniline **57** (5.00 g, 29.1 mmol) and nitrosobenzene **70** (4.05 g, 37.8 mmol), with column chromatography (1:3 CH<sub>2</sub>Cl<sub>2</sub>:Hex) affording the title compound **59** as an orange solid (3.70 g, 49%).

**R<sub>f</sub>** 0.66 (1:1 CH<sub>2</sub>Cl<sub>2</sub>:Hex). **mp:** 43.1 °C – 45.1 °C. **<sup>1</sup>H NMR** (400 MHz, CDCl<sub>3</sub>): δ 8.04 – 7.94 (m, 2H, H-8), 7.75 (dd, *J* = 8.0, 1.4 Hz, 1H, H-6), 7.68 (dd, *J* = 8.0, 1.7 Hz, 1H, H-3), 7.57 – 7.48 (m, 3H, H-9 and H-10), 7.42 – 7.35 (m, 1H, H-4), 7.31 (ddd, *J* = 8.0, 7.3, 1.7 Hz, 1H, H-5). **<sup>13</sup>C NMR** (101 MHz, CDCl<sub>3</sub>): δ 152.7 (C-7), 149.7 (C-1), 133.9 (C-6), 132.0 (C-5), 131.7 (C-9), 129.3 (C-10), 128.1 (C-4), 125.9 (C-2), 123.6 (C-8), 117.9 (C-3). **MS (ESI<sup>+</sup>) m/z:** Found 260.0 Calculated for C<sub>12</sub>H<sub>10</sub>BrN<sub>2</sub><sup>+</sup> [M+H]<sup>+</sup> 259.99.

*Z isomer which spontaneously forms upon light exposure isolated as a minor side product*

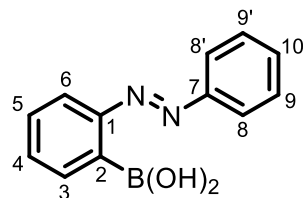
**R<sub>f</sub>** 0.30 (1:1 CH<sub>2</sub>Cl<sub>2</sub>:Hex). **<sup>1</sup>H NMR** (400 MHz, CDCl<sub>3</sub>): δ 7.60 (dd, *J* = 7.8, 1.4 Hz, 1H, H-3), 7.31 – 7.24 (m, 2H, H-9), 7.19 (tt, *J* = 7.4, 1.2 Hz, 1H, H-10), 7.07 (td, *J* = 7.6, 1.4 Hz, 1H, H-5), 7.01 (td, *J* = 7.8, 1.7 Hz, 1H, H-4), 6.97 – 6.92 (m, 2H, H-8), 6.27 (dd, *J* = 7.6, 1.7 Hz, 1H, H-6). **<sup>13</sup>C NMR** (101 MHz, CDCl<sub>3</sub>): δ 153.2 (C-7), 152.9 (C-1), 133.1 (C-3), 128.8 (C-9), 128.3 (C-10), 128.1 (C-4), 127.8 (C-5), 120.4 (C-8), 119.0 (C-6), 115.9 (C-2)

Data in accordance with literature and assignments made based on COSY, HSQC and HMBC data.<sup>215</sup>

## Experimental

---

### (E)-(2-(Phenylaz恒)phenyl)boronic acid **47**



2-bromoazobenzene **59** (2.089 g, 8.000 mmol), bis(pinacolato)-diboron (2.235 g, 8.800 mmol, 1.1 eq), KOAc (1.570 g, 16.00 mmol, 2 eq) and Pd(dppf)Cl<sub>2</sub>•CH<sub>2</sub>Cl<sub>2</sub> (0.065 g, 0.080 mmol, 1 mol%) were dissolved in anhydrous dioxane (80 mL, 0.1 M) under a nitrogen atmosphere. The reaction mixture was then heated to 80 °C and left to stir for 24 h. After stirring overnight, the reaction was cooled to room temperature, diluted with EtOAc (80 mL) and the mixture washed with brine (2 × 50 mL) and water (2 × 25 mL). The organic layer was then dried over MgSO<sub>4</sub>, filtered through Celite, and concentrated *in vacuo* to provide a crude brown oil. The oil was re-dissolved in hexane, cooled to 0 °C and a black solid removed via vacuum filtration. The hexane layer was then reduced *in vacuo* to provide a deep red oil. The crude oil was re-dissolved in THF (40 mL, 0.2 M) in a RBF capped with a pierced rubber septum. Sodium periodate (5.134 g, 24.00 mmol, 3 eq) was dissolved in DI water (40 mL) and added to the reaction mixture. After stirring for 30 min, 1 M HCl (6.4 mL) was added, and the reaction left to stir at room temperature for a further 16 h. The reaction mixture, cloudy with red precipitate, was then diluted with Et<sub>2</sub>O (150 mL) and washed with water (2 × 50 mL). The Et<sub>2</sub>O layer was then washed with 10% w/v sodium thiosulfate solution (3 × 25 mL), brine (25 mL) then water (25 mL). The remaining organic layer was tested for peroxides using starch and potassium iodide paper. The boronic acid was then purified via acid-base extraction of the organic layer using 2 M NaOH to basify/extract and 2 M HCl to neutralise and precipitate the acid. Filtration of the purified precipitate gave the title compound **47** as a peach-coloured solid (1.556 g, 86%).

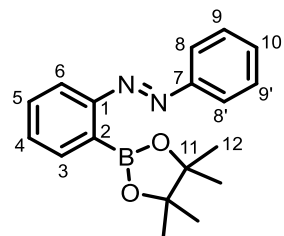
**mp:** 82.1 °C – 85.0 °C (dec.). **<sup>1</sup>H NMR** (400 MHz, DMSO-d<sub>6</sub>) δ 7.88 – 7.80 (m, 3H, H-6 and H-8), 7.75 (s, 2H, H of B(OH)<sub>2</sub>), 7.61 – 7.54 (m, 3H, H-9 and H-10), 7.52 – 7.44 (m, 3H, H-3, H-4 and H-5). **<sup>13</sup>C NMR** (101 MHz, DMSO-d<sub>6</sub>) δ 154.7 (C-1), 151.1 (C-7), 132.8 (C-3), 131.5 (C-10), 130.8 (C-4), 129.5 (C-5), 129.2 (C-9), 122.5 (C-8), 122.4 (C-6). <sup>2</sup>C-2 not observed due to boron relaxation. **<sup>11</sup>B NMR** (128 MHz, DMSO-d<sub>6</sub>) δ 28.9. **UV-Vis** (MeCN) λ<sub>max</sub> 326 (π → π\*), 445 (n → π\*). **MS** (Nanospray) *m/z*: Found 227.1 Calculated for C<sub>12</sub>H<sub>12</sub>BN<sub>2</sub>O<sub>2</sub><sup>+</sup> [M+H]<sup>+</sup> 227.0992.

Data in accordance with literature and assignments made based on COSY, HSQC and HMBC data.<sup>98</sup>

## Experimental

---

(*E*)-1-Phenyl-2-(2-(4,4,5,5-tetramethyl-1,3,2-dioxaborolan-2-yl)phenyl)diazene **48**



Synthesized according to the **General Boron Esterification Procedure A** from (*E*)-(2-(phenyldiazenyl)phenyl)boronic acid **47** (0.250 g, 1.11 mmol) and pinacol (0.131 g, 1.11 mmol), to give the title compound **48** as a red-orange oil (0.334 g, 98%).

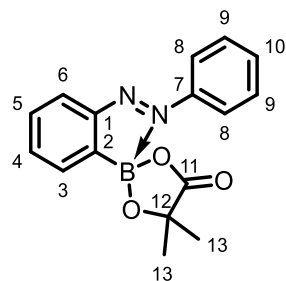
**<sup>1</sup>H NMR** (400 MHz, CDCl<sub>3</sub>): δ 7.92 – 7.87 (m, 2H, H-8), 7.79 (dd, *J* = 8.0, 1.2 Hz, 1H, H-6), 7.72 (dd, *J* = 7.3, 1.6 Hz, 1H, H-3), 7.54 – 7.42 (m, 5H, H-4, H-5, H-9 and H-10), 1.34 (s, 12H, H-12). **<sup>13</sup>C NMR** (101 MHz, CDCl<sub>3</sub>): δ 157.2 (C-1), 152.9 (C-7), 134.5 (C-3), 130.8 (C-10), 130.8 (C-4), 130.0 (C-5), 129.0 (C-9), 123.1 (C-8), 120.3 (C-6), 84.0 (C-11), 25.1 (C-12). \*C-2 not observed due to boron relaxation **<sup>11</sup>B NMR** (128 MHz, CDCl<sub>3</sub>): δ 30.4. **UV-Vis** (MeCN) λ<sub>max</sub> 317 (π → π\*) 438 (n → π\*). **HRMS** (ESI<sup>+</sup>) *m/z*: Found 331.1597 Calculated for C<sub>18</sub>H<sub>21</sub>BN<sub>2</sub>O<sub>2</sub>Na<sup>+</sup> [M+Na]<sup>+</sup> 331.1588. Δ = 1.5 ppm.

Data in accordance with literature and assignments made based on COSY, HSQC and HMBC data.<sup>98</sup>

## Experimental

---

(*E*)-5,5-Dimethyl-2-(2-(phenyldiazenyl)phenyl)-1,3,2-dioxaborolan-4-one **66**



Synthesized according to the **General Boron Esterification Procedure A** from (*E*)-(2-(phenyldiazenyl)phenyl)boronic acid **47** (0.250 g, 1.11 mmol) and  $\alpha$ -hydroxyisobutyric acid (0.115 g, 1.11 mmol), to give the title compound **66** as a light brown solid, which was subsequently recrystallized from hexane (0.318 g, 98%).

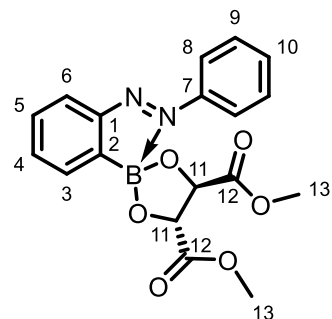
**mp:** 108.0 °C – 113.1 °C. **<sup>1</sup>H NMR** (400 MHz, CDCl<sub>3</sub>):  $\delta$  8.08 (d,  $J$  = 7.6 Hz, 1H, H-6), 7.91 – 7.84 (m, 2H, H-8), 7.65 – 7.59 (m, 2H, H-4 and H-10), 7.59 – 7.54 (m, 3H, H-5 and H-9), 7.52 (dd,  $J$  = 7.4, 1.4 Hz, 1H, H-3), 1.44 (s, 6H, H-13). **<sup>13</sup>C NMR** (101 MHz, CDCl<sub>3</sub>):  $\delta$  181.4 (C-11), 155.9 (C-1), 144.6 (C-7), 135.8 (C-4), 133.1 (C-10), 130.9 (C-3), 130.4 (C-5), 129.9 (C-9), 128.5 (C-6), 122.9 (C-8), 76.6 (C-12), 27.3 (C-13). <sup>13</sup>C-2 not observed due to boron relaxation. **<sup>11</sup>B NMR** (128 MHz, CDCl<sub>3</sub>):  $\delta$  14.6. **UV-Vis** (MeCN)  $\lambda_{\text{max}}$  336 ( $\pi \rightarrow \pi^*$ ), n →  $\pi^*$  transition not observed as a resolved band. **IR**  $\nu$  (cm<sup>-1</sup>): 2989, 1754, 1376, 1292, 1178, 1096, 1032, 1013, 977, 783, 764, 736. **HRMS** mass not found by ESI<sup>+</sup>, ESI<sup>-</sup> or APCI.

Assignments made based on COSY, HSQC and HMBC data.

## Experimental

---

Dimethyl (4*R*,5*R*)-2-(2-((*E*)-phenyldiazenyl)phenyl)-1,3,2-dioxaborolane-4,5-dicarboxylate  
**63**



Synthesized according to the **General Boron Esterification Procedure B** from (*E*)-(2-(phenyldiazenyl)phenyl)boronic acid **47** (0.250 g, 1.11 mmol) and (+)-dimethyl-L-tartrate (0.197 g, 1.11 mmol), to give the title compound **63** as an orange oil (Purity <90%).

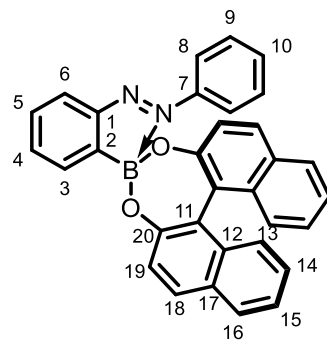
*Due to water and silica instability issues, and its state as an oil, this compound was unable to be generated in good purity (>90%) and as such was analysed directly from the crude mixture. Selected data from the crude mixture is presented below.*

**<sup>1</sup>H NMR** (400 MHz, CDCl<sub>3</sub>): δ 8.00 (d, *J* = 7.1 Hz, 1H, H-6), 7.87 (dd, *J* = 5.7, 3.3 Hz, 2H, H-8), 7.63 (d, *J* = 6.6 Hz, 1H, H-3), 7.53 (m, H-4; H-5; H-9 and H-10), 5.09 (s, 2H, H-11), 3.66 (s, 6H, H-13). **<sup>11</sup>B NMR** (128 MHz, CDCl<sub>3</sub>): δ 22.7. **HRMS** not found by Nanospray or APCI.

## Experimental

---

(*S,E*)-*N*-(2-(Dinaphtho[2,1-d:1',2'-f][1,3,2]dioxaborepin-4-yl)phenyl)-*N*-phenyldiazene **68**



Synthesized according to the **General Boron Esterification Procedure B** from (*E*)-(2-(phenyldiazenyl)phenyl)boronic acid **47** (0.250 g, 1.11 mmol) and (*S*)-BINOL (0.317 g, 1.11 mmol), to give a crude mixture of the title compound **68**, the starting boronic acid and (*S*)-BINOL as a red oil (Purity <90%).

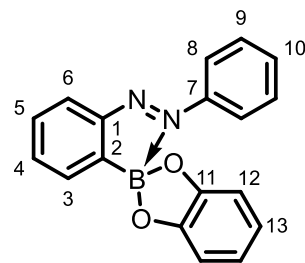
*Due to water and silica instability issues, and its state as an oil, this compound was unable to be generated in good purity (>90%) and as such was analysed directly from the crude mixture. Selected data from the crude mixture is presented below.*

**<sup>11</sup>B NMR** (128 MHz, CDCl<sub>3</sub>): δ 12.6.

## Experimental

---

(*E*)-1-(2-(Benzo[d][1,3,2]dioxaborol-2-yl)phenyl)-2-phenyldiazene **46**



Synthesized according to the **General Boron Esterification Procedure A** from (*E*)-(2-(phenyldiazenyl)phenyl)boronic acid **47** (0.250 g, 1.11 mmol) and catechol (0.122 g, 1.11 mmol), to give the title compound **46** as a red-brown solid, which was subsequently recrystallized from hexane (0.319 g, 96%).

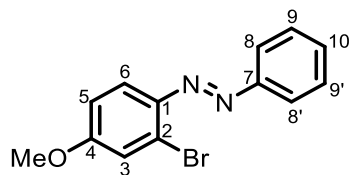
**mp:** 113.6 °C – 114.7°C. **<sup>1</sup>H NMR** (400 MHz, CDCl<sub>3</sub>): δ 8.17 – 8.09 (m, 1H, H-6), 7.67 – 7.63 (m, 3H, H-8 and H-5), 7.63 – 7.56 (m, 2H, H-4 and H-3), 7.50 – 7.43 (m, 1H, H-10), 7.39 – 7.31 (m, 2H, H-9), 7.05-7.00 (m, 2H, H-13), 6.97-6.92 (m, 2H, H-12). **<sup>13</sup>C NMR** (101 MHz, CDCl<sub>3</sub>): δ 156.0 (C-1), 150.5 (C-11), 144.8 (C-7), 134.6 (C-4), 133.0 (C-10), 132.0 (C-5), 130.6 (C-3), 129.7 (C-9), 128.4 (C-6), 123.3 (C-8), 121.0 (C-12), 111.6 (C-13). \*C-2 not observed due to boron relaxation. **<sup>11</sup>B NMR** (128 MHz, CDCl<sub>3</sub>): δ 19.6. **HRMS** Not found by Nanospray or APCI.

Data in accordance with literature and assignments made based on COSY, HSQC and HMBC data.<sup>98</sup>

## Experimental

---

### (E)-1-(2-Bromo-4-methoxyphenyl)-2-phenyldiazene **60**



Synthesized according to the **General Mills Reaction** from 2-bromo-4-methoxyaniline **58** (2.00 g, 9.90 mmol) and nitrosobenzene **70** (1.38 g, 12.9 mmol), with column chromatography (1:3 CH<sub>2</sub>Cl<sub>2</sub>:Hex) affording the title compound **60** as an orange crystalline solid (2.70 g, 94%).

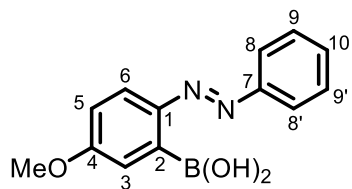
**R<sub>f</sub>** 0.69 (1:1 CH<sub>2</sub>Cl<sub>2</sub>:Hex). **mp:** 64.1 °C – 64.2 °C. **<sup>1</sup>H NMR** (400 MHz, CDCl<sub>3</sub>): δ 7.97 – 7.92 (m, 2H, H-8), 7.76 (d, *J* = 9.0 Hz, 1H, H-6), 7.54 – 7.49 (m, 2H, H-9), 7.48 – 7.43 (m, 1H, H-10), 7.28 (d, *J* = 2.7 Hz, 1H, H-3), 6.93 (dd, *J* = 9.0, 2.7 Hz, 1H, H-5), 3.88 (s, 3H, MeO). **<sup>13</sup>C NMR** (101 MHz, CDCl<sub>3</sub>): δ 162.3 (C-4), 152.9 (C-7), 143.8 (C-1), 131.1 (C-10), 129.3 (C-9), 128.2 (C-2), 123.3 (C-8), 118.7 (C-6), 118.0 (C-3), 114.7 (C-5), 56.0 (MeO). **IR** *v* (cm<sup>-1</sup>): 3084, 1593, 1569, 1479, 1275, 1232, 1034, 519. **HRMS** (ESI<sup>+</sup>) *m/z*: Found 312.9947 Calculated for C<sub>13</sub>H<sub>11</sub>BrN<sub>2</sub>ONa<sup>+</sup> [M+Na]<sup>+</sup> 312.9947 Δ = 2.1 ppm.

Assignments made based on COSY, HSQC and HMBC data.

## Experimental

---

### (E)-(5-Methoxy-2-(phenyldiazenyl)phenyl)boronic acid **62**



The 2-bromo-4-methoxyazobenzene **60** (2.18 g, 7.50 mmol), bis(pinacolato)-diboron (2.10 g, 8.25 mmol, 1.1 eq), KOAc (1.47 g, 15.0 mmol, 2 eq) and Pd(dppf)Cl<sub>2</sub>•CH<sub>2</sub>Cl<sub>2</sub> (0.061 g, 0.075 mmol, 1 mol%) were dissolved in anhydrous dioxane (75 mL, 0.1 M) under a nitrogen atmosphere. The reaction mixture was then heated to 80 °C and left to stir for 24 h. The reaction was cooled to room temperature, diluted with EtOAc (80 mL) and the mixture washed with brine (2 × 50 mL) and water (2 × 25 mL). The organic layer was then dried over MgSO<sub>4</sub>, filtered through Celite, and concentrated *in vacuo* to provide a crude brown oil. The oil was re-dissolved in hexane, cooled to 0 °C, a black solid was then removed via vacuum filtration and the hexane layer reduced *in vacuo* to provide a deep red oil. The crude oil was re-dissolved in THF (37.5 mL, 0.2 M) in a RBF capped with a pierced rubber septum. Sodium periodate (4.81 g, 22.5 mmol, 3 eq) was dissolved in DI water (37.5 mL) and added to the reaction mixture. After stirring for 30 min, 1 M HCl (6.0 mL) was added, and the reaction was left to stir at room temperature for a further 14 h. The reaction mixture, now cloudy with red precipitate, was then diluted with Et<sub>2</sub>O (150 mL) and washed with water (2 × 50 mL). The Et<sub>2</sub>O layer was then washed with 10% w/v sodium thiosulfate solution (3 × 25 mL), brine (25 mL) and water (25 mL) and the remaining organic layer tested for peroxides using starch and potassium iodide paper. The boronic acid was then purified via acid-base extraction of the organic layer using 2 M NaOH to basify/extract and 2 M HCl to neutralise and precipitate the acid. Filtration of the purified precipitate gave the title compound **62** as a light-yellow solid (1.63 g, 85%).

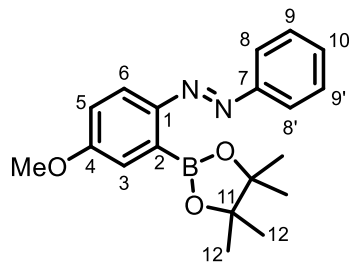
**mp:** 119.2 °C – 122.4 °C (dec.). **<sup>1</sup>H NMR** (400 MHz, DMSO-d<sub>6</sub>) δ 7.88 (d, *J* = 8.5 Hz, 1H, H-6), 7.83 (d, *J* = 7.4 Hz, 2H, H-8), 7.77 (s, 2H, B(OH)<sub>2</sub>), 7.61 – 7.56 (m, 2H, H-9), 7.55 – 7.50 (m, 1H, H-10), 7.08 (dd, *J* = 8.7, 2.8 Hz, 1H, H-5), 7.05 (d, *J* = 3.0 Hz, 1H, H-3), 3.86 (s, 3H, OMe). **<sup>13</sup>C NMR** (101 MHz, DMSO-d<sub>6</sub>) δ 161.6 (C-4), 151.0 (C-7), 149.0 (C-1), 130.9 (C-10), 129.4 (C-9), 124.5 (C-6), 122.2 (C-8), 117.5 (C-3), 114.4 (C-5), 55.6 (OMe). **<sup>2</sup>B NMR** (128 MHz, DMSO-d<sub>6</sub>) δ 28.2. **UV-Vis** (MeCN) λ<sub>max</sub> 374 (π → π\*), 421 (n → π\*). **IR ν (cm<sup>-1</sup>)**: 3350, 3158, 2938, 1595, 1485, 1391, 1324, 123, 1095, 1033, 762, 679. **HRMS** (Nanospray) *m/z*: Found 291.0712 Calculated for C<sub>13</sub>H<sub>13</sub>N<sub>2</sub>O<sub>3</sub>ClB<sup>+</sup> [M+Cl]<sup>+</sup> 291.072. Δ = 1.5 ppm.

Assignments made based on COSY, HSQC and HMBC data.

## Experimental

---

(*E*)-1-(4-Methoxy-2-(4,4,5,5-tetramethyl-1,3,2-dioxaborolan-2-yl)phenyl)-2-phenyldiazene  
**61**



Synthesized according to the **General Boron Esterification Procedure A** from (*E*)-(5-methoxy-2-(phenyldiazenyl)phenyl)boronic acid **62** (0.250 g, 0.977 mmol) and pinacol (0.115 g, 0.977 mmol), to give the title compound **61** as a red-orange oil (0.326 g, 99%).

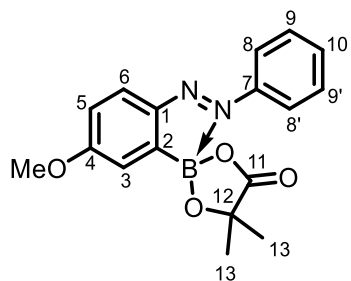
**<sup>1</sup>H NMR** (400 MHz, CDCl<sub>3</sub>): δ 7.90 – 7.81 (m, 3H, H-8 and H-6), 7.50 – 7.45 (m, 2H, H-9), 7.44 – 7.39 (m, 1H, H-10), 7.16 (d, *J* = 2.8 Hz, 1H, H-3), 7.02 (dd, *J* = 8.8, 2.8 Hz, 1H, H-5), 3.89 (s, 3H, OMe), 1.37 (s, 12H, H-12). **<sup>13</sup>C NMR** (101 MHz, CDCl<sub>3</sub>): δ 161.4 (C-4), 153.0 (C-7), 151.0 (C-1), 130.2 (C-10), 128.9 (C-9), 122.8 (C-8), 122.6 (C-6), 118.4 (C-3), 116.2 (C-5), 84.1 (C-11), 55.7 (MeO), 25.1 (C-12). <sup>11</sup>B NMR (128 MHz, CDCl<sub>3</sub>): δ 30.4. **UV-Vis** (MeCN)  $\lambda_{\text{max}}$  372 ( $\pi \rightarrow \pi^*$ ), 424 (n → π\*). **IR**  $\nu$  (cm<sup>-1</sup>): 2978, 1593, 1569, 1479, 1275, 1232, 1034. **HRMS** (EI) *m/z*: Found 338.1793 Calculated for C<sub>19</sub>H<sub>23</sub>N<sub>2</sub>O<sub>3</sub>B<sup>+</sup> [M]<sup>+</sup> 338.1796 Δ = 0.9 ppm.

Assignments made based on COSY, HSQC and HMBC data.

## Experimental

---

(*E*)-2-(5-Methoxy-2-(phenyldiazenyl)phenyl)-5,5-dimethyl-1,3,2-dioxaborolan-4-one **67**



Synthesized according to the **General Boron Esterification Procedure A** from (*E*)-(2-(phenyldiazenyl)phenyl)boronic acid **62** (0.250 g, 0.977 mmol) and  $\alpha$ -hydroxyisobutyric acid (0.102 g, 0.977 mmol), to give the title compound **67** as a red solid, which was subsequently recrystallized from hexane (0.257 g, 78%).

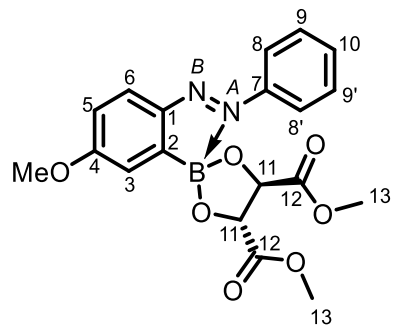
**mp:** 145.9 °C – 147.1 °C. **<sup>1</sup>H NMR** (400 MHz, CDCl<sub>3</sub>):  $\delta$  8.00 (d, *J* = 8.6 Hz, 1H, H-6), 7.82 (dm, *J* = 8.1 Hz, 2H, H-8), 7.57 – 7.48 (m, 3H, H-9 and H-10), 7.04 (d, *J* = 2.5 Hz, 1H, H-3), 6.93 (dd, *J* = 8.6, 2.5 Hz, 1H, H-5), 3.94 (s, 3H, MeO), 1.44 (s, 6H, H-13). **<sup>13</sup>C NMR** (101 MHz, CDCl<sub>3</sub>):  $\delta$  181.5 (C-11), 167.0 (C-4), 150.6 (C-1), 144.2 (C-7), 132.0 (C-10), 131.2 (C-6), 129.7 (C-9), 122.5 (C-8), 117.3 (C-3), 114.8 (C-5), 76.5 (C-12), 56.2 (MeO), 27.5 (C-13). **<sup>11</sup>B NMR** (128 MHz, CDCl<sub>3</sub>):  $\delta$  12.6. **IR v** (cm<sup>-1</sup>): 2978, 1749, 1579, 1426, 1291, 1185, 1104, 1019, 883, 824, 772, 693. **HRMS** not found by Nanospray, EI or APCI.

Assignments made based on COSY, HSQC and HMBC data.

## Experimental

---

Dimethyl (4*R*,5*R*)-2-(5-methoxy-2-((*E*)-phenyldiazenyl)phenyl)-1,3,2-dioxaborolane-4,5-dicarboxylate **64**



Synthesized according to the **General Boron Esterification Procedure B** from (*E*)-(2-phenyldiazenyl)phenylboronic acid **62** (0.250 g, 0.977 mmol) and (+)-dimethyl L-tartrate (0.174 g, 0.977 mmol), to give the title compound **64** as an orange oil (0.385 g, 99%).

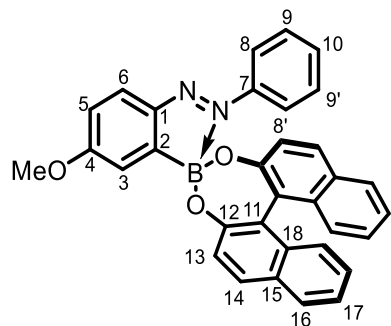
**<sup>1</sup>H NMR** (400 MHz, CDCl<sub>3</sub>): δ 7.93 (d, *J* = 8.5 Hz, 1H, H-6), 7.91 – 7.83 (m, 2H, H-8), 7.52 – 7.46 (m, 3H, H-9 and H-10), 7.17 – 7.15 (m, 1H, H-3), 6.92 (dd, *J* = 8.5, 2.7 Hz, 1H, H-5), 5.04 (s, 2H, H-11), 3.93 (s, 3H, MeO) 3.65 (s, 6H, H-13). **<sup>13</sup>C NMR** (101 MHz, CDCl<sub>3</sub>): δ 172.1 (C-12), 165.9 (C-4), 150.7 (C-1), 146.4 (C-7), 131.3 (C-10), 130.2 (C-6), 129.4 (C-9), 122.5 (C-8), 117.4 (C-3), 115.1 (C-5), 77.4 (C-11), 56.0 (MeO), 52.6. (C-13). <sup>13</sup>C-<sup>15</sup>N HMBC (600 MHz, *Cryo-probe*, MeCN-d<sub>3</sub>, *J*<sub>H-N</sub> = 5 Hz): δ 399.6 (N-A), 478.0 (N-B). **UV-Vis** (MeCN)  $\lambda_{\text{max}}$  355 nm ( $\pi \rightarrow \pi^*$ ), 436 nm (n → π\*) observed as a shoulder. **IR v** (cm<sup>-1</sup>): 2953, 1731, 1574, 1426, 1349, 1204, 1087, 1022, 769, 689. **HRMS** not found by Nanospray, ESI or APCI.

Assignments made based on COSY, HSQC and HMBC data.

## Experimental

---

(*S,E*)-N-(2-(Dinaphtho[2,1-d:1',2'-f][1,3,2]dioxaborepin-4-yl)-4-methoxyphenyl)-N-phenyldiazene **69**



Synthesized according to the **General Boron Esterification Procedure B** from (*E*)-(5-methoxy-2-(phenyldiazenyl)phenyl)boronic acid **62** (0.250 g, 0.977 mmol) and (*S*)-BINOL (0.280 g, 0.977 mmol), to give a crude mixture of the title compound **69**, the starting boronic acid and (*S*)-BINOL as a red oil (Purity <90%).

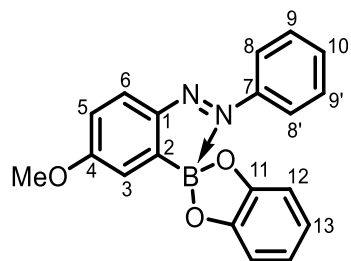
*Due to water and silica instability issues, and its state as an oil, this compound was unable to be generated in good purity (>90%) and as such was analysed directly from the crude mixture. Selected data from the crude mixture is presented below.*

**<sup>11</sup>B NMR** (128 MHz, CDCl<sub>3</sub>): δ 11.7.

## Experimental

---

(*E*)-1-(2-(Benzo[d][1,3,2]dioxaborol-2-yl)-4-methoxyphenyl)-2-phenyldiazene **65**



Synthesized according to the **General Boron Esterification Procedure A** from (*E*)-(2-(phenyldiazenyl)phenyl)boronic acid **62** (0.250 g, 0.977 mmol) and catechol (0.108 g, 0.977 mmol), to give the title compound **65** as a red solid, which was subsequently recrystallized from hexane (0.315 g, 98%).

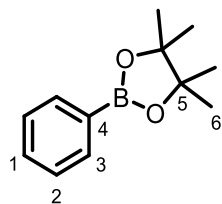
**mp:** 129.9 °C – 131.1 °C (dec.). **<sup>1</sup>H NMR** (400 MHz, CDCl<sub>3</sub>): δ 8.03 (d, *J* = 8.6 Hz, 1H, H-6), 7.69 – 7.61 (m, 2H, H-8), 7.45 – 7.39 (m, 1H, H-10), 7.36 – 7.30 (m, 2H, H-9), 7.18 (d, *J* = 2.6 Hz, 1H, H-3), 7.03 – 6.99 (m, 1H, H-5), 6.99 – 6.95 (m, 2H, C-13), 6.90 (dd, *J* = 5.6, 3.4 Hz, 2H, C-12), 3.92 (s, 3H, OMe). **<sup>13</sup>C NMR** (101 MHz, CDCl<sub>3</sub>): δ 166.4 (C-4), 151.0 (C-11), 150.4 (C-1), 143.9 (C-7), 132.0 (C-10), 130.7 (C-6), 129.7 (C-9), 122.6 (C-8), 120.5 (C-12), 117.1 (C-3), 116.1 (C-5), 111.4 (C-13), 56.1 (OMe). **<sup>11</sup>B NMR** (128 MHz, CDCl<sub>3</sub>): δ 16.2. **IR v** (cm<sup>-1</sup>): 2925, 1573, 1475, 1379, 1293, 1201, 1104, 1015, 864. **HRMS** not found by Nanospray, EI or APCI.

Assignments made based on COSY, HSQC and HMBC data.

## Experimental

---

### 4,4,5,5-Tetramethyl-2-phenyl-1,3,2-dioxaborolane **72**



Synthesized according to the **General Boron Esterification Procedure A** from phenylboronic acid **71** (0.250 g, 2.05 mmol) and pinacol (0.242 g, 2.05 mmol), to give the title compound **72** as a white solid, which was subsequently recrystallized from CHCl<sub>3</sub> (0.418 g, 99%).

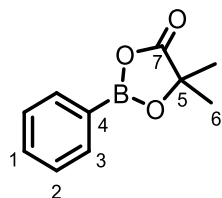
**mp:** 28.3 °C – 31.8°C **<sup>1</sup>H NMR** (400 MHz, CDCl<sub>3</sub>): δ 7.82 (dt, *J* = 8.0, 1.1 Hz, 2H, H-3), 7.50 – 7.44 (m, 1H, H-1), 7.41 – 7.34 (m, 2H, H-2), 1.36 (s, 12H, H-6). **<sup>13</sup>C NMR** (101 MHz, CDCl<sub>3</sub>): δ 134.9 (C-3), 131.4 (C-1), 127.9 (C-2), 83.9 (C-5), 25.0 (C-6). \*C-4 not observed due to boron relaxation. **<sup>11</sup>B NMR** (128 MHz, CDCl<sub>3</sub>): δ 30.0. **MS (EI<sup>+</sup>)** *m/z*: Found 204.13 Calculated for C<sub>12</sub>H<sub>17</sub>BO<sub>2</sub> [M]<sup>+</sup> 204.13.

Data in accordance with literature with assignments made based on COSY, HMBC and HSQC data.<sup>216</sup>

## Experimental

---

### 5,5-Dimethyl-2-phenyl-1,3,2-dioxaborolan-4-one **73**



Synthesized according to the **General Boron Esterification Procedure A** from phenylboronic acid **71** (0.250 g, 2.05 mmol) and  $\alpha$ -hydroxyisobutyric acid (0.214 g, 2.05 mmol), to give the title compound **73** as a white solid, which was subsequently recrystallized from CHCl<sub>3</sub> (0.385 g, 99%).

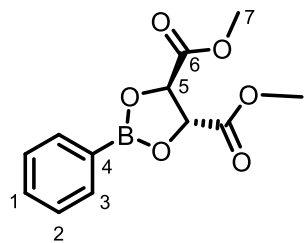
**mp:** 39.8 °C – 43.3 °C. **<sup>1</sup>H NMR** (400 MHz, CDCl<sub>3</sub>):  $\delta$  7.96 – 7.86 (m, 2H, H-3), 7.61 – 7.56 (m, 1H, H-1), 7.49 – 7.42 (m, 2H, H-2), 1.60 (s, 6H, H-6). **<sup>13</sup>C NMR** (101 MHz, CDCl<sub>3</sub>):  $\delta$  179.0 (C-7), 135.4 (C-3), 133.3 (C-1), 128.3 (C-2), 79.7 (C-5), 25.6 (C-6). \*C-4 not observed due to boron relaxation. **<sup>11</sup>B NMR** (128 MHz, CDCl<sub>3</sub>):  $\delta$  33.0. **IR v** (cm<sup>-1</sup>): 2978, 1808, 1603, 1376, 1176, 1052, 1025, 870, 832, 703. **HRMS (ESI<sup>+</sup>) m/z:** Found 190.0793 Calculated for C<sub>10</sub>H<sub>11</sub>BO<sub>3</sub> [M]<sup>+</sup> 190.0801  $\Delta$  = 1.6 ppm.

Assignments made based on COSY, HMBC and HSQC data.

## Experimental

---

Dimethyl (*4R,5R*)-2-phenyl-1,3,2-dioxaborolane-4,5-dicarboxylate **74**



Synthesized according to the **General Boron Esterification Procedure A** from phenylboronic acid **71** (0.250 g, 2.05 mmol) and (+)-dimethyl L-tartrate (0.365 g, 2.05 mmol), to give the title compound **74** as a white solid, which was subsequently recrystallized from CHCl<sub>3</sub> (0.531 g, 98%).

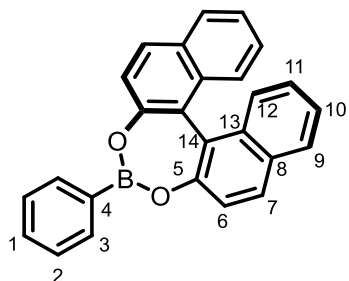
**mp:** 57.9 °C – 59.0°C. **<sup>1</sup>H NMR** (400 MHz, CDCl<sub>3</sub>): δ 7.98 – 7.83 (m, 2H, H-3), 7.55 – 7.50 (m, 1H, H-1), 7.40 (ddd, *J* = 8.1, 6.6, 1.5 Hz, 2H, H-2), 5.11 (s, 2H, H-5), 3.85 (s, 6H, H-7). **<sup>13</sup>C NMR** (101 MHz, CDCl<sub>3</sub>): δ 169.9 (C-6), 135.3 (C-3), 132.4 (C-1), 128.0 (C-2), 77.9 (C-5), 53.1 (C-7). \*C-4 not observed due to boron relaxation. **<sup>11</sup>B NMR** (128 MHz, CDCl<sub>3</sub>): δ 31.1. **IR** *v* (cm<sup>-1</sup>): 2963, 1759, 1739, 1602, 1437, 1372, 1278, 1199, 1108, 1018, 698. **HRMS** (ESI<sup>+</sup>) *m/z*: Found 264.0800 Calculated for C<sub>12</sub>H<sub>13</sub>BO<sub>6</sub><sup>+</sup> [M+H]<sup>+</sup> 264.0805. Δ = 0.0 ppm.

Assignments made based on COSY, HSQC and HMBC data.

## Experimental

---

### (S)-4-Phenylidinaphtho[2,1-d:1',2'-f][1,3,2]dioxaborepine **75**



Synthesized according to the **General Boron Esterification Procedure B** from phenylboronic acid **72** (0.250 g, 2.05 mmol) and (*S*)-BINOL (0.365 g, 2.05 mmol), to give a crude mixture of the title compound **75**, the starting boronic acid and (*S*)-BINOL as a white solid (Purity <90%).

*Due to water and silica instability issues, and its state as an oil, this compound was unable to be generated in good purity (>90%) and as such was analysed directly from the crude mixture. Selected data from the crude mixture is presented below.*

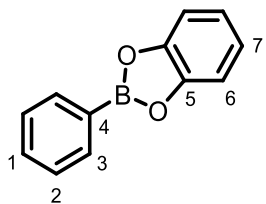
**<sup>11</sup>B NMR** (128 MHz, CDCl<sub>3</sub>): δ 25.1.

Data in accordance with literature.<sup>217</sup>

## Experimental

---

### 2-Phenylbenzo[d][1,3,2]dioxaborole **45**



Synthesized according to the **General Boron Esterification Procedure A** from phenylboronic acid **72** (0.250 g, 2.05 mmol) and catechol (0.226 g, 2.05 mmol), to give the title compound **45** as a white solid, which was subsequently recrystallized from CHCl<sub>3</sub> (0.397 g, 99%).

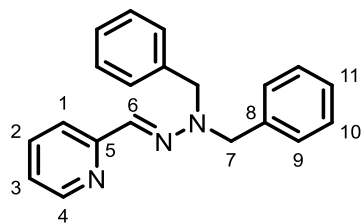
**mp:** 109.9 °C – 112.0 °C **<sup>1</sup>H NMR** (400 MHz, CDCl<sub>3</sub>): δ 8.14 – 8.05 (m, 2H, H-3), 7.63 – 7.55 (m, 1H, H-1), 7.53 – 7.47 (m, 2H, H-2), 7.35 – 7.29 (m, 2H, H-7), 7.17 – 7.10 (m, 2H, H-6). **<sup>13</sup>C NMR** (101 MHz, CDCl<sub>3</sub>): δ 148.7 (C-5), 135.1 (C-3), 132.5 (C-1), 128.4 (C-2), 122.9 (C-6), 112.7 (C-7). \*C-4 not observed due to boron relaxation. **<sup>11</sup>B NMR** (128 MHz, CDCl<sub>3</sub>): δ 31.3. **MS (EI) m/z:** Found 196.07 Calculated for C<sub>12</sub>H<sub>9</sub>BO<sub>2</sub><sup>+</sup> [M]<sup>+</sup> 196.07.

Data in accordance with literature with assignments made based on COSY, HMBC and HSQC data.<sup>218</sup>

## Experimental

---

### (E)-2-((2,2-Dibenzylhydrazineylidene)methyl)pyridine **92**



N,N-dibenzylhydrazine (1.49 g, 7.00 mmol, 1.5 eq) was added to a solution of pyridine-2-carbaldehyde **107** (0.500 g, 4.67 mmol) in MeOH (23 mL, 0.2 M) and the mixture stirred for 16 h at room temperature. The solvent was then removed under reduced pressure and the resulting residue was purified by column chromatography (1:3 EtOAc:Hex) to give the title compound **92** as a white solid (1.32 g, 94%).

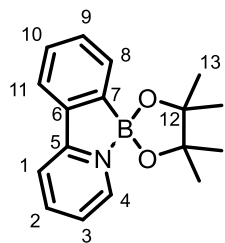
**R<sub>f</sub>** 0.18 (1:5 EtOAc:Hex). **mp:** 55.9 °C – 58.1 °C. **<sup>1</sup>H NMR** (400 MHz, CDCl<sub>3</sub>): δ 8.43 (dt, *J* = 4.9, 1.1 Hz, 1H, H-4), 7.82 (d, *J* = 8.1 Hz, 1H, H-1), 7.60 (td, *J* = 7.7, 2.0 Hz, 1H, H-2), 7.36 – 7.19 (m, 11H, H-11, H-10, H-9, and H-6), 7.05 (ddd, *J* = 7.5, 4.9, 1.5 Hz, 1H, H-3), 4.61 (s, 4H, H-7). **<sup>13</sup>C NMR** (101 MHz, CDCl<sub>3</sub>): δ 156.2 (C-5), 149.1 (C-4), 137.1 (C-8), 136.1 (C-2), 131.4 (C-6), 128.8 (C-10), 127.7 (C-9), 127.5 (C-11), 121.5 (C-3), 119.0 (C-1), 57.9 (C-7). **MS (ESI<sup>+</sup>)** *m/z*: Found 302.17 Calculated for C<sub>20</sub>H<sub>20</sub>N<sub>3</sub><sup>+</sup> [M+H]<sup>+</sup> 302.17.

Data in accordance with literature with assignments made based on COSY, HMBC and HSQC data.<sup>115</sup>

## Experimental

---

### 2-(2-(4,4,5,5-Tetramethyl-1,3,2-dioxaborolan-2-yl)phenyl)pyridine **76**



An oven-dried Schlenk tube was charged with  $[\text{Rh}(\text{COD})\text{Cl}]_2$  (0.009 g, 0.02 mmol, 2.5 mol%), 1,3-bis-(2,6-diisopropylphenyl)imidazolinium chloride (0.015 g, 0.035 mmol, 5 mol%),  $^t\text{BuOK}$  (0.004 g, 0.04 mmol, 5 mol%) and anhydrous hexane (3.5 mL, 0.1 M). The reaction mixture was allowed to stir for 2 h at room temperature, followed by the addition of 2-phenylpyridine (0.10 mL, 0.70 mmol) and  $\text{B}_2\text{pin}_2$  (0.21 g, 0.84 mmol, 1.2 eq). The reaction was then stirred overnight at room temperature. The reaction was concentrated *in vacuo*, and the product purified by silica chromatography (3:1 EtOAc:Hexane) to give the title compound **76** as a white solid (0.182 g, 71%).

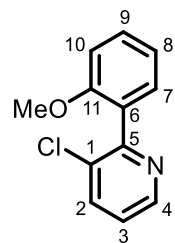
**R<sub>f</sub>** 0.38 (EtOAc). **mp:** 74.1 °C – 76.5 °C. **<sup>1</sup>H NMR** (400 MHz,  $\text{CDCl}_3$ ):  $\delta$  8.66 (ddd,  $J = 5.6, 1.5, 0.9$  Hz, 1H, H-4), 7.96 (td,  $J = 7.6, 1.5$  Hz, 1H, H-2), 7.79 (dt,  $J = 8.0, 0.9$  Hz, 1H, H-1), 7.72 (d,  $J = 7.2$  Hz, 1H, H-8), 7.65 (dt,  $J = 7.6, 0.9$  Hz, 1H, H-11), 7.40 (td,  $J = 7.2, 1.1$  Hz, 1H, H-9), 7.36 (ddd,  $J = 7.3, 5.6, 1.2$  Hz, 1H, H-3), 7.29 (td,  $J = 7.5, 1.1$  Hz, 1H, H-10), 1.42 (s, 12H, H-13). **<sup>13</sup>C NMR** (101 MHz,  $\text{CDCl}_3$ ):  $\delta$  156.6 (C-5), 143.3 (C-4), 142.0 (C-2), 137.2 (C-6), 131.6 (C-9), 131.5 (C-8), 127.9 (C-10), 122.8 (C-3), 121.3 (C-11), 117.5 (C-1), 80.3 (C-12), 27.1 (C-13). \*C-7 not observed due to boron relaxation. **<sup>11</sup>B NMR** (128 MHz,  $\text{CDCl}_3$ ):  $\delta$  12.4. **MS (ESI<sup>+</sup>)** *m/z*: Found 282.2 Calculated for  $\text{C}_{17}\text{H}_{21}\text{BNO}_2^+ [\text{M}+\text{H}]^+$  282.17.

Data in accordance with literature and assignments made based on COSY, HSQC and HMBC data.<sup>124</sup>

## Experimental

---

### 1-Chloro-5-(11-methoxyphenyl)pyridine **87**



Synthesized according to the **General Suzuki Cross-Coupling Procedure A** from 3-chloro-2-bromopyridine **83** (3.00 g, 15.6 mmol), methoxy boronic acid **81** (2.72 g, 17.9 mmol), Pd(OAc)<sub>2</sub> (0.175 g, 0.780 mmol), SPhos (0.640 g, 1.56 mmol) and Cs<sub>2</sub>CO<sub>3</sub> (10.2 g, 31.2 mmol), with column chromatography (1:6 EtOAc:Hex) affording the title compound **87** as a colourless oil (2.98 g, 87%).

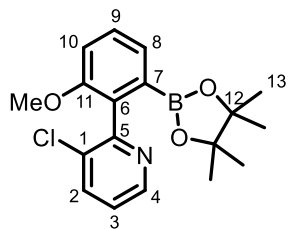
**R<sub>f</sub>** 0.30 (1:4, EtOAc:Hex). **<sup>1</sup>H NMR** (400 MHz, CDCl<sub>3</sub>):  $\delta$  8.58 (dd, *J* = 4.7, 1.5 Hz, 1H, H-4), 7.76 (dd, *J* = 8.1, 1.5 Hz, 1H, H-2), 7.42 (ddd, *J* = 8.3, 7.4, 1.8 Hz, 1H, H-9), 7.31 (dd, *J* = 7.5, 1.8 Hz, 1H, H-7), 7.23 (dd, *J* = 8.1, 4.7 Hz, 1H, H-3), 7.06 (td, *J* = 7.5, 1.0 Hz, 1H, H-8), 7.00 (dd, *J* = 8.3, 1.0 Hz, 1H, H-10), 3.80 (s, 3H, MeO). **<sup>13</sup>C NMR** (101 MHz, CDCl<sub>3</sub>):  $\delta$  156.9 (C-11), 155.8 (C-5), 147.4 (C-4), 137.1 (C-2), 132.3 (C-1), 130.5 (C-9/7), 130.4 (C-9/7), 128.0 (C-6), 123.3 (C-3), 120.7 (C-8), 111.1 (C-10), 55.7 (MeO). **HRMS** (ESI<sup>+</sup>) *m/z*: Found 220.0526 Calculated for C<sub>12</sub>H<sub>11</sub>ClNO [M+H]<sup>+</sup> 220.0526.  $\Delta$  = 1.1 ppm.

Data in accordance with literature and assignments made based on COSY, HSQC and HMBC data.<sup>219</sup>

## Experimental

---

3-Chloro-2-(2-methoxy-6-(4,4,5,5-tetramethyl-1,3,2-dioxaborolan-2-yl)phenyl)pyridine **93**



Synthesized according to the **General Ir-Catalysed Borylation Procedure** from biaryl-pyridine **87** (2.00 g, 9.10 mmol),  $B_2pin_2$  (11.6 g, 45.5 mmol),  $[Ir(OMe)(cod)]_2$  (0.151 g, 0.228 mmol), hemilabile ligand **92** (0.137 g, 0.455 mmol) and  $HBpin$  (0.291 g, 2.28 mmol), with column chromatography (1:4 EtOAc:Hex) affording the title compound **93** as a white solid (1.32 g, 42%).

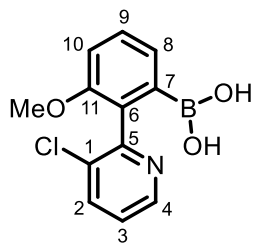
**R<sub>f</sub>** 0.25 (1:4 EtOAc:Hex). **mp:** 106.2 °C – 108.9 °C. **<sup>1</sup>H NMR** (400 MHz,  $CDCl_3$ ):  $\delta$  8.52 (dd,  $J$  = 4.7, 1.5 Hz, 1H, H-4), 7.70 (dd,  $J$  = 8.0, 1.5 Hz, 1H, H-2), 7.46 (dd,  $J$  = 7.4, 1.3 Hz, 1H, H-8), 7.40 (dd,  $J$  = 8.3, 7.3 Hz, 1H, H-9), 7.20 (dd,  $J$  = 8.0, 4.7 Hz, 1H, H-3), 7.07 (dd,  $J$  = 8.1, 1.4 Hz, 1H, H-10), 3.75 (s, 3H, MeO), 1.08 (s, 12H, H-13). **<sup>13</sup>C NMR** (101 MHz,  $CDCl_3$ ):  $\delta$  157.1 (C-5), 156.5 (C-11), 146.6 (C-4), 136.1 (C-2), 133.7 (C-6), 132.5 (C-1), 129.4 (C-9), 127.3 (C-8), 122.7 (C-3), 113.8 (C-10), 83.4 (C-12), 56.0 (MeO), 24.7 (C-13). \*C-7 not observed due to boron relaxation. **<sup>11</sup>B NMR** (128 MHz,  $CDCl_3$ ):  $\delta$  29.6. **IR v** ( $cm^{-1}$ ): 2978, 1577, 1411, 1347, 1316, 1256, 1140, 1043, 852, 799, 756. **HRMS** (ESI<sup>+</sup>) *m/z*: Found 346.1396 Calculated for  $C_{18}H_{22}BClNO_3^+$  [M+H]<sup>+</sup> 346.1379.  $\Delta$  = 4.9 ppm.

Assignments made based on COSY, HSQC and HMBC data.

## Experimental

---

### (2-(3-Chloropyridin-2-yl)-3-methoxyphenyl)boronic acid **97**



Synthesized according to the **General Biaryl Boronic Ester Hydrolysis Procedure** from Bpin–biaryl-pyridine **93** (0.250 g, 0.723 mmol), and NaIO<sub>4</sub> (0.464 g, 2.17 mmol) to afford the title compound **97** as a white solid (0.170 g, 89%).

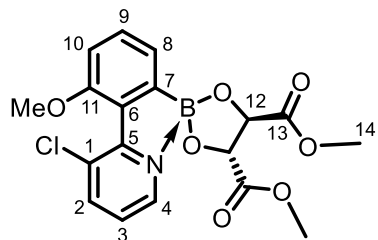
**mp:** 113.9 °C – 117.8 °C (dec.). **<sup>1</sup>H NMR** (400 MHz, CDCl<sub>3</sub>): δ 8.07 (dd, *J* = 4.9, 1.5 Hz, 1H, H-4), 7.47 (dd, *J* = 8.1, 1.5 Hz, 1H, H-2), 7.36 (dd, *J* = 8.2, 7.3 Hz, 1H, H-9), 7.23 (dd, *J* = 7.3, 1.1 Hz, 1H, H-8), 6.97 (dd, *J* = 8.2, 1.1 Hz, 1H, H-10), 6.89 (dd, *J* = 8.1, 4.9 Hz, 1H, H-3), 3.79 (s, 3H, MeO). **<sup>13</sup>C NMR** (101 MHz, CDCl<sub>3</sub>): δ 156.5 (C-5), 156.4 (C-11), 144.0 (C-4), 138.8 (C-2), 131.1 (C-1), 130.7 (C-9), 130.4 (C-6), 126.1 (C-8), 122.0 (C-3), 112.8 (C-10), 55.7 (MeO). \*C-7 not observed due to boron relaxation. **<sup>11</sup>B NMR** (128 MHz, CDCl<sub>3</sub>): δ 19.7. **IR** *v* (cm<sup>-1</sup>): 3058, 2835, 1575, 1410, 1314, 1256, 1034, 789. **HRMS** (Nanospray) *m/z*: Found 264.0604 Calculated for C<sub>12</sub>H<sub>12</sub>NO<sub>3</sub>Cl<sup>(11)B</sup> [M+H]<sup>+</sup> 264.0599. Δ = 1.9 ppm.

Assignments made based on COSY, HSQC and HMBC data

## Experimental

---

Dimethyl (*4R,5R*)-2-(2-(3-chloropyridin-2-yl)-3-methoxyphenyl)-1,3,2-dioxaborolane-4,5-dicarboxylate **104**



Synthesized according to the **General Boron Esterification Procedure B** from boronic acid **97** (0.140 g, 0.531 mmol) and (+)-dimethyl L-tartrate (0.095 g, 0.531 mmol), to give the title compound **104** as white solid (0.215 g, 99%).

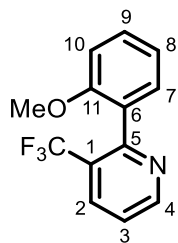
**mp:** 112.0 °C – 114.3 °C. **<sup>1</sup>H NMR** (400 MHz, CDCl<sub>3</sub>): δ 8.77 (dd, *J* = 5.3, 1.7 Hz, 1H, H-4), 8.02 (dd, *J* = 8.1, 1.7 Hz, 1H, H-2), 7.47 (dd, *J* = 8.3, 7.0 Hz, 1H, H-9), 7.33 (dd, *J* = 8.1, 5.3 Hz, 1H, H-3), 7.28 (d, *J* = 7.0 Hz, 1H, H-8), 6.90 (d, *J* = 8.3 Hz, 1H, H-10), 4.93 (s, 2H, H-12), 3.91 (s, 3H, MeO), 3.84 (s, 6H, H-14). **<sup>13</sup>C NMR** (101 MHz, CDCl<sub>3</sub>): δ 173.6 (C-13), 156.7 (C-11), 154.1 (C-5), 145.6 (C-2), 142.2 (C-4), 134.3 (C-9), 129.7 (C-1), 124.9 (C-6), 123.2 (C-8), 122.5 (C-3), 112.3 (C-10), 77.8 (C-12), 54.9 (OMe), 52.5 (C-14). \*C-7 not observed due to boron relaxation **<sup>11</sup>B NMR** (128 MHz, CDCl<sub>3</sub>): δ 12.6. **IR** *v* (cm<sup>-1</sup>): 3552, 3095, 2948, 1742, 1602, 1454, 1263, 1217, 1122, 1084, 989, 789. **HRMS** not found by Nanospray, EI or APCI.

Assignments made based on COSY, HSQC and HMBC data.

## Experimental

---

### 2-(2-Methoxyphenyl)-3-(trifluoromethyl)pyridine **88**



Synthesized according to the **General Suzuki Cross-Coupling Procedure A** from 3-(trifluoromethyl)-2-bromopyridine **84** (5.00 g, 22.1 mmol), methoxy boronic acid **81** (3.87 g, 25.4 mmol), Pd(OAc)<sub>2</sub> (0.248 g, 1.11 mmol), SPhos (0.908 g, 2.21 mmol) and Cs<sub>2</sub>CO<sub>3</sub> (14.4 g, 44.2 mmol), with column chromatography (1:6 EtOAc:Hex) affording the title compound **88** as a white solid (4.64 g, 83%).

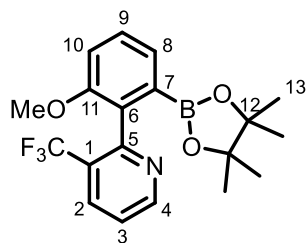
**R<sub>f</sub>** 0.30 (1:5 EtOAc:Hex) **mp:** 74.6 °C – 75.7 °C. **<sup>1</sup>H NMR** (400 MHz, CDCl<sub>3</sub>): δ 8.85 (dm, *J* = 5.7 Hz, 1H, H-4), 8.05 (dm, *J* = 8.1 Hz, 1H, H-2), 7.46 – 7.36 (m, 2H, H-3 and H-9), 7.23 (d, *J* = 7.5 Hz, 1H, H-7), 7.03 (t, *J* = 7.5 Hz, 1H, H-8), 6.97 (d, *J* = 8.2 Hz, 1H, H-10). 3.74 (s, 1H, OMe). **<sup>13</sup>C NMR** (126 MHz, *Cryo-probe*, CDCl<sub>3</sub>) δ 156.9 (C-11), 156.1 (q, *J* = 1.8 Hz, C-5), 152.0 (C-4), 134.6 (q, *J* = 4.9 Hz, C-2), 130.3 (C-3), 130.1 (C-7), 128.3 (C-6), 126.2 (q, *J* = 31 Hz, C-1), 123.6 (q, *J* = 274 Hz, CF<sub>3</sub>), 122.0 (C-9), 120.2 (C-8), 110.9 (C-10), 55.6 (OMe). **<sup>19</sup>F NMR** (376 MHz, CDCl<sub>3</sub>): δ -60.2. **<sup>1</sup>H-<sup>15</sup>N HMBC** (600 MHz, *Cryo-probe*, MeCN-d<sub>3</sub>, *J*<sub>H-N</sub> = 5 Hz): δ 323.7. **IR v** (cm<sup>-1</sup>): 3009, 2846, 1569, 1498, 1433, 1317, 1275, 1121, 1083, 1021, 746. **HRMS** (ESI<sup>+</sup>) *m/z*: Found 254.0787 Calculated for C<sub>13</sub>H<sub>11</sub>F<sub>3</sub>NO [M+H]<sup>+</sup> 254.0787. Δ = 0.3 ppm.

Assignments made based on COSY, HSQC and HMBC data.

## Experimental

---

3-Trifluoromethyl-2-(2-methoxy-6-(4,4,5,5-tetramethyl-1,3,2-dioxaborolan-2-yl)phenyl)pyridine **94**



Synthesized according to the **General Ir-Catalysed Borylation Procedure** from biaryl-pyridine **88** (1.00 g, 3.95 mmol),  $B_2\text{pin}_2$  (5.01 g, 19.7 mmol),  $[\text{Ir}(\text{OMe})(\text{cod})]_2$  (0.065 g, 0.099 mmol), hemilabile ligand **92** (0.060 g, 0.20 mmol) and  $\text{HBpin}$  (0.126 g, 0.987 mmol), with column chromatography (1:4 EtOAc:Hex) affording the title compound **94** as a white solid (0.963 g, 64 %).

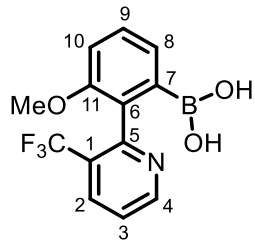
**R<sub>f</sub>** 0.63 (1:1 EtOAc:Hex) **mp:** 72.9 °C – 74.5 °C **<sup>1</sup>H NMR** (400 MHz,  $\text{CDCl}_3$ ):  $\delta$  8.78 (ddd,  $J = 4.9, 1.8, 0.8$  Hz, 1H, H-4), 7.98 (ddd,  $J = 7.9, 1.8, 0.7$  Hz, 1H, H-2), 7.47 (dd,  $J = 7.5, 1.2$  Hz, 1H, H-8), 7.42 – 7.34 (m, 2H, H-9 and H-3), 7.06 (dd,  $J = 8.1, 1.2$  Hz, 1H, H-10), 3.71 (s, 3H, MeO), 1.03 (s, 12H, H-13). **<sup>13</sup>C NMR** (126 MHz, *Cryo-probe*,  $\text{CDCl}_3$ ):  $\delta$  157.5 (q,  $J = 1.7$  Hz, C-5), 156.6 (C-11) 151.2 (C-4), 133.9 (C-6), 133.5 (q,  $J = 5.1$  Hz, C-2), 129.4 (C-9), 127.2 (C-8), 126.3 (q,  $J = 32$  Hz, C-1), 123.7 (q,  $J = 274$  Hz,  $\text{CF}_3$ ), 121.3 (C-3), 113.7 (C-10), 83.4 (C-12), 55.8 (MeO), 24.7 (C-13). \*C-7 not observed due to boron relaxation **<sup>11</sup>B NMR** (128 MHz,  $\text{CDCl}_3$ ):  $\delta$  29.4. **<sup>19</sup>F NMR** (376 MHz,  $\text{CDCl}_3$ ):  $\delta$  -60.7 **IR v (cm<sup>-1</sup>)**: 2978, 1573, 1427, 1351, 1317, 1258, 1114, 1047, 1029, 965, 852, 758. **HRMS (EI)** *m/z*: Found 364.1323 Calculated for  $\text{C}_{18}\text{H}_{18}\text{BF}_3\text{NO}_3^+$  [M-CH<sub>3</sub>]<sup>+</sup> 364.1326.  $\Delta = 0.8$  ppm.

Assignments made based on COSY, HSQC and HMBC data.

## Experimental

---

(3-Methoxy-2-(3-(trifluoromethyl)pyridin-2-yl)phenyl)boronic acid **98**



Synthesized according to the **General Biaryl Boronic Ester Hydrolysis Procedure** from Bpin-biaryl-pyridine **94** (0.400 g, 1.05 mmol), and NaIO<sub>4</sub> (0.677 g, 3.16 mmol) to afford the title compound **98** as a white solid (0.275 g, 88%).

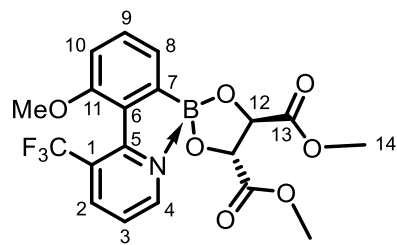
**mp:** 151.8 °C – 154.9 °C (dec.). **<sup>1</sup>H NMR** (400 MHz, CD<sub>3</sub>CN) δ 8.25 (d, *J* = 5.2 Hz, 1H, H-4), 7.86 (d, *J* = 7.6 Hz, 1H, H-2), 7.42 (t, *J* = 7.7 Hz, 1H, H-9), 7.18 – 7.09 (m, 2H, H-3 and H-8), 7.07 (d, *J* = 8.3 Hz, 1H, H-10), 3.72 (s, 3H, OMe). **<sup>13</sup>C NMR** (101 MHz, CD<sub>3</sub>CN) δ 157.7 (C-11), 156.9 (q, *J* = 2.0 Hz, C-5), 149.7 (C-4), 137.7 (q, *J* = 5.1 Hz, C-2), 131.7 (C-9), 131.0 (C-6), 125.9 (C-8), 125.6 (q, *J* = 33 Hz, C-1), 124.7 (q, *J* = 271 Hz, CF<sub>3</sub>), 122.4 (C-3), 113.5 (C-10), 55.9 (OMe). \*C-7 not observed due to boron relaxation **<sup>11</sup>B NMR** (128 MHz, CD<sub>3</sub>CN): δ 19.3. **<sup>19</sup>F NMR** (376 MHz, CD<sub>3</sub>CN) δ -60.71. **IR v** (cm<sup>-1</sup>): 3337, 3014, 2845, 1589, 1466, 1427, 1321, 1265, 1165, 1116, 1033, 797, 779, 746. **HRMS** (Nanospray, negative ion) *m/z*: Found 332.0488 Calculated for C<sub>13</sub>H<sub>11</sub>BClF<sub>3</sub>NO<sub>3</sub><sup>-</sup> [M+Cl]<sup>-</sup> 332.0478. Δ = 4.5 ppm.

Assignments made based on COSY, HMBC and HSQC data.

## Experimental

---

Dimethyl (4*R*,5*R*)-2-(3-methoxy-2-(3-(trifluoromethyl)pyridin-2-yl)phenyl)-1,3,2-dioxaborolane-4,5-dicarboxylate **103**



Synthesized according to the **General Boron Esterification Procedure B** from boronic acid **98** (0.140 g, 0.471 mmol) and (+)-dimethyl L-tartrate (0.084 g, 0.471 mmol), to give the title compound **103** as an off-white film (0.205 g, 99%).

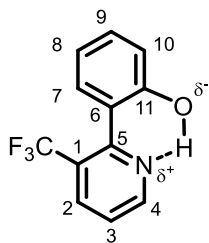
**<sup>1</sup>H NMR** (400 MHz, CD<sub>3</sub>CN) δ 8.89 (d, *J* = 5.2 Hz, 1H, H-4), 8.40 (d, *J* = 8.1 Hz, 1H, H-2), 7.64 (dd, *J* = 8.1, 5.2 Hz, 1H, H-3), 7.50 (t, *J* = 7.6 Hz, 1H, H-9), 7.26 (d, *J* = 7.0 Hz, 1H, H-10), 7.04 (d, *J* = 8.3 Hz, 1H, H-8), 4.82 (s, 2H, H-12), 3.84 (s, 3H, MeO), 3.76 (s, 6H, H-4). **<sup>13</sup>C NMR** (101 MHz, CD<sub>3</sub>CN) δ 173.5 (C-13), 157.8 (C-11), 153.9 (C-5), 148.2 (C-4), 142.2 (q, *J* = 3.9 Hz, C-2), 134.4 (C-9), 127.8 (C-6), 125.5 (q, *J* = 34 Hz, C-1) 124.6 (C-10), 123.7 (q, *J* = 273 Hz, CF<sub>3</sub>), 123.5 (C-3), 113.0 (C-8), 78.5 (C-12), 55.4 (MeO), 52.9 (C-14). \*C-7 not observed due to boron relaxation **<sup>11</sup>B NMR** (128 MHz, CDCl<sub>3</sub>) δ 13.3. **<sup>19</sup>F NMR** (376 MHz, CD<sub>3</sub>CN) δ -60.44 **IR** *v* (cm<sup>-1</sup>): 3213, 2955, 1749, 1737, 1590, 1466, 1437, 1319, 1121, 1086, 1023, 755. **HRMS** (APCI<sup>+</sup>) *m/z*: Found 440.1131 Calculated for C<sub>19</sub>H<sub>18</sub>BF<sub>3</sub>NO<sub>7</sub><sup>+</sup> [M+H]<sup>+</sup> 440.1123. Δ = 1.8 ppm.

Assignments made based on COSY, HMBC and HSQC data.

## Experimental

---

### 2-(3-(Trifluoromethyl)pyridin-2-yl)phenol **190**



In a flame-dried Schlenk tube, 2-(2-methoxyphenyl)-3-(trifluoromethyl)pyridine **88** (0.100 g, 0.395 mmol) was dissolved in CH<sub>2</sub>Cl<sub>2</sub> (2 mL, 0.2 M) and cooled to 0 °C, whereupon BBr<sub>3</sub> (1 M solution in heptane, 1.2 mL, 1.18 mmol, 3 eq) was added slowly. After addition, the reaction mixture was allowed to warm to room temperature and left to stir overnight. The reaction was cooled to 0 °C, and quenched with 2 M NaOH (2 mL). 2 M HCl (~2 mL) was then added until the reaction mixture reached ~pH = 7, further diluted with sat. aq. NH<sub>4</sub>Cl (5 mL), and the mixture extracted with CH<sub>2</sub>Cl<sub>2</sub>. The organic layer was dried with MgSO<sub>4</sub>, filtered through Celite®, and evaporated *in vacuo*. The residue was purified by column chromatography (1:3 EtOAc:Hex) to give the title compound **190** as a white solid (0.093 g, 99%).

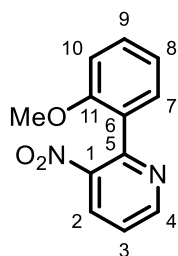
**R<sub>f</sub>** 0.60 (1:1 EtOAc:Hex). **mp:** 64.7 °C – 66.9 °C. **<sup>1</sup>H NMR** (400 MHz, CDCl<sub>3</sub>): δ 10.29 (s, 1H, OH), 8.77 (dd, *J* = 4.8, 2.0 Hz, 1H, H-4), 8.21 (dd, *J* = 8.0, 2.0 Hz, 1H, H-2), 7.53 (dt, *J* = 8.0, 1.5 Hz, 1H, H-7), 7.45 (dd, *J* = 8.0, 4.8 Hz, 1H, H-3), 7.36 (ddd, *J* = 8.2, 7.4, 1.8 Hz, 1H, H-9), 7.07 (dd, *J* = 8.2, 1.6 Hz, 1H, H-10), 6.96 (td, *J* = 7.8, 1.6 Hz, 1H, H-8). **<sup>13</sup>C NMR** (126 MHz, *Cryo-probe*, CDCl<sub>3</sub>) δ 156.6 (q, *J* = 1.6 Hz, C-5), 156.2 (C-11), 150.2 (C-4), 137.6 (q, *J* = 5.3 Hz, C-2), 131.9 (C-9), 130.4 (q, *J* = 4.5 Hz, C-7), 130.3 (C-7), 125.0 (q, *J* = 32 Hz, C-1), 123.6 (q, *J* = 274 Hz, C of CF<sub>3</sub>), 121.8 (C-6), 121.8 (C-3), 119.7 (C-8), 117.9 (C-10). **<sup>19</sup>F NMR** (376 MHz, CDCl<sub>3</sub>): δ -56.6. **<sup>1</sup>H-<sup>15</sup>N HMBC** (600 MHz, *Cryo-probe*, MeCN-d<sub>3</sub>, *J<sub>H-N</sub>* = 10 Hz): δ 317.4. **IR v** (cm<sup>-1</sup>): 3081, 2717, 1578, 1443, 1380, 1322, 1229, 1112, 1084, 1035, 843, 751. **HRMS** (ESI<sup>+</sup>) *m/z*: Found 262.0448 Calculated for C<sub>12</sub>H<sub>8</sub>F<sub>3</sub>NONa<sup>+</sup> [M+Na]<sup>+</sup> 262.0450. Δ = 0.6 ppm.

Assignments made based on COSY, HSQC and HMBC data.

## Experimental

---

### 2-(2-Methoxyphenyl)-3-nitropyridine **89**



Synthesized according to the **General Suzuki Cross-Coupling Procedure A** from 3-nitro-2-bromopyridine **85** (4.00 g, 19.7 mmol), methoxy boronic acid **81** (3.44 g, 22.7 mmol), Pd(OAc)<sub>2</sub> (0.221 g, 0.985 mmol), SPhos (0.809 g, 1.97 mmol) and Cs<sub>2</sub>CO<sub>3</sub> (12.8 g, 39.4 mmol), with column chromatography (1:6 EtOAc:Hex) affording the title compound **89** as a white solid (4.10 g, 90%).

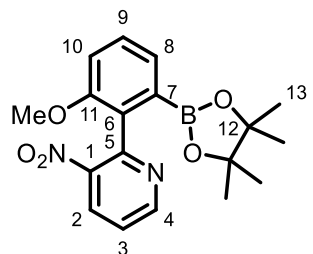
**R<sub>f</sub>** 0.23 (1:1 CH<sub>2</sub>Cl<sub>2</sub>:Hex). **mp:** 126.9 °C – 129.1 °C. **<sup>1</sup>H NMR** (400 MHz, CDCl<sub>3</sub>): δ 8.88 (dt, *J* = 4.8, 1.5 Hz, 1H, H-4), 8.22 (dt, *J* = 8.1, 1.5 Hz, 1H, H-2), 7.68 (dt, *J* = 7.5, 1.5 Hz, 1H, H-10), 7.48 – 7.40 (m, 2H, H-8 and H-3), 7.15 (tt, *J* = 7.5, 1.2 Hz, 1H, H-9), 6.92 (dd, *J* = 8.3, 1.1 Hz, 1H, H-7), 3.72 (s, 3H, OMe). **<sup>13</sup>C NMR** (101 MHz, CDCl<sub>3</sub>): δ 156.3 (C-11), 152.6 (C-4), 150.7 (C-5), 147.1 (C-1), 131.8 (C-2), 131.4 (C-8), 130.7 (C-10), 126.3 (C-6), 122.3 (C-3), 121.6 (C-9), 110.7 (C-7), 55.1 (OMe). **MS (ESI<sup>+</sup>)** *m/z*: Found 231.1 Calculated for C<sub>12</sub>H<sub>11</sub>N<sub>2</sub>O<sub>3</sub><sup>+</sup> [M+H]<sup>+</sup> 231.1.

Data in accordance with literature and assignments made based on COSY, HMBC and HSQC data.<sup>220</sup>

## Experimental

---

2-(2-Methoxy-6-(4,4,5,5-tetramethyl-1,3,2-dioxaborolan-2-yl)phenyl)-3-nitropyridine **95**



Synthesized according to the **General Ir-Catalysed Borylation Procedure** from biaryl-pyridine **89** (2.00 g, 8.69 mmol),  $B_2\text{pin}_2$  (11.0 g, 43.4 mmol),  $[\text{Ir}(\text{OMe})(\text{cod})]_2$  (0.144 g, 0.217 mmol), hemilabile ligand **92** (0.131 g, 0.434 mmol) and  $\text{HBpin}$  (0.278 g, 2.17 mmol), with filtration through a pad of silica affording a mixture of the title compound **95** and  $B_2\text{pin}_2$  as a crude white solid which was used directly in the next reaction.

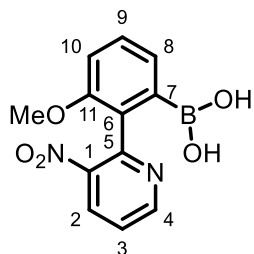
*Selected data from the crude mixture presented below:*

**R<sub>f</sub>** 0.23 (1:1  $\text{CH}_2\text{Cl}_2$ :Hex). **<sup>1</sup>H NMR** (400 MHz,  $\text{CDCl}_3$ ):  $\delta$  8.79 (dd,  $J = 4.7, 1.5$  Hz, 1H), 8.29 (dd,  $J = 8.2, 1.6$  Hz, 1H), 7.45 (dd,  $J = 7.4, 1.3$  Hz, 1H), 7.42 – 7.37 (m, 2H), 7.00 (dd,  $J = 8.2, 1.4$  Hz, 1H), 3.68 (s, 3H), 1.10 (s, 12H). **<sup>11</sup>B NMR** (128 MHz,  $\text{CDCl}_3$ ):  $\delta$  29.7.

## Experimental

---

### (3-Methoxy-2-(3-nitropyridin-2-yl)phenyl)boronic acid **99**



Synthesized according to the **General Biaryl Boronic Ester Hydrolysis Procedure** from the crude Bpin-biaryl-pyridine **95** mixture (*est.* 8.69 mmol), and NaIO<sub>4</sub> (5.57 g, 26.1 mmol) to afford the title compound **99** as a white solid (0.238 g 10% over 2 steps).

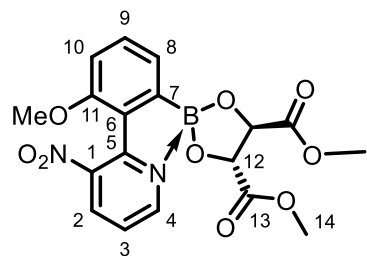
**mp:** 215.8 °C – 218.0 °C **<sup>1</sup>H NMR** (500 MHz, *Cryo-probe*, CDCl<sub>3</sub>) 8.47 (dd, *J* = 5.0, 1.6 Hz, 1H, H-4), 7.98 (dd, *J* = 8.1, 1.5 Hz, 1H, H-2), 7.39 (dd, *J* = 8.2, 7.2 Hz, 1H, H-9), 7.23 – 7.16 (m, 2H, H-3 and H-8), 6.90 (dd, *J* = 8.2, 0.8 Hz, 1H, H-10), 3.76 (s, 3H, MeO) **<sup>13</sup>C NMR** (126 MHz, *Cryo-probe*, CDCl<sub>3</sub>): δ 156.8 (C-11), 151.1 (C-5), 147.4 (C-4), 145.9 (C-1), 133.9 (C-2), 132.4 (C-9), 127.4 (C-6), 124.8 (C-8), 121.9 (C-3), 111.8 (C-10), 55.2 (MeO). \*C-7 not observed due to boron relaxation. **<sup>11</sup>B NMR** (128 MHz, CDCl<sub>3</sub>): δ 16.8 **IR v** (cm<sup>-1</sup>): 2970, 2949, 2845, 1739, 1724, 1546, 1525, 1458, 1348, 1311, 1265, 1170, 1092, 1041, 859, 737. **HRMS** not found by ESI or Nanospray (Neagitive ion).

Assignments made based on COSY, HMBC and HSQC data.

## Experimental

---

Dimethyl (4*R*,5*R*)-2-(3-methoxy-2-(3-nitropyridin-2-yl)phenyl)-1,3,2-dioxaborolane-4,5-dicarboxylate **104**



Synthesized according to the **General Boron Esterification Procedure B** from boronic acid **99** (0.100 g, 0.365 mmol) and (+)-dimethyl L-tartrate (0.065 g, 0.365 mmol), to give the title compound **104** as white solid (0.150 g, 99%).

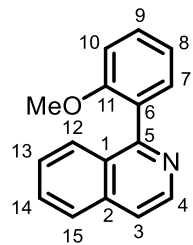
**mp:** 205.1 °C – 207.3 °C **<sup>1</sup>H NMR** (400 MHz, CDCl<sub>3</sub>): δ 9.10 (dd, *J* = 5.4, 1.4 Hz, 1H, H-4), 8.23 (dd, *J* = 8.1, 1.4 Hz, 1H, H-2), 7.56 – 7.51 (m, 2H, H-9 and H-3), 7.35 (dd, *J* = 7.1, 0.9 Hz, 1H, H-8), 6.87 (dd, *J* = 8.4, 0.9 Hz, 1H, H-10), 4.96 (s, 2H, H-12), 3.89 (s, 6H, H-14), 3.84 (s, 3H, OMe). **<sup>13</sup>C NMR** (101 MHz, CDCl<sub>3</sub>): δ 173.7 (C-13), 157.3 (C-11), 148.6 (C-5), 146.3 (C-4), 145.2 (C-1), 137.4 (C-2), 135.8 (C-9), 123.8 (C-8), 123.0 (C-6), 122.1 (C-3), 111.7 (C-10), 78.0 (C-12), 54.6 (MeO), 52.7 (C-14). \*C-7 not observed due to boron relaxation. **<sup>11</sup>B NMR** (128 MHz, CDCl<sub>3</sub>): δ 13.1. **<sup>1</sup>H-<sup>15</sup>N HMBC** (600 MHz, *Cryo-probe*, MeCN-d<sub>3</sub>, *J*<sub>H-N</sub> = 5 Hz): δ 252.4 (N-Pyridine), 370.9 (N-Nitro). **IR v** (cm<sup>-1</sup>): 3106, 3076, 2958, 1729, 1591, 1579, 1545, 1465, 1373, 1288, 1275, 1207, 1123, 1083, 1011, 795, 722. **HRMS** (Nanospray) *m/z*: Found 417.1112 Calculated for C<sub>18</sub>H<sub>18</sub>BN<sub>2</sub>O<sub>9</sub><sup>+</sup> [M+H]<sup>+</sup> 417.1105. Δ = 1.7 ppm.

Assignments made based on COSY, HMBC and HSQC data.

## Experimental

---

### 1-(2-Methoxyphenyl)isoquinoline **90**



Synthesized according to the **General Suzuki Cross-Coupling Procedure A** from 1-chloroisoquinoline **86** (2.50 g, 15.3 mmol), methoxy boronic acid **81** (2.67 g, 17.6 mmol), Pd(OAc)<sub>2</sub> (0.172 g, 0.764 mmol), SPhos (0.627 g, 1.53 mmol) and Cs<sub>2</sub>CO<sub>3</sub> (9.96 g, 30.6 mmol), with column chromatography (1:6 EtOAc:Hex) affording the title compound **90** as a white solid (2.84 g, 79%).

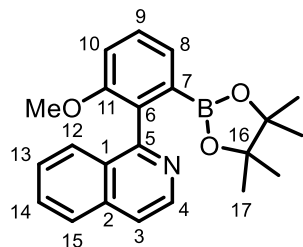
**R<sub>f</sub>** 0.32 (1:3 EtOAc:Hex) **mp:** 76.9 °C – 78.1 °C **<sup>1</sup>H NMR** (400 MHz, CDCl<sub>3</sub>): δ 8.62 (d, *J* = 5.8 Hz, 1H, H-4), 7.86 (d, *J* = 8.3 Hz, 1H, H-15), 7.71 (d, *J* = 8.6 Hz, 1H, H-12), 7.69 – 7.63 (m, 2H, H-3 and H-14), 7.51 – 7.44 (m, 2H, H-13 and H-9), 7.39 (dd, *J* = 7.6, 2.0 Hz, 1H, H-7), 7.12 (t, *J* = 7.6 Hz, 1H, H-8), 7.06 (d, *J* = 8.3 Hz, 1H, H-10), 3.70 (s, 3H, MeO). **<sup>13</sup>C NMR** (101 MHz, CDCl<sub>3</sub>): δ 159.2 (C-5), 157.3 (C-11), 142.4 (C-4), 136.3 (C-2), 131.3 (C-7), 130.1 (C-9), 130.0 (C-14), 128.8 (C-6), 128.0 (C-12), 127.9 (C-1), 127.0 (C-13), 126.8 (C-15), 120.9 (C-8), 120.2 (C-3), 111.2 (C-10), 55.7 (MeO). **HRMS** (ESI<sup>+</sup>) *m/z*: Found 236.1065 Calculated for C<sub>16</sub>H<sub>14</sub>NO<sup>+</sup> [M+H]<sup>+</sup> 236.1070. Δ = 2.1 ppm.

Data in accordance with literature and assignments made based on COSY, HMBC and HSQC data. <sup>115</sup>

## Experimental

---

1-(2-Methoxy-6-(4,4,5,5-tetramethyl-1,3,2-dioxaborolan-2-yl)phenyl)isoquinoline **96**



Synthesized according to the **General Ir-Catalysed Borylation Procedure** from biaryl-pyridine **90** (0.150 g, 0.638 mmol), B<sub>2</sub>pin<sub>2</sub> (0.810 g, 3.19 mmol), [Ir(OMe)(cod)]<sub>2</sub> (0.011 g, 0.016 mmol), hemilabile ligand **92** (0.010 g, 0.032 mmol) and HBpin (0.020 g, 0.159 mmol), with column chromatography (1:3 EtOAc:Hex) affording the title compound **96** as a white solid (0.150 g, 65 %).

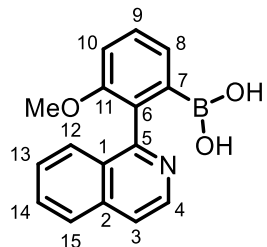
**R<sub>f</sub>** 0.23 (1:3 EtOAc:Hex) **mp:** 39.1 °C – 42.9 °C **<sup>1</sup>H NMR** (500 MHz, *Cryo-probe*, CDCl<sub>3</sub>) 8.57 (d, *J* = 5.6 Hz, 1H, H-4), 7.83 (dt, *J* = 7.9, 1.1 Hz, 1H, H-15), 7.65 – 7.59 (m, 3H, H-3, H-12 and H-14), 7.49 – 7.44 (m, 2H, H-9 and H-8), 7.41 (ddd, *J* = 8.1, 7.0, 1.3 Hz, 1H, H-13), 7.13 (dd, *J* = 7.4, 1.9 Hz, 1H, H-10), 3.68 (s, 3H, MeO), 0.85 (s, 12H, H-17). **<sup>13</sup>C NMR** (126 MHz, *Cryo-probe*, CDCl<sub>3</sub>): δ 160.3 (C-5), 157.1 (C-11), 141.8 (C-4), 136.2 (C-2), 134.0 (C-6), 129.6 (C-14), 129.4 (C-9), 129.0 (C-1), 127.9 (C-12), 127.1 (C-8), 126.58 (C-15), 126.56 (C-13), 119.6 (C-3), 113.8 (C-10), 83.2 (C-16), 56.0 (OMe), 24.5 (C-17). \*C-7 not observed due to boron relaxation. **<sup>11</sup>B NMR** (128 MHz, CDCl<sub>3</sub>): δ 29.3. **HRMS** (ESI<sup>+</sup>) *m/z*: Found 362.1930 Calculated for C<sub>22</sub>H<sub>25</sub>NO<sub>3</sub>B<sup>+</sup> [M+H]<sup>+</sup> 362.1922. Δ = 2.2 ppm.

Data in accordance with literature and assignments made based on COSY, HMBC and HSQC data.<sup>115</sup>

## Experimental

---

### (2-(Isoquinolin-1-yl)-3-methoxyphenyl)boronic acid **100**



Synthesized according to the **General Biaryl Boronic Ester Hydrolysis Procedure** from Bpin-biaryl-pyridine **96** (0.100 g, 0.277 mmol), and NaIO<sub>4</sub> (0.178 g, 0.831 mmol) to afford the title compound **100** as a white foam (0.053 g, 69%).

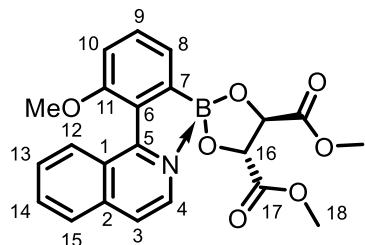
**mp:** 56 °C (dec) **<sup>1</sup>H NMR** (400 MHz, CD<sub>3</sub>OD) δ 9.31 (dd, *J* = 8.8, 1.0 Hz, 1H, H-12), 8.26 (d, *J* = 6.1 Hz, 1H, H-4), 8.09 (dt, *J* = 8.4, 0.9 Hz, 1H, H-15), 8.02 (dd, *J* = 6.2, 0.8 Hz, 1H, H-3), 7.96 (ddd, *J* = 8.3, 6.9, 1.2 Hz, 1H, H-14), 7.82 (ddd, *J* = 8.4, 6.9, 1.5 Hz, 1H, H-13), 7.58 (dd, *J* = 8.3, 6.9 Hz, 1H, H-9), 7.28 (dd, *J* = 7.0, 1.0 Hz, 1H, H-10), 7.17 (dd, *J* = 8.3, 0.9 Hz, 1H, H-8), 4.03 (s, 3H, MeO). **<sup>13</sup>C NMR** (101 MHz, CD<sub>3</sub>OD) δ 159.3 (C-5), 158.1 (C-11), 141.5 (C-2), 134.9 (C-9), 134.6 (C-14), 133.5 (C-4), 131.8 (C-12), 128.9 (C-13), 128.4 (C-15), 128.2 (C-6), 126.1 (C-1), 123.8 (C-10), 123.7 (C-3), 113.4 (C-8), 55.8 (MeO). \*C-7 not observed due to boron relaxation. **<sup>11</sup>B NMR** (128 MHz, CD<sub>3</sub>OD): δ 8.65. **IR v** (cm<sup>-1</sup>): 3436, 2836, 1645, 1621, 1434, 1384, 1247, 1089, 1017, 976, 828, 748. **HRMS** not found by Nanospray or APCI (positive or negative ion).

Assignments made based on COSY, HMBC and HSQC data.

## Experimental

---

Dimethyl (4*R*,5*R*)-2-(2-(isoquinolin-1-yl)-3-methoxyphenyl)-1,3,2-dioxaborolane-4,5-dicarboxylate **105**



Synthesized according to the **General Boron Esterification Procedure B** from boronic acid **100** (0.100 g, 0.358 mmol) and (+)-dimethyl L-tartrate (0.064 g, 0.358 mmol), to give the title compound **105** as an off-white film (0.150 g, 99%).

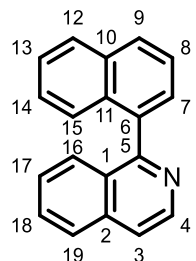
**<sup>1</sup>H NMR** (400 MHz, CDCl<sub>3</sub>): δ 9.22 (d, *J* = 8.8 Hz, 1H, H-12), 8.52 (d, *J* = 6.3 Hz, 1H, H-4), 7.89 – 7.81 (m, 2H, H-14 and H-15), 7.74 (d, *J* = 6.3 Hz, 1H, H-3), 7.67 (ddd, *J* = 8.3, 6.6, 1.8 Hz, 1H, H-13), 7.50 (dd, *J* = 8.6, 6.9 Hz, 1H, H-9), 7.38 (dd, *J* = 6.9, 1.0 Hz, 1H, H-8), 6.96 (dd, *J* = 8.6, 1.1 Hz, 1H, H-10), 5.00 (s, 2H, H-16), 3.94 (s, 3H, MeO), 3.86 (s, 6H, H-18). **<sup>13</sup>C NMR** (101 MHz, CDCl<sub>3</sub>): δ 173.9 (C-17), 158.9 (C-5), 156.1 (C-11), 140.2 (C-2), 134.4 (C-9), 133.9 (C-4), 133.3 (C-14), 131.0 (C-12), 127.3 (C-13), 127.0 (C-15), 126.9 (C-6), 125.1 (C-1), 123.8 (C-8), 122.0 (C-3), 112.6 (C-10), 77.9 (C-16), 55.5 (MeO), 52.5 (C-18). \*C-7 not observed due to boron relaxation. **<sup>11</sup>B NMR** (128 MHz, CDCl<sub>3</sub>): δ 11.6. **IR** *v* (cm<sup>-1</sup>): 2952, 1736, 1623, 1473, 1436, 1357, 1262, 1214, 1122, 1015, 709. **HRMS** (APCI<sup>+</sup>) Found 422.1419 Calculated for C<sub>22</sub>H<sub>21</sub>BNO<sub>7</sub><sup>+</sup> [M]<sup>+</sup> 422.1406. Δ = 3.1 ppm.

Assignments made based on COSY, HMBC and HSQC data.

## Experimental

---

### 1-(Naphthalen-1-yl)isoquinoline **91**



Synthesized according to the **General Suzuki Cross-Coupling Procedure A** from 1-chloroisoquinoline **86** (7.21 g, 44.1 mmol), naphthyl boronic acid **82** (8.72 g, 50.7 mmol), Pd(OAc)<sub>2</sub> (0.495 g, 2.20 mmol), SPhos (1.81 g, 4.40 mmol) and Cs<sub>2</sub>CO<sub>3</sub> (28.7 g, 88.1 mmol), with column chromatography (1:6 EtOAc:Hex) affording the title compound **91** as a white solid (11.2 g, 99%).

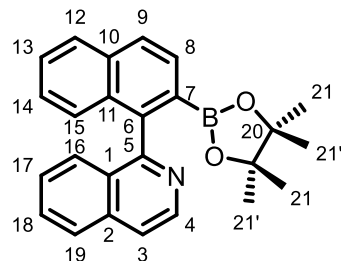
**R<sub>f</sub>** 0.40 (1:4 CH<sub>2</sub>Cl<sub>2</sub>:Hex) **mp:** 103.6 °C – 105.2 °C. **<sup>1</sup>H NMR** (400 MHz, CDCl<sub>3</sub>): δ 8.72 (d, *J* = 5.8 Hz, 1H, H-4), 8.01 (dt, *J* = 7.9, 1.2 Hz, 1H, H-13), 7.96 (dd, *J* = 8.4, 1.1 Hz, 1H, H-15), 7.95 (dt, *J* = 8.2, 0.9 Hz, 1H, H-19), 7.76 (dd, *J* = 5.8, 1.0 Hz, 1H, H-3), 7.68 (ddd, *J* = 8.1, 6.8, 1.2 Hz, 1H, H-18), 7.65 – 7.61 (m, 2H, H-12 and H-7), 7.60 (dd, *J* = 7.0, 1.7 Hz, 1H, H-16) 7.49 (ddd, *J* = 8.2, 6.7, 1.4 Hz, 1H, H-9), 7.43 – 7.37 (m, 2H, H-17 and H-14), 7.33 (ddd, *J* = 8.2, 6.7, 1.4 Hz, 1H, H-8). **<sup>13</sup>C NMR** (101 MHz, CDCl<sub>3</sub>): δ 160.6 (C-5), 142.5 (C-4), 137.1 (C-6), 136.6 (C-2), 133.8 (C-11), 132.4 (C-10), 130.3 (C-18), 128.9 (C-13), 128.4 (C-1), 128.4 (C-15), 127.9 (C-16), 127.8 (C-12), 127.3 (C-17), 127.0 (C-19), 126.4 (C-8), 126.1 (C-9), 126.0 (C-7), 125.3 (C-14), 120.3 (C-3). **MS (ESI<sup>+</sup>)** *m/z:* Found 256.1 Calculated for C<sub>19</sub>H<sub>14</sub>N<sup>+</sup> [M+H]<sup>+</sup> 256.1.

Data in accordance with literature and assignments made based on COSY, HMBC and HSQC data. <sup>115</sup>

## Experimental

---

1-(2-(4,4,5,5-Tetramethyl-1,3,2-dioxaborolan-2-yl)naphthalen-1-yl)isoquinoline **79**



Synthesized according to the **General Ir-Catalysed Borylation Procedure** from biaryl-pyridine **91** (6.00 g, 23.5 mmol), B<sub>2</sub>pin<sub>2</sub> (8.95 g, 35.2 mmol)\*, [Ir(OMe)(cod)]<sub>2</sub> (0.389 g, 0.588 mmol), hemilabile ligand **92** (0.354 g, 1.18 mmol) and HBpin (0.752 g, 5.88 mmol), with column chromatography (1:3 EtOAc:Hex) affording the title compound **79** as an off-white/light yellow oil which foamed into an off white solid upon drying (8.35g, 93%).

\*1.5 eq used rather than 5.0 eq specified in the General Procedure

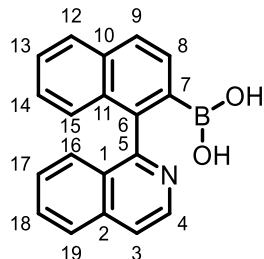
**R<sub>f</sub>** 0.20 (1:3 EtOAc:Hex) **mp:** 52.8 °C – 57.8 °C **<sup>1</sup>H NMR** (600 MHz, *Cryo-probe*, CDCl<sub>3</sub>) 8.66 (d, *J* = 5.7 Hz, 1H, H-4), 7.97 (d, *J* = 8.4 Hz, 1H, H-9), 7.95 (d, *J* = 8.4 Hz, 1H, H-8), 7.92 (d, *J* = 8.2 Hz, 1H, H-12), 7.89 (d, *J* = 8.3 Hz, 1H, H-19), 7.73 (d, *J* = 5.7 Hz, 1H, H-3), 7.62 (ddd, *J* = 8.3, 6.8, 1.4 Hz, 1H, H-18), 7.48 (ddd, *J* = 8.2, 6.4, 1.5 Hz, 1H, H-13), 7.42 (dd, *J* = 8.5, 1.0 Hz, 1H, H-16), 7.34 – 7.27 (m, 3H, H-14, H-15 and H-17), 0.94 (s, 6H, H-21 or H-21'), 0.74 (s, 6H, H-21 or H-21'). **<sup>13</sup>C NMR** (151 MHz, *Cryo-probe*, CDCl<sub>3</sub>): 161.9 (C-5), 144.5 (C-6), 142.1 (C-4), 136.1 (C-2), 135.0 (C-10), 132.4 (C-11), 130.5 (C-8), 129.81 (C-18), 129.79 (C-1), 128.1 (C-12), 127.7 (C-15), 127.6 (C-9), 127.0 (C-16), 126.85 (C-13), 126.82 (C-17), 126.6 (C-19), 126.2 (C-14), 119.7 (C-3), 83.3 (C-20), 24.6 (C-21 or C-21'), 24.3 (C-21 or C-21'). \*C-7 not observed due to boron relaxation. **<sup>11</sup>B NMR** (128 MHz, CDCl<sub>3</sub>): δ 30.0 **<sup>1</sup>H-<sup>15</sup>N HMBC** (600 MHz, *Cryo-probe*, CDCl<sub>3</sub>, *J*<sub>H-N</sub> = 5Hz): δ 308.8. **HRMS** (ESI<sup>+</sup>) *m/z*: Found 382.1969 Calculated for C<sub>25</sub>H<sub>25</sub>NO<sub>2</sub>B<sup>+</sup> [M+H]<sup>+</sup> 382.1973. Δ = 0.1 ppm. **HPLC** Chiral OD-H, hexane:isopropanol = 99:1, flow = 1.0 mL/min, λ = 254 nm, t<sub>R</sub> = 20.33, 23.25 min.

Data in accordance with literature and assignments made based on COSY, HMBC and HSQC data.<sup>115</sup>

## Experimental

---

### (1-(Isoquinolin-1-yl)naphthalen-2-yl)boronic acid **101**



Synthesized according to the **General Biaryl Boronic Ester Hydrolysis Procedure** from Bpin-biaryl-pyridine **79** (3.00 g, 7.87 mmol), and NaIO<sub>4</sub> (5.05 g, 23.6 mmol) to afford the title compound **101** as a white solid (1.65 g, 92%).

**mp:** 218 °C – 250 °C (dec.) **<sup>1</sup>H NMR** (400 MHz, CD<sub>3</sub>OD) δ 8.43 (d, *J* = 6.0 Hz, 1H, H-4), 8.27 (d, *J* = 7.3 Hz, 1H H-16/19 or H-12/15), 8.15 (d, *J* = 8.4 Hz, 1H, H-16/19 or H-12/15), 8.10 (d, *J* = 7.9 Hz, 1H, H-9/8), 8.06 (d, *J* = 6.0 Hz, 1H, H-3), 8.02 (dd, *J* = 8.0, 1.6 Hz, 1H, H-12/15 or H-16/19), 7.94 (t, *J* = 7.6 Hz, 1H, H-17/18 or H-13/14), 7.88 (d, *J* = 7.8 Hz, 1H H-12/15 or H-16/19), 7.79 (d, *J* = 7.9 Hz, 1H, H-9/8), 7.70 (t, *J* = 7.5 Hz, 1H, H-17/18 or H-13/14), 7.54 (ddd, *J* = 8.3, 6.9, 1.4 Hz, 1H, H-13/14 or H-17/18), 7.48 (ddd, *J* = 8.3, 6.7, 1.5 Hz, 1H, H-13/14 or H-17/18). **<sup>13</sup>C NMR** (101 MHz, CD<sub>3</sub>OD) δ 160.8 (C-Ar), 142.2 (C-Ar), 140.4 (C-Ar), 138.2 (C-Ar), 136.7 (C-Ar), 136.0 (C-Ar), 133.8 (C-Ar), 132.1 (C-Ar), 131.6 (C-Ar), 130.1 (C-Ar), 129.9 (C-Ar), 128.9 (C-Ar), 128.7 (C-Ar), 128.6 (C-Ar), 127.3 (C-Ar), 126.9 (C-Ar), 126.6 (C-Ar), 123.0 (C-Ar). \*C-7 not observed due to boron relaxation. **<sup>11</sup>B NMR** (128 MHz, CD<sub>3</sub>OD): δ 14.7. **IR** *v* (cm<sup>-1</sup>): 3047, 1556, 1401, 1243, 1139, 1073, 955, 867, 745. **HRMS** (Negative Ion Nanospray) *m/z*: Found 334.0804 Calculated for C<sub>19</sub>H<sub>14</sub>BNO<sub>2</sub>Cl<sup>-</sup> [M+Cl]<sup>-</sup> 334.0806. Δ = -0.6 ppm.

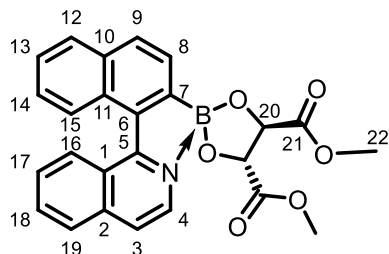
\*Assignments made based on COSY, HMBC and HSQC data.

*Line broadening in spectra preventing unambiguous assignment.*

## Experimental

---

Dimethyl (*4R,5R*)-2-(1-(isoquinolin-1-yl)naphthalen-2-yl)-1,3,2-dioxaborolane-4,5-dicarboxylate **106**



Synthesized according to the **General Boron Esterification Procedure B** from boronic acid **101** (0.100 g, 0.334 mmol) and (+)-dimethyl-L-tartrate (0.060 g, 0.334 mmol), to give the title compound **106** as a white solid (0.144 g, 98%).

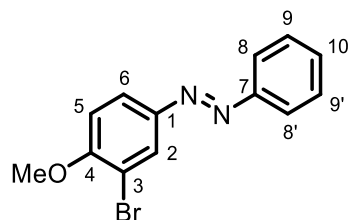
**mp:** 130 °C (dec.). **<sup>1</sup>H NMR** (400 MHz, CDCl<sub>3</sub>): δ 8.63 (d, *J* = 6.3 Hz, 1H, H-4), 8.56 (dd, *J* = 8.6, 1.0 Hz, 1H, H-16), 8.09 – 8.04 (m, 1H, H-12), 8.03 (dd, *J* = 7.8, 0.6 Hz, 1H, H-9), 7.97 (dt, *J* = 8.2, 0.7 Hz, 1H, H-19), 7.96 – 7.93 (m, 1H, H-15), 7.91 (d, *J* = 7.8 Hz, 1H, H-8), 7.89 (ddd, *J* = 8.3, 6.8, 1.1 Hz, 1H, H-18), 7.82 (dd, *J* = 6.3, 0.8 Hz, 1H, H-3), 7.67 (ddd, *J* = 8.6, 6.8, 1.3 Hz, 1H, H-17), 7.51 – 7.44 (m, 2H, H-13 and H-14), 5.03 (s, 2H, H-20), 3.89 (s, 6H, H-22). **<sup>13</sup>C NMR** (101 MHz, CDCl<sub>3</sub>): δ 173.8 (C-21), 160.0 (C-5), 140.4 (C-2), 135.4 (C-11), 135.3 (C-6), 134.7 (C-4), 133.4 (C-18), 133.1 (C-9), 130.2 (C-16), 129.5 (C-10), 129.2 (C-15), 128.2 (C-8), 127.6 (C-17), 127.3 (C-19), 126.0 (C-13), 125.42 (C-14 or C-12), 125.38 (C-14 or C-12), 124.4 (C-1), 121.6 (C-3), 78.0 (C-20), 52.6 (C-22). \*C-7 not observed due to boron relaxation. **<sup>11</sup>B NMR** (128 MHz, CDCl<sub>3</sub>): δ 12.5. **IR v** (cm<sup>-1</sup>): 3404, 3016, 2951, 1738, 1558, 1433, 1363, 1216, 1128, 1090, 1019, 823, 748. **HRMS** not found by Nanospray or EI.

Assignments made based on COSY, HMBC and HSQC data.

## Experimental

---

### (E)-1-(3-Bromo-4-methoxyphenyl)-2-phenyldiazene **119**



Synthesized according to the **General Mills Reaction** from 3-bromo-4-methoxyaniline **118** (15.0 g, 74.2 mmol) and nitrosobenzene **70** (10.3 g, 96.5 mmol), with column chromatography (1:3 CH<sub>2</sub>Cl<sub>2</sub>:Hex) affording the title compound **119** as an orange crystalline solid (20.3 g, 94%).

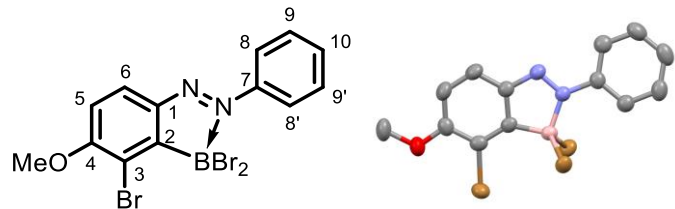
**R<sub>f</sub>** 0.58 (1:1 CH<sub>2</sub>Cl<sub>2</sub>:Hex) **mp:** 69.6 °C – 71.2 °C. **<sup>1</sup>H NMR** (400 MHz, CDCl<sub>3</sub>): δ 8.20 (d, *J* = 2.3 Hz, 1H, H-2), 7.93 (dd, *J* = 8.7, 2.3 Hz, 1H, H-6), 7.91 – 7.86 (m, 2H, H-8), 7.54 – 7.48 (m, 2H, H-9), 7.48 – 7.43 (m, 1H, H-10), 7.00 (d, *J* = 8.7 Hz, 1H, H-5), 3.96 (s, 3H, MeO). **<sup>13</sup>C NMR** (101 MHz, CDCl<sub>3</sub>): δ 158.1 (C-4), 152.6 (C-7), 147.2 (C-1), 131.0 (C-10), 129.2 (C-9), 126.2 (C-2), 125.9 (C-6), 122.9 (C-8), 112.7 (C-3), 111.5 (C-5), 56.7 (MeO). **HRMS** (EI<sup>+</sup>) *m/z*: Found 290.0048 Calculated for C<sub>13</sub>H<sub>11</sub>N<sub>2</sub>OBr<sup>+</sup> [M]<sup>+</sup> 290.0049. Δ = 0.3 ppm.

Data in accordance with literature and assignments made based on COSY, HMBC and HSQC data.<sup>137</sup>

## Experimental

---

### (E)-1-(3-Bromo-2-(dibromoboraneyl)-4-methoxyphenyl)-2-phenyldiazene **126**



In a 2-neck RBF, azo-compound **119** (0.500 g, 1.72 mmol) was dissolved in CH<sub>2</sub>Cl<sub>2</sub> (17 mL) and cooled to 0 °C, whereupon BBr<sub>3</sub> (1 M solution in heptane, 6.87 mL, 4.0 eq) was added slowly. After addition, the reaction mixture was removed from the ice bath and allowed to slowly warm to room temperature. After stirring for 16 h, the mixture was cooled to 0 °C and quenched with DI water (15 mL). The mixture was then extracted with CH<sub>2</sub>Cl<sub>2</sub> (2 × 10 mL), dried with MgSO<sub>4</sub>, filtered through Celite® and the organic layer reduced *in vacuo*. The resulting solid was then purified by column chromatography (1:4 EtOAc:Hexane) to give the title compound **126** as a red crystalline solid (0.289 g, 36%).

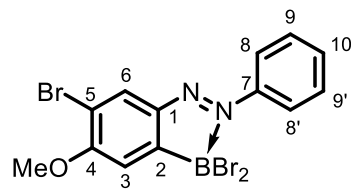
**R<sub>f</sub>** 0.42 (1:3 EtOAc:Hex). **mp:** 220 °C – >300 °C (dec.). **<sup>1</sup>H NMR** (400 MHz, CDCl<sub>3</sub>): δ 8.59 – 8.47 (m, 2H, H-8), 8.21 (d, *J* = 8.6 Hz, 1H, H-6), 7.61 – 7.53 (m, 3H, H-9 and H-10), 7.05 (d, *J* = 8.6 Hz, 1H, H-5), 4.09 (s, 3H, MeO). **<sup>13</sup>C NMR** (126 MHz, *Cryo-probe*, CDCl<sub>3</sub>): δ 163.4 (C-4), 148.3 (C-1), 141.6 (C-7), 132.9 (C-10), 130.4 (C-6), 129.5 (C-9), 124.2 (C-8), 115.9 (C-3), 112.1 (C-5), 57.5 (MeO). \*C-2 not observed due to boron relaxation **<sup>11</sup>B NMR** (128 MHz, CDCl<sub>3</sub>): δ -3.4. **IR v** (cm<sup>-1</sup>): 2944, 1591, 1555, 1460, 1341, 1245, 1127, 1047, 1002, 886, 810, 766. **HRMS** Not found by ESI<sup>+</sup>, APCI or Nanospray. Compound identity validated by single crystal **X-Ray** analysis.

Assignments made based on COSY, HMBC and HSQC data.

## Experimental

---

(*E*)-1-(5-Bromo-2-(dibromoboraneyl)-4-methoxyphenyl)-2-phenyldiazene **127**



*Identified as a side product of the above reaction.*

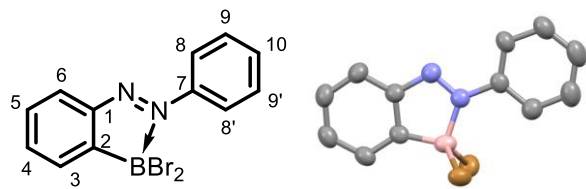
**R<sub>f</sub>** 0.52 (1:4 EtOAc:Hex). **mp:** 142.8 °C – 177.2 °C (dec.). **<sup>1</sup>H NMR** (400 MHz, CDCl<sub>3</sub>): δ 8.53 – 8.48 (m, 2H, H-8), 8.41 (s, 1H, H-6), 7.60 – 7.55 (m, 3H, H-9 and H-10), 7.32 (s, 1H, H-3), 4.14 (s, 3H, MeO). **<sup>13</sup>C NMR** (126 MHz, *Cryo-probe*, CDCl<sub>3</sub>): δ 163.5 (C-4), 148.2 (C-1), 141.7 (C-7), 133.4 (C-6), 132.9 (C-10), 129.6 (C-9), 123.9 (C-8), 113.4 (C-5), 111.7 (C-3), 57.6 (MeO). \*C-2 not observed due to boron relaxation **<sup>11</sup>B NMR** (128 MHz, CDCl<sub>3</sub>): δ -4.4 **IR** *v* (cm<sup>-1</sup>): 3344, 3074, 1739, 1575, 1555, 1475, 1377, 1244, 1111, 1056, 1024, 898, 761, 676. **HRMS** Not found by ESI<sup>+</sup>, MALDI or Nanospray.

Assignments made based on COSY, HMBC and HSQC data.

## Experimental

---

### (E)-1-(2-(Dibromoboraneyl)phenyl)-2-phenyldiazene **155**



In a flame dried RBF, azobenzene **26** (0.100 g, 0.549 mmol) was dissolved in CH<sub>2</sub>Cl<sub>2</sub> (5 mL) and cooled to 0 °C, whereupon BBr<sub>3</sub> (1 M solution in heptane, 1.65 mL, 3 eq) was added slowly. After addition, the reaction mixture was removed from the ice bath and allowed to slowly warm to room temperature. After stirring for 16 h, the mixture was cooled to 0 °C and quenched with sat. aq. K<sub>2</sub>CO<sub>3</sub> (5 mL). The mixture was then extracted with CH<sub>2</sub>Cl<sub>2</sub> (2 × 5 mL), dried with MgSO<sub>4</sub>, filtered through Celite® and the organic layer evaporated. The resulting solid was then washed with 1:4 Et<sub>2</sub>O:hexane to give the title compound **155** as a red crystalline solid (0.075 g, 39%).

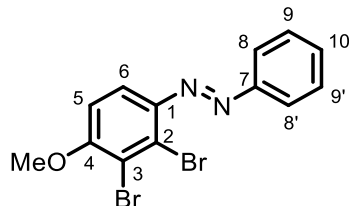
**R<sub>f</sub>** 0.57 (1:4 EtOAc:Hex) **mp:** 175.4 °C – 178.2 °C (dec.). **<sup>1</sup>H NMR** (400 MHz, CDCl<sub>3</sub>): δ 8.67 – 8.60 (m, 2H, H-8), 8.25 (d, *J* = 7.7 Hz, 1H, H-6), 7.84 (d, *J* = 7.2 Hz, 1H, H-3), 7.75 (td, *J* = 7.2, 0.8 Hz, 1H, H-4), 7.67 – 7.59 (m, 3H, H-9 and H-10), 7.56 (td, *J* = 7.7, 1.2 Hz, 1H, H-5). **<sup>13</sup>C NMR** (126 MHz, *Cryo-probe*, CDCl<sub>3</sub>): δ 153.5 (C-1), 141.8 (C-7), 137.0 (C-4), 133.9 (C-10), 129.8 (C-5), 129.7 (C-3), 129.6 (C-9), 128.5 (C-6), 124.7 (C-8). \*C-2 not observed due to boron relaxation. **<sup>11</sup>B NMR** (128 MHz, CDCl<sub>3</sub>): δ -3.4. **IR** *v* (cm<sup>-1</sup>): 3058, 1599, 1462, 1345, 1227, 1162, 921, 882, 825, 768. **HRMS** Not found by ESI<sup>+</sup>, APCI or Nanospray. Compound identity validated by single crystal **X-Ray** analysis.

Assignments made based on COSY, HMBC and HSQC data.

## Experimental

---

### ((E)-1-(2,3-Dibromo-4-methoxyphenyl)-2-phenyldiazene **159**



A mixture of boryl-azobenzene **126** (0.060 g, 0.13 mmol) and CuBr<sub>2</sub> (0.087 g, 0.39 mmol, 3.0 eq) was dissolved in MeOH (1 mL)/H<sub>2</sub>O (1 mL) and stirred at 80 °C for 16 h under an air atmosphere. The mixture was then cooled to r.t. and diluted with Et<sub>2</sub>O (5 mL). The organic layer washed with brine (3 mL), dried over MgSO<sub>4</sub>, filtered through Celite®, and concentrated *in vacuo*. The crude mixture was purified by column chromatography (1:6 EtOAc:Hex) to afford the title compound **159** as an orange solid (0.022 g, 47%).

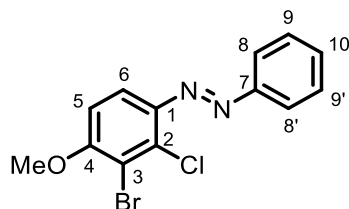
**R<sub>f</sub>** 0.82 (1:1 EtOAc:Hex) **mp:** 95.1 °C – 97.0 °C. **<sup>1</sup>H NMR** (500 MHz, CDCl<sub>3</sub>): δ 7.97 – 7.93 (m, 2H, H-8), 7.75 (d, *J* = 9.0 Hz, 1H, H-6), 7.54 – 7.47 (m, 3H, H-9 and H-10), 6.97 (d, *J* = 9.0 Hz, 1H, H-5), 3.99 (s, 3H, MeO). **<sup>13</sup>C NMR** (101 MHz, CDCl<sub>3</sub>): δ 159.1 (C-4), 152.7 (C-7), 145.6 (C-1), 131.4 (C-10), 130.9 (C-2), 129.3 (C-9), 123.5 (C-8), 117.0 (C-6), 116.3 (C-3), 110.3 (C-5), 57.1 (MeO). **IR v** (cm<sup>-1</sup>): 2921, 2851, 1736, 1578, 1471, 1458, 1427, 1377, 1271, 1230, 1180, 1147, 1070, 1032, 810, 768. **HRMS** (ESI<sup>+</sup>) *m/z*: Found 368.9231 Calculated for C<sub>13</sub>H<sub>11</sub>Br<sub>2</sub>N<sub>2</sub>O<sup>+</sup> [M+H]<sup>+</sup> 368.9233. Δ = 0.5 ppm

Assignments made based on COSY, HMBC and HSQC data.

## Experimental

---

((E)-1-(3-Bromo-2-chloro-4-methoxyphenyl)-2-phenyldiazene **158**



A mixture of boryl-azobenzene **126** (0.100 g, 0.217 mmol) and CuCl<sub>2</sub> (0.088 g, 0.651 mmol, 3.0 eq) was dissolved in MeOH (1.1 mL)/H<sub>2</sub>O (1.1 mL) and stirred at 80 °C for 16 h under an air atmosphere. The mixture was then cooled to r.t. and diluted with Et<sub>2</sub>O (5 mL). The organic layer was washed with brine (3 mL), dried over MgSO<sub>4</sub>, filtered through Celite®, and concentrated *in vacuo*. The crude mixture was purified by column chromatography (1:6 EtOAc:Hex) to afford the title compound **158** as an orange solid (0.033 g, 47%).

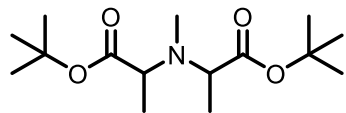
**R<sub>f</sub>** 0.82 (1:1 EtOAc:Hex) **mp:** 83.1 °C – 87.6 °C. **<sup>1</sup>H NMR** (400 MHz, CDCl<sub>3</sub>): δ 7.96 – 7.93 (m, 2H, H-8), 7.76 (d, *J* = 9.1 Hz, 1H, H-6), 7.54 – 7.48 (m, 3H, H-9 and H-10), 6.91 (d, *J* = 9.1 Hz, 1H, H-5), 3.99 (s, 3H, MeO). **<sup>13</sup>C NMR** (101 MHz, CDCl<sub>3</sub>): δ 159.1 (C-4), 152.6 (C-7), 145.5 (C-1), 137.9 (C-2) 131.4 (C-10), 129.3 (C-9), 123.5 (C-8), 117.9 (C-3) 117.0 (C-6), 110.3 (C-5), 57.1 (MeO). **IR v** (cm<sup>-1</sup>): 2976, 2937, 2835, 1737, 1578, 1472, 1459, 1428, 1384, 1274, 1232, 1147, 1071, 1042, 809, 768. **HRMS** (ESI<sup>+</sup>) *m/z*: Found 324.9735 Calculated for C<sub>13</sub>H<sub>11</sub>BrClN<sub>2</sub>O<sup>+</sup> [M+H]<sup>+</sup> 324.9735. Δ = 0.9 ppm

Assignments made based on COSY, HMBC and HSQC data.

## Experimental

---

### Di-tert-butyl 2,2'-(methylazanediyl)dipropionate **165**

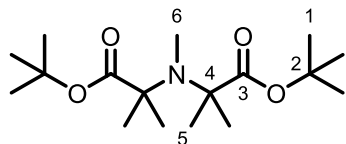


In a flame-dried RBF under an atmosphere of N<sub>2</sub>, tert-butyl-2-bromopropanoate **164** (20.4 g, 97.7 mmol, 2.2 eq), K<sub>2</sub>CO<sub>3</sub> (36.8 g, 266 mmol, 6.0 eq) and MeNH<sub>3</sub>Cl **163** (3.00 g, 44.4 mmol) were dissolved in MeCN (89 mL), the mixture heated 60 °C and left to stir for 16 h. The reaction was then cooled to room temperature, filtered through Celite®, and concentrated *in vacuo*. The crude material containing both diastereomers was then taken onto the subsequent methylation and deprotection steps with no further purification or analysis.

## Experimental

---

### Di-tert-butyl 2,2'-(methylazanediyl)bis(2-methylpropanoate) **166**



Two flame-dried two-neck RBFs under N<sub>2</sub> were charged with diisopropylamine (1.25 mL, 8.89 mmol, 2.4 eq, per flask) and THF (9.5 mL, per flask). These solutions were cooled to -78 °C to which 1.45 M N–Butyllithium in hexane (6.13 mL, 8.89 mmol, 2.4 eq, per flask) was added dropwise. The reactions were warmed to 0 °C and stirred for a further 30 min to form LDA. To each flask was added a portion of the crude material **165** from the previous step (1.07 g, 3.71 mmol, per flask) dissolved in THF (9.5 mL per flask). The resulting solutions were stirred at 0 °C for a further 20 min, yielding golden, clear solutions. The reactions were then cooled to -78 °C and another portion of 1.45 M N–Butyllithium in hexanes (5.11 mL, 7.41 mmol, 2.0 eq, per flask) was added dropwise. The mixtures were stirred for 5 min at -78 °C and then stirred another 30 min at 0 °C. To these solutions methyl iodide (1.38 mL, 22.2 mmol, 6.0 eq) was added dropwise over 10 min. The reactions were warmed to room temperature with stirring for 3.5 hours. The reactions were then quenched with sat. aq. NH<sub>4</sub>Cl (40 mL) and stirred for a further 15 min. The solutions were combined, diluted with EtOAc (50 mL) and washed with water (20 mL). The layers were separated, and the resulting aqueous layer was extracted with EtOAc (50 mL × 2). The combined organics were washed brine (100 mL), dried over MgSO<sub>4</sub>, filtered, and concentrated to give the title compound **166** as a yellow oil (1.45g, 62%).

**R<sub>f</sub>** 0.45 (1:9 EtOAc:Hex). **<sup>1</sup>H NMR** (400 MHz, CDCl<sub>3</sub>): δ 2.42 (s, 3H, H-6), 1.45 (s, 18H, H-1), 1.31 (s, 12H, H-5). **<sup>13</sup>C NMR** (101 MHz, CDCl<sub>3</sub>): δ 177.2 (C-3), 80.3 (C-2), 63.9 (C-4), 32.8 (C-6), 28.0 (C-1), 25.6 (C-5).

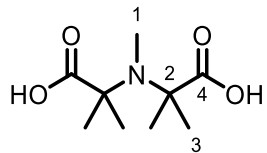
Data in accordance with literature and assignments made based on COSY, HMBC and HSQC

data.<sup>164</sup>

## Experimental

---

### 2,2'-(Methylazanediyl)bis(2-methylpropanoic acid) **167**



The diester **166** (1.45 g, 4.60 mmol) was added to a 50 mL flask and dissolved in 97% formic acid (4.74 mL, 122 mmol, 26.5 eq). The solution was stirred 80 °C under an atmosphere of N<sub>2</sub> for 4 hours and then cooled to room temperature. The reaction was concentrated *in vacuo* to yield a brown/white solid. Water (5 mL) was added to fully solubilize all solids and to this aqueous solution was added acetone (50 mL) to precipitate the bis-acid as a white solid. This mixture was stirred at 0 °C for approximately 1 hour and subsequently filtered to isolate the title compound **167** as a white powder (0.663 g, 71%).

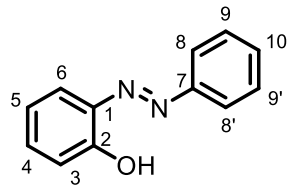
**mp:** 206 °C – 250 °C (dec.) **<sup>1</sup>H NMR** (400 MHz, D<sub>2</sub>O): δ 2.78 (s, 3H, H-1), 1.57 (s, 12H, H-3). **<sup>13</sup>C NMR** (101 MHz, D<sub>2</sub>O): δ 176.3 (C-4), 71.5 (C-2), 35.2 (C-1), 22.5 (C-3), 20.1 (C-3).

Data in accordance with literature and assignments made based on COSY, HMBC and HSQC data.<sup>164</sup>

## Experimental

---

### (E)-2-(Phenyldiazenyl)phenol **156**



In a flame-dried Schlenk tube at 0 °C, a 30% (w/w) H<sub>2</sub>O<sub>2</sub> solution (0.23 mL, 2.00 mmol) was added dropwise to a mixture of boryl-azobenzene **155** (0.070 g, 0.199 mmol) and NaOH (0.080 g, 2.00 mmol) in Et<sub>2</sub>O (1.0 mL, 0.2 M) and left to stir at room temperature behind a safety shield. After stirring for 2 hours, the solution was cooled to 0 °C, neutralized with 1 M HCl and extracted (gently) with CH<sub>2</sub>Cl<sub>2</sub> (10 mL × 3). The combined organic layers were washed with 10% Na<sub>2</sub>S<sub>3</sub>O<sub>4</sub> (10 mL) and H<sub>2</sub>O (5 mL), dried over MgSO<sub>4</sub>, tested for peroxides using starch paper and concentrated *in vacuo*. The residue was purified by column chromatography (1:40 EtOAc:Hex) to afford the title compound **156** as an orange solid (0.035 g, 87%).

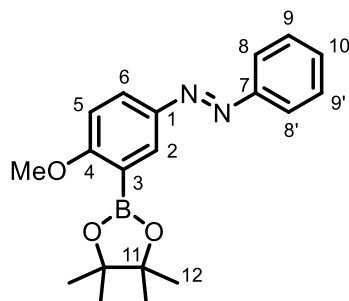
**R<sub>f</sub>** 0.80 (1:4 EtOAc:Hex) **mp:** 75.8 °C – 77.9 °C. **<sup>1</sup>H NMR** (400 MHz, CDCl<sub>3</sub>): δ 12.94 (s, 1H, OH), 7.96 (dd, *J* = 8.0, 1.7 Hz, 1H, H-6), 7.92 – 7.84 (m, 2H, H-8), 7.57 – 7.46 (m, 3H, H-9 and H-10), 7.36 (ddd, *J* = 8.5, 7.2, 1.7 Hz, 1H, H-4), 7.08 (ddd, *J* = 8.0, 7.2, 1.5 Hz, 1H, H-5), 7.04 (dd, *J* = 8.5, 1.5 Hz, 1H, H-3). **<sup>13</sup>C NMR** (101 MHz, CDCl<sub>3</sub>): δ 152.9 (C-2), 150.7 (C-7), 137.5 (C-1), 133.4 (C-6), 133.4 (C-4), 131.3 (C-10), 129.5 (C-9), 122.4 (C-8), 120.1 (C-5), 118.3 (C-3). **UV-Vis** (MeCN)  $\lambda_{\text{max}}$  = 324 nm ( $\epsilon$  = 13,536 M<sup>-1</sup>cm<sup>-1</sup>), 373 nm ( $\epsilon$  = 8,454 M<sup>-1</sup>cm<sup>-1</sup>). **MS** (ESI<sup>+</sup>) *m/z*: Found 199.1 Calculated for C<sub>12</sub>H<sub>11</sub>N<sub>2</sub>O<sup>+</sup> [M+H]<sup>+</sup> 199.1

Data in accordance with literature and assignments made based on COSY, HMBC and HSQC data.<sup>221, 222</sup>

## Experimental

---

(*E*)-1-(4-Methoxy-3-(4,4,5,5-tetramethyl-1,3,2-dioxaborolan-2-yl)phenyl)-2-phenyldiazene  
**120**



In a flame-dried RBF, bromoazobenzene **119** (7.10 g, 24.4 mmol), bis(pinacolato)-diboron (7.43 g, 29.3 mmol, 1.2 eq), potassium acetate (4.79 g, 48.8 mmol, 2.0 eq) and Pd(dppf)Cl<sub>2</sub>•CH<sub>2</sub>Cl<sub>2</sub> (0.996 g, 1.22 mmol, 5 mol%) were dissolved in dioxane (120 mL) under an atmosphere of N<sub>2</sub>. The reaction mixture was then stirred at reflux for 16 h. After cooling to room temperature, water (80 mL) was added, and the mixture extracted with CH<sub>2</sub>Cl<sub>2</sub> (3 × 100 mL). The combined organic extracts were washed with brine (80 mL), dried over MgSO<sub>4</sub>, filtered through Celite®, and concentrated *in vacuo*. The crude mixture was then purified by column chromatography (1:6 EtOAc:Hex) to afford the title compound **120** as an orange solid (7.57 g, 92%).

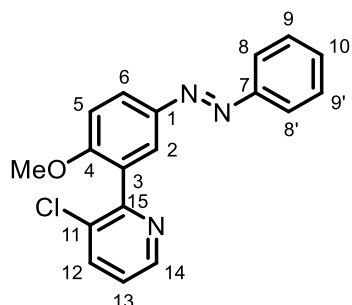
**R<sub>f</sub>** 0.46 (1:5 EtOAc:Hex). **mp:** 98.8 °C – 99.8 °C. **<sup>1</sup>H NMR** (400 MHz, CDCl<sub>3</sub>): δ 8.31 (d, *J* = 2.8 Hz, 1H, H-2), 8.01 (dd, *J* = 8.9, 2.8 Hz, 1H, H-6), 7.91 – 7.86 (m, 2H, H-8), 7.50 (tm, *J* = 7.6 Hz, 2H, H-9), 7.46 – 7.40 (tm, *J* = 7.2 Hz, 1H, H-10), 6.98 (d, *J* = 8.9 Hz, 1H, H-5), 3.92 (s, 3H, OMe), 1.39 (s, 12H, H-12). **<sup>13</sup>C NMR** (101 MHz, CDCl<sub>3</sub>): 166.6 (C-4), 153.0 (C-7), 146.5 (C-1), 132.2 (C-2), 130.4 (C-10), 129.1 (C-9), 127.3 (C-6), 122.7 (C-8), 110.7 (C-5), 83.9 (C-11), 56.3 (OMe), 25.0 (C-12). \*C-3 not observed due to boron relaxation. **<sup>11</sup>B NMR** (128 MHz, CDCl<sub>3</sub>): δ 30.0. **IR v** (cm<sup>-1</sup>): 2973, 1602, 1569, 1492, 1412, 1341, 1255, 1132, 1062, 965, 830, 825, 771. **HRMS** (ESI<sup>+</sup>) *m/z*: Found 339.1867 Calculated for C<sub>19</sub>H<sub>24</sub>BNO<sub>3</sub> [M+H]<sup>+</sup> 339.1878. Δ = -3.2 ppm.

Assignments made based on COSY, HMBC and HSQC data.

## Experimental

---

(*E*)-3-Chloro-2-(2-methoxy-5-(phenyldiazenyl)phenyl)pyridine **121**



Synthesized according to the **General Suzuki Cross-Coupling Procedure A** from Bpin-azobenzene **120** (3.00 g, 8.87 mmol), bromide **83** (2.05 g, 10.6 mmol), Pd(OAc)<sub>2</sub> (0.100 g, 0.444 mmol), SPhos (0.364 g, 0.887 mmol) and Cs<sub>2</sub>CO<sub>3</sub> (5.78 g, 17.7 mmol), with column chromatography (1:3 EtOAc:Hex) affording the title compound **121** as an orange solid (2.21 g, 77%).

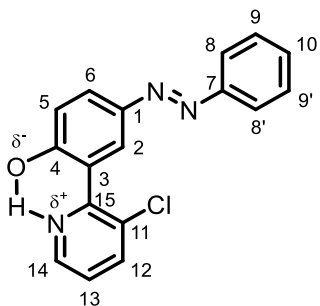
**R<sub>f</sub>** 0.22 (1:4 EtOAc:Hex). **mp:** 92.0 °C – 93.2 °C. **<sup>1</sup>H NMR** (400 MHz, CDCl<sub>3</sub>): δ 8.61 (dd, *J* = 4.7, 1.5 Hz, 1H, H-14), 8.09 (dd, *J* = 8.8, 2.5 Hz, 1H, H-6), 8.01 (d, *J* = 2.4 Hz, 1H, H-2), 7.89 (dm, *J* = 7.2 Hz 2H, H-8), 7.78 (dd, *J* = 8.1, 1.5 Hz, 1H, H-12), 7.49 (tm, *J* = 7.3 Hz, 2H, H-9), 7.44 (tm, *J* = 7.3 Hz, 1H, H-10), 7.26 (dd, *J* = 8.1, 4.7 Hz, 1H, H-13), 7.12 (d, *J* = 8.9 Hz, 1H, H-5), 3.88 (s, 3H, MeO). **<sup>13</sup>C NMR** (101 MHz, CDCl<sub>3</sub>): δ 159.3 (C-4), 155.0 (C-15), 152.8 (C-7), 147.4 (C-14), 146.6 (C-1), 137.1 (C-12), 132.2 (C-11), 130.5 (C-10), 129.1 (C-9), 128.6 (C-3), 126.9 (C-6), 124.3 (C-2), 123.6 (C-13), 122.7 (C-8), 111.1 (C-5), 56.0 (MeO). **IR v** (cm<sup>-1</sup>): 2937, 2838, 1599, 1493, 1435, 1269, 1245, 1130, 1020, 759, 688. **HRMS** (ESI<sup>+</sup>) *m/z*: Found 324.0905 Calculated for C<sub>18</sub>H<sub>15</sub>ClN<sub>3</sub>O<sup>+</sup> [M+H]<sup>+</sup> 324.0898. Δ = 2.3 ppm.

Assignments made based on COSY, HMBC and HSQC data.

## Experimental

---

### (E)-2-(3-Chloropyridin-2-yl)-4-(phenyldiazenyl)phenol **132**



In a Schlenk tube, azo-biaryl **121** (0.050 g, 0.15 mmol) was dissolved in CH<sub>2</sub>Cl<sub>2</sub> (1.5 mL) and cooled to 0 °C, whereupon BBr<sub>3</sub> (1 M solution in heptane, 0.60 mL, 4 eq) was added slowly. After addition, the reaction mixture was removed from the ice bath and allowed to slowly warm to room temperature. After stirring for 16 h, the mixture was cooled to 0 °C and quenched with 2M NaOH (1 mL). The mixture was then neutralized with 2M HCl (2 mL) and extracted with CH<sub>2</sub>Cl<sub>2</sub> (2 × 5 mL). The organic layer was dried with MgSO<sub>4</sub>, filtered through Celite®, and evaporated *in vacuo*. The resulting solid was then purified *via* column chromatography (1:4 EtOAc:Hex) to give the title compound **132** as an orange solid (0.039 g, 82%).

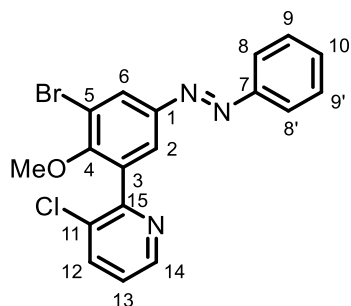
**R<sub>f</sub>** 0.20 (1:4 EtOAc:Hex). **mp:** 109.2 °C – 111.8 °C. **<sup>1</sup>H NMR** (400 MHz, CDCl<sub>3</sub>): δ 12.57 (s, 1H, OH proton) 8.92 (d, *J* = 2.3 Hz, 1H, H-2), 8.52 (dd, *J* = 4.9, 1.5 Hz, 1H, H-14), 7.98 (dd, *J* = 8.8, 2.3 Hz, 1H, H-6), 7.96 (dd, *J* = 8.1, 1.5 Hz, 1H, H-12), 7.92 – 7.87 (m, 2H, H-8), 7.51 (ddt, *J* = 8.3, 6.1, 1.8 Hz, 2H, H-9), 7.47 – 7.41 (m, 1H, H-10), 7.29 (dd, *J* = 8.1, 4.9 Hz, 1H, H-13), 7.18 (d, *J* = 8.8 Hz, 1H, H-5). **<sup>13</sup>C NMR** (101 MHz, CDCl<sub>3</sub>): δ 161.1 (C-4), 153.7 (C-15), 152.8 (C-7), 145.3 (C-1), 145.0 (C-14), 141.1 (C-12), 130.5 (C-10), 129.8 (C-11), 129.2 (C-9), 127.5 (C-2), 125.1 (C-6), 123.2 (C-13), 122.7 (C-8), 119.3 (C-3), 119.0 (C-5). **UV-Vis** (MeCN)  $\lambda_{\text{max}}$  = 346 nm ( $\epsilon$  = 27,930 M<sup>-1</sup>cm<sup>-1</sup>), 434 nm ( $\epsilon$  = 1,410 M<sup>-1</sup>cm<sup>-1</sup>) **IR**  $\nu$  (cm<sup>-1</sup>): δ 3061, 2923, 1736, 1573, 1438, 1259, 1131, 1027, 906, 764. **HRMS** (ESI<sup>+</sup>) *m/z*: Found 310.0728 Calculated for C<sub>17</sub>H<sub>13</sub>ClN<sub>3</sub>O<sup>+</sup> [M+H]<sup>+</sup> 310.0742. Δ = -4.6 ppm.

Assignments made based on COSY, HMBC and HSQC data.

## Experimental

---

(*E*)-2-(3-Bromo-2-methoxy-5-(phenyldiazenyl)phenyl)-3-chloropyridine **124**



A mixture of azo-biaryl **121** (0.050 g, 0.15 mmol), Pd(OAc)<sub>2</sub> (0.002 g, 0.008 mmol, 5 mol%), NBS (0.033 g, 0.19 mmol, 1.2 eq), and TsOH·H<sub>2</sub>O (0.015 g, 0.077 mmol, 50 mol%) were dissolved in acetonitrile (1.5 mL, 0.1M) and stirred at 50 °C. After stirring for 16 h, the mixture was cooled, reduced *in vacuo* and purified by column chromatography (1:9 EtOAc:Hex), to afford the title compound **124** as a sticky orange oil (0.018 g, 29 %).

**R<sub>f</sub>** 0.28 (1:9 EtOAc:Hex). **<sup>1</sup>H NMR** (400 MHz, CDCl<sub>3</sub>): δ 8.63 (dd, *J* = 4.7, 1.5 Hz, 1H, H-14), 8.26 (d, *J* = 2.3 Hz, 1H, H-6), 7.93 (d, *J* = 2.4 Hz, 1H, H-2), 7.91 – 7.88 (m, 2H, H-8), 7.86 (dd, *J* = 8.2, 1.5 Hz, 1H, H-12), 7.56 – 7.44 (m, 3H, H-9 and H-10), 7.35 (dd, *J* = 8.2, 4.7 Hz, 1H, H-13), 3.65 (s, 3H, MeO). **<sup>13</sup>C NMR** (101 MHz, CDCl<sub>3</sub>): δ 157.0 (C-4), 154.5 (C-15), 152.5 (C-7), 149.0 (C-1), 147.5 (C-14), 137.6 (C-12), 134.4 (C-3), 132.0 (C-11), 131.5 (C-10), 129.3 (C-9), 127.9 (C-6), 125.7 (C-2), 124.2 (C-13), 123.1 (C-8), 118.4 (C-5), 61.9 (MeO). **IR** *v* (cm<sup>-1</sup>): 2921, 2850, 1571, 1470, 1414, 1393, 1248, 1035, 997, 795, 769. **HRMS** (ESI<sup>+</sup>) *m/z*: Found 423.9833 Calculated for C<sub>18</sub>H<sub>13</sub>BrClN<sub>3</sub>NaO<sup>+</sup> [M+Na]<sup>+</sup> 423.9823. Δ = 2.5 ppm.

*Z isomer:*

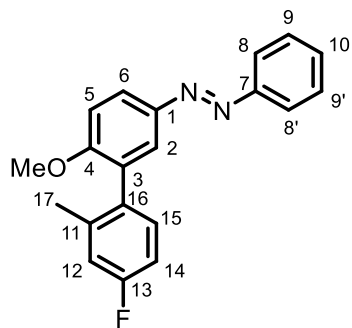
**<sup>1</sup>H NMR** (400 MHz, CDCl<sub>3</sub>): 8.55 (dd, *J* = 4.7, 1.5 Hz, 1H), 7.75 (dd, *J* = 8.2, 1.5 Hz, 1H), 7.34 – 7.27 (m, 3H), 7.23 – 7.17 (m, 2H), 6.91 (dt, *J* = 8.3, 1.1 Hz, 2H), 6.76 (d, *J* = 2.4 Hz, 1H), 3.56 (s, 3H).

Assignments made based on COSY, HMBC and HSQC data.

## Experimental

---

(E)-1-(4'-Fluoro-6-methoxy-2'-methyl-[1,1'-biphenyl]-3-yl)-2-phenyldiazene **130**



Synthesized according to the **General Suzuki Cross-Coupling Procedure A** from bromo-BBr<sub>2</sub>-azobenzene **126** (0.100 g, 0.217 mmol), boronic acid **128** (0.040 g, 0.26 mmol), Pd(OAc)<sub>2</sub> (0.002 g, 0.011 mmol), SPhos (0.009 g, 0.022 mmol) and Cs<sub>2</sub>CO<sub>3</sub> (0.141 g, 0.434 mmol), with column chromatography (1:4 EtOAc:Hex) affording the title compound **130** as an orange solid (0.024 g, 35%).

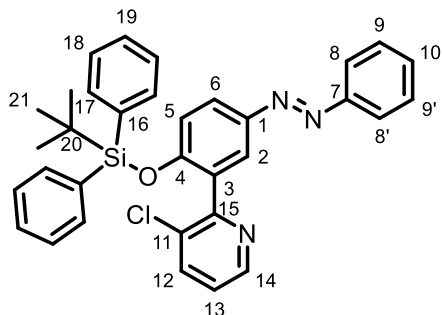
**R<sub>f</sub>** 0.28 (1:4 CH<sub>2</sub>Cl<sub>2</sub>:Hex). **mp:** 61.3 °C – 64.9 °C. **<sup>1</sup>H NMR** (400 MHz, CDCl<sub>3</sub>): δ 7.99 (dd, *J* = 8.8, 2.5 Hz, 1H, H-6), 7.90 – 7.85 (m, 2H, H-8), 7.77 (d, *J* = 2.5 Hz, 1H, H-2), 7.52 – 7.47 (m, 2H, H-9), 7.47 – 7.41 (m, 1H, H-10), 7.20 (dd, *J* = 8.3, 6.0 Hz, 1H, H-15), 7.09 (d, *J* = 8.8 Hz, 1H, H-5), 6.99 (dd, *J* = 9.9, 2.7 Hz, 1H, H-12), 6.95 (tdd, *J* = 8.4, 2.7, 0.6 Hz, 1H, H-14), 3.87 (s, 3H, MeO), 2.16 (s, 3H, H-17). **<sup>13</sup>C NMR** (126 MHz, CDCl<sub>3</sub>) δ 162.4 (d, <sup>1</sup>J<sub>C-F</sub> = 245.3 Hz, C-13), 159.3 (C-4), 152.9 (C-7), 146.8 (C-1), 139.4 (d, <sup>3</sup>J<sub>C-F</sub> = 8.0 Hz, C-11), 133.8 (d, <sup>4</sup>J<sub>C-F</sub> = 3.1 Hz, C-16), 131.5 (d, <sup>3</sup>J<sub>C-F</sub> = 8.4 Hz, C-15), 130.7 (C-3), 130.6 (C-10), 129.2 (C-9), 125.5 (C-6), 124.9 (C-2), 122.7 (C-8), 116.5 (d, <sup>2</sup>J<sub>C-F</sub> = 21.0 Hz, C-12), 112.5 (d, <sup>2</sup>J<sub>C-F</sub> = 20.9 Hz, C-14), 110.8 (C-5), 56.0 (MeO), 20.2 (d, <sup>5</sup>J<sub>C-F</sub> = 1.6 Hz, C-17). **<sup>19</sup>F NMR** (376 MHz, CDCl<sub>3</sub>): δ -115.7 (td, *J* = 9.2, 6.0 Hz) **IR v s(cm<sup>-1</sup>)**: 2936, 2835, 1585, 1482, 1265, 1237, 1126, 1034, 1019, 958, 816, 765. **HRMS** (ESI<sup>+</sup>) *m/z*: Found 321.1400 Calculated for C<sub>20</sub>H<sub>18</sub>FN<sub>2</sub>O<sup>+</sup> [M+H]<sup>+</sup> 321.1398. Δ = 0.6 ppm.

Assignments made based on COSY, HMBC and HSQC data.

## Experimental

---

(E)-2-((Tert-butyldiphenylsilyl)oxy)-5-(phenyldiazenyl)phenyl)-3-chloropyridine **134**



In a flame dried Schlenk tube, hydroxy-azo-biaryl **132** (0.080 g, 0.258 mmol) and imidazole (0.004 g, 0.06 mmol, 20 mol%) were dissolved in CH<sub>2</sub>Cl<sub>2</sub> (2.5 mL) and cooled to 0 °C under an atmosphere of N<sub>2</sub>. Triethylamine (0.11 mL, 0.77 mmol, 3.0 eq) and tert-butylchlorodiphenylsilane (0.213 g, 0.775 mmol, 3.0 eq) were then added and the resulting mixture was heated to reflux and left to stir. After 16 h the reaction was cooled to room temperature, quenched with water (2 mL), diluted with CH<sub>2</sub>Cl<sub>2</sub> (2.5 mL), and washed with brine (3 × 10 mL). The organic layer was then separated, dried over MgSO<sub>4</sub>, filtered through Celite® and concentrated *in vacuo*. The orange residue was purified by column chromatography (1:6 EtOAc:Hex) to give the title compound **134** as a yellow oil (0.140 g, 99%)

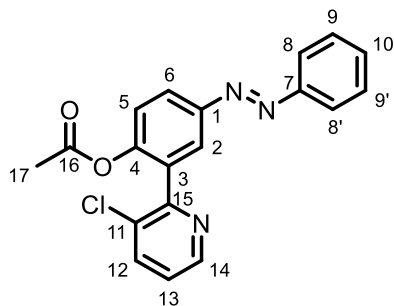
**R<sub>f</sub>** 0.40 (1:6 EtOAc:Hex). **<sup>1</sup>H NMR** (400 MHz, CDCl<sub>3</sub>): δ. 8.69 (dd, *J* = 4.7, 1.5 Hz, 1H, H-14), 8.03 (d, *J* = 2.5 Hz, 1H, H-2), 7.87 (dd, *J* = 8.1, 1.5 Hz, 1H, H-12), 7.85 – 7.81 (m, 2H, H-8), 7.75 – 7.70 (m, 4H H-18 or H-17), 7.65 (dd, *J* = 8.7, 2.5 Hz, 1H, H-6), 7.50 – 7.36 (m, 9H, H-9 + H-10 + H-19 + H-18 or H-17), 7.34 (dd, *J* = 8.1, 4.7 Hz, 1H, H-13), 6.60 (d, *J* = 8.7 Hz, 1H, H-5), 0.79 (s, 9H, H-21). **<sup>13</sup>C NMR** (101 MHz, CDCl<sub>3</sub>): δ 155.8 (C-15), 155.5 (C-1), 152.8 (C-7), 147.5 (C-14), 146.8 (C-4), 137.0 (C-12), 135.5 (C-17 or C-18), 132.7 (C-11), 130.9 (C-3), 130.5 (C-10), 130.2 (C-19), 129.7 (C-16), 129.1 (C-9), 128.1 (C-17 or C-18), 125.3 (C-6), 124.6 (C-2), 123.7 (C-13), 122.7 (C-8), 119.6 (C-5), 25.9 (C-21), 19.2 (C-20). **IR ν (cm<sup>-1</sup>)**: 3049, 2929, 2857, 1598, 1488, 1471, 1448, 1428, 1277, 1114, 1077, 1031, 919, 821, 771, 700. **HRMS (ESI<sup>+</sup>) m/z:** Found 548.1912 Calculated for C<sub>33</sub>H<sub>30</sub>ClN<sub>3</sub>OSi<sup>+</sup> [M+H]<sup>+</sup> 548.1919. Δ = 1.3 ppm.

Assignments made based on COSY, HMBC and HSQC data.

## Experimental

---

### (E)-2-(3-Chloropyridin-2-yl)-4-(phenyldiazenyl)phenyl acetate **135**



In a flame dried Schlenk tube, hydroxy-azo-biaryl **132** (0.063 g, 0.20 mmol) was dissolved in CH<sub>2</sub>Cl<sub>2</sub> (2 mL) and cooled to 0 °C under an atmosphere of N<sub>2</sub>. Triethylamine (0.14 mL, 1.0 mmol, 5.0 eq) and acetyl chloride (1 M in CH<sub>2</sub>Cl<sub>2</sub>, 0.51 mL, 2.5 eq) were then added and the resulting mixture warmed to room temperature and left to stir. After 16 h the reaction was quenched with water (2 mL), and the aqueous layer extracted with CH<sub>2</sub>Cl<sub>2</sub> (3 × 2.5 mL). The combined organic layers were then separated, dried over MgSO<sub>4</sub>, filtered through Celite® and concentrated *in vacuo*. The residue was purified by column chromatography (1:6 EtOAc:Hex) to give the title compound **135** as a red oil (0.070 g, 98%).

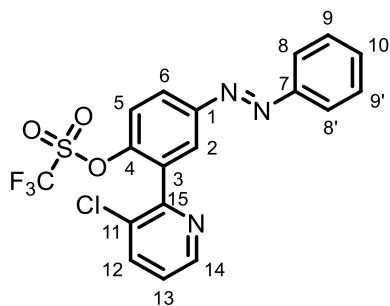
**R<sub>f</sub>** 0.25 (1:3 EtOAc:Hex). **<sup>1</sup>H NMR** (400 MHz, CDCl<sub>3</sub>): δ. 8.63 (dd, *J* = 4.6, 1.5 Hz, 1H, H-14), 8.11 (d, *J* = 2.4 Hz, 1H, H-2), 8.07 (dd, *J* = 8.6, 2.4 Hz, 1H, H-6), 7.91 (dd, *J* = 8.4, 1.5 Hz, 2H, H-8), 7.84 (dd, *J* = 8.1, 1.5 Hz, 1H, H-12), 7.54 – 7.49 (m, 2H, H-9), 7.49 – 7.42 (m, 2H, H-10 and H-5), 7.30 (dd, *J* = 8.1, 4.7 Hz, 1H, H-13), 2.11 (s, 3H, H-17). **<sup>13</sup>C NMR** (101 MHz, CDCl<sub>3</sub>): δ 168.5 (C-16), 153.7 (C-15), 152.6 (C-7), 150.1 (C-4), 150.0 (C-1), 147.6 (C-14), 137.6 (C-12), 131.9 (C-3), 131.7 (C-11), 131.3 (C-10), 129.2 (C-9), 125.4 (C-2), 124.8 (C-6), 124.0 (C-13), 123.6 (C-5), 123.0 (C-8), 21.0 (C-17). **IR** *v* (cm<sup>-1</sup>): 3062, 1766, 1572, 1445, 1367, 1180, 1077, 1028, 909, 769. **HRMS** (ESI<sup>+</sup>) *m/z*: Found 352.0850 Calculated for C<sub>19</sub>H<sub>15</sub>ClN<sub>3</sub>O<sub>2</sub><sup>+</sup> [M+H]<sup>+</sup> 352.0847. Δ = 0.9 ppm.

Assignments made based on COSY, HMBC and HSQC data.

## Experimental

---

### (E)-2-(3-Chloropyridin-2-yl)-4-(phenyldiazenyl)phenyl trifluoromethanesulfonate **136**



In a flame dried Schlenk tube, hydroxy-azo-biaryl **132** (0.100 g, 0.323 mmol) was dissolved in CH<sub>2</sub>Cl<sub>2</sub> (3 mL) and cooled to 0 °C under an atmosphere of N<sub>2</sub>. Triethylamine (0.11 mL, 0.81 mmol, 2.5 eq) and triflic anhydride (1 M in CH<sub>2</sub>Cl<sub>2</sub>, 0.81 mL, 2.5 eq) were then added and the resulting mixture warmed to room temperature and left to stir. After 16 h the reaction was quenched with water (2 mL), and the aqueous layer extracted with CH<sub>2</sub>Cl<sub>2</sub> (3 × 2.5 mL). The combined organic layers were then separated, dried over MgSO<sub>4</sub>, filtered through Celite® and concentrated *in vacuo*. The residue was purified by column chromatography (1:9 EtOAc:Hex) to give the title compound **136** as a red oil (0.116 g, 81 %).

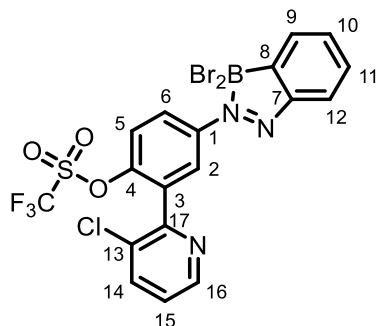
**R<sub>f</sub>** 0.30 (1:9 EtOAc:Hex) **<sup>1</sup>H NMR** (400 MHz, CDCl<sub>3</sub>): δ. 8.68 (dd, *J* = 4.7, 1.6 Hz, 1H, H-14), 8.18 (d, *J* = 2.4 Hz, 1H, H-2), 8.10 (dd, *J* = 8.8, 2.5 Hz, 1H, H-6), 7.94 (dd, *J* = 7.8, 1.9 Hz, 2H, H-8), 7.88 (dd, *J* = 8.1, 1.6 Hz, 1H, H-12), 7.59 (d, *J* = 8.8 Hz, 1H, H-5), 7.56 – 7.48 (m, 3H, H-9 and H-10), 7.36 (dd, *J* = 8.1, 4.7 Hz, 1H, H-13). **<sup>13</sup>C NMR** (101 MHz, CDCl<sub>3</sub>): δ 152.4 (C-7), 151.8 (C-15), 151.4 (C-1), 148.1 (C-4), 147.8 (C-14), 137.8 (C-12), 133.0 (C-3), 131.93 (C-10), 131.88 (C-11), 129.3 (C-9), 126.1 (C-2), 125.2 (C-6), 124.7 (C-13), 123.3 (C-8), 122.8 (C-5), 118.5 (q, <sup>1</sup>*J*<sub>C-F</sub> = 320 Hz, CF<sub>3</sub>) **<sup>19</sup>F NMR** (376 MHz, CDCl<sub>3</sub>): δ -73.90 **IR v** (cm<sup>-1</sup>): 3384, 3062, 2924, 1423, 1210, 1139, 1074, 1027, 888, 858, 767. **HRMS** (ESI<sup>+</sup>) *m/z*: Found 442.0227 Calculated for C<sub>18</sub>H<sub>12</sub>N<sub>3</sub>O<sub>3</sub>SClF<sub>3</sub><sup>+</sup> [M+H]<sup>+</sup> 442.0235 Δ = 1.8 ppm

Assignments made based on COSY, HMBC and HSQC data.

## Experimental

---

(E)-2-(3-Chloropyridin-2-yl)-4-(phenyldiazenyl)phenyl trifluoromethanesulfonate **139**



In a flame dried RBF, triflyl-azo-biaryl **136** (0.113 g, 0.256 mmol) was dissolved in CH<sub>2</sub>Cl<sub>2</sub> (2.5 mL) and cooled to 0 °C, whereupon BBr<sub>3</sub> (1 M solution in heptane, 0.77 mL, 3 eq) was added slowly. After addition, the reaction mixture was removed from the ice bath and allowed to slowly warm to room temperature. After stirring for 16 h, the mixture was cooled to 0 °C and quenched with sat. aq. K<sub>2</sub>CO<sub>3</sub> (5 mL). The mixture was then extracted with CH<sub>2</sub>Cl<sub>2</sub> (2 × 5 mL), dried with MgSO<sub>4</sub>, filtered through Celite® and the organic layer evaporated *in vacuo*. The resulting solid was then purified by column chromatography (1:1 EtOAc:Hex) to give the title compound **139** as an orange solid (0.032 g, 21%).

**R<sub>f</sub>** 0.25 (1:1 EtOAc:Hex) **mp** >250 °C (slow and incomplete decomposition) **<sup>1</sup>H NMR** (400 MHz, CDCl<sub>3</sub>): δ. 8.89 (dd, *J* = 9.2, 2.8 Hz, 1H, H-6), 8.81 (d, *J* = 2.8 Hz, 1H, H-2), 8.69 (dd, *J* = 4.6, 1.5 Hz, 1H, H-16), 8.28 (d, *J* = 7.9 Hz, 1H, H-12), 7.92 (dd, *J* = 8.2, 1.5 Hz, 1H, H-14), 7.86 (d, *J* = 7.3 Hz, 1H, H-9), 7.80 (t, *J* = 7.3, 1H, H-10), 7.68 (d, *J* = 9.2 Hz, 1H, H-5), 7.62 – 7.56 (m, 1H, H-11), 7.42 (dd, *J* = 8.2, 4.6 Hz, 1H, H-15). **<sup>13</sup>C NMR\*** **<sup>11</sup>B NMR** (128 MHz, CDCl<sub>3</sub>): δ -3.5. **<sup>19</sup>F NMR** (376 MHz, CDCl<sub>3</sub>): δ -73.71. **IR v** (cm<sup>-1</sup>): 3355, 2924, 1523, 1423, 1210, 1137, 1073, 1029, 1015, 891, 609. **HRMS** not found by ESI or Nanospray

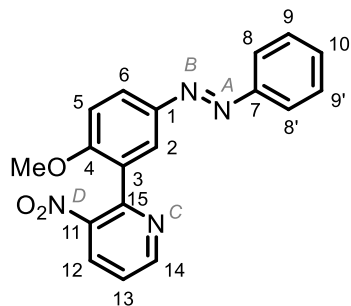
\*<sup>13</sup>C data not obtained due to compound degradation. Subsequent attempts at re-synthesising the material for characterisation proved unsuccessful.

Assignments made based on COSY data.

## Experimental

---

### (E)-2-(2-Methoxy-5-(phenyldiazenyl)phenyl)-3-nitropyridine **188**



Synthesized according to the **General Suzuki Cross-Coupling Procedure A** from Bpin-azobenzene **120** (1.50 g, 4.44 mmol), bromide **85** (1.08 g, 5.32 mmol), Pd(OAc)<sub>2</sub> (0.050 g, 0.22 mmol), SPhos (0.182 g, 0.444 mmol) and Cs<sub>2</sub>CO<sub>3</sub> (2.89 g, 8.87 mmol), with column chromatography (1:9 EtOAc:Hex) affording the title compound **188** as an orange solid (0.946 g, 64%).

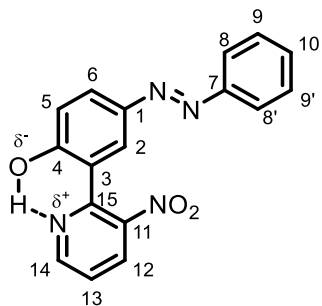
**R<sub>f</sub>** 0.50 (1:9 EtOAc:Hex) **mp:** 110.1 °C – 113.2 °C. **<sup>1</sup>H NMR** (400 MHz, CDCl<sub>3</sub>): δ 8.92 (dd, *J* = 4.7, 1.7 Hz, 1H, H-14), 8.32 (d, *J* = 2.4 Hz, 1H, H-2), 8.26 (dd, *J* = 8.3, 1.5 Hz, 1H, H-12), 8.09 (dd, *J* = 8.8, 2.5 Hz, 1H, H-6), 7.90 (dd, *J* = 8.4, 1.4 Hz, 2H, H-8), 7.54 – 7.44 (m, 4H, H-13, H-9 and H-10), 7.05 (d, *J* = 8.9 Hz, 1H, H-5), 3.81 (s, 3H, OMe). **<sup>13</sup>C NMR** (125 MHz, *Cryo-probe* CDCl<sub>3</sub>): δ 158.5 (C-4), 152.8 (C-14 and C-7), 150.0 (C-15), 147.3 (C-1), 147.1 (C-11), 132.0 (C-12), 130.7 (C-10), 129.2 (C-9), 127.6 (C-6), 127.3 (C-3), 124.5 (C-2), 122.8 (C-8 and C-13), 110.9 (C-5), 55.7 (OMe). **<sup>1</sup>H-<sup>15</sup>N HMBC** (600 MHz, *Cryo-probe*, MeCN-d<sub>3</sub>, *J<sub>H-N</sub>* = 3 Hz): δ 503.0 (N-B), 499.4 (N-A), 373.0 (N-D), 322.9 (N-C). **IR v** (cm<sup>-1</sup>) 2944, 1596, 1523, 1486, 1359, 1270, 1244, 1017, 821, 762, 750, 684. **HRMS** (ESI<sup>+</sup>) *m/z*: Found 335.1132 Calculated for C<sub>18</sub>H<sub>15</sub>N<sub>4</sub>O<sub>3</sub><sup>+</sup> [M+H]<sup>+</sup> 335.1132. Δ = 2.1 ppm.

Assignments made based on COSY, HMBC and HSQC data.

## Experimental

---

### (E)-2-(3-Nitropyridin-2-yl)-4-(phenyldiazenyl)phenol **193**



In a flame-dried RBF, azo-biaryl **188** (0.500 g, 1.50 mmol) was dissolved in CH<sub>2</sub>Cl<sub>2</sub> (15 mL) and cooled to 0 °C, whereupon BBr<sub>3</sub> (1 M solution in heptane, 4.49 mL, 3 eq) was added slowly. After addition, the reaction mixture was removed from the ice bath and allowed to slowly warm to room temperature. After stirring for 16 h, the mixture was cooled to 0 °C and quenched with 2 M NaOH (5 mL). The mixture was then neutralized with 2M HCl (10 mL) and extracted with CH<sub>2</sub>Cl<sub>2</sub> (2 × 25 mL). The organic layer was dried with MgSO<sub>4</sub>, filtered through Celite®, and evaporated *in vacuo*. The resulting solid was then purified *via* column chromatography (1:4 EtOAc:Hex) to give title compound **193** as a crystalline orange solid (0.335 g, 70%).

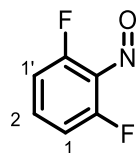
**R<sub>f</sub>** 0.60 (1:1 EtOAc:Hex). **mp:** 209.8 °C – 211.9 °C. **<sup>1</sup>H NMR** (500 MHz, CDCl<sub>3</sub>): δ 11.46 (s, 1H, OH), 8.79 (dd, *J* = 4.9, 1.5 Hz, 1H, H-14), 8.22 (dd, *J* = 8.1, 1.6 Hz, 1H, H-12), 8.00 (dd, *J* = 8.8, 2.3 Hz, 1H, H-6), 7.95 (d, *J* = 2.3 Hz, 1H, H-2), 7.91 – 7.85 (m, 2H, H-8), 7.55 – 7.47 (m, 3H, H-13 and H-9), 7.47 – 7.41 (m, 1H, H-10), 7.18 (d, *J* = 8.8 Hz, 1H, H-5). **<sup>13</sup>C NMR** (126 MHz, *Cryo-probe*, CDCl<sub>3</sub>): δ 160.1 (C-4), 152.6 (C-7), 150.6 (C-15), 149.8 (C-14), 146.2 (C-1), 145.7 (C-11), 134.0 (C-12), 130.8 (C-10), 129.2 (C-9), 126.2 (C-6), 125.9 (C-2), 122.9 (C-8), 122.6 (C-13), 119.5 (C-5), 117.5 (C-3). **UV-Vis** (THF)  $\lambda_{\text{max}}$  = 348 nm ( $\epsilon$  = 24,450 M<sup>-1</sup>cm<sup>-1</sup>), 435 nm ( $\epsilon$  = 1,670 M<sup>-1</sup>cm<sup>-1</sup>). **IR**  $\nu$  (cm<sup>-1</sup>): 3024, 1738, 1604, 1528, 1469, 1355, 1288, 1227, 1122, 1091, 929, 853, 817, 770, 695. **HRMS** (ESI<sup>+</sup>) *m/z*: Found 321.0979 Calculated for C<sub>17</sub>H<sub>13</sub>N<sub>4</sub>O<sub>3</sub><sup>+</sup> [M+H]<sup>+</sup> 321.0988. Δ = -2.8 ppm.

Assignments made based on COSY, HMBC and HSQC data.

## Experimental

---

### 1,3-Difluoro-2-nitrosobenzene **144**



Across two RBFs, 2,6-difluoroaniline **143** (1.30 g, 10.1 mmol, per flask) was dissolved in CH<sub>2</sub>Cl<sub>2</sub> (20 mL, per flask) and cooled to 0 °C. A solution of Oxone® (6.19 g, 2 eq, 20.1 mmol, per flask) in DI water (20 mL, per flask) was then added to each flask and the reactions left to warm to room temperature with stirring behind a blast shield. The reactions were diluted with CH<sub>2</sub>Cl<sub>2</sub> (20 mL per flask) and washed with 1 M NaOH (2 × 10 mL), 1 M HCl (2 × 10 mL) and finally 10 % Na<sub>2</sub>S<sub>2</sub>O<sub>3</sub> solution (10 mL). The organic layers were combined to give a single crude mixture, dried over MgSO<sub>4</sub> and concentrated *in vacuo* (being cautious of compound volatility). The crude mixture was then carried directly into the following reaction without purification.

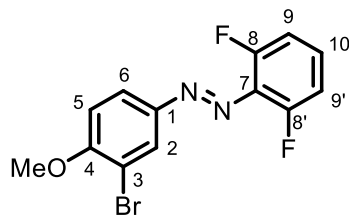
*Selected data presented from the crude material:*

**R<sub>f</sub>** 0.50 (1:4 EtOAc:Hex) **<sup>1</sup>H NMR** (300 MHz, CDCl<sub>3</sub>) δ 7.63 (tt, *J* = 8.5, 5.9 Hz, 1H, H-2), 7.12 (t, *J* = 8.6 Hz, 2H, H-1) **<sup>19</sup>F NMR** (283 MHz, CDCl<sub>3</sub>) δ -130.08 (dd, *J* = 8.7, 5.9 Hz).

## Experimental

---

(*E*)-1-(3-Bromo-4-methoxyphenyl)-2-(2,6-difluorophenyl)diazene **145**



Synthesized according to the **General Mills Reaction** from 3-bromo-4-methoxyaniline **118** (4.88 g, 24.2 mmol, 1.2 eq) and the crude nitrosobenzene **144** (*est.* 20.2 mmol), with column chromatography (1:9-to-1:4 EtOAc:Hex) affording the title compound **145** as an orange crystalline solid (4.53 g, 69% over 2 steps).

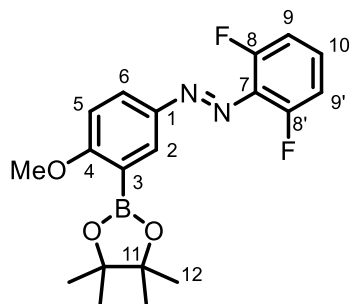
**R<sub>f</sub>** 0.45 (1:4 EtOAc:Hex) **mp:** 110.2 °C – 112.8 °C. **<sup>1</sup>H NMR** (400 MHz, CDCl<sub>3</sub>): δ 8.18 (d, *J* = 2.3 Hz, 1H, H-2), 7.96 (dd, *J* = 8.7, 2.3 Hz, 1H, H-6), 7.38 – 7.27 (m, 1H, H-10), 7.08 – 7.00 (m, 3H, H-9 and H-5), 4.00 (s, 3H. MeO). **<sup>13</sup>C NMR** (101 MHz, CDCl<sub>3</sub>): δ 158.9 (C-4), 155.9 (dd, <sup>1/3</sup>J<sub>C-F</sub> = 259.0, 4.2 Hz, C-8), 147.9 (C-1), 131.3 (t, <sup>2</sup>J<sub>C-F</sub> = 10.1 Hz, C-7), 130.2 (t, <sup>3</sup>J<sub>C-F</sub> = 10.3 Hz, C-10), 126.32 (C-6 or C-2), 126.30 (C-6 or C-2), 112.9 (C-3), 112.6 (dd, <sup>2/4</sup>J<sub>C-F</sub> = 19.7, 4.3 Hz, C-9), 111.4 (C-5), 56.8 (OMe). **<sup>19</sup>F NMR** (376 MHz, CDCl<sub>3</sub>): δ -121.46 (dd, <sup>1</sup>J<sub>C-F</sub> = 8.7, 5.9 Hz). **IR v** (cm<sup>-1</sup>): 2946, 1615, 1585, 1463, 1392, 1271, 1244, 1137, 1024, 886, 785, 712. **HRMS** (ESI<sup>+</sup>) *m/z*: Found 326.9936 Calculated for C<sub>13</sub>H<sub>10</sub>BrF<sub>2</sub>N<sub>2</sub>O [M+H]<sup>+</sup> 326.9936. Δ = 0.9 ppm.

Assignments made based on COSY, HMBC and HSQC data.

## Experimental

---

(*E*)-1-(2,6-Difluorophenyl)-2-(4-methoxy-3-(4,4,5,5-tetramethyl-1,3,2-dioxaborolan-2-yl)phenyl)diazene **146**



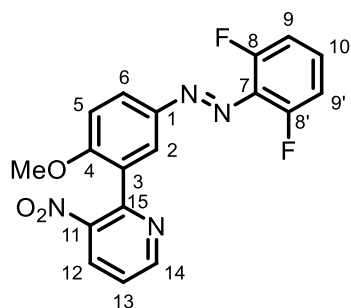
**R<sub>f</sub>** 0.33 (1:4 EtOAc:Hex). **mp:** 123.4 °C – 125.2 °C. **<sup>1</sup>H NMR** (400 MHz, CDCl<sub>3</sub>): δ 8.31 (d, *J* = 2.6 Hz, 1H, H-2), 8.01 (dd, *J* = 8.9, 2.6 Hz, 1H, H-6), 7.30 – 7.22 (m, 1H, H-10), 7.06 – 6.94 (m, 3H, H-9 and H-5), 3.92 (s, 3H, OMe), 1.37 (s, 12H, H-12). **<sup>13</sup>C NMR** (101 MHz, CDCl<sub>3</sub>) : δ 167.3 (C-4), 155.8 (dd, <sup>1/3</sup>*J*<sub>C-F</sub> = 257.6, 4.6 Hz, C-8), 147.2 (C-1), 132.9 (C-2), 131.8 (t, <sup>2</sup>*J*<sub>C-F</sub> = 10.4 Hz, C-7), 129.4 (t, <sup>3</sup>*J*<sub>C-F</sub> = 9.6 Hz, C-10), 127.2 (C-6), 112.5 (dd, <sup>2/4</sup>*J*<sub>C-F</sub> = 18.7, 5.3 Hz, C-9), 110.6 (C-5), 84.0 (C-11), 56.3 (MeO), 25.0 (C-12). \*C-3 not observed due to boron relaxation. **<sup>11</sup>B NMR** (128 MHz, CDCl<sub>3</sub>): δ 29.9. **<sup>19</sup>F NMR** (376 MHz, CDCl<sub>3</sub>): δ -122.20 (dd, *J* = 8.4, 5.7 Hz). **IR v** (cm<sup>-1</sup>): 2980, 1587, 1464, 1442, 1372, 1320, 1256, 1132, 1059, 1012, 817, 786. **HRMS** (ESI<sup>+</sup>) *m/z*: Found 375.1679 Calculated for C<sub>19</sub>H<sub>22</sub>BF<sub>2</sub>N<sub>2</sub>O<sub>3</sub> [M+H]<sup>+</sup> 375.1686. Δ = 1.9 ppm.

Assignments made based on COSY, HMBC and HSQC data.

## Experimental

---

(*E*)-2-((2,6-Difluorophenyl)diazenyl)-2-methoxyphenyl)-3-nitropyridine **147**



Synthesized according to the **General Suzuki Cross-Coupling Procedure A** from Bpin-azobenzene **146** (3.00 g, 8.02 mmol), bromide **85** (1.85 g, 9.62 mmol), Pd(OAc)<sub>2</sub> (0.090 g, 0.40 mmol), SPhos (0.329 g, 0.802 mmol) and Cs<sub>2</sub>CO<sub>3</sub> (5.22 g, 16.0 mmol), with column chromatography (1:4 EtOAc:Hex) affording the title compound **147** as an orange solid (2.64 g, 89%).

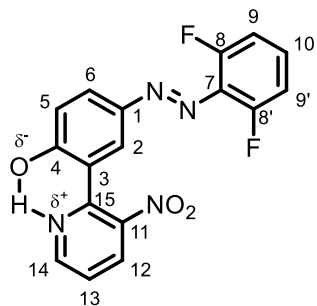
**R<sub>f</sub>** 0.19 (1:4 EtOAc:Hex). **mp:** 139.6 °C – 142.0 °C. **<sup>1</sup>H NMR** (400 MHz, CDCl<sub>3</sub>): δ 8.91 (dt, *J* = 4.7, 1.2 Hz, 1H, H-14), 8.30 (d, *J* = 2.4 Hz, 1H, H-2), 8.26 (dt, *J* = 8.3, 1.3 Hz, 1H, H-12), 8.10 (ddd, *J* = 8.7, 2.4, 0.9 Hz, 1H, H-6), 7.47 (ddd, *J* = 8.1, 4.8, 1.0 Hz, 1H, H-13), 7.30 – 7.23 (m, 1H, H-10), 7.08 – 6.98 (m, 3H, H-5 and H-9), 3.81 (s, 3H, MeO). **<sup>13</sup>C NMR** (101 MHz, CDCl<sub>3</sub>): δ 159.3 (C-4), 155.8 (dd, <sup>1/3</sup>*J*<sub>C-F</sub> = 258.4, 4.4 Hz, C-8), 152.9 (C-14), 149.8 (C-15), 148.0 (C-1), 147.0 (C-11), 132.0 (C-12), 131.6 (t, <sup>2</sup>*J*<sub>C-F</sub> = 10.2 Hz, C-7), 129.9 (t, <sup>3</sup>*J*<sub>C-F</sub> = 10.2 Hz, C-10), 127.9 (C-6), 127.4 (C-3), 124.6 (C-2), 122.9 (C-13), 112.5 (dd, <sup>2/4</sup>*J*<sub>C-F</sub> = 18.8, 4.9 Hz, C-9), 110.9 (C-5), 55.8 (MeO). **<sup>19</sup>F NMR** (376 MHz, CDCl<sub>3</sub>): δ -121.70 (dd, *J* = 9.2, 5.4 Hz). **IR v** (cm<sup>-1</sup>): 2982, 1600, 1526, 1352, 1276, 1239, 1129, 1014, 822, 782. **HRMS (ESI<sup>+</sup>) m/z:** Found 371.0947 Calculated for C<sub>18</sub>H<sub>13</sub>F<sub>2</sub>N<sub>4</sub>O<sub>3</sub><sup>+</sup> [M+H]<sup>+</sup> 371.0950. Δ = 0.8 ppm.

Assignments made based on COSY, HMBC and HSQC data.

## Experimental

---

### (E)-4-((2,6-Difluorophenyl)diazenyl)-2-(3-nitropyridin-2-yl)phenol **148**



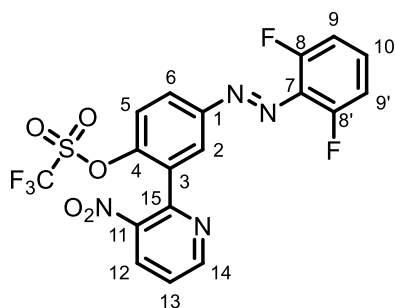
In a flame-dried RBF, azo-biaryl **147** (0.500 g, 1.35 mmol) was dissolved in CH<sub>2</sub>Cl<sub>2</sub> (6.8 mL) and cooled to 0 °C, whereupon BBr<sub>3</sub> (1 M solution in heptane, 4.05 mL, 3 eq) was added slowly. After addition, the reaction mixture was removed from the ice bath and allowed to slowly warm to room temperature. After stirring for 16 h, the mixture was cooled to 0 °C and quenched with 2 M NaOH (5 mL). The mixture was then neutralized with 2 M HCl (10 mL) and extracted with CH<sub>2</sub>Cl<sub>2</sub> (2 × 25 mL). The organic layer was dried with MgSO<sub>4</sub>, filtered through Celite®, and evaporated *in vacuo*. The resulting solid was then purified *via* column chromatography (1:4-to-1:1 EtOAc:Hex) to give the title compound **148** as an orange solid (0.336 g, 70%).

**R<sub>f</sub>** 0.38 (1:1 EtOAc:Hex). **mp:** 165.7 °C – 167.0 °C. **<sup>1</sup>H NMR** (400 MHz, CDCl<sub>3</sub>):  $\delta$  11.45 (s, 1H, OH), 8.79 (dd,  $J$  = 4.9, 1.6 Hz, 1H, H-14), 8.23 (dd,  $J$  = 8.2, 1.6 Hz, 1H, H-12), 8.00 (dd,  $J$  = 8.8, 2.3 Hz, 1H, H-6), 7.97 (dd,  $J$  = 2.3, 0.5 Hz, 1H, H-2), 7.51 (dd,  $J$  = 8.2, 4.9 Hz, 1H, H-13), 7.33 – 7.26 (m, 1H, H-10), 7.19 (dd,  $J$  = 8.8, 0.5 Hz, 1H, H-5), 7.05 – 6.99 (m, 2H, H-9). **<sup>13</sup>C NMR** (126 MHz, *Cryo-probe*, CDCl<sub>3</sub>):  $\delta$  160.8 (C-4), 155.9 (dd,  $^{1/3}J_{C-F}$  = 258.4, 4.4 Hz, C-8), 150.4 (C-15), 149.8 (C-14), 147.0 (C-1), 145.7 (C-11), 134.0 (C-12), 131.4 (t,  $^2J_{C-F}$  = 10.2 Hz, C-7), 130.0 (t,  $^3J_{C-F}$  = 10.2 Hz, C-10), 126.3 (C-2 or 6), 126.2 (C-2 or 6), 122.7 (C-13), 119.5 (C-5), 117.8 (C-3), 112.5 (dd,  $^{2/4}J_{C-F}$  = 18.8, 4.9 Hz, C-9). **<sup>19</sup>F NMR** (376 MHz, CDCl<sub>3</sub>):  $\delta$  -121.46 (dd,  $J$  = 9.2, 6.0 Hz). **IR v** (cm<sup>-1</sup>):  $\delta$  3361, 1588, 1528, 1483, 1363, 1280, 1247, 1089, 1026, 819, 784. **HRMS (ESI<sup>+</sup>) m/z:** Found 357.0790 Calculated for C<sub>17</sub>H<sub>11</sub>F<sub>2</sub>N<sub>4</sub>O<sub>3</sub><sup>+</sup> [M+H]<sup>+</sup> 357.0794.  $\Delta$  = 1.1 ppm.

Assignments made based on COSY, HMBC and HSQC data.

## Experimental

(*E*)-4-((2,6-Difluorophenyl)diazenyl)-2-(3-nitropyridin-2-yl)phenyl trifluoromethanesulfonate **149**



In a flame dried Schlenk tube, hydroxy-azo-biaryl **148** (0.150 g, 0.421 mmol) was dissolved in CH<sub>2</sub>Cl<sub>2</sub> (4.2 mL) and cooled to 0 °C under an atmosphere of N<sub>2</sub>. Triethylamine (0.15 mL, 1.05 mmol, 2.5 eq) and triflic anhydride (1 M in CH<sub>2</sub>Cl<sub>2</sub>, 1.05 mL, 2.5 eq) were then added and the resulting mixture warmed to room temperature and left to stir. After 16 h the reaction was quenched with water (2 mL), and the aqueous layer extracted with CH<sub>2</sub>Cl<sub>2</sub> (3 × 2.5 mL). The combined organic layers were then separated, dried over MgSO<sub>4</sub>, filtered through Celite® and concentrated *in vacuo*. The residue was purified by column chromatography (1:9 EtOAc:Hex) to give the title compound **149** as a red solid (0.156 g, 76%).

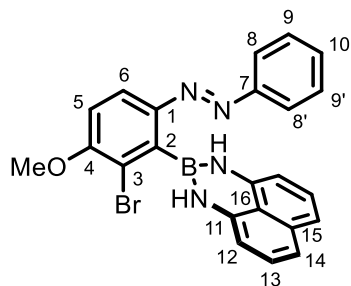
**Rf** 0.48 (1:4 EtOAc:Hex). **mp:** 115.9 °C – 117.6 °C. **<sup>1</sup>H NMR** (400 MHz, CDCl<sub>3</sub>): δ 9.01 (dd, *J* = 4.7, 1.5 Hz, 1H, H-14), 8.51 (dd, *J* = 8.3, 1.6 Hz, 1H, H-12), 8.24 (d, *J* = 2.4 Hz, 1H, H-2), 8.16 (dd, *J* = 8.8, 2.5 Hz, 1H, H-6), 7.64 (dd, *J* = 8.4, 4.7 Hz, 1H, H-13), 7.57 (d, *J* = 8.9 Hz, 1H, H-5), 7.43 – 7.33 (m, 1H, H-10), 7.11 – 7.03 (m, 2H, H-9). **<sup>13</sup>C NMR** (126 MHz, *Cryo-probe*, CDCl<sub>3</sub>): δ 156.1 (dd, <sup>1/3</sup>*J*<sub>C-F</sub> = 261.2, 4.4 Hz, C-8), 153.5 (C-14), 152.3 (C-1), 148.1 (C-15 or C-4), 148.0 (C-15 or C-4), 146.0 (C-11), 133.1 (C-12), 132.6 (C-3), 131.6 (t, <sup>3</sup>*J*<sub>C-F</sub> = 10.4 Hz, C-10), 131.1 (t, <sup>2</sup>*J*<sub>C-F</sub> = 9.7 Hz, C-7), 126.0 (C-6), 125.3 (C-2), 124.4 (C-13), 122.6 (C-5), 118.6 (q, <sup>1</sup>*J*<sub>C-F</sub> = 320.1 Hz, CF<sub>3</sub>), 112.8 (dd, <sup>2/4</sup>*J*<sub>C-F</sub> = 20.0, 4.0 Hz, C-9). **<sup>19</sup>F NMR** (376 MHz, CDCl<sub>3</sub>): -73.61 (s, 3F, CF<sub>3</sub>), -120.17 (dd, *J* = 9.2, 6.0 Hz, 2F, F-8). **IR v** (cm<sup>-1</sup>): δ 3061, 1615, 1526, 1404, 1351, 1217, 1130, 1087, 1023, 858, 841, 780. **HRMS** (ESI<sup>+</sup>) *m/z*: Found 489.0275 Calculated for C<sub>18</sub>H<sub>10</sub>F<sub>5</sub>N<sub>4</sub>O<sub>5</sub>S<sup>+</sup> [M+H]<sup>+</sup> 489.0275. Δ = 2.5 ppm.

Assignments made based on COSY, HMBC and HSQC data.

## Experimental

---

(*E*)-2-(2-Bromo-3-methoxy-6-(phenyldiazenyl)phenyl)-2,3-dihydro-1H-naphtho[1,8-de][1,3,2]diazaborinine **169**



In a flame-dried flask, boryl-azobenzene **126** (7.50 g, 16.3 mmol) and 1,8-diaminonaphthelene (3.86 g, 24.4 mmol, 1.5 eq) were dissolved in CH<sub>2</sub>Cl<sub>2</sub> (85 mL) to which was added NEt<sub>3</sub> (4.54 mL, 32.6 mmol, 2 eq). After being stirred at room temperature for 1 h, the solution was concentrated *in vacuo* and purified *via* silica chromatography (1:4 EtOAc:Hexane) to give the title compound **169** as a red solid (7.21 g, 97%).

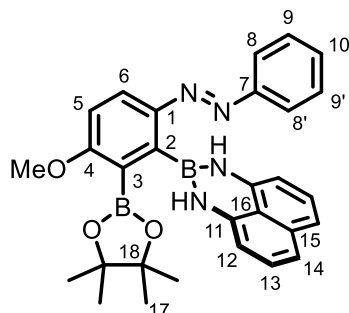
**R<sub>f</sub>** 0.30 (1:4 EtOAc:Hex). **mp:** 203.4 °C – 204.6 °C. **<sup>1</sup>H NMR** (400 MHz, CDCl<sub>3</sub>): δ 7.95 (d, *J* = 8.7 Hz, 1H, H-6), 7.75 – 7.66 (m, 2H, H-8), 7.35 – 7.30 (m, 3H, H-9 and H-10), 7.14 (dd, *J* = 8.3, 7.1 Hz, 2H, H-13), 7.08 (dd, *J* = 8.3, 1.2 Hz, 2H, H-14), 7.03 (d, *J* = 8.7 Hz, 1H, H-5), 6.32 (dd, *J* = 7.2, 1.2 Hz, 2H, H-12), 5.69 (s, 2H, NH of Bdan), 3.98 (s, 3H, MeO). **<sup>13</sup>C NMR** (101 MHz, CDCl<sub>3</sub>) 157.7 (C-4), 151.2 (C-7), 150.4 (C-1), 141.3 (C-11), 136.6 (C-15), 131.1 (C-10), 129.3 (C-9), 127.7 (C-13), 123.9 (C-6), 122.9 (C-8), 119.5 (C-16), 117.5 (C-14), 117.4 (C-3), 112.0 (C-5), 106.0 (C-12), 56.7 (MeO). \*C-2 not observed due to boron relaxation. **<sup>11</sup>B NMR** (128 MHz, CDCl<sub>3</sub>): δ 28.7. **IR v** (cm<sup>-1</sup>): 3404, 3322, 2930, 1596, 1509, 1409, 1269, 1127, 1060, 817, 759. **HRMS** (ESI<sup>+</sup>) *m/z*: Found 456.0764 Calculated for C<sub>23</sub>H<sub>18</sub>BBrN<sub>4</sub>O [M]<sup>+</sup> 456.0752. Δ = 2.6 ppm.

Assignments made based on COSY, HMBC and HSQC data.

## Experimental

---

(*E*)-2-(3-Methoxy-6-(phenyldiazenyl)-2-(4,4,5,5-tetramethyl-1,3,2-dioxaborolan-2-yl)phenyl)-2,3-dihydro-1H-naphtho[1,8-de][1,3,2]diazaborinine **170**



Synthesized according to the **General Miyaura Borylation Procedure** from bromoazobenzene **169** (0.040 g, 0.088 mmol),  $B_2\text{Pin}_2$  (4.71 g, 18.5 mmol),  $\text{PdCl}_2(\text{PPh}_3)_2$  (0.434 g, 0.618 mmol),  $^t\text{BuPPH}_2$  (0.299 g, 1.24 mmol) and  $\text{K}_2\text{CO}_3$  (3.41 g, 24.7 mmol). After a 16 h reaction time, column chromatography (1:4 EtOAc:Hex) affording the title compound **170** as an orange solid (5.88 g, 94%).

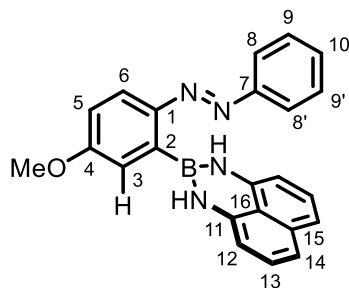
$R_f$  0.28 (1:4 EtOAc:Hex). **mp:** 226.9 °C – 228.3 °C.  **$^1\text{H NMR}$**  (400 MHz,  $\text{CDCl}_3$ ):  $\delta$  7.96 (d,  $J = 9.0$  Hz, 1H, H-6), 7.82 – 7.69 (m, 2H, H-8), 7.41 – 7.33 (m, 3H, H-9 and H-10), 7.11 (dd,  $J = 8.3, 7.3$  Hz, 2H, H-13), 7.03 (dd,  $J = 8.3, 1.1$  Hz, 2H, H-14), 6.98 (d,  $J = 9.0$  Hz, 1H, H-5), 6.28 (dd,  $J = 7.3, 1.1$  Hz, 2H, H-12), 5.96 (s, 2H, 2x NH of Bdan), 3.90 (s, 3H, MeO), 1.26 (s, 12H, H-17).  **$^{13}\text{C NMR}$**  (126 MHz, *Cryo-probe*,  $\text{CDCl}_3$ ) 164.9 (C-4), 152.1 (C-7), 150.0 (C-1), 141.5 (C-11), 136.5 (C-15), 130.6 (C-10), 129.3 (C-9), 127.7 (C-13), 123.0 (C-6), 122.8 (C-8), 119.6 (C-16), 117.3 (C-14), 111.0 (C-5), 105.8 (C-12), 84.5 (C-18), 56.0 (MeO), 25.0 (C-17). \*C-2 and C-3 not observed due to boron relaxation.  **$^{11}\text{B NMR}$**  (128 MHz,  $\text{CDCl}_3$ ):  $\delta$  29.7. **IR  $\nu$  (cm<sup>-1</sup>)**: 3381, 2923, 2852, 1600, 1562, 1514, 1313, 1252, 1131, 1062, 819, 761. **HRMS (ESI<sup>+</sup>)  $m/z$ :** Found 505.2588 Calculated for  $\text{C}_{29}\text{H}_{31}\text{B}_2\text{N}_4\text{O}_3$  [M+H]<sup>+</sup> 505.2577.  $\Delta = 2.0$  ppm.

Assignments made based on COSY, HMBC and HSQC data.

## Experimental

---

(*E*)-2-(5-Methoxy-2-(phenyldiazenyl)phenyl)-2,3-dihydro-1H-naphtho[1,8-de][1,3,2]diazaborinine **171**



*Isolated as an undesired side product during the Miyaura borylation screening.*

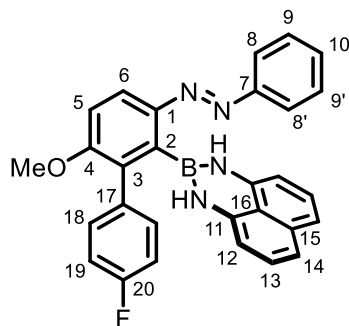
**R<sub>f</sub>** 0.45 (1:4 EtOAc:Hex). **mp:** 154.8 °C – 156.6 °C. **<sup>1</sup>H NMR** (400 MHz, CDCl<sub>3</sub>): δ 7.94 (d, *J* = 9.0 Hz, 1H, H-6), 7.88 – 7.81 (m, 2H, H-8), 7.55 – 7.49 (m, 2H, H-9), 7.49 – 7.44 (m, 1H, H-10), 7.21 (d, *J* = 2.8 Hz, 1H, H-3), 7.14 (dd, *J* = 8.3, 7.2 Hz, 2H, H-13), 7.07 – 7.03 (m, 3H, H-5 and H-14), 6.54 (s, 2H, NHs of B dan), 6.36 (dd, *J* = 7.2, 1.1 Hz, 2H, H-12), 3.94 (s, 3H, MeO). **<sup>13</sup>C NMR** (126 MHz, *Cryo-probe*, CDCl<sub>3</sub>) 161.8 (C-4), 152.8 (C-7), 150.8 (C-1), 141.5 (C-11), 136.5 (C-15), 130.8 (C-10), 129.4 (C-9), 127.8 (C-13), 122.8 (C-8), 119.9 (C-16), 119.3 (C-6), 117.9 (C-3), 117.7 (C-14), 115.8 (C-5), 106.0 (C-12), 55.8 (MeO). \*C-2 not observed due to boron relaxation. **<sup>11</sup>B NMR** (128 MHz, CDCl<sub>3</sub>): δ 28.6. **IR v** (cm<sup>-1</sup>): 3385, 3345, 2935, 1599, 1514, 1464, 1409, 1371, 1328, 1205, 1152, 1070, 816, 756. **HRMS** (ESI<sup>+</sup>) *m/z*: Found 379.1731 Calculated for C<sub>23</sub>H<sub>20</sub>BN<sub>4</sub>O [M+H]<sup>+</sup> 379.1725. Δ = 1.6 ppm.

Assignments made based on COSY, HMBC and HSQC data.

## Experimental

---

(*E*)-2-(2-Bromo-3-methoxy-6-(phenyldiazenyl)phenyl)-2,3-dihydro-1H-naphtho[1,8-de][1,3,2]diazaborinine **173**



Synthesized according to the **General Suzuki Cross-Coupling Procedure B** from bromo-azobenzene **169** (0.040 g, 0.088 mmol, *1.0 eq.*)\*, boronic acid **172** (0.015 g, 0.011 mmol, *1.2 eq.*)\*, Pd(OAc)<sub>2</sub> (0.001 g, 0.004 mmol), PPh<sub>3</sub> (0.002 g, 0.008 mmol) and Cs<sub>2</sub>CO<sub>3</sub> (0.057 g, 0.18 mmol), with column chromatography (1:9 EtOAc:Hex) affording the title compound **173** as an orange solid (0.036 g, 87%).

\*Aryl bromide used as limiting reagent instead of boron coupling partner as described in the general procedure

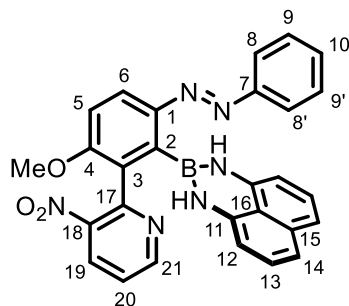
**R<sub>f</sub>** 0.41 (1:3 EtOAc:Hex). **mp:** 207.2 °C – 208.9 °C. **<sup>1</sup>H NMR** (400 MHz, CDCl<sub>3</sub>): δ 7.99 (d, *J* = 8.9 Hz, 1H, H-6), 7.81 – 7.72 (m, 2H, H-8), 7.42 – 7.34 (m, 5H, H-18, H-10 and H-9), 7.12 (d, *J* = 8.9 Hz, 1H, H-5), 7.08 – 7.02 (m, 4H, H-19 and H-13), 6.98 (dd, *J* = 8.2, 1.1, 2H, H-14), 6.11 (dd, *J* = 7.2, 1.1 Hz, 2H, C-12), 5.51 (s, 2H, 2 NH groups of Bdan), 3.85 (s, 3H, MeO). **<sup>13</sup>C NMR** (126 MHz, *Cryo-probe*, CDCl<sub>3</sub>) δ 162.3 (d, *J* = 245 Hz, C-20), 158.9 (C-4), 152.1 (C-7), 150.2 (C-1), 141.2 (C-11), 136.3 (C-15), 134.5 (C-3), 133.8 (d, *J* = 3.4 Hz, C-17), 131.7 (d, *J* = 8.5 Hz, C-18), 130.7 (C-10), 129.3 (C-9), 127.7 (C-13), 122.9 (C-8), 120.5 (C-6), 119.2 (C-16), 117.3 (C-14), 115.2 (d, *J* = 22.1 Hz C-19), 111.9 (C-5), 105.5 (C-12), 56.1 (MeO). \*C-2 not observed due to boron relaxation. **<sup>11</sup>B NMR** (128 MHz, CDCl<sub>3</sub>): δ 29.4. **<sup>19</sup>F NMR** (376 MHz, CDCl<sub>3</sub>): δ -114.65 (tt, *J* = 9.2, 5.4 Hz). **IR v** (cm<sup>-1</sup>): 3415, 3007, 1596, 1512, 1404, 1394, 1255, 1216, 1055, 819, 761, 748. **HRMS** (ESI<sup>+</sup>) *m/z*: Found 473.1944 Calculated for C<sub>29</sub>H<sub>23</sub>BFN<sub>4</sub>O [M+H]<sup>+</sup> 473.1943. Δ = 0.2 ppm.

Assignments made based on COSY, HMBC and HSQC data.

## Experimental

---

(E)-2-(3-Methoxy-2-(3-nitropyridin-2-yl)-6-(phenyldiazenyl)phenyl)-2,3-dihydro-1H-naphtho[1,8-de][1,3,2]diazaborinine **174**



Synthesized according to the **General Suzuki Cross-Coupling Procedure B** from Bpin-azobenzene **170** (1.00 g, 1.98 mmol), pyridyl-bromide **85** (0.483 g, 2.38 mmol), Pd(OAc)<sub>2</sub> (0.022 g, 0.099 mmol), PPh<sub>3</sub> (0.052 g, 0.20 mmol,) and Cs<sub>2</sub>CO<sub>3</sub> (1.29 g, 3.97 mmol), with column chromatography (1:3 EtOAc:Hex) affording the title compound **174** as an orange solid (0.885 g, 89%).

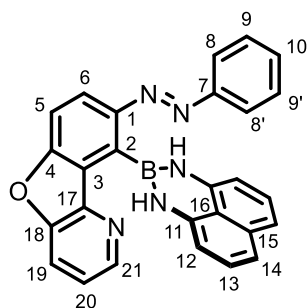
**R<sub>f</sub>** 0.14 (1:3 EtOAc:Hex). **mp:** >250 °C (equipment max.). **<sup>1</sup>H NMR** (400 MHz, CDCl<sub>3</sub>): δ 8.79 (dd, *J* = 4.7, 1.5 Hz, 1H, H-21), 8.24 (dd, *J* = 8.3, 1.5 Hz, 1H, H-19), 8.08 (d, *J* = 8.9 Hz, 1H, H-6), 7.77 – 7.70 (m, 2H, H-8), 7.39 – 7.33 (m, 4H, H-9, H-10 and H-20), 7.10 (d, *J* = 8.9 Hz, 1H, H-5), 7.03 (dd, *J* = 8.3, 7.1 Hz, 2H, H-13), 6.97 (dd, *J* = 8.3, 1.2 Hz, 2H, H-14), 6.14 (dd, *J* = 7.2, 1.2 Hz, 2H, H-12), 5.70 (s, 2H, NH of Bdan), 3.80 (s, 3H, MeO). **<sup>13</sup>C NMR** (126 MHz, *Cryo-probe*, CDCl<sub>3</sub>) δ 158.2 (C-4), 152.7 (C-21), 151.8 (C-7), 151.5 (C-17), 150.4 (C-1), 147.1 (C-18), 141.2 (C-11), 136.3 (C-15), 131.8 (C-19), 131.1 (C-3), 130.8 (C-10), 129.3 (C-9), 127.7 (C-13), 123.6 (C-6), 123.2 (C-20), 122.9 (C-8), 119.2 (C-16), 117.2 (C-14), 111.8 (C-5), 105.6 (C-12), 56.0 (MeO). \*C-2 not observed due to boron relaxation. **<sup>11</sup>B NMR** (128 MHz, CDCl<sub>3</sub>): δ 29.1. **IR v** (cm<sup>-1</sup>): 2921, 2095, 1592, 1504, 1397, 1353, 1262, 1060, 819, 763. **HRMS** (ESI<sup>+</sup>) *m/z*: Found 501.1847 Calculated for C<sub>28</sub>H<sub>22</sub>BN<sub>6</sub>O<sub>3</sub> [M+H]<sup>+</sup> 501.1841. Δ = 1.2 ppm.

Assignments made based on COSY, HMBC and HSQC data.

## Experimental

---

(*E*)-9-(1H-Naphtho[1,8-de][1,3,2]diazaborinin-2(3H)-yl)-8-(phenyldiazenyl)benzofuro[3,2-b]pyridine **175**



Under an atmosphere of N<sub>2</sub>, azo-biaryl **174** (0.800 g, 1.82 mmol) and LiCl (0.309 g, 7.28 mmol) were dissolved in DMF (18 mL) and the solution heated to 140 °C for 16 h. After cooling to room temperature, the reaction was diluted with H<sub>2</sub>O (40 mL) and extracted with EtOAc (3 × 40 mL). The organic layer was dried over MgSO<sub>4</sub>, filtered through Celite®, reduced *in vacuo*. The residue was then purified by column chromatography (1:5 EtOAc:Hex) to give the title compound **175** as an orange solid (0.118 g, 13%).

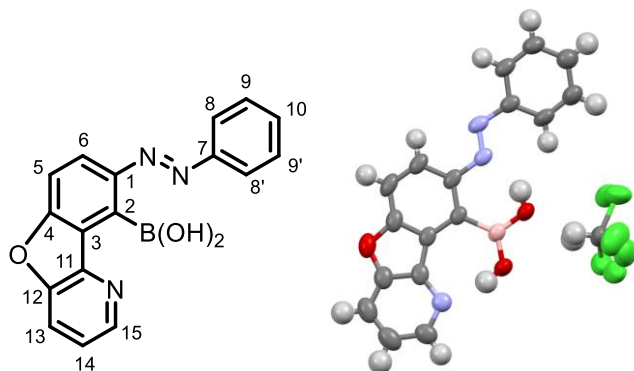
**R<sub>f</sub>** 0.65 (1:2 EtOAc:Hex). **mp:** 206.5 – 209.0 °C. **<sup>1</sup>H NMR** (400 MHz, DMSO-d<sub>6</sub>): 8.66 (dd, *J* = 4.8, 1.4 Hz, 1H, H-21), 8.28 (s, 2H, NH of dan), 8.23 (dd, *J* = 8.4, 1.4 Hz, 1H, H-19), 8.21 (d, *J* = 8.8 Hz, 1H, H-6), 7.99 (d, *J* = 8.8 Hz, 1H, H-5), 7.82 – 7.76 (m, 2H, H-8), 7.56 (dd, *J* = 8.4, 4.8 Hz, 1H, H-20), 7.52 – 7.47 (m, 3H, H-9 and H-10), 7.07 (dd, *J* = 8.3, 7.4 Hz, 2H, H-13), 6.93 (dd, *J* = 8.3, 1.0 Hz, 2H, H-14), 6.37 (dd, *J* = 7.4, 1.0 Hz, 2H, H-12). **<sup>13</sup>C NMR** (126 MHz, *Cryo-probe*, DMSO-d<sub>6</sub>) δ 157.5 (C-4), 151.61 (C-1 or C-7), 151.59 (C-1 or C-7), 150.0 (C-18), 146.0 (C-21), 144.4 (C-17), 142.9 (C-11), 136.2 (C-15), 131.2 (C-10), 129.5 (C-9), 127.7 (C-13), 126.2 (C-3), 122.31 (C-8), 122.26 (C-20), 119.9 (C-16), 119.8 (C-19), 119.3 (C-6), 115.7 (C-14), 113.3 (C-5), 105.1 (C-12). \*C-2 not observed due to boron relaxation. **<sup>11</sup>B NMR** (128 MHz, CDCl<sub>3</sub>): δ 28.4. **IR v** (cm<sup>-1</sup>): 3359, 3041, 2923, 2852, 1631, 1595, 1504, 1400, 1371, 1212, 1057, 818, 759. **HRMS** (Nanospray) *m/z*: Found 440.1697 Calculated for C<sub>27</sub>H<sub>19</sub>BN<sub>5</sub>O [M+H]<sup>+</sup> 440.1683. Δ = 3.2 ppm.

Assignments made based on COSY, HMBC and HSQC data.

## Experimental

---

### (E)-(8-(Phenyldiazenyl)benzofuro[3,2-b]pyridin-9-yl)boronic acid **176**



To a 6 mL THF solution of Bd-an-azo-biaryl **175** (0.200 g, 0.455 mmol) was added a 6N HCl aq. (0.5 mL) solution and the solution was stirred under air at room temperature overnight. The mixture was then neutralized using 2M NaOH and sat. aq. NH<sub>4</sub>Cl. The aqueous phase was then extracted with Et<sub>2</sub>O. The organic layer was washed with brine, dried over MgSO<sub>4</sub>, and filtered. The filtrate was concentrated under reduced pressure and the residue recrystallized from chloroform/n-hexane to give the title compound **176** as an orange solid (0.116 g, 80%)

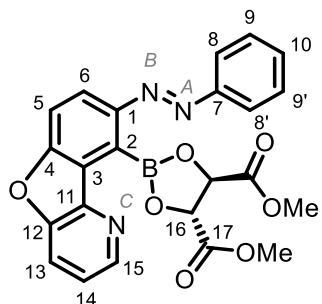
**mp:** 168.3 – 170.6 °C. **<sup>1</sup>H NMR** (400 MHz, CDCl<sub>3</sub>): δ 8.68 (dd, *J* = 4.9, 1.3 Hz, 1H, H-15), 8.34 (d, *J* = 9.1 Hz, 1H, H-6), 8.02 (dd, *J* = 8.4, 1.3 Hz, 1H, H-13), 7.93 – 7.85 (m, 2H, H-8), 7.80 (d, *J* = 9.1 Hz, 1H, H-5), 7.62 – 7.53 (m, 4H, H-14, H-9 and H-10). **<sup>13</sup>C NMR** (126 MHz, *Cryo-probe*, CDCl<sub>3</sub>) δ. 159.2 (C-4), 154.0 (C-7), 152.2 (C-1), 150.9 (C-12), 144.2 (C-11), 143.4 (C-15), 132.2 (C-10), 129.8 (C-9), 127.3 (C-3), 123.3 (C-8), 122.4 (C-14), 120.5 (C-13), 118.7 (C-6), 115.4 (C-5). \*C-2 not observed due to boron relaxation. **<sup>11</sup>B NMR** (128 MHz, CD<sub>3</sub>CN): δ 28.1. **IR v** (cm<sup>-1</sup>): 3358, 3038, 1623, 1596, 1459, 1399, 1313, 1238, 1213, 1183, 1077. **HRMS** (Nanospray) *m/z*: Found 316.0891 Calculated for C<sub>17</sub>H<sub>11</sub>BN<sub>3</sub>O<sub>3</sub> [M+H]<sup>+</sup> 316.0891. Δ = -0.6 ppm. Compound identity validated by single crystal **X-Ray** analysis.

Assignments made based on COSY, HMBC and HSQC data.

## Experimental

---

Dimethyl (4*R*,5*R*)-2-((*E*)-phenyldiazenyl)benzofuro[3,2-b]pyridin-9-yl)-1,3,2-dioxaborolane-4,5-dicarboxylate **177**



(*E*)-(8-(phenyldiazenyl)benzofuro[3,2-b]pyridin-9-yl)boronic acid **176** (23 mg, 0.063 mmol) and dimethyl tartrate (7.1 mg, 0.064 mmol, 1 eq) were dissolved in anhydrous PhMe (5 mL) which was then evaporated under an atmosphere of N<sub>2</sub> using a short path distillation apparatus. After repeating the distillation three times, the compound was dried under vacuum to give a crude film of title compound **177** which was analysed without further purification. (28 mg, 99%)

*Data presented from the crude mixture of title compound **177** and dimethyl tartrate:*

**<sup>1</sup>H NMR** (500 MHz, CD<sub>3</sub>CN): 8.58 (dd, *J* = 4.7, 1.3 Hz, 1H, H-15), 8.31 (d, *J* = 8.6 Hz, 1H, H-6), 8.11 – 8.07 (m, 2H, H-8), 7.97 (dd, *J* = 8.5, 1.3 Hz, 1H, H-13), 7.80 (d, *J* = 8.6 Hz, 1H, H-5), 7.65 – 7.60 (m, 3H, H-9 and H-10), 7.48 (dd, *J* = 8.5, 4.7 Hz, 1H, H-14), 5.37 (s, 2H, H-16), 3.71 (s, 6H, OMe) **<sup>13</sup>C NMR** (126 MHz, *Cryo-probe*, CD<sub>3</sub>CN) δ. 172.0 (C-17), 160.8 (C-4), 152.9 (C-12), 152.3 (C-1), 148.1 (C-7), 147.1 (C-15), 145.2 (C-11), 133.4 (C-10), 130.6 (C-9), 130.5 (C-6), 127.7 (C-3), 123.8 (C-8), 123.6 (C-14), 120.1 (C-13), 114.4 (C-5), 78.4 (C-16), 52.9 (OMe). \*C-2 not observed due to boron relaxation. **<sup>11</sup>B NMR** (128 MHz, CD<sub>3</sub>CN): δ 18.7. **<sup>1</sup>H-<sup>15</sup>N HMBC** (600 MHz, *Cryo-probe*, CDCl<sub>3</sub>, *J*<sub>H-N</sub> = 5 Hz): δ 476.3 (N - B), 392.7 (N - A), 302.9 (N - C). **IR v** (cm<sup>-1</sup>): 2954, 1749, 1623, 1460, 1399, 1313, 1213, 1095, 823. **HRMS** not found by Nanospray or APCI

Assignments made based on COSY, HMBC and HSQC data.

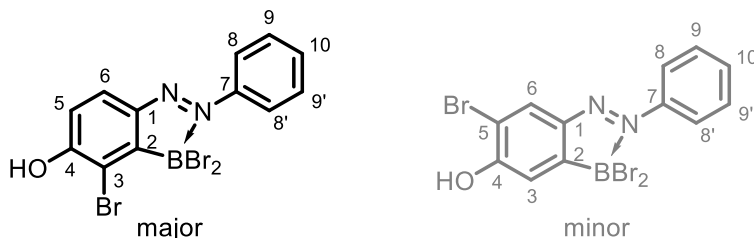
## Experimental

---

(*E*)-2-Bromo-3-(dibromoboraneyl)-4-(phenyldiazenyl)phenol **178**

and

(*E*)-2-Bromo-5-(dibromoboraneyl)-4-(phenyldiazenyl)phenol **179**



Across three RBFs, azobenzene **119** (1.50 g, 5.15 mmol per flask) was dissolved in dichloroethane (35 mL, per flask) and cooled to 0 °C, whereupon BBr<sub>3</sub> (1 M solution in Heptane 20.6 mL, 4 eq, per flask) was added slowly. The reaction mixtures were left to stir at r.t for 5 min and then heated slowly to 70 °C. After an overnight stir, the mixtures were cooled to room temperature and the solvent reduced using a continuous flow of N<sub>2</sub> with the outflows bubbled through successive quenching baths of ice-cold isopropanol and ice-cold 2M NaOH. Once reduced, the crude mixtures were brought into suspension using minimal hot CHCl<sub>3</sub> (10 mL), combined, and cold hexane added (100 mL) to precipitate a deep-red, free-flowing, crystalline solid containing both title compounds **178** and **179**. The material was exceedingly insoluble and therefore carried through without further purification.

*Selected data presented for the major isomer from the crude material:*

**<sup>1</sup>H NMR** (400 MHz, CDCl<sub>3</sub>) δ 8.57 – 8.46 (m, 2H, H-8), 8.15 (d, *J* = 8.5 Hz, 1H, H-6), 7.64 – 7.55 (m, 3H, H-9 and H-10), 7.20 (d, *J* = 8.5 Hz, 1H, H-5), 6.73 (s, 1H, OH). **<sup>11</sup>B NMR** (128 MHz, CDCl<sub>3</sub>) δ -3.7

*Selected data presented for the minor isomer from the crude material:*

**<sup>1</sup>H NMR** (400 MHz, CDCl<sub>3</sub>) δ 8.58 – 8.44 (m, 2H, H-8), 8.39 (s, 1H, H-6), 7.62 – 7.54 (m, 3H, H-9 and H-10), 7.43 (s, 1H, H-3), 6.55 (s, 1H, OH).

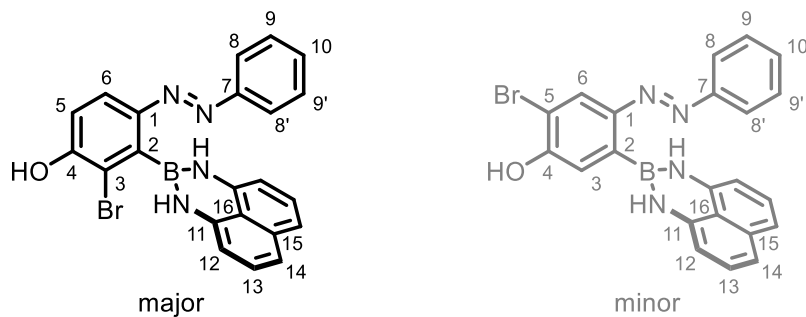
## Experimental

---

((E)-2-Bromo-3-(1H-naphtho[1,8-de][1,3,2]diazaborinin-2(3H)-yl)-4-(phenyldiazenyl)phenol  
**180**

and

((E)-2-Bromo-5-(1H-naphtho[1,8-de][1,3,2]diazaborinin-2(3H)-yl)-4-(phenyldiazenyl)phenol  
**181**

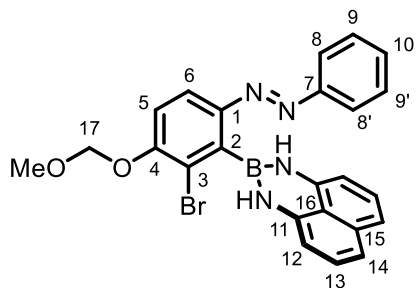


In a flame-dried flask, the crude boryl azobenzene mixture (*est.* 15.5 mmol) and 1,8-diaminonaphthelene (3.67 g, 23.2 mmol, 1.5 eq) were dissolved in CH<sub>2</sub>Cl<sub>2</sub> (150 mL, 0.1 M) which was cooled to 0 °C. NEt<sub>3</sub> (3.13 mL, 23.2 mmol, 1.5 eq) was then added dropwise and the reaction left to warm to room temperature. After being stirred at room temperature for 16 h, the solution was reduced *in vacuo*, and the residue was brought into suspension with warm EtOAc and subsequently precipitated using hexane to give a free-flowing, light-brown solid containing both title compounds **180** and **181**. The resulting material was then carried into the next reaction without further purification.

## Experimental

---

(E)-2-(2-Bromo-3-(methoxymethoxy)-6-(phenyldiazenyl)phenyl)-2,3-dihydro-1H-naphtho[1,8-de][1,3,2]diazaborinine **181**



In a flame-dried RBF under an atmosphere of N<sub>2</sub>, the crude boryl azobenzene mixture of **179** and **180** (*est.* 15.5 mmol) was dissolved in CH<sub>2</sub>Cl<sub>2</sub> (150 mL, 0.1 M), NEt(i-Pr)<sub>2</sub> (8.08 mL, 46.4 mmol, 3 eq) added, and the reaction cooled to 0 °C. MOM-bromide (90% technical grade, 3.50 mL, 38.6 mmol, 2.5 eq) was then added dropwise and the reaction was left to warm to room temperature with stirring. After 16 h, the reaction mixture was quenched with 2M NaOH, and left to stir for a further 15 min. The reaction mixture was extracted with CH<sub>2</sub>Cl<sub>2</sub> (3 × 50 mL), the combined organic phases dried over MgSO<sub>4</sub>, filtered through Celite®, and concentrated *in vacuo*. The residue was then purified by column chromatography (1:4 EtOAc:Hex) to give the title compound **181** as a red solid (4.97 g, 66% yield over 3 steps).

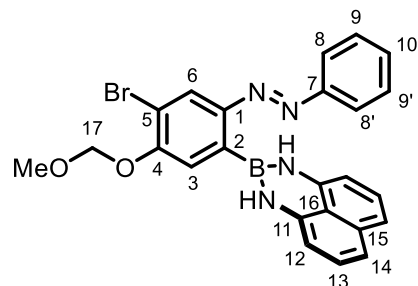
**R<sub>f</sub>** 0.31 (1:4 EtOAc:Hex). **mp:** 127.9 – 132.4 °C. **<sup>1</sup>H NMR** (400 MHz, CDCl<sub>3</sub>): δ 7.93 (d, *J* = 8.8 Hz, 1H, H-6), 7.75 – 7.68 (m, 2H, H-8), 7.37 – 7.32 (m, 3H, H-9 and H-10), 7.31 (d, *J* = 8.8 Hz, 1H, H-5), 7.14 (dd, *J* = 8.3, 7.2 Hz, 2H, H-13), 7.08 (dd, *J* = 8.3, 1.2 Hz, 2H, H-14), 6.31 (dd, *J* = 7.2, 1.2 Hz, 2H, H-12), 5.69 (s, 2H, NH of dan), 5.35 (s, 2H, H-17), 3.56 (s, 3H, OMe). **<sup>13</sup>C NMR** (126 MHz, *Cryo-probe*, CDCl<sub>3</sub>) δ. 155.5 (C-4), 151.3 (C-1/C-7), 151.2 (C-1/C-7), 141.3 (C-11), 136.6 (C-15), 131.2 (C-10), 129.3 (C-9), 127.7 (C-13), 123.4 (C-6), 122.9 (C-8), 119.5 (C-16), 118.3 (C-3), 117.5 (C-14), 116.0 (C-5), 106.0 (C-12), 95.1 (C-17), 56.7 (OMe). \*C-2 not observed due to boron relaxation. **<sup>11</sup>B NMR** (128 MHz, CDCl<sub>3</sub>): δ 28.9. **IR ν (cm<sup>-1</sup>)**: 3401, 3051, 2904, 1726, 1596, 1553, 1500, 1411, 1399, 1313, 1259, 1149, 1081, 1029, 977, 818, 762. **HRMS (ESI)** *m/z*: Found 486.0858 Calculated for C<sub>24</sub>H<sub>20</sub>BBrN<sub>4</sub>O<sub>2</sub> [M]<sup>+</sup> 486.0857. Δ = 0.2 ppm.

Assignments made based on COSY HSQC and HMBC data.

## Experimental

---

((E)-2-(4-Bromo-5-(methoxymethoxy)-2-(phenyldiazenyl)phenyl)-2,3-dihydro-1H-naphtho[1,8-de][1,3,2]diazaborinine **182**



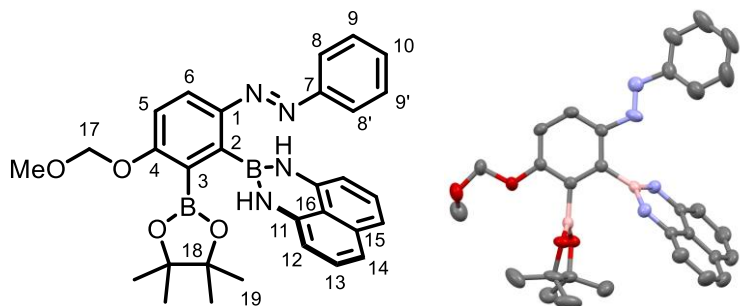
Isolated as a minor side product from the previous reaction sequence (0.440 g, 6% yield over 3 steps).

**R<sub>f</sub>** 0.85 (1:1 EtOAc:Hex). **mp:** 133.6 °C – 135.0 °C. **<sup>1</sup>H NMR** (400 MHz, CDCl<sub>3</sub>): δ 8.17 (s, 1H, H-6), 7.88 – 7.83 (m, 2H, H-8), 7.55 – 7.47 (m, 3H, H-9 and H-10), 7.42 (s, 1H, H-3), 7.14 (dd, *J* = 8.3, 7.2 Hz, 2H, H-13), 7.06 (dd, *J* = 8.3, 1.1 Hz, 2H, H-14), 6.53 (s, 2H, NH of Bdan), 6.37 (dd, *J* = 7.2, 1.1 Hz, 2H, H-12), 5.39 (s, 2H, H-17), 3.59 (s, 3H, MeO). **<sup>13</sup>C NMR** (126 MHz, *Cryo-probe*, CDCl<sub>3</sub>) δ. 155.7 (C-4), 152.6 (C-7), 151.4 (C-1), 141.2 (C-11), 136.5 (C-15), 131.4 (C-10), 129.5 (C-9), 127.8 (C-13), 123.1 (C-8), 122.4 (C-6), 120.0 (C-16), 118.5 (C-3), 117.9 (C-14), 116.1 (C-5), 106.1 (C-12), 95.2 (C-17), 56.8 (MeO). \*C-2 not observed due to boron relaxation. **<sup>11</sup>B NMR** (128 MHz, CDCl<sub>3</sub>): δ 28.6. **IR v** (cm<sup>-1</sup>): 3390, 3049, 2951, 1738, 1597, 1505, 1471, 1361, 1239, 1148, 1018, 977, 964, 816, 756. **HRMS** (ESI) *m/z*: Found 487.0949 Calculated for C<sub>24</sub>H<sub>21</sub>BBrN<sub>4</sub>O<sub>2</sub> [M+H]<sup>+</sup> 487.0935. Δ = 2.9 ppm.

Assignments made based on COSY HSQC and HMBC data.

## Experimental

(E)-2-(3-(Methoxymethoxy)-6-(phenyldiazenyl)-2-(4,4,5,5-tetramethyl-1,3,2-dioxaborolan-2-yl)phenyl)-2,3-dihydro-1H-naphtho[1,8-de][1,3,2]diazaborinine **183**



Synthesized according to the **General Miyaura Borylation Procedure** from bromoazobenzene **181** (3.15 g, 7.18 mmol),  $B_2\text{pin}_2$  (2.91 g, 11.5 mmol),  $\text{PdCl}_2(\text{PPh}_3)_2$  (0.252 g, 0.359 mmol),  $^t\text{BuPPh}_2$  (0.174 g, 0.718 mmol) and  $\text{K}_2\text{CO}_3$  (1.99 g, 14.4 mmol). After a 16 h reaction time, column chromatography (1:4 EtOAc:Hex) affording the title compound **183** as an orange solid (3.33 g, 87%).

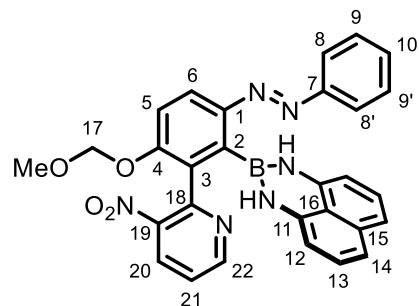
**R<sub>f</sub>** 0.28 (1:4 EtOAc:Hex). **mp:** 169.8 °C – 172.9 °C. **<sup>1</sup>H NMR** (400 MHz,  $\text{CDCl}_3$ ):  $\delta$  7.93 (d,  $J$  = 9.0 Hz, 1H, H-6), 7.82 – 7.72 (m, 2H, H-8), 7.41 – 7.34 (m, 3H, H-9 and H-10), 7.18 (d,  $J$  = 9.0 Hz, 1H, H-5), 7.12 (dd,  $J$  = 8.4, 7.2 Hz, 2H, H-13), 7.04 (dd,  $J$  = 8.4, 1.0 Hz, 2H, H-14), 6.28 (dd,  $J$  = 7.2, 1.0 Hz, 2H, H-12), 5.97 (s, 2H, NH of Bdan), 5.26 (s, 2H, H-17), 3.52 (s, 3H, MeO), 1.27 (s, 12H, H-19). **<sup>13</sup>C NMR** (126 MHz, *Cryo-probe*,  $\text{CDCl}_3$ ):  $\delta$  162.2 (C-4), 152.0 (C-7), 150.7 (C-1), 141.4 (C-11), 136.5 (C-15), 130.7 (C-10), 129.3 (C-9), 127.7 (C-13), 122.9 (C-6), 122.7 (C-8), 119.6 (C-16), 117.4 (C-14), 114.4 (C-5), 105.9 (C-12), 94.2 (C-17), 84.5 (C-18), 56.4 (MeO), 25.0 (C-19). \*C-2 and C-3 not observed due to boron. **<sup>11</sup>B NMR** (128 MHz,  $\text{CDCl}_3$ ):  $\delta$  30.0. **IR v** ( $\text{cm}^{-1}$ ): 3366, 3049, 2977, 1597, 1562, 1515, 1328, 1310, 1261, 1205, 1162, 1128, 1038, 983, 966, 848, 819, 811, 761. **HRMS** (ESI) *m/z*: Found 535.2685 Calculated for  $\text{C}_{30}\text{H}_{32}\text{B}_2\text{N}_4\text{O}_4$  [ $\text{M}+\text{H}]^+$  535.2682.  $\Delta$  = 0.6 ppm.

Assignments made based on COSY HSQC and HMBC data.

## Experimental

---

(*E*)-2-(3-(Methoxymethoxy)-2-(3-nitropyridin-2-yl)-6-(phenyldiazenyl)phenyl)-2,3-dihydro-1H-naphtho[1,8-de][1,3,2]diazaborinine **185a**



Synthesized according to the **General Suzuki Cross-Coupling Procedure B** from Bpin-azobenzene **183** (1.60 g, 3.00 mmol), pyridyl-bromide **85** (0.730 g, 3.59 mmol), Pd(OAc)<sub>2</sub> (0.034 g, 0.15 mmol), PPh<sub>3</sub> (0.079 g, 0.30 mmol,) and Cs<sub>2</sub>CO<sub>3</sub> (1.95 g, 5.99 mmol), with column chromatography (1:3 EtOAc:Hex) affording the title compound **185a** as an orange solid (1.25g, 79%).

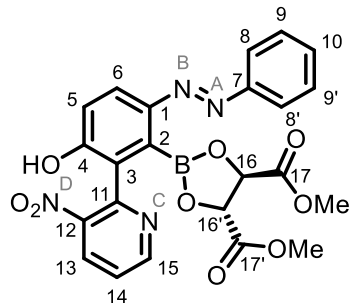
**R<sub>f</sub>** 0.24 (1:3 EtOAc:Hex). **mp:** 191.2 °C – 192.3 °C. **<sup>1</sup>H NMR** (400 MHz, CDCl<sub>3</sub>): δ 8.80 (dd, *J* = 4.8, 1.6 Hz, 1H, H-22), 8.26 (dd, *J* = 8.2, 1.6 Hz, 1H, H-20), 8.05 (d, *J* = 8.9 Hz, 1H, H-6), 7.79 – 7.72 (m, 2H, H-8), 7.39 – 7.31 (m, 5H, H-5, H-9, H-10 and H-21), 7.03 (dd, *J* = 8.3, 7.1 Hz, 2H, H-13), 6.97 (dd, *J* = 8.3, 1.1 Hz, 2H, H-14), 6.14 (dd, *J* = 7.2, 1.2 Hz, 2H, H-12), 5.71 (s, 2H, NH of Bdan), 5.12 (s, 2H, H-17), 3.36 (s, 3H. OMe). **<sup>13</sup>C NMR** (101 MHz, CDCl<sub>3</sub>) δ 155.8 (C-4), 152.7 (C-22), 151.8 (C-7), 151.5 (C-18), 151.0 (C-1), 147.0 (C-19), 141.2 (C-11), 136.3 (C-15), 131.8 (C-20), 131.6 (C-3), 130.9 (C-10), 129.3 (C-9), 127.7 (C-13), 123.4 (C-6), 123.2 (C-21), 123.0 (C-8), 119.2 (C-16), 117.3 (C-14), 115.1(C-5), 105.7 (C-12), 94.7 (C-17), 56.4 (MeO). \*C-2 not observed due to boron relaxation. **<sup>11</sup>B NMR** (128 MHz, CDCl<sub>3</sub>): δ 28.7. **IR** *v* (cm<sup>-1</sup>): 3411, 3053, 2925, 1737, 1596, 1526, 1474, 1397, 1353, 1254, 1155, 1084, 1069, 1033, 980, 922, 848, 819, 765. **HRMS** (ESI) *m/z*: Found 531.1942 Calculated for C<sub>29</sub>H<sub>24</sub>BN<sub>6</sub>O<sub>4</sub> [M+H]<sup>+</sup> 531.1942. Δ = 0.9 ppm.

Assignments made based on COSY HSQC and HMBC data.

## Experimental

---

Dimethyl (4*R*,5*R*)-2-(3-hydroxy-2-(3-nitropyridin-2-yl)-6-((*E*)-phenyldiazenyl)phenyl)-1,3,2-dioxaborolane-4,5-dicarboxylate **187a**



In a 2 mL vial, protected-Azo-Biaryl **185a** (0.020 g, 0.033 mmol) was dissolved in THF (1 mL) to which was added 6M HCl (28  $\mu$ L, 5 eq). The solution was then sonicated and left to stir at 50 °C for 3h. The solution was then reduced to dryness, redissolved in 1:1 methanol/THF to which pyridine (24  $\mu$ L, 6eq) was added and left to stir for a further 10 min (To neutralise the solution and prevent formation of the motor's HCl salt). The solution was then reduced *in vacuo*, redissolved in 1:1 EtOAc/THF, filtered through Celite® and again reduced to dryness. Dimethyl tartrate (0.007g, 1 eq) was then added to the residue and dissolved in anhydrous PhMe which was then boiled off under nitrogen using a short path distillation apparatus. After repeating 4 times, the residue was left to dry *in vacuo* and analysed directly without further purification.

*Data presented from the crude mixture of title compound **187a** and dimethyl tartrate:*

**<sup>1</sup>H NMR** (600 MHz, CD<sub>3</sub>CN):  $\delta$  9.01 (dd, J = 5.3, 1.4 Hz, 1H, H-15), 8.45 (dd, J = 8.2, 1.4 Hz, 1H, H-13), 7.83 – 7.78 (m, 3H, H-8 and H-6), 7.71 (dd, J = 8.2, 5.3 Hz, 1H, H-14), 7.55 – 7.51 (m, 2H, H-9), 7.50 – 7.47 (m, 1H, H-10), 6.93 (d, J = 8.8 Hz, 1H, H-5), 4.85 (s, 2H, H-16), 3.62 (s, 6H, MeO). **<sup>13</sup>C NMR** (151 MHz, *Cryo-probe*, CD<sub>3</sub>CN):  $\delta$  173.4 (C-17), 161.3 (C-4), 153.1 (C-7), 148.7 (C-1), 148.4 (C-11), 147.8 (C-15), 146.5 (C-12), 138.7 (C-13), 131.2 (C-10), 130.1 (C-9), 124.6 (C-14), 124.4 (C-6), 124.0 (C-3), 123.3 (C-8), 119.4 (C-5), 78.6 (C-16), 52.8 (MeO). \*C-2 not observed due to boron relaxation. **<sup>11</sup>B NMR** (128 MHz, CD<sub>3</sub>CN):  $\delta$  13.4. **<sup>1</sup>H-<sup>15</sup>N HMBC** (600 MHz, *Cryo-probe*, CD<sub>3</sub>CN,  $J_{\text{H-N}}$  = 12 Hz):  $\delta$  370 (N-D), 261 (N-C). **HRMS** not found by Nanospray.

*Boronic acid intermediate:*

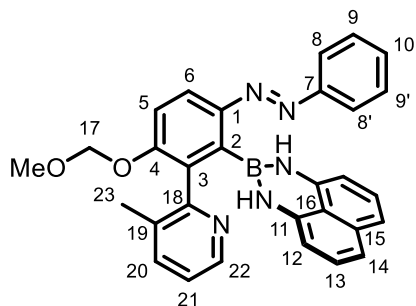
**HRMS** (Nanospray) *m/z*: Found 365.1063 Calculated for C<sub>17</sub>H<sub>14</sub>N<sub>4</sub>O<sub>5</sub>B [M+H]<sup>+</sup> 365.1055.  $\Delta$  = 2.2 ppm.

Assignments made based on COSY HSQC and HMBC data.

## Experimental

---

(E)-2-(3-(Methoxymethoxy)-2-(3-methylpyridin-2-yl)-6-(phenyldiazenyl)phenyl)-2,3-dihydro-1H-naphtho[1,8-de][1,3,2]diazaborinine **185d**



Synthesized according to the **General Suzuki Cross-Coupling Procedure B** from Bpin-azobenzene **183** (0.040 g, 0.075 mmol), pyridyl-bromide **184d** (0.016 g, 0.090 mmol), Pd(OAc)<sub>2</sub> (0.001 g, 0.004 mmol), *rac*-BIDME (0.003 g, 0.008 mmol,) and Cs<sub>2</sub>CO<sub>3</sub> (0.049 g, 0.15 mmol), with column chromatography (1:3 EtOAc:Hex) affording the title compound **185d** as an orange solid (0.015g, 40%).

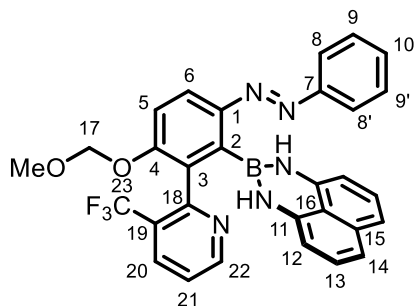
**R<sub>f</sub>** 0.30 (1:1 EtOAc:Hex). **mp:** 213.2 °C – 214.3 °C. **<sup>1</sup>H NMR** (400 MHz, CDCl<sub>3</sub>): δ 8.52 (dd, *J* = 4.9, 1.3 Hz, 1H, H-22), 7.99 (d, *J* = 9.0 Hz, 1H, H-6), 7.85 – 7.73 (m, 2H, H-8), 7.53 (dd, *J* = 7.7, 1.3 Hz, 1H, H-20), 7.42 – 7.32 (m, 4H, H-9, H-10 and H-5), 7.14 (dd, *J* = 7.7, 4.9 Hz, 1H, H-21), 7.02 (dd, *J* = 8.3, 7.3 Hz, 2H, H-13), 6.94 (dd, *J* = 8.3, 1.1 Hz, 2H, H-14), 6.09 (dd, *J* = 7.3, 1.1 Hz, 2H, H-12), 5.74 (s, 2H, NH of Bdan), 5.16 (s, 2H, H-17), 3.36 (s, 3H, MeO), 2.18 (s, 3H, H-23). **<sup>13</sup>C NMR** (126 MHz, *Cryo-probe*, CDCl<sub>3</sub>): δ 156.9 (C-18), 156.5 (C-4), 152.2 (C-7), 151.1 (C-1), 146.5 (C-22), 141.4 (C-11), 137.9 (C-20), 136.3 (C-15), 135.2 (C-3), 132.7 (C-19), 130.8 (C-10), 129.3 (C-9), 127.7 (C-13), 123.0 (C-21 and C-8), 120.5 (C-6), 119.4 (C-16), 117.1 (C-14), 116.0 (C-5), 105.4 (C-12), 94.7 (C-17), 56.3 (OMe), 19.2 (C-23). \*C-2 not observed due to boron relaxation. **<sup>11</sup>B NMR** (128 MHz, CDCl<sub>3</sub>): δ 29.2. **IR** *v* (cm<sup>-1</sup>): 3364, 3293, 2922, 1599, 1520, 1414, 1330, 1249, 1155, 1075, 1033, 998, 917, 818, 764, 689. **HRMS** (ESI) *m/z*: Found 500.2246 Calculated for C<sub>30</sub>H<sub>27</sub>BN<sub>5</sub>O<sub>2</sub> [M+H]<sup>+</sup> 500.2252. Δ = 1.2 ppm.

Assignments made based on COSY HSQC and HMBC data.

## Experimental

---

(*E*)-2-(3-(Methoxymethoxy)-2-(3-nitro-5-(trifluoromethyl)pyridin-2-yl)-6-(phenyldiazenyl)phenyl)-2,3-dihydro-1H-naphtho[1,8-de][1,3,2]diazaborinine **185e**



Synthesized according to the **General Suzuki Cross-Coupling Procedure B** from Bpin-azobenzene **183** (0.030 g, 0.056 mmol), pyridyl-bromide **184e** (0.015 g, 0.067 mmol), Pd(OAc)<sub>2</sub> (0.001 g, 0.004 mmol), *rac*-BIDME (0.002 g, 0.006 mmol,) and Cs<sub>2</sub>CO<sub>3</sub> (0.037 g, 0.11 mmol), with column chromatography (1:1 EtOAc:Hex) affording the title compound **185e** as an orange solid (0.015g, 46%).

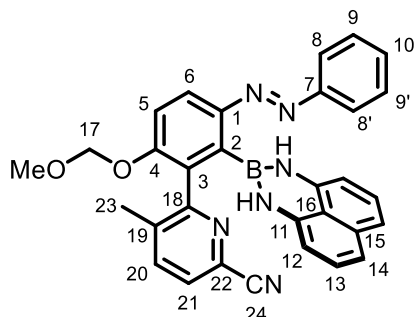
**R<sub>f</sub>** 0.18 (1:2 EtOAc:Hex). **mp:** 176.9 °C – 179.2 °C. **<sup>1</sup>H NMR** (400 MHz, CDCl<sub>3</sub>): δ 8.84 (d, *J* = 4.9 Hz, 1H, H-22), 8.04 (d, *J* = 9.0 Hz, 1H, H-6), 8.01 (d, *J* = 8.1 Hz, 1H, H-20), 7.82 – 7.67 (m, 2H, H-8), 7.40 (d, *J* = 9.0 Hz, 1H, H-5), 7.38 – 7.32 (m, 4H, H-9, H-10 and H-21), 7.05 (dd, *J* = 8.3, 7.3 Hz, 2H, H-13), 6.95 (d, *J* = 8.3 Hz, 2H, H-14), 6.11 (d, *J* = 7.3 Hz, 2H, H-12), 5.65 (s, 2H, NH of Bdan), 5.14 (s, 2H, H-17), 3.38 (s, 3H, MeO). **<sup>13</sup>C NMR** (126 MHz, *Cryo-probe*, CDCl<sub>3</sub>) 156.9 (C-4), 155.5 (q, <sup>3</sup>*J*<sub>C-F</sub> = 1.6 Hz, C-18), 151.9 (C-22/7), 151.8 (C-22/7), 150.3 (C-1), 141.2 (C-11), 136.3 (C-15), 134.8 (q, <sup>3</sup>*J*<sub>C-F</sub> = 4.3 Hz, C-20), 132.8 (C-3), 130.9 (H-10), 129.3 (H-9), 127.7 (C-13), 126.4 (q, <sup>2</sup>*J*<sub>C-F</sub> = 32.4 Hz, C-19), 123.7 (q, <sup>1</sup>*J*<sub>C-F</sub> = 273.4 Hz, CF<sub>3</sub>) 122.9 (C-8), 122.72 (C-6/21), 122.66 (C-6/21), 119.2 (C-16), 117.2 (C-14), 115.2 (C-5), 105.5 (C-12), 94.8 (C-17), 56.3 (MeO). δ \*C-2 not observed due to boron relaxation. **<sup>11</sup>B NMR** (128 MHz, CDCl<sub>3</sub>): δ 28.9. **<sup>19</sup>F NMR** (376 MHz, CDCl<sub>3</sub>): -60.0 **IR** *v* (cm<sup>-1</sup>): 3379, 2922, 2852, 1598, 1505, 1471, 1318, 1257, 1153, 1117, 1029, 983, 818, 763. **HRMS** (ESI) *m/z*: Found 554.1957 Calculated for C<sub>30</sub>H<sub>24</sub>BF<sub>3</sub>N<sub>5</sub>O<sub>2</sub> [M+H]<sup>+</sup> 554.1970. Δ = 2.4 ppm.

Assignments made based on COSY HSQC and HMBC data

## Experimental

---

(*E*)-2-(3-(Methoxymethoxy)-2-(3-nitro-5-(trifluoromethyl)pyridin-2-yl)-6-(phenyldiazenyl)phenyl)-2,3-dihydro-1H-naphtho[1,8-de][1,3,2]diazaborinine **185g**



Synthesized according to the **General Suzuki Cross-Coupling Procedure B** from Bpin-azobenzene **183** (0.030 g, 0.056 mmol), pyridyl-bromide **184g** (0.013 g, 0.067 mmol), Pd(OAc)<sub>2</sub> (0.001 g, 0.004 mmol), *rac*-BIDME (0.002 g, 0.006 mmol,) and Cs<sub>2</sub>CO<sub>3</sub> (0.037 g, 0.11 mmol), with column chromatography (1:1 EtOAc:Hex) affording the title compound **185g** as an orange film (0.012g, 41%).

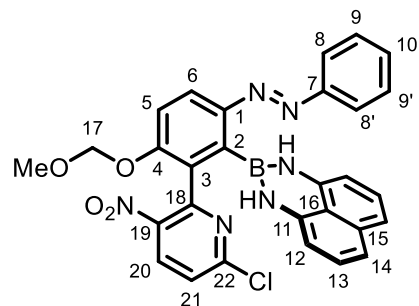
**R<sub>f</sub>** 0.25 (1:3 EtOAc:Hex). **<sup>1</sup>H NMR** (400 MHz, CDCl<sub>3</sub>): δ 8.04 (d, *J* = 8.9 Hz, 1H, H-6), 7.82 – 7.75 (m, 2H, H-8), 7.62 (d, *J* = 7.9 Hz, 1H, H-20), 7.52 (d, *J* = 7.9 Hz, 1H, H-21), 7.41 – 7.35 (m, 4H, H-5, H-9 and H-10), 7.04 (dd, *J* = 8.2, 7.2 Hz, 2H, H-13), 6.97 (d, *J* = 8.2 Hz, 2H, H-14), 6.17 (d, *J* = 7.2 Hz, 2H, H-12), 5.66 (s, 2H, NH of dan), 5.17 (s, 2H, H-17), 3.39 (s, 3H, MeO), 2.25 (s, 3H, H-23). **<sup>13</sup>C NMR** (126 MHz, *Cryo-probe*, CDCl<sub>3</sub>): δ 159.1 (C-18), 156.2 (C-4), 151.9 (C-7), 150.9 (C-1), 141.0 (C-11), 138.5 (C-20), 137.9 (C-19), 136.3 (C-15), 133.0 (C-22), 131.1 (C-10), 130.3 (C-3), 129.3 (C-9), 127.8 (C-13), 127.6 (C-21), 123.0 (C-8), 122.5 (C-6), 119.2 (C-16), 117.5 (C-24), 117.4 (C-14), 115.7 (C-5), 105.7 (C-12), 94.7 (C-17), 56.5 (MeO), 19.6 (C-23). \*C-2 not observed due to boron relaxation. **<sup>11</sup>B NMR** (128 MHz, CDCl<sub>3</sub>): δ 28.2. **IR ν (cm<sup>-1</sup>)**: 3380, 2922, 2851, 2234, 1597, 1505, 1471, 1398, 1252, 1152, 1037, 980, 819, 764. **HRMS (ESI) m/z:** Found 525.2197 Calculated for C<sub>31</sub>H<sub>26</sub>BN<sub>6</sub>O<sub>2</sub> [M+H]<sup>+</sup> 525.2197. Δ = 1.5 ppm.

Assignments made based on COSY HSQC and HMBC data.

## Experimental

---

(E)-2-(2-(6-Chloro-3-nitropyridin-2-yl)-3-(methoxymethoxy)-6-(phenyldiazenyl)phenyl)-2,3-dihydro-1H-naphtho[1,8-de][1,3,2]diazaborinine **185c**



Synthesized according to the **General Suzuki Cross-Coupling Procedure B** from Bpin-azobenzene **183** (0.030 g, 0.056 mmol), pyridyl-bromide **184c** (0.016 g, 0.067 mmol), Pd(OAc)<sub>2</sub> (0.001 g, 0.004 mmol), PPh<sub>3</sub> (0.002 g, 0.006 mmol,) and Cs<sub>2</sub>CO<sub>3</sub> (0.037 g, 0.11 mmol), with column chromatography (1:1 EtOAc:Hex) affording the title compound **185c** as an orange film (0.027g, 85%).

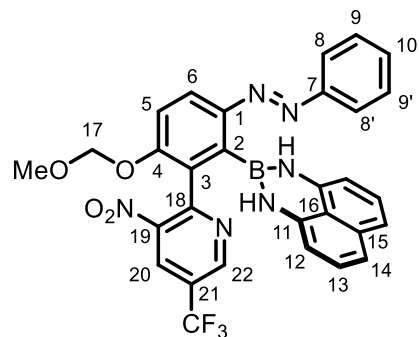
**R<sub>f</sub>** 0.30 (1:4 EtOAc:Hex). **mp:** 201.9 °C – 204.1 °C. **<sup>1</sup>H NMR** (400 MHz, CDCl<sub>3</sub>) δ 8.21 (d, *J* = 8.6 Hz, 1H, H-20), 8.07 (d, *J* = 8.9 Hz, 1H, H-6), 7.78 – 7.69 (m, 2H, H-8), 7.39 – 7.32 (m, 5H, H-5, H-9, H-10 and H-21), 7.05 (dd, *J* = 8.3, 7.2 Hz, 2H, H-13), 6.99 (dt, *J* = 8.3, 1.8 Hz, 2H, H-14), 6.19 (dt, *J* = 7.2, 1.8 Hz, 2H, H-12), 5.73 (s, 2H, NH of Bdan), 5.13 (s, 2H, H-17), 3.38 (s, 3H, MeO). **<sup>13</sup>C NMR** (126 MHz, *Cryo-probe*, CDCl<sub>3</sub>): δ 155.7 (C-4), 154.0 (C-18), 152.2 (C-22), 151.6 (C-7), 150.9 (C-1), 145.6 (C-19), 141.1 (C-11), 136.3 (C-15), 134.6 (C-20), 131.0 (C-10), 130.5 (C-3), 129.3 (C-9), 127.7 (C-13), 124.66 (C-6), 124.0 (C-21), 122.9 (C-8), 119.2 (C-16), 117.3 (C-14), 115.0 (C-5), 105.8 (C-12), 94.7 (C-17), 56.4 (MeO) \*C-2 not observed due to boron relaxation. **<sup>11</sup>B NMR** (128 MHz, CDCl<sub>3</sub>): δ 28.6. **IR ν** (cm<sup>-1</sup>): 3402, 2919, 2850, 1598, 1586, 1525, 1347, 1258, 1155, 1082, 1035, 980, 819, 763. **HRMS** (ESI) *m/z*: Found 565.1548 Calculated for C<sub>29</sub>H<sub>23</sub>BClN<sub>6</sub>O<sub>4</sub> [M+H]<sup>+</sup> 565.1557. Δ = 1.6 ppm.

Assignments made based on COSY HSQC and HMBC data.

## Experimental

---

(*E*)-2-(3-(Methoxymethoxy)-2-(3-nitro-5-(trifluoromethyl)pyridin-2-yl)-6-(phenyldiazenyl)phenyl)-2,3-dihydro-1H-naphtho[1,8-de][1,3,2]diazaborinine **185b**



Synthesized according to the **General Suzuki Cross-Coupling Procedure B** from Bpin-azobenzene **183** (0.250g, 0.468 mmol), pyridyl-bromide **184b** (0.152 g, 0.562 mmol), Pd(OAc)<sub>2</sub> (0.005 g, 0.023 mmol), *rac*-BIDME (0.016 g, 0.047 mmol,) and Cs<sub>2</sub>CO<sub>3</sub> (0.305 g, 0.936 mmol), with column chromatography (1:1 EtOAc:Hex) affording the title compound **185b** as an orange film (0.133 g, 47%).

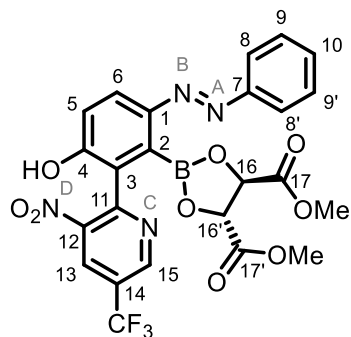
**R<sub>f</sub>** 0.40 (1:4 EtOAc:Hex). **mp:** 101.2 °C – 107.3 °C. **<sup>1</sup>H NMR** (400 MHz, CDCl<sub>3</sub>): δ 9.04 (d, *J* = 1.7 Hz, 1H, H-22), 8.49 (d, *J* = 1.7 Hz, 1H, H-20), 8.08 (d, *J* = 8.9 Hz, 1H, H-6), 7.77 – 7.73 (m, 2H, H-8), 7.40 – 7.34 (m, 4H, H-9, H-10 and H-5), 7.05 (dd, *J* = 8.3, 7.2 Hz, 2H, H-13) 7.00 (dd, *J* = 8.3, 1.1 Hz, 2H, H-14), 6.16 (dd, *J* = 7.2, 1.1 Hz, 2H, H-12), 5.70 (s, 2H, NH of Bdan), 5.12 (s, 2H, H-17), 3.37 (s, 3H, MeO). **<sup>13</sup>C NMR** (126 MHz, *Cryo-probe*, CDCl<sub>3</sub>): δ 155.7 (C-4), 154.9 (C-18), 151.7 (C-7), 151.1 (C-1), 149.0 (q, <sup>3</sup>J<sub>C-F</sub> = 3.6 Hz, C-22), 146.5 (C-19), 141.0 (C-11), 136.3 (C-15), 131.1 (C-10), 130.2 (C-3), 129.4 (q, <sup>3</sup>J<sub>C-F</sub> = 3.6 Hz, C-20), 129.3 (C-9), 127.7 (C-13), 126.3 (q, <sup>2</sup>J<sub>C-F</sub> = 34.8 Hz, C-21), 124.0 (C-6), 123.0 (C-8), 122.3 (q, <sup>1</sup>J<sub>C-F</sub> = 273.4 Hz, CF<sub>3</sub>), 119.3 (C-16), 117.6 (C-14), 115.2 (C-5), 105.8 (C-12), 94.9 (C-17), 56.5 (MeO). \*C-2 not observed due to boron relaxation. **<sup>11</sup>B NMR** (128 MHz, CDCl<sub>3</sub>): δ 28.8. **<sup>19</sup>F NMR** (376 MHz, CDCl<sub>3</sub>): -62.0 **IR** *v* (cm<sup>-1</sup>): 3416, 2956, 2925, 1737, 1598, 1505, 1400, 1318, 1255, 1143, 1092, 1034, 979, 820, 761. **HRMS** (ESI) *m/z*: Found 599.1807 Calculated for C<sub>30</sub>H<sub>23</sub>BF<sub>3</sub>N<sub>6</sub>O<sub>4</sub> [M+H]<sup>+</sup> 599.1820. Δ = 2.2 ppm.

Assignments made based on COSY HSQC and HMBC data.

## Experimental

---

Dimethyl (4*R*,5*R*)-2-(3-hydroxy-2-(3-nitro-5-(trifluoromethyl)pyridin-2-yl)-6-((*E*)-phenyldiazenyl)phenyl)-1,3,2-dioxaborolane-4,5-dicarboxylate **187b**



In a 2 mL vial, protected-azo-biaryl **185b** (0.020 g, 0.033 mmol) was dissolved in THF (1 mL) to which was added 6M HCl (28  $\mu$ L, 5 eq). The solution was then sonicated and left to stir at 50 °C for 3h. The solution was then reduced to dryness, redissolved in 1:1 methanol/THF to which pyridine (24  $\mu$ L, 6eq) was added and left to stir for a further 10 min (To neutralise the solution and prevent formation of the motor's HCl salt). The solution was then reduced *in vacuo*, redissolved in 1:1 EtOAc/THF, filtered through Celite® and again reduced to dryness. Dimethyl tartrate (0.007g, 1 eq) was added to the residue and redissolved in anhydrous PhMe which was then boiled off under nitrogen using a short path distillation apparatus. After repeating 4 times, the residue was left to dry *in vacuo* and analysed directly without further purification.

*Data presented from the crude mixture of title compound **187b** and dimethyl tartrate:*

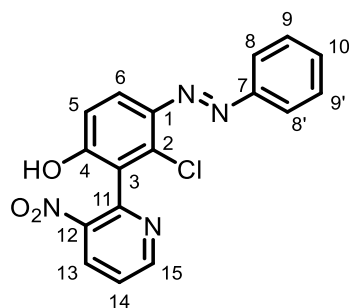
**<sup>1</sup>H NMR** (400 MHz, CD<sub>3</sub>CN):  $\delta$  9.26 (d, J = 1.3 Hz, 1H, H-15), 8.73 (d, J = 1.3 Hz, 1H, H-13), 8.02 (d, J = 8.5 Hz, 1H, H-6), 7.82 – 7.79 (m, 2H, H-8), 7.58 – 7.52 (m, 3H, H-9 and H-10), 7.10 (d, J = 8.5 Hz, 1H, H-5), 4.70 (s, 2H, H-16), 3.54 (s, 6H, MeO). **<sup>13</sup>C NMR** (126 MHz, *Cryo-probe*, CD<sub>3</sub>CN):  $\delta$  172.2 (C-17), 160.4 (C-4), 153.5 (C-11), 150.5 (C-1), 149.6 (C-7), 148.8 (q, <sup>3</sup>J<sub>C-F</sub> = 3.9 Hz, C-15), 146.6 (C-12), 133.4 (q, <sup>3</sup>J<sub>C-F</sub> = 3.6 Hz, C-13), 132.4 (C-10), 130.8 (C-3), 130.5 (C-9), 130.1 (C-6), 126.6 (q, <sup>2</sup>J<sub>C-F</sub> = 34.8 Hz, C-14), 123.4 (C-8), 122.5 (q, <sup>1</sup>J<sub>C-F</sub> = 273.4 Hz, CF<sub>3</sub>), 118.0 (C-5), 78.0 (C-16), 52.8 (MeO). \*C-2 not observed due to boron relaxation. **<sup>11</sup>B NMR** (128 MHz, CD<sub>3</sub>CN):  $\delta$  18.6 **<sup>19</sup>F NMR** (376 MHz, CD<sub>3</sub>CN): -62.6 **<sup>1</sup>H-<sup>15</sup>N HMBC** (600 MHz, *Cryo-probe*, CD<sub>3</sub>CN, J<sub>H-N</sub> = 10 Hz):  $\delta$  480 (N-B), 367 (N-D), 307 (N-C). \*N-A correlation not identified. **HRMS** not found by nanospray.

Assignments made based on COSY HSQC and HMBC data.

## Experimental

---

(*E*)-2-(3-(Methoxymethoxy)-2-(3-nitro-5-(trifluoromethyl)pyridin-2-yl)-6-(phenyldiazenyl)phenyl)-2,3-dihydro-1H-naphtho[1,8-de][1,3,2]diazaborinine **194**



A mixture of Bdan-azo-biaryl **185a** (0.100 g, 0.190 mmol) and CuCl<sub>2</sub> (0.076 g, 0.57 mmol, 3eq) was dissolved in MeOH (1.0 mL)/H<sub>2</sub>O (1.0 mL) and stirred at 80 °C for 16 h under air. The mixture was then cooled to r.t. and diluted with Et<sub>2</sub>O (5 mL). The organic layer washed with brine (5 mL), dried over MgSO<sub>4</sub>, filtered through Celite®, and concentrated *in vacuo*. The crude mixture was purified by column chromatography (1:3 EtOAc:Hex) to give the title compound **194** as an orange solid (0.013 g, 20%).

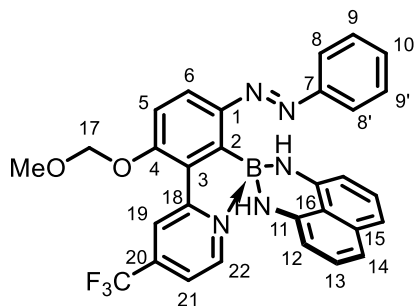
**R<sub>f</sub>** 0.40 (1:1 EtOAc:Hex). **mp:** 212.4 °C – 214.0 °C. **<sup>1</sup>H NMR** (400 MHz, CDCl<sub>3</sub>): δ 8.96 (dd, *J* = 4.7, 1.7 Hz, 1H, H-15), 8.56 (dd, *J* = 8.4, 1.7 Hz, 1H, H-13), 8.17 (s, 1H, OH), 7.93 – 7.86 (m, 2H, H-8), 7.81 (d, *J* = 8.9 Hz, 1H, H-6), 7.65 (dd, *J* = 8.4, 4.7 Hz, 1H, H-14), 7.57 – 7.42 (m, 3H, H-9 and H-10), 6.96 (d, *J* = 8.9 Hz, 1H, H-5). **<sup>13</sup>C NMR** (126 MHz, *Cryo-probe*, CDCl<sub>3</sub>): δ 157.3 (C-4), 152.9 (C-7), 152.5 (C-15), 149.2 (C-11), 146.9 (C-12) 143.1 (C-1), 136.2 (C-2), 133.8 (C-13), 131.3 (C-10), 129.3 (C-9), 124.0 (C-14), 123.4 (C-8), 122.9 (C-3), 120.1 (C-6), 116.7 (C-5). **IR v** (cm<sup>-1</sup>): 3067, 2710, 1737, 1591, 1532, 1414, 1359, 1305, 1217, 1067, 830, 766, 753. **HRMS** (ESI) *m/z*: Found 355.0586 Calculated for C<sub>17</sub>H<sub>12</sub>ClN<sub>4</sub>O<sub>3</sub> [M+H]<sup>+</sup> 355.0586. Δ = 1.7 ppm.

Assignments made based on COSY HSQC and HMBC data.

## Experimental

---

(*E*)-2-(3-(Methoxymethoxy)-2-(3-nitro-5-(trifluoromethyl)pyridin-2-yl)-6-(phenyldiazenyl)phenyl)-2,3-dihydro-1H-naphtho[1,8-de][1,3,2]diazaborinine **185f**



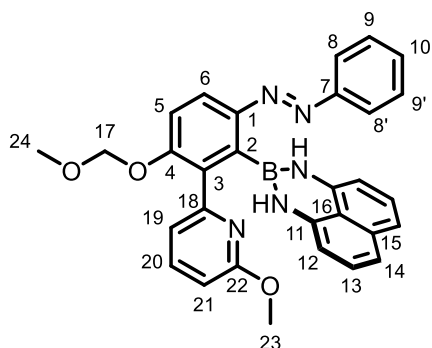
Synthesized according to the **General Suzuki Cross-Coupling Procedure B** from Bpin-azobenzene **183** (0.040 g, 0.075 mmol), pyridyl-bromide **184f** (0.020 g, 0.090 mmol), Pd(OAc)<sub>2</sub> (0.001 g, 0.004 mmol), *rac*-BIDME (0.003 g, 0.008 mmol,) and Cs<sub>2</sub>CO<sub>3</sub> (0.049 g, 0.15 mmol), with column chromatography (1:3 EtOAc:Hex) affording the title compound **185f** as an orange film (0.019g, 46%).

**R<sub>f</sub>** 0.35 (1:2 EtOAc:Hex). **<sup>1</sup>H NMR** (400 MHz, CD<sub>3</sub>CN): δ 8.69 (d, *J* = 5.2 Hz, 1H, H-22), 8.36 (s, 1H, H-19), 7.93 (d, *J* = 9.2 Hz, 1H, H-6), 7.58 (dd, *J* = 5.2, 2.1 Hz, 1H, H-21), 7.56 – 7.47 (m, 2H, H-8), 7.38 – 7.31 (m, 2H, H-10 and H-5), 7.31 – 7.25 (m, 2H, H-9), 7.00 (dd, *J* = 8.3, 7.3 Hz, 2H, H-13), 6.84 (d, *J* = 8.3 Hz, 2H, H-14), 6.12 (d, *J* = 7.3 Hz, 2H, H-12), 5.53 (s, 2H, NH of Bdan), 5.41 (s, 2H, H-17), 3.47 (s, 3H, MeO). **<sup>13</sup>C NMR** (126 MHz, *Cryo-probe*, CD<sub>3</sub>CN): δ 157.7 (C-4), 157.0 (C-18), 153.4 (C-7), 150.9 (C-1), 148.0 (C-22), 144.6 (C-11), 137.6 (C-15), 131.5 (C-10), 130.5 (C-3), 130.1 (C-9), 128.5 (C-13), 123.4 (C-8), 121.9 (C-6), 120.9 (q, <sup>3</sup>*J*<sub>C-F</sub> = 4.2 Hz, C-19), 119.6 (q, <sup>3</sup>*J*<sub>C-F</sub> = 3.2 Hz, C-21), 117.3 (C-16) 116.2 (C-5), 115.6 (C-14), 105.3 (C-12), 95.6 (C-17), 57.0 (MeO). \*C-2 not observed due to boron relaxation, C-20 and CF<sub>3</sub> not observed due to large peak splitting from fluorine spin coupling. **<sup>11</sup>B NMR** (128 MHz, CD<sub>3</sub>CN): δ 17.3. **<sup>19</sup>F NMR** (376 MHz CD<sub>3</sub>CN): -65.3 **IR v** (cm<sup>-1</sup>): 2931, 1627, 1567, 1454, 1322, 1243, 1146, 1083, 945, 818. **HRMS** not found by ESI.

Assignments made based on COSY HSQC and HMBC data.

## Experimental

(*E*)-2-(3-(Methoxymethoxy)-2-(6-methoxypyridin-2-yl)-6-(phenyldiazenyl)phenyl)-2,3-dihydro-1H-naphtho[1,8-de][1,3,2]diazaborinine **185g**



Synthesized according to the **General Suzuki Cross-Coupling Procedure B** from Bpin-azobenzene **183** (0.050 g, 0.094 mmol), pyridyl-bromide **184g** (0.021 g, 0.11 mmol), Pd(OAc)<sub>2</sub> (0.001 g, 0.004 mmol), *rac*-BIDME (0.003 g, 0.008 mmol,) and Cs<sub>2</sub>CO<sub>3</sub> (0.061 g, 0.19 mmol), with column chromatography (1:4 EtOAc:Hex) affording the title compound **185g** as an orange film (0.039 g, 81%).

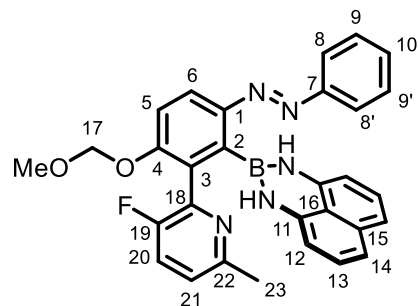
**R<sub>f</sub>** 0.37 (1:3 EtOAc:Hex). **<sup>1</sup>H NMR** (400 MHz, CDCl<sub>3</sub>): δ 7.95 (d, *J* = 8.9 Hz, 1H, H-6), 7.84 – 7.73 (m, 2H, H-8), 7.59 (dd, *J* = 8.3, 7.3 Hz, 1H, H-20), 7.40 – 7.34 (m, 4H, H-9 H-10 and H-5), 7.18 (dd, *J* = 7.3, 0.8 Hz, 1H, H-19), 7.04 (dd, *J* = 8.3, 7.2 Hz, 2H, H-13), 6.98 (dd, *J* = 8.3, 1.2 Hz, 2H, H-14), 6.62 (dd, *J* = 8.3, 0.8 Hz, 1H, H-21), 6.10 (dd, *J* = 7.2, 1.2 Hz, 2H, H-12), 5.62 (s, 2H, NH of Bdan), 5.22 (s, 2H, H-17), 3.80 (s, 3H, H-23), 3.45 (s, 3H, H-24). **<sup>13</sup>C NMR** (126 MHz, *Cryo-probe*, CDCl<sub>3</sub>): δ 163.8 (C-22), 156.5 (C-4), 153.8 (C-18), 152.3 (C-7), 151.1 (C-1), 141.5 (C-11), 138.4 (C-20), 136.4 (C-15), 135.1 (C-3), 130.8 (C-10), 129.3 (C-9), 127.7 (C-13), 123.0 (C-8), 119.5 (C-6), 119.2 (C-16), 118.5 (C-19), 117.1 (C-14), 116.4 (C-5), 109.6 (C-21), 105.3 (C-12), 94.9 (C-17), 56.4 (C-24), 53.4 (C-23). \*C-2 not observed due to boron relaxation. **<sup>11</sup>B NMR** (128 MHz, CDCl<sub>3</sub>): δ 28.9. **IR v** (cm<sup>-1</sup>): 3414, 2925, 1738, 1597, 1503, 1462, 1395, 1312, 1247, 1149, 1080, 1042, 986, 819, 762. **HRMS** (ESI) *m/z*: Found 516.2178 Calculated for C<sub>30</sub>H<sub>27</sub>BN<sub>5</sub>O<sub>3</sub> [M+H]<sup>+</sup> 516.2201. Δ = 4.5 ppm.

Assignments made based on COSY HSQC and HMBC data.

## Experimental

---

(E)-2-(2-(3-Fluoro-6-methylpyridin-2-yl)-3-(methoxymethoxy)-6-(phenyldiazenyl)phenyl)-2,3-dihydro-1H-naphtho[1,8-de][1,3,2]diazaborinine **185i**



Synthesized according to the **General Suzuki Cross-Coupling Procedure B** from Bpin-azobenzene **183** (0.050 g, 0.094 mmol), pyridyl-bromide **184i** (0.021 g, 0.11 mmol), Pd(OAc)<sub>2</sub> (0.001 g, 0.004 mmol), *rac*-BIDME (0.003 g, 0.008 mmol,) and Cs<sub>2</sub>CO<sub>3</sub> (0.061 g, 0.19 mmol), with column chromatography (1:4 EtOAc:Hex) affording the title compound **185i** as an orange film (0.038 g, 78%).

**R<sub>f</sub>** 0.25 (1:3 EtOAc:Hex). **<sup>1</sup>H NMR** (400 MHz, CDCl<sub>3</sub>): δ 8.04 (d, *J* = 8.9 Hz, 1H, H-6), 7.78 – 7.73 (m, 2H, H-8), 7.38 (d, *J* = 8.9 Hz, 1H, H-5), 7.37 – 7.34 (m, 3H, H-9 and H-10), 7.30 (t, *J* = 8.7 Hz, 1H, H-20), 7.06 – 7.02 (m, 3H, H-13 and H-21), 6.97 (dd, *J* = 8.3, 1.0 Hz, 2H, H-14), 6.15 (dd, *J* = 7.3, 1.0 Hz, 2H, H-12), 5.75 (s, 2H, NH of Bdan), 5.21 (s, 2H, H-17), 3.42 (s, 3H, MeO), 2.46 (s, 3H, H-23). **<sup>13</sup>C NMR** (126 MHz, *Cryo-probe*, CDCl<sub>3</sub>): δ 157.1 (C-4), 156.2 (d, <sup>1</sup>*J*<sub>C-F</sub> = 252 Hz, C-19), 153.8 (d, <sup>4</sup>*J*<sub>C-F</sub> = 5.1 Hz, C-22), 152.0 (C-7), 150.9 (C-1), 144.3 (d, <sup>2</sup>*J*<sub>C-F</sub> = 20.4 Hz, C-18), 141.4 (C-11), 136.4 (C-15), 130.8 (C-10), 130.0 (C-3), 129.3 (C-9), 127.7 (C-13), 123.9 (d, <sup>3</sup>*J*<sub>C-F</sub> = 2.5 Hz, C-21), 123.3 (d, <sup>2</sup>*J*<sub>C-F</sub> = 20.7 Hz, C-20), 122.9 (C-8), 122.7 (C-6), 119.3 (C-16), 117.0 (C-14), 115.5 (C-5), 105.4 (C-12), 94.6 (C-17), 56.2 (MeO), 23.8 (C-23). \*C-2 not observed due to boron relaxation. **<sup>11</sup>B NMR** (128 MHz, CDCl<sub>3</sub>): δ 28.6. **<sup>19</sup>F NMR** (128 MHz, CDCl<sub>3</sub>): δ -126.49 (dd, *J* = 8.9, 4.1 Hz). **IR v** (cm<sup>-1</sup>): 3408, 3051, 2924, 1595, 1505, 1466, 1397, 1255, 1245, 1152, 1038, 988, 818, 762. **HRMS** (ESI) *m/z*: Found 518.2136 Calculated for C<sub>30</sub>H<sub>26</sub>BFN<sub>5</sub>O<sub>2</sub> [M+H]<sup>+</sup> 518.2158. Δ = 4.3 ppm.

Assignments made based on COSY HSQC and HMBC data.

## Experimental

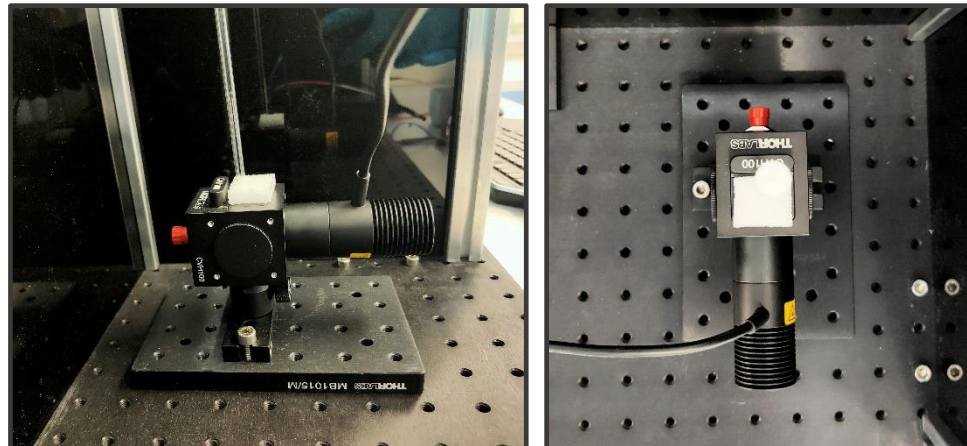
---

### 8.4 Photochemistry

#### 8.4.1 Photochemistry – Initial Irradiation Experiments

*Sample Preparation.* For a typical experiment, ~4-6 mg of material was dissolved in 0.6 mL of CDCl<sub>3</sub>, C<sub>6</sub>D<sub>6</sub> or MeCN-d<sub>3</sub>.

*Equipment.* Samples were contained in a Norrell quartz NMR tube (Boron content 0.0 - 0.1 ppm, Ø = 5 mm) and irradiated *via* the front port of the sample holder (window size: W×H = 9 mm × 14 mm). Irradiations were performed at, 365 nm using Thorlabs M365L3 LED (FWHM = 9 nm, 1000 mA, typ. power output = 1290 mW), or 430 nm using Thorlabs M430L4 LED (FWHM = 15 nm, 500 mA, typ. power output = 758 mW) and driven at their maximum current using ThorLabs DC2200 High-Power LED Driver. After 3 hours of irradiation, the irradiation was halted, the tubes placed in a dark container and transported to the NMR suite where <sup>1</sup>H and <sup>11</sup>B NMR spectra were recorded.



## Experimental

---

### 8.4.2 Photochemistry - Online UV-Vis Experiments

*Sample Preparation.* For a typical experiment, 1 mM stock solutions of the material of interest were prepared in MeCN, THF, PhMe or CH<sub>2</sub>Cl<sub>2</sub> and were used in turn to make further diluted solutions until the absorbance of the diluted solution (3 mL) was  $\leq 1.0$  a.u.

*UV-Vis Equipment.* Spectra were generated using an Ocean Optics Deep-UV Deuterium & Tungsten Halogen (DH-2000-S-DUV-TTL) or Thorlabs Stabilized Deuterium UV (SLS204) light source to provide broad-spectrum light (*See manufacturer websites for details of the spectral outputs*). The broad-spectrum light was then carried *via* a Ø600 µm, MM fibre optic patch cable (M114L01) to the sample holder where the light was collimated by a ThorLabs plano-convex lens (LA4647). After the collimated light passes through the sample contained in a 4-sided quartz cuvette, it is focused by a second ThorLabs plano-convex lens (LA4647) into a Ø200 µm, MM fibre optic patch cable (M151L01). The light is then carried to a Compact Czerny-Turner CCD Spectrometer (CCS200/M) where the broad-spectrum light is dispersed and analysed using a CCD array. The CCD data output is then sent to a PC for analysis.

*LED Irradiation Equipment.* Samples were contained in ThorLabs quartz 4-sided cuvettes (CV10Q35FAE, path length  $10.00 \pm 0.05$  mm) and irradiated *via* the front port (window size: W×H = 9 mm × 14 mm). Irradiations were performed at 300 nm using Thorlabs M300L4 LED (FWHM = 20 nm, 350 mA, typ. power output = 32 mW), 365 nm using Thorlabs M365L3 LED (FWHM = 9 nm, 1000 mA, typ. power output = 1290 mW), 405 nm using Thorlabs M405L4 LED (FWHM = 12.5 nm, 1000 mA, typ. power output = 1300 mW) or 430 nm using Thorlabs M430L4 LED (FWHM = 15 nm, 500 mA, typ. power output = 758 mW) and driven at their maximum current using ThorLabs DC2200 High-Power LED Driver. The cuvette mount temperature was controlled by mounting the cuvette holder directly onto a ThorLabs temperature-controlled mini-series breadboard (PTC1/M). The temperature controlled-breadboard and LED Driver were both controlled using a PC running the respective ThorLabs control programs.

## Experimental

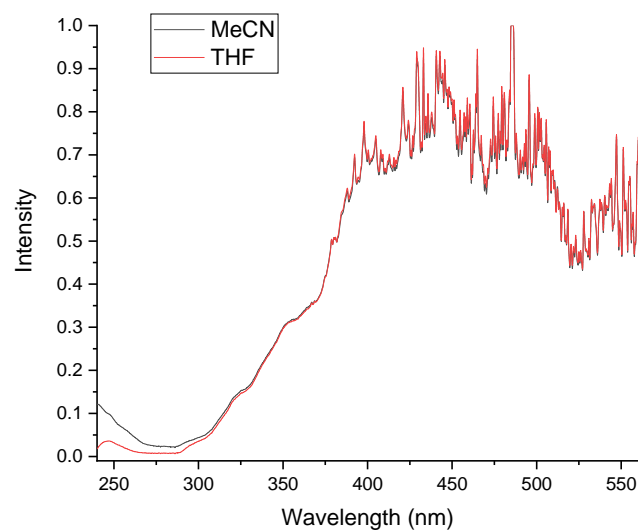
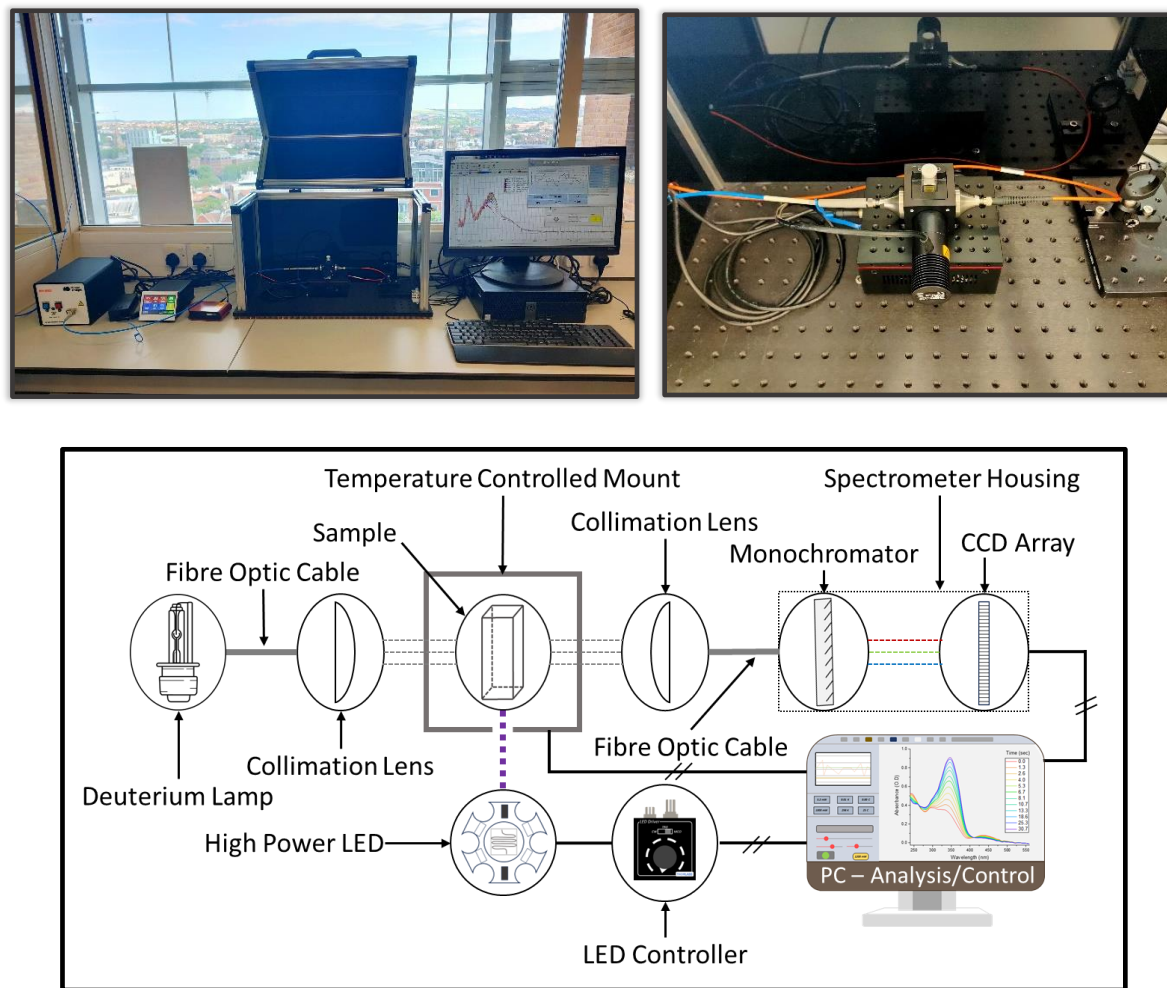


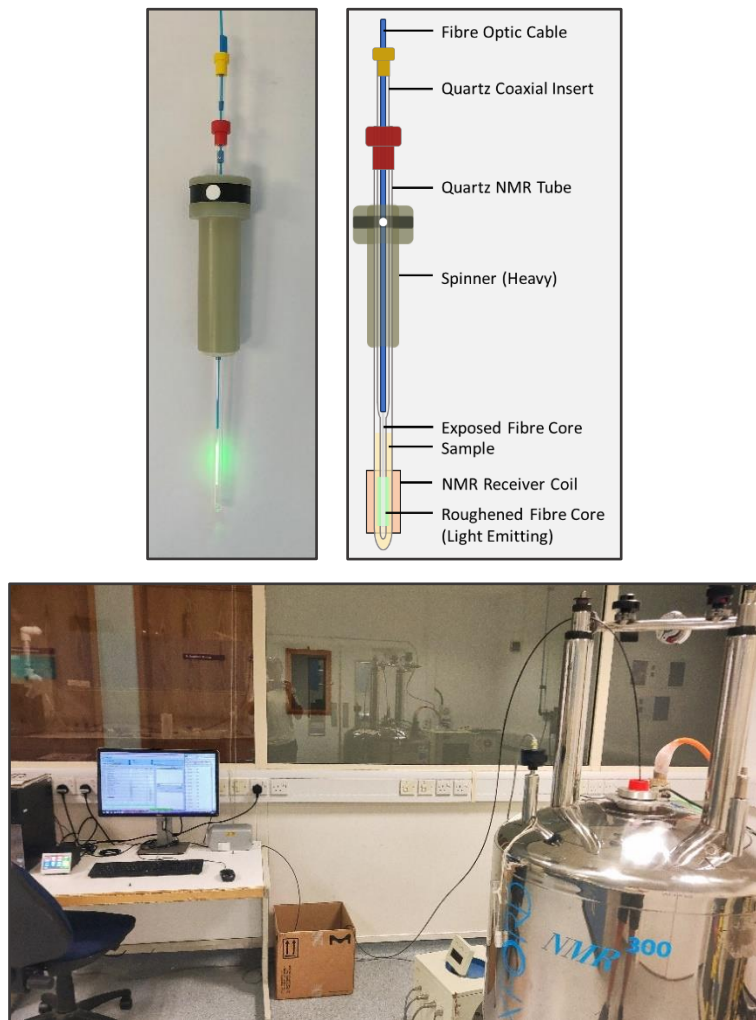
**Figure 50.** Light intensity detected with MeCN or THF solutions used for UV-vis absorption spectra background.

## Experimental

### 8.4.3 Photochemistry – *in situ* NMR Experiments

*Sample Preparation.* For a typical experiment, ~2mg of the material was dissolved in 0.3 mL of deuterated MeCN, THF, CDCl<sub>3</sub> or CD<sub>2</sub>Cl<sub>2</sub> under an atmosphere of nitrogen.

*Equipment.* A custom 5 m long, Ø800 µm MM Optical Fiber (FT800UMT) was built with an SMA adaptor on one end and the other with ± 1 cm of fibre exposed above a flat cleave. The exposed tip was then roughened with 100 grit sandpaper to cause the light to be emitted uniformly from the tip. The exposed fibre optic tip was then housed in a Norell Quartz Coaxial Insert (NI5CCI-V-QTZ) which was then inserted directly into the samples. Irradiations were performed at 365 nm using Thorlabs M365FP1 Fibre-Coupled LED (FWHM = 9 nm, 1400 mA, typical power output = 15.5 mW for Ø400 µm fibre) driven by ThorLabs DC2200 High-Power LED Driver.



## Experimental

### 8.4.4 Photochemistry –Photostationary States Established by $^1\text{H}$ NMR

#### Azobenzene **26**

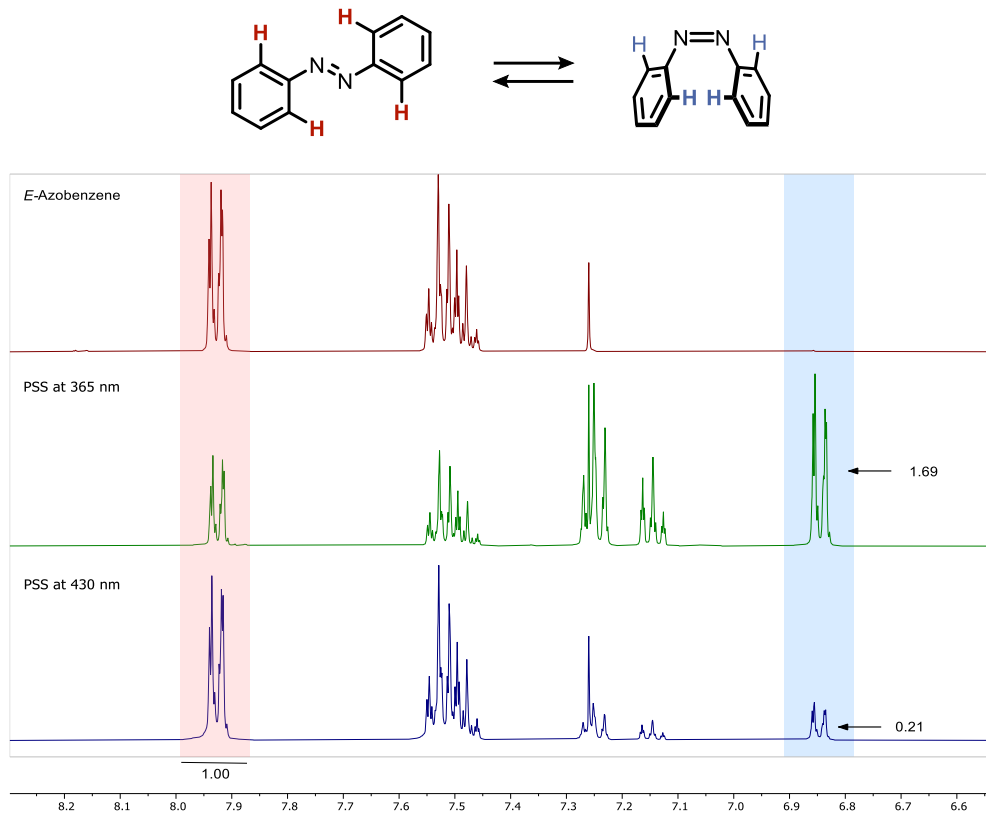


**Figure 51.** Photostationary State composition of Azobenzene **26** under 365 nm and 430 nm irradiation.

## Experimental

### (+)-DMT-MeO-Azobenzene **64**

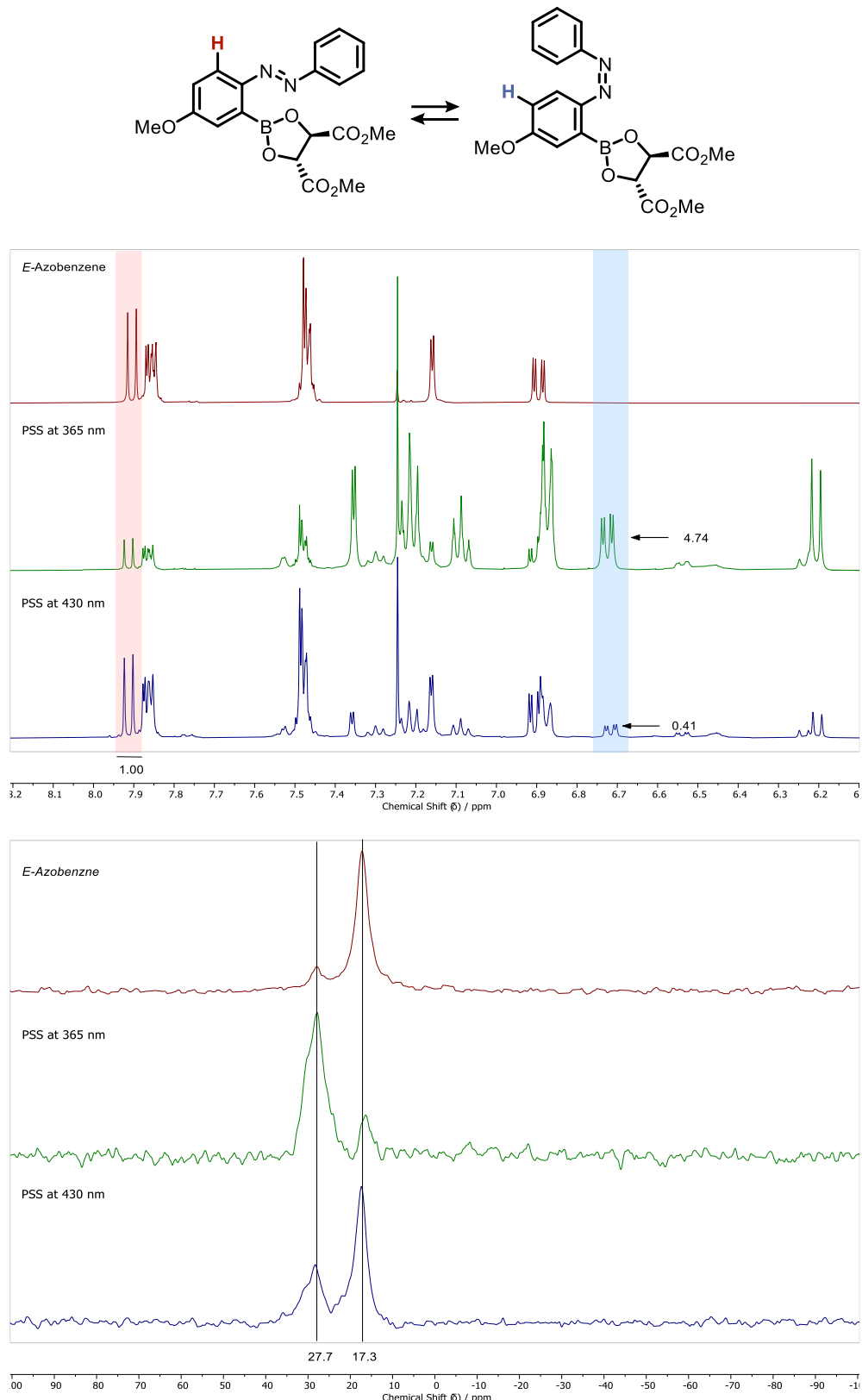


**Figure 52.** Photostationary State composition of Azobenzene **64** under 365 nm and 430 nm irradiation.

## Experimental

(+)-DMT-MeO-Azobenzene **64** + Pyridine

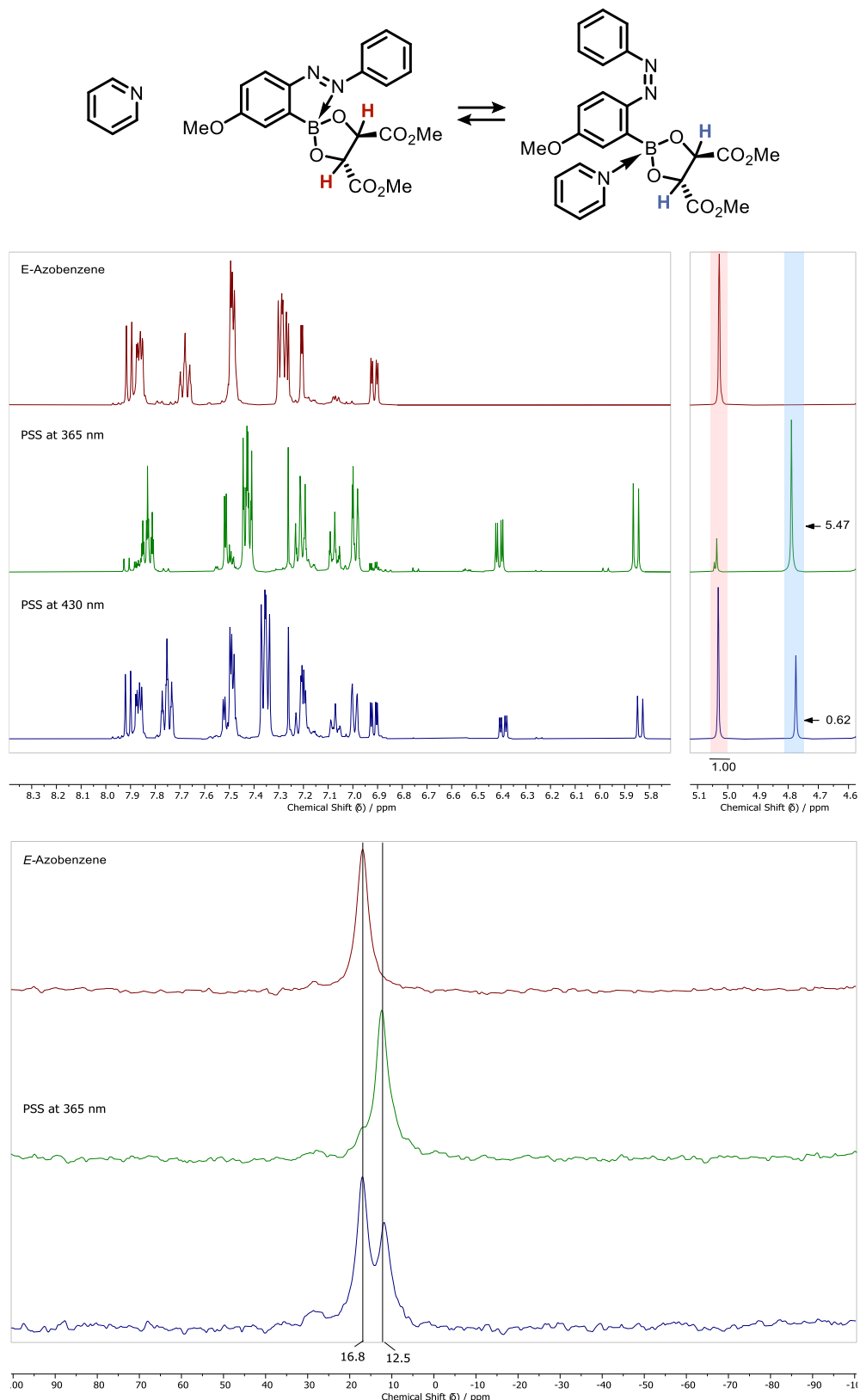


**Figure 53.** Photostationary State composition of Azobenzene **64** under 365 nm and 430 nm irradiation in the presence of pyridine.

## Experimental

### Pinacol-MeO-Azobenzene **61**

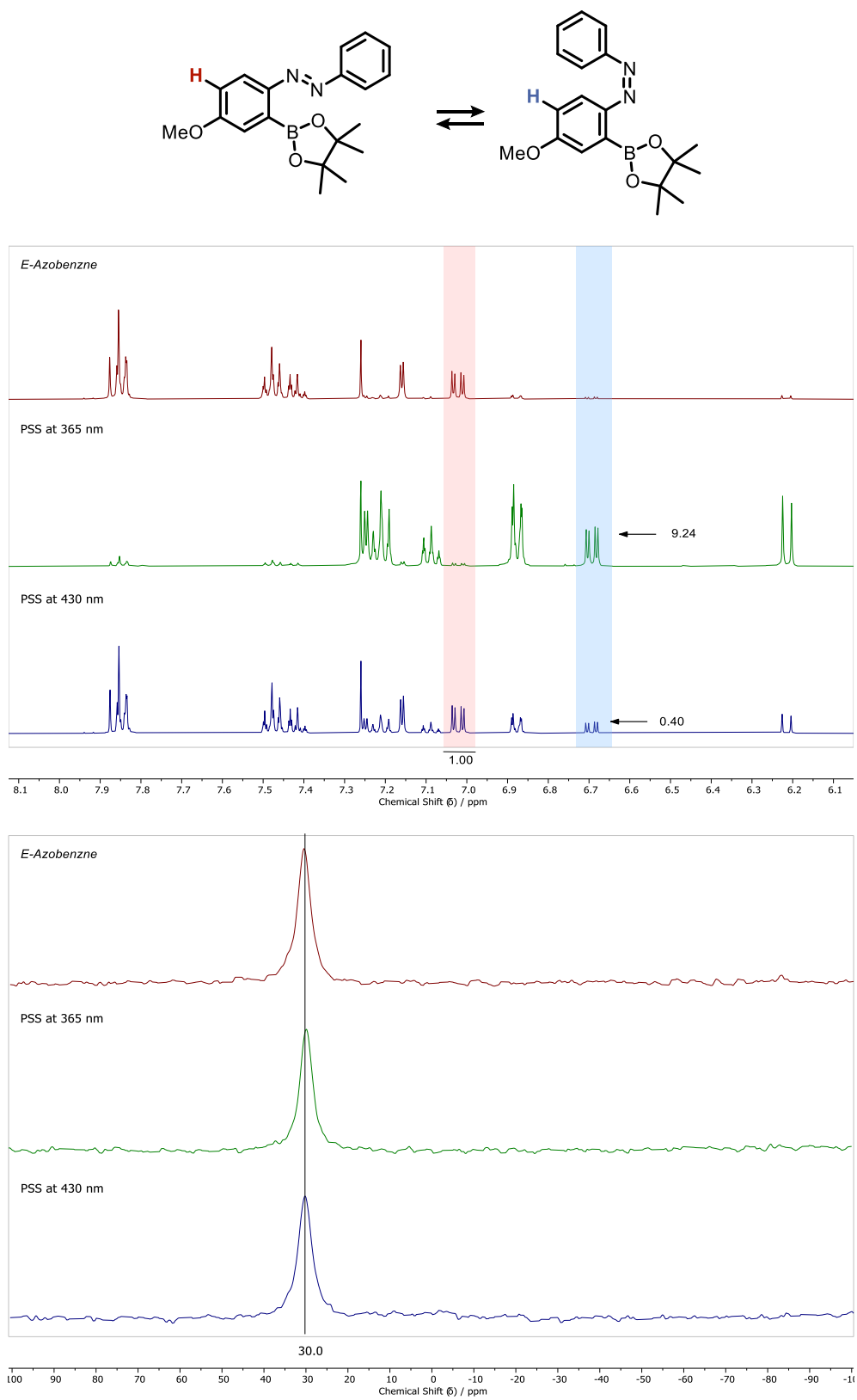


**Figure 54.** Photostationary State composition of Azobenzene **61** under 365 nm and 430 nm irradiation.

## Experimental

### Catechol-MeO-Azobenzene **65**

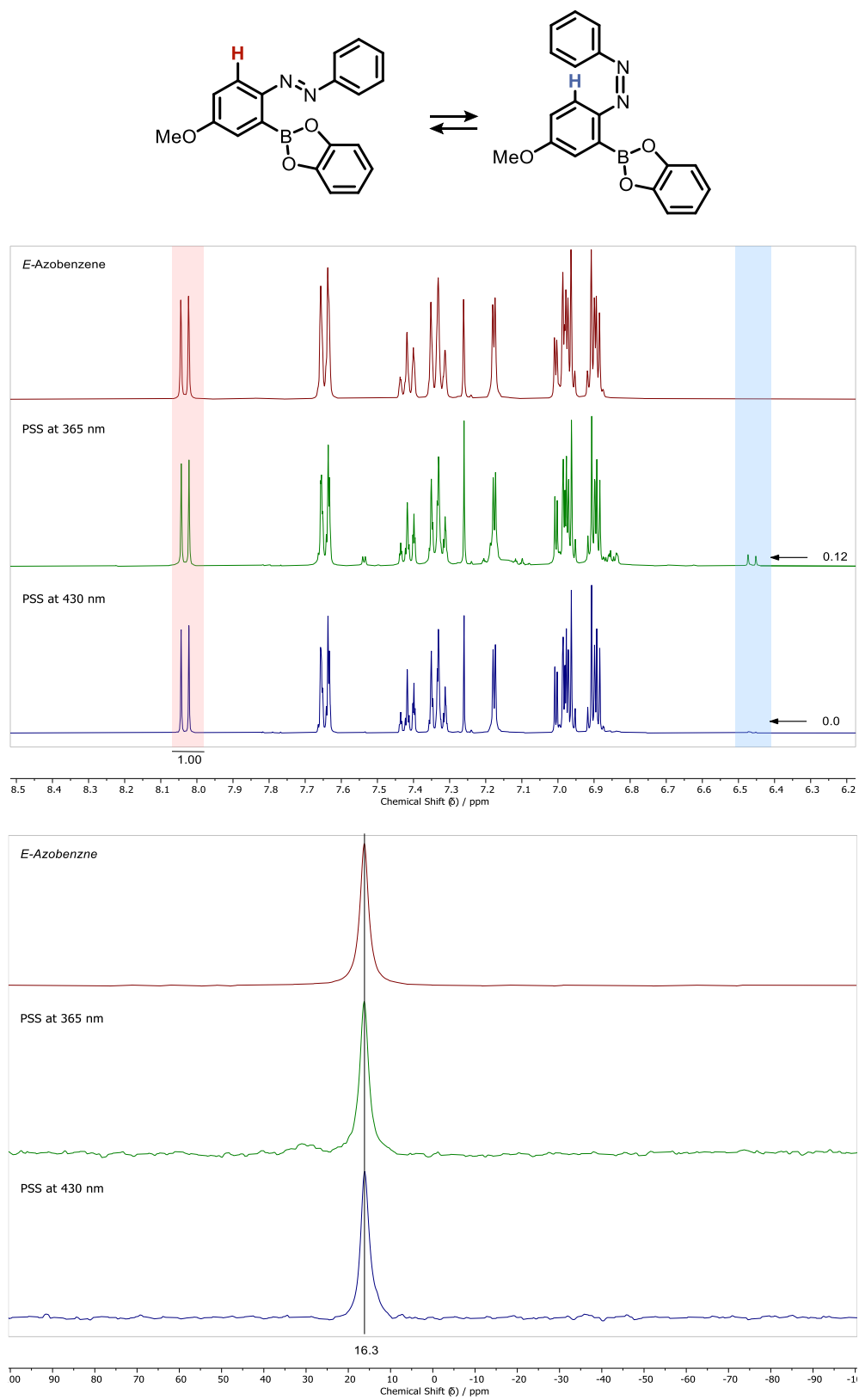


**Figure 55.** Photostationary State composition of Azobenzene **65** under 365 nm and 430 nm irradiation.

## Experimental

$\alpha$ -Hydroxyisobutyric acid-MeO-Azobenzene **66** + Pyridine

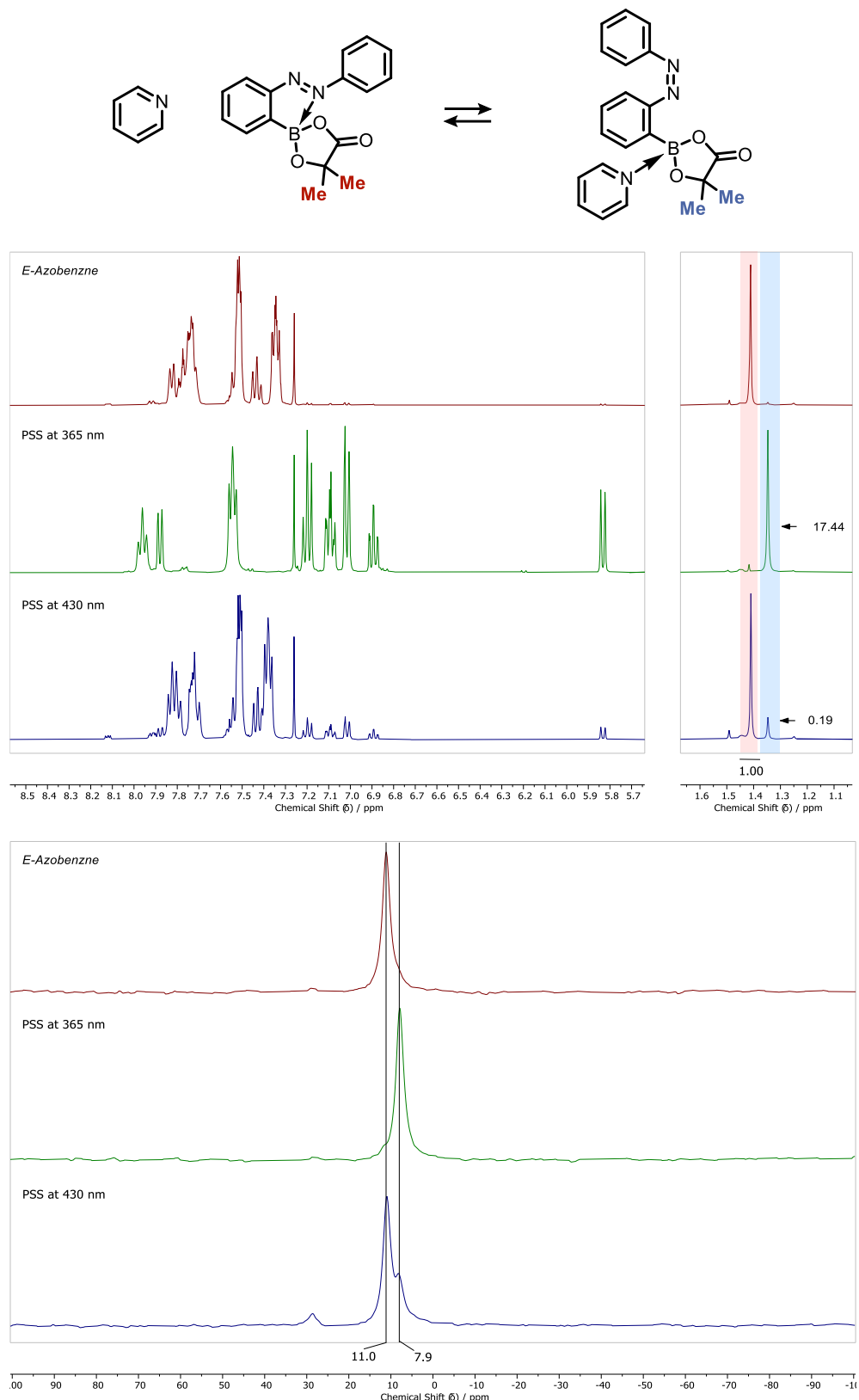


**Figure 56.** Photostationary State composition of Azobenzene **66** under 365 nm and 430 nm irradiation in the presence of pyridine.

## Experimental

### Pinacol-Azobenzene **48**

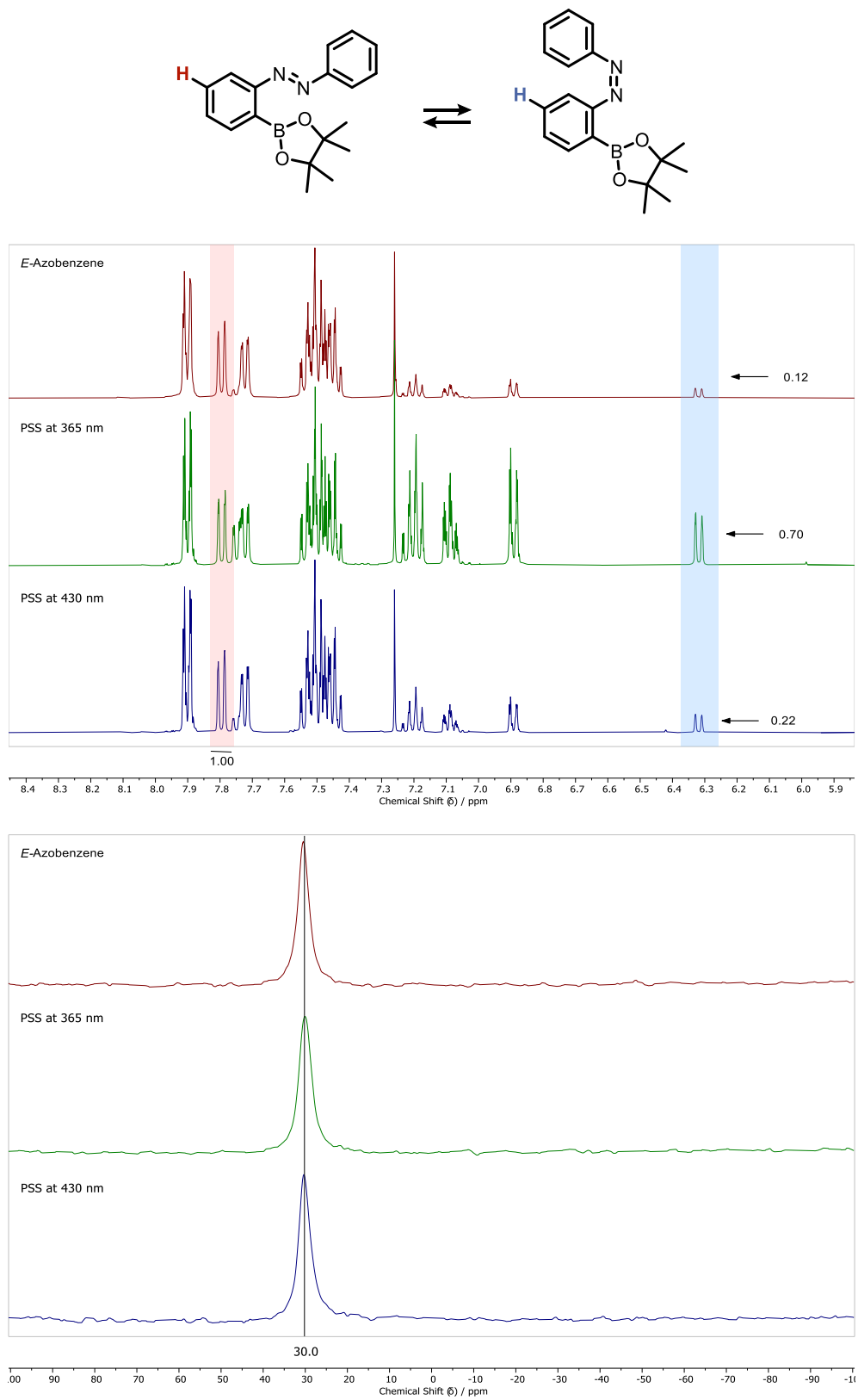


**Figure 57.** Photostationary State composition of Azobenzene **48** under 365 nm and 430 nm irradiation.

## Experimental

### Catechol-Azobenzene **49**

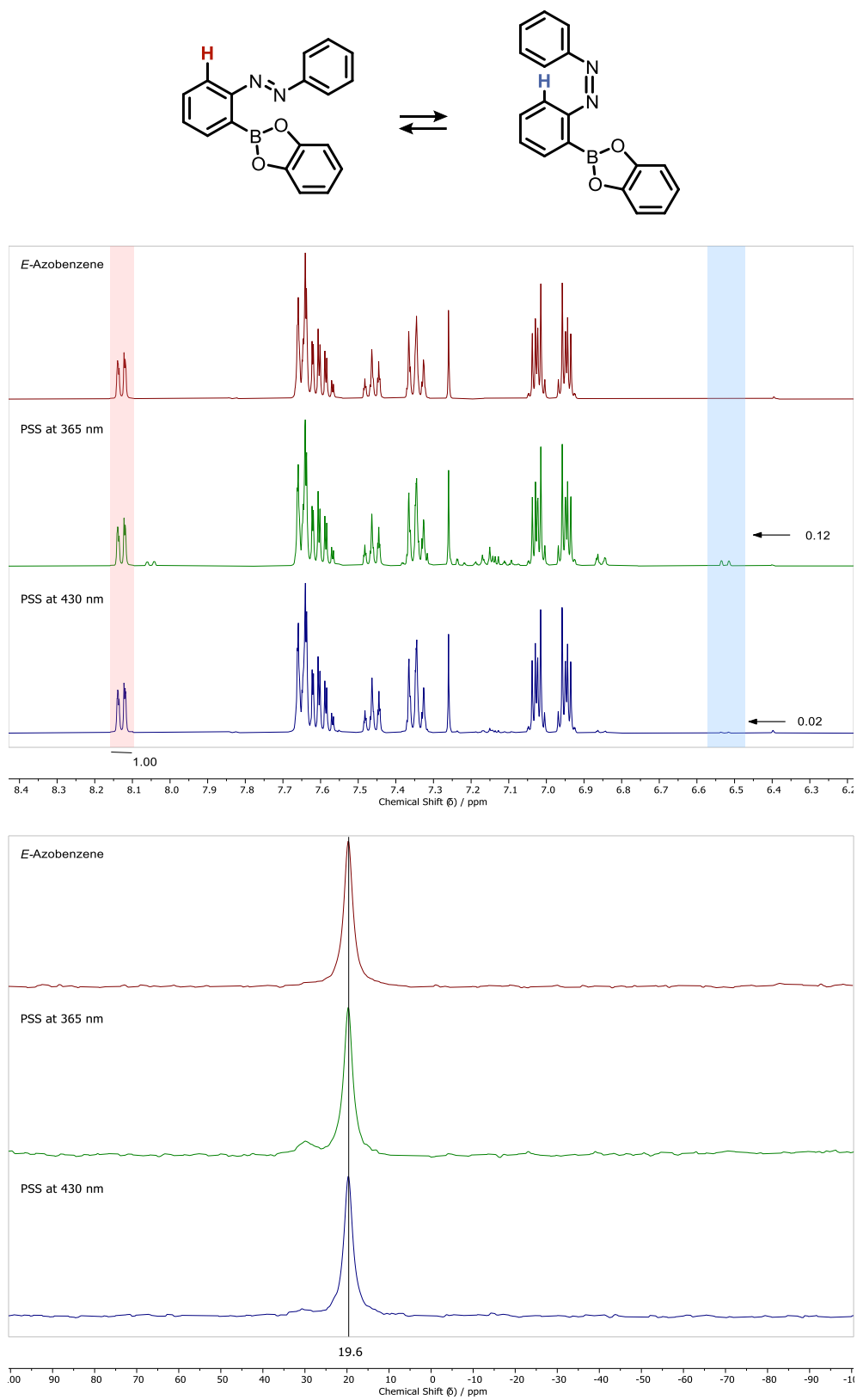


**Figure 58.** Photostationary State composition of Azobenzene **49** under 365 nm and 430 nm irradiation.

## Experimental

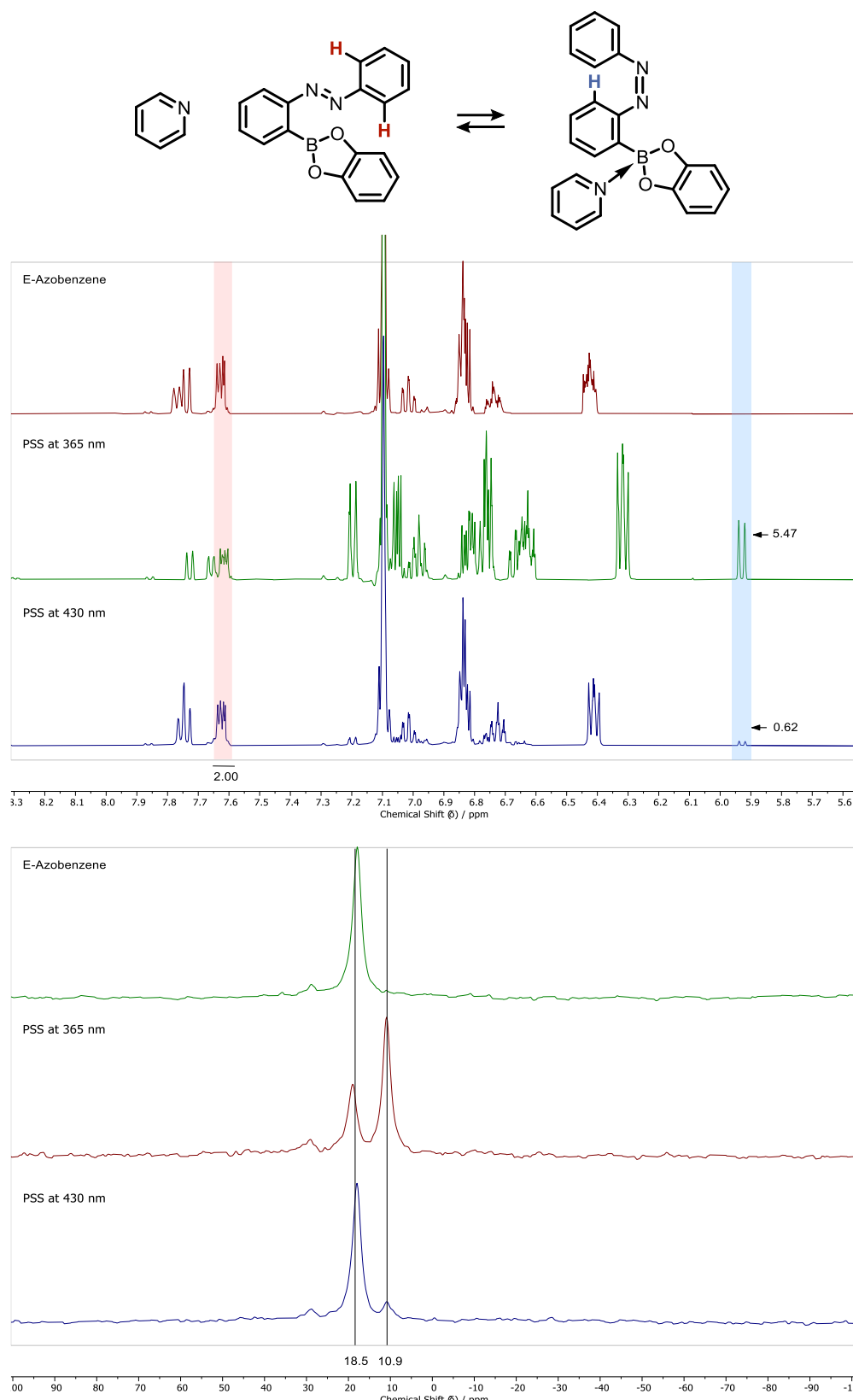


**Figure 59.** Photostationary State composition of Azobenzene 49 under 365 nm and 430 nm irradiation in the presence of pyridine.

## Experimental

### 8.5 XRD Crystallographic data

(*E*)-1-(3-bromo-2-(dibromoboraneyl)-4-methoxyphenyl)-2-phenyldiazene **126**

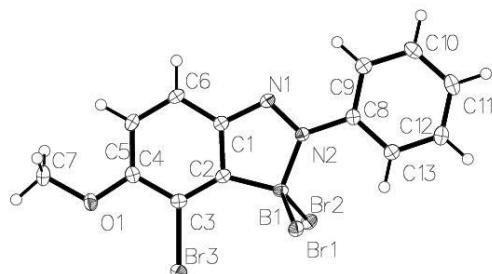


**Figure 60.** Crystal structure of **126** with the anisotropic displacement parameters depicted at the 50% probability level and hydrogens omitted for clarity.

(*E*)-(8-(phenyldiazenyl)benzofuro[3,2-b]pyridin-9-yl)boronic acid **177**

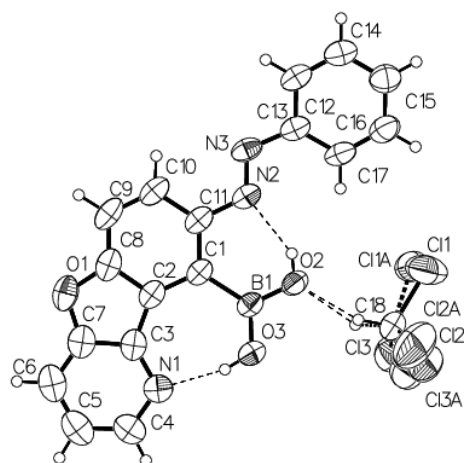


**Figure 61.** Crystal structure of **177** with the anisotropic displacement parameters depicted at the 50% probability level. Solvent molecule and hydrogens, except those on the heteroatoms, omitted for clarity.

(*E*)-1-(2-(dibromoboraneyl)phenyl)-2-phenyldiazene **155**

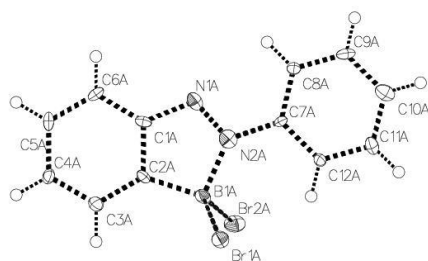


**Figure 62.** Crystal structure of **155** with the anisotropic displacement parameters depicted at the 50% probability level. Disorder and hydrogens omitted for clarity.

## Experimental

---

(*E*)-2-(3-(methoxymethoxy)-6-(phenyldiazenyl)-2-(4,4,5,5-tetramethyl-1,3,2-dioxaborolan-2-yl)phenyl)-2,3-dihydro-1H-naphtho[1,8-de][1,3,2]diazaborinine **183**

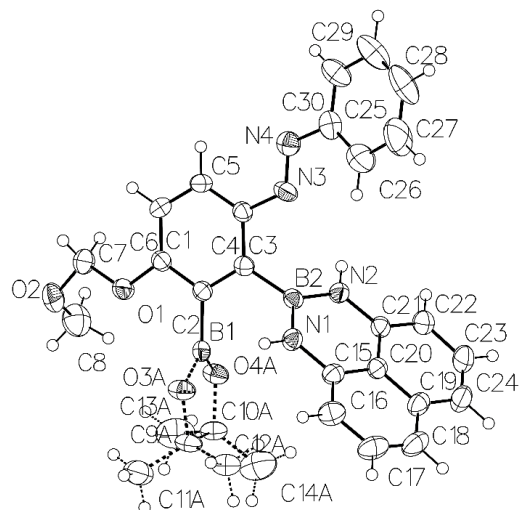


**Figure 63.** Crystal structure of **183** with the anisotropic displacement parameters depicted at the 50% probability level.  
Disorder and hydrogens, except those on the heteroatoms, omitted for clarity.

## Experimental

---

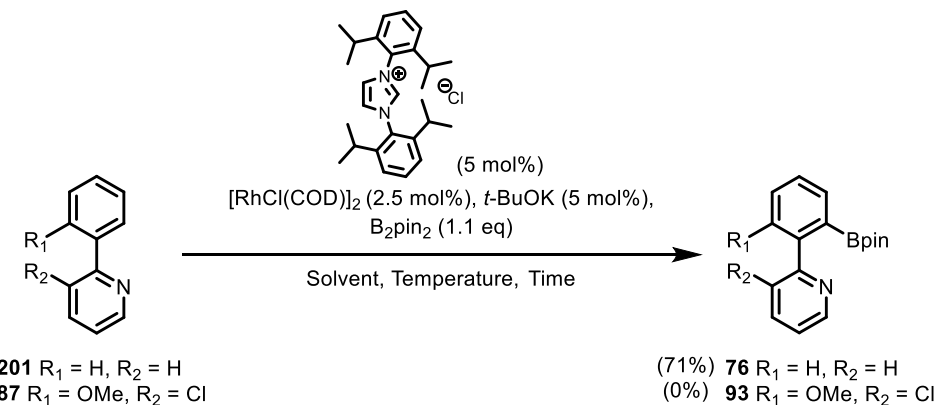
Reference	<b>177</b>	<b>183</b>	<b>126</b>	<b>155</b>
Empirical formula	C <sub>18</sub> H <sub>13</sub> BCl <sub>3</sub> N <sub>3</sub> O <sub>3</sub>	C <sub>30</sub> H <sub>32</sub> B <sub>2</sub> N <sub>4</sub> O <sub>4</sub>	C <sub>13</sub> H <sub>10</sub> BN <sub>2</sub> OB <sub>3</sub>	C <sub>12</sub> H <sub>9</sub> BN <sub>2</sub> Br <sub>2</sub>
Formula weight	436.47	534.21	460.77	351.84
Temperature/K	200(2)	200(2)	100.0	100.0
Crystal system	triclinic	monoclinic	monoclinic	triclinic
Space group	P-1	P <sub>2</sub> 1/c	P <sub>2</sub> 1/n	P-1
a/Å	7.1965(4)	12.7275(4)	8.9023(3)	7.6080(3)
b/Å	10.2760(5)	12.1656(5)	7.2552(3)	8.6313(3)
c/Å	13.6219(6)	19.0364(7)	22.7751(9)	9.7846(3)
$\alpha/^\circ$	94.983(3)	90	90	101.0660(10)
$\beta/^\circ$	93.622(3)	104.8180(10)	91.1400(10)	100.6090(10)
$\gamma/^\circ$	105.007(3)	90	90	94.7650(10)
Volume/Å <sup>3</sup>	965.47(8)	2849.52(18)	1470.71(10)	615.11(4)
Z	2	4	4	2
$\rho_{\text{calc}}/\text{g/cm}^3$	1.501	1.245	2.081	1.900
$\mu/\text{mm}^{-1}$	0.500	0.082	8.223	6.564
F(000)	444.0	1128.0	880.0	340.0
Crystal size/mm <sup>3</sup>	0.426 × 0.358 × 178	0.362 × 0.187 × 0.152	0.228 × 0.184 × 0.012	0.371 × 0.186 × 0.08
Radiation	MoKα ( $\lambda = 0.71073$ )	MoKα ( $\lambda = 0.71073$ )	MoKα ( $\lambda = 0.71073$ )	MoKα ( $\lambda = 0.71073$ )
2θ range for data collection/°	4.128 to 50.698 -8 ≤ h ≤ 8, -12 ≤ k ≤ 12, -16 ≤ l ≤ 16	4.014 to 50.696 -15 ≤ h ≤ 15, -14 ≤ k ≤ 14, -22 ≤ l ≤ 22	3.578 to 56.564 -11 ≤ h ≤ 11, -9 ≤ k ≤ 9, -30 ≤ l ≤ 30	4.334 to 57.556 -10 ≤ h ≤ 10, -11 ≤ k ≤ 11, -13 ≤ l ≤ 13
Reflections collected	14571	140196	95754	28355
Independent reflections	3539 [ $R_{\text{int}} = 0.0473$ , $R_{\sigma} = 0.0418$ ]	5222 [ $R_{\text{int}} = 0.1132$ , $R_{\sigma} = 0.0344$ ]	3652 [ $R_{\text{int}} = 0.0592$ , $R_{\sigma} = 0.0190$ ]	3196 [ $R_{\text{int}} = 0.0425$ , $R_{\sigma} = 0.0268$ ]
Data/restraints/parameters	3539/36/289	5222/317/437	3652/0/182	3196/545/278
Goodness-of-fit on F <sup>2</sup>	1.026	1.074	1.069	1.048
Final R indexes [ $ I  \geq 2\sigma(I)$ ]	$R_1 = 0.0457$ , $wR_2 = 0.1051$	$R_1 = 0.0532$ , $wR_2 = 0.1391$	$R_1 = 0.0187$ , $wR_2 = 0.0367$	$R_1 = 0.0211$ , $wR_2 = 0.0400$
Final R indexes [all data]	$R_1 = 0.0926$ , $wR_2 = 0.1261$	$R_1 = 0.0848$ , $wR_2 = 0.1588$	$R_1 = 0.0242$ , $wR_2 = 0.0379$	$R_1 = 0.0303$ , $wR_2 = 0.0419$
Largest diff. peak/hole / e Å <sup>-3</sup>	0.22/-0.24	0.28/-0.30	0.44/-0.35	0.33/-0.38

**Table 9.** Crystal data and structure refinement.

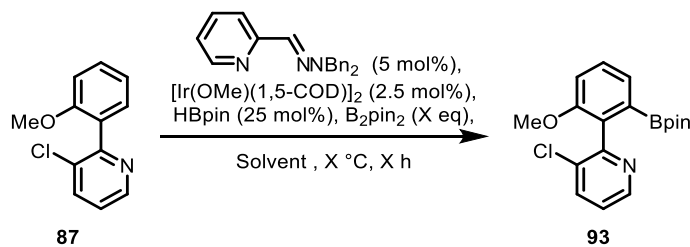
## Experimental

### 8.6 Supplementary Data and Optimization Tables

#### 8.6.1 C–H Borylation Testing



**Scheme 43.** Rhodium catalysed borylation from Crudden and co-workers which was only viable on the planar biaryl-pyridine **201** with attempts at the borylation of **87** proving unsuccessful.<sup>124</sup>



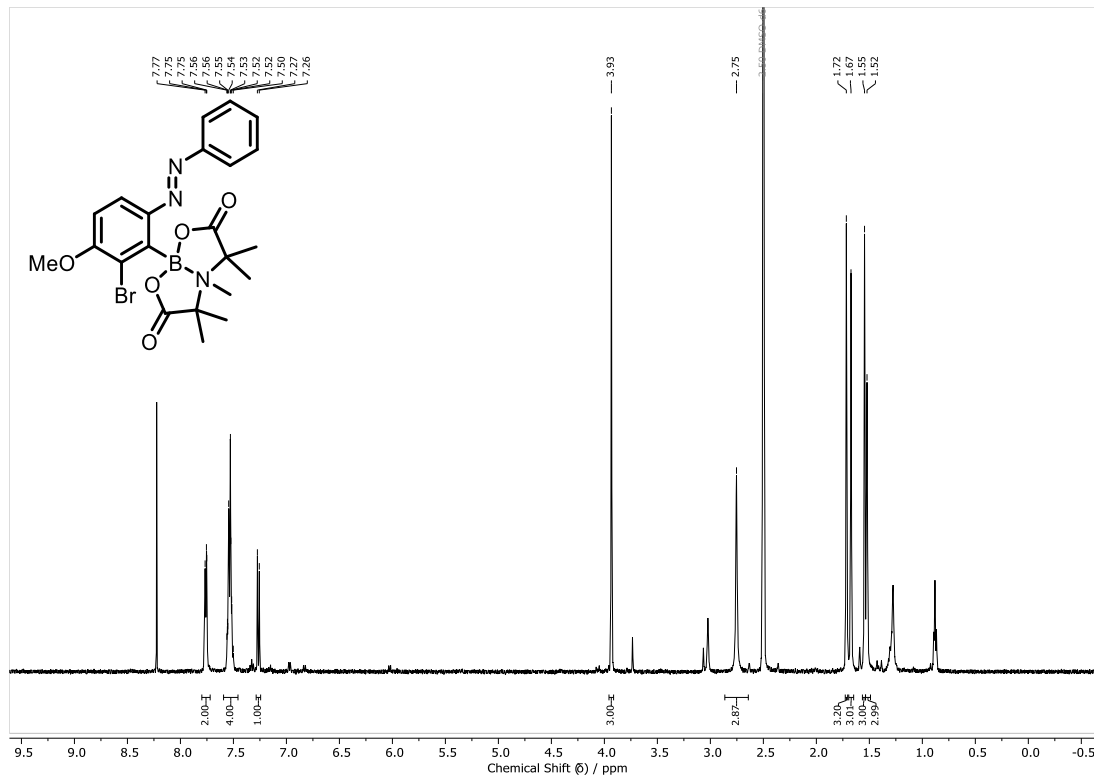
Entry	Solvent	Temp (°C)	B <sub>2</sub> pin <sub>2</sub> (eq)	Time (h)	Yield (%)
1	PhMe	100	5.0	18	57.3
2	Xylene	100	5.0	18	64.2
3	Xylene	100	2.5	18	41.3
4	Xylene	100	1.2	18	38.1
5	Xylene	60	1.2	18	20.0
6	PhMe	60	1.2	18	28.0
7	THF	60	1.2	18	17.4

**Table 10.** Short reoptimization of the borylation methodology from Lassaletta and co-workers to use more forcing conditions as it was noted in their paper that electron deficient pyridyl rings were more challenging to borylate.<sup>115</sup>

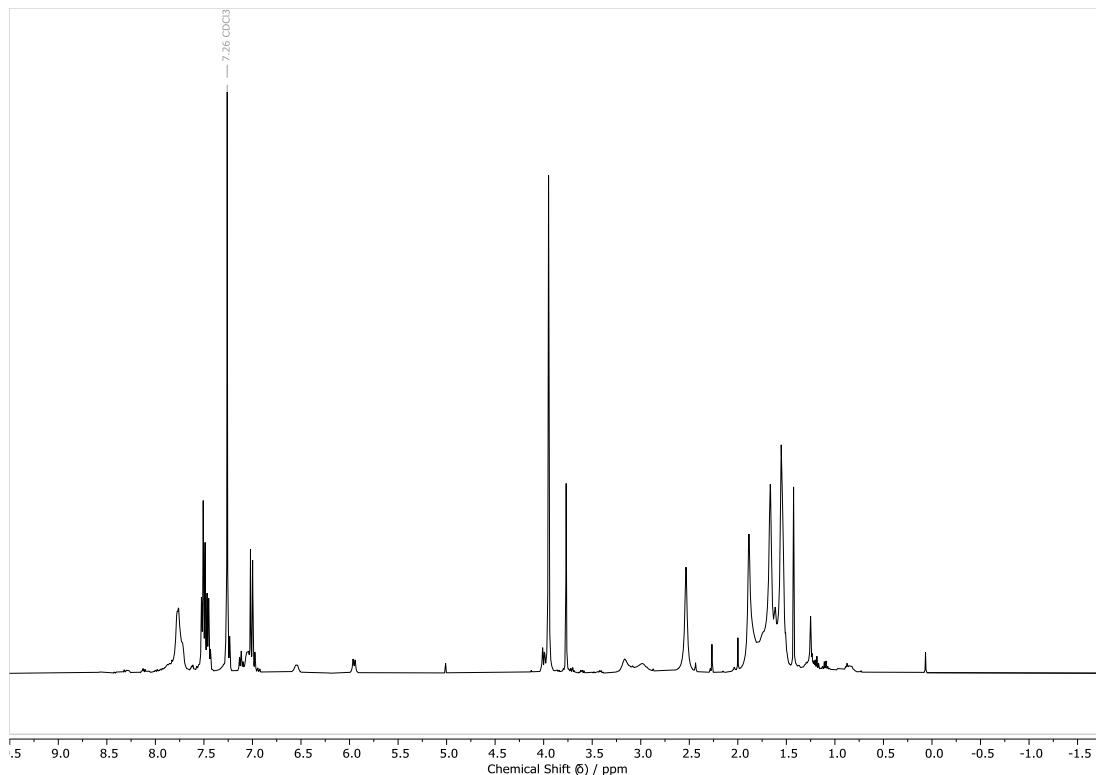
## Experimental

### 8.6.2 Azobenzene-TIDA NMR

$^1\text{H}$  NMR (400 MHz, DMSO-d<sub>6</sub>, 100 °C)

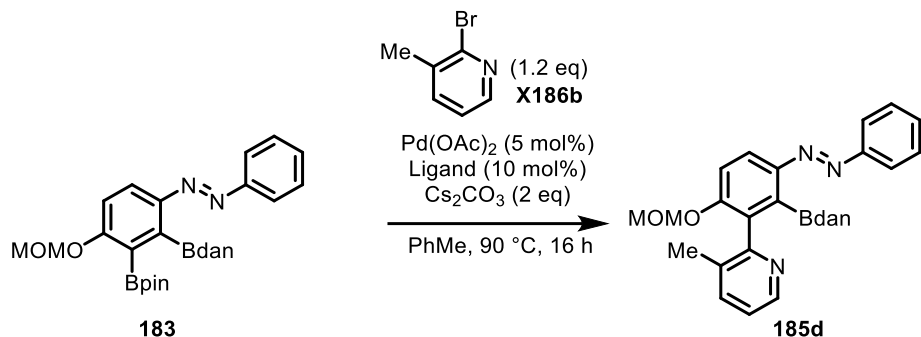


$^1\text{H}$  NMR (400 MHz, CDCl<sub>3</sub>, 25 °C)



## Experimental

### 8.6.3 Second Hindered Suzuki cross-coupling Ligand Screen



Entry	Pd source	Ligand	dehalogenated	185b
1	Pd(OAc) <sub>2</sub>	SPhos	25	0
2	Pd(OAc) <sub>2</sub>	Xphos	41	0
3	Pd(OAc) <sub>2</sub>	CyJohnPhos	92	0
4	Pd(OAc) <sub>2</sub>	tBuPPh <sub>2</sub>	32	0
5	Pd(OAc) <sub>2</sub>	P(o-Tol) <sub>3</sub>	78	0
6	Pd(OAc) <sub>2</sub>	P(C <sub>6</sub> F <sub>5</sub> ) <sub>3</sub>	0	0
7	Pd(OAc) <sub>2</sub>	(R)-BIDME	0	26

**Table 11.** Second screen of the hindered Suzuki cross-coupling with pyridine rings lacking an *ortho* Nitro substituent

## Experimental

### 8.6.4 Addition of Water to Twisted H-bonding Compound 194

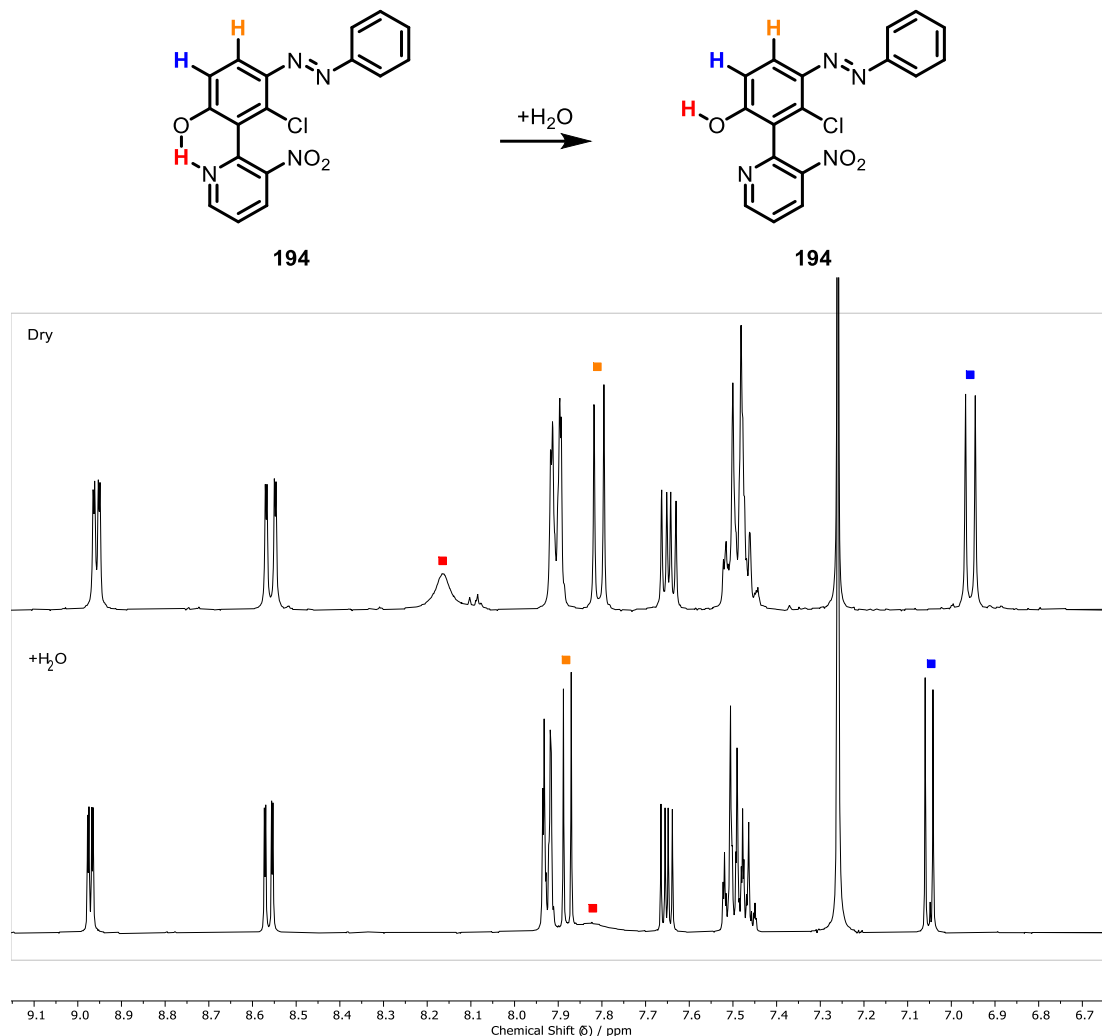


**Figure 64.** Addition of excess water to compound **194** to disturb the H-bond thereby proving its presence in the anhydrous conditions. Borad peak corresponding to the H-bond in the top spectrum (red label) shifts upfield and shows significant line broadening indicating the H-bond is disturbed by the presence of water. Significant upfield shifting is also observed for the peaks corresponding to the azo hydrogens labelled in orange and blue.

## Experimental

---

### 8.6.5 Python Script for UV-Vis data acquisition.

```
import os
import time
import matplotlib.pyplot as plt
import math
from ctypes import *
import tkinter as tk
from tkinter import filedialog
import csv
import time

# os.chdir(r"C:\Program Files\IVI Foundation\VISA\Win64\Bin")
lib = cdll.LoadLibrary("TLCCS_64.dll")

# For the initialization, the resource name needs to be changed to the name of the
# connected device.
# The resource name has this format: USB0::0x1313::<product ID>::<serial number>::RAW
ccs_handle = c_int(0)
lib.tlccs_init(b"USB0::0x1313::0x8089::M00781050::RAW", 1, 1, byref(ccs_handle))

# Specify the integration time, number of measurements, the sleep time between
# measurements, and the number of scans to average
int_t = 65                      # Integration time in milliseconds per scan.
scan_av = 10                     # Number of scans to average per measurement.
num_measurements = 720           # Total number of measurements.
measurement_delay = 0.0          # Time delay in seconds between each measurement (if
# desired).

# Set integration time in seconds, ranging from 1e-5 to 6e1
integration_time = c_double(int_t * 0.001) # For convenience, the integration time is
# entered here in ms, but please note that tlccs_setIntegrationTime has seconds as
# input, hence the factor of 0.001.
lib.tlccs_setIntegrationTime(ccs_handle, integration_time)

# Ask the user to select the reference file
ref_select = input("Press 'm' to measure a reference spectrum or 'o' to open a
reference spectrum from a .csv file.")
if ref_select == "o":
    root = tk.Tk()
    root.withdraw()
    solv_default_dir = 'C:/Users/is20508/OneDrive - University of
Bristol/Desktop/Photochem Data and Guides/Oddy/Solvent Backgrounds'
    reference_file = filedialog.askopenfilename(title="Select Reference File",
filetypes=(("CSV Files", "*.csv"),), initialdir=solv_default_dir, )

    # Check if a file was selected
    if not reference_file:
        print("No reference file selected. Exiting.")
        exit()

    # Load the reference spectrum from the .csv file
    with open(reference_file, "r") as file:
        reader = csv.reader(file)
        data_array_ref = [float(row[1]) for row in reader]

    print("Reference spectrum loaded.")
    print()
elif ref_select == "m":
    #Reference measurement
    input("Press ENTER to start measurement of reference spectrum.")
    lib.tlccs_startScan(ccs_handle)
```

## Experimental

---

```
data_array_ref=(c_double*3648)()
status = c_int(0)

while (status.value & 0x0010) == 0:
    lib.tlccs_getDeviceStatus(ccs_handle, byref(status))

lib.tlccs_getScanData(ccs_handle, byref(data_array_ref))
print("Reference spectrum recorded.")
print()

# Measurement with sample
input("Press ENTER to start measurement of spectrum with sample.")
print("Running Sample Collection...")

measurements_list = [] #contains the averaged intensities for each measurement
completion_times = [] #contains a list of the times (given in seconds since the epoch) each measurement was recorded

for i in range(num_measurements):
    single_measurement_list = []

    for j in range(scan_av):
        lib.tlccs_startScan(ccs_handle)
        single_scan_data_array = (c_double * 3648)()
        status = c_int(0)

        while (status.value & 0x0010) == 0:
            lib.tlccs_getDeviceStatus(ccs_handle, byref(status))

        lib.tlccs_getScanData(ccs_handle, byref(single_scan_data_array))
        single_measurement_list.append(list(single_scan_data_array[:]))

    # Calculate the average intensity for each element
    averaged_scan = []
    for k in range(3648):
        sum_intensity = sum(scan_data[k] for scan_data in single_measurement_list)
        avg_intensity = sum_intensity / scan_av
        averaged_scan.append(avg_intensity)

    measurements_list.append(averaged_scan) # Adds light intensity data to list
    end_time = time.time()
    completion_times.append(end_time) # Adds time since epoch to time list

    print("Measurement " + str(i+1) + " complete.")
    time.sleep(measurement_delay)

print("series of {} spectra, recorded {} seconds apart with an acquisition time of {} seconds".format(num_measurements, measurement_delay, scan_av * integration_time.value))
print()

# Get the wavelength array.
#
# Each cell in the wavelength array corresponds to a cell in the data arrays.
# E.g. wavelength[5] is the wavelength for the scan data in data_array_sample[5]
wavelengths = (c_double * 3648)()
lib.tlccs_getWavelengthData(ccs_handle, 0, byref(wavelengths), c_void_p(None),
c_void_p(None))

# Calculate the absorption and optical density of the sample.
#
# Formulas:
```

## Experimental

---

```
# Absorption[%] = ((Reference Spectrum - Sample Spectrum) / Reference Spectrum) * 100
# Optical density = -log_10(Transmission) ≈ -log_10(1 - Absorption)
#
# try and except is necessary to prevent errors due to impossible mathematical
operations.
absorption_list = []
OD_list = []

for measurement in measurements_list:
    absorption_measurement = []
    for i in range(3648):
        try:
            absorption = float(((data_array_ref[i] - measurement[i]) /
data_array_ref[i]) * 100)
            absorption_measurement.append(absorption)
        except ZeroDivisionError:
            absorption_measurement.append(0)
    absorption_list.append(list(absorption_measurement))

    od_measurement = []
    for j in range(3648):
        try:
            od = -math.log10(1 - (absorption_measurement[j] / 100))
            od_measurement.append(od)
        except (ValueError, ZeroDivisionError):
            od_measurement.append(0)

    OD_list.append(list(od_measurement))

# Create plots of the spectra. Matplotlib is used to create the plots.
# See this website for further information: https://matplotlib.org/stable/index.html
fig, ax = plt.subplots()

ax.set_title('Optical density')
for j in range(num_measurements):
    ax.plot(wavelengths, OD_list[j], label="Measurement {}".format(j+1))

ax.set_xlabel('Wavelength [nm]')
ax.set_ylabel('Optical density')
ax.grid(True)
ax.legend()

plt.show()

# GUI to specify save location and file name for exporting optical density data
root = tk.Tk()
root.withdraw()
default_save_dir = 'C:/Users/is20508/OneDrive - University of
Bristol/Desktop/Photochem Data and Guides/Olly/CSV Output'
file_name = filedialog.asksaveasfilename(title="Save As", defaultextension=".csv",
filetypes=(("CSV Files", "*.csv"),), initialdir=default_save_dir)
if not file_name:
    print("No file name specified. Exiting.")
    exit()
output_filename = file_name

# Prepare data for export
data_export = []
data_export.append(["Wavelength [nm]"] + ["{:.2f}".format(completion_times[i] -
completion_times[0]) for i in range(num_measurements)]) # Header row
```

## Experimental

---

```
for i in range(len(wavelengths)):
    row = [wavelengths[i]]
    for j in range(num_measurements):
        row.append(OD_list[j][i])
    data_export.append(row)

# Export optical density data to a CSV file
with open(output_filename, "w", newline="") as file:
    writer = csv.writer(file)
    writer.writerows(data_export)

print("Optical density data exported to {}".format(output_filename))
```

### References

- (1) Kassem, S.; van Leeuwen, T.; Lubbe, A. S.; Wilson, M. R.; Feringa, B. L.; Leigh, D. A. Artificial molecular motors. *Chem. Soc. Rev.* **2017**, *46* (9), 2592-2621. DOI: 10.1039/c7cs00245a.
- (2) Pezzato, C.; Cheng, C.; Stoddart, J. F.; Astumian, R. D. Mastering the non-equilibrium assembly and operation of molecular machines. *Chem. Soc. Rev.* **2017**, *46* (18), 5491-5507. DOI: 10.1039/c7cs00068e.
- (3) Erbas-Cakmak, S.; Leigh, D. A.; McTernan, C. T.; Nussbaumer, A. L. Artificial Molecular Machines. *Chem. Rev.* **2015**, *115* (18), 10081-10206. DOI: 10.1021/acs.chemrev.5b00146.
- (4) Corra, S.; Curcio, M.; Baroncini, M.; Silvi, S.; Credi, A. Photoactivated Artificial Molecular Machines that Can Perform Tasks. *Adv. Mater.* **2020**, e1906064. DOI: 10.1002/adma.201906064.
- (5) Okuno, D.; Iino, R.; Noji, H. Rotation and structure of FoF1-ATP synthase. *J Biochem* **2011**, *149* (6), 655-664. DOI: 10.1093/jb/mvr049.
- (6) Vale, R. D. The Molecular Motor Toolbox for Intracellular Transport. *Cell* **2003**, *112*, 467-480.
- (7) Feringa, B. L. Vision Statement: Materials in Motion. *Adv. Mater.* **2020**, *32* (20), 1906416. DOI: <https://doi.org/10.1002/adma.201906416>.
- (8) Coskun, A.; Banaszak, M.; Astumian, R. D.; Stoddart, J. F.; Grzybowski, B. A. Great expectations: can artificial molecular machines deliver on their promise? *Chem. Soc. Rev.* **2012**, *41* (1), 19-30. DOI: 10.1039/c1cs15262a.
- (9) Feringa, B. L. The Art of Building Small: From Molecular Switches to Motors (Nobel Lecture). *Angew. Chem. Int. Edit.* **2017**, *56* (37), 11060-11078. DOI: 10.1002/anie.201702979.
- (10) Sauvage, J. P. From Chemical Topology to Molecular Machines (Nobel Lecture). *Angew. Chem. Int. Edit.* **2017**, *56* (37), 11080-11093. DOI: 10.1002/anie.201702992.
- (11) Stoddart, J. F. Mechanically Interlocked Molecules (MIMs)-Molecular Shuttles, Switches, and Machines (Nobel Lecture). *Angew. Chem. Int. Edit.* **2017**, *56* (37), 11094-11125. DOI: 10.1002/anie.201703216.
- (12) Kay, E. R.; Leigh, D. A.; Zerbetto, F. Synthetic molecular motors and mechanical machines. *Angew. Chem. Int. Edit.* **2007**, *46* (1-2), 72-191. DOI: 10.1002/anie.200504313.
- (13) Feringa, B. L.; Delden, R. A. v.; Koumura, N.; Geertsema, E. M. Chiroptical Molecular Switches. *Chem. Rev.* **2000**, *100* (5), 1789-1816.
- (14) McNaught, A. D.; Wilkinson, A. *IUPAC Compendium of Chemical Terminology*, 2nd ed. (the "Gold Book"); Blackwell Scientific Publications, 1997. DOI: <https://doi.org/10.1351/goldbook>.

## References

---

- (15) Moss, G. P. Basic terminology of stereochemistry (IUPAC Recommendations 1996). *Pure Appl. Chem.* **1996**, *68* (12), 2193-2222. DOI: doi:10.1351/pac199668122193.
- (16) Koumura, N.; Geertsema, E. M.; Meetsma, A.; Feringa, B. L. Light-Driven Molecular Rotor: Unidirectional Rotation Controlled by a Single Stereogenic Center. *J. Am. Chem. Soc.* **2000**, *122* (48), 12005-12006.
- (17) Kistemaker, J. C.; Stacko, P.; Visser, J.; Feringa, B. L. Unidirectional rotary motion in achiral molecular motors. *Nature Chemistry* **2015**, *7* (11), 890-896. DOI: 10.1038/nchem.2362.
- (18) Ruangsrapichat, N.; Pollard, M. M.; Harutyunyan, S. R.; Feringa, B. L. Reversing the direction in a light-driven rotary molecular motor. *Nature Chemistry* **2011**, *3* (1), 53-60. DOI: 10.1038/nchem.872.
- (19) Koumura, N.; Zijlstra, R. W. J.; Delden, R. A. v.; Harada, N.; Feringa, B. L. Light-driven monodirectional molecular rotor. *Nature* **1999**, *401*, 152-155.
- (20) Wezenberg, S. J.; Feringa, B. L. Supramolecularly directed rotary motion in a photoresponsive receptor. *Nat. Commun.* **2018**, *9* (1), 1984. DOI: 10.1038/s41467-018-04249-x.
- (21) Leigh, D. A.; Wong, J. K. Y.; Dehez, F. o.; Zerbetto, F. Unidirectional rotation in a mechanically interlocked molecular rotor. *Nature* **2003**, *424*, 174–179.
- (22) Wilson, M. R.; Sola, J.; Carbone, A.; Goldup, S. M.; Lebrasseur, N.; Leigh, D. A. An autonomous chemically fuelled small-molecule motor. *Nature* **2016**, *534* (7606), 235-240. DOI: 10.1038/nature18013.
- (23) Hernández, J. V.; Kay, E. R.; Leigh, D. A. A Reversible Synthetic Rotary Molecular Motor. *Science* **2004**, *306* (5701), 1532-1537. DOI: 10.1126/science.1103949.
- (24) Cheng, C.; McGonigal, P. R.; Schneebeli, S. T.; Li, H.; Vermeulen, N. A.; Ke, C.; Stoddart, J. F. An artificial molecular pump. *Nature Nanotechnology* **2015**, *10* (6), 547-553. DOI: 10.1038/nnano.2015.96.
- (25) Ragazzon, G.; Baroncini, M.; Silvi, S.; Venturi, M.; Credi, A. Light-powered autonomous and directional molecular motion of a dissipative self-assembling system. *Nature Nanotechnology* **2015**, *10* (1), 70-75. DOI: 10.1038/nnano.2014.260.
- (26) Bissell, R. A.; Cordova, E.; Kaifer, A. E.; Stoddart, J. F. A chemically and electrochemically switchable molecular shuttle. *Nature* **1994**, *369*, 133-137.
- (27) Beves, J. E.; Blanco, V.; Blight, B. A.; Carrillo, R.; D'Souza, D. M.; Howgego, D.; Leigh, D. A.; Slawin, A. M.; Symes, M. D. Toward metal complexes that can directionally walk along tracks: controlled stepping of a molecular biped with a palladium(II) foot. *J. Am. Chem. Soc.* **2014**, *136* (5), 2094-2100. DOI: 10.1021/ja4123973.
- (28) von Delius, M.; Geertsema, E. M.; Leigh, D. A. A synthetic small molecule that can walk down a track. *Nature Chemistry* **2010**, *2* (2), 96-101. DOI: 10.1038/nchem.481.
- (29) Iwamura, H.; Mislow, K. Stereochemical consequences of dynamic gearing. *Acc. Chem. Res.* **1988**, *21* (4), 175-182. DOI: 10.1021/ar00148a007.

## References

---

- (30) Koga, N.; Kawada, Y.; Iwamura, H. Recognition of the phase relationship between remote substituents in 9,10-bis(3-chloro-9-trptycylloxy)trptycene molecules undergoing rapid internal rotation cooperatively. *J. Am. Chem. Soc.* **1983**, *105* (16), 5498-5499. DOI: 10.1021/ja00354a063.
- (31) Stevens, A. M.; Richards, C. J. A metallocene molecular gear. *Tetrahedron Letters* **1997**, *38* (44), 7805-7808. DOI: 10.1016/S0040-4039(97)10042-9.
- (32) Frantz, D. K.; Linden, A.; Baldridge, K. K.; Siegel, J. S. Molecular Spur Gears Comprising Triptycene Rotators and Bibenzimidazole-Based Stators. *J. Am. Chem. Soc.* **2012**, *134* (3), 1528-1535. DOI: 10.1021/ja2063346.
- (33) Kelly, T. R.; Bowyer, M. C.; Bhaskar, K. V.; Bebbington, D.; Garcia, A.; Lang, F.; Kim, M. H.; Jette, M. P. A Molecular Brake. *J. Am. Chem. Soc.* **1994**, *116* (8), 3657-3658. DOI: 10.1021/ja00087a085.
- (34) Kelly, T. R.; Tellitu, I.; Sestelo, J. P. In Search of Molecular Ratchets. *Angew. Chem. Int. Edit.* **1997**, *36* (17), 1866-1868.
- (35) Kelly, T. R.; Silva, H. D.; Silva, R. A. Unidirectional rotary motion in a molecular system. *Nature* **1999**, *401*, 150-152.
- (36) Davis, A. P. Tilting at Windmills? The Second Law Survives. *Angew. Chem. Int. Edit.* **1998**, *37* (7), 909-910. DOI: 10.1002/(sici)1521-3773(19980420)37:7<909::Aid-anie909>3.0.Co;2-x.
- (37) Mock, W. L.; Ochwat, K. J. Theory and example of a small-molecule motor. *J. Phys. Org. Chem.* **2003**, *16* (3), 175-182. DOI: 10.1002/poc.591.
- (38) Kariyawasam, L. S.; Hartley, C. S. Dissipative Assembly of Aqueous Carboxylic Acid Anhydrides Fueled by Carbodiimides. *J. Am. Chem. Soc.* **2017**, *139* (34), 11949-11955. DOI: 10.1021/jacs.7b06099.
- (39) Jayalath, I. M.; Wang, H.; Mantel, G.; Kariyawasam, L. S.; Hartley, C. S. Chemically Fueled Transient Geometry Changes in Diphenic Acids. *Org. Lett.* **2020**, *22* (19), 7567-7571. DOI: 10.1021/acs.orglett.0c02757.
- (40) Jayalath, I. M.; Gerken, M. M.; Mantel, G.; Hartley, C. S. Substituent Effects on Transient, Carbodiimide-Induced Geometry Changes in Diphenic Acids. *J. Org. Chem.* **2021**, *86* (17), 12024-12033. DOI: 10.1021/acs.joc.1c01385.
- (41) Dahl, B. J.; Branchaud, B. P. Synthesis and characterization of a functionalized chiral biaryl capable of exhibiting unidirectional bond rotation. *Tetrahedron Letters* **2004**, *45* (52), 9599-9602. DOI: 10.1016/j.tetlet.2004.10.147.
- (42) Bringmann, G.; Price Mortimer, A. J.; Keller, P. A.; Gresser, M. J.; Garner, J.; Breuning, M. Atroposelective synthesis of axially chiral biaryl compounds. *Angew. Chem. Int. Edit.* **2005**, *44* (34), 5384-5427. DOI: 10.1002/anie.200462661.
- (43) Lin, Y.; Dahl, B. J.; Branchaud, B. P. Net directed 180° aryl–aryl bond rotation in a prototypical achiral biaryl lactone synthetic molecular motor. *Tetrahedron Letters* **2005**, *46* (48), 8359-8362. DOI: 10.1016/j.tetlet.2005.09.151.

## References

---

- (44) Stephen P. Fletcher, F. D., Michael M. Pollard, Ben L. Feringa. A Reversible, Unidirectional Molecular Rotary Motor Driven by Chemical Energy. *Science* **2005**, *310* (5745), 80-82.
- (45) Dahl, B. J.; Branchaud, B. P. 180° Unidirectional Bond Rotation in a Biaryl Lactone Artificial Molecular Motor Prototype. *Org. Lett.* **2006**, *8* (25), 5841-5844.
- (46) Collins, B. S. L.; Kistemaker, J. C. M.; Otten, E.; Feringa, B. L. A chemically powered unidirectional rotary molecular motor based on a palladium redox cycle. *Nature Chemistry* **2016**, *8* (9), 860-866. DOI: 10.1038/nchem.2543.
- (47) Gerhard Bringmann\*, H. B., Ulrich Dauer, Stefan Giissregen and Martin Stahl. Structure and Enantiomerization of Helically Twisted Lactone--Bridged Biaryls: a Theoretical Study. *Tetrahedron* **1995**, *51* (11), 3149-3158.
- (48) Bringmann, G.; Hartung, T. First Atropo-Enantioselective Ring Opening of Achiral Biaryls Containing Lactone Bridges with Chiral Hydride-Transfer Reagents Derived from Borane. *Angew. Chem. Int. Edit.* **1992**, *31* (6), 761-762. DOI: 10.1002/anie.199207611 (acccessed 2020/05/20).
- (49) Bringmann, G.; Hartung, T. Atropo-enantioselective biaryl synthesis by stereocontrolled cleavage of configuratively labile lactone-bridged precursors using chiral H-nucleophiles. *Tetrahedron* **1993**, *49* (36), 7891-7902. DOI: 10.1016/S0040-4020(01)88014-5.
- (50) Zhang, Y.; Chang, Z.; Zhao, H.; Crespi, S.; Feringa, B. L.; Zhao, D. A Chemically Driven Rotary Molecular Motor Based on Reversible Lactone Formation with Perfect Unidirectionality. *Chem* **2020**, *6* (9), 2420-2429. DOI: 10.1016/j.chempr.2020.07.025.
- (51) Borsley, S.; Kreidt, E.; Leigh, D. A.; Roberts, B. M. W. Autonomous fuelled directional rotation about a covalent single bond. *Nature* **2022**, *604* (7904), 80-85. DOI: 10.1038/s41586-022-04450-5.
- (52) Tena-Solsona, M.; Rieß, B.; Grötsch, R. K.; Löhrer, F. C.; Wanzke, C.; Käsdorf, B.; Bausch, A. R.; Müller-Buschbaum, P.; Lieleg, O.; Boekhoven, J. Non-equilibrium dissipative supramolecular materials with a tunable lifetime. *Nat. Commun.* **2017**, *8* (1), 15895. DOI: 10.1038/ncomms15895.
- (53) Mo, K.; Zhang, Y.; Dong, Z.; Yang, Y.; Ma, X.; Feringa, B. L.; Zhao, D. RETRACTED ARTICLE: Intrinsically unidirectional chemically fuelled rotary molecular motors. *Nature* **2022**, *609* (7926), 293-298. DOI: 10.1038/s41586-022-05033-0.
- (54) Balzani, V. Photochemical molecular devices. *Photochem Photobiol Sci* **2003**, *2* (5), 459-476. DOI: 10.1039/b300075n.
- (55) Balzani, V.; Credi, A.; Venturi, M. Light powered molecular machines. *Chem. Soc. Rev.* **2009**, *38* (6), 1542-1550. DOI: 10.1039/b806328c.
- (56) Baroncini, M.; Silvi, S.; Credi, A. Photo- and Redox-Driven Artificial Molecular Motors. *Chem. Rev.* **2020**, *120* (1), 200-268. DOI: 10.1021/acs.chemrev.9b00291.

## References

---

- (57) Baroncini, M.; Canton, M.; Casimiro, L.; Corra, S.; Groppi, J.; La Rosa, M.; Silvi, S.; Credi, A. Photoactive Molecular-Based Devices, Machines and Materials: Recent Advances. *Eur. J. Inorg. Chem.* **2018**, 2018 (42), 4589-4603. DOI: 10.1002/ejic.201800923.
- (58) Koumura, N.; Geertsema, E. M.; van Gelder, M. B.; Meetsma, A.; Feringa, B. L. Second Generation Light-Driven Molecular Motors. Unidirectional Rotation Controlled by a Single Stereogenic Center with Near-Perfect Photoequilibria and Acceleration of the Speed of Rotation by Structural Modification. *J. Am. Chem. Soc.* **2002**, 124 (18), 5037-5051. DOI: 10.1021/ja012499i.
- (59) Filatov, M.; Paolino, M.; Min, S. K.; Kim, K. S. Fulgides as Light-Driven Molecular Rotary Motors: Computational Design of a Prototype Compound. *J. Phys. Chem. Lett.* **2018**, 9 (17), 4995-5001. DOI: 10.1021/acs.jpclett.8b02268.
- (60) Pang, X.; Jiang, C.; Qi, Y.; Yuan, L.; Hu, D.; Zhang, X.; Zhao, D.; Wang, D.; Lan, Z.; Li, F. Ultrafast unidirectional chiral rotation in the Z-E photoisomerization of two azoheteroarene photoswitches. *Phys. Chem. Chem. Phys.* **2018**, 20 (40), 25910-25917. DOI: 10.1039/c8cp04762f.
- (61) Wang, J.; Durbeej, B. Toward Fast and Efficient Visible-Light-Driven Molecular Motors: A Minimal Design. *ChemistryOpen* **2018**, 7 (8), 583-589. DOI: 10.1002/open.201800089.
- (62) Filatov, M.; Paolino, M.; Min, S. K.; Choi, C. H. Design and photoisomerization dynamics of a new family of synthetic 2-stroke light driven molecular rotary motors. *Chem. Commun. (Camb)* **2019**, 55 (36), 5247-5250. DOI: 10.1039/c9cc01955c.
- (63) Guentner, M.; Schildhauer, M.; Thumser, S.; Mayer, P.; Stephenson, D.; Mayer, P. J.; Dube, H. Sunlight-powered kHz rotation of a hemithioindigo-based molecular motor. *Nat. Commun.* **2015**, 6, 8406. DOI: 10.1038/ncomms9406.
- (64) Gerwien, A.; Mayer, P.; Dube, H. Photon-Only Molecular Motor with Reverse Temperature-Dependent Efficiency. *J. Am. Chem. Soc.* **2018**, 140 (48), 16442-16445. DOI: 10.1021/jacs.8b10660.
- (65) Petermayer, C.; Dube, H. Indigoid Photoswitches: Visible Light Responsive Molecular Tools. *Acc. Chem. Res.* **2018**, 51 (5), 1153-1163. DOI: 10.1021/acs.accounts.7b00638.
- (66) Wilcken, R.; Schildhauer, M.; Rott, F.; Huber, L. A.; Guentner, M.; Thumser, S.; Hoffmann, K.; Oesterling, S.; de Vivie-Riedle, R.; Riedle, E.; et al. Complete Mechanism of Hemithioindigo Motor Rotation. *J. Am. Chem. Soc.* **2018**, 140 (15), 5311-5318. DOI: 10.1021/jacs.8b02349.
- (67) Gerwien, A.; Mayer, P.; Dube, H. Green light powered molecular state motor enabling eight-shaped unidirectional rotation. *Nat. Commun.* **2019**, 10 (1), 4449. DOI: 10.1038/s41467-019-12463-4.
- (68) Greb, L.; Lehn, J.-M. Light-Driven Molecular Motors: Imines as Four-Step or Two-Step Unidirectional Rotors. *J. Am. Chem. Soc.* **2014**, 136 (38), 13114-13117. DOI: 10.1021/ja506034n.

## References

---

- (69) Greb, L.; Eichhofer, A.; Lehn, J. M. Synthetic Molecular Motors: Thermal N Inversion and Directional Photoinduced C=N Bond Rotation of Camphorquinone Imines. *Angew. Chem. Int. Edit.* **2015**, *54* (48), 14345-14348. DOI: 10.1002/anie.201506691.
- (70) Roke, D.; Sen, M.; Danowski, W.; Wezenberg, S. J.; Feringa, B. L. Visible-Light-Driven Tunable Molecular Motors Based on Oxindole. *J. Am. Chem. Soc.* **2019**, *141* (18), 7622-7627. DOI: 10.1021/jacs.9b03237.
- (71) Roke, D.; Stuckhardt, C.; Danowski, W.; Wezenberg, S. J.; Feringa, B. L. Light-Gated Rotation in a Molecular Motor Functionalized with a Dithienylethene Switch. *Angew. Chem. Int. Edit.* **2018**, *57* (33), 10515-10519. DOI: 10.1002/anie.201802392.
- (72) Faulkner, A.; van Leeuwen, T.; Feringa, B. L.; Wezenberg, S. J. Allosteric Regulation of the Rotational Speed in a Light-Driven Molecular Motor. *J. Am. Chem. Soc.* **2016**, *138* (41), 13597-13603. DOI: 10.1021/jacs.6b06467.
- (73) Gerwien, A.; Schildhauer, M.; Thumser, S.; Mayer, P.; Dube, H. Direct evidence for hula twist and single-bond rotation photoproducts. *Nat. Commun.* **2018**, *9* (1), 2510. DOI: 10.1038/s41467-018-04928-9.
- (74) Basheer, M. C.; Oka, Y.; Mathews, M.; Tamaoki, N. A Light-Controlled Molecular Brake with Complete ON-OFF Rotation. *Chem.-Eur. J.* **2010**, *16* (11), 3489-3496, Article. DOI: 10.1002/chem.200902123.
- (75) Hashim, P. K.; Thomas, R.; Tamaoki, N. Induction of Molecular Chirality by Circularly Polarized Light in Cyclic Azobenzene with a Photoswitchable Benzene Rotor. *Chem.-Eur. J.* **2011**, *17* (26), 7304-7312, Article. DOI: 10.1002/chem.201003526.
- (76) Thomas, R.; Yoshida, Y.; Akasaka, T.; Tamaoki, N. Influence of a Change in Helical Twisting Power of Photoresponsive Chiral Dopants on Rotational Manipulation of Micro-Objects on the Surface of Chiral Nematic Liquid Crystalline Films. *Chem.-Eur. J.* **2012**, *18* (39), 12337-12348, S12337/12331-S12337/12313, 10.1002/chem.201200836. DOI: 10.1002/chem.201200836.
- (77) Commins, P.; Garcia-Garibay, M. A. Photochromic Molecular Gyroscope with Solid State Rotational States Determined by an Azobenzene Bridge. *J. Org. Chem.* **2014**, *79* (4), 1611-1619, Article. DOI: 10.1021/jo402516n.
- (78) Kim, Y.; Tamaoki, N. A photoresponsive planar chiral azobenzene dopant with high helical twisting power. *J. Mater. Chem. C* **2014**, *2* (43), 9258-9264, 10.1039/C4TC01851F. DOI: 10.1039/C4TC01851F.
- (79) Mafy, N. N.; Kim, Y.; Thomas, R.; Akasaka, T.; Tamaoki, N. Molecular crankshaft effect converting piston-like molecular motion to continuous rotation of macro objects. *ACS Appl. Mater. Interfaces* **2019**, *11* (16), 15097-15102, 10.1021/acsami.9b03706. DOI: 10.1021/acsami.9b03706.
- (80) Ter Wiel, M. K.; van Delden, R. A.; Meetsma, A.; Feringa, B. L. Control of rotor motion in a light-driven molecular motor: towards a molecular gearbox. *Org. Biomol. Chem.* **2005**, *3* (22), 4071-4076. DOI: 10.1039/b510641a.

## References

---

- (81) Nilsson, J. R.; O'Sullivan, M. C.; Li, S.; Anderson, H. L.; Andreasson, J. A photoswitchable supramolecular complex with release-and-report capabilities. *Chem. Commun. (Camb)* **2015**, *51* (5), 847-850. DOI: 10.1039/c4cc08513b.
- (82) Foy, J. T.; Li, Q.; Goujon, A.; Colard-Itte, J. R.; Fuks, G.; Moulin, E.; Schiffmann, O.; Dattler, D.; Funeriu, D. P.; Giuseppone, N. Dual-light control of nanomachines that integrate motor and modulator subunits. *Nature Nanotechnology* **2017**, *12* (6), 540-545. DOI: 10.1038/nnano.2017.28.
- (83) Muraoka, T.; Kinbara, K.; Kobayashi, Y.; Aida, T. Light-driven open-close motion of chiral molecular scissors. *J. Am. Chem. Soc.* **2003**, *125* (19), 5612-5613, Article. DOI: 10.1021/ja034994f.
- (84) Nilsson, A. H. a. J.-E. The determination of the barrier to internal rotation in ferrocene and ruthenocene by means of electron diffraction. *Chem. Commun. (London)* **1968**, (2), 88-89. DOI: 10.1039/C19680000088.
- (85) Muraoka, T.; Kinbara, K.; Aida, T. Reversible operation of chiral molecular scissors by redox and UV light. *Chem. Commun.* **2007**, (14), 1441-1443, Article. DOI: 10.1039/b618248h.
- (86) Muraoka, T.; Kinbara, K.; Wakamiya, A.; Yamaguchi, S.; Aida, T. Crystallographic and chiroptical studies on tetraarylferrocenes for use as chiral rotary modules for molecular machines. *Chem.-Eur. J.* **2007**, *13* (6), 1724-1730, Article. DOI: 10.1002/chem.200601098.
- (87) Muraoka, T.; Kinbara, K.; Aida, T. Mechanical twisting of a guest by a photoresponsive host. *Nature* **2006**, *440* (7083), 512-515, Article. DOI: 10.1038/nature04635.
- (88) Kai, H.; Nara, S.; Kinbara, K.; Aida, T. Toward long-distance mechanical communication: Studies on a ternary complex interconnected by a bridging rotary module. *J. Am. Chem. Soc.* **2008**, *130* (21), 6725-, Article. DOI: 10.1021/ja801646b.
- (89) Štacko, P.; Kistemaker, J. C. M.; Leeuwen, T. v.; Chang, M.-C.; Otten, E.; B. L. Feringa. Locked synchronous rotor motion in a molecular motor. *Science* **2017**, *356* (6341), 964-968.
- (90) Uhl, E.; Mayer, P.; Dube, H. Active and Unidirectional Acceleration of Biaryl Rotation by a Molecular Motor. *Angew. Chem. Int. Edit.* **2020**, *59* (14), 5730-5737. DOI: 10.1002/anie.201913798.
- (91) Uhl, E.; Thumser, S.; Mayer, P.; Dube, H. Transmission of Unidirectional Molecular Motor Rotation to a Remote Biaryl Axis. *Angew. Chem. Int. Edit.* **2018**, *57* (34), 11064-11068. DOI: 10.1002/anie.201804716.
- (92) Uhl, E.; Thumser, S.; Mayer, P.; Dube, H. Transmission of Unidirectional Molecular Motor Rotation to a Remote Biaryl Axis. *Angew. Chem. Int. Edit.* **2018**, *57* (34), 11064-11068. DOI: 10.1002/anie.201804716.
- (93) Uhl, E.; Mayer, P.; Dube, H. Active and Unidirectional Acceleration of Biaryl Rotation by a Molecular Motor. *Angew. Chem. Int. Edit.* **2020**, *59* (14), 5730-5737. DOI: 10.1002/anie.201913798.

## References

---

- (94) Regen-Pregizer, B. L.; Dube, H. Defining Unidirectional Motions and Structural Reconfiguration in a Macrocyclic Molecular Motor. *J. Am. Chem. Soc.* **2023**, *145* (24), 13081-13088. DOI: 10.1021/jacs.3c01567.
- (95) Yoshino, J.; Kano, N.; Kawashima, T. Synthesis of the most intensely fluorescent azobenzene by utilizing the B-N interaction. *Chem. Commun. (Camb)* **2007**, (6), 559-561. DOI: 10.1039/b615966d.
- (96) Yoshino, J.; Furuta, A.; Kambe, T.; Itoi, H.; Kano, N.; Kawashima, T.; Ito, Y.; Asashima, M. Intensely fluorescent azobenzenes: synthesis, crystal structures, effects of substituents, and application to fluorescent vital stain. *Chemistry* **2010**, *16* (17), 5026-5035. DOI: 10.1002/chem.201000258.
- (97) Yoshino, J.; Kano, N.; Kawashima, T. Synthesis of organoboron compounds bearing an azo group and substituent effects on their structures and photoisomerization. *Tetrahedron* **2008**, *64* (33), 7774-7781. DOI: 10.1016/j.tet.2008.05.128.
- (98) Kano, N.; Yoshino, J.; Kawashima, T. Photoswitching of the Lewis Acidity of a Catecholborane Bearing an Azo Group Based on the Change in Coordination Number of Boron. *Org. Lett.* **2005**, *7* (18), 3909-3911.
- (99) Luisier, N.; Scopelliti, R.; Severin, K. Supramolecular gels based on boronate esters and imidazolyl donors. *Soft Matter* **2016**, *12* (2), 588-593, 10.1039/C5SM02298C. DOI: 10.1039/C5SM02298C.
- (100) Diemer, S. L.; Kristensen, M.; Rasmussen, B.; Beeren, S. R.; Pittelkow, M. Simultaneous Disulfide and Boronic Acid Ester Exchange in Dynamic Combinatorial Libraries. *International Journal of Molecular Sciences* **2015**, *16* (9), 21858-21872.
- (101) Spencer, J. N.; Andrefsky, J. C.; Grushow, A.; Naghdi, J.; Patti, L. M.; Trader, J. F. Hydrogen bond equilibria of phenol-pyridine in cyclohexane, carbon tetrachloride, and benzene solvents. *J. Phys. Chem.* **1987**, *91* (6), 1673-1674. DOI: 10.1021/j100290a076.
- (102) Beezer, A. E.; Hawksworth, W. A.; Orban, M.; Tyrrell, H. J. V. Hydrogen-bonded complexes between pyridine and phenol in carbon tetrachloride solutions. *Journal of the Chemical Society, Faraday Transactions 1: Physical Chemistry in Condensed Phases* **1977**, *73* (0), 1326-1333, 10.1039/F19777301326. DOI: 10.1039/F19777301326.
- (103) Strueben, J.; Lipfert, M.; Springer, J.-O.; Gould, C. A.; Gates, P. J.; Sönnichsen, F. D.; Staubitz, A. High-Yield Lithiation of Azobenzenes by Tin–Lithium Exchange. *Chem.-Eur. J.* **2015**, *21* (31), 11165-11173. DOI: 10.1002/chem.201500003.
- (104) Strueben, J.; Gates, P. J.; Staubitz, A. Tin-Functionalized Azobenzenes as Nucleophiles in Stille Cross-Coupling Reactions. *J. Org. Chem.* **2014**, *79* (4), 1719-1728. DOI: 10.1021/jo402598u.
- (105) Ruslim, C.; Ichimura, K. Spectroscopic and thermal isomerization characteristics of 3,3'-dialkoxy and dialkanoyloxy azobenzenes. *J. Mat. Chem.* **2000**, *10* (12), 2704-2707, 10.1039/B003975F. DOI: 10.1039/B003975F.

## References

---

- (106) Thongpaen, J.; Manguin, R.; Dorcet, V.; Vives, T.; Duhayon, C.; Mauduit, M.; Baslé, O. Visible Light Induced Rhodium(I)-Catalyzed C–H Borylation. *Angew. Chem. Int. Edit.* **2019**, *58* (43), 15244-15248. DOI: 10.1002/anie.201905924.
- (107) Kawamorita, S.; Miyazaki, T.; Ohmiya, H.; Iwai, T.; Sawamura, M. Rh-Catalyzed Ortho-Selective C–H Borylation of N-Functionalized Arenes with Silica-Supported Bridgehead Monophosphine Ligands. *J. Am. Chem. Soc.* **2011**, *133* (48), 19310-19313. DOI: 10.1021/ja208364a.
- (108) He, Z.-C.; Mellerup, S. K.; Liu, L.; Wang, X.; Dao, C.; Wang, S. Reversible Photoisomerization from Borepin to Boratanorcaradiene and Double Aryl Migration from Boron to Carbon. *Angew. Chem. Int. Edit.* **2019**, *58* (20), 6683-6687. DOI: 10.1002/anie.201902231.
- (109) Wang, G.; Liu, L.; Wang, H.; Ding, Y.-S.; Zhou, J.; Mao, S.; Li, P. N,B-Bidentate Boryl Ligand-Supported Iridium Catalyst for Efficient Functional-Group-Directed C–H Borylation. *J. Am. Chem. Soc.* **2017**, *139* (1), 91-94. DOI: 10.1021/jacs.6b11867.
- (110) Okada, S.; Namikoshi, T.; Watanabe, S.; Murata, M. Ruthenium-Catalyzed Ortho-Selective Aromatic C-H Borylation of 2-Arylpyridines with Pinacolborane. *ChemCatChem* **2015**, *7* (10), 1531-1534. DOI: <https://doi.org/10.1002/cctc.201500110>.
- (111) Keske, E. C.; Moore, B. D.; Zenkina, O. V.; Wang, R.; Schatte, G.; Crudden, C. M. Highly selective directed arylation reactions via back-to-back dehydrogenative C–H borylation/arylation reactions. *Chem. Commun.* **2014**, *50* (69), 9883-9886, 10.1039/C4CC02499K. DOI: 10.1039/C4CC02499K.
- (112) Ros, A.; Estepa, B.; López-Rodríguez, R.; Álvarez, E.; Fernández, R.; Lassaletta, J. M. Use of Hemilabile N,N Ligands in Nitrogen-Directed Iridium-Catalyzed Borylations of Arenes. *Angew. Chem. Int. Edit.* **2011**, *50* (49), 11724-11728. DOI: <https://doi.org/10.1002/anie.201104544>.
- (113) Lu, J.-s.; Ko, S.-B.; Walters, N. R.; Wang, S. Decorating BODIPY with Three- and Four-Coordinate Boron Groups. *Org. Lett.* **2012**, *14* (22), 5660-5663. DOI: 10.1021/ol302633s.
- (114) Ishida, N.; Moriya, T.; Goya, T.; Murakami, M. Synthesis of Pyridine–Borane Complexes via Electrophilic Aromatic Borylation. *J. Org. Chem.* **2010**, *75* (24), 8709-8712. DOI: 10.1021/jo101920p.
- (115) Ros, A.; Estepa, B.; Lopez-Rodriguez, R.; Alvarez, E.; Fernandez, R.; Lassaletta, J. M. Use of hemilabile N,N ligands in nitrogen-directed iridium-catalyzed borylations of arenes. *Angew. Chem. Int. Edit.* **2011**, *50* (49), 11724-11728. DOI: 10.1002/anie.201104544.
- (116) Gladiali, S.; Fabbri, D. Atropisomeric Binaphthalene-Core Phosphacyclic Derivatives in Coordination Chemistry and Homogeneous Catalysis. *Chemische Berichte* **1997**, *130* (5), 543-554. DOI: <https://doi.org/10.1002/cber.19971300503>.
- (117) Tani, K.; Tashiro, H.; Yoshida, M.; Yamagata, T. Stereoselective reaction of  $\pm$ -7-Phenyldinaphtho[2,1-b;1',2'-d]phosphole with an optically active palladium complex. Molecular structure and fluxional behavior of Pd(S)-C<sub>6</sub>H<sub>4</sub>CH(CH<sub>3</sub>)N(CH<sub>3</sub>)<sub>2</sub>(P)-PPh(C<sub>20</sub>H<sub>12</sub>) Cl. *J. Organomet. Chem.* **1994**, *469* (2), 229-236. DOI: [https://doi.org/10.1016/0022-328X\(94\)88077-8](https://doi.org/10.1016/0022-328X(94)88077-8).

## References

---

- (118) Gladiali, S.; Dore, A.; Fabbri, D.; De Lucchi, O.; Valle, G. Synthesis, Crystal Structure, Dynamic Behavior and Reactivity of Dinaphtho[2,1-b:1',2'-d]phospholes and Related Atropisomeric Phosphacyclic Derivatives. *J. Org. Chem.* **1994**, *59* (21), 6363-6371. DOI: 10.1021/jo00100a044.
- (119) Watson, A. A.; Willis, A. C.; Wild, S. B. Atropisomerism in ( $\pm$ )-7-methyl- and -phenyl-substituted dinaphtho[2,1-b;1',2'-d]phospholes and dinaphth[2,1-b;1',2'-d]arsoles. *J. Organomet. Chem.* **1993**, *445* (1), 71-78. DOI: 10.1016/0022-328X(93)80189-I.
- (120) Dore, A.; Fabbri, D.; Gladiali, S.; Valle, G. New axially chiral sulfur compounds: Synthesis and conformational stability of enantiopure 4,4'-biphenanthrene-3,3'-dithiol and related atropisomeric derivatives. *Tetrahedron: Asymmetry* **1995**, *6* (3), 779-788. DOI: 10.1016/0957-4166(95)00074-Y.
- (121) Xue, X.; Gu, Z. Synthesis of Bridged Biaryl Atropisomers via Sequential Cu- and Pd-Catalyzed Asymmetric Ring Opening and Cyclization. *Org. Lett.* **2019**, *21* (11), 3942-3945. DOI: 10.1021/acs.orglett.9b01062.
- (122) Heeb, J.-P.; Clayden, J.; Smith, M. D.; Armstrong, R. J. Interrogating the configurational stability of atropisomers. *Nature Protocols* **2023**. DOI: 10.1038/s41596-023-00859-y.
- (123) Pais, V. F.; Neumann, T.; Vayá, I.; Jiménez, M. C.; Ros, A.; Pischel, U. Arylisoquinoline-derived organoboron dyes with a triaryl skeleton show dual fluorescence. *Beilstein J. Org. Chem.* **2019**, *15*, 2612-2622. DOI: 10.3762/bjoc.15.254.
- (124) Keske, E. C.; Moore, B. D.; Zenkina, O. V.; Wang, R.; Schatte, G.; Crudden, C. M. Highly selective directed arylation reactions via back-to-back dehydrogenative C-H borylation/arylation reactions. *Chem. Commun. (Camb)* **2014**, *50* (69), 9883-9886. DOI: 10.1039/c4cc02499k.
- (125) Hammett, L. P. The Effect of Structure upon the Reactions of Organic Compounds. Benzene Derivatives. *J. Am. Chem. Soc.* **1937**, *59* (1), 96-103. DOI: 10.1021/ja01280a022.
- (126) Kost, D.; Carlson, E. H.; Raban, M. The validity of approximate equations for  $k_c$  in dynamic nuclear magnetic resonance. *Journal of the Chemical Society D: Chemical Communications* **1971**, (13), 656-657, 10.1039/C29710000656. DOI: 10.1039/C29710000656.
- (127) Bergman, J. J.; Chandler, W. D. A Study of the Barriers to Rotation in Some Highly Substituted Diphenyl Ethers. *Canadian Journal of Chemistry* **1972**, *50* (3), 353-363. DOI: 10.1139/v72-053.
- (128) Parada, G. A.; Glover, S. D.; Orthaber, A.; Hammarström, L.; Ott, S. Hydrogen Bonded Phenol-Quinolines with Highly Controlled Proton-Transfer Coordinate. *Eur. J. Org. Chem.* **2016**, *2016* (20), 3365-3372. DOI: 10.1002/ejoc.201600460.
- (129) Fugard, A. J.; Lahdenperä, A. S. K.; Tan, J. S. J.; Mekareeya, A.; Paton, R. S.; Smith, M. D. Hydrogen-Bond-Enabled Dynamic Kinetic Resolution of Axially Chiral Amides Mediated by a Chiral Counterion. *Angew. Chem. Int. Edit.* **2019**, *58* (9), 2795-2798. DOI: 10.1002/anie.201814362.

## References

---

- (130) Bhat, V.; Wang, S.; Stoltz, B. M.; Virgil, S. C. Asymmetric Synthesis of QUINAP via Dynamic Kinetic Resolution. *J. Am. Chem. Soc.* **2013**, *135* (45), 16829-16832. DOI: 10.1021/ja409383f.
- (131) Tucker, S. C.; Brown, J. M.; Oakes, J.; Thorntwaite, D. Resolution and coupling of 1-(2'-hydroxy-1'-naphthyl)isoquinolines. *Tetrahedron* **2001**, *57* (13), 2545-2554. DOI: 10.1016/S0040-4020(01)00064-3.
- (132) Cox, P. A.; Leach, A. G.; Campbell, A. D.; Lloyd-Jones, G. C. Protodeboronation of Heteroaromatic, Vinyl, and Cyclopropyl Boronic Acids: pH–Rate Profiles, Autocatalysis, and Disproportionation. *J. Am. Chem. Soc.* **2016**, *138* (29), 9145-9157. DOI: 10.1021/jacs.6b03283.
- (133) Okada, S.; Namikoshi, T.; Watanabe, S.; Murata, M. Ruthenium-Catalyzed Ortho-Selective Aromatic C $\square$ H Borylation of 2-Arylpyridines with Pinacolborane. *ChemCatChem* **2015**, *7* (10), 1531-1534. DOI: 10.1002/cctc.201500110.
- (134) Fu, X.; Wei, Z.; Xia, C.; Shen, C.; Xu, J.; Yang, Y.; Wang, K.; Zhang, P. Palladium-Catalyzed Direct Ortho C–O bond construction of Azobenzenes with Iodobenzene diacetate via C–H Activation. *Catalysis Letters* **2017**, *147* (2), 400-406. DOI: 10.1007/s10562-016-1955-7.
- (135) Fahey, D. R. The homogeneous palladium-catalysed ortho-chlorination of azobenzene. *Journal of the Chemical Society D: Chemical Communications* **1970**, (7), 417a-417a, 10.1039/C2970000417A. DOI: 10.1039/C2970000417A.
- (136) Yong, W.-S.; Park, S.; Yun, H.; Lee, P. H. Synthesis of 2H-Indazoles via Tandem Palladium-Catalyzed Deacylative Cross-Coupling and Denitrogenative Cyclization of 2-Iodoazoarenes and 2-Iodoaryltriazenes with Acyldiazoacetates in One-Pot. *Advanced Synthesis & Catalysis* **2016**, *358* (12), 1958-1967. DOI: 10.1002/adsc.201600351.
- (137) Ma, X.-T.; Tian, S.-K. Palladium-Catalyzed Regioselective Halogenation of Aromatic Azo Compounds. *Advanced Synthesis & Catalysis* **2013**, *355* (2-3), 337-340. DOI: 10.1002/adsc.201200902.
- (138) Seth, K.; Nautiyal, M.; Purohit, P.; Parikh, N.; Chakraborti, A. K. Palladium catalyzed Csp<sup>2</sup>-H activation for direct aryl hydroxylation: the unprecedented role of 1,4-dioxane as a source of hydroxyl radicals. *Chem. Commun.* **2015**, *51* (1), 191-194, 10.1039/C4CC06864E. DOI: 10.1039/C4CC06864E.
- (139) Wang, Z.-J.; Chen, X.; Wu, L.; Wong, J. J.; Liang, Y.; Zhao, Y.; Houk, K. N.; Shi, Z. Metal-Free Directed C–H Borylation of Pyrroles. *Angew. Chem. Int. Edit.* **2021**, *60* (15), 8500-8504. DOI: 10.1002/anie.202016573.
- (140) Iqbal, S. A.; Cid, J.; Procter, R. J.; Uzelac, M.; Yuan, K.; Ingleson, M. J. Acyl-Directed ortho-Borylation of Anilines and C7 Borylation of Indoles using just BBr<sub>3</sub>. *Angew. Chem. Int. Edit.* **2019**, *58* (43), 15381-15385. DOI: 10.1002/anie.201909786.
- (141) Niu, L.; Yang, H.; Wang, R.; Fu, H. Metal-Free Ortho C–H Borylation of 2-Phenoxyprydines under Mild Conditions. *Org. Lett.* **2012**, *14* (10), 2618-2621. DOI: 10.1021/o1300950r.

## References

---

- (142) Rej, S.; Chatani, N. Transient Imine as a Directing Group for the Metal-Free o-C–H Borylation of Benzaldehydes. *J. Am. Chem. Soc.* **2021**, *143* (7), 2920-2929. DOI: 10.1021/jacs.0c13013.
- (143) Wu, G.; Fu, X.; Wang, Y.; Deng, K.; Zhang, L.; Ma, T.; Ji, Y. C–H Borylation of Diphenylamines through Adamantane-1-carbonyl Auxiliary by BBr<sub>3</sub>. *Org. Lett.* **2020**, *22* (17), 7003-7007. DOI: 10.1021/acs.orglett.0c02552.
- (144) Lv, J.; Chen, X.; Xue, X.-S.; Zhao, B.; Liang, Y.; Wang, M.; Jin, L.; Yuan, Y.; Han, Y.; Zhao, Y.; et al. Metal-free directed sp<sup>2</sup>-C–H borylation. *Nature* **2019**, *575* (7782), 336-340. DOI: 10.1038/s41586-019-1640-2.
- (145) Lv, J.; Zhao, B.; Yuan, Y.; Han, Y.; Shi, Z. Boron-mediated directed aromatic C–H hydroxylation. *Nat. Commun.* **2020**, *11* (1), 1316. DOI: 10.1038/s41467-020-15207-x.
- (146) Shigeno, M.; Imamatsu, M.; Kai, Y.; Kiriyama, M.; Ishida, S.; Nozawa-Kumada, K.; Kondo, Y. Construction of 1,2,3-Benzodiazaborole by Electrophilic Borylation of Azobenzene and Nucleophilic Dialkylative Cyclization. *Org. Lett.* **2021**, *23* (20), 8023-8027. DOI: 10.1021/acs.orglett.1c03033.
- (147) Yamazaki, K.; Rej, S.; Ano, Y.; Chatani, N. Origin of the Enhanced Reactivity in the ortho C–H Borylation of Benzaldehydes with BBr<sub>3</sub>. *Org. Lett.* **2022**, *24* (1), 213-217. DOI: 10.1021/acs.orglett.1c03829.
- (148) Smith, M. O.; March, J.; Smith, M. O. *March's advanced organic chemistry : reactions, mechanisms, and structure*; Wiley-Interscience, 2007.
- (149) Hansen, T.; Vermeeren, P.; Bickelhaupt, F. M.; Hamlin, T. A. Stability of alkyl carbocations. *Chem. Commun.* **2022**, *58* (86), 12050-12053, 10.1039/D2CC04034D. DOI: 10.1039/D2CC04034D.
- (150) Arnett, E. M.; Hofelich, T. C. Stabilities of carbocations in solution. 14. An extended thermochemical scale of carbocation stabilities in a common superacid. *J. Am. Chem. Soc.* **1983**, *105* (9), 2889-2895. DOI: 10.1021/ja00347a060.
- (151) Houle, F. A.; Beauchamp, J. L. Photoelectron spectroscopy of methyl, ethyl, isopropyl, and tert-butyl radicals. Implications for the thermochemistry and structures of the radicals and their corresponding carbonium ions. *J. Am. Chem. Soc.* **1979**, *101* (15), 4067-4074. DOI: 10.1021/ja00509a010.
- (152) Olah, G. A. 100 Years of Carbocations and Their Significance in Chemistry1. *J. Org. Chem.* **2001**, *66* (18), 5943-5957. DOI: 10.1021/jo010438x.
- (153) Demuynck, M.; De Clercq, P.; Vandewalle, M. (.-.-)-Hysterin: revised structure and total synthesis. *J. Org. Chem.* **1979**, *44* (26), 4863-4866. DOI: 10.1021/jo00394a025.
- (154) Grieco, P. A.; Nishizawa, M.; Oguri, T.; Burke, S. D.; Marinovic, N. Sesquiterpene lactones: total synthesis of (.-.-)-vernolepin and (.-.-)-vernomenin. *J. Am. Chem. Soc.* **1977**, *99* (17), 5773-5780. DOI: 10.1021/ja00459a039.

## References

---

- (155) Pfizenmayer, A. J.; Ramanjulu, J. M.; Vera, M. D.; Ding, X.; Xiao, D.; Wei-Chuan, C.; Joullié, M. M. Synthesis and biological activities of [N-MeLeu5]- and [N-MePhe5]-didemnin B. *Tetrahedron* **1999**, *55* (2), 313-334. DOI: 10.1016/S0040-4020(98)01042-4.
- (156) Buchanan, G. S.; Cole, K. P.; Tang, Y.; Hsung, R. P. Total Synthesis of ( $\pm$ )-Phomactin A. Lessons Learned from Respecting a Challenging Structural Topology. *J. Org. Chem.* **2011**, *76* (17), 7027-7039. DOI: 10.1021/jo200936r.
- (157) Tokunaru, H.; Takashi, K.; Yasuhiko, K.; Isao, Y.; Hideaki, T.; Kazuyo, Y. Studies of the Selective O-Alkylation and Dealkylation of Flavonoids. XVIII. A Convenient Method for Synthesizing 3,5,6,7-Tetrahydroxyflavones. *Bulletin of the Chemical Society of Japan* **1995**, *68* (7), 2033-2041. DOI: 10.1246/bcsj.68.2033.
- (158) Wuts, T. W. G. a. P. G. M. *Greene's Protective Groups in Organic Synthesis*; Wiley, 2014.
- (159) Hassan, M. M. M.; Hoque, M. E.; Dey, S.; Guria, S.; Roy, B.; Chattopadhyay, B. Iridium-Catalyzed Site-Selective Borylation of 8-Arylquinolines. *Synthesis* **2021**, *53* (18), 3333-3342. DOI: 10.1055/a-1506-3884.
- (160) Littke, A. F.; Fu, G. C. Palladium-Catalyzed Coupling Reactions of Aryl Chlorides. *Angew. Chem. Int. Edit.* **2002**, *41* (22), 4176-4211. DOI: 10.1002/1521-3773(20021115)41:22<4176::AID-ANIE4176>3.0.CO;2-U.
- (161) Lehmann, J. W.; Blair, D. J.; Burke, M. D. Towards the generalized iterative synthesis of small molecules. *Nat. Rev. Chem.* **2018**, *2* (2), 0115. DOI: 10.1038/s41570-018-0115.
- (162) Knapp, D. M.; Gillis, E. P.; Burke, M. D. A General Solution for Unstable Boronic Acids: Slow-Release Cross-Coupling from Air-Stable MIDA Boronates. *J. Am. Chem. Soc.* **2009**, *131* (20), 6961-6963. DOI: 10.1021/ja901416p.
- (163) Gillis, E. P.; Burke, M. D. A Simple and Modular Strategy for Small Molecule Synthesis: Iterative Suzuki–Miyaura Coupling of B-Protected Haloboronic Acid Building Blocks. *J. Am. Chem. Soc.* **2007**, *129* (21), 6716-6717. DOI: 10.1021/ja0716204.
- (164) Blair, D. J.; Chitti, S.; Trobe, M.; Kostyra, D. M.; Haley, H. M. S.; Hansen, R. L.; Ballmer, S. G.; Woods, T. J.; Wang, W.; Mubayi, V.; et al. Automated iterative Csp<sub>3</sub>–C bond formation. *Nature* **2022**, *604* (7904), 92-97. DOI: 10.1038/s41586-022-04491-w.
- (165) Ihara, H.; Koyanagi, M.; Sugimoto, M. Anthranilamide: A Simple, Removable ortho-Directing Modifier for Arylboronic Acids Serving also as a Protecting Group in Cross-Coupling Reactions. *Org. Lett.* **2011**, *13* (10), 2662-2665. DOI: 10.1021/ol200764g.
- (166) Noguchi, H.; Hojo, K.; Sugimoto, M. Boron-Masking Strategy for the Selective Synthesis of Oligoarenes via Iterative Suzuki–Miyaura Coupling. *J. Am. Chem. Soc.* **2007**, *129* (4), 758-759. DOI: 10.1021/ja067975p.
- (167) Li, C.; Xiao, G.; Zhao, Q.; Liu, H.; Wang, T.; Tang, W. Sterically demanding aryl–alkyl Suzuki–Miyaura coupling. *Organic Chemistry Frontiers* **2014**, *1* (3), 225-229, 10.1039/C4QO00024B. DOI: 10.1039/C4QO00024B.

## References

---

- (168) Zhao, Q.; Li, C.; Senanayake, C. H.; Tang, W. An Efficient Method for Sterically Demanding Suzuki–Miyaura Coupling Reactions. *Chem.– Eur. J.* **2013**, *19* (7), 2261-2265. DOI: 10.1002/chem.201203898.
- (169) Yin, J.; Rainka, M. P.; Zhang, X.-X.; Buchwald, S. L. A Highly Active Suzuki Catalyst for the Synthesis of Sterically Hindered Biaryls: Novel Ligand Coordination. *J. Am. Chem. Soc.* **2002**, *124* (7), 1162-1163. DOI: 10.1021/ja017082r.
- (170) Barder, T. E.; Walker, S. D.; Martinelli, J. R.; Buchwald, S. L. Catalysts for Suzuki–Miyaura Coupling Processes: Scope and Studies of the Effect of Ligand Structure. *J. Am. Chem. Soc.* **2005**, *127* (13), 4685-4696. DOI: 10.1021/ja042491j.
- (171) Martin, R.; Buchwald, S. L. Palladium-Catalyzed Suzuki–Miyaura Cross-Coupling Reactions Employing Dialkylbiaryl Phosphine Ligands. *Acc. Chem. Res.* **2008**, *41* (11), 1461-1473. DOI: 10.1021/ar800036s.
- (172) Ishiyama, T.; Murata, M.; Miyaura, N. Palladium(0)-Catalyzed Cross-Coupling Reaction of Alkoxydiboron with Haloarenes: A Direct Procedure for Arylboronic Esters. *J. Org. Chem.* **1995**, *60* (23), 7508-7510. DOI: 10.1021/jo00128a024.
- (173) Jakt, M.; Johannissen, L.; Rzepa, H. S.; Widdowson, D. A.; Wilhelm, R. A computational study of the mechanism of palladium insertion into alkynyl and aryl carbon–fluorine bonds. *Journal of the Chemical Society, Perkin Transactions 2* **2002**, (3), 576-581, 10.1039/B108727B. DOI: 10.1039/B108727B.
- (174) Huq, M. M.; Robiur Rahman, M.; Naher, M.; Khan, M. M. R.; Masud, M. K.; Hossain, G. M. G.; Zhu, N.; Lo, Y. H.; Younus, M.; Wong, W.-Y. Synthesis, Characterization and Catalytic Activities of Palladium(II) Nitroaryl Complexes. *Journal of Inorganic and Organometallic Polymers and Materials* **2016**, *26* (6), 1243-1252. DOI: 10.1007/s10904-016-0434-3.
- (175) Cavanagh, J. *Protein NMR spectroscopy : principles and practice*, 2nd ed.; Academic Press, 2007.
- (176) <https://chem.ch.huji.ac.il/nmr/techniques/1d/row2/n.html>
- (177) Y.Vasavi, N. P., D.Sathis Kumar, David Banji, N.Srisutherson, Somsubhara Ghosh, M. Vinay Kumar Chakravarthy. Heteronuclear Multible Bond Correlation Spectroscopy- An Overview. *International Journal of PharmTech Research* **2011**, *3* (3), 14101422.
- (178) AD BAX, K. A. F., GREGORY S. WALKER. Increased HMBC Sensitivity for Correlating Poorly Resolved Proton Multiplets to Carbon-13 Using Selective or Semi-selective Pulses. *Journal of Magnetic Resonance, Series A* **1996**, *119*, 134-138.
- (179) Furrer, J. A comprehensive discussion of HMBC pulse sequences. 2. Some useful variants. *Concepts in Magnetic Resonance Part A* **2012**, *40A* (3), 146-169. DOI: 10.1002/cmr.a.21231.
- (180) Günther, H. *NMR spectroscopy : basic principles, concepts, and applications in chemistry*; Wiley-VCH, 2013.

## References

---

- (181) Furrer, J. A comprehensive discussion of hmbc pulse sequences, part 1: The classical HMBC. *Concepts in Magnetic Resonance Part A* **2012**, *40A* (3), 101-127. DOI: 10.1002/cmr.a.21232.
- (182) Lambert, J. B.; Binsch, G.; Roberts, J. D. NITROGEN-15 MAGNETIC RESONANCE SPECTROSCOPY, I. CHEMICAL SHIFTS<sup>\*</sup>. *Proceedings of the National Academy of Sciences* **1964**, *51* (5), 735-737. DOI: 10.1073/pnas.51.5.735.
- (183) Ros, A.; Fernández, R.; Lassaletta, J. M. Functional group directed C–H borylation. *Chem. Soc. Rev.* **2014**, *43* (10), 3229-3243, 10.1039/C3CS60418G. DOI: 10.1039/C3CS60418G.
- (184) Emmler, T.; Gieschler, S.; Limbach, H. H.; Buntkowsky, G. A simple method for the characterization of OHO-hydrogen bonds by <sup>1</sup>H-solid state NMR spectroscopy. *Journal of Molecular Structure* **2004**, *700* (1), 29-38. DOI: 10.1016/j.molstruc.2004.01.045.
- (185) Kumar, G. A.; McAllister, M. A. Theoretical Investigation of the Relationship between Proton NMR Chemical Shift and Hydrogen Bond Strength. *J. Org. Chem.* **1998**, *63* (20), 6968-6972. DOI: 10.1021/jo980759h.
- (186) Liepiņš, E.; Petrova, M. V.; Gudriniece, E.; Pauliņš, J.; Kuznetsov, S. L. Relationships between <sup>1</sup>H, <sup>13</sup>C and <sup>17</sup>O NMR chemical shifts and H/D isotope effects on <sup>13</sup>C and <sup>17</sup>O nuclear shielding in intramolecular hydrogen-bonded systems. *Magnetic Resonance in Chemistry* **1989**, *27* (10), 907-915. DOI: 10.1002/mrc.1260271002.
- (187) Garcia-Amorós, J.; Díaz-Lobo, M.; Nonell, S.; Velasco, D. Fastest Thermal Isomerization of an Azobenzene for Nanosecond Photoswitching Applications under Physiological Conditions. *Angew. Chem. Int. Edit.* **2012**, *51* (51), 12820-12823. DOI: 10.1002/anie.201207602.
- (188) García-Amorós, J.; Velasco, D. Recent advances towards azobenzene-based light-driven real-time information-transmitting materials. *Beilstein J. Org. Chem.* **2012**, *8*, 1003-1017. DOI: 10.3762/bjoc.8.113.
- (189) Garcia-Amorós, J.; Sánchez-Ferrer, A.; Massad, W. A.; Nonell, S.; Velasco, D. Kinetic study of the fast thermal cis-to-trans isomerisation of para-, ortho- and polyhydroxyazobenzenes. *Phys. Chem. Chem. Phys.* **2010**, *12* (40), 13238-13242, 10.1039/C004340K. DOI: 10.1039/C004340K.
- (190) Steinwand, S.; Halbritter, T.; Rastädter, D.; Ortiz-Sánchez, J. M.; Burghardt, I.; Heckel, A.; Wachtveitl, J. Ultrafast Spectroscopy of Hydroxy-Substituted Azobenzenes in Water. *Chem.– Eur. J.* **2015**, *21* (44), 15720-15731. DOI: 10.1002/chem.201501863.
- (191) Millefiori, S.; Millefiori, A. Intramolecular hydrogen bond in ortho-hydroxyazobenzenes. *Journal of the Chemical Society, Faraday Transactions 2: Molecular and Chemical Physics* **1980**, *76* (0), 827-833, 10.1039/F29807600827. DOI: 10.1039/F29807600827.
- (192) Gentili, P. L.; Capaccioni, A.; Germani, R.; Fantacci, S. The Versatile Photo-Thermal Behaviour of a 2-Hydroxyazobenzene. *Molecules* **2023**, *28* (3), 1183.

## References

---

- (193) Trost, B. M.; Kinson, P. L.; Maier, C. A.; Paul, I. C. Structure of 4,8-dihydrodibenzo[cd,gh] pentalene. *J. Am. Chem. Soc.* **1971**, *93* (26), 7275-7281. DOI: 10.1021/ja00755a026.
- (194) Takeshi, K.; Yasuhiro, I.; Naomichi, F. The First Preparation and Structures of Dibenzo[bc,fg][1,4]-diselenapentalene and -selenathiapentalene. *Chem. Lett.* **1993**, *22* (4), 635-636. DOI: 10.1246/cl.1993.635.
- (195) Kimura, T.; Ishikawa, Y.; Ogawa, S.; Nishio, T.; Iida, I.; Furukawa, N. First preparation of dibenzo[bc,fg][1,4]dithiapentalene and determination of the structure by X-ray analysis. *Tetrahedron Letters* **1992**, *33* (42), 6355-6358. DOI: 10.1016/S0040-4039(00)60972-3.
- (196) Shimizu, M.; Tatsumi, H.; Mochida, K.; Oda, K.; Hiyama, T. Silicon-Bridge Effects on Photophysical Properties of Silafluorenes. *Chem.- Asian J.* **2008**, *3* (8-9), 1238-1247. DOI: 10.1002/asia.200800094.
- (197) Mazzanti, V.; Della Pia, E. A.; Jevric, M.; Jepsen, T. H.; Kadziola, A.; Hammerich, O.; Nielsen, M. B. Dibenzo[bc,fg][1,4]oxathiapentalene: an elusive molecule? *Journal of Sulfur Chemistry* **2013**, *34* (6), 588-595. DOI: 10.1080/17415993.2013.789515.
- (198) Vetráková, L.; Ladányi, V.; Al Anshori, J.; Dvořák, P.; Wirz, J.; Heger, D. The absorption spectrum of cis-azobenzene. *Photochemical & Photobiological Sciences* **2017**, *16* (12), 1749-1756, 10.1039/C7PP00314E. DOI: 10.1039/C7PP00314E.
- (199) Czerny, M.; Turner, A. F. Über den Astigmatismus bei Spiegelspektrometern. *Zeitschrift für Physik* **1930**, *61* (11), 792-797. DOI: 10.1007/BF01340206.
- (200) Skoog, D. A.; Holler, F. J.; Crouch, S. R.; Crouch, S. R.; Holler, F. J. *Principles of instrumental analysis*; Thomson, 2007.
- (201) Kerckhoffs, A.; Christensen, K. E.; Langton, M. J. Fast relaxing red and near-IR switchable azobenzenes with chalcogen and halogen substituents: periodic trends, tuneable thermal half-lives and chalcogen bonding. *Chem. Sci.* **2022**, *13* (39), 11551-11559, 10.1039/D2SC04601F. DOI: 10.1039/D2SC04601F.
- (202) Victor Talrose, A. N. Y., Alexy A. Usov, Antonina A. Goncharova, Axlexander N. Leskin, Natalia A. Messineva, Natalia V. Trusova, Margarita V. Efimkina. NIST Chemistry WebBook, NIST Standard Reference Database Number 69, Eds. P.J. Linstrom and W.G. Mallard.
- (203) Mayerhöfer, T. G.; Pahlow, S.; Popp, J. The Bouguer-Beer-Lambert Law: Shining Light on the Obscure. *ChemPhysChem* **2020**, *21* (18), 2029-2046. DOI: 10.1002/cphc.202000464.
- (204) Knie, C.; Utecht, M.; Zhao, F.; Kulla, H.; Kovalenko, S.; Brouwer, A. M.; Saalfrank, P.; Hecht, S.; Bléger, D. ortho-Fluoroazobenzenes: Visible Light Switches with Very Long-Lived Z Isomers. *Chem.- Eur. J.* **2014**, *20* (50), 16492-16501. DOI: 10.1002/chem.201404649.
- (205) Erekath, S.; Chordiya, K.; Vidhya, K. V.; Kahaly, M. U.; Kalpathy, S. K. Self-aggregation, H-bonding, and photoresponse in film and solution states of azobenzene containing polyurea. *Phys. Chem. Chem. Phys.* **2022**, *24* (38), 23447-23459, 10.1039/D2CP01200F. DOI: 10.1039/D2CP01200F.

## References

---

- (206) Harbron, E. J.; Hadley, D. H.; Imm, M. R. Solvent effects on phototriggered conformational changes in an azobenzene-functionalized poly(p-phenylene vinylene). *Journal of Photochemistry and Photobiology A: Chemistry* **2007**, *186* (2), 151-157. DOI: 10.1016/j.jphotochem.2006.08.002.
- (207) Klán, P.; Wirz, J.; Klán, P. *Photochemistry of Organic Compounds : From Concepts to Practice*; John Wiley & Sons, Incorporated, 2009.
- (208) Stranius, K.; Börjesson, K. Determining the Photoisomerization Quantum Yield of Photoswitchable Molecules in Solution and in the Solid State. *Sci. Rep.* **2017**, *7* (1), 41145. DOI: 10.1038/srep41145.
- (209) Hall, D. G. Structure, Properties, and Preparation of Boronic Acid Derivatives. In *Boronic Acids*, 2011; pp 1-133.
- (210) Bruker, *SAINT+ v8.39.0 Integration Engine, Data Reduction Software*; WI, USA, 2018. (accessed).
- (211) Bruker, *SADABS, 2018, Bruker AXS area detector scaling and absorption correction*; WI, USA, 2018. (accessed).
- (212) Sheldrick, G. SHELXT - Integrated space-group and crystal-structure determination. *Acta Crystallographica Section A* **2015**, *71* (1), 3-8. DOI: 10.1107/S2053273314026370.
- (213) Sheldrick, G. A short history of SHELX. *Acta Crystallographica Section A* **2008**, *64* (1), 112-122. DOI: 10.1107/S0108767307043930.
- (214) Dolomanov, O. V.; Bourhis, L. J.; Gildea, R. J.; Howard, J. A. K.; Puschmann, H. OLEX2: a complete structure solution, refinement and analysis program. *Journal of Applied Crystallography* **2009**, *42* (2), 339-341. DOI: 10.1107/S0021889808042726.
- (215) Lv, H.; Laishram, R. D.; Yang, Y.; Li, J.; Xu, D.; Zhan, Y.; Luo, Y.; Su, Z.; More, S.; Fan, B. TEMPO catalyzed oxidative dehydrogenation of hydrazobenzenes to azobenzenes. *Organic & Biomolecular Chemistry* **2020**, *18* (18), 3471-3474, 10.1039/D0OB00103A. DOI: 10.1039/D0OB00103A.
- (216) Murata, M.; Oyama, T.; Watanabe, S.; Masuda, Y. Palladium-Catalyzed Borylation of Aryl Halides or Triflates with Dialkoxyborane: A Novel and Facile Synthetic Route to Arylboronates. *J. Org. Chem.* **2000**, *65* (1), 164-168. DOI: 10.1021/jo991337q.
- (217) Thormeier, S.; Carboni, B.; Kaufmann, D. E. Chiral boronates—versatile reagents in asymmetric synthesis. *J. Organomet. Chem.* **2002**, *657* (1), 136-145. DOI: [https://doi.org/10.1016/S0022-328X\(02\)01323-2](https://doi.org/10.1016/S0022-328X(02)01323-2).
- (218) Rochette, É.; Desrosiers, V.; Soltani, Y.; Fontaine, F.-G. Isodesmic C–H Borylation: Perspectives and Proof of Concept of Transfer Borylation Catalysis. *J. Am. Chem. Soc.* **2019**, *141* (31), 12305-12311. DOI: 10.1021/jacs.9b04305.
- (219) Pierrat, P.; Gros, P.; Fort, Y. Hiyama Cross-Coupling of Chloro-, Fluoro-, and Methoxypyridyltrimethylsilanes: Room-Temperature Novel Access to Functional Bi(het)aryl. *Org. Lett.* **2005**, *7* (4), 697-700. DOI: 10.1021/o1047482u.

## **References**

---

- (220) Peng, H.; Chen, X.; Chen, Y.; He, Q.; Xie, Y.; Yang, C. Solvent-free synthesis of  $\delta$ -carbolines/carbazoles from 3-nitro-2-phenylpyridines/2-nitrobiphenyl derivatives using DPPE as a reducing agent. *Tetrahedron* **2011**, *67* (32), 5725-5731. DOI: <https://doi.org/10.1016/j.tet.2011.06.027>.
- (221) Shigeno, M.; Imamatsu, M.; Kai, Y.; Kiriyama, M.; Ishida, S.; Nozawa-Kumada, K.; Kondo, Y. Construction of 1,2,3-Benzodiazaborole by Electrophilic Borylation of Azobenzene and Nucleophilic Dialkylative Cyclization. *Org. Lett.* **2021**, *23* (20), 8023-8027. DOI: [10.1021/acs.orglett.1c03033](https://doi.org/10.1021/acs.orglett.1c03033).
- (222) Wu, Y.; Zhou, B. Rhodium(III)-Catalyzed Selective C–H Acetoxylation and Hydroxylation Reactions. *Org. Lett.* **2017**, *19* (13), 3532-3535. DOI: [10.1021/acs.orglett.7b01494](https://doi.org/10.1021/acs.orglett.7b01494).